Insights into the development of peri-biliary fibrosis following hepatic ischaemia-reperfusion injury and the ameliorating effect of PXR activation

Aimen O Amer

Student Number: 109252476

Doctor of Philosophy

School of Medicine

Newcastle University

Submitted September 2017

Abstract

Despite progress in liver transplantation, biliary complications such as non-anastomotic biliary strictures (NABS) remain its “Achilles heel” and our understanding of the pathogenesis of these lesions remains limited. An inflammatory process following reperfusion injury of the liver is a possible cause for this pathology. The pregnane X receptor (PXR) has gained interest in recent years as a potential therapeutic target for inflammatory bowel and liver conditions. Its role in ischaemia reperfusion injury (IRI) following liver transplantation remains unexplored. The aim of this project was to investigate the development of biliary pathology following ischaemia reperfusion injury and the potential beneficial effect of PXR activation on these lesions.

In vitro studies on the pro-fibrotic effect of varying oxygen conditions on human biliary epithelial cells were carried out initially, followed by an in vivo rat model of hepatic ischaemia reperfusion injury to sequentially examine the progression of fibrosis following hepatic IRI and the potential ameliorating effect of PXR activation on this. The project culminates in a retrospective clinical study to confirm the benefit of PXR activation in a cohort of liver transplant recipients

The in vitro studies highlighted an active pro-inflammatory role for biliary epithelial cells when subjected to oxygen after a period of hypoxia. Moreover, hepatic IRI was found to cause persistent inflammatory and fibrotic changes beyond the initial ischaemic insult in the in vivo rat model. Activation of the PXR led to a reduction in post-IRI cellular damage, inflammation and fibrosis in the animal model and these promising findings were supported in the clinical study which highlighted a beneficial role for PXR activation in reducing anastomotic biliary strictures and ultimately improving patient survival following liver transplantation

This project provides further insight into the pathogenesis of biliary lesions following reperfusion injury and shed further light on the potential role for PXR activation in improving graft outcomes following liver transplantation. It also opens the door for novel therapies such as the use of PXR activators in perfusion fluid, potentially optimising the organ donation pool.

Dedication

I would like to dedicate this work to my father, whose lifetime achievements and work ethics have inspired me to embark on this project, and to my mother and wife, whose patience and support enabled me to complete it.

Acknowledgments

I would like to express my utmost gratitude and appreciation to Professor Matthew Wright for his constant guidance and support throughout this project. I enjoyed our scientific (and theological) debates and found working with him an absolute pleasure. He might also say the same had it not been for my terrible bookkeeping which he tolerated with great patience!

I would equally like to thank my clinical supervisor, Professor Steve White, without whom this work would not have been possible in the first place. His fatherly support and patience has helped see me through some difficult times, and his clinical and academic accomplishments continue to inspire me. He has helped me become the person that I am today and for that I am forever grateful.

I would also like to thank my laboratory colleagues and friends: Emma Fairhall, Izzy Swidenbank, Phillip Probert, Stephen Hill, Michael White, Audrey Brown, Karen Wallace, Stephanie Meyer and Anne Lakey for all their help. Beanbags, abandoned coffee machines and our ‘wall of fame’ still stand testament to the wonderful times we spent working under one lab roof.

I must also thank Kirsty McColl and Abigail Vallance for their assistance in completing parts of this project and for ‘gently’ correcting my grammatical and spelling mistakes.

In addition, I would like to extend my gratitude and appreciation to Professors Andrew Fisher and John Kirby for their regular guidance as reviewers of my project; to Professor Paul Flecknell, Dr Aurelie Thomas and other members of the Comparative Biology Centre for their assistance with the animal procedures; and to the biobank and electron microscopy staff for their support. I also wish to thank the staff at both the Robinson library and the Library of University Hospital of North Durham for their tremendous effort at sourcing otherwise unobtainable literature for me, and the research team at the National Institute for Health Chemical Genomics Centre in Maryland, USA for providing the drug PXR profiling data.

Importantly, I wish to thank the transplant coordinators at the Freeman Hospital for all the effort and time they have put into helping me with the clinical research.

Declaration and sources of funding

I declare that the work in this project is original research that I have conducted and that no aspect of this thesis has been accepted as part of a degree elsewhere.

This project has been partly funded by the Libyan Ministry of Higher Education and Scientific Research

Publications and presentations

Publications

Amer, A. O., Probert, P. M., Dunn, M., Knight, M., Vallance, A. E., Flecknell, P. A., Oakley, F., Cameron, I., White, S. A., Blain, P. G. & Wright, M. C. 2015. Sustained Isoprostane E2 Elevation, Inflammation and Fibrosis after Acute Ischaemia-Reperfusion Injury Are Reduced by Pregnane X Receptor Activation. PloS one, 10, e0136173.

Presentations

Dunn M, **Amer A**, Knight M, Roper C, Wright MC. Lipid Peroxidation Profiles in Acute Hepatic Ischaemia-Reperfusion Injury. J Am Soc Mass Spectrom. 2016 Jun; 27(S1). Poster presentation at the American Society for Mass Spectrometry conference in San Antonio, USA, June 2016

Amer A, McColl KN, Vallance AE, Kanwar A, Wright MC, White SA. Reducing the risk of early allograft dysfunction in liver transplant recipients by activation of the pregnane x receptor (PXR). Transpl Int. 2015 Nov; 28(S4). Oral presentation at the European Society of Organ Transplantation International Transplant Congress in Brussels, September 2015

Amer A, Vallance AE, Wright MC, White SA. Activation of the pregnane x receptor (PXR) reduces the risk of early allograft dysfunction following liver transplantation. GUT. 2015 Jun; 64(S1). Poster presentation at the Digestive Disease Federation meeting in London, June 2015

Amer A, Vallance AE, Manas DM, Wright MC, White SA. The PXR as a drug target for the prevention of early graft loss following liver transplantation. BJS. 2014 May; 101(S4). Oral presentation at the annual meeting of the Society of Academic and Research Surgery (SARS) in Cambridge, January 2014 (Patey prize session)

Amer A, Vallance AE, Wright MC, White SA. Peri-portal fibrosis: the role of biliary epithelial cells following ischaemia-reperfusion injury during DCD liver transplantation. Transpl Int. 2013 Nov; 26(S2). Oral presentation at the 16th Congress of the European Society for Organ Transplantation (ESOT), Vienna, Austria, September 2013

Vallance AE, **Amer A,** White SA, Wright MC. Transpl Int. 2013 Nov; 26(S2). The PXR as a drug target for the prevention of early graft loss after severe liver ischaemia reperfusion injury. Oral presentation at the 16th Congress of the European Society for Organ Transplantation (ESOT), Vienna, Austria, September 2013

Amer A, Wright MC, White SA. In vivo alterations to cholangiocyte microvilli and bile composition in response to hepatic ischaemia reperfusion injury. Transpl Int. 2013 Nov; 26(S2). Poster presentation at the 16th Congress of the European Society for Organ Transplantation (ESOT), Vienna, Austria, September 2013

Amer A, Wright MC, White SA. The effect of ischaemia-reperfusion injury on the morphology of biliary epithelial cell microvilli and bile regulation in vivo. J Hepatol. 2013 Apr; 58(S1). Poster presentation at the International Liver Congress of the European Association for the Study of the Liver (EASL), Amsterdam, The Netherlands, April 2013

Amer A, Vallance AE, Wright MC, White SA. The PXR: A drug target for the prevention of early graft loss after severe liver ischaemia reperfusion injury. Oral presentation at the Royal College of Surgeons of England and North of England Surgical Society joint meeting. Newcastle upon Tyne, UK

Amer A, Wright MC, White SA. Peri-portal fibrosis: the role of biliary epithelial cells following ischaemia-reperfusion injury in the liver. Oral presentation for the Ella Foster Memorial Award at the Freeman Hospital, Newcastle upon Tyne, March 2013

Amer A, Manas DM, Wright MC, White SA. Activated hepatic stellate cell chemotaxis in-vitro: The role of ischaemia-reperfusion injury. BJS. 2013 May; 100(S4):24. Presented at the Society of Academic and Research Surgery (SARS) and the Section of Surgery of the Royal Society of Medicine (RSM) Joint Meeting 2013, London

Amer A, Wright MC, White SA. In vivo alterations to cholangiocyte microvilli and bile composition in response to hepatic ischaemia-reperfusion injury. BJS. 2013 May; 100(S4):24. Presented at the Society of Academic and Research Surgery (SARS) and the Section of Surgery of the Royal Society of Medicine (RSM) Joint Meeting 2013, London

Amer A, Manas DM, Wright MC, White SA. The effect of hypoxic stress on activated HSC chemotaxis in-vitro. GUT. Jul 2012;61(S2). Poster presentation at the Digestive Disorders Federation Annual Conference, Liverpool, June 2012

Amer A, Manas DM, Wright MC, White SA. The effect of hypoxic stress on activated hepatic stellate cell (HSC) chemotaxis in-vitro. HPB. 2012 Jul;14(S2). Poster presentation at the International Hepato-Pancreato-Biliary Association (IHPBA) World Congress, Paris, France, July 2012

Table of contents

Chapter 1. Introduction 1

1.1. The current state of orthotopic liver transplantation (OLT) 2

1.2. Non-anastomotic biliary strictures (NABS) and liver transplantation 3

1.3. A potential role for reperfusion injury in the development of NABS 5

1.4. Activation of the pregnane X receptor as a potential target in the prevention of NABS 7

1.5. Hypotheses and aims of project 9

Chapter 2. Biliary epithelial cells and peri-ductal fibrosis following ischaemia-reperfusion injury: Innocent bystanders or central players? An in vitro study 10

2.1. Introduction 11

2.1.1. The role of biliary epithelial cells in the development of transplantation-related peri-biliary fibrosis 11

2.1.2. Isolation of primary biliary epithelial cells in culture: Techniques and challenges 13

2.1.3. Hypotheses and aims 15

2.2. Materials and methods 16

2.2.1. Ethical considerations 16

2.2.2. Cell isolation protocols 16

2.2.3. Cell culture conditions 19

2.2.4. Cell culture in hypoxia 20

2.2.5. Chemotaxis assays 21

2.2.6. Sample processing and preservation 24

2.2.7. Methods for protein analysis 25

2.2.8. Methods for cell staining 29

2.2.9. Statistical analysis 30

2.3. Results 32

2.3.1. Confirmation of isolated cell phenotype in culture 32
2.3.2. Results of chemotaxis assays 38
2.3.3. Results of cytokine quantification in conditioned cell media 48
2.4. Discussion 49
Chapter 3. In vivo rat hepatic ischaemia-reperfusion injury models: A literature review 53
3.1. Introduction 54
3.1.1. The ideal species 54
3.1.2. Anatomy of the rat liver 57
3.1.3. In vivo rat models of hepatic IRI 65
3.1.4. Aim of review 69
3.2. Methods 70
3.2.1. Study design 70
3.2.2. Inclusion criteria 70
3.2.3. Search strategy 71
3.2.4. Exclusion of ineligible studies 72
3.2.5. Data extraction 72
3.2.6. Data expression and statistical analysis 74
3.3. Results 75
3.3.1. Overview of eligible studies 75
3.3.2. Description of model methodology 75
3.3.3. Chronological evolvement of methodologies 86
3.3.4. Associations between hepatic IRI models and other variables 102
3.3.5. Survival analysis 109
3.4. Discussion 115
Chapter 4. In vivo IRI model 121
4.1. Introduction 122
4.1.1. Stages of hepatic IRI 122

4.1.2. Ischaemia reperfusion injury and biliary epithelial cells 126
4.1.3. Susceptibility of the biliary epithelium to ischaemic injury: anatomical, physiological and embryological considerations 127
4.1.4. Challenges to understanding NABS 128
4.1.5. Aim of study 129
4.2. Materials and methods 130
4.2.1. Ethical considerations 130
4.2.2. Rat model of hepatic ischaemia-reperfusion injury and ischaemic cholangiopathy 130
4.2.3. Sample processing and preservation 134
4.2.4. Methods for protein analysis 136
4.2.5. Methods for mRNA quantification 137
4.2.6. Methods for tissue staining 138
4.2.7. Examination of biliary epithelial cell microvilli under transmission electron microscopy (TEM) 142
4.2.8. Thiobarbituric Acid Reactive Substances (TBARS) assay 142
4.2.9. Bile acid assay 143
4.2.10. Phospholipid assay 144
4.2.11. Glutamate dehydrogenase assay 145
4.2.12. Serum liver function tests 146
4.2.13. Statistical analysis 146
4.3. Results 147
4.3.1. Results from the pilot hepatic ischaemia-reperfusion injury model 147
4.3.2. Results from the optimised hepatic ischaemia reperfusion injury and cholangiopathy model 149
4.4. Discussion 198
Chapter 5. PXR study 204
5.1. Introduction 205
5.1.1. The nuclear receptor superfamily 205

5.1.2. Discovery of the PXR 207
5.1.3. The structure of the PXR and its mechanism of action 208
5.1.4. PXR ligand selectivity between species 212
5.1.5. Role of the PXR 213
5.1.6. Risks associated with PXR activation 217
5.1.7. Hypothesis and aim of study 219
5.2. Materials and methods 220
5.2.1. Ethical considerations 220
5.2.2. Model to investigate the effect of PXR activation on hepatic ischaemia-reperfusion injury 220
5.2.3. Sample processing and preservation 223
5.2.4. Protein analysis 223
5.2.5. mRNA quantification 223
5.2.6. Methods for tissue staining 223
5.2.7. Other biochemical analyses 223
5.2.8. Statistical analysis 223
5.3. Results 224
5.3.1. Mortality 224
5.3.2. Evidence of PXR activation 224
5.3.3. Effect of PXR activation on lipid peroxidation 226
5.3.4. Effect of PXR activation on bile flow 226
5.3.5. Effect of PXR activation on hepatocellular necrosis 228
5.3.6. Effect of PXR activation on liver function tests 230
5.3.7. Effect of PXR activation on inflammatory cell infiltration 231
5.3.8. Effect of PXR activation on dry liver weight 233
5.3.9. Effect of PXR activation on IRI-induced fibrogenesis 235
5.3.10. Effect of PXR activation on IRI-induced ductular reaction 241
5.4. Discussion 243

Chapter 6. Clinical PXR study 246

6.1. Introduction 247

6.1.1. Rat versus human PXR 247

6.1.2. Identification of clinically relevant PXR activators 247

6.1.3. PXR polymorphism 249

6.1.4. Designing a clinical study 250

6.1.5. Hypothesis and aim of study 252

6.2. Methods 253

6.2.1. Study design 253

6.2.2. Data extraction 253

6.2.3. Exclusion criteria 259

6.2.4. Calculation of Predicted hPXR activation value on day 7 ($PPAV_7$) 260

6.2.5. Outcomes 262

6.2.6. Data expression and statistical analysis 264

6.3. Results 266

6.3.1. Overview of patient inclusion 266

6.3.2. Characteristics of study population 267

6.3.3. hPXR activation 270

6.3.4. Early allograft dysfunction (EAD) and hPXR activation 275

6.3.5. Post-transplant complications and hPXR activation 278

6.3.6. The impact of hPXR activation on survival following OLT 281

6.3.7. Subgroup analyses 293

6.4. Discussion 297

Conclusion 301

Appendices 302

References 313

List of figures

Figure 1.1. Deceased donor liver transplant trends in the adult and paediatric populations over the past 10 years. Data from NHSBT (2015).....3
Figure 1.2. Non-anastomotic biliary strictures identified on cholangiography. Lesions can range from solitary and mild (left) to diffuse and severe (right). From Buis et al (Buis et al., 2007) 4
Figure 1.3. Blood supply to the bile duct. Adapted from Deltenre and Valla 2006 (Deltenre and Valla, 2006).....5
Figure 1.4 The effects of PXR activation in the liver.....8
Figure 2.1 The expression of TLRs by BECs and the NFkB-mediated immune response 12
Figure 2.2 Percoll gradient centrifugation results in a HSC/hepatocyte ring (top) and a BEC ring (bottom).....17
Figure 2.3 Separation of HSC layer in Optiprep gradient 18
Figure 2.4 Multigas incubator for in vitro hypoxia studies (left). To maintain hypoxia, oxygen in this incubator is replaced with nitrogen delivered via a nitrogen generator (right).....21
Figure 2.5 Testing for the expression of chemoattractants by hBECs in various oxygen states 23
Figure 2.6 Assembly of chemotaxis assay components.....24
Figure 2.7 Assembly of transfer layers in holding cassette 29
Figure 2.8 Human BECs visualised in cell culture using immunofluorescence staining at 20X objective magnification. Solid white arrows denote duct-like arrangements...32
Figure 2.9 Immunofluorescence staining for surface markers of BECs (transporters and tight junctions). Note the presence of Dynabeads from the cell isolation process which auto-fluoresce and do not represent antigen-antibody binding sites (as demonstrated in control images). CFTR: Cystic fibrosis transmembrane conductance regulator; AE2: Anion exchange protein 2; OSTα: Organic solute transporter alpha; ZO1: Zonula occludens-1; TRITC: Tetramethylrhodamine; FITC: Fluorescein isothiocyanate 34
Figure 2.10 Immunofluorescence staining for markers of mesenchymal cells (α-SMA and vimentin) along with CK19 in hBECs. Note auto-fluorescence of Dynabeads in control images. TRITC: Tetramethylrhodamine; FITC: Fluorescein isothiocyanate...34

Figure 2.11 Immunofluorescence imaging showing CK19 and α-SMA positivity in freshly-cultured hBECS in comparison to mature hBECs and H69 cells. TRITC: Tetramethylrhodamine; FITC: Fluorescein isothiocyanate 35
Figure 2.12 hHSCs at 20X objective magnification under light microscopy after 5 days in culture with (left) and withought (right) MatrigelTM. 36
Figure 2.13 Immunofluorescence imaging of activated hHSCs. Neural crest markers (GFAP and synaptophysin) are stained along with α-SMA. TRITC: Tetramethylrhodamine; FITC: Fluorescein isothiocyanate 37
Figure 2.14 Light microscopy of cell culture insert showing size of stellate cell relative to pore diameter. Left: image taken at the time the cells were seeded onto insert. White arrowhead marks one pore. Black arrow marks one hHSC. Right: image takes after 20 hours of incubation. Black arrow shows previously marked cell has now migrated to lower surface of insert 38
Figure 2.15 Migration of hHSCs towards PDGF (left) versus VEGF (middle) and MCP-1 (right). Cells were used at passage 4 and seeded at 60,000 cell/ml. 39
Figure 2.16 Migration of hHSCs towards various cytokines. Concentrations of cytokines in this example were all 62.5ng/ml. Cells were used at passage 3 and seeded at 100,000 cell/ml. Average absorbance of washed crystal violet stain was used in preliminary experiments rather than actual cell count. *P<0.05 versus negative control. 39
Figure 2.17 Migration of hHSCs towards high and low concentrations of various bile components. Cells were used at passage 4 and seeded at 60,000 cell/ml. PDGF used as positive control is not shown (average count >80). High concentrations=100ng/ml; Low concentrations=10ng/ml. PC: Phosphatidylcholine; CL: Cholesterol; CDCA: Chenodeoxycholic acid; CA: Cholic acid; Bil: Bilirubin. *P<0.05 versus negative control; $P<0.05 versus high concentration 40
Figure 2.18 Comparison of hHSC migration to bile components and known cytokines. Concentrations of cytokines in this example were all 62.5ng/ml. Cells were used at passage 3 and seeded at 100,000 cell/ml. Average absorbance of washed crystal violet stain was used in preliminary experiments rather than actual cell count. High concentrations=100ng/ml; Low concentrations=10ng/ml. PC: Phosphatidylcholine; CL: Cholesterol; CDCA: Chenodeoxycholic acid; CA: Cholic acid; Bil: Bilirubin. *P<0.05 versus negative control; $P<0.05 versus high concentration 41
Figure 2.19 hHSC migration to media from hypoxic versus normoxic Kupffer cells. *P<0.05 versus negative control; $P<0.05 versus normoxic conditions 42

Figure 2.20 hHSC migration to media from hypoxic versus normoxic human biliary epithelial cells at 1 and 7 days in culture. Cells were used at passage 4 and seeded at 100,000 cell/ml. *P<0.05 versus negative control; ^P<0.05 versus later timepoint; $P<0.05 versus normoxic conditions....43
Figure 2.21 hHSC migration to media from hypoxic versus normoxic human hepatic stellate cells at 3 and 7 days in coated culture. Cells were used at passage 4 and seeded at 100,000 cell/ml. *P<0.05 versus negative control; ^P<0.05 versus later timepoint; $P<0.05 versus normoxic conditions....44
Figure 2.22 hHSC migration to media from hypoxic versus normoxic human hepatic stellate cells at 3 and 7 days in uncoated culture. Cells were used at passage 4 and seeded at 100,000 cell/ml. *P<0.05 versus negative control; ^P<0.05 versus later timepoint; $P<0.05 versus normoxic conditions....45
Figure 2.23 hHSC migration to media from human biliary epithelial cells (passage 0) at 1 and 3 days in culture. Hypoxic to normoxic conditions were compared to hypoxia or normoxia alone. hHSCs were used at passage 3 and seeded at 60,000 cell/ml. *P<0.05 versus negative control; ^P<0.05 versus later timepoint; $P<0.05 versus normoxia or hypoxia alone....46
Figure 2.24 hHSC migration to bile sample obtained from rats exposed to hepatic IRI versus control rats. hHSCs were used at passage 3 and seeded at 30,000 cell/ml. *P<0.05 versus negative control....47
Figure 3.1 The frequency of published research on hepatic IRI studies since 1950 according to mammalian species (results are based on PubMed search conducted in May 2016)....55
Figure 3.2 Time-trend of animal choice in published in vivo hepatic IRI studies. (results are based on PubMed search conducted in May 2016)....56
Figure 3.3 The falciform ligament (arrow) divides the median lobe of rat liver into right and left portions....58
Figure 3.4 Passage of vascular and biliary structures via the transverse hepatic fissure (porta hepatis) (arrow). The hepatogastric ligament can also be seen on the left....58
Figure 3.5 Anatomy and relative mass of rat liver lobes. Modified from Martins and Neuhaus 2007 (Martins and Neuhaus 2007)....60
Figure 3.6 Right lobe (superior and inferior) joined to Spiegel lobe (anterior and posterior) through caudate process....61

Figure 3.7 Portal venous anatomy in the rat. RML: Right median lobe; LML: Left median lobe; LLL: Left lateral lobe; SRL: Superior right lobe; IRL: Inferior right lobe; ACL: Anterior caudate lobe; PCL: Posterior caudate lobe. Paracaval caudate tissue is omitted for simplification 62
Figure 3.8 Hepatic venous anatomy in the rat. RML: Right median lobe; LML: Left median lobe; LLL: Left lateral lobe; SRL: Superior right lobe; IRL: Inferior right lobe; ACL: Anterior caudate lobe; PCL: Posterior caudate lobe; IVC: Inferior vena cava. Paracaval caudate tissue is omitted for simplification 64
Figure 3.9 Biliary tree anatomy in the rat. RML: Right median lobe; LML: Left median lobe; LLL: Left lateral lobe; SRL: Superior right lobe; IRL: Inferior right lobe; ACL: Anterior caudate lobe; PCL: Posterior caudate lobe; CBD: Common bile duct. Paracaval caudate tissue is omitted for simplification 65
Figure 3.10 Selective inflow occlusion models. Flow represents portal venous and hepatic arterial inflow combined. Black rectangles represent level of occlusion. Ischaemic lobes represented in purple. RML: Right median lobe; LML: Left median lobe; LLL: Left lateral lobe; SRL: Superior right lobe; IRL: Inferior right lobe; ACL: Anterior caudate lobe; PCL: Posterior caudate lobe. Paracaval caudate tissue is omitted for simplification 67
Figure 3.11 Study-inclusion flowchart 76
Figure 3.12 Distribution of rat strains utilised in hepatic IRI studies 77
Figure 3.13 Frequency distribution of anaesthetic agents used in rat hepatic IRI studies 78
Figure 3.14 Frequency distribution of heparin doses administered in rat hepatic IRI studies 79
Figure 3.15 Frequency distribution of models adopted in rat hepatic IRI studies 80
Figure 3.16 Frequency distribution of ischaemia times in hepatic IRI rat studies 83
Figure 3.17 Frequency distribution of minimum reperfusion times in hepatic IRI rat studies 84
Figure 3.18 Frequency distribution of maximum reperfusion times in hepatic IRI rat studies (excluding survival analyses) 84
Figure 3.19 Summary of intervention types adopted in rat hepatic IRI studies 86
Figure 3.20 Time-trends in the adoption of total inflow occlusion models 87
Figure 3.21 Time-trends in the adoption of 70% inflow occlusion models 88
Figure 3.22 Time-trends in the adoption of 20% inflow occlusion models 89

Figure 3.23 Time-trends in the adoption of isolated portal vein and hepatic artery occlusion models 90
Figure 3.24 Time-trends in the reporting of the three most commonly used anaesthetics in rat hepatic IRI models 91
Figure 3.25 Time-trends in the reporting of less commonly used anaesthetics in rat hepatic IRI models 92
Figure 3.26 Time-trends in the reporting of rarely used anaesthetics in rat hepatic IRI models 93
Figure 3.27 Time-trends in reported use of heparin in hepatic IRI models in rats. (A) Number of reports describing heparin use compared to those where heparin is not given or not mentioned. (B) Percentage of reports describing heparin use in comparison to the overall published hepatic IRI studies in rat during the same period of time 94
Figure 3.28 Time-trends in reported adoption of bile duct exclusion method in rat hepatic IRI studies. (A) Number of reports reporting bile duct exclusion compared to those where the technique is not performed or not mentioned. (B) Percentage of reports describing bile duct exclusion in comparison to the overall published hepatic IRI studies in rat during the same period of time 95
Figure 3.29 Time trends in reporting commonly chosen ischaemia times in rat hepatic IRI studies 96
Figure 3.30 Time trends in reporting less commonly chosen ischaemia times in rat hepatic IRI studies 97
Figure 3.31 Time trends in reporting minimum reperfusion times in rat hepatic IRI studies 98
Figure 3.32 Time trends in reporting short-term (upto 24hr) maximum reperfusion times in rat hepatic IRI studies 99
Figure 3.33 Time trends in reporting long-term (>24hr) maximum reperfusion times in rat hepatic IRI studies 99
Figure 3.34 Time trends for number of models within report in rat hepatic IRI studies 100
Figure 3.35 Time trends for intervention type in rat hepatic IRI studies 101
Figure 4.1 Partial hepatic ischaemia with bile duct isolation 131
Figure 4.2 Bile duct cannulation. Cannula insertion point magnified. 132
Figure 4.3 Average percentage of fibrosis in each study group in the pilot model based on Sirius red staining 148

Figure 4.4 CT cholangiogram showing low-resolution outline of biliary tree (black arrow) but also showing leakage of contrast into systemic circulation as evident in the outlined renal vein (white arrow) 149
Figure 4.5 Percentage of postoperative weight change in relation to preoperative weight. With the exception of day 1, both the IRI and control groups demonstrated statistically comparable weight changes. *p=0.003 (versus control). 150
Figure 4.6 A comparison of bile flow rates (normalised to total body weight) between the IRI and control groups. Bile flow was significantly lower in the IRI group after 5 hours and 1 day of reperfusion. *p<0.05 (versus control). 151
Figure 4.7 A comparison of serum total protein concentration between IRI and control groups. The graph includes preoperative and immediate postoperative time points and demonstrates no significant difference between the two groups at any time point. 152
Figure 4.8 A comparison of serum total albumin concentration between IRI and control groups. The graph illustrates that there is no significant difference between the two groups at any timepoint. 153
Figure 4.9 A comparison of serum bilirubin concentration between IRI and control groups. Although average bilirubin levels are higher in the IRI group on day 1 the difference is not statistically significant. 154
Figure 4.10 A comparison of serum bile acid concentration between the IRI and control groups. Serum bile acids were significantly higher in the IRI group after 1 day of reperfusion. *p<0.01 (versus control). 155
Figure 4.11 A comparison of serum alkaline phosphatase (ALP) activity between the IRI and control groups. Serum ALP activity was significantly higher in the IRI group between postoperative day 1 and 3. *p<0.01 (versus control). 156
Figure 4.12 A comparison of serum γ-glutamyl transferase (GGT) activity between IRI and control groups. Although average serum GGT activity is higher in the IRI group within the first 24 hours post-reperfusion, the difference is not statistically significant. 157
Figure 4.13 A comparison of serum alanine transaminase (ALT) activity between the IRI and control groups (logscale). Higher average serum ALT activity was demonstrated in the IRI group immediately following surgery up until day 3. *p<0.005 (versus control). 158

Figure 4.14 A comparison of serum hyaluronate concentration between the IRI and control groups. Higher average hyaluronate concentration was demonstrated in the IRI group on day 1 and 3 postoperatively. *p<0.05 (versus control).....159
Figure 4.15 A comparison of tissue hyaluronate concentration in ischaemic and sham ischaemic lobes. Average hyaluronate concentration peaked on day 3 in the IRI group. *p<0.05 (versus control).....159
Figure 4.16 A comparison between biliary bile acid (above) and phospholipid (below) concentrations between the IRI and control groups. A significant increase in biliary bile acid in the IRI group (day 1) is followed by a delayed increase in biliary phospholipid in that group (day 3). *p<0.05 (versus control). 161
Figure 4.17 A comparison between biliary (above) and serum (below) BS/PL ratios between the IRI and control groups. *p<0.05 (versus control).....162
Figure 4.18 RT-PCR analysis in ischaemic and sham ischaemic lobes shows significantly reduced expression of Ntcp in the ischaemic liver lobes between day 1 and 3 post-reperfusion. *p<0.05 versus control.....163
Figure 4.19 RT-PCR analysis in ischaemic and sham ischaemic lobes shows significantly reduced expression of Oatp2b1 in ischaemic liver lobes on day 1 post-reperfusion. *p<0.005 versus control.....164
Figure 4.20 RT-PCR analysis comparing the expression of Bsep in ischaemic and sham ischaemic lobes. 164
Figure 4.21 Serum levels of IL-1α, MIP-1α, IL-6, MCP-1, VEGF and MIP-2 compared between the two study groups. *p<0.05 (versus control).....168
Figure 4.22 Changes in serum RANTES concentration in both the IRI and control groups. *p<0.05 (versus control) 168
Figure 4.23 Biliary levels of MCP-1 (top) and VEGF (bottom) compared between the two study groups. *p<0.05 (versus control) 170
Figure 4.24 Changes in biliary EGF concentration in both the IRI and control groups. *p<0.05 (versus IRI) 171
Figure 4.25 Changes in biliary RANTES concentration in both the IRI and control groups. *p<0.05 (versus control) 171
Figure 4.26 Changes in MIP-1α concentration in ischaemic versus sham ischaemic liver tissue. *p<0.05 (versus control) 173
Figure 4.27 Levels of IL-6, IL-12p70, MIP-2, VEGF and IL-1α in ischaemic versus sham ischaemic liver tissue. *p<0.05 (IRI versus control) 175

Figure 4.28 Levels of IL-2, IL-4, IL-10, IP-10 and IL-1β in ischaemic versus sham ischaemic liver tissue. *p<0.05 (versus IRI) 177
Figure 4.29 Levels of RANTES in ischaemic versus sham ischaemic liver tissue .. 178
Figure 4.30 H&E staining of liver sections in low (A) and high (B) magnification demonstrates early parenchymal injury followed by ductal proliferation and peri-ductal fibrosis persisting up to 28 days following reperfusion in the IRI group. 183
Figure 4.31 Comparison of liver damage severity scores between IRI and control groups assessed on H&E slides (scale of 0–5: normal–extensive damage). *p<0.05 (versus control) 184
Figure 4.32 Comparison of inflammatory cell counts in peri-portal areas between the IRI and control groups. Inflammatory cell counts are significantly higher in the IRI group from day 3 and persist for at least 28 days following reperfusion. *p<0.05 (versus control) 184
Figure 4.33 Comparison of inflammatory cell counts in centrilobular areas between the IRI and control groups. Inflammatory cell counts in centrilobular areas normalise after day 3. *p<0.05 (versus control) 185
Figure 4.34 Comparison of α-SMA immunohistochemistry staining between IRI and sham IRI groups demonstrates a progressive increase in α-SMA-positive myofibroblasts in the IRI group peaking at day 10. 186
Figure 4.35 Quantification of α-SMA immunohistochemistry staining demonstrates significantly higher α-SMA expression in the IRI group between day 3 and 14 post-reperfusion compared to control. *p<0.05 (versus control) 187
Figure 4.36 Comparison of vimentin staining between IRI and sham IRI groups demonstrates a significant increase in vimentin-positivity in the IRI group 188
Figure 4.37 Quantification of vimentin immunohistochemistry staining demonstrates significantly higher vimentin expression in the IRI group between day 1 and 6 post-reperfusion compared to control. *p<0.05 (versus control) 189
Figure 4.38 Sirius red staining demonstrates progressive peri-portal fibrosis in the IRI group persisting up to 28 days following reperfusion with bridging portal tracts at late timepoints. 190
Figure 4.39 Progression of fibrosis in the IRI group compared to control based on quantification of sirius red staining. *p<0.05. *p<0.05 (versus control) 191
Figure 4.40 RT-PCR analysis in ischaemic and sham ischaemic lobes shows significantly increased expression of TGF-β in the ischaemic liver lobes between day 1 and 3 post-reperfusion. *p<0.05 versus control 192

Figure 4.41 RT-PCR analysis in ischaemic and sham ischaemic lobes shows significantly increased expression of vimentin in the ischaemic liver lobes between day 1 and 3 post-reperfusion. *p<0.05 versus control 192
Figure 4.42 RT-PCR analysis in ischaemic and sham ischaemic lobes shows significantly increased expression of Col1A1 in the ischaemic liver lobes between day 3 and 14 post-reperfusion. *p<0.05 versus control 193
Figure 4.43 Comparison of CK19 staining between IRI and sham IRI groups demonstrates a significant increase in CK19-positivity in the IRI group 194
Figure 4.44 Quantification of CK19 immunohistochemistry staining demonstrates significantly higher CK19 expression in the IRI group from day 10 up to day 28 post-reperfusion compared to control. *p<0.05 (versus control) 195
Figure 4.45 TEM images comparing BEC microvilli morphology during early (day 1) and late (day 28) reperfusion timepoints 196
Figure 4.46 Changes in BEC microvillar density following IRI. *p<0.05 (versus control) 197
Figure 5.1 Timeline trend for PXR publications 205
Figure 5.2 The general structure of a nuclear receptor 207
Figure 5.3 Regulation of CYP3A4 transcription by ligand-activation of the PXR. Adapted from Shukla et al (Shukla et al., 2011) 210
Figure 5.4 Northern blot analysis of hPXR expression in various human tissue. From Lehmann et al (Lehmann et al., 1998) 210
Figure 5.5 Comparison of PXR sequences (DBDnr and LBD) between orthologues and other NR1I members. Numbers indicate percentage similarity of amino acid identity. DBDnr for pig, dog and fish were not cloned at the time the original diagram was published and hence are not shown. From Kliewer et al (Kliewer et al., 2002) 213
Figure 5.6 In vivo PXR study: treatment and control groups 222
Figure 5.7 PXR study timeframe 222
Figure 5.8 Western blot of Cyp3A1 expression on day 1 and 10 in IRI+PCN and IRI+vehicle groups 224
Figure 5.9 Corresponding densitometry analysis of Cyp3A1 western blot results in ischaemic and sham ischaemic lobes. *P<0.05 versus IRI+vehicle 225
Figure 5.10 RT-PCR analysis of Cyp3A1 mRNA transcripts in ischaemic and sham ischaemic lobes. *P<0.05 versus IRI+vehicle 225
Figure 5.11 Liver MDA levels. PCN treatment compared to control. *P<0.05 versus IRI+vehicle. 226

Figure 5.12 Bile flow post-IRI. PCN treatment compared to control. *P<0.005 versus IRI+vehicle. 227
Figure 5.13 Serum bile acid levels post-IRI. PCN treatment compared to control. *P<0.05 versus IRI+vehicle..... 228
Figure 5.14 H&E staining of liver sections in PXR study. Scale bar represents 100μm at X20 magnification 229
Figure 5.15 Comparison of liver damage severity scores between IRI+PCN and IRI+vehicle groups assessed on H&E slides (scale of 0–5). *P<0.05 versus IRI+vehicle 229
Figure 5.16 Serum ALT pre and post-IRI. PCN treatment compared to control. *P<0.05 versus IRI+vehicle..... 230
Figure 5.17 Serum ALP levels pre and post-IRI. PCN treatment compared to control. 231
Figure 5.18 Serum total protein levels pre and post-IRI. PCN treatment compared to control. 231
Figure 5.19 A: H&E staining of liver sections in PXR study. Scale bar represents 100μm at X10 magnification 232
Figure 5.20 Comparison of inflammatory cell counts in peri-portal areas between the IRI+PCN and IRI-vehicle groups. *P<0.05 versus IRI+vehicle..... 232
Figure 5.21 Comparison of inflammatory cell counts in centrilobular areas between the IRI+PCN and IRI-vehicle groups. *P<0.05 versus IRI+vehicle..... 233
Figure 5.22 Gross changes in size and features of rat liver lobes (top) subjected to 60 min of partial lobar ischaemia followed by reperfusion for 10 days in PCN-treated animals (left) compared to vehicle-treated controls (right). Non-ischaemic lobes (bottom) are shown for comparison. 234
Figure 5.23 Liver lobe weights on day 10 post-IRI. *P<0.05 versus IRI+vehicle..... 235
Figure 5.24 RT-PCR analysis comparing TGF- β mRNA expression between the IRI+PCN and IRI-vehicle groups. *p<0.05 versus IRI+vehicle 236
Figure 5.25 RT-PCR analysis comparing α-SMA mRNA expression between the IRI+PCN and IRI-vehicle groups. *p<0.05 versus IRI+vehicle 236
Figure 5.26 RT-PCR analysis comparing vimentin mRNA expression between the IRI+PCN and IRI-vehicle groups. 237
Figure 5.27 RT-PCR analysis comparing MMP-2 mRNA expression between the IRI+PCN and IRI-vehicle groups. 237

Figure 5.28 RT-PCR analysis comparing Col1a1 mRNA expression between the IRI+PCN and IRI-vehicle groups. *p<0.05 versus IRI+vehicle.....238
Figure 5.29 Comparison of vimentin staining between IRI+PCN and IRI+vehicle groups on post-reperfusion days 1 and 10 (above) with corresponding stain quantification (below). *P<0.005 versus IRI+vehicle 239
Figure 5.30 Comparison of α-SMA staining between IRI+PCN and IRI+vehicle groups on post-reperfusion days 1 and 10 (above) with corresponding stain quantification (below). *P<0.05 versus IRI+vehicle 240
Figure 5.31 Comparison of Sirius red staining between IRI+PCN and IRI+vehicle groups on post-reperfusion days 1 and 10 (above) with corresponding stain quantification (below). *P<0.05 versus IRI+vehicle 241
Figure 5.32 Comparison of CK19 staining between IRI+PCN and IRI+vehicle groups on post-reperfusion days 1 and 10 (above) with corresponding stain quantification (below). *P<0.05 versus IRI+vehicle 242
Figure 6.1 Procedure-inclusion flowchart 266
Figure 6.2 Kaplan-Meier curve comparing graft survival (death-censored) between EAD and non-EAD groups 276
Figure 6.3 Kaplan-Meier curve comparing patient survival between EAD and non-EAD groups.....276
Figure 6.4 Comparison of EAD risk between low and high hPXR activation groups 277
Figure 6.5 Comparison of average $PPAV_7$ between EAD and non-EAD cohorts 277
Figure 6.6 Kaplan-Meier curve comparing patient survival between low and high hPXR activation groups.....281
Figure 6.7 Kaplan-Meier curve comparing graft survival (death-censored) between low and high hPXR activation groups.....282
Figure 6.8 Kaplan-Meier curve comparing rejection-free survival between low and high hPXR activation groups 282

List of tables

Table 1 List of common PXR activators and relative potencies across species. Adapted from di Masi et al and Shukla et al (di Masi et al., 2009, Shukla et al., 2011) 8
Table 2 Cytokines secreted by BECs 12
Table 3 Correlation between biliary cytokine concentrations (from rats exposed to hepatic IRI and sham surgery) and average hHSC migration in vitro 47
Table 4 List of inclusion criteria for review 70
Table 5 Details of variables collected from studies included in literature review..... 73
Table 6 Frequency distribution of rat hepatic ischaemia reperfusion injury models .. 80
Table 7 First reports of IRI models..... 81
Table 8 Frequency distribution of studies with long-term follow up (excluding survival analyses) 85
Table 9 The distribution of model multiplicity in rat hepatic IRI studies over time ... 100
Table 10 The distribution of intervention type in rat hepatic IRI studies over time .. 102
Table 11 The distribution of chosen strains across IRI models reported (only models with significant associations are displayed) 104
Table 12 The distribution of gender across rat IRI models reported (major models displayed for comparison)..... 105
Table 13 The distribution of reported bile duct involvement across IRI models (major models displayed for comparison). Cases where bile duct involvement was not mentioned are not shown..... 106
Table 14 Average maximum ischaemia times for major IRI models 107
Table 15 Average maximum reperfusion times for major IRI models (excluding reperfusion times for survival analyses)..... 109
Table 16 The frequency distribution of reported observation periods for survival analyses..... 110
Table 17 Summary of coefficient statistics for independent variables in multiple linear regression model 111
Table 18 Breakdown of average survival rates based on reported IRI models and ischaemia times (SEM and range omitted if n<2) 111

Table 19 Summary of cytokines that demonstrated significant differences in serum concentrations between the IRI and control groups. Values are reported as mean±SD. 168
Table 20 Summary of cytokines that demonstrated significant differences in biliary concentrations between the IRI and control groups. Values are reported as mean±SD. 172
Table 21 Summary of cytokines that demonstrated significant differences in ischaemic lobe concentration between the IRI and control groups. Values are reported as mean±SD. 178
Table 22 A comparison of BEC microvilli height and width between study groups..196
Table 23 List of PXR target genes and role in xenobiotic metabolism. Corresponding human orthologues of murine genes reported if known. Phase I: Activation; Phase II: Solubilisation; Phase III: Elimination. Adapted from Rosenfeld et al and Hariparsad et al (Rosenfeld et al., 2003, Hariparsad et al., 2009) 211
Table 24 Details of variables collected for clinical PXR study 253
Table 25 Definition of liver transplant-related complications 262
Table 26 Frequency distribution of recipient characteristics....267
Table 27 Descriptive statistics of recipient characteristics (continuous variables)...267
Table 28 Frequency distribution of donor characteristics 268
Table 29 Descriptive statistics of donor characteristics (continuous variables) 269
Table 30 Frequency distribution of transplant characteristics....269
Table 31 Descriptive statistics of transplant characteristics (continuous variables).270
Table 32 hPXR activators administered within the first 7 days post-transplantation271
Table 33 Administered doses of common hPXR activators during the first 7 days post-transplantation....272
Table 34 Comparison of recipient, donor and transplant variables between low and high hPXR activation groups 273
Table 35 Incidence of post-OLT complications in the study population....278
Table 36 A comparison of average $PPAV_7$ between recipients with and without various post-OLT complications 280
Table 37 Univariate Cox regression for patient survival 284
Table 38 Multivariate Cox regression for patient survival 286
Table 39 Univariate Cox regression for graft survival....287
Table 40 Multivariate Cox regression for graft survival....290
Table 41 Univariate Cox regression for rejection-free survival 291

Table 42 Multivariate Cox regression for rejection-free survival 293
Table 43 Subgroup analyses comparing average $PPAV_7$ between recipients with and without EAD 294
Table 44 Subgroup analyses comparing average $PPAV_7$ between recipients with and without anastomotic biliary strictures 295
Table 45 Subgroup analyses comparing average $PPAV_7$ between recipients with and without sepsis 295
Table 46 Subgroup analyses of patient survival (only Log Rank P values reported) 296

List of Abbreviations

α-SMA	Alpha Smooth Muscle Actin
ACL	Anterior Caudate Lobe
ADP	Adenosine Diphosphate
AF	Activation Function
ALD	Alcoholic Liver Disease
ALP	Alkaline Phosphatase
ALT	Alanine Transaminase
AMR	Antibody-Mediated Rejection
ANOVA	Analysis of Variance
APS	Amonium Persulfate
AST	Aspartate Transaminase
ATP	Adenosine Triphosphate
BEC	Biliary Epithelial Cell
BHT	Butylated Hydroxytoluene
BMI	Body Mass Index
BNF	British National formulary
BS	Bile Salt
BSA	Bovine Serum Albumin
CA	Cholic Acid
CAR	Constitutive androstane Receptor
CARLA	Coactivator Receptor Ligand Assay

CBD Common Bile Duct

CDCA Chenodeoxycholic Acid

CEBP CAMP-Response Element Binding Protein

CFTR Cystic Fibrosis Transmembrane Conductance Regulator

CI Confidence Interval

CIT Cold Ischaemia Time

CL Cholesterol

CMV Cytomegalovirus

COD Cause of Death

CRC Concentration Response Curve

CT Computerised Tomography

CVA Cerebrovascular Accident

DAB 3,3'-Diaminobenzidine

DAPI 4',6-Diamidino-2-Phenylindole

DBD Donation after Brain Death

DCD Donation after Cardiac Death

DMEM Dulbecco's Modified Eagle Medium

DMSO Dimethyl Sulfoxide

DNA Deoxyribonucleic Acid

DTT Dithiothreitol

EAD Early Allograft Dysfunction

ECD Extended Criteria Donor

ECL Enhanced Chemi-Luminescence

ECMO	Extracorporeal Membrane Oxygenation
EDTA	Ethylenediaminetetraacetic Acid
EGF	Epithelial Growth Factor
EGTA	Ethylene Glycol-Bis(B-Aminoethyl Ether)-N,N,N',N'-Tetraacetic Acid
ELISA	Enzyme-Linked Immune Sorbent Assay
EOS	Electronic Offering System
EPV	Event per Variable
ER	Estrogen Receptor
ERC	Ethical Review Committee
FCS	Foetal Calf Serum
FGF	Fibroblast Growth Factor
FITC	Fluorescein Isothiocyanate
FRET	Fluorescence Resonance Energy Transfer
FXR	Farnesoid X Receptor
GFAP	Glial Fibrillary Acidic Protein
GGT	Gamma Glutamyl Transferase
GR	Glucocorticoid Receptor
HA	Hepatic Artery
HAT	Hepatic Artery Thrombosis
HBI	Hypoxic Brain Injury
HBSS	Hanks' Balanced Salt Solution
HEA	Human Epithelial Antigen

HGF Hepatocyte Growth Factor

HR Hazard Ratio

HRP Horseradish Peroxidase

HSC Hepatic Stellate Cell

HSD 3α-Hydroxysteroid Dehydrogenase

HTS High Throughput Screening

ICAM Intercellular Adhesion Molecules

ICC Immunocytochemistry

ICH Intracranial Haemorrhage

IFN Interferon

IHC Immunohistochemistry

IL Interleukin

INR International Normalised Ratio

IO Intraoperative

IOB Intraoperative Blood Transfusion

IRI Ischaemia Reperfusion Injury

IRL Inferior Right Lobe

ITU Intensive Care Unit

IU International Unit

IV Intravenous

IVC Inferior Vena Cava

KC Kupffer Cell

LBD Ligand-Binding Domain

LCA Lithocholic Acid

LDH Lactate Dehydrogenase

LLL Left Lateral Lobe

LML Left Median Lobe

LOS Length of Stay

LXR Liver X Receptor

MCP Monocyte Chemoattractant Protein

MCP Monocyte Chemoattractant Protein

MDA Malondialdehyde

MELD Model for End Stage Liver Disease

MIP Macrophage Inhibitory Protein

MMP Metalloproteinase

MPT Mitochondrial Permeability Transition

MW Molecular Weight

NABS Non-Anastomotic Biliary Strictures

NAD Nicotinamide Adenine Dinucleotide

NADP Nicotinamide Adenine Dinucleotide Phosphate

NAFLD Non-Alcoholic Fatty Liver Disease

NAPQI N-Acetyl-P-Benzoquinone Imine

NHS National Health Service

NHSBT National Health Service Blood and Transplant

NIH National Institute of Health

NO Nitric Oxide

NRES National Research Ethics Service

NVS Named Veterinary Surgeon

OLT Orthotopic Liver Transplantation

PAGE Polyacrylamide Gel Electrophoresis

PBS Phosphate-Buffered Saline

PBVP Peri-Biliary Vascular Plexus

PC Phosphatidylcholine

PCL Posterior Caudate Lobe

PCN Pregnenolone-16α-Carbonitrile

PCNA Proliferating Cell Nuclear Antigen

PDGF Platelet-Derived Growth Factor

PDGFR Platelet-Derived Growth Factor Receptor

PGC PPARγ-Coactivator

PL Phospholipid

PNF Primary Non Function

PO Per Os

POB Postoperative Blood Transfusion

PPAR Peroxisome Proliferator-Activated Receptor

PR Progesterone Receptor

PT Prothrombin Time

PXR Pregnane X Receptor

RCT Randomised Control Trial

RML Right Median Lobe

RNA	Ribonucleic Acid
ROS	Reactive Oxygen Species
RPM	Revolutions per Minute
RT-PCR	Real-Time Polymerase Chain Reaction
RXR	Retinoid X Receptor
SC	Subcutaneous
SD	Standard Deviation
SDF	Stroma-Derived Factor
SDS	Sodium Dodecyl Sulfate
SEC	Sinusoidal Endothelial Cell
SEM	Standard Error of Mean
SHP	Small Heterodimer Partner
SMRT	Silencing Mediator for Retinoid and Thyroid Hormone
SNP	Single Nucleotide Polymorphisms
SOFA	Sequential Organ Failure Assessment
SPA	Scintillation Proximity Assay
SPSS	Statistical Package for Social Sciences
SRC	Steroid Receptor Coactivator
SRL	Superior Right Lobe
SXR	Steroid and Xenobiotic Receptor
TBA	Thiobarbituric Acid
TBARS	Thiobarbituric Acid Reactive Substances

TBS Tris-Buffered Saline

TBW Total Body Weight

TCMR T Cell-Mediated Rejection

TEM Transmission Electron Microscopy

TEMED Tetramethylethylenediamine

TGF Transforming Growth Factor

TNF Tumour Necrosis Factor

TRIS 2-Amino-2-(Hydroxymethyl)-1,3-Propanediol

TRITC Tetramethylrhodamine

VDR Vitamin D Receptor

VEGF Vascular Endothelial Growth Factor

VIF Variance Inflation Factor

VV Veno-Venous

WB Western Blot

WIT Warm Ischaemia Time

XREM Xenobiotic Responsive Enhancer Molecule

Chapter 1. Introduction

1.1. The current state of orthotopic liver transplantation (OLT)

Liver transplantation remains to date the mainstay therapy for patients with acute or chronic end-stage liver disease. Over the past few decades, there has been an increasing demand for liver transplantation in Europe and North America owing to significant developments in immunotherapy, organ preservation, and perioperative care. These improvements have led to more 'high-risk' patients being considered suitable for transplantation, and more patients surviving failed transplants (Lentine and Schnitzler, 2011, Thuluvath et al., 2010). However, the rapid growth in transplant waiting lists is met with only a modest increase in the number of organ donors and thus the gap between organ demand and supply continues to widen, with more patients dying whilst awaiting transplantation (Wertheim et al., 2011, NHSBT, 2015).

Organs from 'marginal' or extended criteria donors (ECD) are increasingly being utilised in an attempt to reduce the gap between organ supply and demand (Burra and Freeman, 2012). These include organs donated after cardiac death (DCD). A number of studies have reported inferior outcomes with the use of DCD organs compared to those donated after brain death (DBD) (Foley et al., 2005, Merion et al., 2006, Jay et al., 2011a, Kaczmarek et al., 2007). A recent systematic review of DCD liver transplantation revealed a significantly increased risk of graft failure and mortality among recipients of DCD liver grafts (Jay et al., 2011b). Nevertheless, while the rate of DBD organs has plateaued over the past decade, the contribution of DCD organs to the deceased donor pool increases every year (Figure 1.1). In the UK, liver transplantation from DCD donors increased by 17% in 2014/2015 whereas liver transplants from DBD donors fell by 3% compared to the previous year (NHSBT, 2015). However, in view of the existing organ shortage and the significant risk associated with DCD liver transplantation, it is imperative that all potential strategies for optimising DCD grafts are examined in order to minimise graft loss and insure the best possible outcome for each recipient.

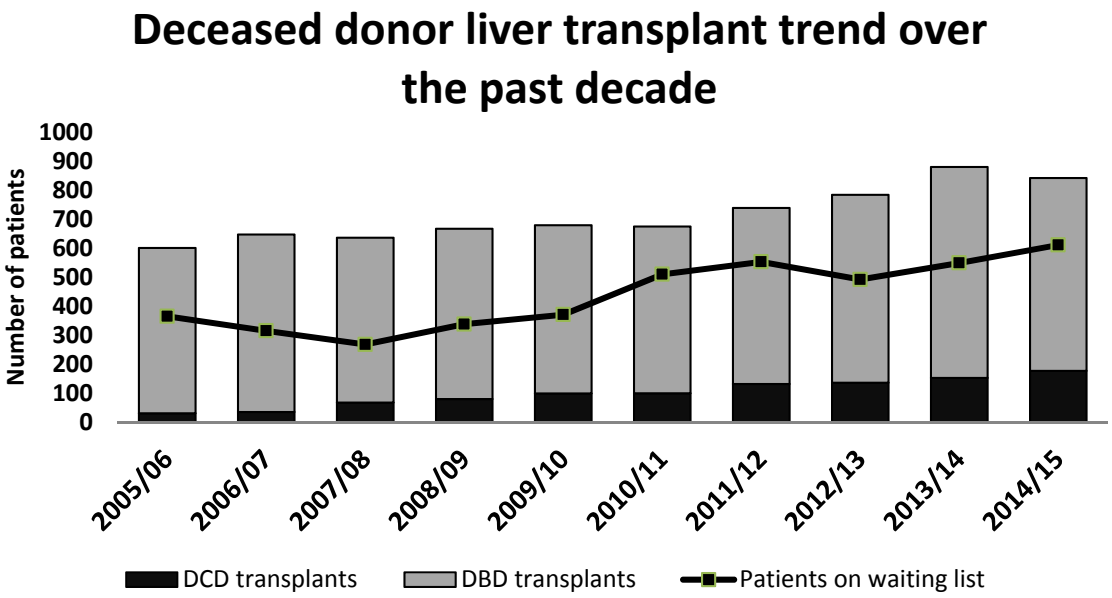

Figure 1.1. Deceased donor liver transplant trends in the adult and paediatric populations over the past 10 years. Data from NHSBT (2015).

1.2. Non-anastomotic biliary strictures (NABS) and liver transplantation

In 1977, Calne described biliary complications as the “Achilles heel” of liver transplantation (Calne, 1977). They remain a major obstacle to successful transplantation to date despite advances in this field (Ayoub et al., 2010, Buck and Zajko, 2008). Reports in recent literature indicate that biliary complications occur in 10 to 40% of all adult cases of liver transplantation (Thethy et al., 2004, Zajko et al., 1985). Non-anastomotic biliary strictures (NABS) account for a significant proportion of these complications, with an incidence ranging between 5-15% (Figure 1.2). They are a significant cause of morbidity, graft failure and death following deceased donor liver transplantation (Sharma et al., 2008). Inadequately treated lesions can lead to lobar atrophy, recurrent cholangitis or secondary biliary cirrhosis (Ayoub et al., 2010). However, despite optimal management, up to 50% of patients with non-anastomotic biliary strictures will eventually require re-transplantation due to graft loss, many of whom die whilst on the waiting list (Ayoub et al., 2010, Sharma et al., 2008).

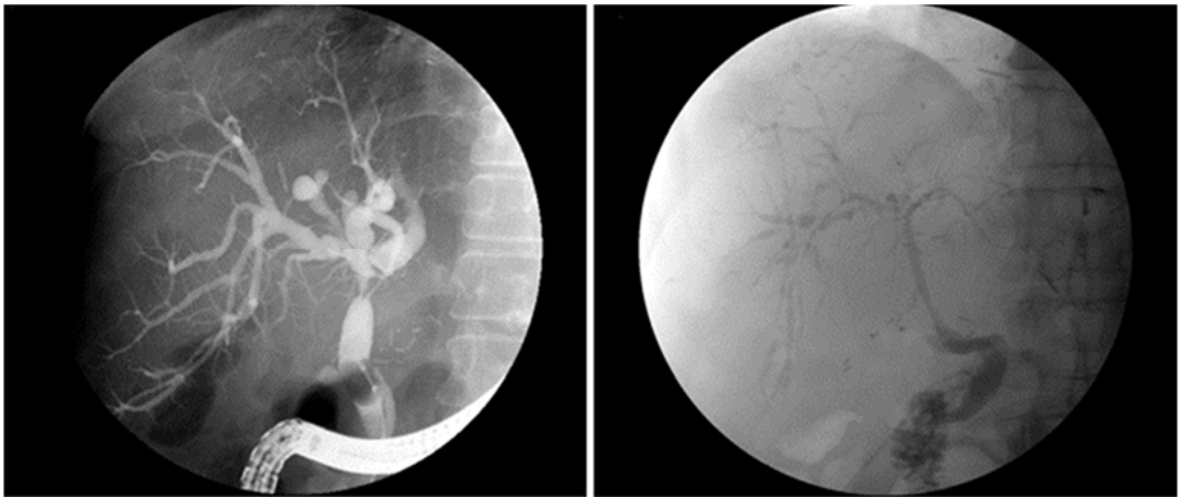

Figure 1.2. Non-anastomotic biliary strictures identified on cholangiography. Lesions can range from solitary and mild (left) to diffuse and severe (right). From Buis et al (Buis et al., 2007)

Liver grafts from DCD donors are particularly prone to NABS (Jay et al., 2011b, Abt et al., 2003, D'Alessandro A et al., 2000, D'Alessandro et al., 2004, Op den Dries et al., 2011, Otero et al., 2003). The association between DCD organs and NABS is not surprising and is reflective of the longer ischaemic periods associated with DCD organs. A number of studies have identified warm ischaemia as a strong risk factor for NABS (Guichelaar et al., 2003, Buis et al., 2007). Moreover, radiographic findings similar to NABS are seen in patients with hepatic artery thrombosis (Zajko et al., 1987). The unique dependence of the biliary tree on arterial blood -which is disrupted during donor hepatectomy- is in contrast to the remainder of the liver parenchyma which receives dual arterial and portal blood (Northover and Terblanche, 1979) (Figure 1.3). This arrangement may explain the increased susceptibility of the biliary tree to ischaemic injury. Therefore, a number of approaches to enhance oxygenation of the liver allograft have been investigated, especially in DCD organs, with the aim of improving the viability of the biliary tree and reducing biliary complications including primary arterial revascularisation, oxygen persufflation and extracorporeal membrane oxygenation (ECMO) of the liver allograft (Brockmann et al., 2005, van As et al., 2002, Suszynski et al., 2012, Choi et al., 2012, Jimenez-Galanes et al., 2009).

However, ischaemia is not the only risk factor linked to development of these lesions. Other factors including ABO incompatibility, CMV infection, enhanced chemokine activity and bile salt injury have also been implicated, reflecting the complex pathogenic nature of these lesions (Op den Dries et al., 2011).

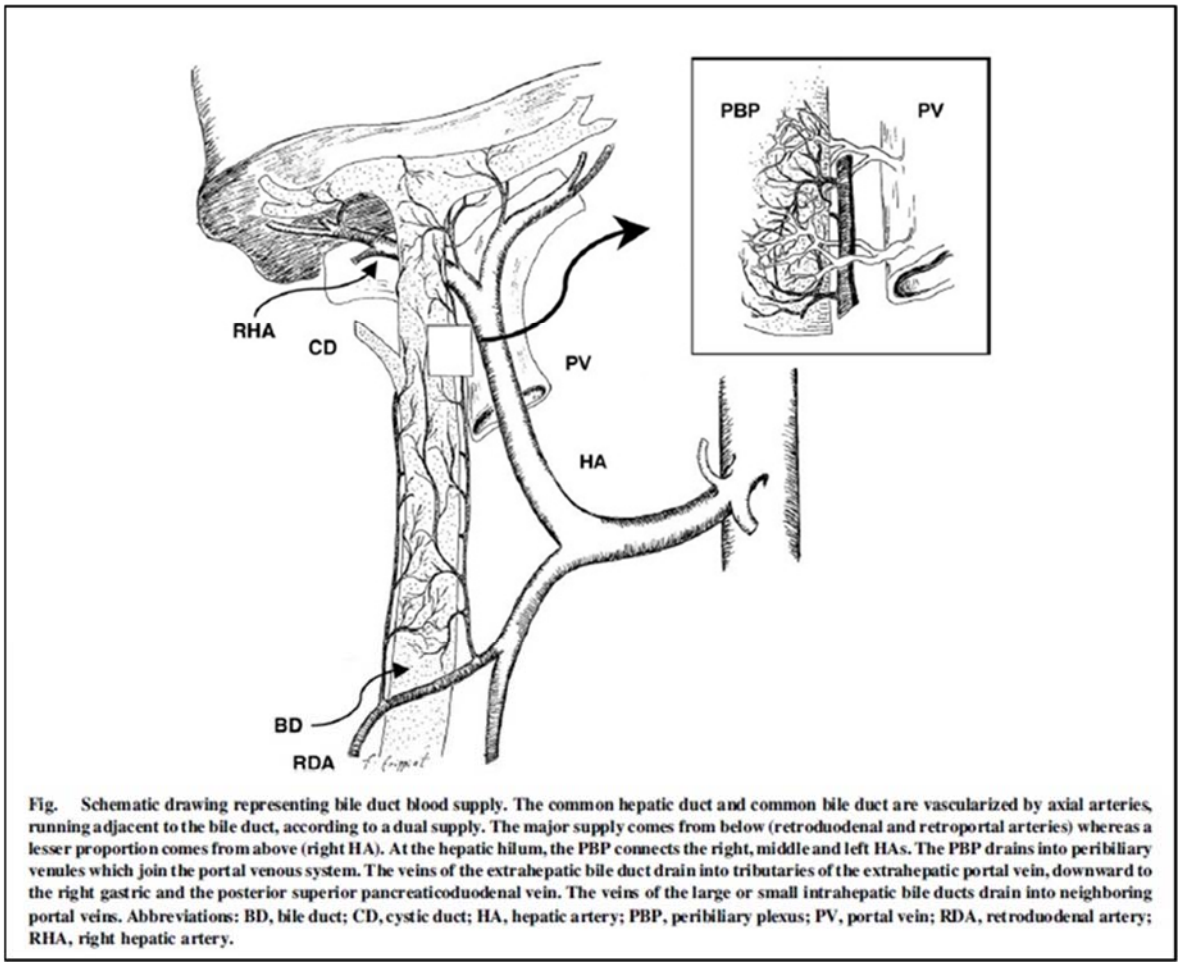

Fig. Schematic drawing representing bile duct blood supply. The common hepatic duct and common bile duct are vascularized by axial arteries, running adjacent to the bile duct, according to a dual supply. The major supply comes from below (retroduodenal and retroportal arteries) whereas a lesser proportion comes from above (right HA). At the hepatic hilum, the PBP connects the right, middle and left HAs. The PBP drains into peribiliary venules which join the portal venous system. The veins of the extrahepatic bile duct drain into tributaries of the extrahepatic portal vein, downward to the right gastric and the posterior superior pancreaticoduodenal vein. The veins of the large or small intrahepatic bile ducts drain into neighboring portal veins. Abbreviations: BD, bile duct; CD, cystic duct; HA, hepatic artery; PBP, peribiliary plexus; PV, portal vein; RDA, retroduodenal artery; RHA, right hepatic artery.

Figure 1.3. Blood supply to the bile duct. Adapted from Deltenre and Valla 2006 (Deltenre and Valla, 2006)

1.3. A potential role for reperfusion injury in the development of NABS

In addition to the effect of ischaemia on the biliary tree, reperfusion injury may play an important part in the development of NABS (Op den Dries et al., 2011) given that significant intrahepatic cellular damage following transplantation is now known to be caused by reperfusion injury (Teoh and Farrell, 2003).

The process of IRI represents a complex interplay between resident intrahepatic (parenchymal and non-parenchymal) cells and circulating inflammatory cells resulting in oxidative stress injury and cell death (Teoh and Farrell, 2003). The effects of reperfusion on the various cell types resident in the liver and their individual roles in graft injury vary considerably (Kukan and Haddad, 2001).

Kupffer cells are activated following warm or cold ischaemia and play a central role in early reperfusion injury (Teoh, 2011). These cells release reactive oxygen species (ROS) and cytokines, leading to the recruitment of inflammatory cells and parenchymal damage. Sinusoidal endothelial cells (SECs) and hepatocytes have been shown to be susceptible to direct injury following cold and warm ischaemia respectively (Noack et al., 1993, Schon et al., 1998, Ikeda et al., 1992, Massip-Salcedo et al., 2007, McKeown et al., 1988). Hepatocytes and SECs play an important role in ROS production and propagation of the inflammatory response (Saiman and Friedman, 2012, Peralta et al., 2013). In addition, SECs are implicated in the microcirculatory disturbances that occur upon reperfusion. A more detailed description of the cellular response to hepatic ischaemia reperfusion injury can be found in section 4.1.1.

Despite extensive research in recent years, much remains to be uncovered about the effect of ischaemia reperfusion injury on hepatocytes, sinusoidal endothelial cells and Kupffer cells. However, even less is known about its effect on BECs. In vitro studies have shown that BECs are more resistant to ischaemia and more vulnerable to re-oxygenation and reperfusion compared to hepatocytes (Noack et al., 1993). The reasons for such contrasting effect of oxygen on BECs is not entirely understood but may be a result of lower basal glutathione levels and enhanced glutathione breakdown during reperfusion in comparison to hepatocytes (Noack et al., 1993, Accatino et al., 2003).

There is evidence to suggest that reperfusion injury to the biliary epithelium persists for days to weeks following transplantation and that recovery from such insult is prolonged compared to hepatocytes or sinusoidal endothelial cells (Kukan and Haddad, 2001, Cutrin et al., 1996). This may explain the often delayed presentation of biliary complications such as NABS following liver transplantation (Ayoub et al., 2010).

1.4. Activation of the pregnane X receptor as a potential target in the prevention of NABS

The pregnane X receptor (PXR) is a promising drug target for the treatment of inflammatory liver disease. PXR is a member of the nuclear receptor gene superfamily of ligand-activated transcription factors. It is highly expressed in hepatocytes and is activated by a wide range of xenobiotics (e.g. cyclosporin and rifampicin) and endobiotics (e.g. bile acids) (Pavek, 2016). In its active form, PXR regulates the expression of genes involved in the metabolism, transport and excretion of these compounds (Kliewer et al., 2002). PXR activation stimulates detoxification pathways that minimise the harmful effects of toxic bile salts and facilitate their excretion (Jonker et al., 2012, Uppal et al., 2005). In addition to these functions, PXR activation has been shown to produce an anti-inflammatory effect and has been explored as a promising therapeutic target in inflammatory bowel disease (di Masi et al., 2009). Researchers in our laboratory have previously demonstrated that PXR activation can promote hepatocyte growth and significantly reduce Nf-κB-induced peri-portal inflammation and fibrosis (Marek et al., 2005, Haughton et al., 2006, Wright, 2006, Wallace et al., 2010, Wallace et al., 2008). In addition, Iannelli and co-workers (Iannelli et al., 2011) have demonstrated that PXR activation results in reduced hepatocyte damage following ischaemia-reperfusion injury. PXR has been shown to regulate the expression of proteins that are implicated in the oxidative stress response such as glutathione-S-transferase (Rosenfeld et al., 2003).

Although some animal studies have linked PXR activation with the development of hepatic steatosis (Lee et al., 2008), this effect has not been observed in clinical practice with common human PXR ligands such as rifampicin even with long-term administration (di Masi et al., 2009). Figure 1.4 summarises the established beneficial effects of PXR activation in the liver.

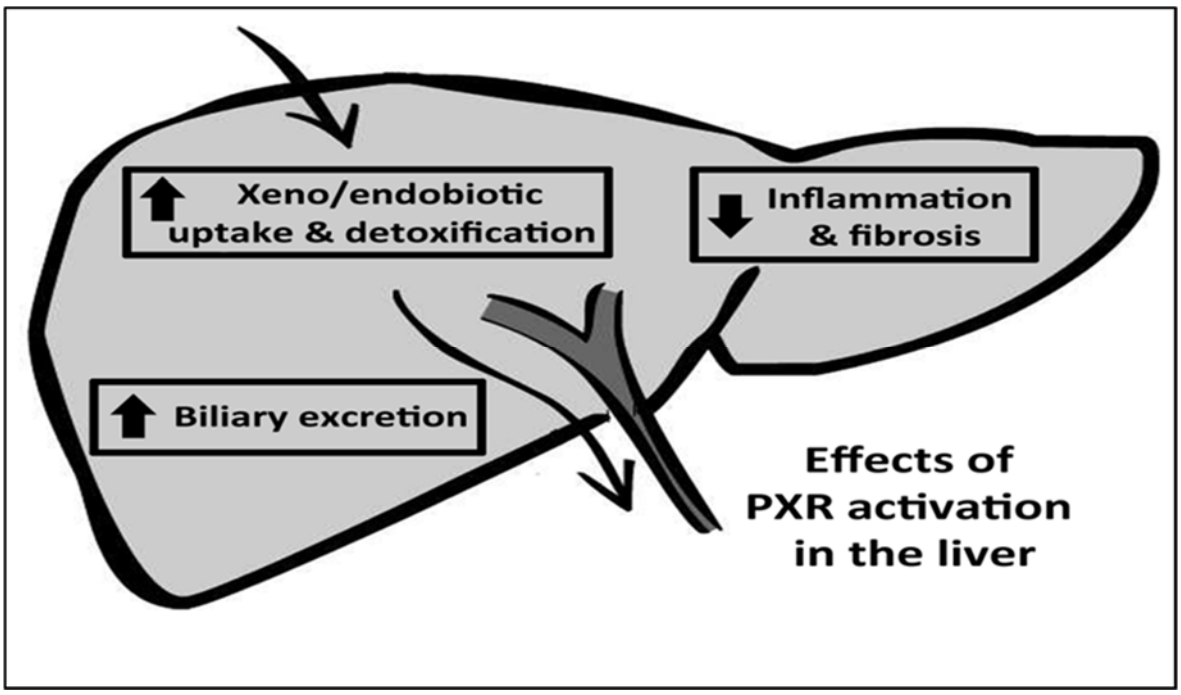

Figure 1.4 The effects of PXR activation in the liver

A number of drugs have been reported to activate the PXR. These vary widely in potency and species selectivity (Table 1).

Table 1 List of common PXR activators and relative potencies across species. Adapted from di Masi et al and Shukla et al (di Masi et al., 2009, Shukla et al., 2011)

Drug	PXR activation potency: EC50* (nM)	
	Human PXR	Mouse PXR
Carbamazepine	15,600	-
Ciglitazone	4,500	-
Clotrimazole	800–5,000	1,000
Dexamethasone	5,000–10,000	>10,000
Hyperforin	23	-
Mifepristone	5,500–10,000	1,000–20,000
PCN	> 10,000	200–700
Progesterone	-	5,000–20,000
Phenobarbital	169,000–370,000	-
Rifampicin	200–3,000	-

*EC50=Dose resulting in half maximal activation; - denotes value unavailable for species

The anti-inflammatory and anti-fibrotic effects of PXR activation could potentially play an important role in liver transplantation by reducing the incidence of NABS and consequently improving graft survival.

1.5. Hypotheses and aims of project

Based on current available evidence, the hypotheses of this project are that

1. BECs play an active role in the inflammatory response to ischaemia-reperfusion injury
2. Ischaemia-reperfusion injury plays a central role in the pathogenesis of NABS
3. The administration of PXR activators will reduce the cytotoxic, inflammatory and pro-fibrotic effects potentially associated with hepatic ischaemia-reperfusion injury

The aim is to develop an in vitro cellular model of hypoxia in addition to an in vivo rodent animal model of hepatic ischaemia-reperfusion injury that are reliable and reproducible in order to test hypotheses 1 and 2. The results of the in vitro and in vivo experiments are detailed in Chapter 2 and Chapter 3 respectively.

The effect of PXR activation on liver function following ischaemia-reperfusion injury is examined in the in vivo animal model in the first instance (Chapter 5). This is followed by a translational retrospective clinical study in order to investigate the relevance of these findings in clinical liver transplantation (Chapter 6).

Chapter 2. Biliary epithelial cells and peri-ductal fibrosis following ischaemia-reperfusion injury: Innocent bystanders or central players? An in vitro study

2.1. Introduction

2.1.1. The role of biliary epithelial cells in the development of transplantation-related peri-biliary fibrosis

Our understanding of the role that BECs play in liver biology has expanded greatly in recent years. In addition to maintaining bile homeostasis in physiological conditions, these cells have been shown to play a central role in liver regeneration and immunity (Strazzabosco et al., 2005). BEC damage and peri-biliary inflammation and fibrosis are central features in a spectrum of liver diseases known collectively as cholangiopathies (Portmann and Zen, 2012). These range from immune-mediated to toxin-induced pathologies of the biliary tree and include NABS (often referred to as ischaemic cholangiopathy) that can complicate liver transplantation. The interrelation between ischaemic stress, BEC damage and peri-biliary inflammation remains poorly understood and is clearly essential to understand the development of NABS.

Recent studies suggest that ischaemia may result in 'toxic bile' formation leading to bile salt-induced damage to BECs which could contribute to peri-ductal inflammation/fibrosis and potentially NABS (Chen et al., 2009a, Buis et al., 2009, Geuken et al., 2004, Hertl et al., 1995, Hertl et al., 2000, Hoekstra et al., 2006, Knoop et al., 1993, Yska et al., 2008). In this respect, BEC damage is viewed as a secondary event in the ischaemic stress response.

Bile salts have potent detergent properties causing cell membrane injury and may also induce mitochondria-mediated toxicity (Palmeira and Rolo, 2004) and apoptosis (Schmucker et al., 1990). Hertl et al demonstrated that porcine livers flushed with saline containing hydrophobic bile salts at the time of procurement develop significantly worse intrahepatic bile duct injury even after short periods of ischemia, compared to control livers flushed with saline alone (Hertl et al., 1995).

Under physiological conditions, the detrimental effect of bile salts is largely neutralised by phospholipids through the formation of mixed micelles in bile (Tsuboi et al., 2004). A number of clinical and experimental studies have shown that the ratio of bile salts to phospholipids increases in bile to above critical micellar concentrations during the first two weeks following OLT and that this may lead to increased bile salt toxicity (Chen et al., 2009a, Buis et al., 2009, Geuken et al., 2004, Hoekstra et al.,

2006, Yska et al., 2008). This is thought to be a result of altered expression of hepatocyte bile salt transporters following OLT.

An alternative and equally plausible hypothesis to the development of peri-biliary fibrosis postulates a more central and active role played by BECs following ischaemic stress. BECs have been shown to express CD1d and can act as antigen-presenting cells (Schrumpf et al., 2015). A number of studies have demonstrated that BECs can recognise pathogen-associated molecular patterns (PAMPs) –and potentially damage-associated molecular patterns (DAMPs) - through the expression of toll-like receptors (TLRs) in pathological states. This results in the activation of downstream pathways vital to the immune response including the expression of adhesion molecules and chemokines (Syal et al., 2012) (Figure 2.1). The evidence for cytokine production by BECs is summarised in Table 2.

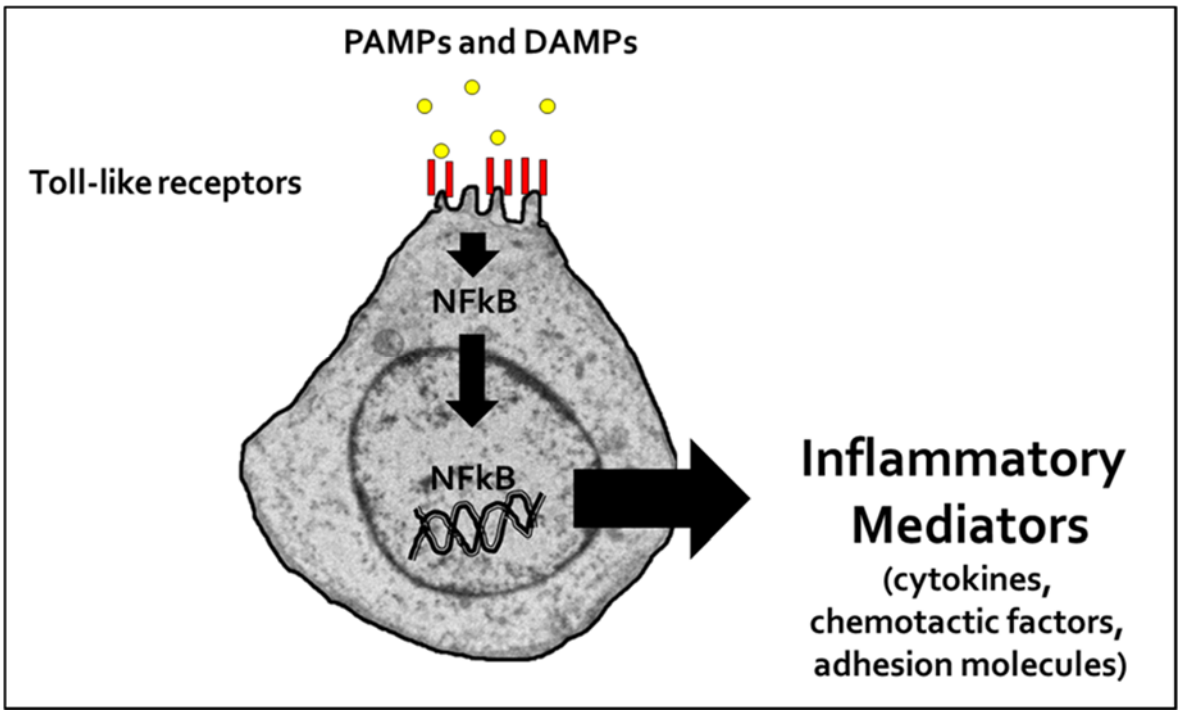

Figure 2.1 The expression of TLRs by BECs and the NFkB-mediated immune response

Table 2 Cytokines secreted by BECs

Cytokine	**Reference**

IL-1β	(Kamihira et al., 2005)
IL-6	(Matsumoto et al., 1994, Yasoshima et al., 1998)
IL-8	(Morland et al., 1997)
CX3CL1 (Fractalkine)	(Isse et al., 2005)
CXCL12 (SDF-1)	(Terada et al., 2003, Wald et al., 2004)
CCL20 (MIP-3α)	(Harada et al., 2011)
CCL2 (MCP-1)	(Morland et al., 1997)
TNF-α	(Yasoshima et al., 1998)
TGF-β	(Milani et al., 1991)

The potential expression of chemokines by BECs may explain the preferential peri-biliary inflammation and fibrosis observed in ischaemia-induced cholangiopathy. However, it is yet to be investigated whether a causal link between ischaemia-reperfusion injury and BEC chemokine expression exists or not.

2.1.2. Isolation of primary biliary epithelial cells in culture: Techniques and challenges

The use of immortalised biliary epithelial cell lines (such as H69 cells) is a relatively practical approach to study BECs in vitro (Dianat et al., 2014). However, given the heterogeneity of intrahepatic biliary epithelial cell populations in size and phenotype, the isolation and culture of primary BECs remain the gold standard for the selective study of BEC subpopulations (Joplin and Kachilele, 2009). The challenges associated with primary BEC isolation and culture are mainly related to the difficulty in maintaining the normal phenotype of these cells in vitro given their propensity to de-differentiate and, in the case of human cholangiocytes, due to the paucity of supply in comparison to cholangiocyte-like cell lines (Joplin, 1994). BECs represent only 5% of the intrahepatic cellular component in a healthy liver (Grant and Billing, 1977). This poses the additional challenge of obtaining adequate cell yields for culture. Nevertheless, a number of methods have been developed to facilitate primary BEC isolation and maximise cell yield for in vitro research. These are listed below.

Density-based isolation techniques

Such techniques utilise the differential density of intrahepatic biliary epithelial cells compared to parenchymal cells (Grant and Billing, 1977). Density gradient centrifugation of a cell suspension using a medium such as Percoll is usually preceded by a method that promotes BEC proliferation such as bile duct ligation in order to maximise cell yield (Sirica and Gainey, 1997). Such techniques are relatively simple and provide cells that retain typical BEC phenotypes. Purity levels of >95% have been reported (Sirica and Gainey, 1997). However, these techniques usually involve a 2-stage process and yield hyperplastic, pathologically involved BECs which could limit their utility (Joplin, 1994). Moreover, although high purity BEC cultures can be obtained from isolation of rat BECs using density gradient centrifugation, similar techniques in human produce significantly contaminated cultures (Joplin, 1994).

Size-based isolation techniques

Centrifugal elutriation has been employed to isolate BECs based on the size of the cell subpopulation of interest (Yaswen et al., 1984). Similar to density-based techniques, this method can be combined with cell-proliferating techniques to maximise cell yield. Occasionally centrifugal elutriation and density gradient centrifugation methods are combined to produce more refined extraction (Ishii et al., 1989).

Selective digestion of the biliary tree

Selective application of connective tissue digestive enzymes within the biliary tree can be used to obtain a high purity, mixed population BEC culture (Demetris et al., 1988). This technique can produce high yields in livers of larger species and does not involve whole liver cell suspension, therefore minimising cell contamination. However, it requires an intact liver which is not always available.

Immuno-isolation techniques

BECs can be selectively isolated based on their unique expression of surface antigens such as epithelial cell adhesion molecule (EpCAM). Immune-isolation techniques utilise antibodies conjugated to particles (such as magnetic beads) that allow cell extraction following antibody-antigen binding. These techniques are usually combined with some form of size/density-based preliminary purification. They are unsurprisingly more selective than exclusive density-based techniques and produce higher purity cultures (Ishii et al., 1989, Joplin et al., 1989). Immuno-isolation can allow isolation of specific BEC subpopulation if necessary. However, antibodies can remain bound to BECs for many days in culture and their effect on cultured BECs remains unclear (Joplin et al., 1989). Therefore a further step is occasionally introduced in order to cleave bound antibodies from the isolated cells (Ishii et al., 1989).

Immuno-isolation was the chosen method for BEC isolation in this project due to the selective nature of the technique, its applicability in human tissue and its relative ease of application and reproducibility.

2.1.3. Hypotheses and aims

Based on the above, it was hypothesized that hepatic IRI alters biliary epithelial cells and/or the peri-biliary environment resulting in attraction of inflammatory and collagen-producing cells

The aim of this study was to examine the roles of BECs and hepatic stellate cells (HSCs) in a simulated ischaemia-reperfusion injury environment in vitro (hypoxia and subsequent re-oxygenation) by investigating:

1. the ability of hepatic stellate cells to migrate towards bile constituents
2. the ability of BECs to produce chemokines in response to hypoxia and re-oxygenation

2.2. Materials and methods

2.2.1. Ethical considerations

National Research Ethics Service (NRES) approval was obtained for the use of human tissue (NRES 07/Q0906/15) in this project. All experiments were carried out in accordance with the Human Tissue Act 2004, and in strict compliance with other local and national guidelines and policies.

2.2.2. Cell isolation protocols

Human hepatic stellate cells (HSCs) and biliary epithelial cells (BECs) were isolated from fresh liver resection specimens obtained from the Freeman Hospital. Care was taken to not include the resection margins of the specimen or grossly abnormal tissue in the samples used for cell isolation.

Resected samples were weighted and transferred from the hospital in ice cold 0.9% saline. Samples were occasionally stored in Dulbecco's modified Eagle medium (DMEM) at 4°C overnight for cell isolation the following day.

Reagents used for cell isolation

Phosphate-buffered saline (PBS – product code 70011044) was purchased from Thermo Fisher Scientific (Waltham, MA, USA). Dulbecco's modified Eagle medium (DMEM) low and high glucose content (product codes D5546 and D5671 respectively), collagenase IA (product code C9891), DNAase I (product code D5025), Optiprep™ (product code D1556) and Hanks' balanced salt solution (HBSS – product code H9269) were purchased from Sigma-Aldrich (St. Louis, MO, USA). Percoll® density gradient medium (product code 17-0891-01) was purchased from GE Healthcare (Chicago, IL, USA). EpCam Dynabeads (CELLection Epithelial Enrich – product code 16203) were purchased from Life Technologies (Carlsbad, CA, USA).

Isolation of human biliary epithelial cells (hBECs) by immuno-magnetic selection

Specimens are diced to fine pieces using a pair of scissors or scalpel blade and then incubated in 0.1% collagenase A and 0.2% DNAse in Phosphate-buffered saline (PBS) for 30-45 minutes at 37°C for digestion. The resultant digest is then filtered through an 80μm pore Nybolt mesh and washed twice in PBS with centrifugation. Semi-purification is achieved by overlaying the cell suspension on a 33%:77% Percoll gradient and centrifuging at 2000rpm for 30 minutes (80% acceleration and 0% deceleration). The resultant BEC ring (Figure 2.2) is then extracted from the Percoll gradient and washed once in PBS with centrifugation. The cells are then incubated with Dynabead-conjugated Human Epithelial Antigen HEA-125 for 30 minutes at 4°C. Dynabead-bound cells are then extracted and washed twice using a magnet to remove supernatant. The resultant hBECs are re-suspended in hBEC media and transferred to a T25 flask for cell culture.

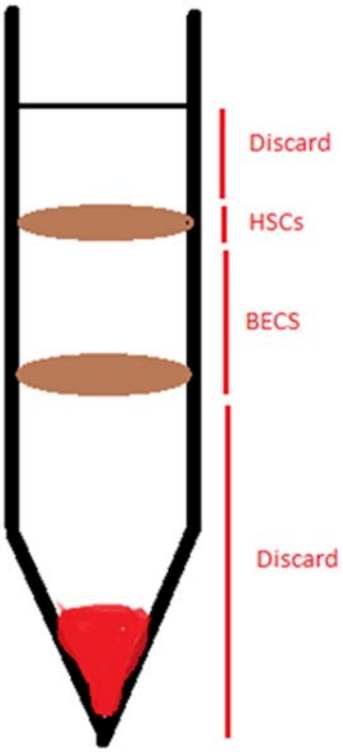

Figure 2.2 Percoll gradient centrifugation results in a HSC/hepatocyte ring (top) and a BEC ring (bottom)

Isolation of human hepatic stellate cells (hHSCs) by differential density separation

Liver tissue is diced, digested, filtered and washed as per the hBEC isolation method. Cells are suspended in Hank's balanced salt solution (HBSS) with or without calcium/magnesium and are then mixed with optiprep (60% solution of Iodixanol in water) to form a 15% Iodixanol crude cell suspension. This is gently overlaid with a 5-10 ml layer of 10% Iodixanol in HBSS followed by a 5 ml layer of HBSS to create a discontinuous Optiprep gradient. The gradient is centrifuged at 2000rpm for 30 minutes (80% acceleration and 0% deceleration). The resultant hHSC ring (Figure 2.3) is extracted from the Optiprep gradient and is washed once in PBS with centrifugation. Washed hHSCs are re-suspended in hHSC media and transferred to T75 flasks for cell culture.

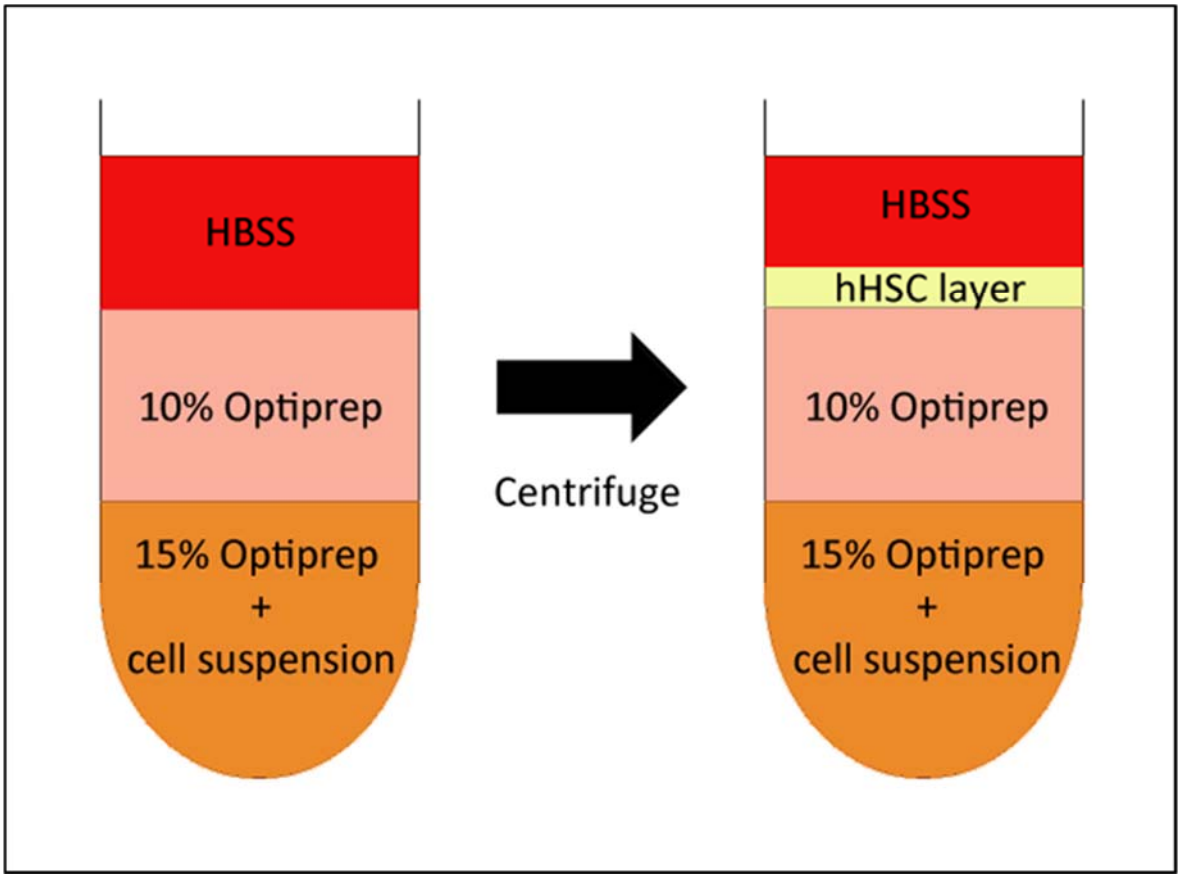

Figure 2.3 Separation of HSC layer in Optiprep gradient

Isolation of human Kupffer cells (KCs) by selective adherence

Kupffer cells were isolate by allowing the final cell suspension obtained during hHSC isolation to settle in a cell culture flask for 60 minutes before rinsing with PBS and

transferring the non-adherent hHSCs to fresh culture flasks. This method utilises the capacity of KCs to adhere to plastic more rapidly than other non-parenchymal cells (Zeng et al., 2013).

H69 cell line

H69 cells (immortalised human intrahepatic cholangiocyte cell line) were kindly provided by Professor Matthew Wright (Newcastle University, UK) and cultured using similar media and culture conditions as hBECs.

2.2.3. Cell culture conditions

Reagents used for cell culture

Dulbecco's modified Eagle medium (DMEM) low and high glucose content, Ham's F12 nutrient mixture medium (product code 51653C), foetal calf serum (product code F2442), epidermal growth factor (product code E9644), hepatocyte growth factor (product code H1404), hydrocortisone (product code H0888), 3,3′,5-Triiodo-L-thyronine (product code T2877), recombinant human insulin (product code I2643), cholera toxin (product code C8052), trypsin-EDTA (product code 59418C), penicillin-streptomycin (product code P4333) and L-glutamine (product code G7513) were purchased from Sigma-Aldrich. Matrigel™ extracellular matrix (product code 354234) was purchased from Corning Inc. (Corning, NY, USA).

Cell culture protocols

Human biliary epithelial cell growth and proliferation in cell culture requires hBEC media which is composed of DMEM and Ham's F12 media 1:1 mixture supplemented with 5% foetal calf serum (FCS), insulin (5µg/ml), hepatocyte growth factor (HGF) (10 ng/ml), Epithelial growth factor (EGF) (10ng/ml), hydrocortisone (0.4µg/ml), tri-iodothyronine (2 nmol/L), cholera toxin (10 ng/ml), 1% glutamine and and 1% penicillin/streptomycin. hBECs were cultured in 5% CO2 at 37°C for optimal growth and proliferation and were sub-cultured using 1X trypsin-EDTA once a confluence of

70-80% was reached. hBECs maintained epithelial phenotype for at least one passage after isolation.

Human hepatic hepatic stellate cells were also cultured in 5% CO2 at 37°C. hHSCs were cultured on gel matrix, rat tail collagen or uncoated plastic depending on the experiment. hHSC media was composed of high glucose-DMEM supplemented with 16% FCS, 1% glutamine and 1% penicillin/streptomycin. hHSCs were split at approximately70-80% confluence using 1X trypsin-EDTA and were maintained in culture for up to 5 passages.

2.2.4. Cell culture in hypoxia

A multi-gas incubator (Sanyo MCO-19M) was used to create a hypoxic environment for cells in culture (Figure 2.4). Cells were cultured in 1% oxygen either continuously or for a set period (8 hours) followed by culture in 21% oxygen in order to simulate ischaemia and reperfusion. CO2 and temperature were maintained at 5% and 37°C respectively throughout the hypoxia experiments.

Figure 2.4 Multigas incubator for in vitro hypoxia studies (left). To maintain hypoxia, oxygen in this incubator is replaced with nitrogen delivered via a nitrogen generator (right)

2.2.5. Chemotaxis assays

Reagents used for chemotaxis assays

Bovine serum albumin (BSA – product code A2153), fibronectin (product code F2006), crystal violet stain (product code C0775), bilirubin (product code B4126), cholate (product code C1129), glycocholate (product code G2878), taurocholate (product code T4009), chenodeoxycholate (product code C9377), deoxycholate (product code D2510), lithocholate (product code L6250), phosphatidyl choline (product code P3556) and cholesterol (product code C8667) were purchased from Sigma-Aldrich. Monocyte chemoattractant protein-1 (product code 279-MC), stroma-derived factor-1 (product code 350-NS), interleukin-6 (product code 206-IL), tumour necrosis factor-α (product code 210-TA), transforming growth factor-β (product code 240-B), interferon-γ (product code 285-IF), vascular endothelial growth factor (product code 293-VE), fibroblast growth factor (product code 233-FB) and epithelial growth factor (product code 236-EG) were purchased from R&D Systems

(Minneapolis, MN, USA). Falcon® 8µm pore cell culture inserts and 24-well companion plates were purchased from Corning Inc.

Chemotaxis protocol

A modified Boyden chamber protocol was followed for the chemotaxis assays using sterile 8µm pore 24-well culture inserts (BD Falcon) coated with fibronectin (2.5µg/ml).

Companion 24-well plates for the inserts were blocked with 1% bovine serum albumin (BSA) in PBS for one hour. Compounds, cells or conditioned cell media were added to the wells after blocking to induce cell migration across the insert filters.

Culture-activated HSCs (passage 3-5) were used as migrating cells. These were kept in serum-free DMEM for 24 hours prior to the assay in order to reduce cell proliferation. HSCs were then detached using 1X trypsin-EDTA, washed and re-suspended in serum-free medium at a concentration of 5-25 x 10^4cell/ml. The cells were subsequently seeded onto the fibronectin-coated inserts placed in the wells of the companion plate at concentrations ranging between 30,000-100,000 cell/ml. Platelet-derived growth factor (PDGF) was used as a positive control at a concentration of 1ng/ml in all migration assays. 1% BSA in PBS was used as a negative control. Cells were incubated for 18-24 hours following which the migrated cells were fixed, stained and counted under low power magnification (X10). Each experiment was typically performed on two occasions at least and the average cell count was measured from 30 field views for each variable of interest.

In early migration assay experiments, cell counts were estimated using spectrophotometric analysis of solubilised crystal violet staining. Briefly, cells adherent to cell culture inserts were fixed in formalin and stained using 0.05% crystal violet stain for 30 minutes. Inserts were then washed with tap water and dried at room temperature for 20 minutes. The dye was then solubilised by reintroducing the cell inserts into the companion plate after adding 2ml of methanol to each well. The plate is then read at OD_{540} and colour intensities are compared to positive and negative control readings.

Chemotaxis experiments

Compounds tested for hHSC chemo-attraction included cytokines such as monocyte chemoattractant protein-1 (MCP-1), stroma-derived factor-1 (SDF-1), interleukin-6 (IL-6), tumour necrosis factor-α (TNF-α), transforming growth factor-β (TGF-β), interferon-γ (IFN-γ), vascular endothelial growth factor (VEGF), fibroblast growth factor (FGF), and epithelial growth factor (EGF) in addition to bile components such as bilirubin, cholate, glycocholate, taurocholate, chenodeoxycholate, deoxycholate, lithocholate, phosphatidyl choline and cholesterol.

hBECs were also tested for expression of hHSC chemoattractants in various oxygen states. hBECs were cultured in 4 wells of 6-well plates in serum-free DMEM for 24 hours in hypoxia (1% O2), normoxia (21% O2) or hypoxia for 8 hours followed by normoxia in order to mimic IRI. Conditioned serum-free media was collected after 24 hours from 2 wells whilst the remainder of cells were re-cultured in hBEC media for 24 hours and then in serum-free DMEM for a further 24 hours under the same oxygen state. Conditioned media was then collected at the 72 hour time point. This process is illustrated in Figure 2.5. Conditioned media from each oxygen state at each time point were diluted 1:8 in serum-free media and added to the companion plate wells to assess chemokine expression (Figure 2.6).

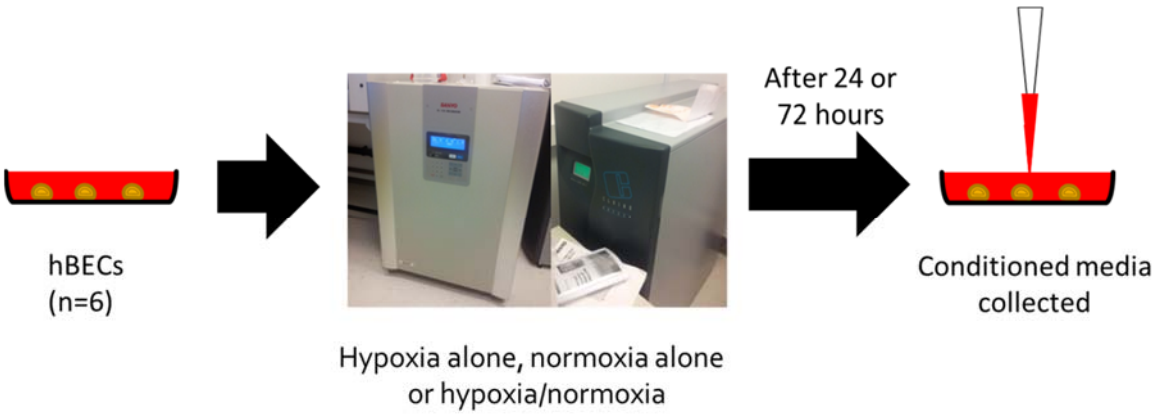

Figure 2.5 Testing for the expression of chemoattractants by hBECs in various oxygen states

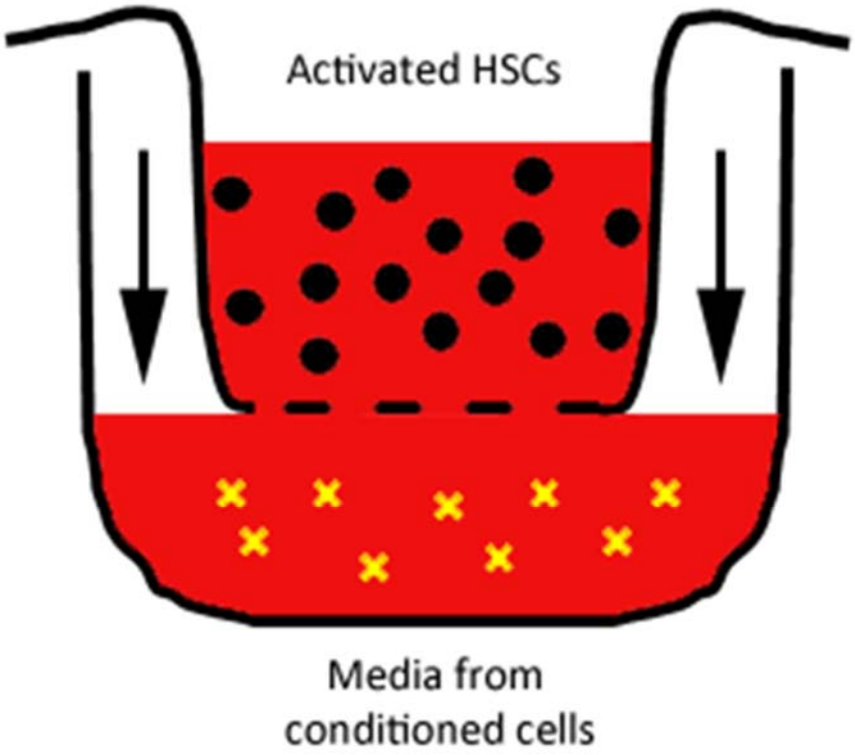

Figure 2.6 Assembly of chemotaxis assay components

2.2.6. Sample processing and preservation

Reagents used for sample processing

RIPA buffer: Purchased from New England Biolabs (Ipswich, MA, USA) as a 10X stock solution (product code 9806) and diluted in deionised water to make a 1X solution. The 1X buffer is composed of Tris-HCl (20 mM; pH 7.5), Sodium chloride (150 mM), EDTA disodium (1 mM), EGTA (1 mM), NP-40 (1%), sodium deoxycholate (1%), sodium pyrophosphate (2.5 mM), beta-glycerophosphate (1 mM), sodium orthovanadate (1 mM) and leupeptin (1 µg/ml).

Cell lysis buffer: Purchased from New England Biolabs as a 10X stock solution (product code 9803) and diluted in deionised water to make a 1X solution. The 1X buffer is composed of Tris-HCl (20 mM; pH 7.5), Sodium chloride (150 mM), EDTA

disodium (1 mM), EGTA (1 mM), Triton (1%), sodium pyrophosphate (2.5 mM), beta-glycerophosphate (1 mM), sodium orthovanadate (1 mM) and leupeptin (1 µg/ml).

Protease inhibitor cocktail (product code P8340) was purchased from Sigma-Aldrich).

Processing of samples from cell culture harvest

Samples for protein extraction were obtained by scraping cultured cells from culture plates on ice in 1X RIPA or lysis buffer. Protease inhibitor cocktail was added to the buffer for a 1X final concentration. The extracted cells were left for 30 minutes at 4°C for complete lysis and then centrifuged at 5000 RPM for 5 minutes at 4°C. Supernatants were extracted and kept at -80°C for long-term storage.

Conditioned serum-free media samples were collected from cell culture and centrifuged at 5000 RPM for 5 minutes at 4°C. Supernatants were transferred to clean tubes and kept at -80°C for long-term storage.

2.2.7. Methods for protein analysis

Reagents used for protein analysis

Lowry ABC reagent: Composed of 2% Sodium carbonate in 0.1N NaOH (Lowry A solution), 1% sodium potassium tartrate in water (Lowry B solution) and 0.5% copper(II) sulphate pentahydrate in water (Lowry C solution) in a 100:1:1 mixture.

Folin and Ciocalteu's phenol reagent: Purchased from Sigma-Aldrich (product code F9252). Reagent is diluted 1:1 in water for the Lowry method.

Acrylamide/bis-acrylamide (37.5:1 ratio; 40% solution): Purchased from Sigma-Aldrich (product code A7168). Used in various concentrations as an electrophoresis matrix to enable protein separation by size.

Tris base: Purchased from Sigma-Aldrich (product code TRIS-RO). Prepared as 1.5M (pH 8.8) and 0.5M (pH 6.8) solutions in deionised water. These are used as components of the separation and stacking gel solutions respectively.

Tetramethylethylenediamine (TEMED): Purchased from Sigma-Aldrich (product code T9281). This facilitates the polymerisation of acrylamide to polyacrylamide in electrophoresis gels.

Amonium Persulfate (APS): Purchased from Sigma-Aldrich (product code A3678). This facilitates the polymerisation of acrylamide to polyacrylamide in electrophoresis gels.

Sodium dodecyl sulfate (SDS): Purchased from Sigma-Aldrich (product code L3771). SDS is used as a component of electrophoresis gels. It acts as a strong detergent and denatures proteins. It also binds to polypeptides at a constant ratio of 1.4:1 (SDS:polypeptide)

Electrophoresis running buffer: Prepared as a stock 10X solution composed of Tris base (250mM), glycine (1.92M) and SDS (1% w/v) in deionised water. Buffer is diluted to 1X concentration in deionised water prior to use in electrophoresis.

NuPage LDS sample buffer: Purchased from Life Technologies (product code NP0007) as a 4X solution. It is mixed with protein samples for a final 1X buffer concentration and is used as a loading buffer to prepare protein samples for denaturing gel electrophoresis.

Dithiothreitol (DTT): Purchased from Sigma-Aldrich (product code D0632). Prepared as a 1M stock solution stored in aliquots at -20°C. DTT is added to sample buffers if reduction of proteins is required.

ColorBurst electrophoresis marker: Purchased from Sigma-Aldrich (product code C1992) as a ready-to-use solution to identify the molecular mass of protein bands following electrophoresis and Western blots.

Transfer buffer: Composed of Tris base (25mM), glycine (192mM) and 20% methanol in deionised water. Buffer is kept at 4°C and used for wet transfer of proteins from gel to nitrocellulose membrane.

TBS-T: Composed of 1X TBS buffer and 0.05% Tween 20. TBS-T is used as a wash solution for nitrocellulose membranes and a component of as blocking buffer and antibody diluents in Western blots. 1X TBS buffer is prepared from 20X TBS stock buffer (4M sodium chloride and 0.4M Tris-HCl; pH 7.4)

Blocking buffer: Composed of 1X TBS buffer, 0.05% Tween 20 and 3% skimmed milk powder. Used to block the nitrocellulose membrane and minimise non-specific antibody binding to the membrane.

Antibody diluent: Composed of 1X TBS buffer, 0.05% Tween 20 and 0.3% skimmed milk powder. Used as a diluent for primary and secondary antibodies during immune-detection of proteins.

Pierce enhanced chemi-luminescence (ECL) substrate kit: Purchased from Thermo Fisher Scientific (product code 32109). Composed of peroxide buffer and luminescence enhancer. Used to detect horseradish peroxidase (HRP) enzyme activity over protein bands.

Protein quantification

Protein quantity in samples was estimated using the Lowry method (Lowry et al., 1951). Sample or standard (5µl) was incubated with 1ml of Lowry ABC reagent for 10 minutes at room temperature followed by the addition of 100µl of diluted Folin reagent and incubation for a further 20-30 minutes at room temperature. Absorbance of the mixture was read at 750nm using a spectrophotometer. The unknown concentrations were calculated based on the calibration curve plotted using the absorbance readings of the standards.

Sodium Dodecyl Sulfate-Polyacrylamide Gel Electrophoresis (SDS-PAGE)

Separation of sample proteins was achieved by the Laemmli method (Laemmli, 1970) using a discontinuous polyacrylamide gel system. The gel consisted of a stacking gel layer (4% acrylamide w/v) and a lower separating gel layer (between 7-15% acrylamide w/v, depending on the molecular weight of the protein of interest). Separating gel solutions were prepared by mixing different volumes of acrylamide/bisacrylamide, SDS, Tris buffer (1.5M pH 8.8) and water depending on the desired acrylamide concentration of the gel. Stacking gel solutions were prepared by mixing the same reagents as in the separating gels but substituting the 1.5M Tris buffer with 0.5M Tris buffer (pH 6.8). The acrylamide concentration in the stacking gel is 4%.

Gels were hand-cast using a Bio-Rad Mini-Protean Tetra Handcast apparatus. APS and TEMED were added to the gel solutions immediately before transferring the gel solution to the apparatus. The separating gel solution was cast first followed by the stacking gel to create a 0.75mm-thick 10-well gel. Gels were then transferred to a Bio-Rad Mini-Protean Tetra Cell electrophoresis tank filled with electrophoresis running buffer.

Protein samples (from cell extracts or serum-free conditioned media) were mixed with loading buffer (with or without DTT) and heated for 10 minutes at 70C before cooling and loading into the SDS gel wells. Gel electrophoresis was run at a constant voltage of 100V for 1-2 hours.

Western blot

Gels from SDS-PAGE were removed from the electrophoresis tank and soaked in cold transfer buffer along with pre-cut nitrocellulose membranes, foam pads and filter papers for at least 10 minutes. Gel, membrane, pads and filter paper were then assembled in the gel holding cassette in the order outlined in Figure 2.7 ensuring there are no bubbles between the layers. The assembly is then inserted into a Bio-Rad Mini Trans-Blot tank for wet transfer of proteins. Electro-transfer was maintained for at least one hour to ensure adequate protein transfer.

Blotted nitrocellulose membranes were then washed in TBS-T and then blocked for 1 hour in room temperature or overnight at 4°C in blocking buffer. Membranes were then washed and incubated with an optimised concentration of primary antibody against the protein of interest for at least 1 hour in room temperature or overnight at 4°C. Membranes were washed again in TBS-T prior to incubation for 30 minutes at room temperature with a secondary HRP-conjugated antibody against the host species of the primary antibody. This was followed by a final wash and then chemi-luminescent detection of probed protein bands using the ECL substrate kit. Chemi-luminescent bands were visualised using a Syngene G:BOX CCD camera and band densities were quantified using GeneTools analysis software supplied with the camera.

A list of antibodies used in western blot experiments is summarised in Appendix 1.

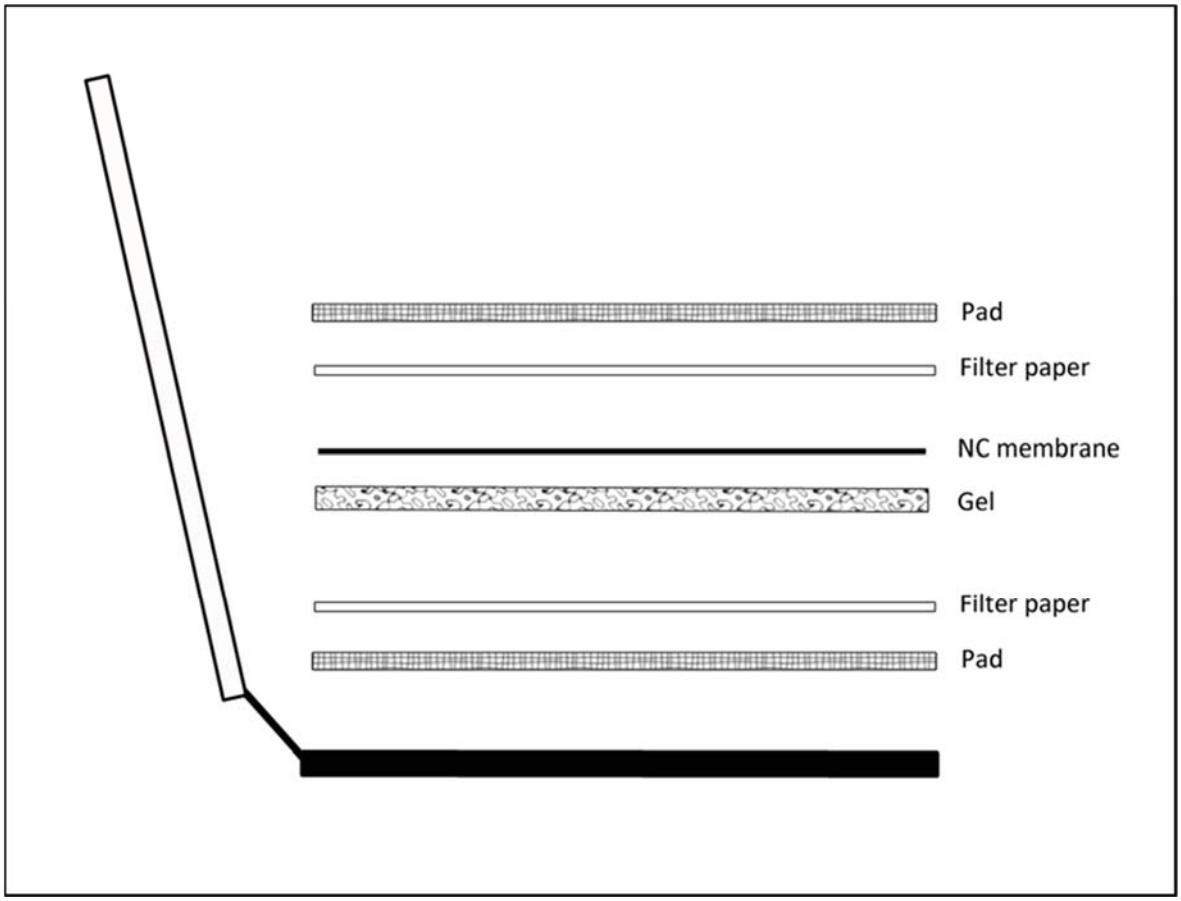

Figure 2.7 Assembly of transfer layers in holding cassette

2.2.8. Methods for cell staining

Reagents used for staining

Fixative solution: Composed of formaldehyde (2% w/v) and glutaraldehyde (0.2% w/v) in PBS (pH 7.4). Used as a fixative for cells prior to immunofluorescence staining.

Blocking solution: Composed of FCS (5%) in PBS. Used as a blocking buffer to prevent non-specific antibody binding during Immunocytofluorescence staining.

Antibody diluent: Composed of FCS (0.5%) in PBS. Used as a diluent for primary and secondary antibodies during Immunocytofluorescence staining.

4',6-diamidino-2-phenylindole (DAPI): Purchased from Sigma-Aldrich (product code D9542).

Methanol (product code 32213) was purchased from Sigma-Aldrich.

Immunocytofluorescence staining

Cells were washed twice with PBS after removal of culture medium and then incubated in ice-cold methanol for 10 minutes at 4°C. Methanol was then decanted and cells washed again with PBS twice before adding the fixative solution and incubating for 10 minutes at room temperature. This was followed by removal of the fixative solution, a further two washes with PBS and then the addition of blocking solution and incubation for 30 minutes at room temperature. Blocked cells were subsequently washed four times with PBS and then incubated for 1 hour with a primary antibody of interest (see Appendix 1) at room temperature (or at 4°C for longer incubation times). After removing the primary antibody and washing the cells twice with PBS, a suitable secondary antibody conjugated to a fluorescent dye (see Appendix 1) was applied to the cells for 30 minutes at room temperature and was covered in foil to prevent dye photobleaching. Finally, the cells were washed four times with PBS and the nuclei counterstained with DAPI for 5 minutes. The cells were kept in PBS and were visualised using a fluorescent microscope (Nikon Eclipse TE2000-S).

A list of antibodies used in immunocytofluorescence staining is summarised in Appendix 1.

2.2.9. Statistical analysis

In the case of parametric data, results were expressed as mean ± SD unless stated otherwise. Means were compared using the Student t-test or the ANOVA test (where multiple variables were analysed or when more than two groups were compared). Tukey's test was used for post-hoc analysis between the groups when significant differences were identified on ANOVA. Non-parametric variables were analysed using the Mann Whitney U test and results expressed as median (mean rank). Correlation between continuous independent variables was performed by measuring Pearson's correlation coefficient. The strength of correlation is described as small, medium or large corresponding to correlation coefficient values below 0.3, between 0.3 and 0.5, and above 0.5 respectively (Cohen, 1988). Test results with p values of

less than 0.05 were accepted as statistically significant. All statistical tests were performed using the Statistical Package for Social Sciences version 19.0 (SPSS Inc., Chicago, IL, USA) and Microsoft Office Excel 2010 (Microsoft Corp., Redmond, WA).

2.3. Results

2.3.1. Confirmation of isolated cell phenotype in culture

Biliary epithelial cells

Biliary epithelial cells had a columnar appearance with elongated nuclei and an overall polar morphology. They exhibited a tendency form duct-like congregations in culture as illustrated in Figure 2.8.

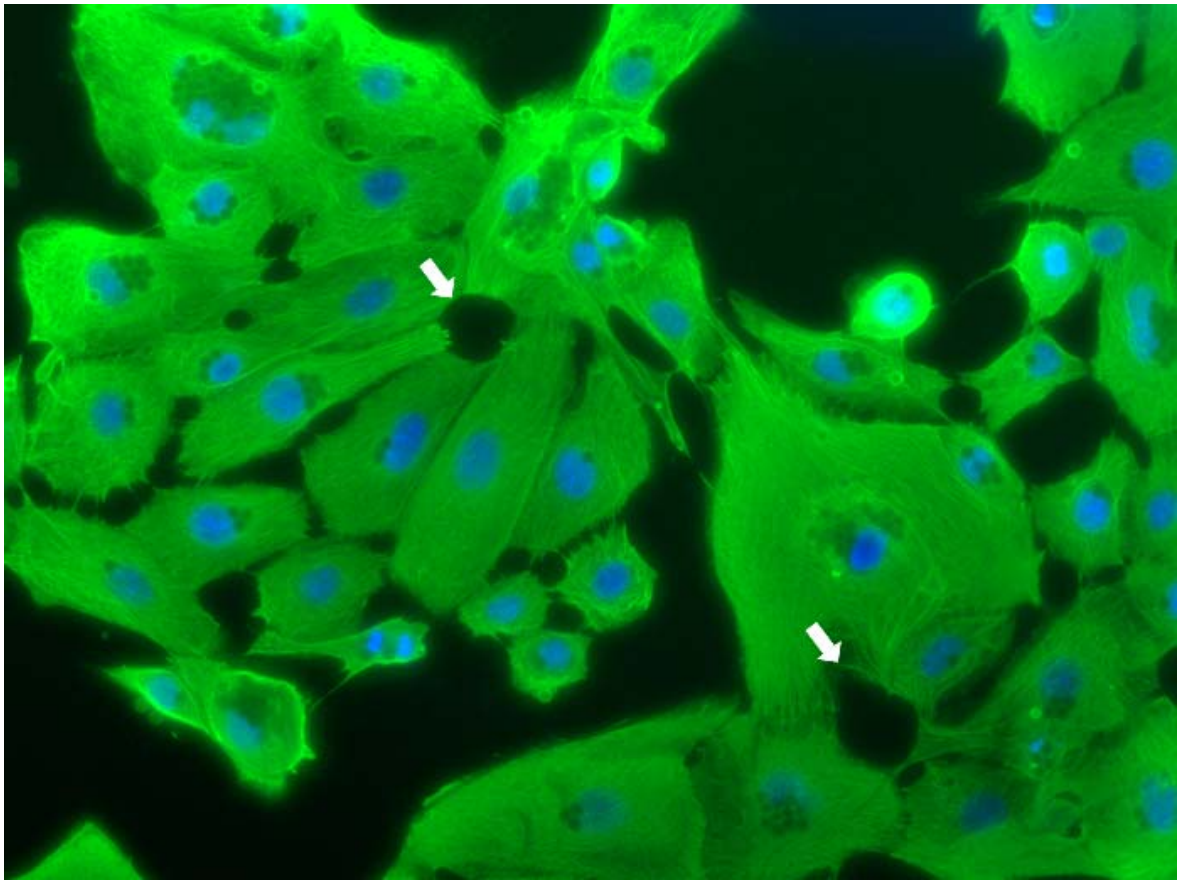

Figure 2.8 Human BECs visualised in cell culture using immunofluorescence staining at 20X objective magnification. Solid white arrows denote duct-like arrangements

In addition to morphological features, BECs were stained at first passage in order to identify typical markers of the biliary epithelium including cytokeratin 19 (CK19) (Figure 2.9), and to exclude markers of mesenchymal cells such as vimentin and α-smooth muscle actin (α-SMA) (Figure 2.10).

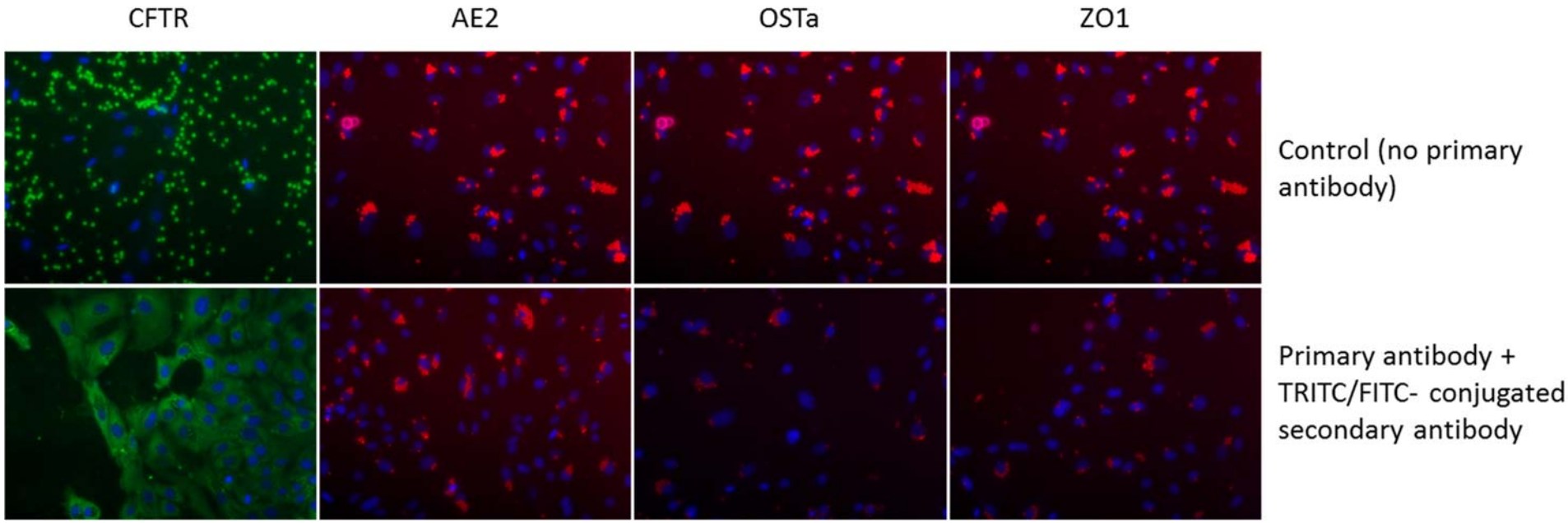
CFTR
AE2
OSTa
ZO1
Control (no primary antibody)
Primary antibody + TRITC/FITC- conjugated secondary antibody

Figure 2.9 Immunofluorescence staining for surface markers of BECs (transporters and tight junctions). Note the presence of Dynabeads from the cell isolation process which auto-fluoresce and do not represent antigen-antibody binding sites (as demonstrated in control images). CFTR: Cystic fibrosis transmembrane conductance regulator; AE2: Anion exchange protein 2; OSTα: Organic solute transporter alpha; ZO1: Zonula occludens-1; TRITC: Tetramethylrhodamine; FITC: Fluorescein isothiocyanate

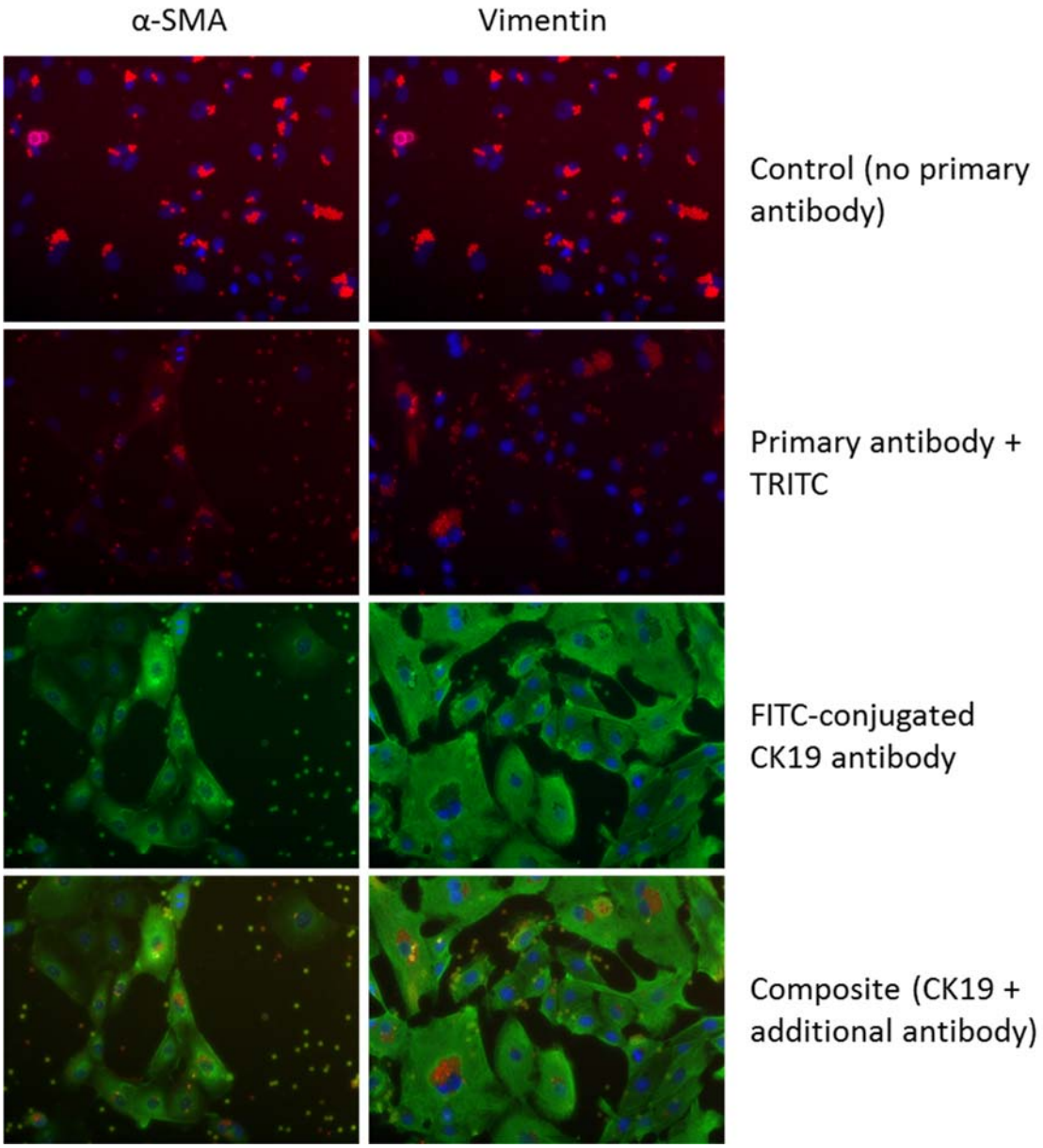

Figure 2.10 Immunofluorescence staining for markers of mesenchymal cells (α-SMA and vimentin) along with CK19 in hBECs. Note auto-fluorescence of Dynabeads in control images. TRITC: Tetramethylrhodamine; FITC: Fluorescein isothiocyanate

Figure 2.10 clearly demonstrates strong expression of CK19 in these cells. Moreover, the cells showed strong positivity for the apical CFTR channel. However, staining for other markers of BECs such as the anion exchange protein 2 (AE2), the organic solute transporter alpha (OSTα) and the tight junction protein zonula occludens 1 (ZO1) was not positive in these cells with the antibody types and concentrations used for these experiments (Figure 2.9). Similar negative results were obtained when stained for platelet-derived growth factor receptor (PDGFR) and multidrug resistance-associated protein 3 (MRP3) (results not shown). On the other hand, staining for vimentin was negative whereas α-SMA staining was faintly positive in comparison to the strong CK19 positivity expressed in the cells as shown in Figure 2.10. This demonstrates the predominant epithelial phenotype in these cells.

Cultured hBECs from first passage were then compared for CK19 and α-SMA positivity to hBECs from fourth passage and to cells from a cholangiocyte-like cell line (H69) (Figure 2.11).

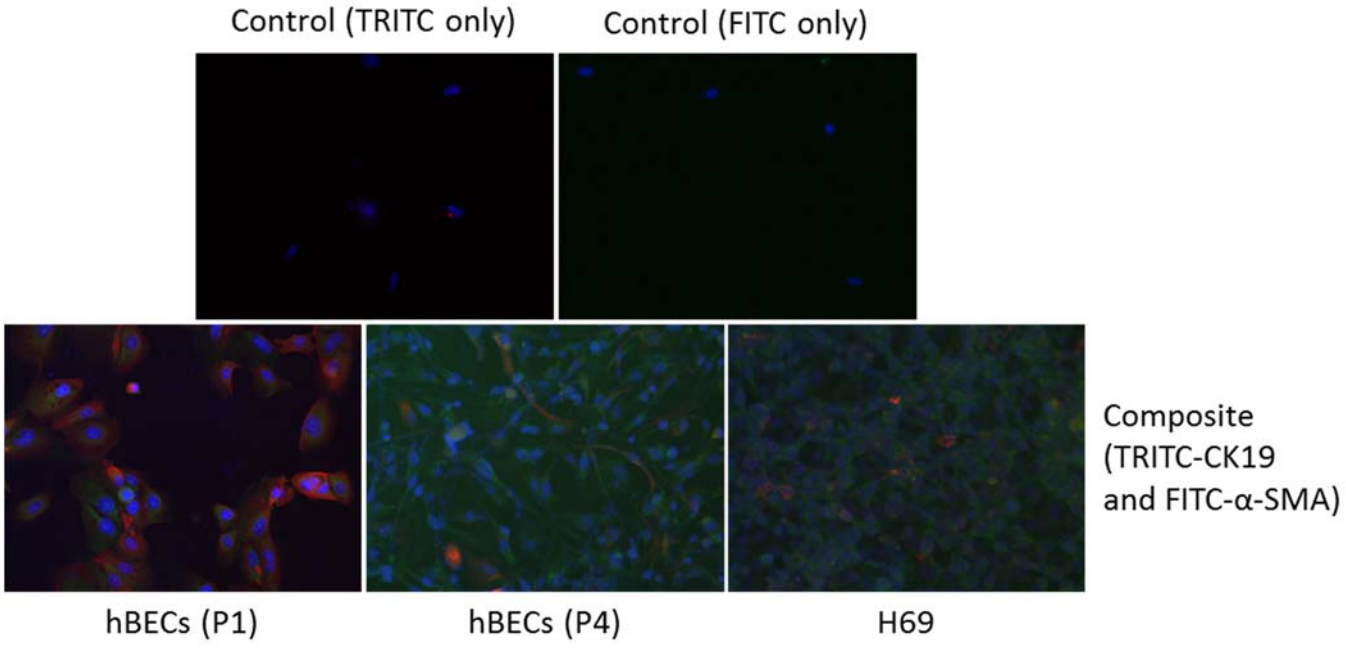

Figure 2.11 Immunofluorescence imaging showing CK19 and α-SMA positivity in freshly-cultured hBECS in comparison to mature hBECs and H69 cells. TRITC: Tetramethylrhodamine; FITC: Fluorescein isothiocyanate

The results suggest that cultured hBECs either slowly lose epithelial phenotype and develop markers of mesenchymal cells when kept in culture for longer periods, or that lower numbers of mesenchymal cells expand after multiple passages in culture. The results also show the stronger expression of CK19 in fresh primary human cholangiocytes in comparison to H69.

Hepatic stellate cells

Human hepatic stellate cells have a branched (occasionally spindle-shaped) appearance with round nuclei in culture. Fresh hHSCs (quiescent hHSCs) demonstrate abundant cytoplasmic fat droplets in keeping with their fat-storing role in normal liver (Friedman, 2008). Activated hHSCs in cell culture lose their lipid droplets and become more flattened. hHSCs become activated after approximately 5 days of growth in cell culture. This spontaneous activation in vitro can be slowed down by coating culture flasks with extracellular matrix products such as Matrigel™ rather than simply growing cells on plastic. These features are illustrated in Figure 2.12.

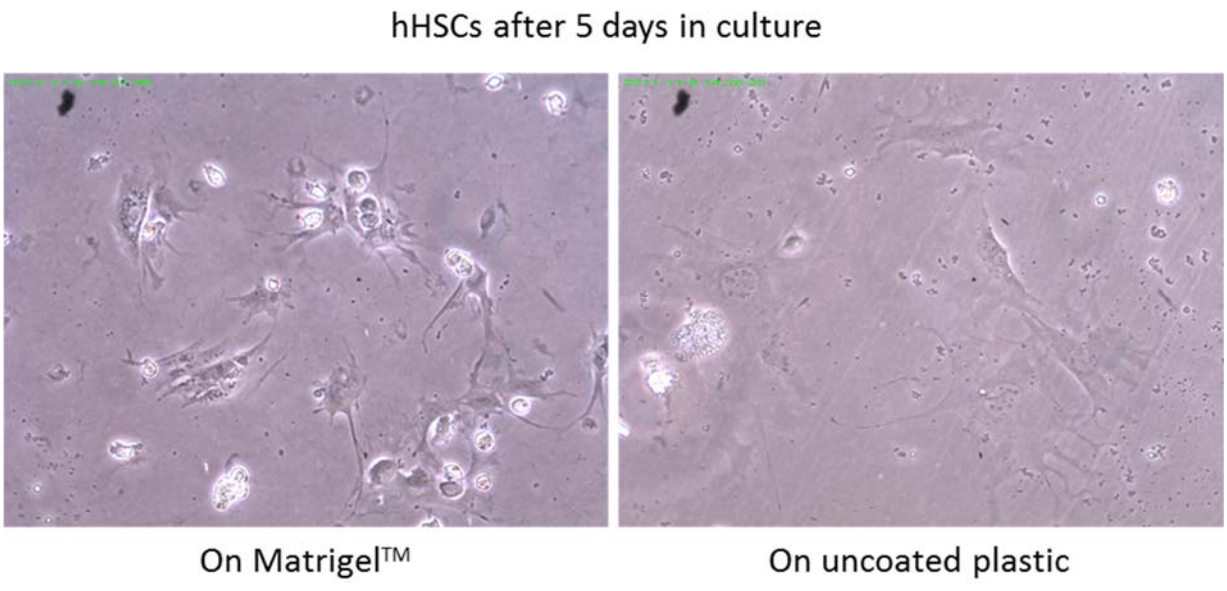

Figure 2.12 hHSCs at 20X objective magnification under light microscopy after 5 days in culture with (left) and withought (right) MatrigelTM.

Activated hHSCs were stained for myofibroblast and neural crest markers including α-SMA, elastin, vimentin, glial fibrillary acidic protein (GFAP) and synaptophysin, in addition to the Kupffer cell marker CD163. Selected examples of these stains are shown in Figure 2.13.

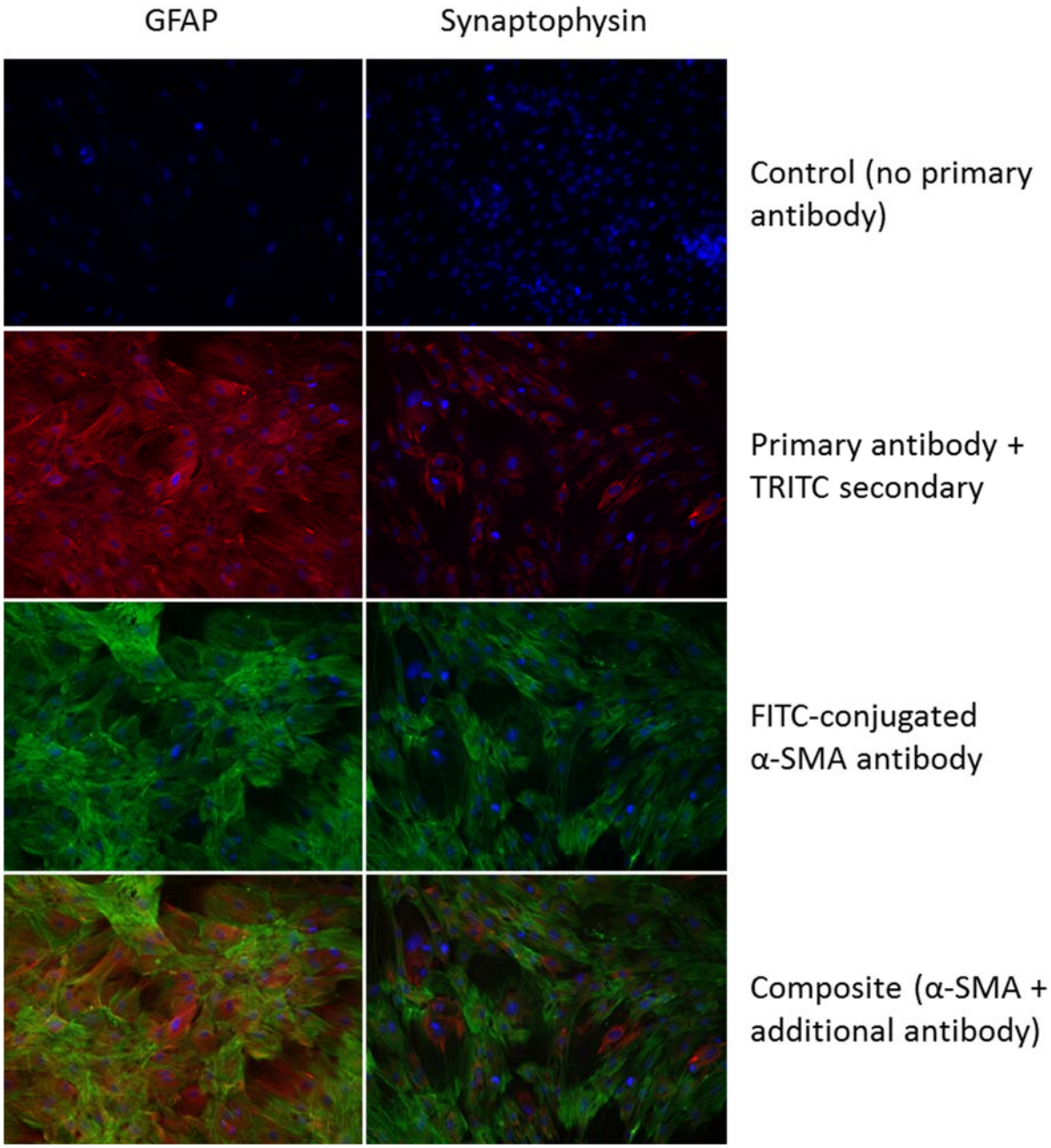

Figure 2.13 Immunofluorescence imaging of activated hHSCs. Neural crest markers (GFAP and synaptophysin) are stained along with α-SMA. TRITC: Tetramethylrhodamine; FITC: Fluorescein isothiocyanate

This clearly demonstrates abundant expression of classic HSC markers such as α-SMA, GFAP and synaptophysin, and confirms HSC activation in culture. Moreover, these cells stained positively for elastin and vimentin, and were negative for CD163 staining (data not shown).

2.3.2. Results of chemotaxis assays

hHSCs were found to measure 20-40μm in culture. Cell culture inserts with a pore diameter of 8μm were therefore used for chemotaxis assays (Kawamoto et al., 1997). The pore diameter allowed active translocation of migrating cells without being prohibitive. A comparison of hHSC size relative to the pores in illustrated in Figure 2.14.

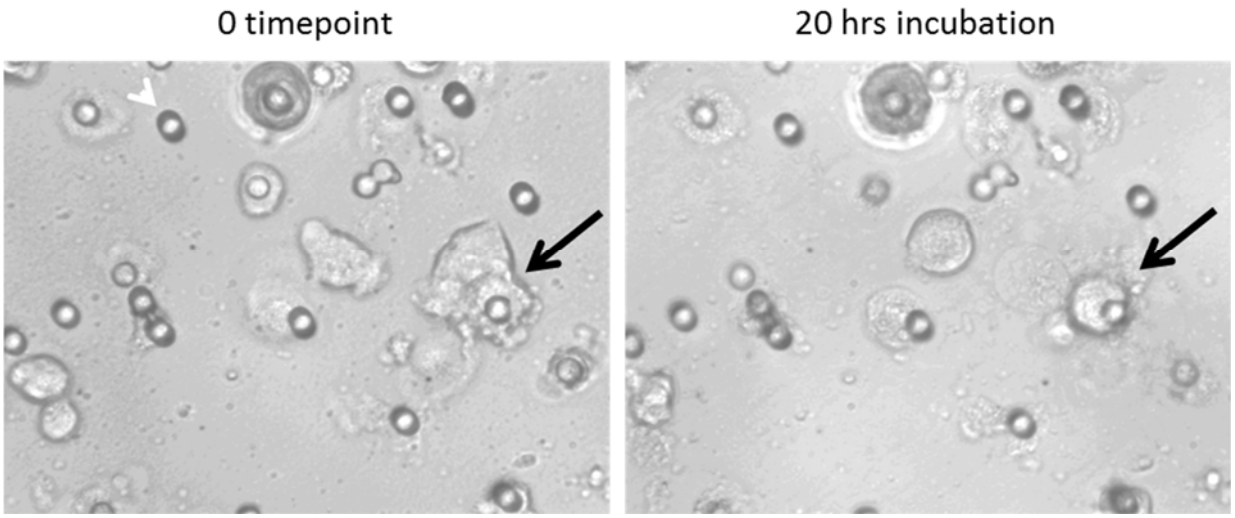

Figure 2.14 Light microscopy of cell culture insert showing size of stellate cell relative to pore diameter. Left: image taken at the time the cells were seeded onto insert. White arrowhead marks one pore. Black arrow marks one hHSC. Right: image takes after 20 hours of incubation. Black arrow shows previously marked cell has now migrated to lower surface of insert

Migration of hHSCs in response known cytokines

hHSC migration was tested against various concentrations of known cytokines and growth factors including PDGF, MCP-1, VEGF, SDF-1, IL-6 and IFN-γ. hHSCs

migration was found to be strikingly greater towards PDGF than any other cytokine tested (Figure 2.15). PDGF was therefore used as a positive control for all subsequent experiments. The results of the initial chemotaxis assays with known cytokines are outlined in Figure 2.16.

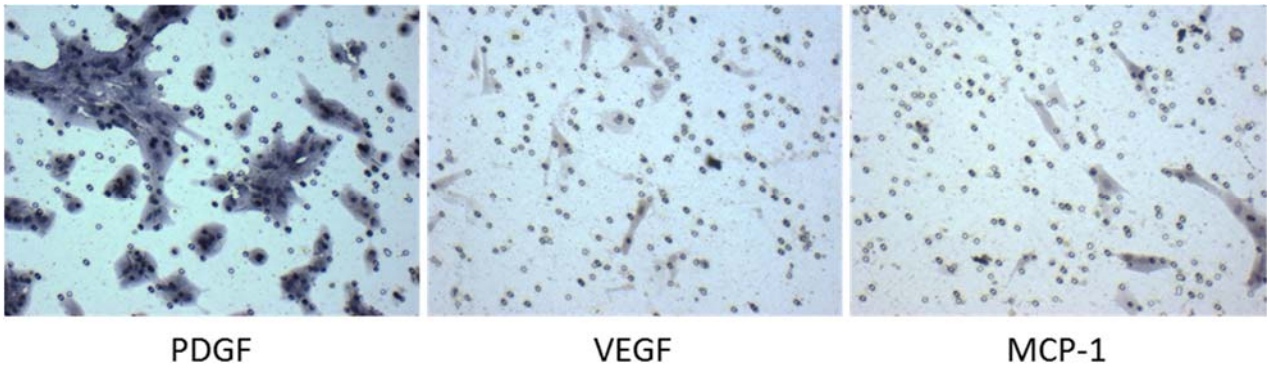

Figure 2.15 Migration of hHSCs towards PDGF (left) versus VEGF (middle) and MCP-1 (right). Cells were used at passage 4 and seeded at 60,000 cell/ml.

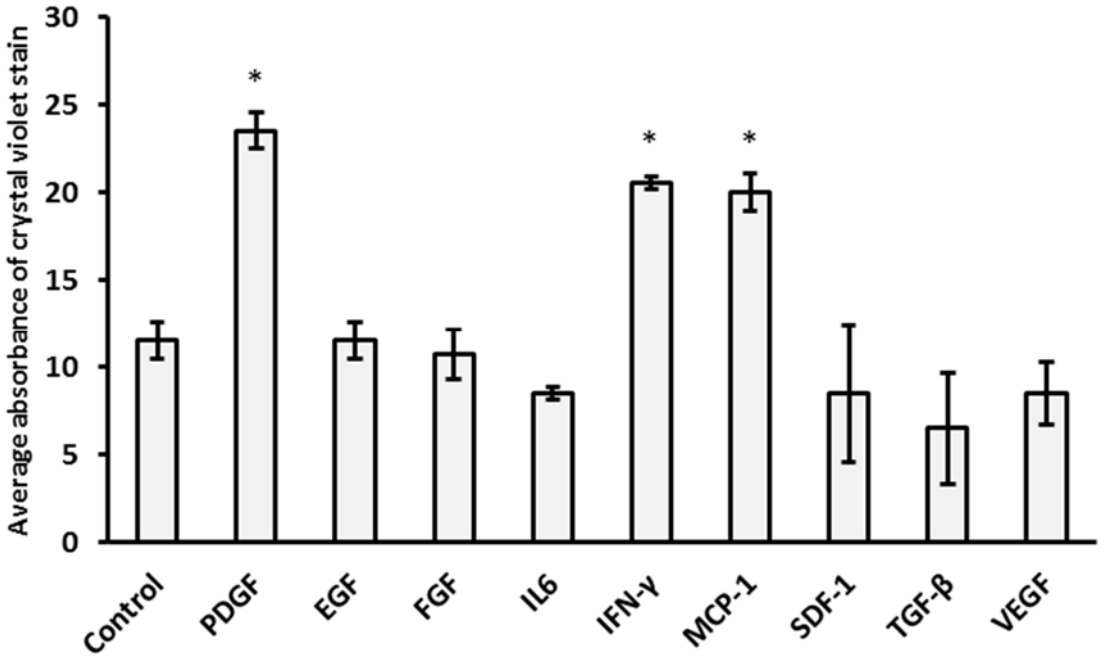

Figure 2.16 Migration of hHSCs towards various cytokines. Concentrations of cytokines in this example were all 62.5ng/ml. Cells were used at passage 3 and seeded at 100,000 cell/ml. Average absorbance of washed crystal violet stain was

used in preliminary experiments rather than actual cell count. *P<0.05 versus negative control.

In addition to PDGF, MCP-1 and IFN-γ were shown to significantly attract hHSCs at the concentrations tested. Interestingly, hHSC migration towards IL-6 was lower than in negative controls but this difference did not reach statistical significance (P=0.06).

Migration of hHSCs in response to various components of bile

Various bile components were used in hHSC migration assays to investigate the potential pro-migratory effect of bile. The compounds tested were cholesterol, phosphatidylcholine, cholic acid, chenodeoxycholic acid and bilirubin at various concentrations. Figure 2.17 outlines the results of these assays.

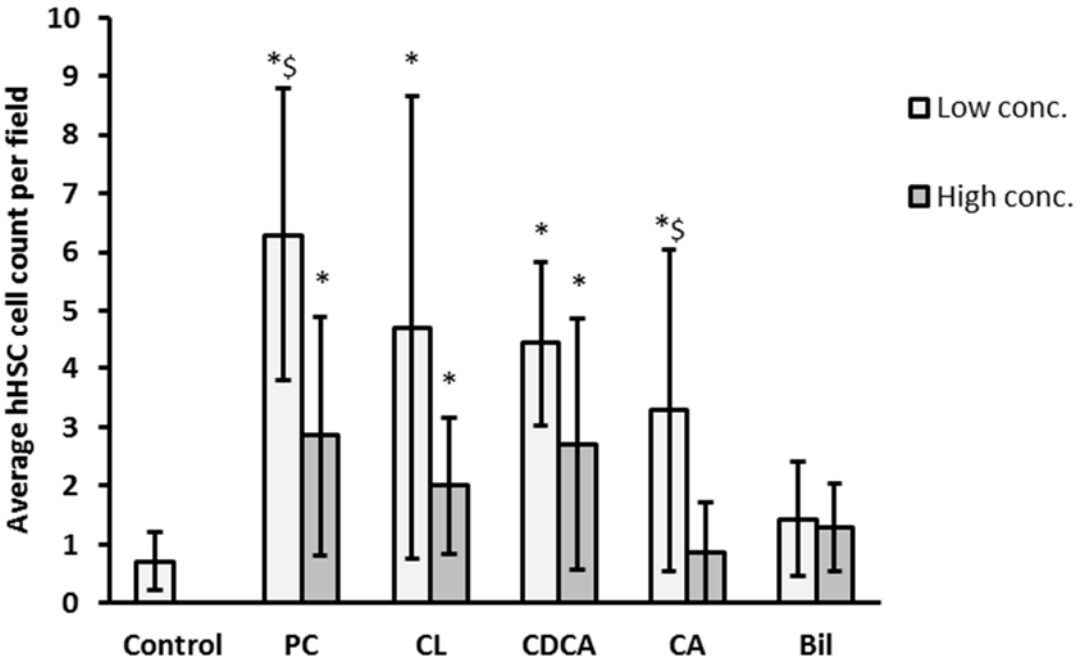

Figure 2.17 Migration of hHSCs towards high and low concentrations of various bile components. Cells were used at passage 4 and seeded at 60,000 cell/ml. PDGF used as positive control is not shown (average count >80). High concentrations=100ng/ml; Low concentrations=10ng/ml. PC: Phosphatidylcholine;

CL: Cholesterol; CDCA: Chenodeoxycholic acid; CA: Cholic acid; Bil: Bilirubin.
*P<0.05 versus negative control; $P<0.05 versus high concentration

The results highlight the chemotactic effect of cholesterol, phosphatidylcholine and the bile acids cholate and chenodeoxycholate on activated hHSCs. Lower concentrations of these compounds appear to be more effective at producing hHSC migration although this is only significantly different in the case of phosphatidylcholine and chenodeoxycholic acid. Bilirubin appears to have no migratory effect on activated hHSCs.

The chemotactic effect of bile components on activated hHSCs was compared to those of known cytokines as part of an assay mentioned previously. Cholesterol, phosphatidylcholine and chenodeoxycholic acid in low concentrations retained significance in attracting hHSCs compared to negative controls, and were comparable in that effect to IFN-γ and MCP-1 (Figure 2.18).

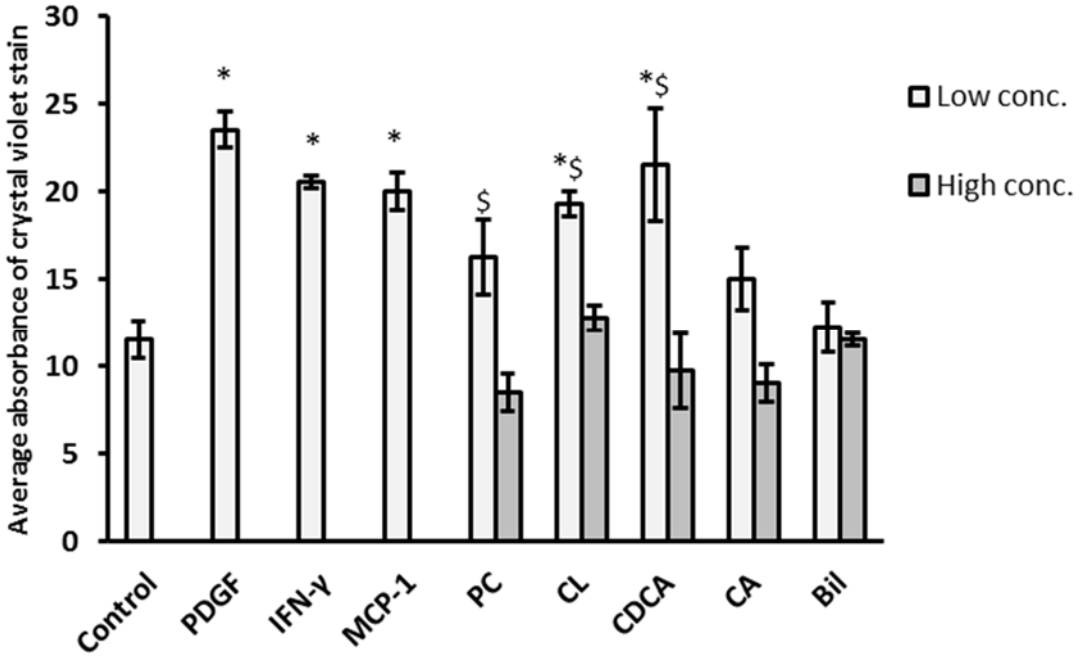

Figure 2.18 Comparison of hHSC migration to bile components and known cytokines. Concentrations of cytokines in this example were all 62.5ng/ml. Cells were used at passage 3 and seeded at 100,000 cell/ml. Average absorbance of washed crystal violet stain was used in preliminary experiments rather than actual cell count. High

concentrations=100ng/ml; Low concentrations=10ng/ml. PC: Phosphatidylcholine; CL: Cholesterol; CDCA: Chenodeoxycholic acid; CA: Cholic acid; Bil: Bilirubin. *P<0.05 versus negative control; $P<0.05 versus high concentration

The effect of cell hypoxia on activated hHSC migration

Conditioned serum-free media from various cell type exposed to hypoxic culture conditions were tested for the presence of potential chemotactic factors to activated hHSCs. The cell types tested included Kupffer cells, hBECs and activated and non-activated hHSCs. Conditioned media from Kupffer cells cultured in hypoxic conditions demonstrated significantly lower migration to activated hHSCs compared to negative controls. On the other hand, hHSCs migrated towards media from Kupffer cells cultured in normoxic conditions in significantly greater numbers compared to media from hypoxic cells and negative controls (Figure 2.19).

It is worth noting that Kupffer cells proved difficult to maintain in culture using standard medium. Therefore they could only be used at an early timepoint in this assay (24 hours in culture) and were not used in further experiments in this project.

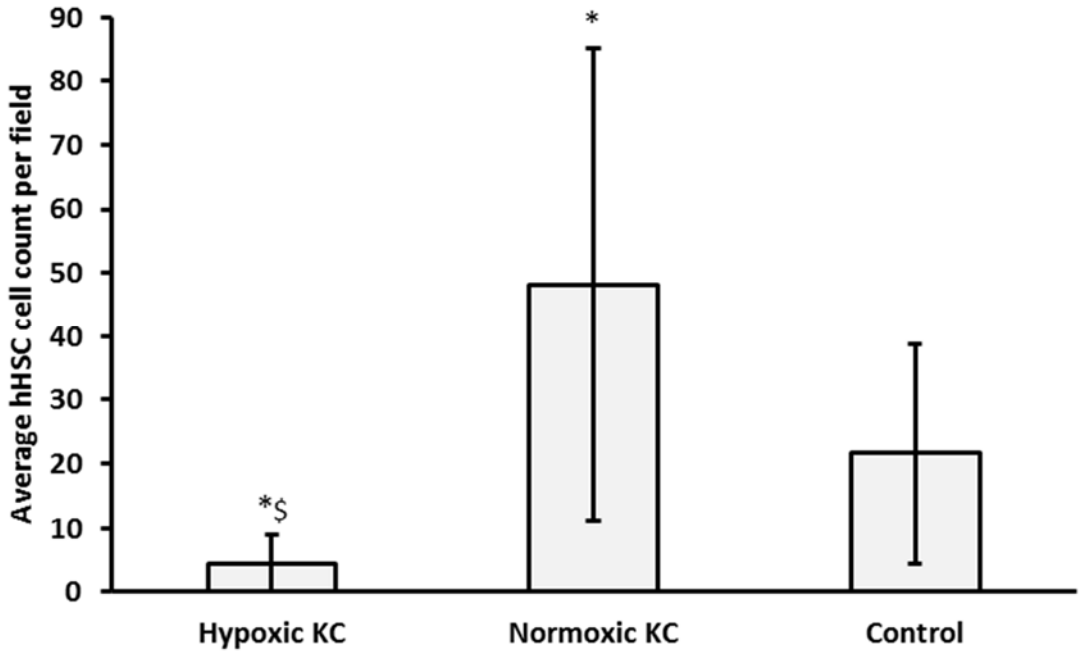

Figure 2.19 hHSC migration to media from hypoxic versus normoxic Kupffer cells. *P<0.05 versus negative control; $P<0.05 versus normoxic conditions

In comparison, conditioned media from hBECs cultured in either hypoxic or normoxic conditions resulted in hHSC migration counts significantly lower than controls. However, for each studied timepoint, hHSC migration was significantly greater to media from the hypoxic group. Moreover, regardless of oxygen condition, cell migration was significantly greater towards media from the later timepoint (Figure 2.20). Far from producing chemotactic factors to hHSCs, this data suggests that hBECs inhibit hHSC migration particularly in normoxic conditions and at earlier timepoints in culture.

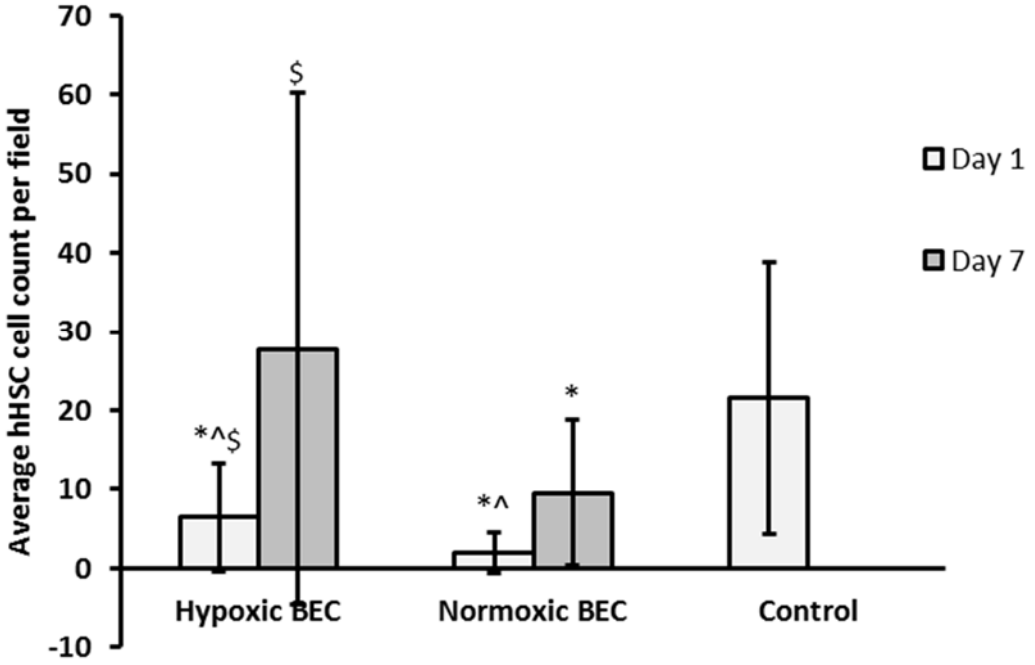

Figure 2.20 hHSC migration to media from hypoxic versus normoxic human biliary epithelial cells at 1 and 7 days in culture. Cells were used at passage 4 and seeded at 100,000 cell/ml. *P<0.05 versus negative control; ^P<0.05 versus later timepoint; $P<0.05 versus normoxic conditions

The ability of quiescent and activated hHSCs to attract activated hHSCs in hypoxic culture conditions was then investigated. Matrigel-coated culture flasks were used to delay the spontaneous hHSC activation in culture. Similar to other cells, the migration effects of quiescent and activated hHSC media on activated hHSCs was mostly

lower than that seen in negative controls. However, contrasting results were obtained with regards to the effect of hypoxia. While quiescent hHSCs produced significantly less attractive media to activated hHSCs in response to hypoxia, a similar effect was not observed when activated hHSCs were cultured in hypoxic conditions. Moreover, later timepoints produced opposite effects on quiescent versus activated hHSCs in comparable oxygen culture conditions (Figure 2.21 and Figure 2.22).

This suggests that quiescent hHSCs produce an environment that suppresses HSC migration and that this effect becomes more pronounced in hypoxic conditions. The data also suggests that the regulatory effect of hypoxia on hHSC migration is lost once these cells become activated.

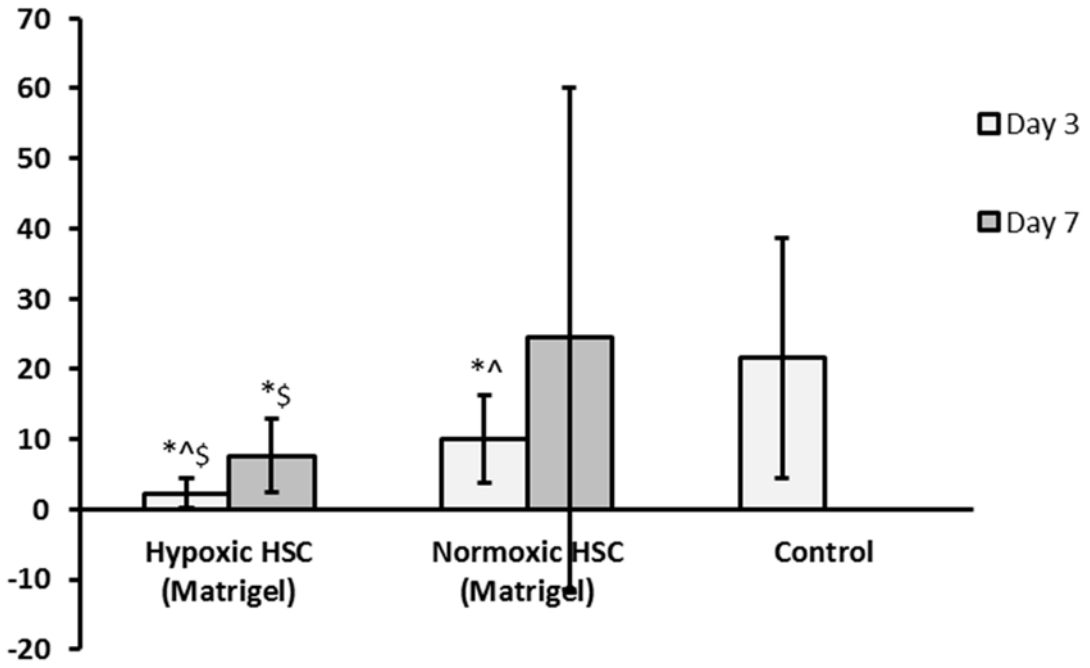

Figure 2.21 hHSC migration to media from hypoxic versus normoxic human hepatic stellate cells at 3 and 7 days in coated culture. Cells were used at passage 4 and seeded at 100,000 cell/ml. *P<0.05 versus negative control; ^P<0.05 versus later timepoint; $P<0.05 versus normoxic conditions

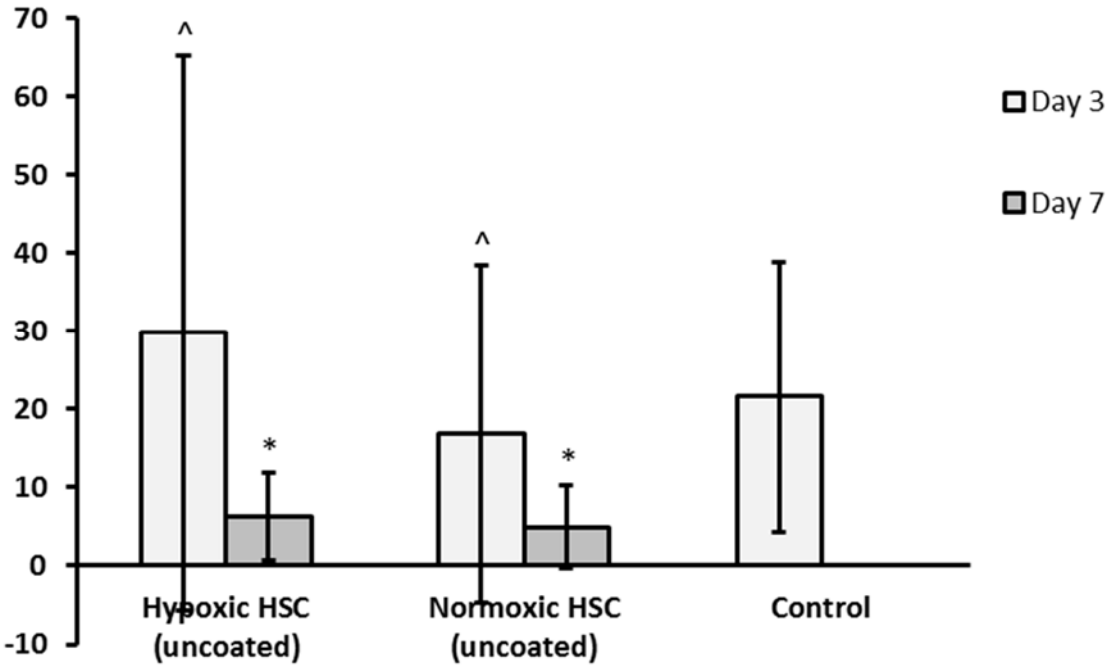

Figure 2.22 hHSC migration to media from hypoxic versus normoxic human hepatic stellate cells at 3 and 7 days in uncoated culture. Cells were used at passage 4 and seeded at 100,000 cell/ml. *P<0.05 versus negative control; ^P<0.05 versus later timepoint; $P<0.05 versus normoxic conditions

The effect of BEC re-oxygenation on activated hHSC migration

In order to simulate the effect of IRI in vitro, hBECs were cultured in hypoxic conditions for 8 hours and then in re-oxygenated conditions. The migratory effect of conditioned media from these cells on hHSCs was compared to that of hBECs kept exclusively in hypoxic or normoxic conditions. This experiment was conducted on hBECs at passage 0 in order to avoid any potential modulatory effect of cell splitting on the biliary epithelial phenotype.

As demonstrated in Figure 2.23, this assay highlighted a significant increase in activated hHSC migration towards media from hBECs that were exposed to hypoxia and subsequently to normal oxygen conditions. However, in contrast to previous results, the inhibitory effect of hBEC culture on hHSC migration in normoxic or hypoxic conditions was not seen here, nor was the improved migratory effect of hypoxia compared to normal oxygen conditions in culture (Figure 2.20).

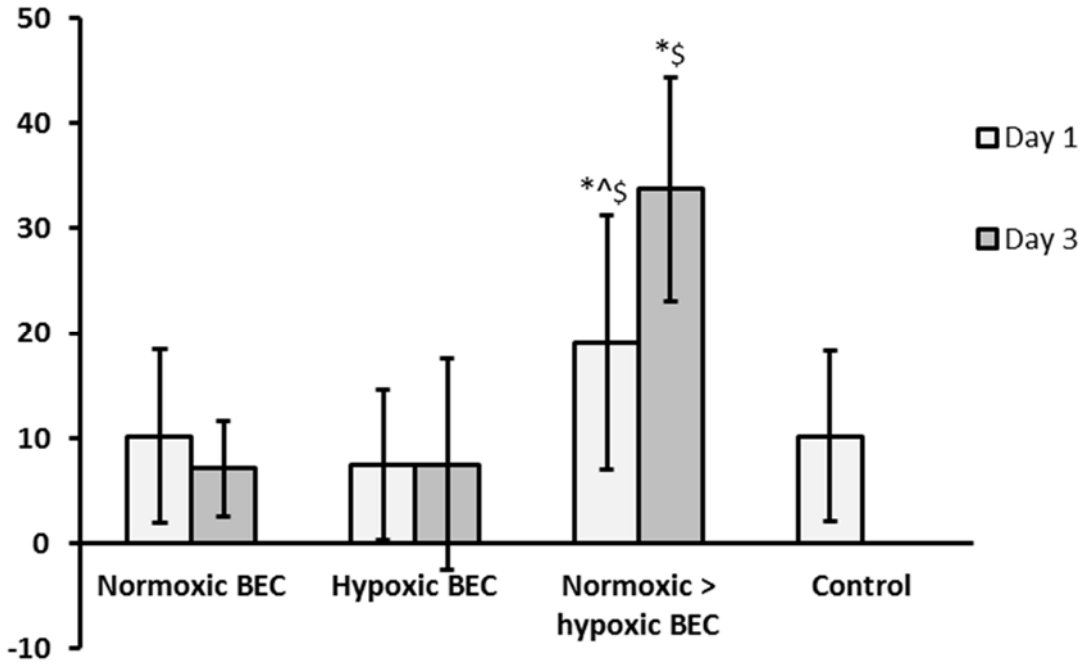

Figure 2.23 hHSC migration to media from human biliary epithelial cells (passage 0) at 1 and 3 days in culture. Hypoxic to normoxic conditions were compared to hypoxia or normoxia alone. hHSCs were used at passage 3 and seeded at 60,000 cell/ml. *P<0.05 versus negative control; ^P<0.05 versus later timepoint; $P<0.05 versus normoxia or hypoxia alone

The effect of in vivo reperfusion injury on activated hHSC migration

In order to investigate the presence of hHSC chemokines in the in vivo environment following IRI, bile samples were obtained from rats exposed to hepatic IRI at early timepoints (5 and 24 hours). These were used in hHSC migration assays in vitro and compared to bile samples obtained from control animals. For further details on the in vivo hepatic IRI model, please refer to Chapter 4.

As demonstrated in Figure 2.24, no obvious difference in hHSC migration was noted in response to bile samples obtained from rats exposed to hepatic IRI compared to control rats. However, when the average migrating hHSC cell count was correlated to the biliary concentrations of various cytokines measured as part of the in vivo hepatic IRI study, a strong correlation was identified between hHSC migration and the level of MCP-1 in bile (Table 3).

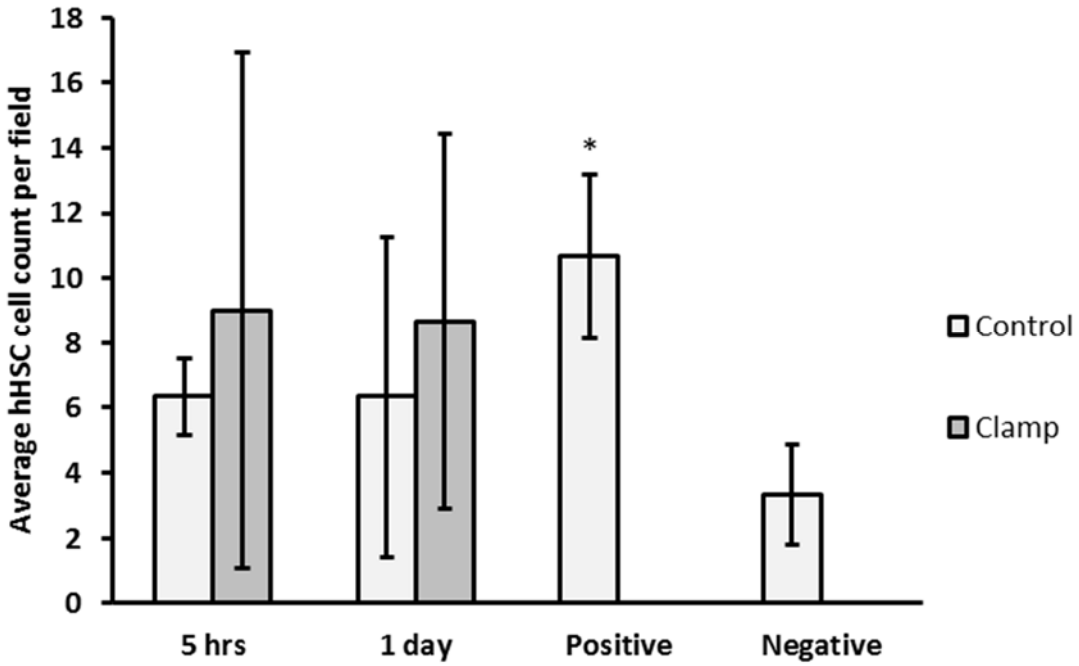

Figure 2.24 hHSC migration to bile sample obtained from rats exposed to hepatic IRI versus control rats. hHSCs were used at passage 3 and seeded at 30,000 cell/ml. *P<0.05 versus negative control

Table 3 Correlation between biliary cytokine concentrations (from rats exposed to hepatic IRI and sham surgery) and average hHSC migration in vitro

	Correlation to average hHSC cell migration	
Cytokine	**Pearson coefficient**	**P value**
IL-1b	0.264	0.408
IL-2	-0.038	0.908
IL-6	-0.203	0.527
EGF	-0.307	0.332
IL-10	-0.116	0.718
IFNγ	-0.147	0.649
MCP-1	0.706	0.01
IP-10	0.42	0.174
VEGF	0.203	0.527
MIP-2	0.284	0.37
RANTES	0.002	0.995

2.3.3. Results of cytokine quantification in conditioned cell media

Despite multiple attempts at isolating commonly known cytokine using gel electrophoresis and western blotting (including at 15% gel percentage), no cytokine was identified using the available antibodies at the manufacturers' recommended doses.

2.4. Discussion

The aim of these in vitro assays was to examine the potential role of BECs in propagating the inflammatory response to ischaemia reperfusion injury. Although a definitive answer to this enquiry may not have been reached, these studies do provide provisional evidence that the peri-biliary environment and BECs in particular can attract HSCs at degrees that vary according to oxygenation levels.

Human BECs were successfully isolated in this study. This was confirmed by the classic morphological features in addition to the strong expression of CK19 and positive staining for CFTR in the isolated cells. Other biliary epithelial proteins such as AE2, OSTα and ZO1 were not detected with immunofluorescence staining. This may be due to the untested antibodies that were used in these experiments or errors in the staining methods, although it could also reflect a loss of these proteins in the isolation process. Staining for vimentin was negative in these cells whereas α-SMA staining was faintly positive, possibly indicating early stages of mesenchymal de-differentiation, a recognised process that BECs gradually undergo in culture (Omenetti et al., 2008). This may also explain the stronger expression of cholangiocyte markers in BECs of earlier culture passages and the predominance of mesenchymal markers at later passages. Immunofluorescence staining has also highlighted the preference of using fresh primary BECs over cell lines such as H69 with regards to conformity to epithelial phenotype.

Non-parenchymal cells were isolated primarily from humans in this study in order to maintain compatibility between cells in culture. hBECs and hHSCs were isolated concurrently from retrieved specimens but same-specimen non-parenchymal cells were used in different experiments due to their distinct optimal utility times.

Activation times for hHSCs in cultures were between 5-7 days from the time of cell isolation. Coating of cell culture flasks with Matrigel™ was shown to delay hHSC activation by approximately one week further. The majority of cultured hHSCs lost their fat droplets and became α-SMA-positive once passaged. Only activated hHSCs were used for the chemotaxis assays in this study.

Among the panel of cytokines studied, PDGF was found to be the most potent chemoattractant to hHSCs in vitro. hHSCs also migrated consistently in response to MCP-1 and IFNγ at the standard concentrations tested. On the other hand, hHSC

migration towards IL-6 was lower than in negative control samples suggesting a possible inhibitory effect against myofibroblast migration, although this difference did not reach statistical significance.

The potential chemotactic effect of bile was also investigated in this study. Although bilirubin was not found to be chemoattractant to hHSCs, hHSC migration was significantly positive towards bile salts, phospholipids and cholesterol in low concentrations in vitro, reaching levels comparable to the chemotactic effect of MCP-1 and IFNγ. This result could be extrapolated to suggest a contributory role of these bile components to the inflammatory and fibrogenic response to hepatic IRI in vivo. It is important to point out however that these components were generally more effective as hHSC chemoattractant at lower doses. This may be a genuine concentration response, although it is equally possible that bile components such as bile salts may have a cytotoxic effect of on hHSCs at higher doses.

Another aspect investigated in this study was the effect of hypoxia on the expression of potential chemokines to hHSCs by various non-parenchymal cells. Generally speaking, Kupffer cells and quiescent hHSCs exposed to hypoxia produced conditioned media that was less attractive to activated hHSCs compared to media from negative controls. This data suggests suppression of activated hHSC migration by these cells during hypoxic conditions. In the case of Kupffer cells, the inhibitory effect of hypoxia on activated hHSCs contrasts with the significantly greater cell migration in normal oxygen conditions in comparison to negative control media, perhaps suggesting a role for reactive oxygen species in the induction of chemokine expression as has been previously proposed (Forman and Torres, 2002). With regards to quiescent hHSCs, suppression of cell migration was greater in hypoxic compared to normal oxygen conditions. However, the regulatory effect of hypoxia on cell migration appears to subside when hHSCs become activated. It remains unclear why activated hHSCs are attractive to other activated hHSCs in vitro regardless of oxygen levels in culture. It is conceivable that in the activated state regardless of stimulant, hHSCs produce “alarm” signals calling for reinforcement and that the pathway for chemokine expression in these cells does not involve oxygen or reactive oxygen species.

Data regarding the effect of hypoxia on hBECs in vitro was inconsistent. However, far from producing chemotactic factors to activated hHSCs in hypoxic or normal oxygen

conditions, these cells produced conditioned media that was either inhibitory or neutral to hHSC migration. Interestingly, the outcome was different when these cells were temporarily exposed to hypoxia and subsequently returned to normal oxygen conditions. Conditioned media in these cells elicited a significantly improved migratory response from activated hHSCs, suggesting a possible active role for these cells in the inflammatory response to hepatic IRI.

The migratory effect of conditioned media altered with time in culture in varying ways according to cell type. On the whole, cells that were thought to be in a non-activated state such as quiescent hHSCs and fresh hBECs became more attractive to activated hHSCs with time in culture, probably as a result of the inevitable spontaneous activation and de-differentiation of these cells in culture. On the other hand, activated hHSCs became less attractive to other activated hHSCs after longer durations in culture, suggesting the presence of negative feedback pathways to chemokine expression in activated hHSCs.

The search for potential chemokine candidates in the conditioned media that would explain the results obtained was generally unsuccessful. It is worth noting that many of the antibodies used in the immunodetection experiments were not previously tested for western blot assays and that optimal antibody dilutions were unknown for this application in many cases. Logistical and financial constraints in this project precluded in-depth testing for the presence of chemokines in vitro, yet it would be inaccurate to conclude that all of the probed chemokines was absent in culture. The application of bile samples obtained from rats exposed to IRI to the migration assays uncovered a strong correlation between hHSC migration and the level of MCP-1 in bile. Although not conclusive, this data suggests that MCP-1 is produced in the vicinity of bile ducts (probably by cholangiocytes) in response to hepatic IRI, and that this contributes to the ensuing peri-biliary inflammation and fibrosis.

One of the main limitations of this in vitro study was the evolving nature of hBECs into mesenchymal-like cells in culture. This necessitated urgency in exposing these cells to test environments even at lower cell concentrations at times, potentially affecting cell-cell signalling and chemokine production. Moreover, hBECs normally require a number of growth factors in culture media in order to maintain their epithelial phenotype for longer periods. The clear need for serum-free and growth factor-free media for migration assays posed a major challenge to hBEC

maintenance in culture particularly for later timepoints (72 hours) which required an interim period of culture in normal hBEC medium. It is possible that this may have impacted on chemokine production and resulted in incomparable early and late samples.

Overall, the results obtained from these experiments are very promising and point to an active role for hBECs and the peri-biliary environment in attracting collagen-producing cells. The in vitro nature of this study required testing of a narrow range of variables. As a result, these experiments pose further questions about the contribution of bile components and of biliary epithelial cells to hepatic IRI and open the door for a wider range of variables to be explored in future studies in order to clarify the pro-inflammatory role for biliary epithelial cells and bile components in vivo.

Chapter 3. In vivo rat hepatic ischaemia-reperfusion injury models: A literature review

3.1. Introduction

Hepatic IRI has been the focus of numerous experimental studies over the years (Spiegel and Bahde, 2006). In vitro studies based on isolated primary liver cells or related cell lines can be useful in investigating the cellular response to hypoxia and re-oxygenation in isolation of other factors and are, broadly speaking, simpler, safer and less expensive to conduct in comparison to in vivo studies (Vignais et al., 2010). However, the isolated nature of such models can limit the extrapolability and relevance of results to the more complex in vivo environment (LeCluyse et al., 2012). An in vitro cellular model to investigate the effect of hypoxia and re-oxygenation on primary liver cells as part of this project is outlined in Chapter 2.

Liver perfusion systems are an alternative method to study hepatic IRI. First described by Claude Bernard in the mid-19th century investigating glycogen metabolism in the liver (Bernard, 1855), the technique has since been modified and improved and is now commonly used investigate liver pathophysiology and drug metabolism (Borchardt et al., 1996). The main variations of the technique are in-situ versus ex-vivo perfusion. The choice of technique depends on the need to preserve or eliminate external physiological influences (Spiegel and Bahde, 2006). However, the substitution of blood with perfusion solution and the lack of interaction with blood components and other external physiological influences render the liver perfusion model less than ideal for studying the pathophysiology of warm ischaemia reperfusion injury, but more useful in investigating organ preservation and perfusate analysis (Bessems et al., 2006, Spiegel and Bahde, 2006).

Various in vivo animal models involving the temporary occlusion of blood flow into the liver have been designed in order to study warm hepatic IRI within a live mammalian system. These models overcome the limitations associated with liver perfusion or in vitro models. Although extrapolation of results from in vivo studies to humans is possible, interspecies variation in liver anatomy, metabolism and hepatic tolerance to ischaemia in addition to variations between and within in vivo models are factors that should be considered in the design of an in vivo model and interpretation of its results (Mendes-Braz et al., 2012).

3.1.1. The ideal species

Various animals have been utilised in in vivo experiments of warm hepatic IRI including pigs, dogs, cats, rabbits, rats and mice. The frequency of published use of each species in hepatic IRI studies is illustrated in Figure 3.1. This shows that rats are the most commonly used species for these studies.

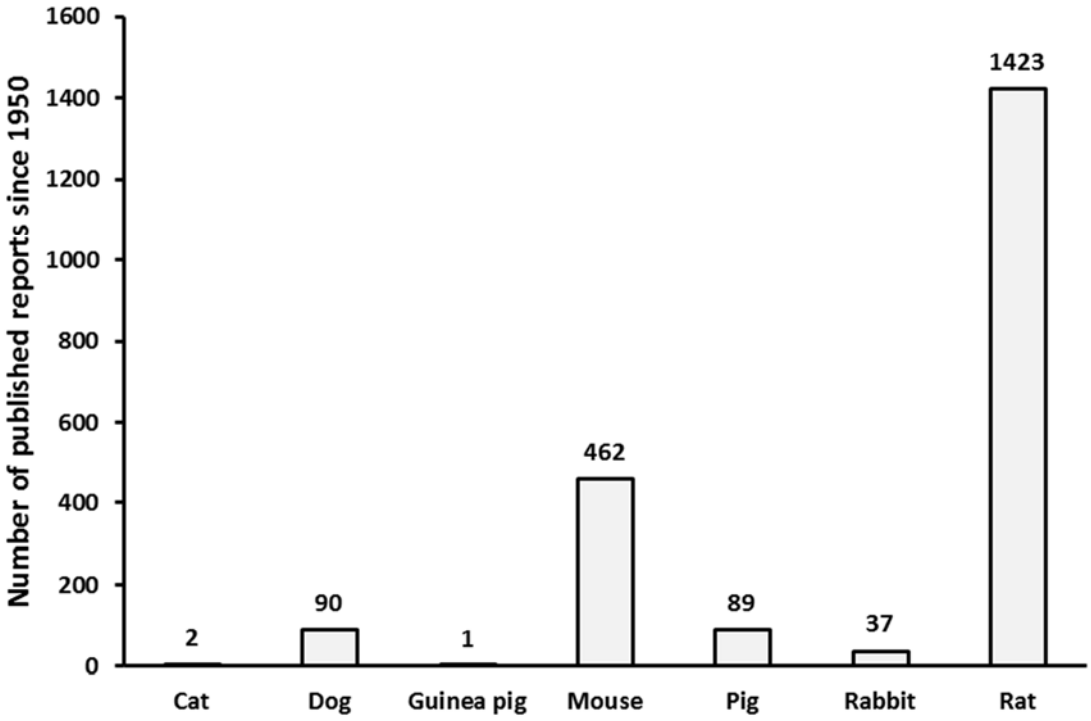

Figure 3.1 The frequency of published research on hepatic IRI studies since 1950 according to mammalian species (results are based on PubMed search conducted in May 2016)

The choice of species for an in vivo hepatic IRI model is influenced by a number of factors including animal size, hepatobiliary anatomy and physiology, technical feasibility, need for genetic modifications, sample size, ethical constraints and cost.

Based on size, animals are classed as either large or small. Large animals include pigs and dogs. Generally speaking, the liver anatomy and metabolism in these animals shows greater resemblance to that of humans, and therefore, can result in data of relatively greater clinical relevance (Abdo et al., 2003). On the other hand, the use of these animals is limited by logistical, financial and ethical constraints. In comparison, smaller animals, such as rats and mice, exhibit distinct differences to

human liver anatomy and more accelerated liver metabolism which can potentially limit data extrapolation to humans. Procedures performed in smaller animals are more likely to be technically demanding which may prove challenging to less experienced investigators. Nevertheless, smaller animals are generally easier to handle in the laboratory setting and present significantly less logistical and financial constraints. Genetically modified strains are most commonly applicable to small animals (Mendes-Braz et al., 2012).

Figure 3.2 displays a time-trend of animal choice in published in vivo hepatic IRI studies. It demonstrates that the utilisation of small animals has increased in the past decade compared to large animals. In particular, the proportion of mice studied has increased the most, although studies of rats remain the highest over the past decade in terms of absolute numbers.

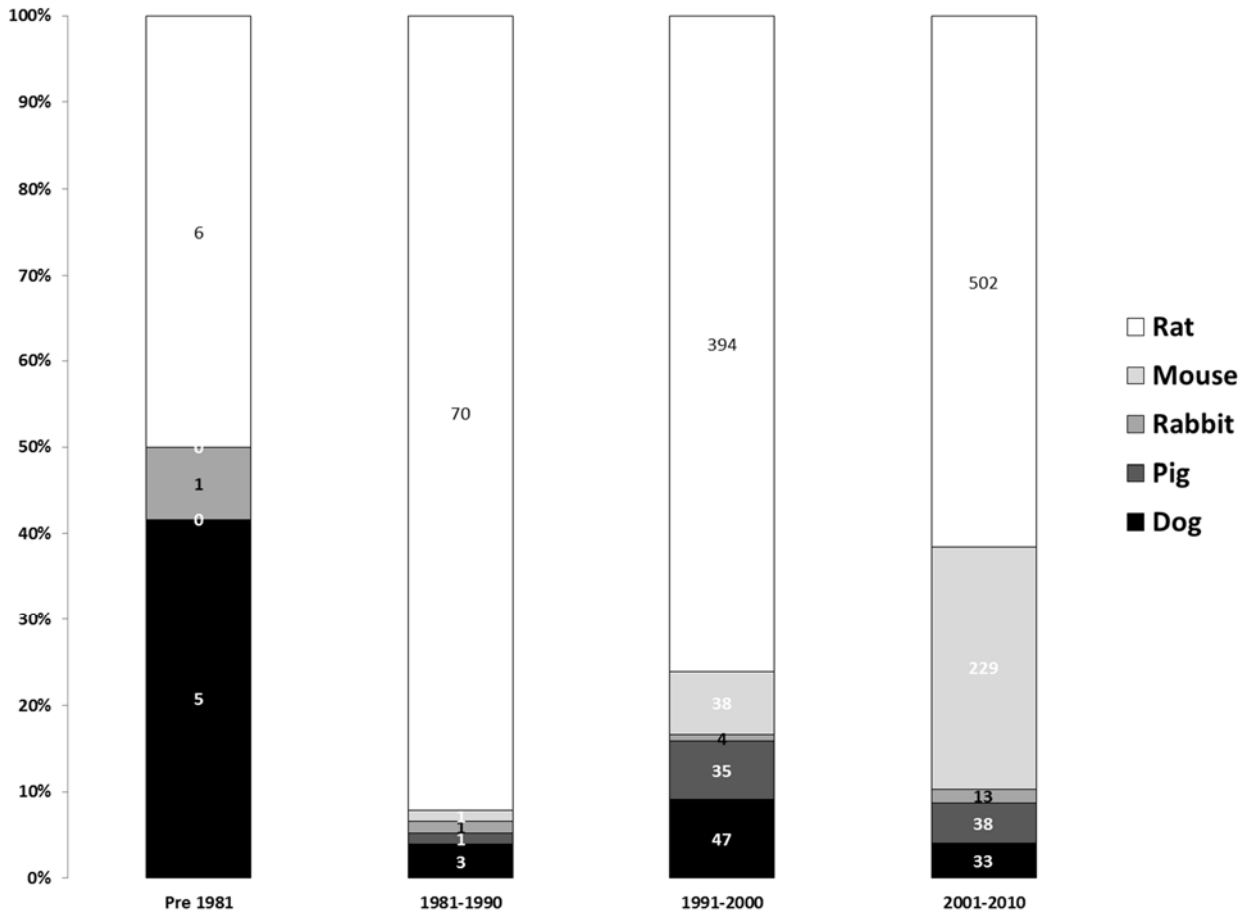

Figure 3.2 Time-trend of animal choice in published in vivo hepatic IRI studies. (results are based on PubMed search conducted in May 2016)

Based on their relative ease of handling, availability and low running costs, rats were selected as the animal of choice for the in vivo hepatic IRI model in this project (Chapter 4).

3.1.2. Anatomy of the rat liver

As is the case in human liver anatomy, the hepatobiliary system in rats exhibits significant anatomical variations. The need to understand the surgical anatomy of the rat liver and its variations is crucial when attempting to design and standardise a live model of hepatic IRI in order to maximise procedure efficiency, prevent complications and minimise skewed results (Martins and Neuhaus, 2007).

General and surface anatomy

The adult rat liver mass is roughly 5% of the total body weight whereas the human liver is proportionately smaller (2.5% of total body weight). In an average-sized rat (250-300g), the mean liver weight is about 13.6g (Vdoviakova et al., 2016, Martins and Neuhaus, 2007).

The rat liver has a superior (diaphragmatic) convex surface and an inferior (visceral) concave surface. The superior surface is covered by peritoneum and is attached to the diaphragm, xiphoid process and supraumbilical anterior abdominal wall (slightly to the right of the midline) via the falciform ligament which forms an interlobular fissure that divides the median lobe of the rat liver into a larger right and smaller left portion by a 2:1 ratio (Madrahimov et al., 2006) (Figure 3.3). Generally speaking, the falciform ligament divides the whole rat liver into two parts, right and left. However, in contrast to humans, the right and left parts of the rat liver are roughly of equal size (Martins and Neuhaus, 2007).

The inferior surface of the rat liver is in relation to the stomach, duodenum, hepatic flexure of the colon, pancreas, right kidney and right adrenal gland. The transverse fissure of the liver (porta hepatis) lies on the inferior surface and is the point of access of portal vein, hepatic artery, bile duct, nerves and lymphatics to the liver (Martins and Neuhaus, 2007, Vdoviakova et al., 2016) (Figure 3.4).

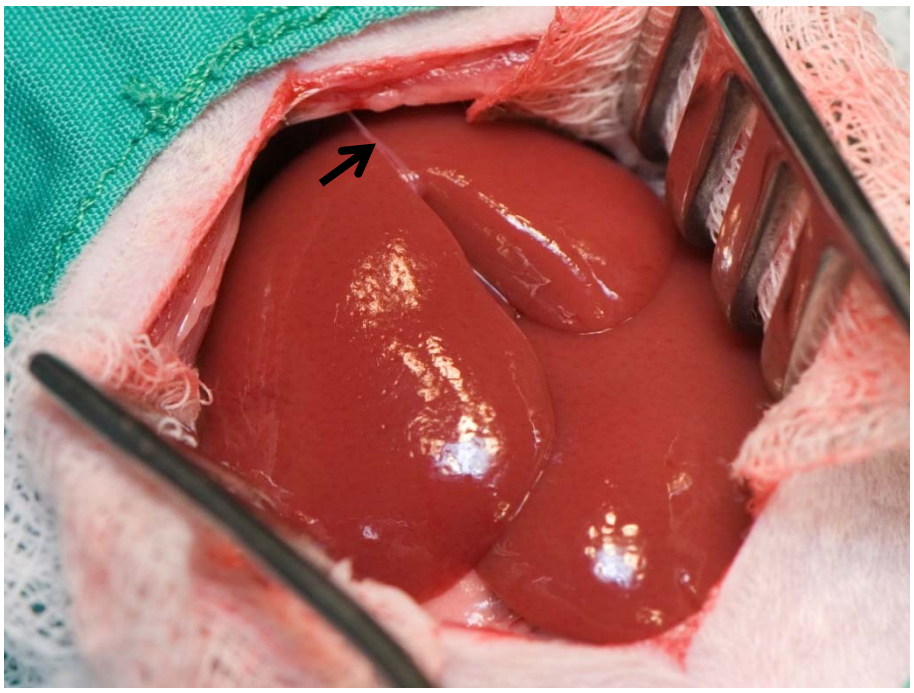

Figure 3.3 The falciform ligament (arrow) divides the median lobe of rat liver into right and left portions

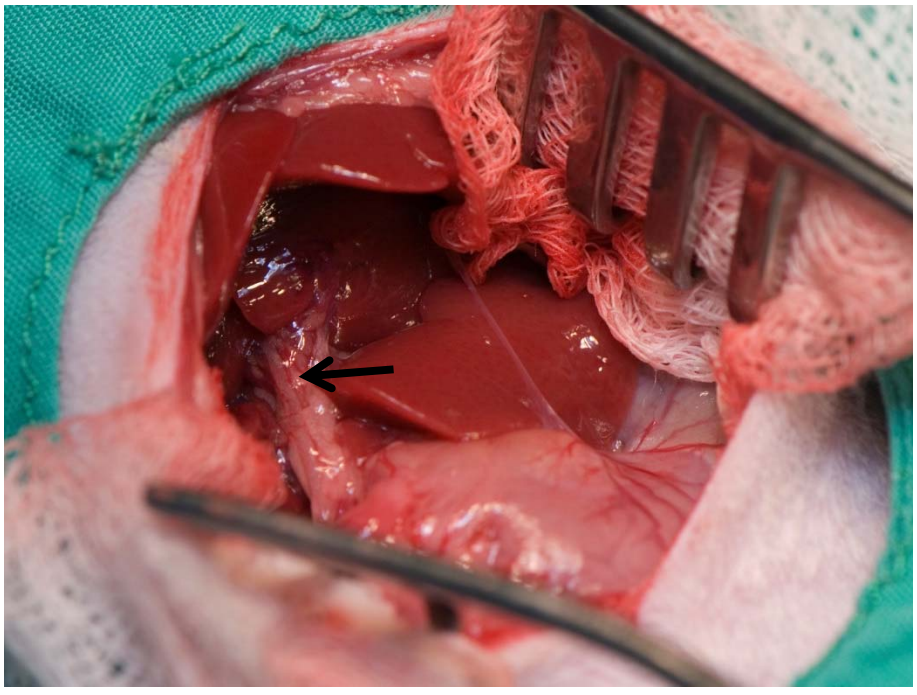

Figure 3.4 Passage of vascular and biliary structures via the transverse hepatic fissure (porta hepatis) (arrow). The hepatogastric ligament can also be seen on the left.

In addition to the falciform ligament, the rat liver communicates with the parietal surface of the abdominal wall and to visceral structures through a number of other ligaments. The round ligament (ligamentum teres hepatis) lies at the free edge of the falciform ligament extending between the umbilicus and the vertical fissure of the median lobe and represents the obliterated embryonic umbilical vein. Similar to humans, the coronal ligament surrounds a bare area of liver dorsally and extends laterally into right and left triangular ligaments which connect the diaphragm to the right and left hepatic lobes respectively. The hepatogastric and hepatoduodenal ligament join the inferior surface to the lesser curvature of the stomach and to the duodenum respectively (Vdoviakova et al., 2016, Martins and Neuhaus, 2007, Kogure et al., 1999).

Lobes of the rat liver

The rat liver is multilobulated in a manner similar to other mammals (Martins and Neuhaus, 2007). It is divided into four lobes: the median, left lateral, right and caudate lobe in descending order of size (Figure 3.5). The rat liver lobes are roughly comparable to segments of the human liver. However, in contrast to human liver segments, rat liver lobes are grossly well defined with deep fissures separating neighbouring lobes (Kogure et al., 1999, Shi et al., 2015). The median lobe comprises about 38% of the rat liver mass. As mentioned above, the falciform ligament connects the diaphragm and anterior abdominal wall to this lobe in line with the vertical (umbilical) fissure dividing the median lobe into a larger right median and smaller left median portion (Madrahimov et al., 2006). The median lobe is dorsally in continuity with the left lateral lobe which comprises roughly 30% of the total liver mass. The left lateral lobe covers most of the anterior surface of the stomach and is itself covered ventromedially by the left portion of the median lobe. The right lobe comprises around 22% of rat liver mass and is almost completely covered ventrally by the right portion of the median lobe. The right lobe is divided by a horizontal fissure into a (slightly larger) superior and an inferior portion. The caudate lobe is situated ventrally and to the left of the IVC and posterior to the stomach. It comprises around 8-10% of the total liver mass and is divided into two distinct portions: the paracaval portion, also known as the caudate process, surrounds a segment of IVC and communicates with the second portion known as the Spiegel lobe. The Spiegel

lobe is itself divided into two leaf-like portions: anterior and posterior, of roughly equal size (Martins and Neuhaus, 2007). The paracaval portion of the caudate lobe bridges the two portions of the Spiegel lobe to the right lobe and for that reason is considered not to be a distinct anatomic unit by some authors (Martins and Neuhaus, 2007, Madrahimov, 2006) (Figure 3.6)

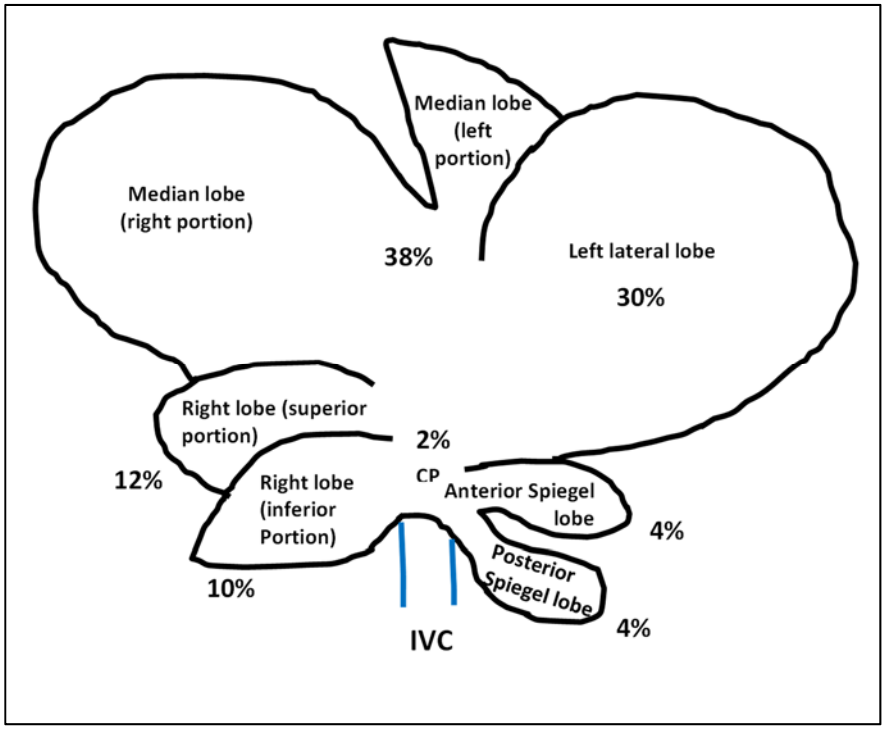

Figure 3.5 Anatomy and relative mass of rat liver lobes. Modified from Martins and Neuhaus 2007 (Martins and Neuhaus 2007)

The right hemi-liver in the rat is comprised of the right lobe and right portion of the median lobe, while the left portion of the median lobe, the left lateral lobe and the caudate lobes form the left hemi-liver. As mentioned above, the right and left hemi-livers are of comparable volumes in the rat (Martins and Neuhaus, 2007).

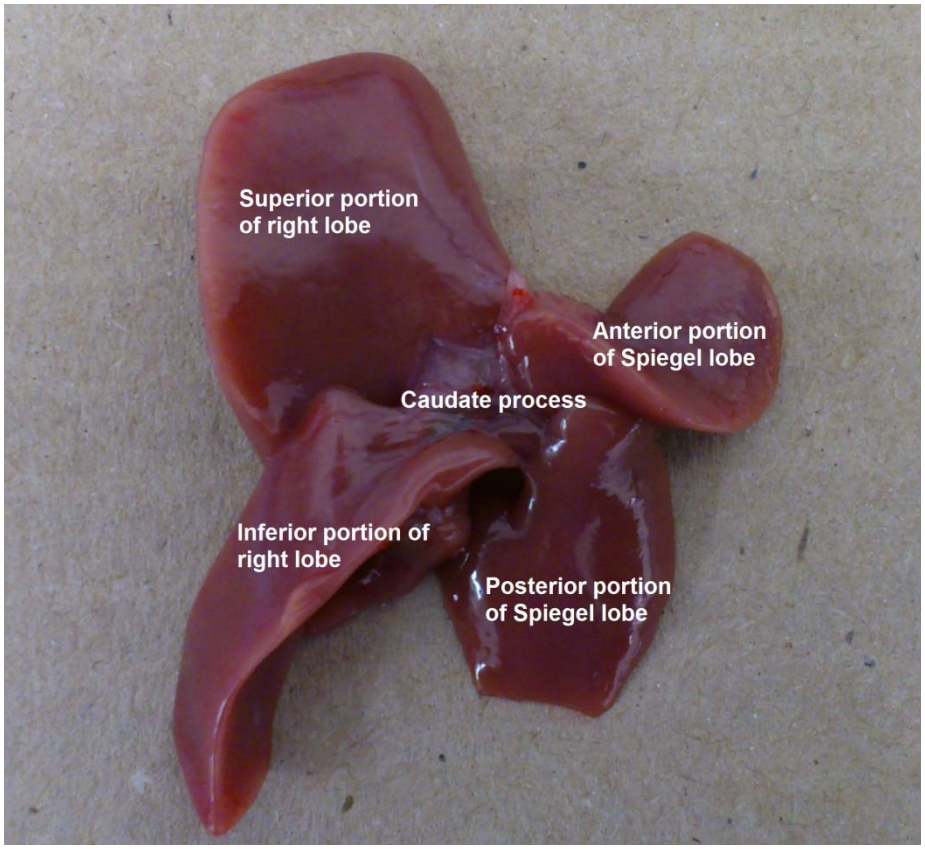

Figure 3.6 Right lobe (superior and inferior) joined to Spiegel lobe (anterior and posterior) through caudate process

Vascular and biliary anatomy

Portal vein

The portal venous system of the rat liver is the most constant anatomic reference, as is the case in mammals, and its branches closely follow the hepatic lobes described in the previous section (Martins and Neuhaus, 2007). The portal vein is formed by the convergence of the superior mesenteric vein, gastrosplenic vein and gastroduodenal vein (Gregerson et al., 1996). At the porta hepatis, the main portal vein first gives branches to right (right portal vein) then caudate lobes (caudate portal vein) followed by the median and finally the left lateral lobe (Martins and Neuhaus, 2007).

The right portal branch divides shortly after its origin into one superior and one (or more) inferior branches. The superior branch frequently supplies both the superior and inferior portions of the right lobe ((Sanger et al., 2015).

The portal branch to the caudate lobe is short and immediately divides into two branches, supplying the anterior and posterior Spiegel lobes. The paracaval caudate is supplied by branches from the right superior and the caudate portal vein (Sanger et al., 2015, Martins and Neuhaus, 2007).

The portal vein then gives off two main branches: the right median and the left portal veins. The right median portal vein supplies the right median lobe while the left portal vein supplies the left median and left lateral lobes. Consequently, the median lobe receives two portal branches whereas each other lobe receives only one branch (Sanger et al., 2015). It is important to note that the division of the left portal vein can either occur proximally in the porta hepatis or deep within the left lateral lobe parenchyma. Therefore, clamping of the pedicle to the left lateral lobe or excision of this lobe may result in inadvertent ischaemia to the left portion of the median lobe (Sanger et al., 2015). Figure 3.4 illustrates the anatomy of the portal vein and its branches in the rat.

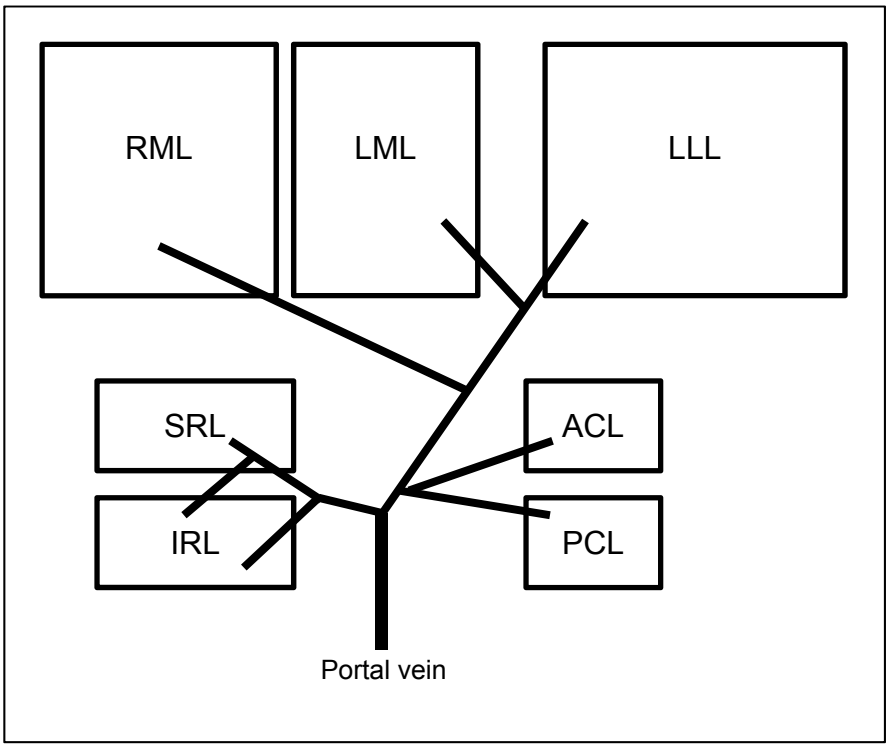

Figure 3.7 Portal venous anatomy in the rat. RML: Right median lobe; LML: Left median lobe; LLL: Left lateral lobe; SRL: Superior right lobe; IRL: Inferior right lobe; ACL: Anterior caudate lobe; PCL: Posterior caudate lobe. Paracaval caudate tissue is omitted for simplification

Hepatic artery

The arterial supply of the liver is supplied by the coeliac trunk. Branches from the coeliac trunk are similar to those in human but run a slightly different course. Hepatic artery branches generally follow the course and pattern of the corresponding portal venous branches lying ventral to the veins ((Madrahimov et al., 2006)). Martins and Neuhaus also describe an accessory left hepatic artery arising from the left gastric artery and supplying the dorsomedial aspect of the left lateral lobe (Martins and Neuhaus, 2007).

Hepatic veins

Examination of the hepatic veins in the rat has helped explain some of the variations in hepatic vein anatomy in humans (Kogure et al., 1999). In contrast to humans, the hepatic parenchyma completely surrounds a segment of IVC (Martins and Neuhaus, 2007). The superior and inferior right lobes drain into the IVC via one (or less commonly two) separate hepatic veins. These correspond to the right hepatic vein and the frequently observed inferior right hepatic vein variant respectively (Martins and Neuhaus, 2007, Kogure et al., 1999, Sanger et al., 2015).

The median lobe drains via two or (more commonly) three veins: the right, middle and left median hepatic veins. The vein draining the left middle lobe (left median vein) may join the IVC separately or, more commonly join the vein draining the left lateral lobe (left hepatic vein) and the middle median vein forming a common trunk prior to entering the IVC. A similar anatomical variation is noted in humans where the middle and left hepatic veins occasionally join and enter the IVC as a common trunk rather than separately (Sanger et al., 2015, Martins and Neuhaus, 2007, Kogure et al., 1999).

The caudate lobe is drained by two veins (anterior and posterior) that can either enter the IVC separately or form a common trunk prior to joining the IVC. The paracaval caudate tissue drains directly into the IVC via multiple small branches (Martins and Neuhaus, 2007, Madrahimov et al., 2006, Sanger et al., 2015). Venous drainage of the rat liver is illustrated in Figure 3.8

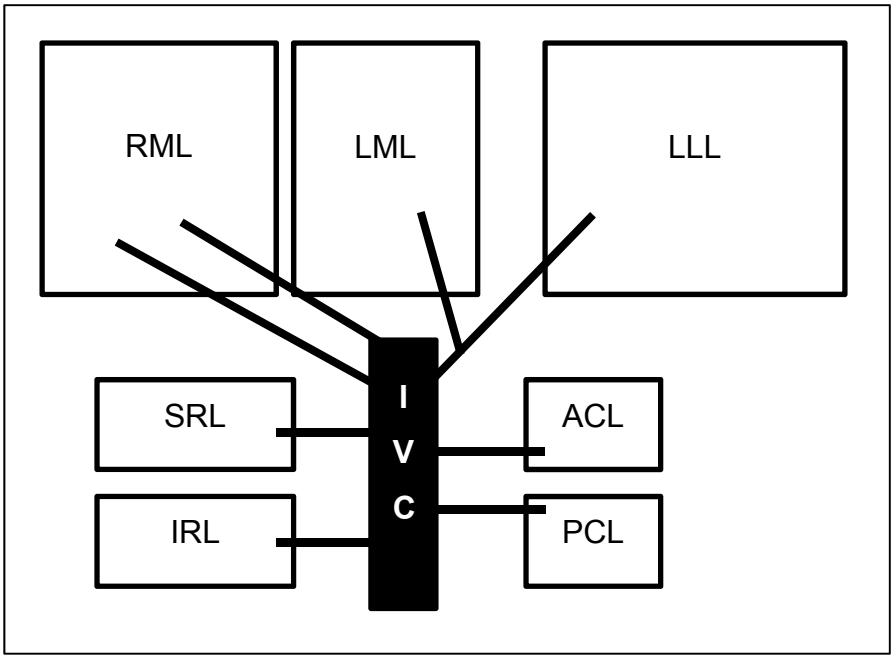

Figure 3.8 Hepatic venous anatomy in the rat. RML: Right median lobe; LML: Left median lobe; LLL: Left lateral lobe; SRL: Superior right lobe; IRL: Inferior right lobe; ACL: Anterior caudate lobe; PCL: Posterior caudate lobe; IVC: Inferior vena cava. Paracaval caudate tissue is omitted for simplification

Biliary tree

Similar to horse and deer, and in contrast to human and mouse liver, the rat liver is devoid of a gallbladder (McMaster, 1922). Biliary branches in the rat liver can vary widely. While most (sub) lobes of the rat liver are drained via one first order biliary ductal branch, the left lateral and median lobes usually drain via two and four first order biliary branches respectively. Branches from the left lateral and left median lobes may converge (Aller and Arias, 2009, Martins and Neuhaus, 2007). Extrahepatic biliary ducts in the rat lie ventral to the portal and arterial vessels. Convergence of the most distal first order biliary branch at the level of the caudate process corresponds to the origin of the common bile duct (CBD). This can either be the right lobe duct (40%), the caudate lobe duct (22.5%) or both simultaneously (37.5%). The common bile duct runs ventral and to the right of the portal vein and then runs within the pancreatic parenchyma before emptying into the duodenum (Aller and Arias, 2009) (Figure 3.9).

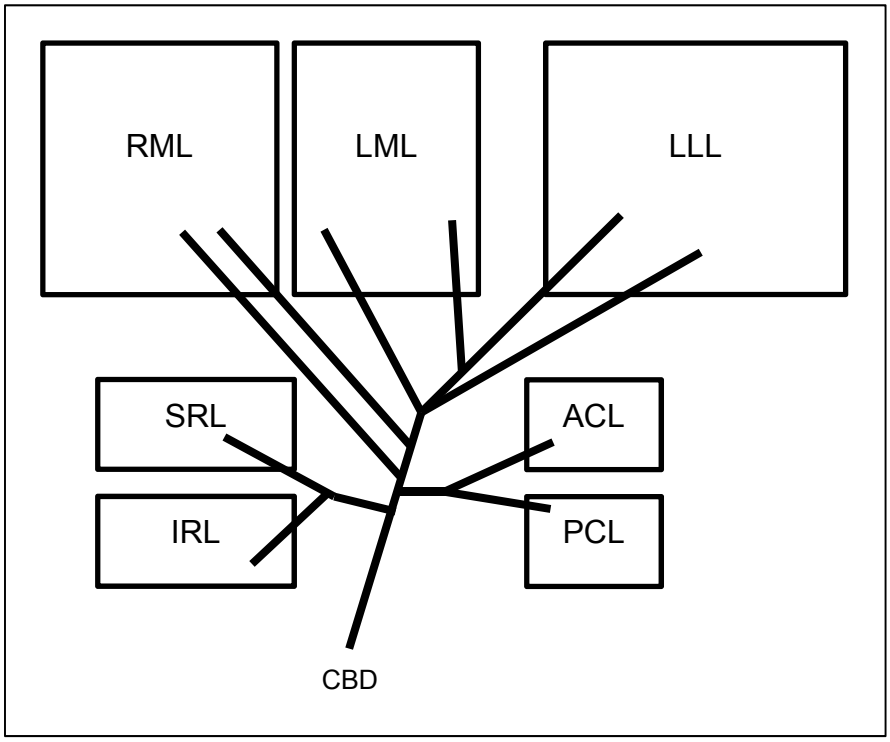

Figure 3.9 Biliary tree anatomy in the rat. RML: Right median lobe; LML: Left median lobe; LLL: Left lateral lobe; SRL: Superior right lobe; IRL: Inferior right lobe; ACL: Anterior caudate lobe; PCL: Posterior caudate lobe; CBD: Common bile duct. Paracaval caudate tissue is omitted for simplification

3.1.3. In vivo rat models of hepatic IRI

Various models of normothermic ischaemia reperfusion injury in the rat liver have been described in the literature. These models vary in procedure severity, technical complexity and degree of injury produced (Expert working group on severity classification of scientific procedures, 2009). An overview of commonly described models is outlined below.

Total inflow occlusion

In total inflow occlusion models, arterial and portal inflow to the rat liver is temporarily interrupted via occlusion of the portal vein and hepatic artery within the hepatoduodenal ligament (porta hepatis) (Figure 3.4). The equivalent technique in clinical surgery is known as the Pringle manoeuvre, first described by James Hogarth

Pringle in 1908 (Pringle, 1908). The porta hepatis also includes the common bile duct which can either be isolated or occluded en-masse with the hepatic inflow vessels. The main limitation of inflow occlusion models is the consequential splanchnic venous congestion resulting from occlusion of the portal vein which can result in intestinal ischaemia, sepsis and remote organ damage due to venous stasis and bacterial translocation (Suzuki et al., 1998, Liu et al., 1992, Liu et al., 1996). The rat liver can only tolerate up to 30 minutes of continuous portal vein clamping (van der Meer et al., 1971). In comparison, the human liver can safely tolerate relatively longer periods of portal venous clamping, due to the existence of a well-developed portosystemic collateral network (Suzuki et al., 1998, Huguet et al., 1992). Therefore, if longer periods of ischaemia are required, total inflow occlusion models are frequently coupled with a procedure that provides portosystemic shunting. A tube portosystemic shunt can be inserted at the time of surgery prior to clamping and usually communicates between a portal venous branch and the IVC or femoral or jugular vein (Spiegel and Bahde, 2006). Alternatively, a direct anastomosis can be created between the IVC and the portal or splenic vein prior to ischaemia. Such shunts are subsequently ligated prior to reperfusion (Kaminski et al., 1997). Single-stage shunt formation procedures are technically challenging and are associated with risks including bleeding and thrombosis. An alternative is a two-stage procedure which results in gradual portosystemic shunt formation. The initial step involves transposition of the spleen into a subcutaneous pouch through a small left upper abdominal incision. The wound is then closed and the rat allowed to recover. After a period of 2-3 weeks, adequate portosystemic anastomoses will have formed. Total inflow occlusion can then be performed as a second stage procedure without the risk of splanchnic congestion (Spiegel and Bahde, 2006). Interestingly, caecal herniation has been reported as an alternative procedure to splenic transposition that may also allow gradual portosystemic shunting (Rhee et al., 2002). The two-stage portosystemic shunt models do not involve microvascular techniques and are thus safer and less technically demanding. However, the consistency of the degree of collateral flow formation and the effect of long-term changes to hepatic inflow on the development of liver IRI remain unknown (Suzuki et al., 1998) and therefore, results arising from these models should be interpreted with caution.

Selective (partial) inflow occlusion

In contrast to total inflow occlusion models, selective (also known as segmental) inflow occlusion involves the temporary interruption of portal venous and hepatic arterial flow to part of the rat liver by occluding the pedicle supplying that part. As demonstrated in Figure 3.10, selective inflow occlusion models can range from 10-90% partial ischaemia models.

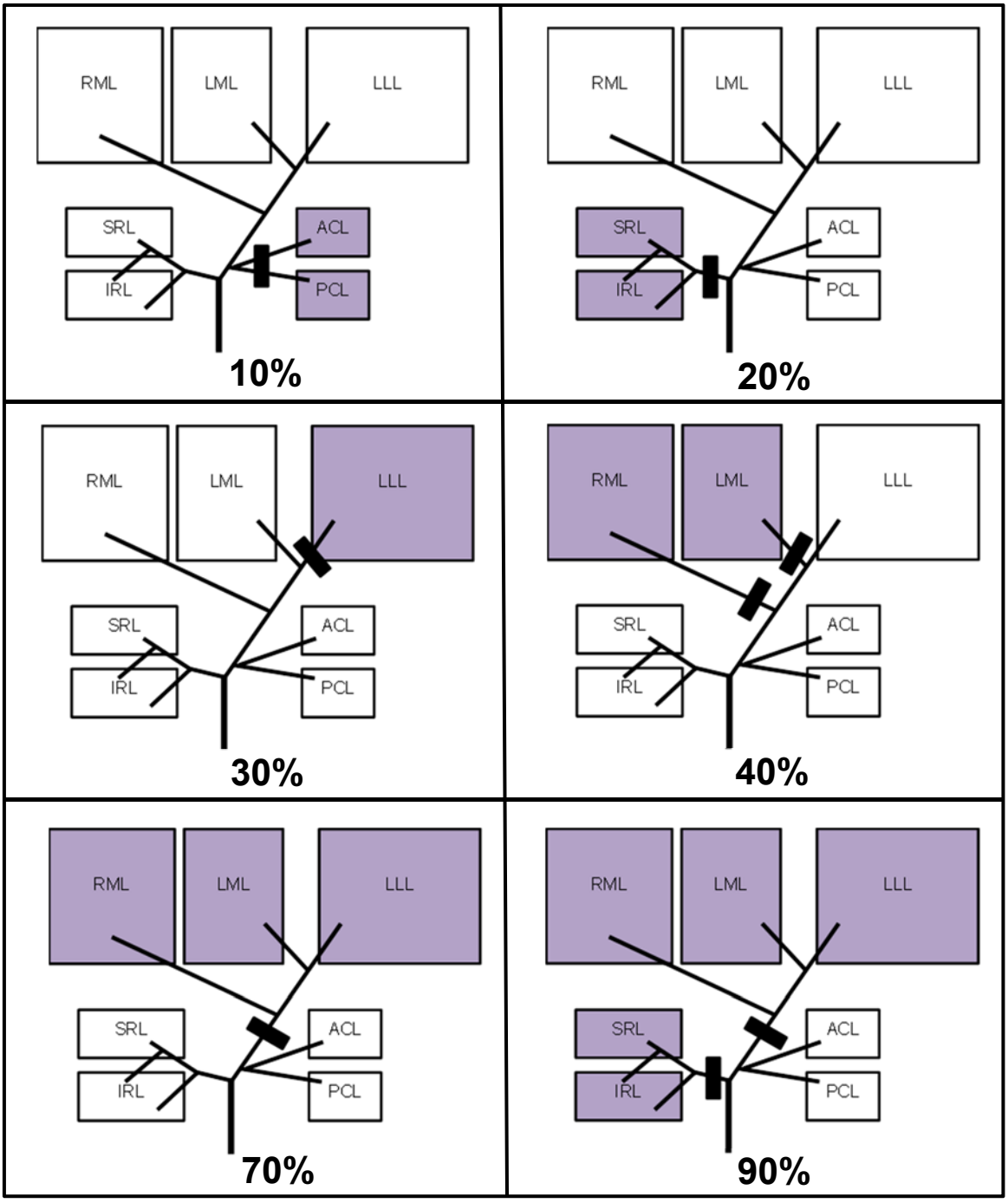

Figure 3.10 Selective inflow occlusion models. Flow represents portal venous and hepatic arterial inflow combined. Black rectangles represent level of occlusion.

Ischaemic lobes represented in purple. RML: Right median lobe; LML: Left median lobe; LLL: Left lateral lobe; SRL: Superior right lobe; IRL: Inferior right lobe; ACL: Anterior caudate lobe; PCL: Posterior caudate lobe. Paracaval caudate tissue is omitted for simplification

Portal venous blood flow is diverted to the non-occluded liver and hence portal stasis and splanchnic congestion is avoided in these models (Karatzas et al., 2014). An additional advantage is the potential to use the remaining non-ischaemic liver as internal control tissue. However, it has been shown that blood flow diverts preferentially into non-ischaemic tissue upon reperfusion in these models (Hayashi et al., 1986). Further effects of the residual non-ischaemic liver tissue on the development of hepatic injury are possible but remain unclear. Therefore, partial inflow occlusion procedures are not uncommonly combined with ligation or resection of the non-ischaemic liver tissue upon reperfusion (Spiegel and Bahde, 2006). Whereas ligation without resection leaves necrotic liver tissue in situ which likely influences the results and inevitably leads to sepsis, resection circumvents that risk and allows for longer follow up durations. Nevertheless, the addition of a resection procedure carries an increased risk of bleeding, liver failure and mortality compared to hepatic IRI alone (Spiegel and Bahde, 2006, Madrahimov, 2006)

Total vascular exclusion

In addition to the temporary interruption of inflow to the rat liver, hepatic venous outflow is also occluded in total vascular exclusion models. Clamps are either applied to the supra/infra hepatic IVC (Kaya et al., 2008) or to individual hepatic veins (Topaloglu et al., 2005). In clinical surgery, this technique is occasionally necessary in order to control excessive bleeding from the liver (Zografos et al., 1999). However, the technique leads to more severe oxidative stress in comparison to inflow occlusion alone (Darilmaz et al., 2005, Sato et al., 1998) and can results in significant haemodynamic instability due to venous pooling in the lower body (Kaya et al., 2008). Therefore some authors have suggested the concomitant application of supracoeliac arterial clamping to mitigate the effect of venous congestion (Stephen et al., 1996, Kaya et al., 2008) although this would lead to lower body ischaemia and carries a paradoxical risk of haemodynamic instability upon reperfusion (Kaya et al.,

2008). Regardless of technique, total vascular exclusion models are more technically challenging and carry greater risks of complications compared to inflow occlusion models.

Isolated portal vein or hepatic artery occlusion

Isolation and temporarily occlusion of either the hepatic artery or the portal vein alone is a recognised technique to investigate normothermic hepatic IRI and can involve either the main vessel or a branch supplying a particular part of the rat liver resulting in global or partial ischaemia respectively. These models result in incomplete ischaemia since blood supply the liver is maintained through the unclamped inflow vessel. Hepatic artery isolation and temporary dearterialisation requires microsurgical expertise and has been employed in experiments that investigate intrahepatic malignancy (Wang et al., 1995) and as an alternative technique to avoid interruption of portal venous flow (Tralhao et al., 2013). Portal vein occlusion is a relatively less technically challenging procedure and is occasionally employed to avoid the severe metabolic injury associated with complete ischaemia models (Matsui and Kojima, 1991). Occlusion of the portal vein results in less biliary damage compared to hepatic artery occlusion (Mancinelli et al., 2015). However, splanchnic congestion remains a limiting factor with this model if flow in the main portal vein is interrupted.

3.1.4. Aim of review

A literature review of all published research on hepatic ischaemia reperfusion injury models in the rat was performed with the following aims:

1. To examine major characteristics related to subject, technique and outcome in the various reported models of hepatic IRI in the rat
2. To identify trends in model adoption and alterations in technique over time
3. To identify risks associated with animal mortality in these models
4. To identify the ideal in vivo hepatic IRI model to address the research aims of this project

3.2. Methods

3.2.1. Study design

A literature review of reported in vivo hepatic ischaemia reperfusion injury studies in rats published in the English language with no restriction on publication date or type of publication.

3.2.2. Inclusion criteria

Table 4 summarises the inclusion criteria of this study.

Table 4 List of inclusion criteria for review

	Criterion	**Comment**
Report criteria	English language publications	
	Adequate description of model	IRI model type reported or referenced
	Original report	Duplicate reports identified and merged
Model criteria	In vivo models	Excludes in-situ reperfusion and ex-vivo isolated perfused rat liver models
	Non-transplant models	To avoid the confounding immunopathological effect of allograft transplantation
	Complete interruption of flow	Excludes low flow models including sepsis, haemorrhage and pneumoperitoneum
	Ten minutes or more of continuous interruption of flow	Excludes studies related to preconditioning alone
	Normothermic reperfusion with blood	Excludes hypothermic reperfusion and reperfusion with blood substitutes or other perfusion solutions
	Ischaemic residual liver	Partial hepatectomy models are included only if the remaining liver is

		exposed to IRI

3.2.3. Search strategy

A comprehensive search was conducted on four medical bibliographic databases (PubMed, MedlinePlus, Embase and Scopus) using the following search syntax:

("rats"[MeSH Terms] OR "rats"[All Fields] OR "rat"[All Fields]) OR ("rodentia"[MeSH Terms] OR "rodentia"[All Fields] OR "rodent"[All Fields]

AND

("liver"[MeSH Terms] OR "liver"[All Fields]) OR (hepate OR hepati* OR hepato*)*

AND

Ischemi OR ischaemi* OR ((interrupt* OR ligat* OR clamp* OR occlu*) AND*

(("blood"[Subheading] OR "blood"[All Fields] OR "blood"[MeSH Terms]) OR ("vessel"[All Fields] OR "blood vessels"[MeSH Terms] OR ("blood"[All Fields] AND "vessels"[All Fields]) OR "blood vessels"[All Fields]) OR porto OR porta* OR arter* OR ("veins"[MeSH Terms] OR "veins"[All Fields] OR "vein"[All Fields]) OR veno* OR vascul*))*

AND

Pringle OR ("reperfusion"[MeSH Terms] OR "reperfusion"[All Fields]) OR unclamp OR revasc* OR releas* OR reflow**

NOT

"shock"[title] OR "sepsis"[title] OR "hemorrhage"[title] OR "haemorrhage"[title] OR "transplantation"[title] OR "allograft" OR "xenotransplantation"[title] OR "graft"[title] OR "preservation"[title] OR "cold ischemia"[title] OR "cold ischaemia"[title] OR "cold ischemic"[title] OR "cold ischaemic"[title] OR "storage"[title] OR "ex vivo"[title] OR "extracorporeal"[title] OR "orthotopic"[title] OR "intestine"[title] OR "intestinal"[title] OR

"renal"[title] OR "kidney"[title] OR “mycardial"[title] OR "myocardium"[title] OR "cardiac"[title] OR "heart"[title] OR "lung"[title] OR "pulmonary"[title]

The search was initially conducted on January the 2nd 2011 and then repeated for updates on May the 15th 2016. Data presented in this chapter is based on the updated search results.

3.2.4. Exclusion of ineligible studies

The inclusion criteria outlined in section 3.2.2 were incorporated into the search strategy (see 3.2.3) in order to filter studies ineligible for inclusion. The list of abstracts obtained from the search was skimmed in order to select studies that met the stated inclusion criteria for review. Full text reports of these selected studies were subsequently obtained (see 3.2.5) and individually examined for suitability for inclusion and any further ineligible studies identified were excluded.

3.2.5. Data extraction

Filing of references and extraction of full-text reports was performed using the bibliographic management software EndNote X4 (Thomson Reuters, London, UK). Full-text reports that could not be extracted using EndNote were either downloaded manually or obtained with library service assistance (Newcastle University and County Durham and Darlington NHS Foundation Trust Libraries). Hard copies of full-text reports were scanned and attached to the corresponding references on EndNote. In the minority of cases where a full-text report was not available, relevant data was extracted from the published abstract if the IRI model was adequately described. Studies where no full-text report or informative abstract was available were excluded from the review.

Data was extracted from individually-examined full-text reports. The variables extracted from each included study were divided into six main domains: Report outlines, animal characteristics, surgical preparation, model technique, intervention details, and outcomes. Details of the individual variables collected within each

domain are outlined in Table 5. The collected data was entered into a Microsoft Office Excel 2010 spreadsheet (Microsoft Corp., Redmond, WA).

Table 5 Details of variables collected from studies included in literature review

Domain	Variable	Details
Report outline	Publication year	YYYY
	Duplicate report	Yes/ No
	Type of publication	Full text/ abstract/ letter/ poster paper/ retracted article/ short communication/ technical brief
Animal characteristics	Strain	Wistar/ Sprague Dawley/ Lewis/ Zucker/ Fischer… etc
	Gender	Male/ Female
	Age*	In weeks
	Weight*	In grams
Surgical preparation	Anaesthetic	Ketamine/ Ether/ Pentobarbital/ Isoflurane… etc
	Heparin administration	Yes/ No; Dose in units/kg and adjusted to average animal weight in study.
Model technique	Method of IRI (model)	Total inflow ischaemia (with or without shunting)/ Selective ischaemia/ Isolated portal vein or hepatic artery clamping… etc
	Bile duct clamping	Yes/ No
	Hepatectomy	Yes/ No; Percentage resected
	Preconditioning	Yes/ No; Number of cycles; Duration of ischaemia; Duration of reperfusion
	Ischaemia time (minimum and maximum)	In minutes
	Reperfusion time (minimum and maximum)	In minutes; Reperfusion for survival studies collected separately
Intervention details	Intervention type	IRI alone; comparison of IRI techniques; other interventions on a background of IRI
Outcomes	Survival data	Survival rates (per model and per ischaemia time if available)
	Main outcome	Free text

3.2.6. Data expression and statistical analysis

In the case of continuous parametric data, results were expressed as mean ± SEM (standard error of mean) unless stated otherwise. Group means were compared using the independent Student t-test or the one-way ANOVA (when more than two groups were compared). ANOVA results are reported as F-value (degrees of freedom between and within groups are indicated within parenthesis) and P value. Post hoc analyses were performed when significant differences between groups were identified on ANOVA (Tukey or Games Howell test for equal or unequal variance respectively).

Categorical data were expressed as frequencies (percentages). Associations between nominal variables were tested using the Chi square or Fisher's exact test as appropriate. Results are reported as Chi-square statistic value X^2 (degrees of freedom are indicated within parenthesis) and P value. The effect size was measured using Cramer's V test with small, medium and large effect size corresponding to values around 0.1, 0.3 and 0.5 respectively (Cohen, 1988).

Multiple regression analysis was performed to identify the relative contribution of multiple independent variables to the prediction of a single continuous independent variable. Results are reported as F-value (regression and residual degrees of freedom are indicated within parenthesis) and P value. The contribution of each individual independent variable to the model is reported as B regression coefficient [lower, upper bound 95% confidence interval for B] and P value.

Test results with p values of less than 0.05 were accepted as statistically significant. All statistical tests were performed using the Statistical Package for Social Sciences version 19.0 (SPSS Inc., Chicago, IL, USA) and Microsoft Office Excel 2010 (Microsoft Corp., Redmond, WA).

3.3. Results

3.3.1. Overview of eligible studies

The search strategy identified 3387 studies that were considered potentially eligible for inclusion into the review. Over half of these (58%) were subsequently excluded during the abstract skimming phase. Of the remaining 1423 studies, a further 248 were excluded following examination of the full-text reports for reasons outlined in the study-inclusion flowchart below (Figure 3.11).

A total of 1175 studies were included in the review. Full-text reports were obtained in 1153 (98.1%) of these studies. Data from the remaining 22 studies was extracted from published abstracts.

3.3.2. Description of model methodology

Rat strain

Wistar rats were utilised in IRI studies in 599 studies (50.8%). The second commonly used strain was Sprague Dawley [432 studies (36.6%)]. Zucker rats were solely utilised in experiments that addressed questions related to obesity and liver steatosis [21 studies (1.8%)]. Figure 3.12 summarises the distribution of rat strains within hepatic IRI models.

Rat gender

Male rats were used in the majority of hepatic IRI studies [1009 studies (85.9%)]. Female rats were in 69 studies (5.9%) and only 14 studies used both genders indiscriminately (1.2%). The gender of rats was not mentioned in 83 reports (7.1%).

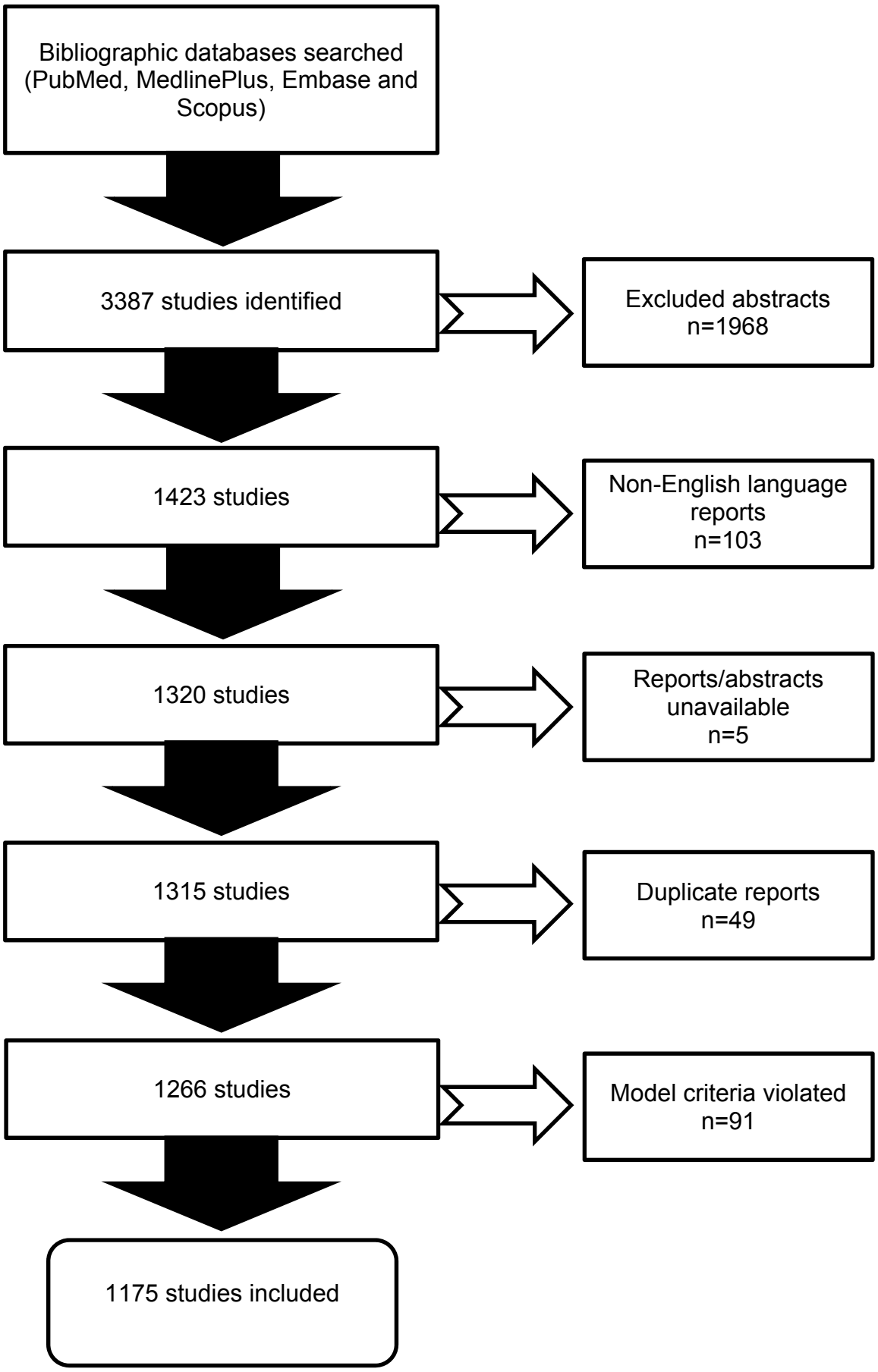

Figure 3.11 Study-inclusion flowchart

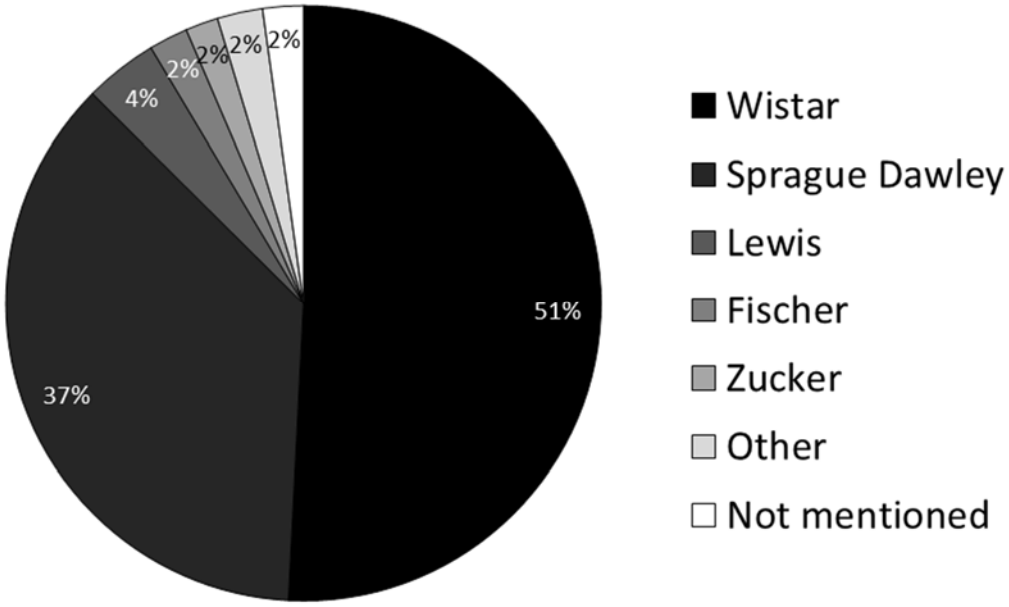

Figure 3.12 Distribution of rat strains utilised in hepatic IRI studies

Rat age

Animal age was the least reported variable among animal characteristics; documented in only 127 reports (10.8%). Age values extracted from the reports refer to animal ages at the time of IRI procedures and are described in weeks. The average age was 10.8±0.5weeks. In studies that addressed questions related to old age [8 studies (0.7%)] the average age in the older groups was 65.7±10.7weeks.

Rat weight

Animal weights were reported in 1063 studies (90.5%). Weight values obtained refer to the average animal weight at the time of IRI procedures and are described in grams. The average weight was 258.3±1.6g. In studies that examined obese animals [9 studies (0.8%)] the average weight in the obese groups was 461.7±54.1g.

Anaesthetic choice

The choice of anaesthetic was reported in 1049 studies (89.3%). The most commonly used single agent anaesthetic for hepatic IRI procedures was

pentobarbital [reported in 351 studies (29.9%)] followed by ether [188 studies (16%)]. The commonest combination anaesthetic was ketamine and xylazine [reported in 132 studies (11.2%)]. The distribution of anaesthetic agents used in hepatic IRI models in rats is summarised in Figure 3.13.

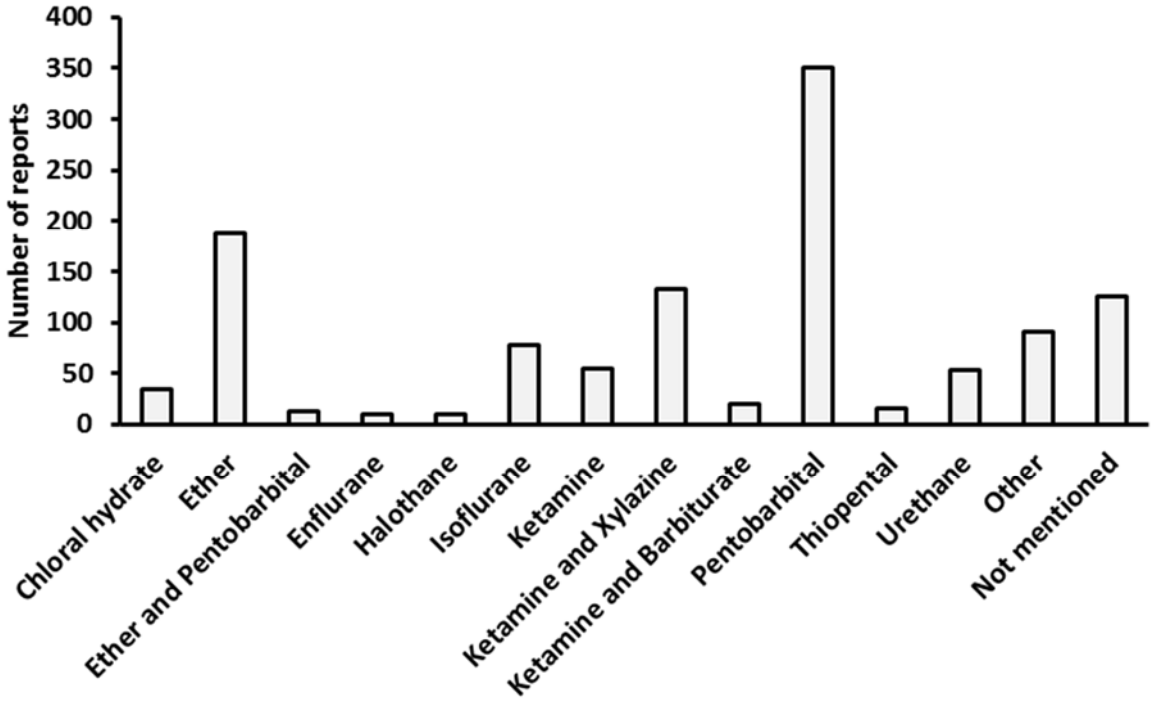

Figure 3.13 Frequency distribution of anaesthetic agents used in rat hepatic IRI studies

Administration of Heparin

The use of heparin to prevent thrombosis at the time of clamping was reported in 162 studies (13.8%). As shown in Figure 3.14, the commonest dose administered was 200U/Kg [14 studies (27.2%)]. The average weight-adjusted dose was 87.7±7.7U and ranged from 5.5-550U. In 3 reports, heparin was administered as a studied intervention (Abe et al., 1993, Shibayama et al., 1991, Harada et al., 2006).

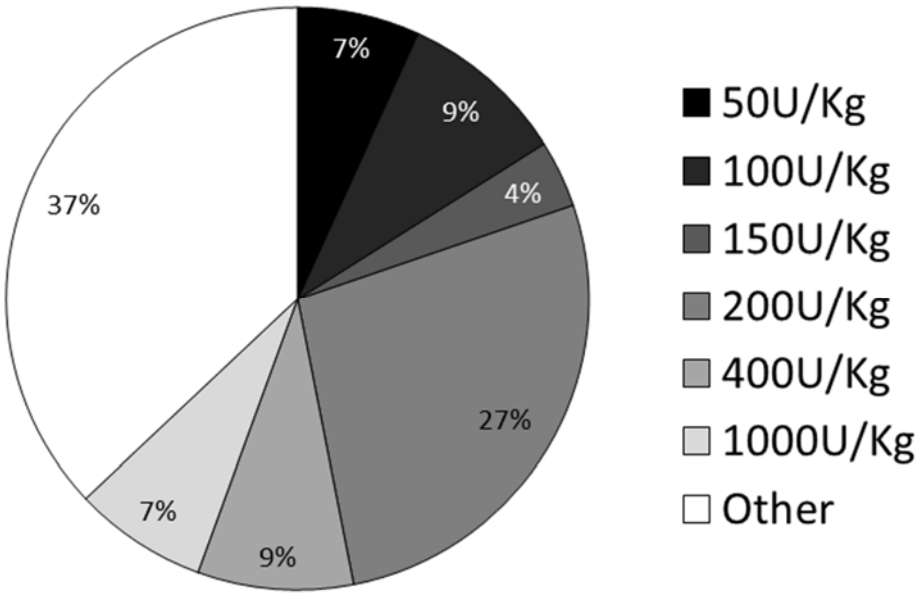

Figure 3.14 Frequency distribution of heparin doses administered in rat hepatic IRI studies

Ischaemia models

As illustrated in Figure 3.15, total inflow occlusion models were utilised in almost a third of hepatic IRI studies in rats [360 studies (30.6%)]. In comparison, studies adopting segmental inflow occlusion models were over twice as commonly adopted [727 (61.9%) studies]. Total hepatic exclusion models (inflow and outflow occlusion) were identified in 9 studies (0.8%) and isolated portal vein or hepatic artery occlusion models were adopted in 32 (2.7%) and 21 (1.8%) studies respectively. The method of ischaemia was unclear in 26 studies (2.2%).

The 70% (left and middle lobe) inflow occlusion model was utilised in 665 studies, making it the most commonly adopted model of hepatic IRI in rats, comprising 91.5% of studies using segmental inflow occlusion models and 56.6% of overall hepatic IRI studies in rats. Within this cohort, hepatectomy or ligation of the remaining 30% non-ischaemic liver was incorporate in 78 (11.7%) and 39 (5.9%) studies respectively.

The second commonest segmental hepatic IRI model was the 20% (right lobe) inflow occlusion model, encountered in 42 studies (5.8% of segmental models). Other segmental models included inflow occlusion of 40% (middle lobe), 30% (left lobe) and 50% (right and right middle lobe) of the liver. These were identified in 1.1%,

0.6% and 0.1% of the studies incorporating segmental hepatic IRI models respectively.

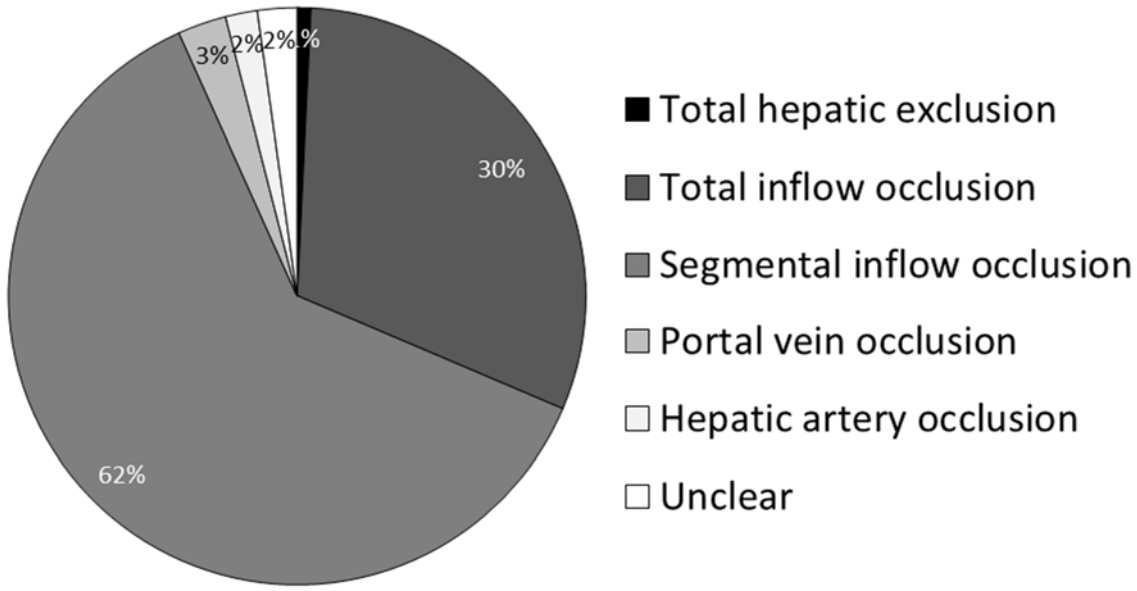

Figure 3.15 Frequency distribution of models adopted in rat hepatic IRI studies

Total inflow occlusion models were commonly performed without the need for portosystemic blood shunting. However, in 91 studies (25.3% of total inflow occlusion studies), some form of portosystemic blood shunting was incorporated. Single-stage shunting was performed using polyethylene tube communication or direct anastomosis between a systemic and portal venous tributary [63 (17.5%) and 4 (1.1%) respectively]. Gradual portosystemic shunts were mostly formed via splenic transposition in 21 studies (5.8%).

Table 6 summarises the frequency distribution of rat hepatic ischaemia reperfusion injury models in this review.

Table 6 Frequency distribution of rat hepatic ischaemia reperfusion injury models

Model		**Frequency (percentage of total)**
Total hepatic exclusion		9 (0.8)

Total inflow occlusion		360 (30.6)
	Without portosystemic shunt	269 (22.9)
	Portosystemic tube shunt	63 (5.4)
	Portosystemic anastomosis	4 (0.3)
	Splenic transposition	21 (1.8)
	Caecal herniation	1 (0.1)
	Cirrhosis model	2 (0.2)
Segmental inflow occlusion		727 (61.9)
	92% inflow occlusion (excluding caudate)	7 (0.6)
	70% inflow occlusion (Left/middle)	665 (56.6)
	50% inflow occlusion (right/right middle)	1 (0.1)
	40% inflow occlusion (middle)	8 (0.7)
	30% inflow occlusion (left)	4 (0.3)
	20% inflow occlusion (right)	42 (3.6)
Portal vein occlusion		32 (2.7)
Hepatic artery occlusion		21 (1.8)
Unclear		26 (2.2)

A single model of hepatic IRI was adopted in the majority of studies [1125 (95.7%)]. The remaining reports included two [42 studies (3.6%)] or three [8 studies (0.7%)] models within the same study.

Initial report of models

Based on the chronological sequence of reports within this review, first describers of models have been identified (in the context of hepatic IRI). These are summarised in Table 7.

Table 7 First reports of IRI models

First author	**Year of publication**	**Procedure**	**Reference**
De Baker	1956	70% IRI	(De Baker, 1956)
van der Meer	1971	Portal vein ligation	(van der Meer et al., 1971)

Hirasawa	1978	Total inflow occlusion with shunt	(Hirasawa et al., 1978)
Clemens	1985	70% IRI and 30% ligation	(Clemens et al., 1985)
Flye	1987	20% IRI and 80% hepatectomy	(Flye and Yu, 1987)
Asakawa	1989	70% IRI and 30% hepatectomy	(Asakawa et al., 1989)
Senga	1990	Splenic transposition	(Senga et al., 1990)
Sjovall	1990	Hepatic artery ligation	(Sjovall et al., 1990)
Linberg	1994	Total hepatic exclusion	(Linberg et al., 1994)
Dong	2002	92% IRI and 8% hepatectomy	(Dong et al., 2002)

Exclusion of bile duct from occlusion

The separation/inclusion of bile duct during vascular occlusion was reported in 494 studies (42%). In 7 reports, the bile duct was ligated prior to IRI in order to investigate the effect of IRI on cholestasis. Of the remaining 487 reports, 86 (17.7%) reported isolation of the bile duct prior to clamping the vascular pedicle in order to avoid the potential confounding effect of cholestasis. The effect of bile duct exclusion versus occlusion in hepatic IRI was studied in one report (Montero et al., 2005).

Ischaemic periods

Ischaemia times were described in 1169 studies (99.5%). Variable ischaemic periods were studied in 162 of these studies (13.9%). The most commonly studied ischaemia times were 60 minutes [417 studies (35.7%)], 30 minutes [260 studies (22.2%)] and 90 minutes [178 studies (15.2%)] in descending order. Reported ischaemia times ranged from 10-2880min and are summarised in Figure 3.16.

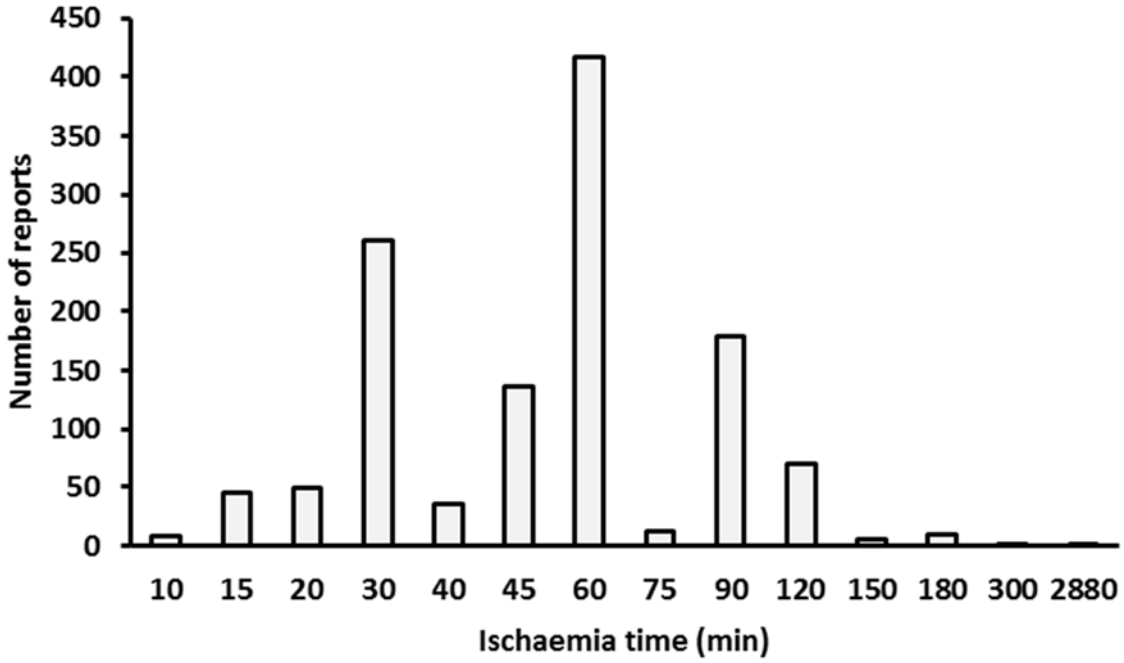

Figure 3.16 Frequency distribution of ischaemia times in hepatic IRI rat studies

Reperfusion periods and long-term follow up (excluding survival analyses)

Reperfusion times were described in 1168 studies (99.4%). In comparison to ischaemia times, variable reperfusion periods were more commonly described within a study [580 of all studies reporting reperfusion times (49.7%)]. Reperfusion periods ranged from 0-259200min (excluding reperfusion periods for survival studies).

The term “minimum reperfusion time” in this review refers to the earliest timepoint for data collection in a study following restoration of blood flow. “Maximum reperfusion time” refers to the latest follow up period in the study (for survival and non-survival outcomes). The most commonly studied minimum reperfusion times in descending order were 60 minutes [266 studies (22.8%)], 0 minutes (immediate post-reperfusion period) [145 studies (12.4%)] and 120 minutes [133 studies (11.4%)]. The most commonly studied maximum reperfusion times (excluding survival analyses) in descending order were 1440 minutes (24hr) [223 studies (22%)], 60 minutes [132 studies (13%)] and 120 minutes[116 studies (11.4%)]. Frequency distribution of minimum and maximum reperfusion times are summarised in Figure 3.17and Figure 3.18.

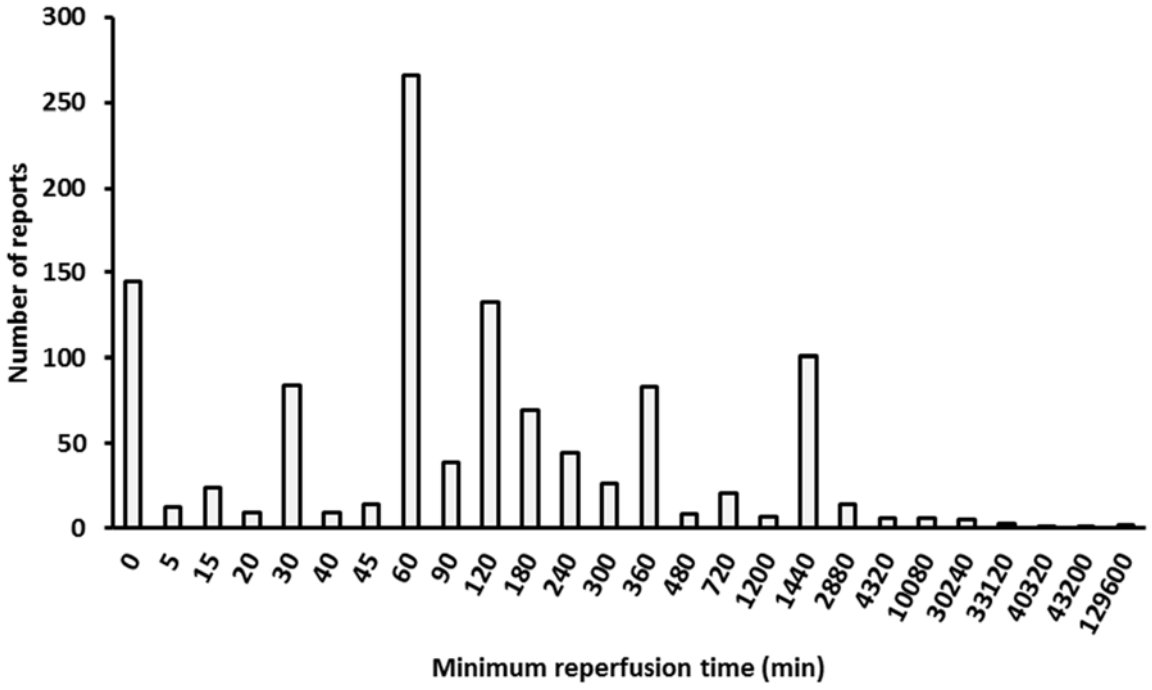

Figure 3.17 Frequency distribution of minimum reperfusion times in hepatic IRI rat studies

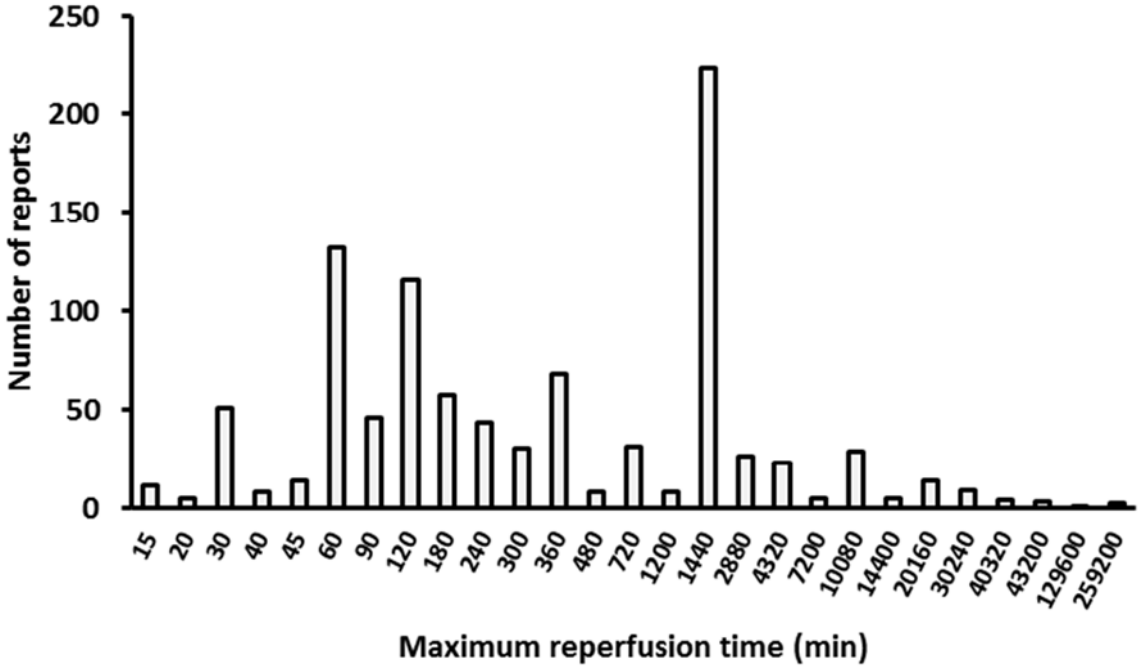

Figure 3.18 Frequency distribution of maximum reperfusion times in hepatic IRI rat studies (excluding survival analyses)

Long-term follow up (≥48hr) for outcomes excluding survival was described in 131 studies. These are summarised in Table 8.

Table 8 Frequency distribution of studies with long-term follow up (excluding survival analyses)

Follow up duration	Number of reports
2 days	26
3 days	23
4 days	4
5 days	5
7 days	29
8 days	1
10 days	5
14 days	14
15 days	2
21 days	9
23 days	3
28 days	4
30 days	3
3 months	1
6 months	2

Fibrosis and long-term biliary pathology

Only 38 studies (3.2%) examined outcomes (excluding survival) for 14 days or longer (see Table 8). Only two of these papers examined the long term effect of hepatic IRI on biliary epithelial cell death and biliary proliferation ((Xu et al., 2004, Hahn et al., 2007). One of these papers also examined the development of delayed fibrotic changes following IRI. However, animals in this study were also exposed to intraoperative radiotherapy (Hahn et al., 2007).

Overview of interventions

Interventions were reported in all studies. In 209 reports (17.8%) IRI was the sole intervention studied. Of these, 154 studies (73.7%) explored outcomes from a single model/method of IRI. In the remaining 55 studies (26.3%), various IRI models and/or ischaemia times were compared. In 966 reports (82.2), other interventions layered on a background of IRI were investigated. Figure 3.19 summarises these intervention groups.

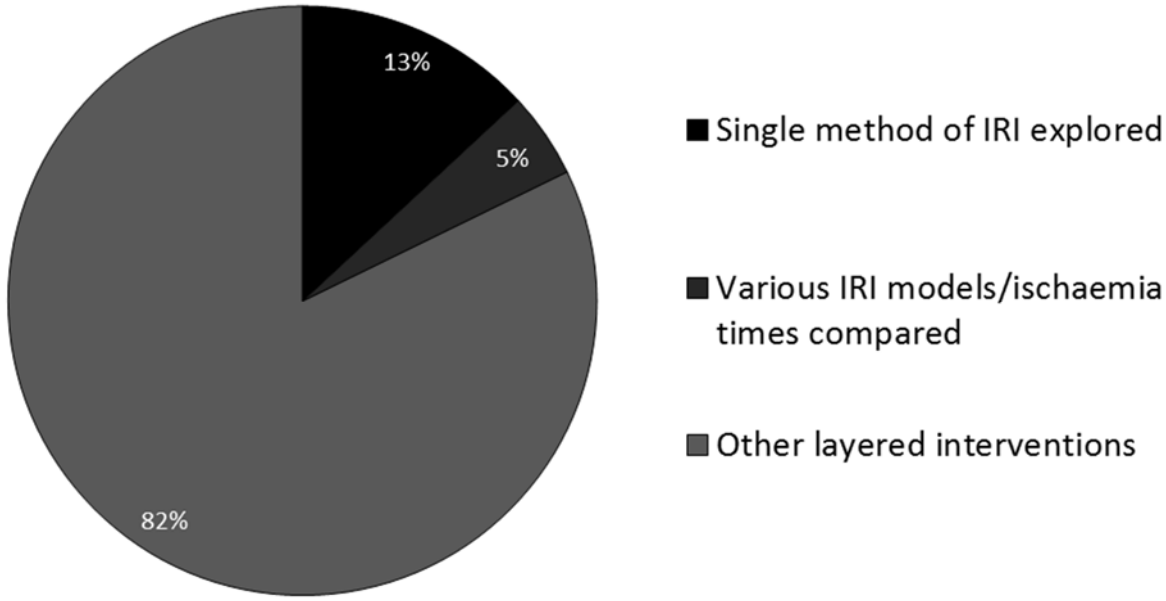

Figure 3.19 Summary of intervention types adopted in rat hepatic IRI studies

3.3.3. Chronological evolvement of methodologies

Trends in hepatic IRI model adoption in rat studies

The distribution of hepatic IRI model adoption over time is summarised in Appendix 2.

Figure 3.20 shows that the use of total inflow occlusion models in hepatic IRI studies in rats has altered over time. The use of immediate or gradual portosystemic shunts had peaked in the late 1990s and has since declined to the extent that the last reported use of a portosystemic tube shunt and of splenic transposition was in 2008

and 2003 respectively. However, the use of total inflow occlusion without portosystemic shunting continues to rise.

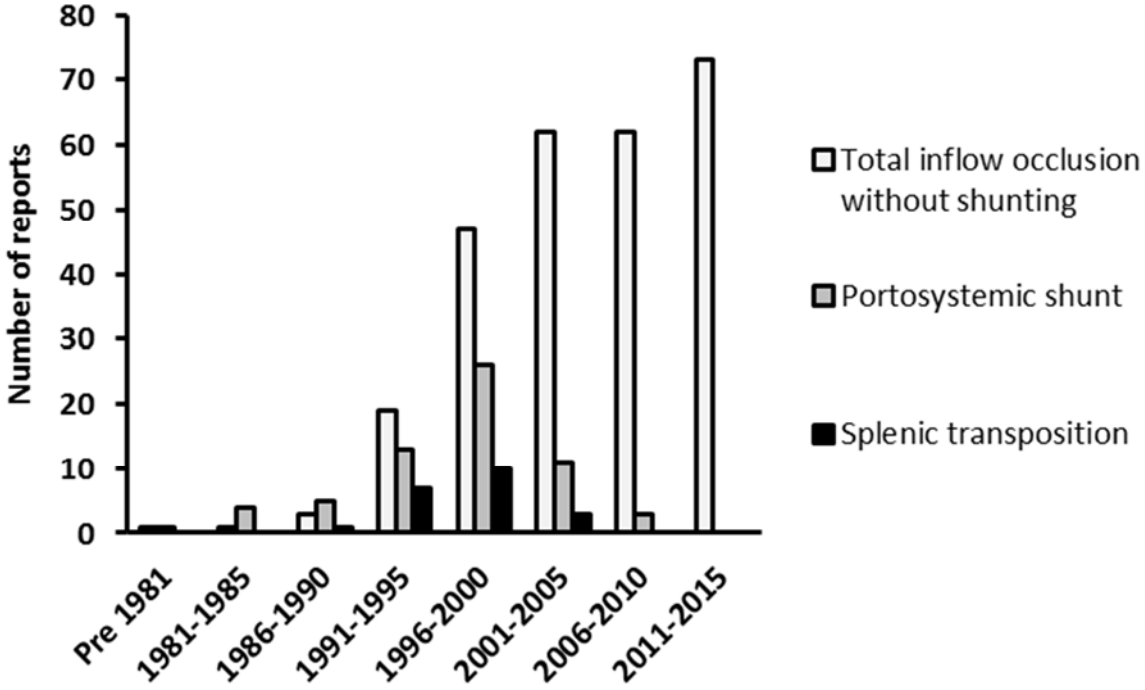

Figure 3.20 Time-trends in the adoption of total inflow occlusion models

A similar difference in time-trend was also noted within 70% inflow occlusion models. The incorporation of 30% hepatectomy (non-ischaemic liver) in hepatic IRI studies in rats peaked in the late 1990s and has been in slow decline since, whereas ligation of non-ischaemic 30% liver peaked later in the early 2000s and has subsequently seen a relatively more acute decline in use. On the other hand, the use of 70% inflow occlusion models without resection or ligation of non-ischaemic liver continues to rise in an approximately linear manner (Figure 3.21).

The first published report of right lobe (20%) inflow occlusion with concomitant 80% resection of non-ischaemic liver was in 1987. The use of this technique had peaked in the early 1990s and subsequent use has been relatively lower but steady. In comparison, publications describing right lobe (20%) inflow occlusion without non-ischaemic liver resection started to emerge in the early 1990s and a relatively greater interest was demonstrated in the technique in the latter half of that decade and in the

early 2000s. The use of this technique has subsequently seen a dramatic fall (Figure 3.22).

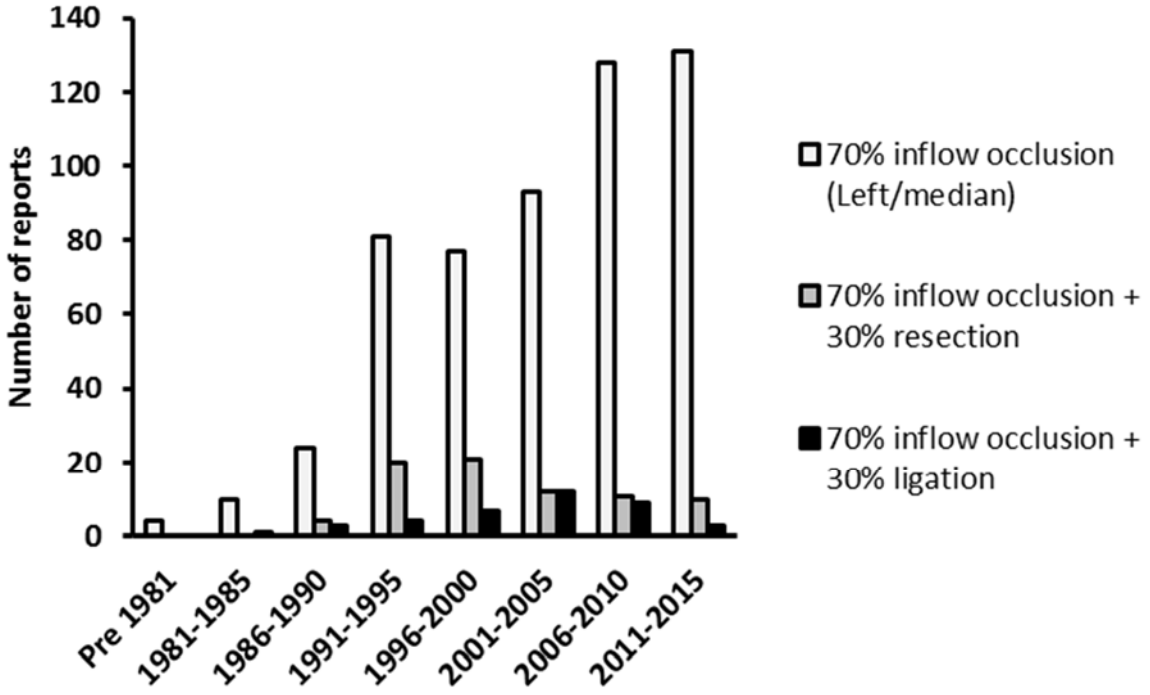

Figure 3.21 Time-trends in the adoption of 70% inflow occlusion models

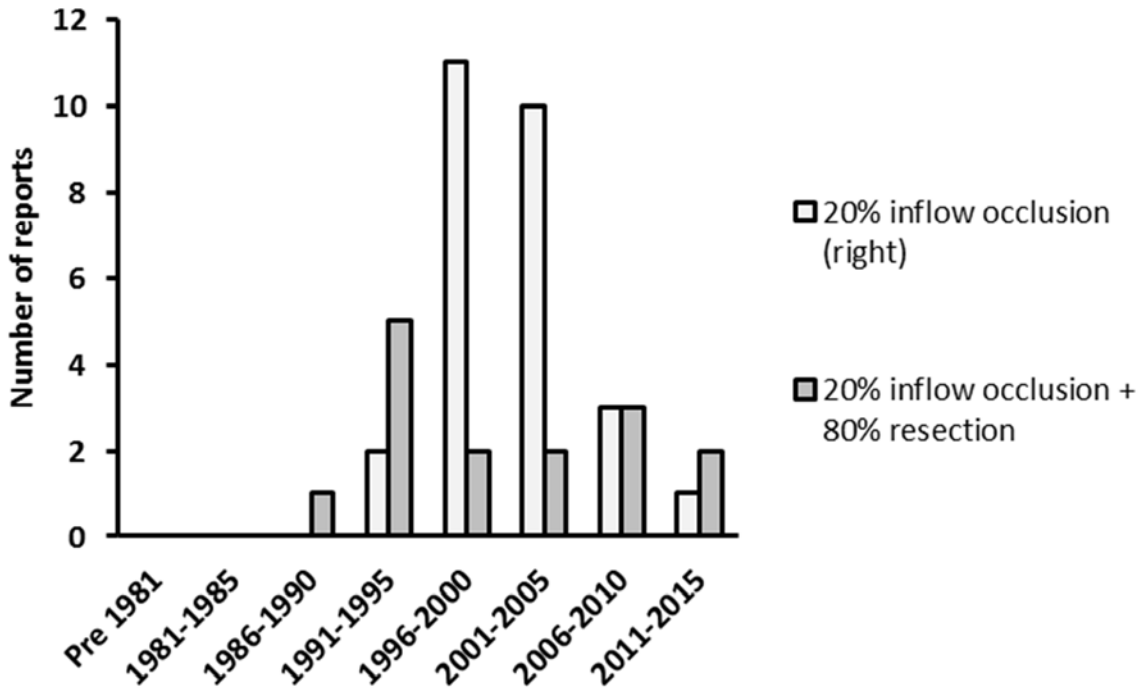

Figure 3.22 Time-trends in the adoption of 20% inflow occlusion models

Similar to right lobe occlusion models, isolated portal vein or hepatic artery occlusion models were adopted relatively later than total or 70% selective occlusion models. The first reports of portal vein and of hepatic artery occlusion were published in 1989 and 1990 respectively. Reports of both these models have subsequently continued at a relatively lower but steady level, although post-2010 has seen a moderate rise in published reports of the isolated portal vein occlusion model (Figure 3.23).

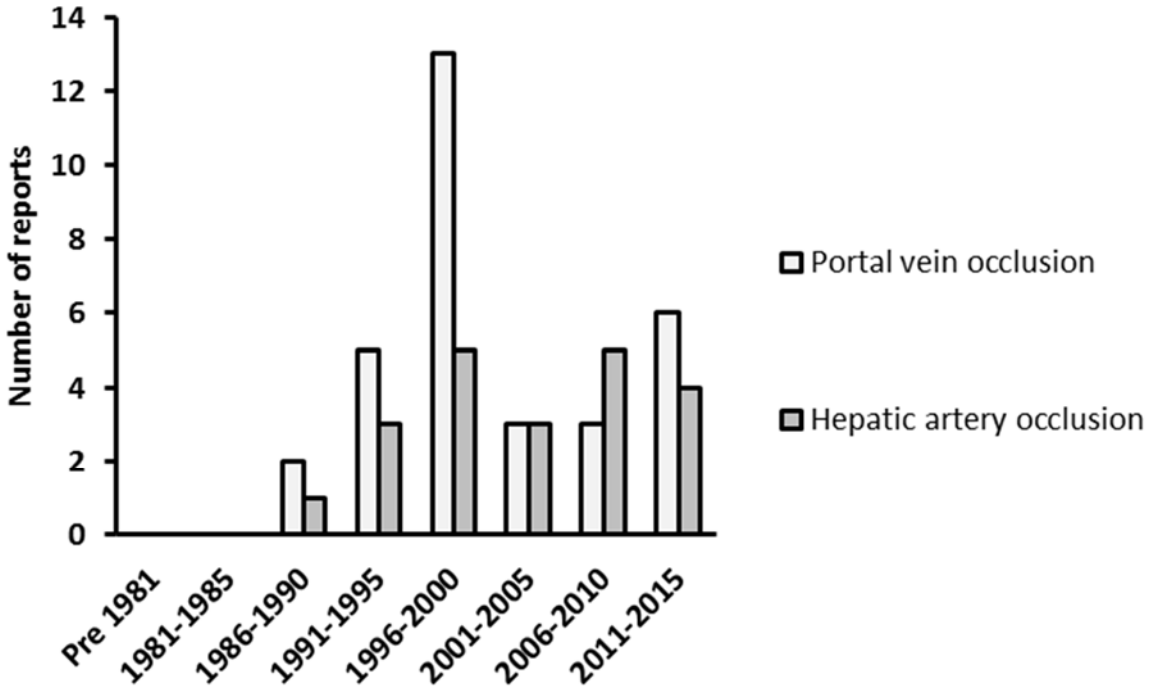

Figure 3.23 Time-trends in the adoption of isolated portal vein and hepatic artery occlusion models

Trends in anaesthetic use in rat hepatic IRI studies

The two most commonly used single anaesthetic agents, pentobarbital and ether (see 3.3.2) were the only anaesthetic agents reported in hepatic IRI studies in rats prior to 1981. However, the reported use of both pentobarbital and ether in rat hepatic IRI studies has been in prominent decline following their peak reported use in the early 2000s and late 1990s respectively. The commonest combination anaesthetic ketamine and xylazine was reportedly first used in a rat hepatic IRI study in1990 and has subsequently seen a linear increase in its use, to the extent that it has surpassed pentobarbital as the most commonly reported anaesthetic used in these studies between 2011 and 2015 (Figure 3.24)

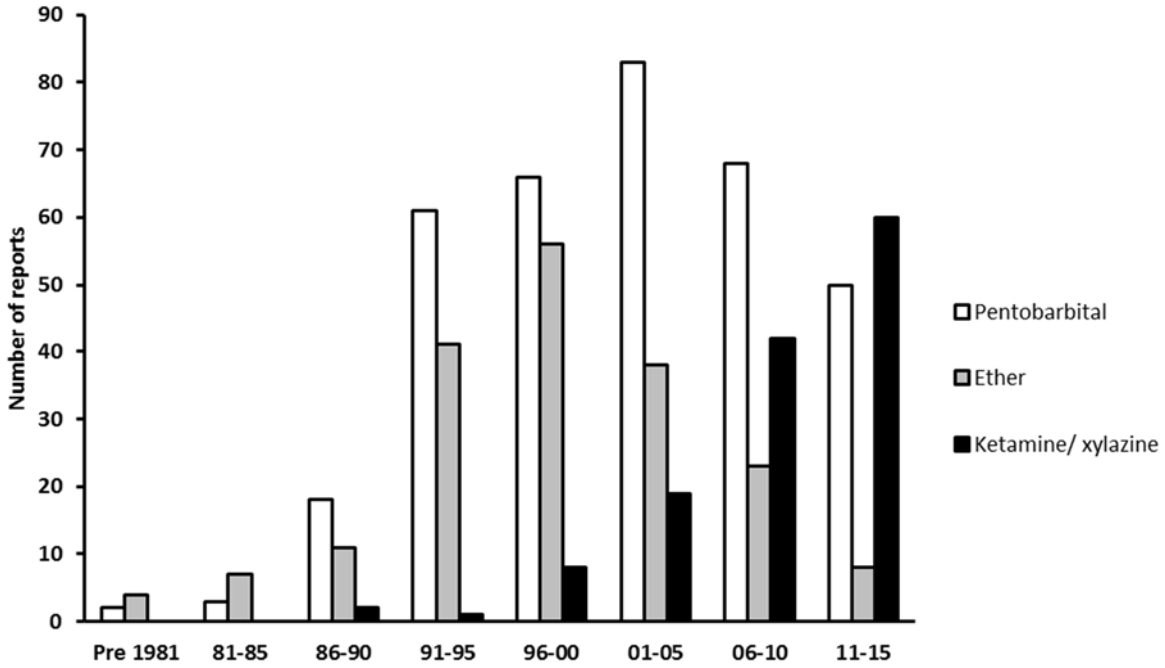

Figure 3.24 Time-trends in the reporting of the three most commonly used anaesthetics in rat hepatic IRI models

In contrast to the striking surge in the use of ketamine in combination with xylazine, the reported use of ketamine alone as an anaesthetic agent for hepatic IRI studies in rats has seen a steady decline subsequent to its peak reported use between 2001 and 2005. A similar pattern to ketamine is seen with the use of urethane as a single-agent in hepatic IRI studies. On the other hand, following its first reported use as single agent anaesthetic in hepatic IRI studies in rats in 1996, isoflurane has seen a substantial increase in its reported use in these studies and has become the third most commonly reported anaesthetic agent used for these procedures between 2011 and 2015. The peak reported use of chloral hydrate in hepatic IRI models in rats was in the late 1990s and subsequently demonstrated a slow decline. Interestingly, the reported use of chloral hydrate has unexpectedly risen in recent years making it the fourth most commonly reported anaesthetic agent in rat hepatic IRI studies between 2011 and 2015 (Figure 3.25).

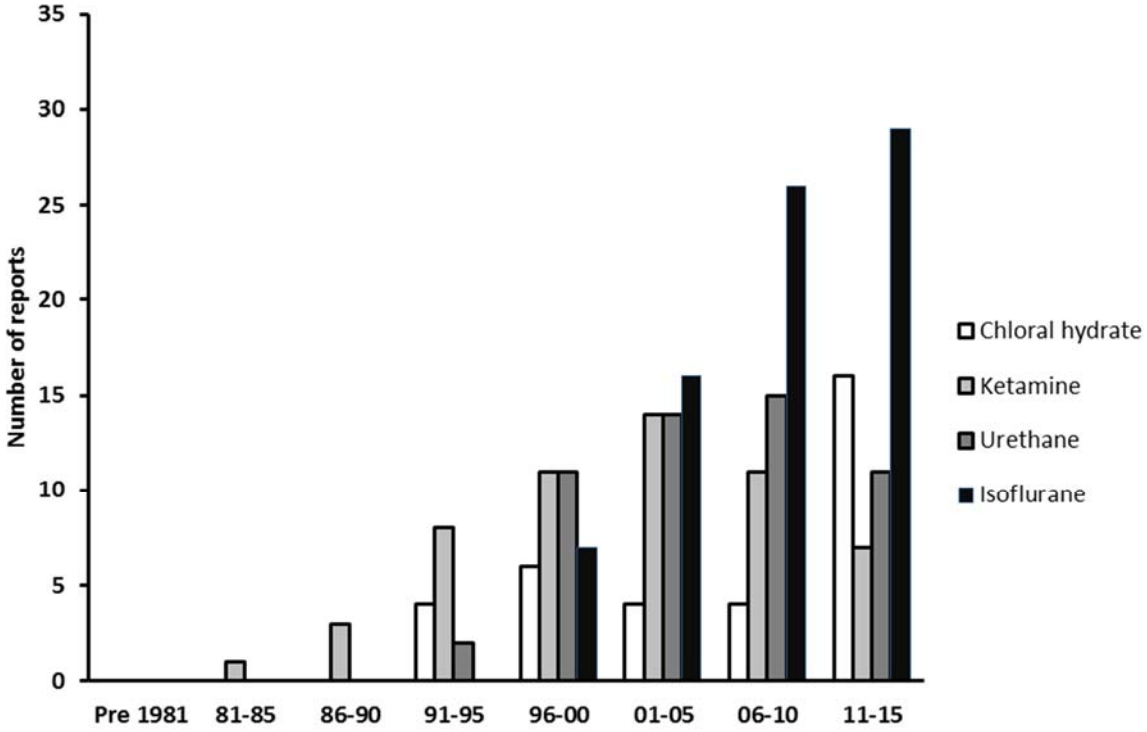

Figure 3.25 Time-trends in the reporting of less commonly used anaesthetics in rat hepatic IRI models

The time-trends of rarely used anaesthetic agents (single and combination anaesthetic agents) are shown in Figure 3.26.

The distribution of reported anaesthetic agents in hepatic IRI studies over time is summarised in Appendix 2.

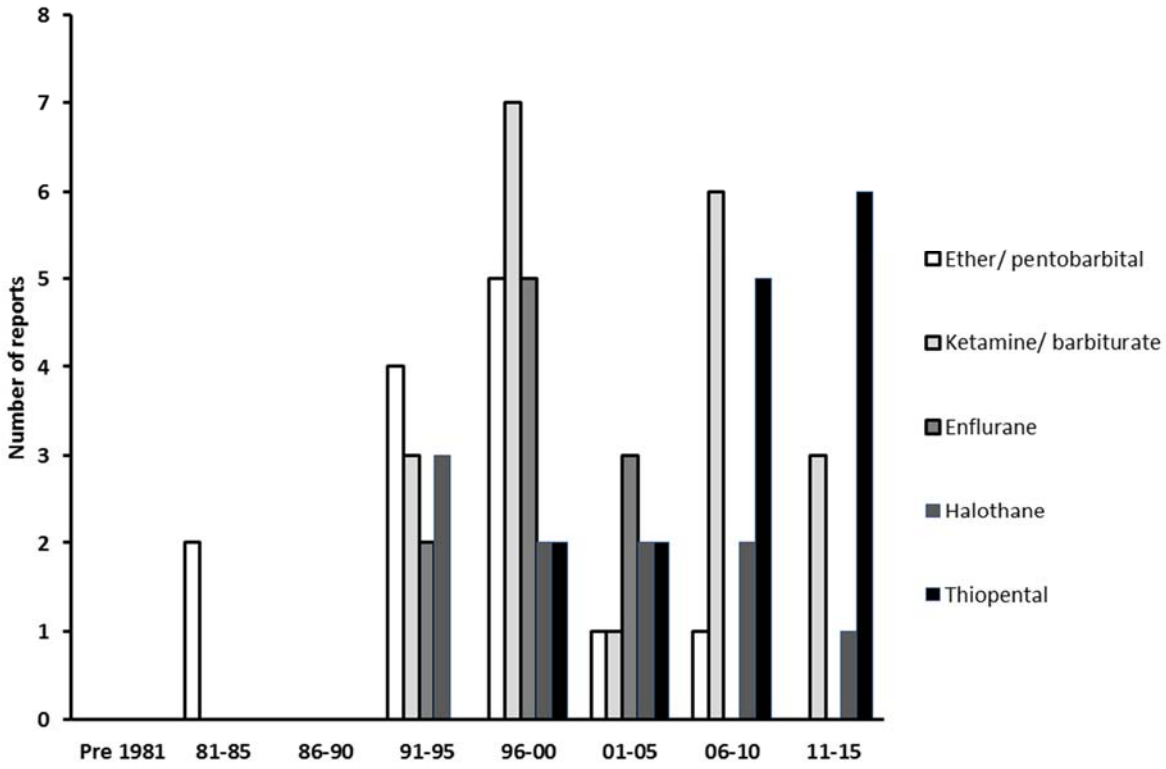

Figure 3.26 Time-trends in the reporting of rarely used anaesthetics in rat hepatic IRI models

Trends in heparin use in rat hepatic IRI studies

The first reported use of heparin to prevent thrombosis in hepatic IRI models in rats was in 1977. The number of reports describing the use of heparin in these studies showed a steady rise up to the early 1990s and declined in subsequent years as shown in Figure 3.27A. However, when the proportion of studies reporting the use of heparin are examined in comparison to the overall published hepatic IRI studies in rat during the same period of time, it becomes apparent that this practice has been in gradual decline over the past four decades as demonstrated in Figure 3.27B.

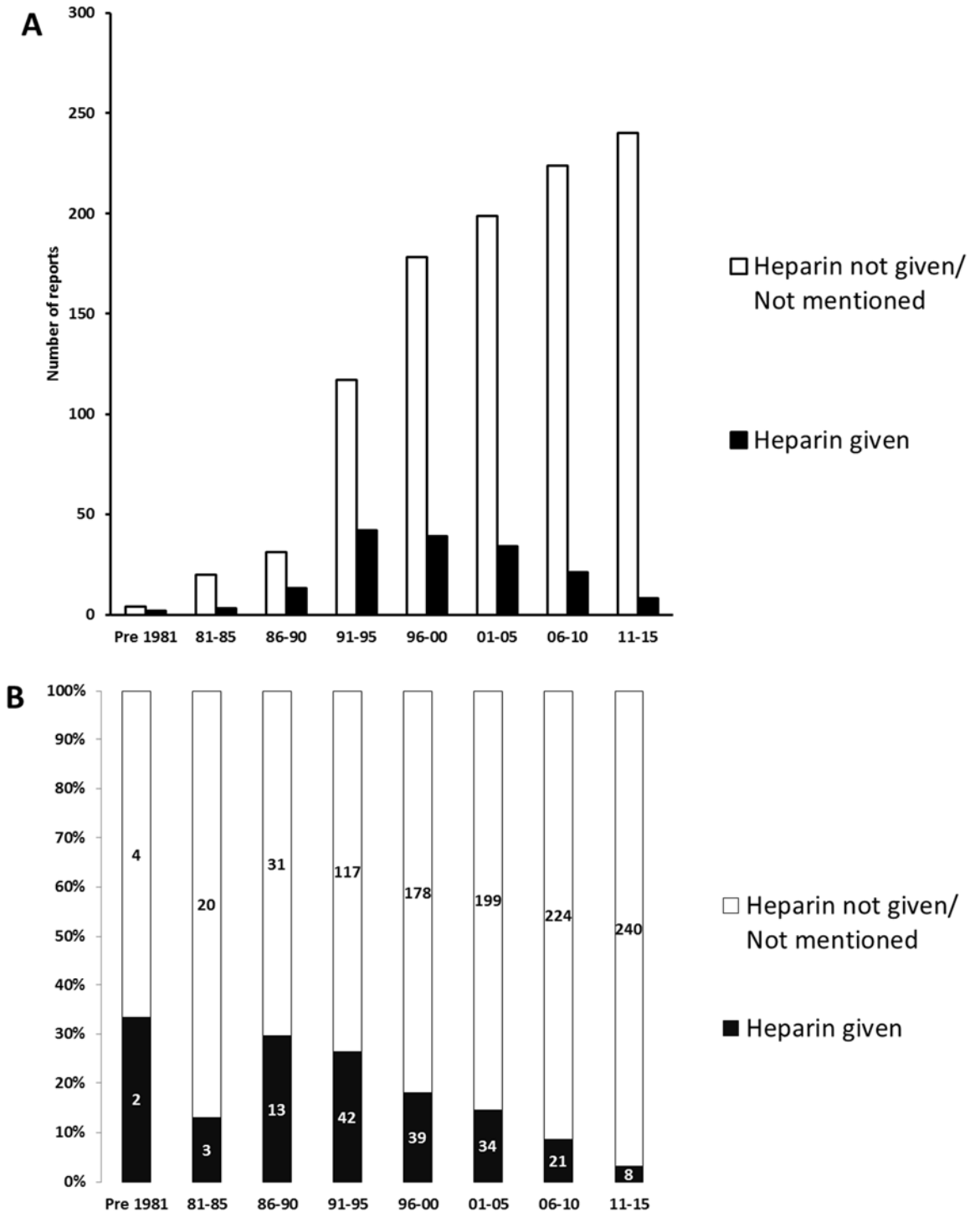

Figure 3.27 Time-trends in reported use of heparin in hepatic IRI models in rats. (A) Number of reports describing heparin use compared to those where heparin is not given or not mentioned. (B) Percentage of reports describing heparin use in comparison to the overall published hepatic IRI studies in rat during the same period of time

Trends in bile duct exclusion in rat hepatic IRI studies

The first reported separation of bile duct prior to vascular occlusion in a rat hepatic IRI study was in 1983. Reports of this technique subsequently increased, reaching a peak in the 1990s and then declined to a stable level, as demonstrated in Figure 3.28A and Figure 3.28B.

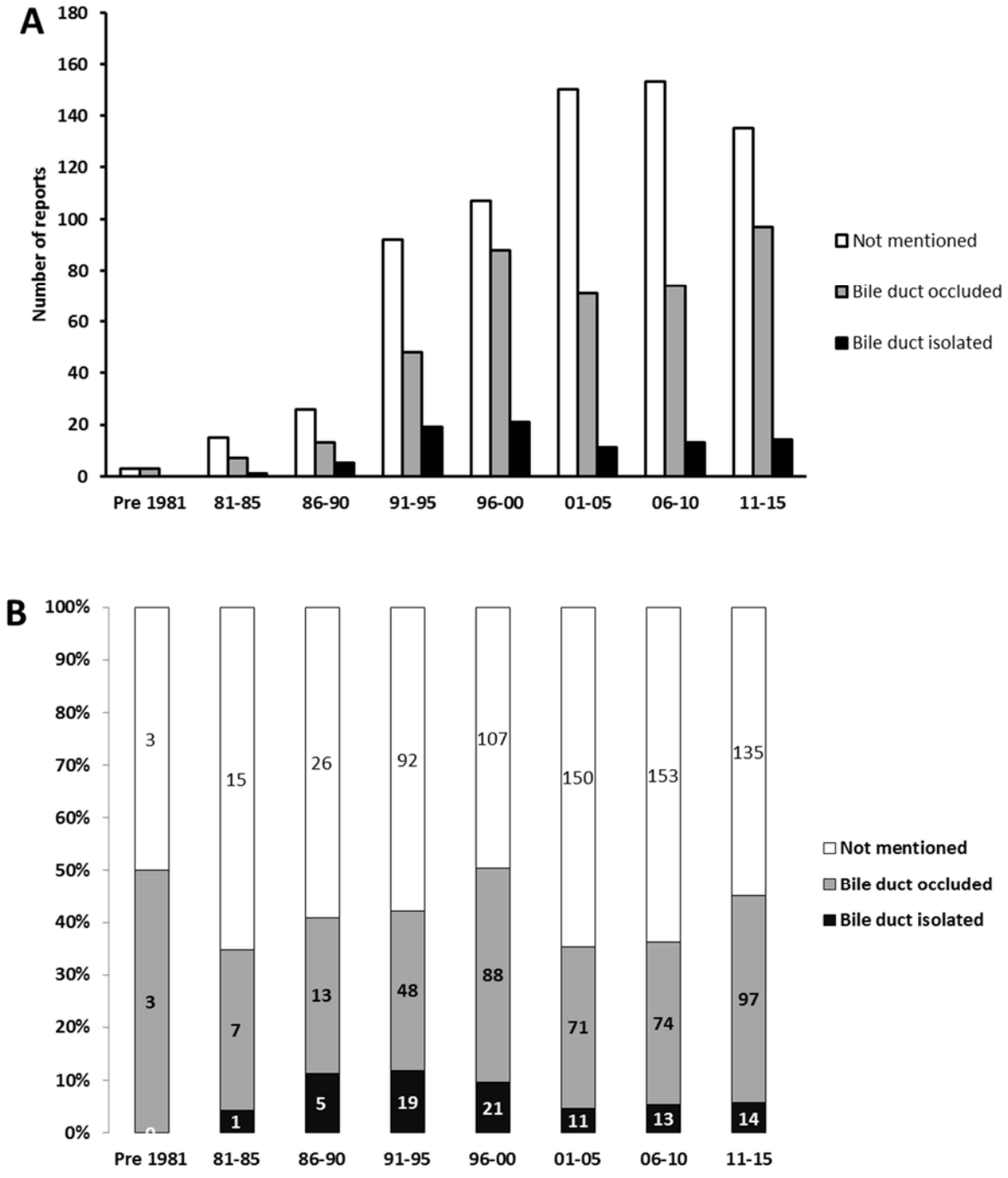

Figure 3.28 Time-trends in reported adoption of bile duct exclusion method in rat hepatic IRI studies. (A) Number of reports reporting bile duct exclusion compared to those where the technique is not performed or not mentioned. (B) Percentage of

reports describing bile duct exclusion in comparison to the overall published hepatic IRI studies in rat during the same period of time

Trends in ischaemia times during rat hepatic IRI studies

As demonstrated in Figure 3.29, the choice of 60 minutes ischaemia time in rat hepatic IRI studies is on an upward linear trend. The number of studies reporting other commonly chosen ischaemia times such as 30 and 45 minutes had previously been on the rise, reaching a plateau over the past two decades. In contrast, reports of 90 minutes ischaemia times have fallen subsequent to a peak in the late 1990s.

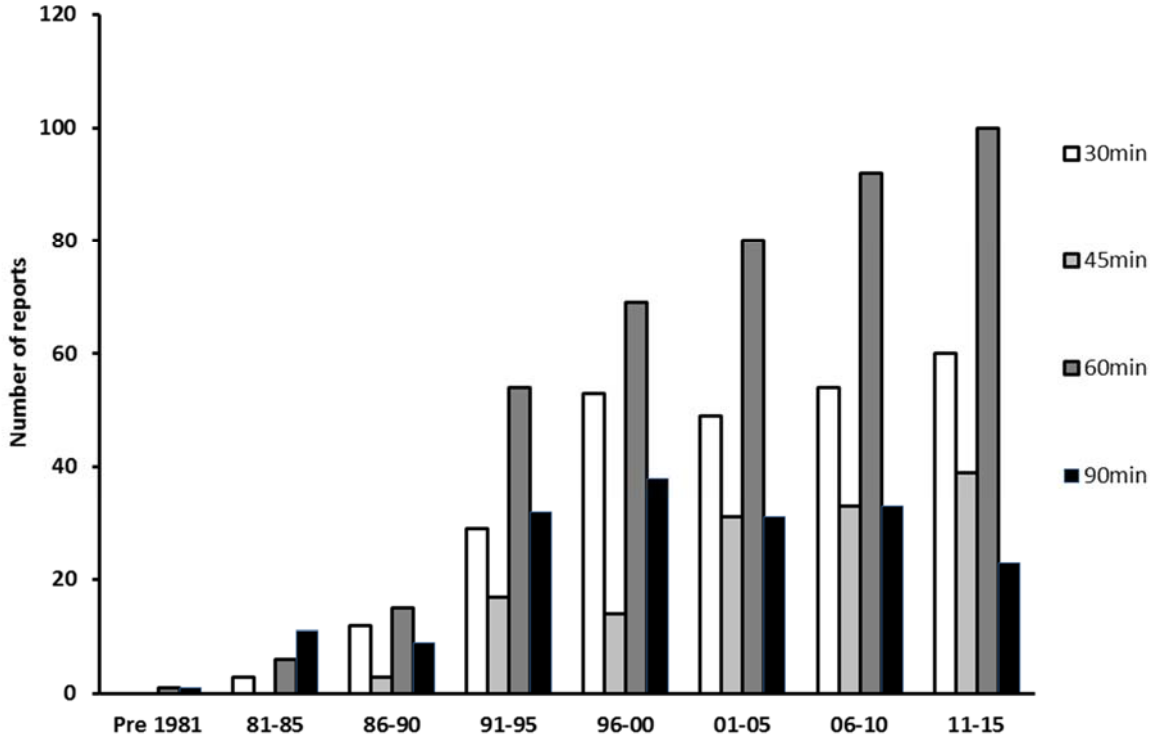

Figure 3.29 Time trends in reporting commonly chosen ischaemia times in rat hepatic IRI studies

Time trends of the less commonly reported ischaemia times (15, 120 and 180 minutes) appear to display a similar upward-downward pattern, peaking in the late 1990s and early 2000s (Figure 3.30).

The distribution of reported ischaemia times in hepatic IRI studies over time is summarised in Appendix 2.

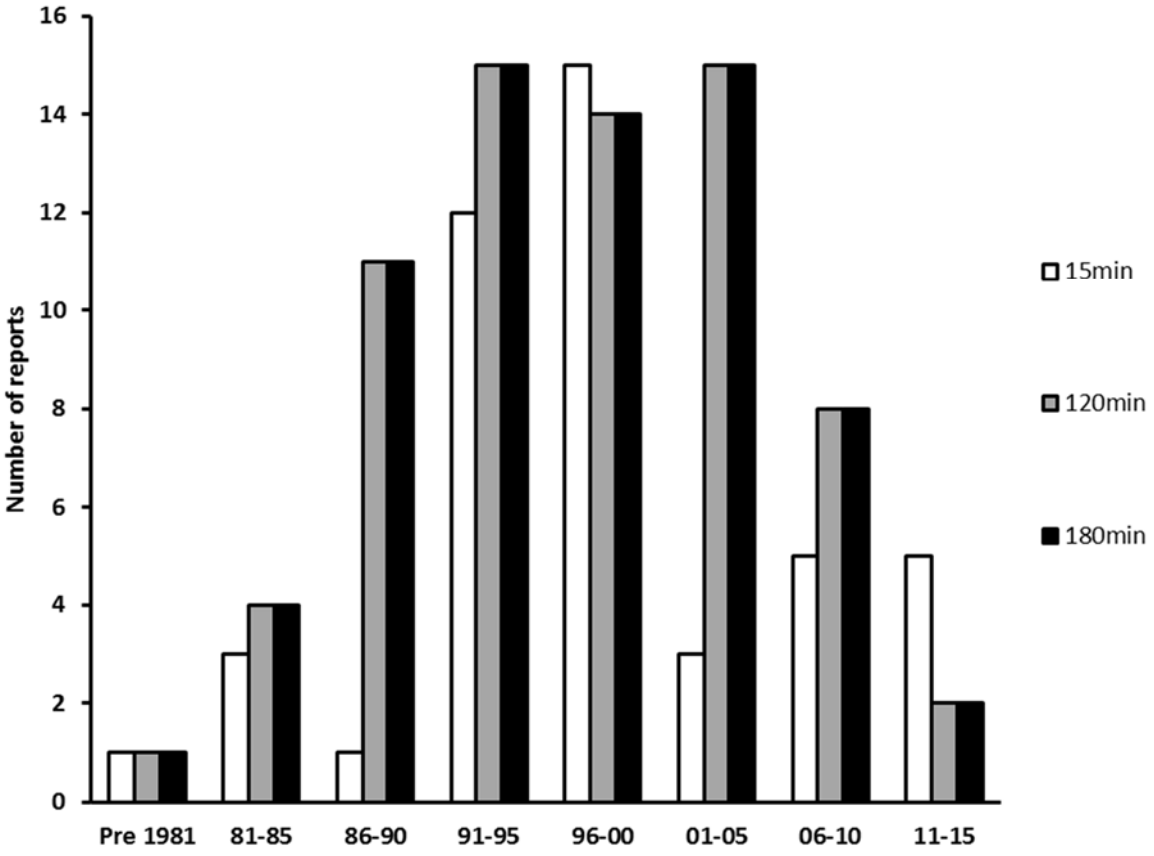

Figure 3.30 Time trends in reporting less commonly chosen ischaemia times in rat hepatic IRI studies

Trends in reperfusion times during rat hepatic IRI studies

Figure 3.31 shows that shorter minimum reperfusion times (0-180 minutes) display an upward-downward trend over time and that the peak of this trend is proportionate to the duration of minimum reperfusion. In other words, reports of reperfusion times of 0 and 30 minutes had peaked in the 1990s whereas those reporting longer reperfusion times of 120 and 180 minutes demonstrated a later peak in the 2000s. Although higher minimum reperfusion times (2-24hrs) are relatively less frequently reported, these appear to be on a continuing upward trend.

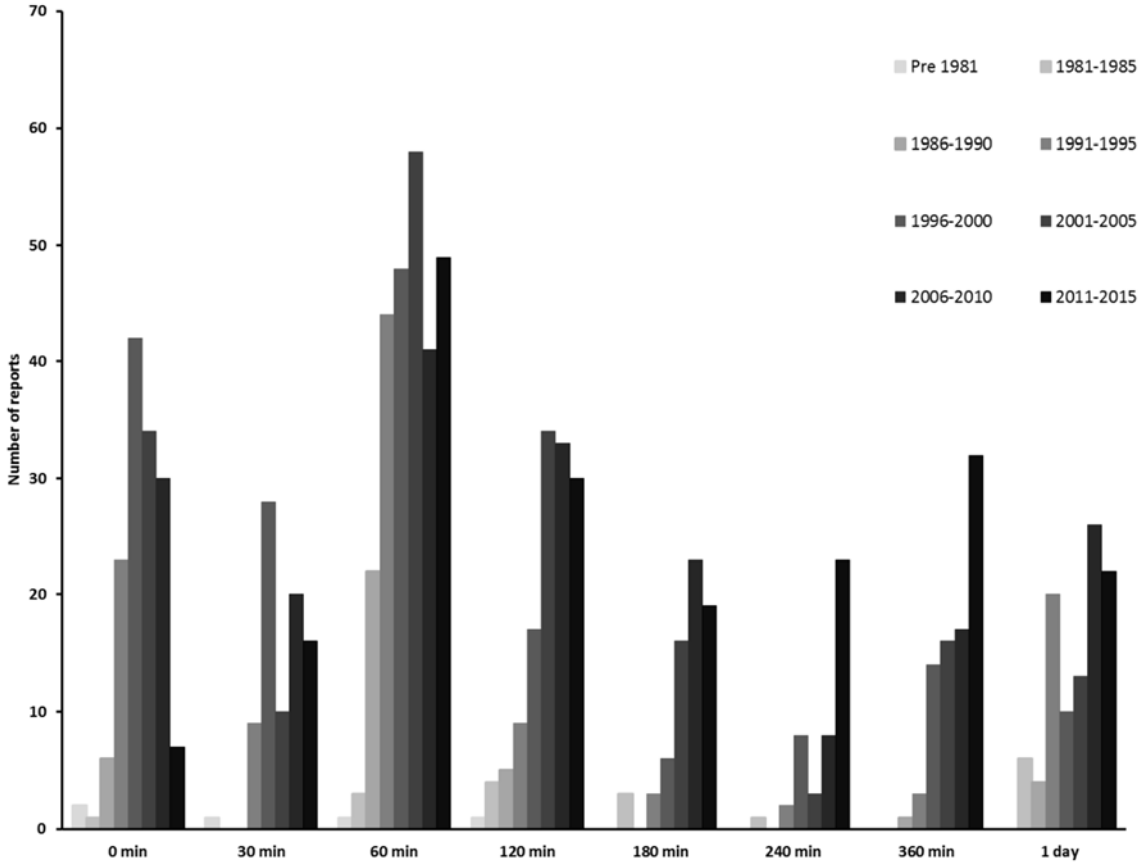

Figure 3.31 Time trends in reporting minimum reperfusion times in rat hepatic IRI studies

In comparison, reported short-term maximum reperfusion times (upto 24hr) have mostly been on an upward trend. The most commonly studied short-term maximum reperfusion times between 2011 and 2015 are 24, 1 and 2 hours in descending order (Figure 3.32).

Time trends for reported long-term maximum reperfusion times are displayed in Figure 3.33. Although an increasing trend can be observe in reports studying long-term follow up times of 2, 7 and 30 days, the numbers within these groups are too small to derive any meaningful conclusion.

A summary of the distribution of reported minimum and maximum reperfusion times in hepatic IRI studies over time is summarised in Appendix 2.

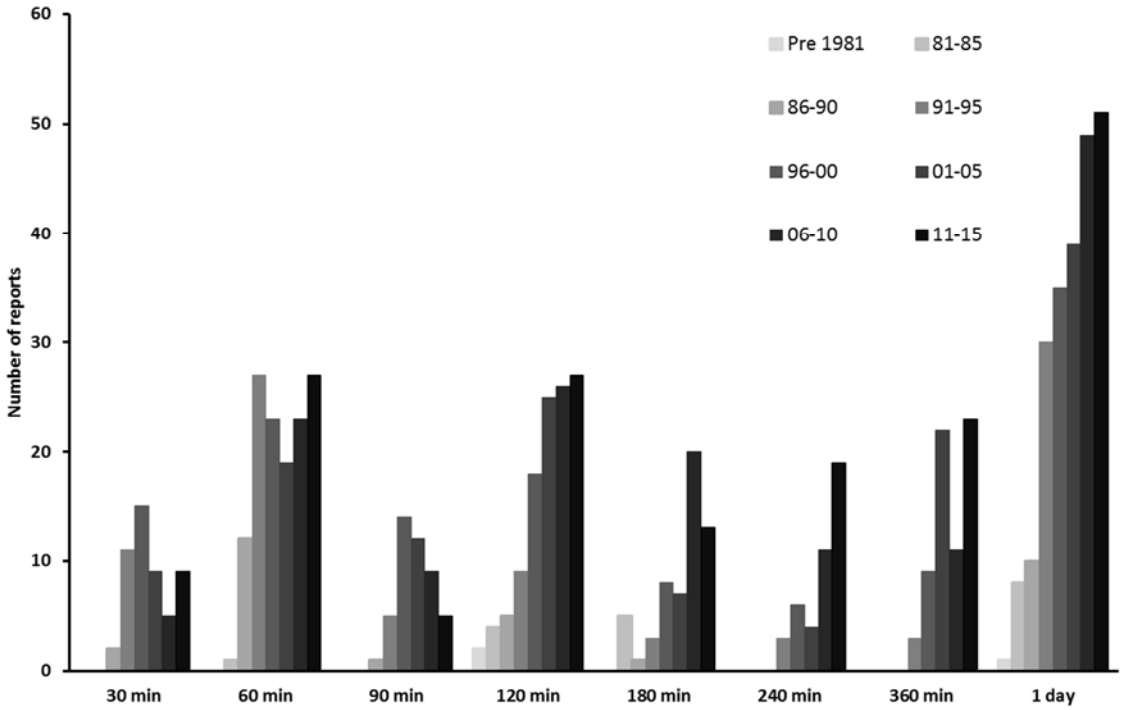

Figure 3.32 Time trends in reporting short-term (upto 24hr) maximum reperfusion times in rat hepatic IRI studies

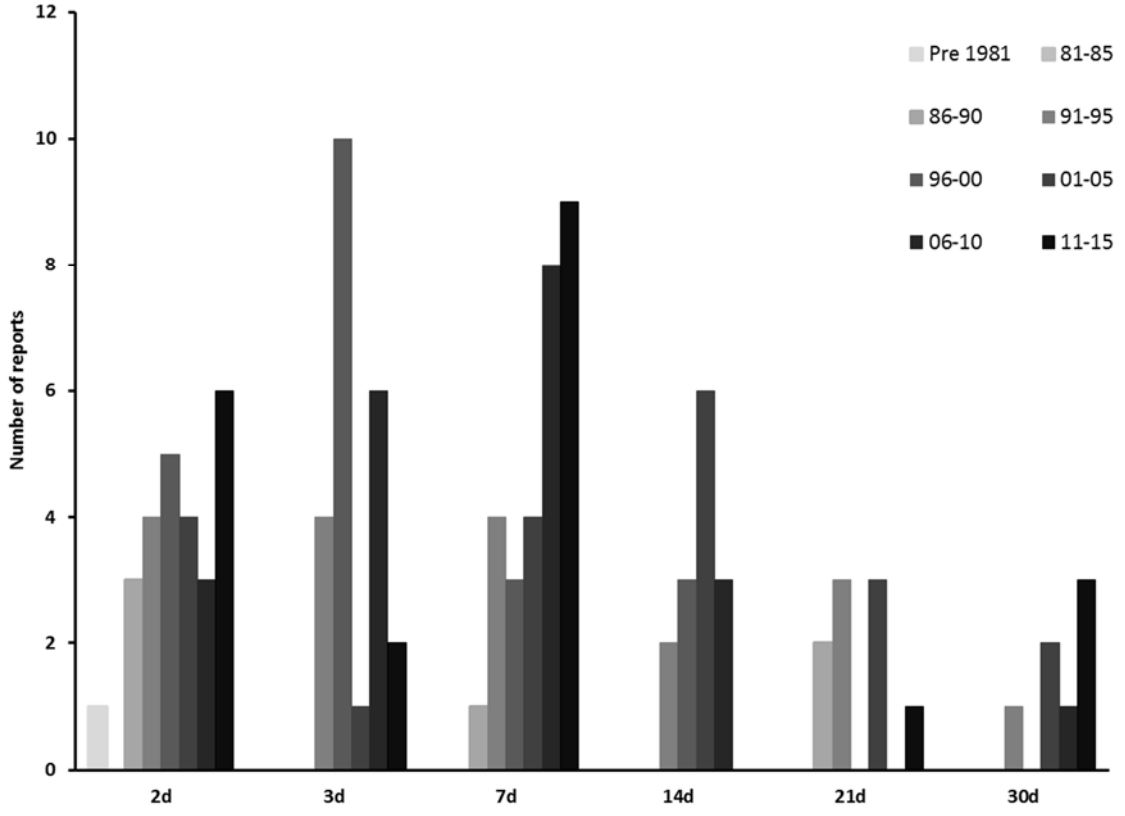

Figure 3.33 Time trends in reporting long-term (>24hr) maximum reperfusion times in rat hepatic IRI studies

Trends in number of models within report for rat hepatic IRI studies

The first study to describe more than one hepatic IRI model in rats within the same report was in 1980. The number of studies reporting multiple models peaked in the late 1990s but remain relatively low compared to single-model reports. Time trends for number of models reported within study are summarised in Figure 3.34 and Table 9

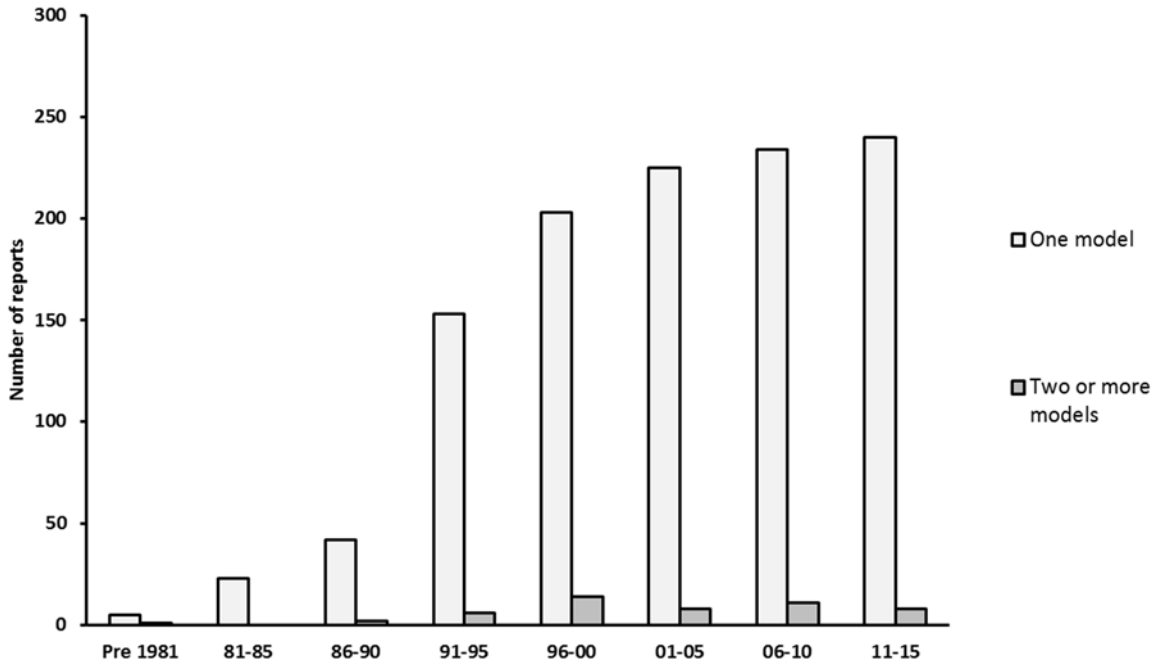

Figure 3.34 Time trends for number of models within report in rat hepatic IRI studies

Table 9 The distribution of model multiplicity in rat hepatic IRI studies over time

Period	Number of models in study		
	One model	Two models	Three models
Pre 1981	5	1	0
1981-1985	23	0	0
1986-1990	42	1	1
1991-1995	153	5	1
1996-2000	203	11	3
2001-2005	225	8	0

2006-2010	234	9	2
2011-2015	240	7	1

Trends in intervention types for rat hepatic IRI studies

As demonstrated in Figure 3.35, reports comparing various rat hepatic IRI models and/or ischaemia times have reduced in numbers since the 1990s. On the other hand, reports exploring outcomes related to a single methodology of hepatic IRI have remained stable in numbers following a relative decline in the early 2000s. In comparison, a prominent rise has been observed in the number of reports investigating other interventions (medicinal/ physical/ pathological … etc) on a background of hepatic IRI following the late 1980s but these numbers have plateaued in the past decade. These studies by far remain more common than investigating hepatic IRI in isolation.

Time trends for intervention types within reports are summarised in Table 10.

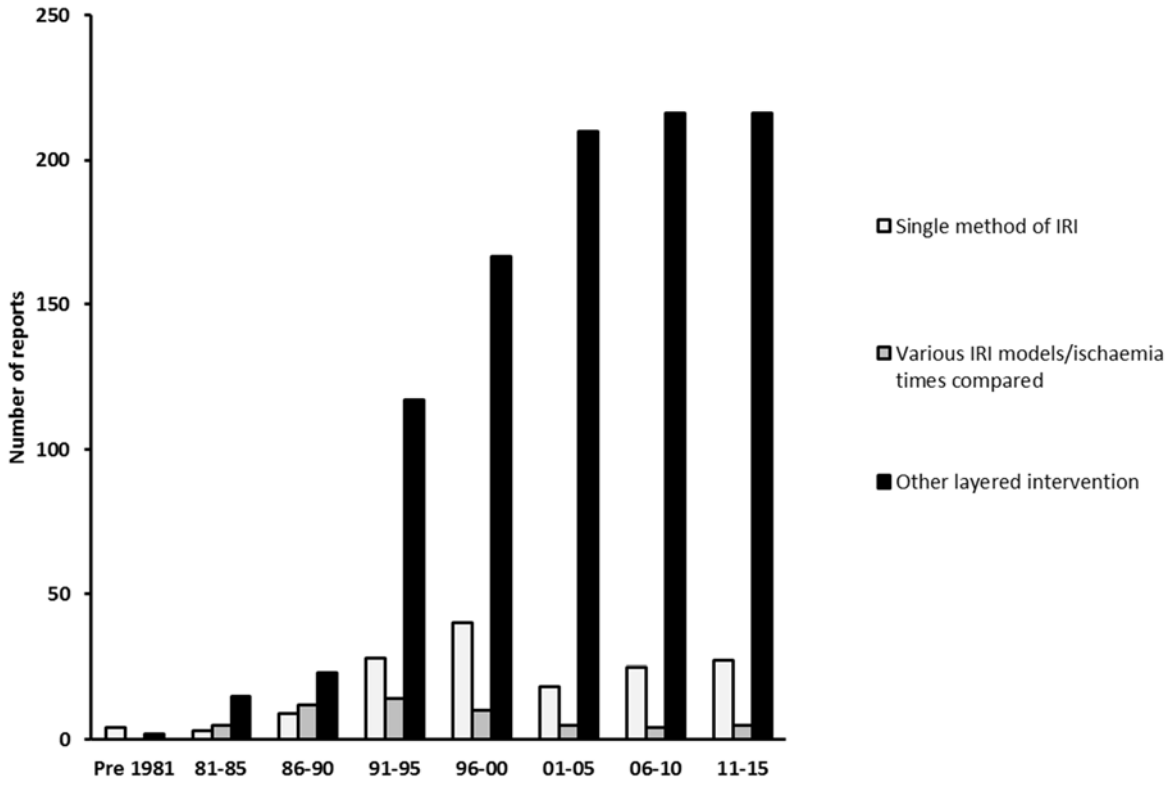

Figure 3.35 Time trends for intervention type in rat hepatic IRI studies

Table 10 The distribution of intervention type in rat hepatic IRI studies over time

Period	Intervention type		
	Single method of IRI	**Various IRI models/ischaemia times compared**	**Other layered intervention**
Pre 1981	4	0	2
1981-1985	3	5	15
1986-1990	9	12	23
1991-1995	28	14	117
1996-2000	40	10	167
2001-2005	18	5	210
2006-2010	25	4	216
2011-2015	27	5	216

3.3.4. Associations between hepatic IRI models and other variables

Use of heparin

There was a statistically significant association between heparin administration and total inflow occlusion models that incorporated immediate portosystemic shunts [X^2 (1)=102.635; P>0.0005]. This association was moderately strong [Cramer's V=0.296]. A further significant association was demonstrated between heparin administration and total inflow occlusion models with splenic transposition [Fisher's exact P=0.001]. On the other hand, 70% inflow occlusion models (with or without 30% hepatectomy) were significantly associated with less use of heparin [X^2(1)=6.946; P=0.008 and X^2 (1)=9.247; P=0.002 respectively]. The associations was small in both groups [Cramer's V<0.1]. Of note, 70% inflow occlusion models with ligation of the non-ischaemic 30% liver were not significantly associated with heparin usage.

No significant association was noted between the use of heparin and any other hepatic IRI model in rat studies.

Choice of rat strain

Total inflow occlusion without portosystemic shunting was significantly associated with the use of Wistar rats [X^2 (1)=6.159; P=0.013]. A significant negative association was demonstrated between this model and the use of Fischer and Zucker rats [X^2 (1)=7.584; P=0.006 and X^2 (1)=6.349; P=0.012 respectively].

Models incorporating splenic transposition for portosystemic shunting were significantly positively associated with the use of Wistar rats [X^2 (1)=7.687; P=0.006] and negatively associated with the use of Sprague Dawley rats [X^2 (1)=4.648; P=0.031].

While 20% (right lobe) hepatic IRI models (without hepatectomy) exhibited a significant positive association with the use of Wistar rats [X^2 (1)=15.893; P<0.0005] and a significant negative association with the use of Sprague Dawley rats [X^2 (1)=12.994; P<0.0005], the reverse was noted with 70% IRI non-hepatectomy models, which were significantly positively associated with Sprague Dawley rat utilisation [X^2 (1)=16.993; P<0.0005] and significantly negatively associated with the use of Wistar rats [X^2 (1)=31.954; P<0.0005]. Non-hepatectomy 70% IRI models were also significantly positively associated with the use of Fischer and Zucker rats [X^2 (1)=18.496; P<0.0005 and X^2 (1)=5.742; P=0.017 respectively]

Lewis rats demonstrated a significant positive association with both 70% and 20% IRI models that incorporated non-ischaemic lobe resection [Fisher's exact P=0.013 and 0.031 respectively]. Zucker rats, on the other hand, demonstrated a significant positive association with 40% (median lobe) IRI models with hepatectomy [Fisher's exact P<0.0005].

Similar to 20% IRI non-hepatectomy models, portal vein occlusion models were significantly positively associated with Wistar rats and negatively associated with Sprague Dawley rats as chosen strain choice[X^2 (1)=8.609; P=0.003 and X^2 (1)=6.739; P=0.009 respectively].

All the above associations were considered small [Cramer's V<0.15]. No other significant association was identified between hepatic IRI models and choice of rat strain.

The distribution of chosen strains across IRI models reported (with significant associations) is summarised in Table 11.

Table 11 The distribution of chosen strains across IRI models reported (only models with significant associations are displayed)

IRI model	Strain						
	Wistar	**Sprague Dawley**	**Fischer**	**Lewis**	**Zucker**	**Other**	**Not mentioned**
Total inflow occlusion (no shunt)	155	94	0	9	0	7	4
Total inflow occlusion (immediate shunt)	30	27	0	3	0	2	2
Total inflow occlusion (splenic transposition)	17	2	0	1	0	0	1
20% IRI	24	1	0	1	0	0	1
20% IRI + hepatectomy	4	4	0	3	0	2	0
70% IRI	225	231	21	26	14	12	7
70% IRI + hepatectomy	42	24	1	7	3	0	1
40% IRI	0	1	0	0	0	0	0
40% IRI + hepatectomy	2	0	0	0	3	2	0
Portal vein	20	3	1	1	0	0	0
Hepatic artery	12	3	1	2	0	0	0

Animal gender

A significant positive association was identified between models that incorporate portosystemic tube shunts or hepatic artery occlusion alone and the choice of female rats [Fisher's exact P=0.002 and 0.006 respectively] compared to males.

In contrast, 70% IRI non-resection models were significantly associated with male rats in comparison to female [$X^2(1)=13.869$; $P<0.0005$].

No statistically significant association was noted between other IRI models and rat gender. The distribution of chosen rat gender across IRI models reported is summarised in Table 12

Table 12 The distribution of gender across rat IRI models reported (major models displayed for comparison)

IRI model	**Gender**	
	Male	**Female**
Total inflow occlusion (no shunt)	231	24
Total inflow occlusion (tube shunt)	47	11
Total inflow occlusion (splenic transposition)	19	0
20% IRI	24	2
20% IRI + hepatectomy	9	1
70% IRI	488	15
70% IRI + hepatectomy	67	8
40% IRI	1	0
40% IRI + hepatectomy	6	0
Portal vein	24	1
Hepatic artery	13	5

Mean age of animals

No statistically significant difference was noted between hepatic IRI models with regards to mean rat age [F(8,118)=0.693; P=0.697].

Mean weight of animals

No statistically significant difference was noted between hepatic IRI models with regards to mean rat weight [F(10,1052)=1.640; P=0.091].

Bile duct involvement

A statistically significant association was found between bile duct clamping and total inflow ischaemia models (without portosystemic shunting or with tube shunts) [$X^2(2)=62.768$ and $X^2(2)=54.690$ respectively; $P<0.0005$]. The association in both cases was moderately strong [Cramer's V=0.2]. A statistically significant association was also found between bile duct clamping and 70% IRI models with 30% hepatectomy [X2(2)=7.026; P=0.03] although the effect size was small [Cramer's V=0.07].

Unsurprisingly, a statistically significant association was noted between isolated portal vein or hepatic artery occlusion models and bile duct sparing. No statistically significant association was noted between other IRI models and bile duct involvement.

The distribution of reported bile duct involvement across IRI models is summarised in Table 13.

Table 13 The distribution of reported bile duct involvement across IRI models (major models displayed for comparison). Cases where bile duct involvement was not mentioned are not shown.

IRI model	**Bile duct involvement**	
	Bile duct clamped	**Bile duct spared**
Total inflow occlusion (no shunt)	144	9

Total inflow occlusion (tube shunt)	47	0
Total inflow occlusion (splenic transposition)	7	1
20% IRI	1	0
20% IRI + hepatectomy	1	0
70% IRI	160	27
70% IRI + hepatectomy	26	0
40% IRI	1	0
40% IRI + hepatectomy	4	0
Portal vein	3	22
Hepatic artery	3	14

Maximum ischaemia time

The average maximum duration of ischaemia was statistically significantly different for the different IRI models reported [Welch's $F(10,105.110)=47.789$; $P<0.0005$]. Post hoc tests showed that the average maximum ischaemic time was significantly lower in total inflow IRI models (without portosystemic shunting) and in portal vein occlusion models compared to most other hepatic IRI models in rats. Interestingly, average maximum ischaemia times were significantly higher in models that incorporated portosystemic shunts compared to selective 70% ischaemia models by a factor of 14.253 (95%CI 0.24-28.27; P=0.043).

A summary of the average maximum ischaemia times for each major IRI model is described in Table 14.

Table 14 Average maximum ischaemia times for major IRI models

IRI model	Average maximum	SEM	95% CI for mean

	ischaemia duration (min)		
Total inflow occlusion (no shunt)	36.21	1.028	[34.19, 38.23]
Total inflow occlusion (tube shunt)	80.6	4.026	[72.56, 88.64]
Total inflow occlusion (splenic transposition)	65.95	6.071	[53.29, 78.62]
20% IRI	91.73	7.173	[76.96, 106.5]
20% IRI + hepatectomy	59.23	7.882	[42.06, 76.4]
70% IRI	66.34	1.296	[63.8, 68.89]
70% IRI + hepatectomy	66.69	2.936	[60.84, 72.54]
Portal vein	36.32	5.254	[25.28, 47.35]
Hepatic artery	62.73	6.338	[48.61, 76.85]

Maximum reperfusion time

The average maximum duration of reperfusion (excluding survival analyses) was statistically significantly different for the different IRI models reported [Welch's $F(10,66.978)=6.270$; $P<0.0005$].

The most striking finding on post hoc tests was that the average maximal reperfusion duration was significantly lower in 70% ischaemia models coupled with 30% liver ligation (rather than resection) when compared to other models such as selective 70% ischaemia alone (1693; 95%CI 350.1-3035.8; P=0.003) or portal vein clamping (2250; 95% CI 260.3-4239.7; P=0.02).

A summary of the average maximum reperfusion times for each major IRI model is described in Table 15

Table 15 Average maximum reperfusion times for major IRI models (excluding reperfusion times for survival analyses)

IRI model	Average maximum reperfusion duration (min)	SEM	95% CI for mean
Total inflow occlusion (no shunt)	1207.78	245.729	[723.54, 1692.01]
Total inflow occlusion (tube shunt)	8045.17	1816.154	[4330.71, 11759.62]
Total inflow occlusion (splenic transposition)	7119.23	3436.152	[-367.5, 14605.96]
20% IRI	1913.65	1652.774	[-1490.3, 5317.61]
20% IRI + hepatectomy	13536	7545.93	[-7414.86, 34486.86]
70% IRI	2472.41	658.558	[1178.47, 3766.35]
70% IRI + hepatectomy	12365.12	6397.327	[-564.36, 25294.6]
70% IRI + 30% ligation	451.62	69.961	[309.73, 593.51]
Portal vein	2701.58	541.637	[1563.64, 3839.52]
Hepatic artery	390	233.624	[-138.49, 918.49]

3.3.5. Survival analysis

Survival analyses were reported in 251 (27.2%) studies. The modal observation (reperfusion) period for survival was 10080min (7 days) and ranged from 20-525600min. The frequency distribution of reported observation periods for survival analyses is summarised in Table 16.

Table 16 The frequency distribution of reported observation periods for survival analyses

Observation period	Number of reports
1 day	27
2 days	5
3 days	13
4 days	1
5 days	7
7 days	113
8 days	3
10 days	8
14 days	8
15 days	6
21 days	5
23 days	2
30 days	14
3 months	1
12 months	1

In order to identify factors related to survival based on this review, multiple linear regression analysis was performed using reported survival rates as a dependent variable. A number of independent variables were considered in this analysis including year of publication, gender, average weight, heparin administration, bile duct involvement, duration of ischaemia, duration of reperfusion and IRI procedure. This model predicted survival rate with statistical significance [$F(8,296)=13.323$; $P<0.0005$).

As demonstrated in Table 17, it is apparent that, of all independent factors, only IRI procedure and duration of ischaemia contributed significantly to the regression model and therefore, to the prediction of animal survival.

Table 17 Summary of coefficient statistics for independent variables in multiple linear regression model

Variable	B (regression coefficient)	95% CI	P value
Year of publication	0.203	[-0.302, 0.709]	0.429
Gender	7.023	[-4.976, 19.021]	0.25
Average weight	0.015	[-0.085, 0.114]	0.774
Heparin administration	-6.389	[-16.112, 3.335]	0.197
Bile duct involvement	3.564	[-0.375, 7.504]	0.076
Duration of ischaemia	-0.510	[-0.628, -0.392]	<0.0005
Duration of reperfusion	-0.00001	[-0.0002, 0.00001]	0.099
IRI procedure	-0.725	[-1.389, -0.062]	0.032

A breakdown of average survival rates based on reported IRI models and ischaemia times is outlined in Table 18.

Table 18 Breakdown of average survival rates based on reported IRI models and ischaemia times (SEM and range omitted if n<2)

Procedure	Ischaemia time	Average survival (%)	SEM	Range (min)	Range (max)
Total hepatic occlusion	30	100			
	45	100			
	60	100			
Total hepatic occlusion + aortic clamp	30	100	0	100	100
	45	42.5	28.5	14	71

	60	0	0	0	0
Total inflow occlusion – no portosystemic shunt	30	61.7	10.1	12	100
	45	56.3	10.9	0	100
	60	32	9.9	0	100
	90	27.8	13.4	0	100
Total inflow occlusion and 70% hepatectomy – no portosystemic shunt	30	57.4	11.2	33.3	100
	60	0			
Total inflow occlusion with single-stage portosystemic shunt	30	100	0	100	100
	45	75			
	60	75.8	5.9	35	100
	90	22.9	3.9	0	100
	120	9.8	5.1	0	62.5
Total inflow occlusion and 70% hepatectomy with single-stage portosystemic shunt	60	30	5.8	20	40
Splenic transposition	60	71.5	16.7	0	100
	90	42.7	18.6	13	77
	120	0	0	0	0
92% inflow occlusion (excluding caudate) + 8% hepatectomy	45	100			
	60	70			
	90	100			

	120	60			
70% inflow occlusion (Left/middle)	30	95.1	4.9	41.7	100
	45	93.3	3.4	80	100
	60	85	4.1	10	100
	90	49	14.3	0	100
	120	61.1	11	14	100
	180	10	0	10	10
70% inflow occlusion (Left/middle) + 30% hepatectomy	30	95.7	2.8	85	100
	60	62.2	7	0	100
	90	33.8	5.8	0	66
	120	30.8	13.4	0	65
70% inflow occlusion (Left/middle) + 30% ligation	60	100	0	100	100
	120	0			
40% inflow occlusion (middle) + 60% hepatectomy	60	90			
	90	0	0	0	0
20% inflow occlusion (right) + 70% hepatectomy	60	32.9	14.3	0	100
	90	5	5	0	10
Portal vein alone	30	100			
	45	100			
	60	100			
	90	100			
	120	70			
Hepatic artery alone	60	92.4			

	120	15			

3.4. Discussion

The main objective of this literature review was to identify the ideal design for an in vivo hepatic IRI model that would be most suited to address the research questions of this project (see section 1.5). The initial task was to identify the most appropriate species for the model and that was resolved following a brief review of the published literature on experimental hepatic IRI. As explained in section 3.1.1, rodent models of hepatic IRI continue to be utilised in significantly larger numbers compared to larger animals due logistical, ethical and financial reasons. Rats were chosen over mice for this project due to relative ease of tissue handling and lesser need for microsurgical expertise. Therefore only reports of hepatic IRI in rats were considered in this literature review.

The choice of animal gender was important as certain-sex-dependent factors have been shown to affect the outcome of hepatic IRI studies (Gasbarrini et al., 2001, Harada et al., 2001, Harada et al., 2004). As evident from the results of this review, the vast majority of studied rats were male. A decision was made to use male rats only in this project in order to avoid the potential confounding effect of cyclic female hormones. The results of this review show that Wistar and Sprague Dawley rats were the two most commonly utilised strains. No clear advantage was demonstrated for the use of either strain over the other. Moreover, there was no requirement for the use of any specialist strain (such as Zucker rats) in this project.

Given that the focus of this project is to investigate long-term complications of hepatic IRI, namely NABS and peri-portal fibrosis, previously published reports investigating these outcomes were sought in the literature review. This highlighted only two reports that had examined the long-term effect of hepatic IRI on biliary pathology. One of these reports identified that hepatic IRI lead initially to an increased rate of biliary epithelial cell apoptosis followed by ductal proliferation of intrahepatic bile ducts (Xu et al., 2004). The second report examined the degree of long-term ductal proliferation and portal fibrosis following intraoperative radiotherapy on a background of hepatic IRI and thus, was not purely focused on direct effects of hepatic IRI (Hahn et al., 2007). Not only was the literature lacking in rat models that addressed the causal relation between hepatic IRI and delayed biliary complications, it was also noted that the vast majority of published reports (96.8%) involved short-term follow up (<14

days). Therefore, there was a clear need for in vivo experimental research on this subject.

As outlined in section 3.1.3, there are a number of well described in vivo models to investigate hepatic IRI in the rat. However, this review has highlighted a handful of other, less commonly known models (or variations thereof), including the use of cirrhosis models (Takeda et al., 2003, Tsuchiya et al., 2003) or caecal herniation (Rhee et al., 2002) in conjunction with total inflow occlusion, or the combined occlusion of main hepatic artery and branch of portal vein (Karwinski et al., 1993, Xiang et al., 2006) in order to avoid splanchnic congestion. These unconventional models are highlighted for academic purposes and were not considered further in this project due to lack of standardisation.

Based on the data presented in Table 6, it is clear that segmental (selective) and total inflow occlusion models are the most commonly reported models in the literature to investigate hepatic IRI in rats, segmental models being twice as commonly reported as total inflow occlusion models (61.9% versus 30.6% of total reports respectively). The remaining ‘conventional’ models include total vascular exclusion and isolated hepatic artery or portal vein occlusion. These models comprised just over 5% of all reported models and were deemed unsuitable for the requirements of this project because of the likely influence of inevitable factors such as partial ischaemia or haemodynamic instability on the validity and applicability of the results.

An ischaemic period longer than 30 minutes is required for a hepatic IRI rat model to produce long-term biliary pathology, (Xu et al., 2004). Given that rat liver cannot tolerate more than 30 minutes of main portal venous occlusion (van der Meer et al., 1971) a total inflow occlusion model would not be appropriate for this project without sufficient portosystemic shunting. However, this review has demonstrated higher rates of mortality associated with single-stage portosystemic shunting at ischaemic durations longer than 30 minutes in comparison to segmental ischaemia of comparable duration (Table 18). For example, 90 minutes of total inflow ischaemia with single-stage portosystemic shunting is associated with an average animal survival rate of 22.9±3.9% compared to 49±14.3% for a similar duration of ischaemia in a 70% segmental IRI model (P=0.017). This may be related to the higher risk of complications associated with portosystemic shunts (including bleeding and shunt thrombosis). The significant association demonstrated between shunt application and

use of heparin in this review highlights the perceived risk of shunt thrombosis by investigators (see section 3.3.4). Although the splenic transposition model demonstrated comparable average survival rates to segmental IRI models in this review, the questionable consistency and applicability of the data produced from such model rendered it less favourable (Suzuki et al., 1998). The inferior survival rates and reliability of data from portosystemic shunt models may explain the reduced popularity of these methods over the past decade (Figure 3.20).

While segmental hepatic IRI models deliver a reasonable balance between procedure severity, technical demand and model applicability, the potential influence of non-ischaemic lobes on results remains an outstanding issue. Investigators have previously overcome this potential problem by combining these procedures with ligation or resection of the non-ischaemic lobes. Bearing in mind that the main focus of this project is long-term biliary pathology and peri-portal fibrosis, a 4-week follow up duration will be necessary in order to adequately investigate these lesions. Such lengthy duration of follow-up will not be feasible if ligation of non-ischaemic lobes is performed due to the inevitable necrosis and abscess formation in the lobes ligated in-situ (Spiegel and Bahde, 2006). An interesting finding from this review is that the reported use of the uncoupled 70% ischaemia model (the most commonly performed segmental model) has continued to rise over the years while models that combine this technique with either ligation or resection of the non-ischaemic liver have been in continuous decline over the past decade despite the presumed superior validity of results associated with the latter models (Figure 3.21). The reasons why the uncoupled model remains more popular with investigators may be related to the relatively lower technical skills required or the reduced risk of complications (Madrahimov et al., 2006). Certainly, this review demonstrates significantly higher average survival rates associated with uncoupled 70% segmental hepatic IRI compared to the same model combined with 30% hepatectomy for ischaemia times above 30 minutes (average survival rate 85±4.1% versus 62.2±7% for 60 minutes ischaemia; P=0.004) (Table 18). Given the increased risk of animal mortality and limited availability of expertise in rat liver resection, a combined ischaemia/hepatectomy model was not considered further in this project.

In order to minimise the potential interference of non-ischaemic lobes in uncoupled segmental hepatic IRI models, and to maximise availability of injured hepatic tissue, it would appear logical to aim for a higher proportion of segmental hepatic ischaemia.

However, as would be expected, greater proportions of segmental ischaemia are associated with lower survival rates (Karatzas et al., 2014). As previously mentioned, the 70% segmental hepatic IRI model was found to be the most commonly reported hepatic IRI model in rats, comprising 56.6% of all reported models identified in this review (Table 6), and its reported use has seen a continuous linear rise over the years (Figure 3.21), despite it being the earliest hepatic IRI model described in rats historically (De Baker, 1956). It is likely that the popularity of this model is related to the balance it delivers between model refinement, ease of procedure and risk. For these reasons, the uncoupled 70% hepatic IRI model was selected as the model of choice for this project.

In addition to the type of hepatic IRI procedure, this review identified ischaemia time as the only other independent factor that predicted animal survival in a regression model (Table 17). Considering the need to develop a reproducible model of long-term biliary pathology and peri-portal fibrosis secondary to hepatic IRI in this project, an attempt was made to identify the longest duration of ischaemia that was associated with acceptable survival outcomes. The review highlighted that the commonest ischaemia times investigated were 30, 60, and 90 minutes (22.2%, 35.7% and 15.2% respectively) (Figure 3.16), and that the average survival rates for these ischaemia times in a 70% segmental hepatic IRI model were 95.1%, 85% and 49% respectively (Table 18). It is worth noting that 2 out of 8 reports of 90 minutes ischaemia using that model reported a survival rate of 100% (Yamada et al., 2007, Koneru et al., 1995). Greater ischaemia times were either insufficiently reported or associated with lower survival rates in this review. The only published report on delayed biliary pathology following hepatic IRI in rats demonstrated only short-lived biliary changes following 30 minutes ischaemia (Xu et al., 2004). On the other hand, this review highlighted a recent decline in the reported use of 90 minutes ischaemia for rat hepatic IRI studies in the literature (Figure 3.29). In spite of the above, and given the acceptable associated survival rates, it was decided to pilot all three common ischaemia times (30, 60 and 90 minutes) in order to identify the safest period that provided consistent long-term biliary and peri-portal pathology. Further details on the pilot in vivo IRI model are provided in Chapter 4.

Based on the information displayed in Figure 3.17, there appears to be an abundance of published data at the 60 and 120 minute reperfusion timepoints, but less data on later sub-24hr timepoints. This may explain the recent rise in reports of

the latter and decline in the former timepoints (Figure 3.31). For this reason a later sub-24hr reperfusion period (5 hours) was chosen as the earliest timepoint in the in vivo model for this project. As mentioned earlier in this section, the maximum reperfusion follow up timepoint was set at 4 weeks to adequately investigate long-term biliary pathology and peri-portal fibrosis.

With regards to anaesthetic use, this review has identified pentobarbital, ether and the combination anaesthetic - ketamine and zylazine as the three most commonly used anaesthetic agents for rat hepatic IRI studies (Figure 3.13). Nevertheless, the review also demonstrates that the use of the former two agents has been in decline over the past decade or so while the latter has seen a steady rise in use over the same period (Figure 3.24). Interestingly, isoflurane has also seen a considerable increase in its reported use since the mid-1990s (Figure 3.25), to the extent that it has recently surpassed ether as the third most commonly reported anaesthetic agent used in studies published between 2011 and 2015. A recent study has reported improved liver functions and reduced mortality associated with the use of isoflurane compared to ketamine and xylazine following hepatic IRI in rats (Steenks et al., 2010). Isoflurane was therefore selected as anaesthetic of choice for this project in view of its safety profile and availability.

The use of heparin was found to be most commonly associated with portosystemic shunt models in this review, which is likely due to the increased risk of thrombosis in these models. On the other hand, 70% partial IRI models were significantly associated with heparin omission from model procedure. In addition, a gradual decline in overall heparin use over the years in rat hepatic IRI models has been demonstrated (Figure 3.27). The growing evidence of anti-inflammatory properties identified in heparin (Zhou et al., 2002, Wang et al., 2002, Xie et al., 2000b) may explain the declining trend in its use in rat IRI models given the potential influence it could have on the results. However, this confounding anti-inflammatory effect remains disputed given the conflicting results on actual rat IRI models (Shibayama et al., 1991, Harada et al., 2006). Furthermore, such effect should be balanced against the potential confounding effect of intravascular coagulation particularly at longer occlusion times. Therefore, heparin was not omitted in the current project and controls were designed in order to balance any potential confounding anti-inflammatory effects from its use.

Although bile duct exclusion was reported in around 18% of studies that reported bile duct handling during rat hepatic IRI procedure, the actual percentage of studies is likely to be lower given that the bile duct would probably be included in the clamped pedicle in the remaining studies that did not report any bile duct procedure within the model design. The technique of bile duct exclusion prior to vascular occlusion requires a degree of technical competence and the rationale behind its use is to avoid the potentially confounding effect of cholestasis on hepatic IRI. However, such effect has not been confirmed in rat models and is countered by the possible altered production of glutathione and/or reactive oxygen species in the absence of bile duct clamping (Montero et al., 2005). Nevertheless, reports of bile duct exclusion in IRI models have continued to be published at a stable rate over the past decade (Figure 3.28). Interestingly, this review also demonstrated that IRI models that are more technically demanding (such as those including shunts or hepatectomy) were significantly associated with bile duct inclusion rather than isolation, possibly reflecting attempts to minimise further delays in operating time. In the current project, bile duct isolation was chosen as part of the model design given the potential for the model to involve longer occlusion times and the availability of expertise to perform the technique.

In conclusion, based on the evidence obtained from the literature review described in this chapter, a 70% segmental hepatic IRI rat model was chosen for the in vivo phase of this project using isoflurane anaesthesia. Various ischaemic times were chosen in the pilot stage of model development and a control arm was designed to balance the potential effects of heparin administration and bile duct exclusion. Delayed follow up timepoints were designated in order to adequately investigate long-term biliary pathology and peri-portal fibrosis. Further details of the in vivo phase of this project are described in Chapter 4.

Chapter 4. In vivo IRI model

4.1. Introduction

Hepatic IRI is an unavoidable process in liver transplantation. The concept was suggested in the late 1970s as a cause for the observed accelerated damage of liver tissue following restoration of oxygen delivery (Chien et al., 1977, Chien et al., 1978, Silver and Szabo, 1983) and the phrase “reperfusion injury” was first used in liver pathology in 1986 by Adkison et al to describe what had previously been attributed to ischaemic liver injury (Adkison et al., 1986). Scientific advances in this field have followed rapidly since then and It has become clear that hepatic IRI pathways are complex and intertwined as more details about the process continue to be unveiled (Gracia-Sancho et al., 2015). Hepatic IRI has been linked to early graft dysfunction and later complications of liver transplantation such as NABS (Mourad et al., 2014, Briceno et al., 2010). Therefore, it is necessary to briefly revisit the current knowledge on the pathogenesis of hepatic IRI in order to better understand its complications.

4.1.1. Stages of hepatic IRI

Hepatic IRI can be divided into three stages based on the predominant pathological feature of each stage.

The cold ischaemic (energy-depletion) stage

In the context of liver transplantation, this stage involves a period of cold preservation following disruption of blood flow to the liver. It is characterised by the rapid depletion of energy substrates leading to cellular damage and microcirculatory failure (Peralta et al., 2013).

Energy depletion

The early consumption of glycogen and the lack of oxygen in the ischaemic period results in a rapid depletion of ATP and other energy substrates within the cell. This triggers a state of homeostatic failure leading to disruption of energy-dependent membrane transport (mainly via the Na/K ATPase pump). This loss of

transmembrane gradient results in cellular swelling notably in Kupffer cells (KCs) and sinusoidal endothelial cells (SECs) (Vollmar et al., 1994).

Cold storage-related SEC damage

It is accepted that cold storage damage to SECs plays a key initiating role in transplant-related hepatic IRI (Gracia-Sancho et al., 2015). SECs are the most susceptible liver cells to cold storage injury, becoming activated, highly pro-inflammatory and apoptotic after 6 hours of cold storage (Russo et al., 2012, Gracia-Sancho et al., 2010). Indeed, in comparison to hepatocytes, where a significant proportion of cells can remain viable even after 48 hours of cold preservation followed by reperfusion, almost half of SECs rapidly lose viability following a brief period of cold ischaemia and reperfusion (Caldwell-Kenkel et al., 1989). SECs activated by cold storage injury promote platelet aggregation, vasoconstriction, KC activation, inflammatory cell recruitment, adhesion molecule expression and hepatocyte damage (Theruvath et al., 2006, Huet et al., 2004). The lack of biological circulatory stimuli in the cold storage environment alters the protective SEC phenotype by rendering it less antioxidant and antithrombotic (Gracia-Sancho et al., 2010).

Microcirculatory changes

Cold storage results in downregulation of the transcription factor Kruppel-like factor2 (KLF2), which amongst many things leads to a reduction of eNOS expression (Gracia-Sancho et al., 2010). As a result, a reduction in SEC production of the vasodilator nitric oxide (NO) ensues. This is also caused by lack of oxygen and energy substrates (Montalvo-Jave et al., 2008), and the increased breakdown of the NO precursor arginine through the enhanced release of arginase (Langle et al., 1995). This results in an imbalance between NO and endothelin formation that leads to vasoconstriction (Goto et al., 1994). In combination with SEC oedema, this leads to sinusoidal narrowing, leukostasis and platelet aggregation (Vollmar et al., 1996), resulting in further impairment of blood flow beyond the period of macrovascular occlusion, a phenomenon known as “no reflow” (Chun et al., 1994)

The early reperfusion (oxidative stress) stage

This stage occurs mainly within the first 2 hours of reperfusion and is characterised by the activation of resident Kupffer cells and by cellular injury mediate primarily through the formation of reactive oxygen species (ROS) (Teoh and Farrell, 2003).

Kupffer cell activation

KCs are activated by a surge in damage-associated molecular patterns (DAMPs) release from nearby necrotic cells (Zhai et al., 2011, Gracia-Sancho et al., 2015, Huang et al., 2011). The binding of these molecules to toll-like receptors (TLRs) on the surface of KCs leads to activation of the NFκB pathway through degradation of the inhibitory component IκB, allowing NFκB to translocate to the nucleus (Teoh, 2011). NFκB induces the synthesis of iNOS and pro-inflammatory cytokines, primarily TNF-α and IL-1, which promote further activation of KCs (and other inflammatory cells), expression of adhesion molecules on leukocytes and SECs and trigger apoptotic pathways (Lichtman and Lemasters, 1999).

Cold preservation has also been shown to induce strong activation of KCs (Arii et al., 1994)

Sources and effects of ROS

Activated KCs (and subsequently PMNs) are major sources of extracellular ROS, generating superoxide anions (O_2^-) through the induction of membrane-bound NADPH oxidase (El-Benna et al., 2008). Moreover, hepatocytes and SECs produce intracellular ROS through impaired mitochondrial function and potentially through the conversion of xanthine dehydrogenase to xanthine oxidase during reperfusion that follows prolonged ischaemic periods (Jaeschke, 2002, Peralta et al., 2013). In addition to simply reacting with macromolecules (leading to peroxidation of membranes, denaturing of proteins and oxidation of DNA), ROS are now also believed to stimulate apoptotic, inflammatory and other signal transduction pathways (Semenza, 2000, Teoh and Farrell, 2003).

The pH paradox, mitochondrial permeability transition and necro-apoptosis

During ischaemia, the intracellular pH within hepatocytes is very low due to anaerobic metabolism, but this paradoxically protects against cellular necrosis. Upon reperfusion, intracellular pH is restored and this leads to accelerated cell death (Lemasters et al., 1998). This phenomenon is explained by the pH-dependent onset of mitochondrial permeability transition (MPT).

In combination with high intra-mitochondrial Ca^{2+} levels, oxidative stress triggers the opening of MPT pores in hepatocytes (Kim et al., 2012). This results in permeability of the inner mitochondrial membrane and collapse of the mitochondrial membrane potential with the consequent swelling and rupture of mitochondria, and aggravation of ATP depletion (Lemasters et al., 2009). In the complete absence of ATP, this results in cellular necrosis. However, in cases of incomplete ATP depletion, the leakage of pro-apoptotic proteins such as cytochrome c, in combination with external activation via TNF-α and other cytokines, leads to the activation of caspase enzymes and initiation of the apoptotic pathway (Kim et al., 2003)

The late reperfusion (inflammatory) stage

This stage is characterised by inflammatory cell infiltration with further cell damage and necro-apoptosis. This stage commences approximately 6 hours after reperfusion (Teoh and Farrell, 2003).

Activation and recruitment of polymorphonuclear leukocytes (PMNs) and lymphocytes

Neutrophils are activated by DAMPs in addition to a number of cytokines (Huang et al., 2015). Moreover, the activation of complement pathways at an early stage in reperfusion results in the priming of KCs and neutrophils for enhanced ROS production and in the attraction of neutrophils (Jaeschke et al., 1993). Neutrophils along with other extrahepatic cellular entities become the predominant source of ROS production at later stages of reperfusion (Datta et al., 2013).

Various subsets of CD4+ T cells are also activated at a relatively early stage during reperfusion. These cells produce cytokines that further activate KCs (such as IFN-γ and GM-CSF) and others that recruit neutrophils (such as IL-17 and MIP-2), thus propagating the inflammatory response (Datta et al., 2013, Peralta et al., 2013).

The role of adhesion molecules

Neutrophils aggregate to the sinusoidal endothelium during the early stages of reperfusion (Sawaya et al., 1999). However, further adhesion is promoted by the expression of adhesion factors on both neutrophils and SECs (Teoh and Farrell, 2003). TNF-α and IL-1 promote the expression of complement receptor 3 (CR3 – CD11b/CD18) on the surface of PMNs (Witthaut et al., 1994) and the expression of intercellular adhesion molecules 1 (ICAM-1) and P-selectins on SECs (Young et al., 2001).

The role of chemokines and metalloproteinases

TNF-α, CXCL1, CXCL8, Macrophage inflammatory protein 2 (MIP-2) and other chemokines are expressed by KCs and parenchymal cells and result in further recruitment of PMNs (Chen et al., 2006, Hisama et al., 1996, Lentsch et al., 1998).

Metalloproteinases (such as MMP-9) produced by neutrophils are responsible for degradation extracellular matrix proteins, particularly fibronectin. This facilitates leukocyte chemotaxis and migration across the extracellular matrix (Hamada et al., 2009)

4.1.2. Ischaemia reperfusion injury and biliary epithelial cells

Despite significant advances in our knowledge on hepatic IRI, little has been established regarding the role of biliary epithelial cells and their interplay with other key cellular players in IRI. It is apparent that BECs are predisposed to cold preservation injury (Kukan et al., 1997) and are more vulnerable to reperfusion injury compared to hepatocytes (Noack et al., 1993). This may be related to greater production of ROS and lower baseline levels of protective glutathione in BECs

compared to hepatocytes (Noack et al., 1993). Moreover, BECs are more exposed to any potential cytotoxic effect of bile salt imbalance that may result from reperfusion injury (Buis et al., 2009), and are likely active drivers of the inflammatory response to reperfusion (see Chapter 2). Regardless of the underlying reason for this susceptibility, biochemical and morphological evidence of BEC injury following reperfusion persists for days to weeks following transplantation, and recovery from such injury is prolonged compared to hepatocytes or SECs (Kukan and Haddad, 2001, Cutrin et al., 1996). This may explain late biliary complications following liver transplantation such as NABS (Ayoub et al., 2010).

4.1.3. Susceptibility of the biliary epithelium to ischaemic injury: anatomical, physiological and embryological considerations

The vascular supply to the biliary tract is solely arterial, in contrast to most of the hepatic parenchyma, which receives both portal and arterial blood. This is delivered via the peri-biliary vascular plexus (PBVP), a complex vascular arrangement that forms multi-layered networks surrounding proximal intra-hepatic bile ducts, tapering into scattered capillaries distally (Nishida et al., 2006). The functions of the intrahepatic biliary tree and the hepatic arterial vasculature are inter-related and inter-dependent. In fact, the numerical correlation between hepatic arterial and biliary profiles in portal tracts is so strong that it has been proposed as an index for bile duct preservation or loss (Strazzabosco and Fabris, 2008).

Embryologically, normal development of the intrahepatic biliary epithelium is found to be crucial to the process of arterial vasculogenesis (Clotman et al., 2003). Moreover, in pathological conditions leading to ductal proliferation, a parallel growth of the intrahepatic arterial vasculature occurs as a result of the expression of angiogenic growth factors such as VEGF by the biliary epithelium, an adaptative mechanism that sustains the growing metabolic demand of the biliary tree (Fabris et al., 2006, Gaudio et al., 1996, Masyuk et al., 2003)

The dependence of the biliary tree on arterial blood supply is highlighted in the case of hepatic artery thrombosis which results in diffuse cholangiopathy due to ischaemia (Tzakis et al., 1985). In addition, biliary complications are almost inevitable in exclusively portal-perfused models of liver transplantation in animals (Li et al., 2011). The susceptibility of the biliary tree to ischaemic injury following orthotopic liver

transplantation in particular is exacerbated by a permanent interruption of more than 60% of the blood supply to the PBVP, originating from proximal vessels including the retroduodenal, retroportal, and gastroduodenal arteries (Northover and Terblanche, 1979) (Figure 1.3).

4.1.4. Challenges to understanding NABS

The pathogenesis of NABS remains largely obscure despite the impact of these lesions on graft survival after liver transplantation (Op den Dries et al., 2011). The diagnosis is made on radiological grounds (Buis et al., 2006) and very few clinical studies have described its underlying histological changes (Buis et al., 2006, Nishida et al., 2006, Abou-Rebyeh et al., 2003) particularly since biopsies are less likely to include medium to large bile ducts where the primary pathological changes occur (Cameron and Busuttil, 2005). This is also complicated by the fact that adjacent peri-portal areas may show marked variability in the severity of pathology (Cameron and Busuttil, 2005).

Animal models have been developed in the past to examine NABS and explore potential therapeutic strategies for these lesions (Cameron and Busuttil, 2005, Cheng et al., 2010b, Chen et al., 2009a, Zhao et al., 2008). However, the majority of these studies have been limited to short term outcomes whereas NABS commonly present late after transplantation. The choice of species for these models has also been problematic. The liver anatomy in larger animals such as pigs resembles more closely that in humans (Nykonenko et al., 2017). Liver transplantation in these animals is relatively less challenging than in small animals such as rats. However, these animals are more difficult to maintain in experimental conditions for longer-term follow up which may be necessary in interventional studies of NABS (Esmaeilzadeh et al., 2012).

Given that ischaemia and/or reperfusion are potentially important risk factors for the development of NABS during liver transplantation (Op den Dries et al., 2011), the substitution of a liver transplantation model with a hepatic IRI model is necessary in order to examine their role in isolation and eliminate the potential effect of allograft immunogenicity and anastomotic complications on the development of NABS. However, no hepatic IRI model with proven reliability to induce NABS has been reported to date.

4.1.5. Aim of study

1. To pilot an animal model of IRI (designed according to results from the literature search) and to identify the optimum ischaemia time in this model
2. To utilise the optimised model in the investigation of short and long term pathological events that occur following reperfusion including the development of NABS

4.2. Materials and methods

4.2.1. Ethical considerations

Local Ethical Review Committee (ERC) and Home Office approval for the animal models were obtained (project license PPL 60/3907; protocol 19b9) in this project.

All experiments were carried out in accordance with the Animals (Scientific Procedures) Act 1986 and in strict compliance with other local and national guidelines and policies.

4.2.2. Rat model of hepatic ischaemia-reperfusion injury and ischaemic cholangiopathy

A rat model of hepatic IRI formed the basis of this project. The procedure used was adapted from the well described partial (70%) ischaemia technique (Arab et al., 2009). In this model, bile duct was separated from the clamped inflow vessels in order to avoid concomitant cholestatic injury (Figure 4.1). Partial hepatic ischaemia avoids portal congestion which, if prolonged, may result in fatal haemodynamic instability and intestinal infarction (Kanazawa et al., 2011).

Animals

Male Sprague Dawley rats (Charles River, Margate, UK), weighting 350-500g were used in all studies. Animals were housed in light- and temperature-controlled conditions and allowed water and standard pelleted chow ad libitum.

Pilot procedure

Ten rats were divided into IRI (n=7) and control groups (n=3). On the day of the procedure, animals in both groups received appropriate analgesia and prophylactic antibiotics subcutaneously upon induction of anaesthesia (0.1mg/100g Meloxicam, 0.05mg/kg Buprinorphine and 150mg/kg Clamoxyl). Anaesthesia was induced in each animal using 5% isoflurane delivered via a vaporiser and mixed with oxygen at

5L/min into an anaesthetic chamber. Isoflurane 1-3% was delivered via a facemask to maintain anaesthesia. Animals were then shaved, cannulated and exposed to a laparotomy. Baseline blood samples were taken immediately prior to skin incision. Lobar vessels to the left and middle hepatic lobes were identified and separated from the corresponding bile duct branch (Figure 4.1). Intra-operative heparin (300IU/kg) was administered intravenously once the vessels were isolated. In the IRI group, these vessels were clamped for a period ranging between 30-90 minutes in order to induce lobar ischaemia-reperfusion injury and cholangiopathy. The lobar vessels in the control group were isolated but not clamped. Apart from clamping, animals in both groups were subjected to similar laparotomy conditions.

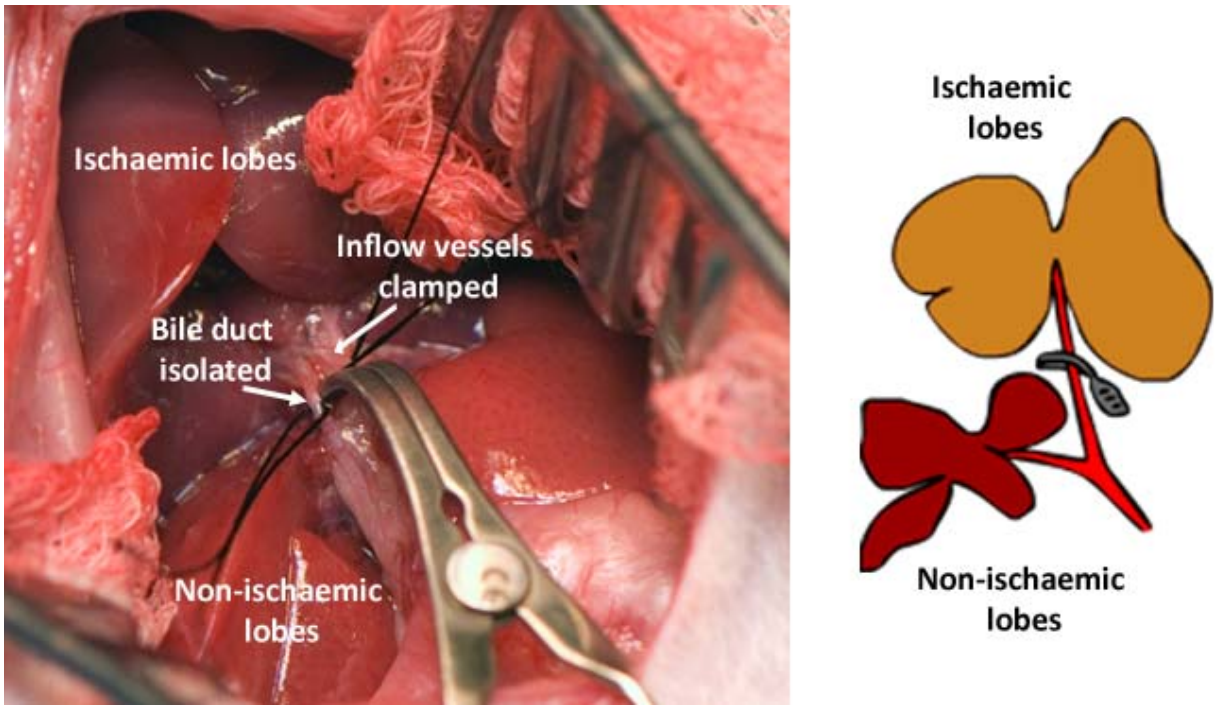

Figure 4.1 Partial hepatic ischaemia with bile duct isolation

During recovery from anaesthesia, a bolus of intravenous fluids was administered subcutaneously (10 ml 0.18% saline/4% glucose). Analgesia (0.05mg/kg Buprinorphine) was administered subcutaneously after 6-8 hours and on day 1 postoperatively while subcutaneous prophylactic antibiotics (150mg/kg Clamoxyl) were given on postoperative day 1 and 3. Further blood samples were taken immediately post-operatively in both groups.

Following recovery, animals were regularly weighed and examined for any deviation from normal health. Animals showing signs of ill health were treated by the named veterinary surgeon (NVS) of the animal unit or, if excessive, killed humanely by a schedule 1 method.

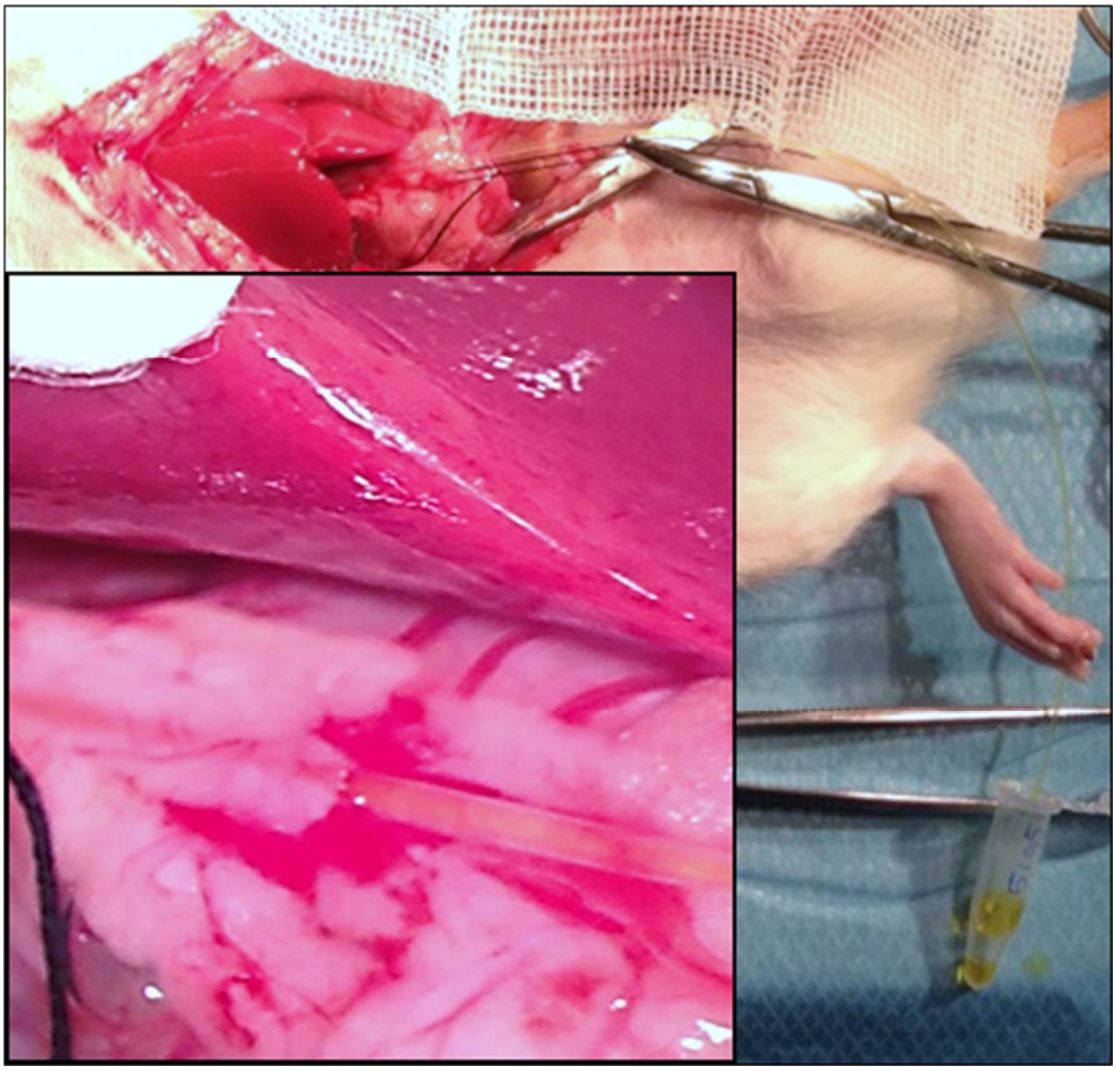

Figure 4.2 Bile duct cannulation. Cannula insertion point magnified.

After 28 days, the animals were exposed to a terminal laparotomy using an anaesthetic regime similar to the initial procedure. During the termination procedure, the common bile duct was cannulated to enable bile collection into pre-weighted tubes for sampling and bile flow measurement (Figure 4.2). Blood samples were also taken and the liver lobes were harvested for tissue analysis.

The pilot phase of the in vitro study focused on developing the IRI and cholangiopathy model. Thirty, sixty and ninety minute clamp times were tested (n=2 each) in order to identify the optimal warm ischaemia period (with maximal biliary damage and minimal mortality) and to ensure model reproducibility.

Cholangiography procedure

Cholangiography was performed by cannulating the common bile duct of an anaesthetised male Sprague Dawley rat and injecting 1ml of diatrizoate meglumine (Gastrograffin) into the bile duct followed by x-ray and CT imaging to assess the condition of the biliary tree. These animals were culled immediately following imaging.

Optimised procedure for hepatic ischaemia reperfusion injury and cholangiopathy

Rats were divided into IRI and control groups (n=21 per group). Peri-operative analgesia, antibiotic and anaesthetic regimes were similar to those described in the pilot procedure, in addition to preoperative preparation and fluids management.

Intraoperatively, lobar vessels to the left and middle hepatic lobes were identified and separated from the corresponding bile duct branch. Intra-operative heparin was administered as described in the pilot procedure. In the IRI group, these vessels were clamped for 90 minutes (identified from the pilot study as the optimal clamp time to induce lobar ischaemia-reperfusion injury and cholangiopathy). The lobar vessels in the control group were isolated but not clamped. In accordance with the pilot procedures, animals in both groups were subjected to similar laparotomy conditions apart from vessel clamping. Baseline blood samples were taken pre- and post-operatively in both groups.

Following recovery, animals were regularly weighed and examined for any deviation from normal health. Animals showing signs of ill health were treated by the NVS or, if excessive, killed humanely by a schedule 1 method.

Every three animals in each group were assigned a certain time point for termination (5 hours, 1, 3, 6, 10, 14 or 28 days postoperatively) where they were exposed to a second laparotomy. Bile, blood and liver tissue procurement was performed in a manner similar to that described in the pilot procedure.

4.2.3. Sample processing and preservation

Reagents used for sample processing

Formalin (product code HT501128), ethanol (product code 459836), xylene (product code A5597) and isopropanol (278475) were purchased from Sigma-Aldrich.

TRIzol reagent: Purchased from Life Technologies (product code 15596-026) as a ready-to-use solution.

RIPA buffer and cell lysis buffer as described in section 2.2.6.

Processing of tissue samples obtained from animals

Liver tissue

For light microscopy tissue imaging, slices of liver from ischaemic and non-ischaemic lobes were fixed in 10% neutral buffered formalin for 48 hours in room temperature and then stored briefly in 70% ethanol. The fixed samples were then dehydrated in increasing concentrations of ethanol followed by xylene and subsequently embedded in paraffin blocks for long-term storage. Sections (5μm thick) were cut from the paraffin blocks using a microtome and then mounted on frosted microscope slides for staining.

Samples obtained from ischaemic and non-ischaemic lobes for protein extraction were placed in 1.5 ml centrifuge tubes and snap-frozen in liquid nitrogen. These samples were stored in -80°C long-term and were used for a range of protein and biochemistry assays. Tissue homogenate was prepared by transferring a small piece (40-100 mg) of sample to RIPA or cell lysis buffer (100 mg/ml) and homogenising the tissue manually using a plastic pestle. Samples were then sonicated on ice in 2 bursts (5 seconds each) with a 30-second interval between sonication bursts in order to prevent sample overheating and protein denaturation (Nelson et al., 2006). The

homogenised samples were left for 30 minutes at 4°C to maximise protein extraction and then centrifuged at 5000 RPM for 5 minutes at 4°C. Supernatants were extracted and kept at -80°C for long-term storage.

Smaller samples from ischaemic and non-ischaemic lobes were obtained for mRNA extraction. These were finely diced and placed in 1.5 ml centrifuge tubes with 1ml Trizol reagent, snap-frozen in liquid nitrogen and kept in -80°C for long-term storage. RNA was extracted from these samples using the guanidinium thiocyanate phenol chloroform extraction method (Chomczynski and Sacchi, 1987). Samples were initially homogenised manually using a plastic pestle and then incubated for 10 minutes at room temperature to maximise permeation of reagent into homogenised tissue and facilitate RNA dissociation. Chloroform (200µl per ml of TRIzol reagent) was added to the homogenate suspension and mixed on a vortex for 15 seconds. The mixture was then left to stand for 5 minutes at room temperature and centrifuged at 12000 X g for 15 minutes at 4°C. The resulting aqueous phase supernatant was transferred to a clean tube and mixed well with 500µl of 100% isopropanol. The mixture was left to stand for 15 minutes at room temperature and subsequently centrifuged at 12000 X g for 10 minutes at 4°C. The resulting RNA pellet was washed with 1ml of 70% ethanol, mixed on a vortex for 5 seconds and then centrifuged at 7500 X g for 5 minutes at 4°C. The ethanol wash was then discarded. The remaining RNA pellet was left to air dry for 10 minutes; resuspended in RNAse-free water and then quantified using a NanoDrop 2000 spectrophotometer (Thermo Fisher Scientific).

For transmission electron microscopy (TEM) imaging, fine samples (less than 2 mm^3) from ischaemic and non-ischaemic lobes were placed in 2% gluteraldehyde in 0.1M sodium cacodylate buffer and stored overnight in 4°C. These samples were subsequently post fixed in 1% osmium tetroxide, dehydrated in increasing concentrations of acetone and then embedded in epoxy resin. Samples were then cut to ultrathin sections (70 nm), mounted on copper grids and stained with 2% uranyl acetate and 1% lead citrate.

Bile

Bile samples were collected in pre-weighted 0.6 ml centrifuge tubes and then weight to determine approximate bile volume. Bile samples were protected from light at all times and were stored long-term in -80°C.

Blood

Blood samples were collected in centrifuge tubes and left to clot for approximately 20 minutes in room temperature. Samples were then centrifuged at 5000 RPM for 5 minutes after which the supernatant serum was collected and stored long-term in -80°C.

4.2.4. Methods for protein analysis

Reagents used for protein analysis

Hyaluronan Quantikine Enzyme-linked immune sorbent assay (ELISA) kit: Purchased from R&D systems (product code DHYAL0). This was used to quantify hyaluronan levels in rat samples.

Muliplex Rat Cytokine/Chemokine Magnetic Bead Panel kit: Purchased from Merck Millipore (Product code RECYTMAG-65K-16). This kit was used to quantify levels of the following cytokines in rat samples using a MagPix system: MCP-1 (CCL2), MIP-1α (CCL3), MIP-1β (CCL4), MIP-2 (CXCL2), RANTES (CCL5), IP-10 (CXCL10), IFN-γ, TNF-α, IL-1α, IL-1β, IL-2, IL-4, IL-5, IL-6, IL-12 p70, IL-10, VEGF and EGF.

Reagents and methods for the Lowry method, gel electrophoresis and western blot are similar to those described in section 2.2.7.

Enzyme-linked immune sorbent assay (ELISA)

Hyaluronan levels in rat samples (serum, bile and liver homogenate) were quantified via ELISA using a kit purchased from R&D Systems. Samples (or standards) were mixed 1:1 with assay diluent in ELISA microplate wells coated with recombinant human aggrecan and incubated on horizontal shaker for 2 hours at room temperature. Wells were then aspirated and washed 5 times. Subsequently,

hyaluronan conjugate (recombinant human aggrecan conjugated to horseradish peroxidase) was added to each well and incubated on horizontal shaker for 2 hours at room temperature. A substrate solution (hydrogen peroxide and stabilised tetramethylbenzidine) was then added to each well and incubated for 30 minutes at room temperature. The chromogenic reaction was then stopped using a diluted hydrochloric acid solution and the absorbance of the resultant product was read at 540nm using a spectrophotometer. The unknown concentrations were calculated based on the calibration curve of the standards using a web-based data analysis programme capable of generating a four parameter logistic curve fit (www.myassays.com).

Cytokine multiplex array

Cytokine levels in rat samples (serum, bile and liver homogenate) were quantified using multiplex cytokine magnetic bead panel purchased from Merck Millipore. The assay is based on the Luminex xMAP technology using fluorescent beads coated with capture antibodies.

Samples (or standards) were mixed with assay buffer, matrix solution and pre-mixed 16-plex beads in equal volumes into appropriate wells of the 96-well plate provided with kit. The plate was then kept to incubate on a plate shaker for 2 hours at room temperature. The plate was then placed on a hand-held magnet and washed twice with wash buffer. Subsequently, pre-mixed detection antibodies were added to the wells and incubated on a plate shaker for 1 hour at room temperature. This was followed by the addition of Streptavidin-Phycoerythrin to the wells and further incubation for 30 minutes on a plate shaker at room temperature. The wells were then washed twice on the magnet with wash buffer and re-suspended in Drive Fluid on a plate shaker for 5 minutes at room temperature. The plate was run on a MagPix system and the results analysed using xPONENT software provided with the system.

4.2.5. Methods for mRNA quantification

Reagents used for mRNA quantification

RQ1 RNase-free DNase I (product code M610A), M-MLV Reverse transcriptase (product code M170B), Random Primers (product code C118A), dNTP Mix (product code U151B) and Pfu DNA Polymerase (product code M774A) were all purchased from Promega. SYBR® Green Jumpstart™ TaqReadyMix™ was purchased from Sigma-Aldrich (product code S9939) as were all gene-specific primers. MicroAmp® Fast Optical 96-Well PCR Reaction plates (product code 4346906) were purchased from Applied Biosystems. Primers were designed using NCBI Primer-Blast (Bethesda, MD, USA).

Real-time polymerase chain reaction (RT-PCR)

Quantitative analysis of mRNA expression was performed using SYBR green-based RT-PCR. RNA samples were treated with DNAse I to remove any contaminating genomic DNA. First strand complimentary DNA was synthesised from RNA samples using random primers and M-MLV Reverse Transcriptase using the manufacturers protocol (Promega, Madison, WI, USA) and a Hybaid PX2 thermal cycler (Thermo Fisher scientific). RT-PCR was performed using an Applied Biosystems 7500 Fast Real-Time PCR thermocycler (Applied Biosystems, Foster City, CA, USA) incorporating the primer sequences summarised in Appendix 3. Standard curves were generated using the included software (SDS 2.0.6) and 18S rRNA was used as reference gene to which the data was normalised.

4.2.6. Methods for tissue staining

Reagents used for staining

Meyer's Haematoxylin solution (product code MHS32), eosin solution (product code 318906) and Scott's tap water (product code S5134) were purchased from Sigma-Aldrich.

Picro-sirius red solution: Composed of 0.1% Sirius red dye in (1.3%) saturated aqueous solution of picric acid and used for collagen staining of tissue sections. Sirius red and saturated aqueous picric acid were both purchased from Sigma-Aldrich (product codes 365548 and P6744).

Tris-EDTA buffer: Composed of Tris base (10mM), EDTA (1mM) and Tween 20 (0.05%) in deionised water (pH 9.0). Used as a buffer for heat-mediated antigen retrieval.

Trypsin solution: Composed of Trypsin (0.05%) in deionised water. Used for enzyme-mediated antigen retrieval.

TBS-Triton X-100 wash buffer: Composed of Triton X-100 (0.025%) in 1X TBS. Used as a wash buffer for immunohistochemistry staining.

Antibody diluent: Composed of BSA (1%) in 1X TBS. Used as a diluent for primary and secondary antibodies during immunohistochemistry staining.

Hydrogen peroxide solution: Composed of hydrogen peroxide (0.3%) in 1X TBS. Used to suppress endogenous peroxidase activity in tissue and reduce background signals during immunohistochemistry staining.

Liquid 3,3'-diaminobenzidine (DAB) and substrate chromogen kit: Purchased from DAKO (product code K3468). The kit is composed of two components: DAB in chromogen solution and a substrate buffer (hydrogen peroxide in imidazole-HCl buffer, pH 7.5). The two components are mixed at a ratio of approximately 1:50 to form the chromogenic reagent which forms a brown stain at the site of the HRP-labelled antigen during immunohistochemistry staining.

DPX mounting medium: Purchased from Sigma-Aldrich (product code 44581) as a ready-to-use medium for cover slip mounting on stained sections.

Rehydration and dehydration of tissue sections

Tissue sections for staining were prepared as described in section 4.2.3. Tissue sections were de-waxed by immersion in 100% xylene followed by rehydration through serial immersion in decreasing concentrations of ethanol and finally in water.

Following staining, tissue sections were again dehydrated through serial immersion in increasing concentrations of ethanol followed by 100% xylene prior to mounting cover slips on slides using DPX mounting medium.

Haematoxylin and Eosin (H&E) staining

Slides containing rehydrated tissue sections were immersed in Meyer's haematoxylin solution for 30 seconds and then rinsed in running water followed by Scott's tap water solution for 10 seconds. Slides were then counterstained by immersion in Eosin solution for 10 seconds and then rinsed in running water for 5 minutes. Finally, sections were dehydrated and covered as previously described.

Sirius red staining

Slides containing rehydrated tissue sections were immersed in picro-sirius red solution for 1 hour in room temperature and then washed twice in acidified water (0.5% glacial acetic acid in deionised water). Tissue sections were then dehydrated and covered as previously described.

Immunohistochemistry

Immunohistochemistry staining was performed on paraffin-embedded tissue sections. Sections were deparaffinised and re-hydrated as described above.

Antigen retrieval

Two methods for antigen retrieval were used in this project. Heat-induced retrieval was the most commonly used method. Enzymatic retrieval was used for immune-detection of Proliferating Cell Nuclear Antigen (PCNA).

For heat-mediated antigen retrieval, rehydrated sections were transferred to a pressure cooker with boiling Tris-EDTA buffer and left for 1 minute under full pressure after which pressure was released and cooker cooled under running water.

Enzyme-mediated antigen retrieval involved the incubation of rehydrated sections in a trypsin solution pre-heated in a water bath at 37°C for 15 minutes. Sections were then removed from the water bath and rinsed in running tap water to remove any residual trypsin.

Immunohistochemistry staining

After antigen retrieval, slides were washed in TBS-Triton X-100 wash buffer twice for 5 minutes on a slow rocker at room temperature. Sections were then blocked using 20% FCS solution in PBS for 1 hour at room temperature. Excess blocking solution was subsequently drained and primary antibody of interest applied to sections and incubated overnight at 4°C.

On the following day, slides were washed in wash buffer twice for 5 minutes on a slow rocker at room temperature and then incubated in a 0.3% hydrogen peroxide solution for 15 minutes. This was followed by application of a suitable HRP-conjugated secondary antibody to the sections and incubation for 1 hour at room temperature. Finally, the slides were washed twice in wash buffer and then covered with a DAB substrate-chromogen solution for a suitable period to develop the enzyme-labelling stain.

Counterstaining

After development of the chromogenic stain, sections were counterstained by immersing slides in Meyer's haematoxylin for 1 minute and then rehydrated as previously described.

Analysis of tissue staining

Stained slides were scanned using a slide scanner (Leica SCN400) to enable remote visualisation and stain quantification. This was achieved using the web-based SlidePath Digital Image Hub and Tissue IA software provided by Leica microsystems (Weltzlar, Germany) and thus eliminated the potential for investigator bias. Inflammatory cell counts in H&E sections were normalised to the size of portal or central vein in each field of view as previously described (Wallace et al., 2010). Liver damage severity was graded on a scale from 0-5 as previously described (Marek et al., 2005). For all morphometric and structural histological analysis, slides were

assessed independently by two investigators blinded to the treatment groups and measurements were taken in at least nine portal tracts per specimen.

4.2.7. Examination of biliary epithelial cell microvilli under transmission electron microscopy (TEM)

TEM sections of rat liver tissue were prepared as described in section 4.2.3. Sections were then visualised using a Philips CM100 Transmission electron microscope (Philips/FEI Corporation, Eindhoven, The Netherlands) and images of the bile ducts and biliary epithelial cells were stored for further analysis. Microvilli were counted and microvillar dimensions and luminal circumferences of bile ducts were measured via ImageJ imaging analysis software (U.S. National Institutes of Health, Bethesda, Maryland, USA) using a scale bar plugin for microscopes. BEC microvillar density was measured by dividing the total number of luminal microvilli by the circumference of the bile ducts lumen in each cross section. This was measured in at least nine bile ducts per specimen.

4.2.8. Thiobarbituric Acid Reactive Substances (TBARS) assay

The TBARS assay protocol was used to estimate lipid peroxidation in rat serum and liver homogenate. The adduct formed from the reaction of malondialdehyde (MDA) with thiobarbituric acid (TBA) is measured spectrophotometrically to determine the level of TBA-reactive substances.

Reagents used for TBARS assay

Malondialdehyde bis(dimethyl acetal) (MDA): Purchased from Sigma-Aldrich (product code 108383). Prepared as a 1mM stock in deionised water and serially diluted to form the assay standard solutions.

Thiobarbituric Acid (TBA): Purchased from Sigma-Aldrich (product code T5500). Working reagent was prepared as a 5.2mg/ml solution in 10% acetic acid and adjusted to pH 3.5 with NaOH solution (10N).

Butylated hydroxytoluene (BHT): Purchased from Sigma-Aldrich (product code W218405) and prepared as a 5% solution in methanol. BHT was used as an anti-oxidant to prevent further oxidation of lipid during sample processing and the TBA reaction.

TBARS protocol

BHT was added to samples during sample processing to minimise ex-vivo lipid peroxidation. TBA reagent was added to each sample or standard in a 1.5ml centrifuge tube with vigorous mixing and then incubated on a heating block at 95°C for 45 minutes. Samples were then allowed to cool on ice for 5 minutes and then centrifuged at 3000 rpm for 15 minutes at room temperature. The supernatants were transferred to a 96-well plate and absorbance was read at 532nm on a microplate absorbance reader. The unknown concentrations were calculated based on the calibration curve of the standards using a web-based data analysis programme (www.myassays.com).

4.2.9. Bile acid assay

Bile acids were measured in rat serum, bile and liver homogenate using an enzymatic recycling method. The enzyme 3α-hydroxysteroid dehydrogenase (3α-HSD) in the presence of Thio-NAD+ converts bile acids to 3-keto steroids and Thio-NADH. This reaction is reversible and the enzyme 3α-HSD can convert the resultant 3-keto steroids in the presence of NADH back to bile acids and NAD+ thus recycling the bile acids. When excess NADH is used, the rate of Thio-NADH production can be measured spectrophotometrically by measuring the change in absorbance over time. Total bile acid concentration is derived from this measurement.

Reagents used for the bile acid assay

Dialab enzymatic recycling bile acid kit: Purchased from Alpha Laboratories (product code 903120). The kit is composed of buffered Thio-NAD (reagent 1) and buffered 3α-HSD mixed with NADH (reagent 2). The reagents were supplied as ready-to-use solutions for bile acid estimation.

Bile acid standard: Purchased from Alpha Laboratories (product code 903210). Used for the estimation of bile acids in conjunction with the Dialab bile acid kit.

Enzymatic recycling bile acid assay protocol

All reagents were pre-warmed to 37°C in a water bath. Reagent 1 was mixed with each samples or standard and incubated for 3 minutes at 37°C. This was followed by the addition of reagent 2 and further incubation at 37°C for 1 minute. Baseline absorbance was then read at 405nm using a spectrophotometer followed by further readings every minute up to 3 minutes. The average change in absorbance per minute was then calculated (δA) and the total bile acid concentration derived using the following formula:

Total bile acid (μM) = δA (sample) X standard concentration (μM) / δA (standard)

The assay is linear up to concentrations of 180μM. Samples with higher concentrations were diluted appropriately in 0.9% saline or PBS (for bile or liver homogenate samples respectively).

4.2.10. Phospholipid assay

Phospatidylcholine levels were measured in rat serum and bile using an enzyme-coupled assay. Phospatidylcholine is hydrolysed enzymatically releasing choline which is then oxidised producing H2O2. This reacts with a probe (Oxi-Red) generating a highly fluorescent product (Resorufin) proportionate to the concentration of phosphatidylcholine in the sample.

Reagents used for the phosphatidylcholine assay

Biovision phosphatidylcholine colorimetric/fluorometric assay kit: Purchased from Cambridge Bioscience (product code K576-100). This kit is composed of the following proprietary reagents: phosphatidylcholine assay buffer, OxyRed probe, phosphatidylcholine hydrolysis enzyme, phosphatidylcholine development mix and phosphatidylcholine standard. OxyRed probe and assay buffer are supplied in a ready-to-use form. Phosphatidylcholine hydrolysis enzyme and phosphatidylcholine

development mix are dissolved in assay buffer prior to use. Phosphatidylcholine standard is dissolved in 200µl of deionised water to prepare a 50mM phosphatidylcholine standard solution from which serial standard dilutions are prepared.

Phosphatidylcholine assay protocol

All reagents were pre-warmed to room temperature prior to use. A reaction mix composed of assay buffer, hydrolysis enzyme, development mix and OxiRed probe were added to each sample or standard in a 96-well plate and incubated for 30 minutes at room temperature. The absorbance was read at 570nm in a microplate reader and the unknown concentrations were calculated based on the calibration curve of the standards using a web-based data analysis programme (www.myassays.com).

4.2.11. Glutamate dehydrogenase assay

Glutamate dehydrogenase (GluDH) levels in rat serum, bile and liver homogenate were measured using a substrate-based assay. GluDH catalyses the reduction of α-ketogluterate to glutamate and the simultaneous oxidation of NADH to NAD+. The rate of reduction of absorbance (due to NADH depletion) is proportionate to GluDH activity in the sample.

Reagents used for the glutamate dehydrogenase assay

Dialab glutamate dehydrogenase assay kit: Purchased from Alpha Laboratories (product code D03773). The kit contains two reagents: reagent 1 is composed of triethanolamine (50mM), α-ketogluterate (7mM), ammonium acetate (100mM), EDTA (2.5mM) , ADP (1mM) and LDH (<1.5mM) and reagent 2 is composed of NADH (0.25mM). Both reagents are supplied as ready-to-use solutions.

Glutamate dehydrogenase assay protocol

All reagents and samples were pre-warmed to 37°C in a water bath. Reagent 1 was mixed with each samples or standard and incubated for 3 minutes at 37°C. Reagent 2 was then added followed by further incubation at 37°C for 1 minute. Baseline absorbance was read after 30 seconds at 340nm using a spectrophotometer followed by further readings every minute up to 5 minutes. The average change in absorbance per minute was then calculated (δA) and the GluDH activity derived using the following formula:

GluDH activity (U/L) = δA X 1485 (constant)

The assay is linear up to concentrations of 120U/L. Samples with higher concentrations were diluted appropriately in 0.9% saline or PBS (for serum/bile or liver homogenate samples respectively).

4.2.12. Serum liver function tests

Measurement of total protein, bilirubin, alkaline phosphatase, alanine transaminase and γ-glutamyl transferase levels in rat serum were performed at the clinical biochemistry laboratories of the Royal Victoria Infirmary in Newcastle upon Tyne.

4.2.13. Statistical analysis

Statistical methods used are those described in section 2.2.9.

4.3. Results

4.3.1. Results from the pilot hepatic ischaemia-reperfusion injury model

Animal survival

Of the ten rats employed in the pilot study, 3 died intraoperatively (30% mortality). Two animals died of sudden respiratory arrest (one rat was exposed to 30 minutes of IRI and the other rat was exposed to a control procedure). A third rat (from the control group) died due to uncontrolled intraoperative haemorrhage.

The procedure was revised in response to these incidents. Abdominal access was limited to a midline incision instead of an inverted T incision. Regular monitoring of vital signs was implemented and abdominal retractors were removed immediately following lobar clamping. Warm pads were kept under the animals throughout the procedure and moist swabs were placed over the abdominal wound during the ischaemic period. Following the implementation of these measures, no further episodes of sudden intra-operative respiratory arrest occurred.

Peri-portal fibrosis

The increase in ischaemia time had a significant effect on the degree of fibrosis on day 28 post IRI based on Sirius red staining [One-way ANOVA $F(4,8)=15.6$, $p=0.0008$]. The degree of fibrosis was found to be more severe and consistent in the 90-minute clamp group. Post hoc comparisons using the Bonferroni-Holm test indicated that average percentage of fibrosis in both the 90 and 30 minute groups (2.3±0.3% and 1.6±0.1% respectively) were significantly higher than those in the control groups and in the non-ischaemic lobes (0.6±0.1% in both; $p<0.05$). The 60-minute clamp group however demonstrated wide variation in fibrosis staining (0.7±0.7%) and was not significantly different from any of the other groups (Figure 4.3).

On that basis, the 90-minute clamp model was chosen due to its consistent results with severe fibrosis and a low incidence of mortality.

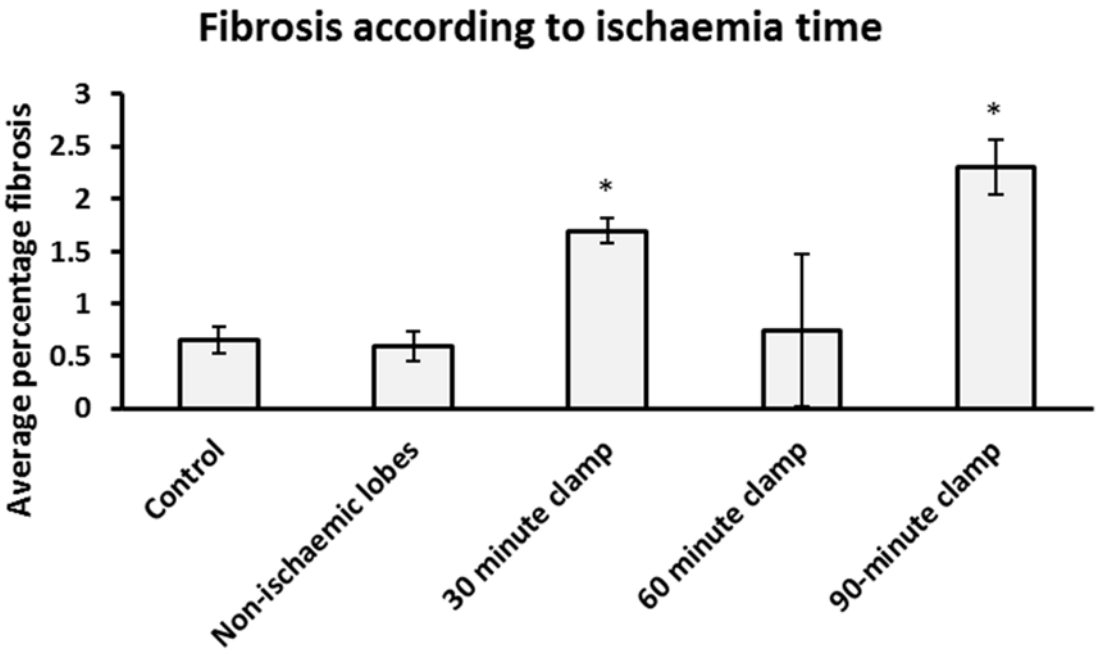

Figure 4.3 Average percentage of fibrosis in each study group in the pilot model based on Sirius red staining

Cholangiography results

Although bile duct cannulation was achieved in all animals with little difficulty, adequate visualisation of the biliary tree was not possible. The apparent reasons for this problem were twofold: Firstly, the diameter of the bile duct prevented downstream displacement of fluid in the biliary tree upon injection of contrast. This resulted in the build-up of pressure within the biliary tree and ultimately the disruption of ductules and leakage of contrast into the systemic circulation. Secondly, the resolution of the small animal CT scanner imaging was still insufficient to delineate any potential stenotic lesions within the biliary tree (Figure 4.4). After experimenting with various perfusion pressures, cannula sizes and cannulation techniques it became clear that no meaningful data could be obtained from rat cholangiography in its current approach and it was decided that the technique would not be further employed to develop the hepatic IRI model.

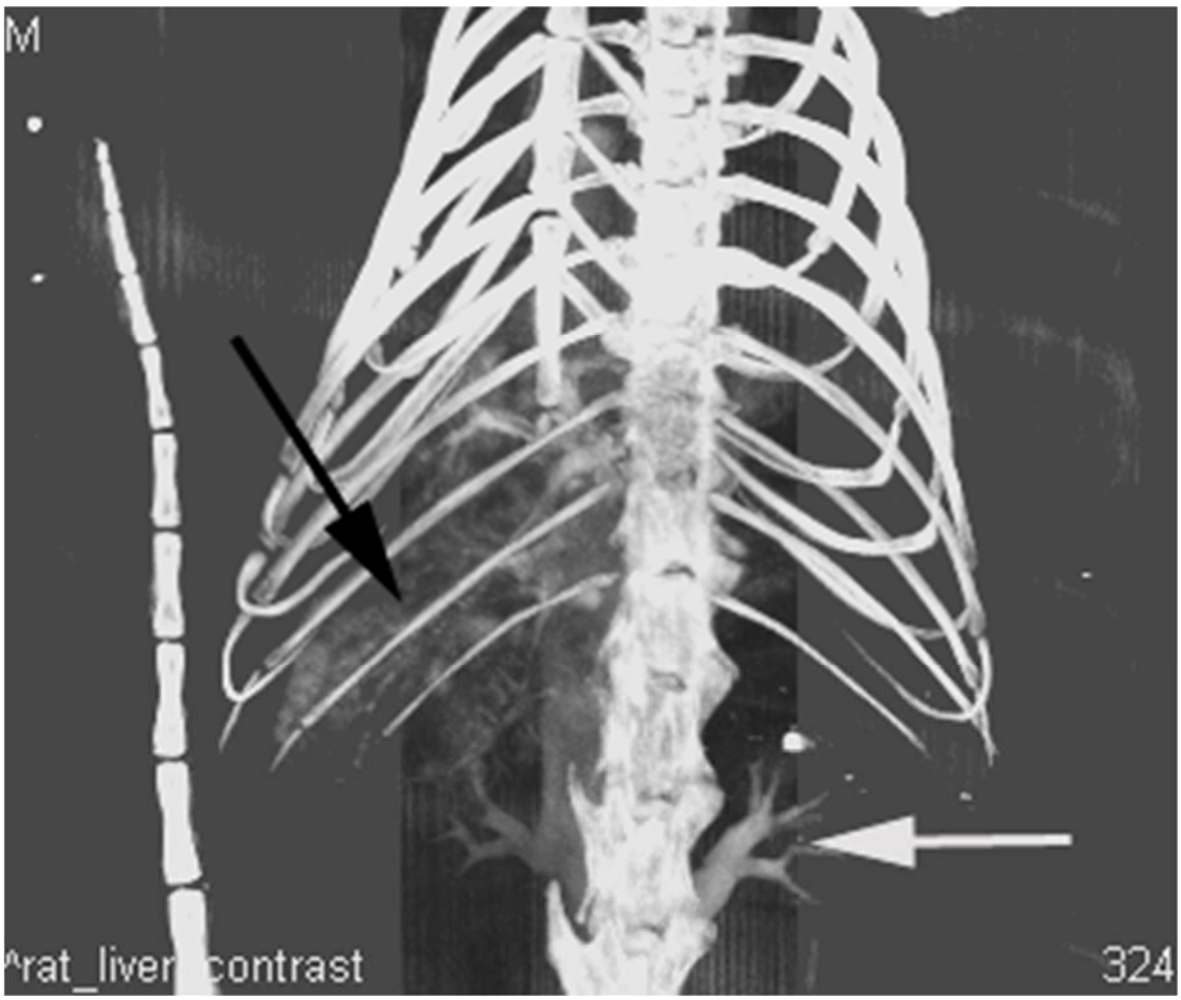

Figure 4.4 CT cholangiogram showing low-resolution outline of biliary tree (black arrow) but also showing leakage of contrast into systemic circulation as evident in the outlined renal vein (white arrow)

4.3.2. Results from the optimised hepatic ischaemia reperfusion injury and cholangiopathy model

Following the pilot study, the hepatic ischaemia reperfusion injury and cholangiopathy model involved an additional 50 rats and the procedure was optimised according to the pilot data. Most importantly, all animals in the clamp group were exposed to 90 minutes of ischaemia.

Mortality rates

Eight out of 50 rats died during the optimised phase of the study. Of these, two rats were killed accidentally (opiate overdose in one case and overheating of faulty

thermal pad in another). The remainder of fatalities were due to uncontrolled intraoperative bleeding (n=4) or unexplained sudden postoperative death (n=2). The exclusion of accidental fatalities resulted in an overall mortality rate of 12.5% in the optimised phase of the study, mainly as a result of uncontrolled intraoperative bleeding (75% of non-accidental deaths). Ultimately, 42 animals survived and were included in the analysis of the IRI model.

Animal weights

Rats in both groups experienced a loss of weight as early as 5 hours postoperatively. Weight loss in relation to preoperative weight was significantly greater in the clamp group than in the control group on postoperative day 1 (6.3±0.7% versus 3.7±0.3% respectively; p=0.003). However, weight gain in the clamp group improved over the subsequent days and was statistically comparable to the control group (Figure 4.5).

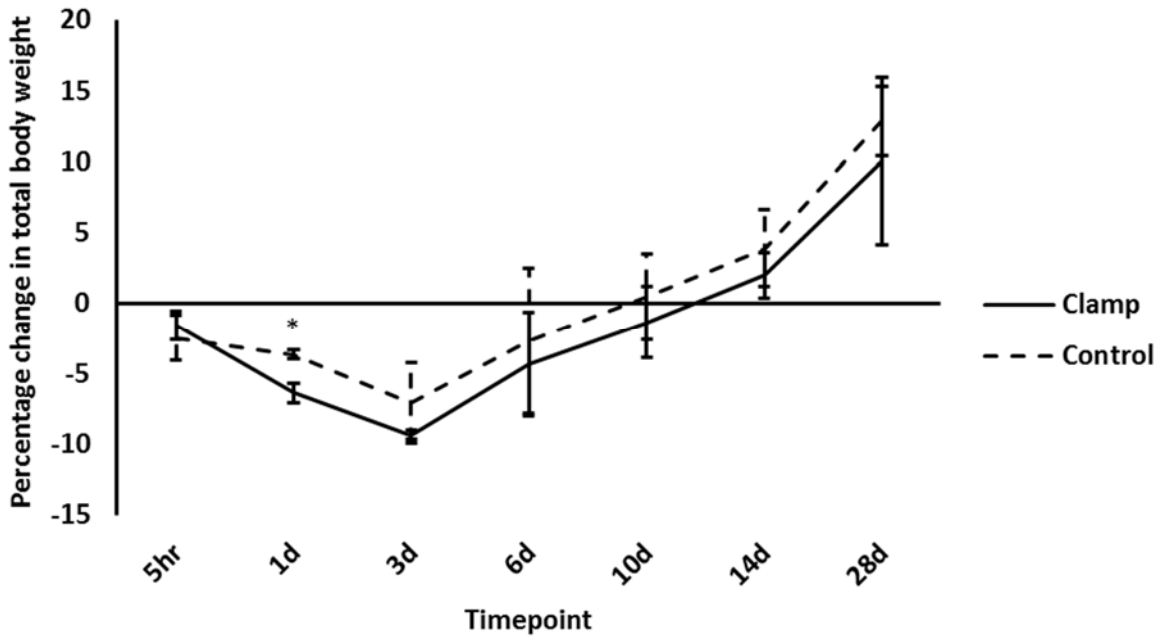

Figure 4.5 Percentage of postoperative weight change in relation to preoperative weight. With the exception of day 1, both the IRI and control groups demonstrated statistically comparable weight changes. *p=0.003 (versus control).

Bile flow

It was not possible to measure lobar bile flow as it was difficult to cannulate each lobar duct separately on a consistent basis. Since common bile duct cannulation was easier to perform consistently, total liver bile production was measured instead. Total bile flow rate normalised to total body weight was significantly reduced in the IRI group compared to the clamp group after 5 hours (13.9±3.0µl/kg/min versus 29.4±7.8µl/kg/min; p=0.03) and 1 day of reperfusion (16.7±5.0µl/kg/min versus 33.9±9.0µl/kg/min; p=0.04). No significant differences between the two groups were apparent when bile flow rates were measured at later time points (Figure 4.6).

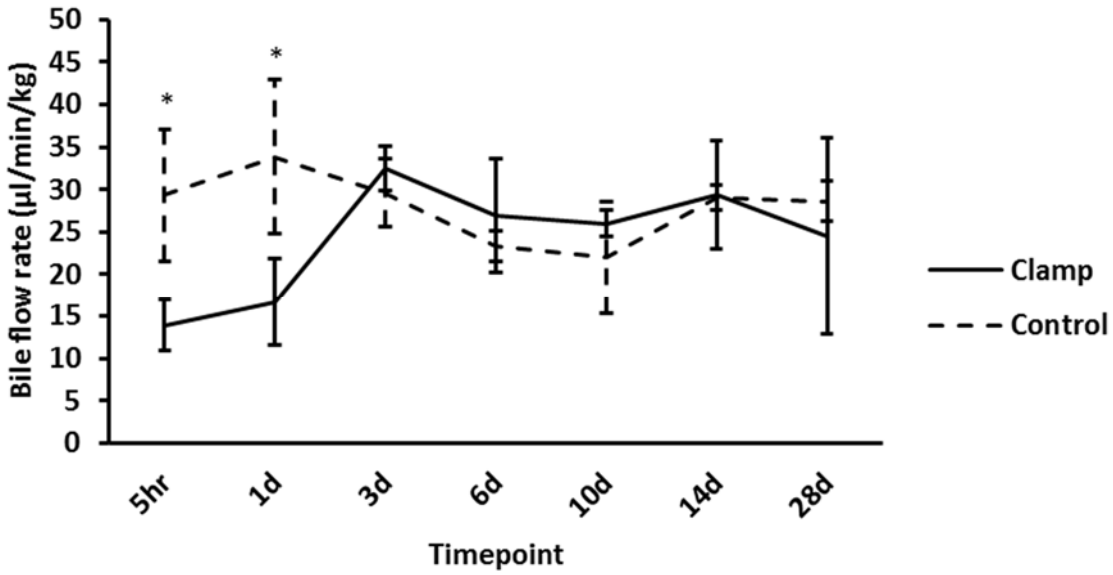

Figure 4.6 A comparison of bile flow rates (normalised to total body weight) between the IRI and control groups. Bile flow was significantly lower in the IRI group after 5 hours and 1 day of reperfusion. *p<0.05 (versus control).

Serum liver function tests

Total protein and albumin

No significant differences in total serum protein or albumin concentrations were noted between the two groups in the peri-operative period and up to 28 days post reperfusion (Figure 4.7 and Figure 4.8 respectively).

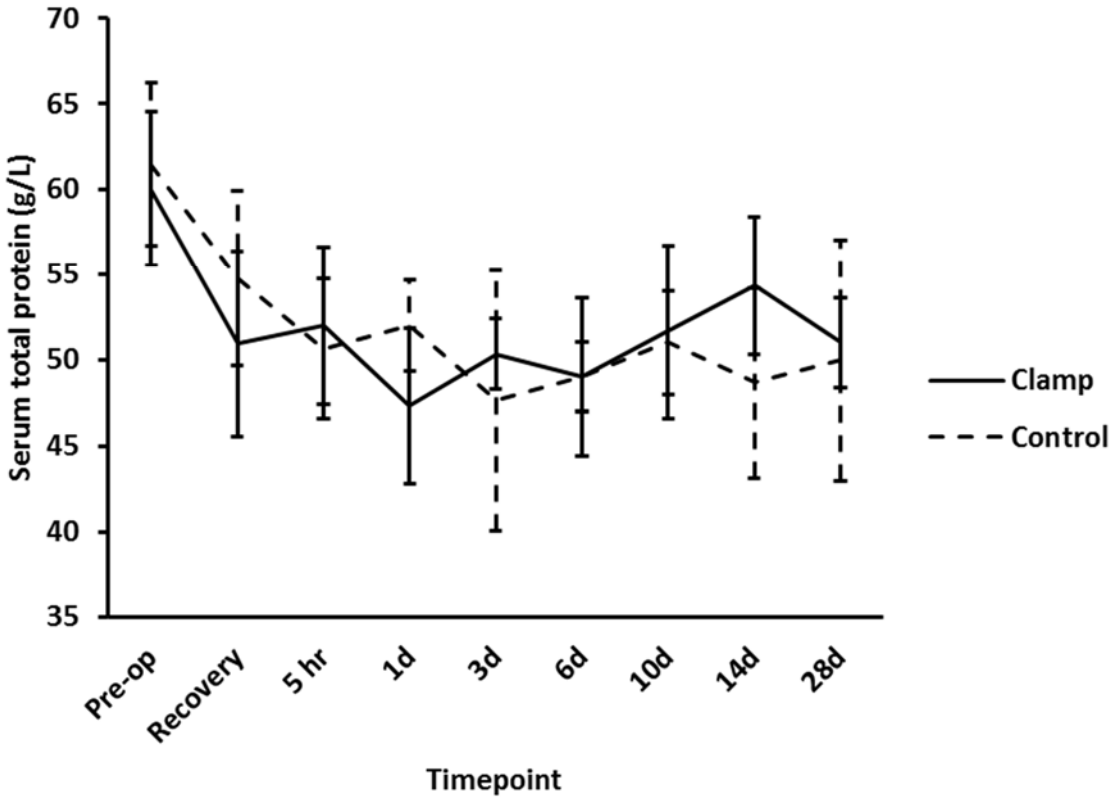

Figure 4.7 A comparison of serum total protein concentration between IRI and control groups. The graph includes preoperative and immediate postoperative time points and demonstrates no significant difference between the two groups at any time point.

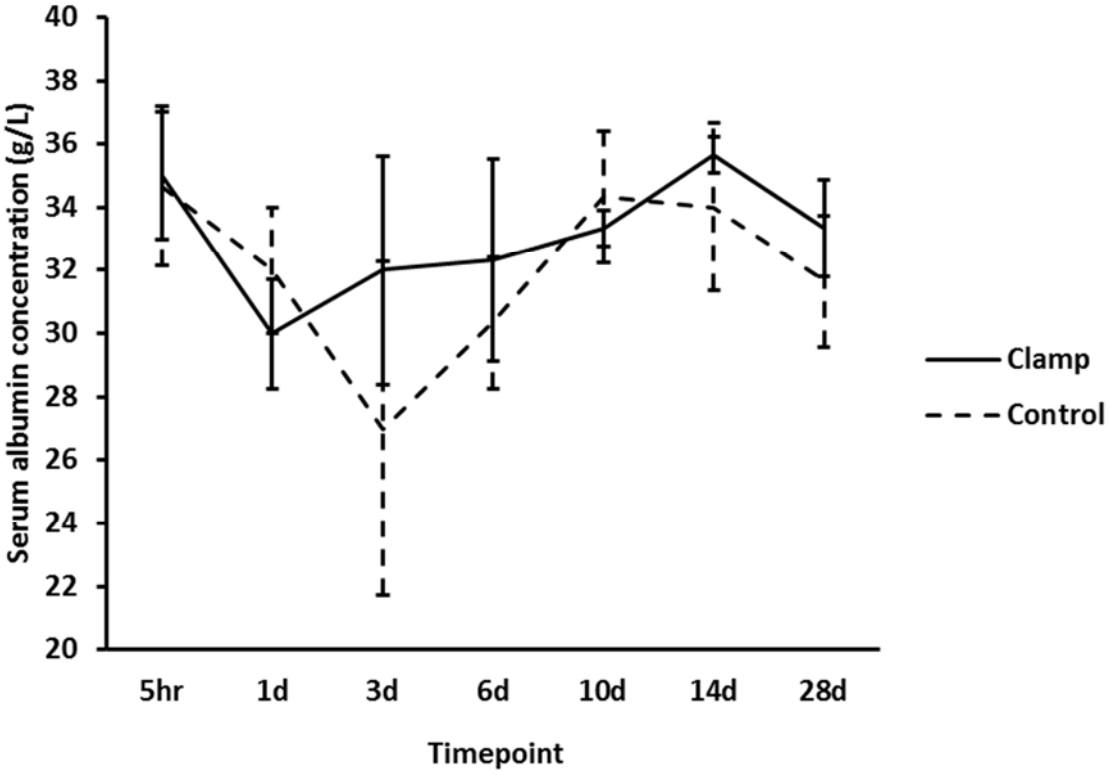

Figure 4.8 A comparison of serum total albumin concentration between IRI and control groups. The graph illustrates that there is no significant difference between the two groups at any timepoint.

.

Bilirubin, bile acids, alkaline phosphatase and γ-glutamyl transferase

Average serum levels of bilirubin were considerably higher in IRI group compared to control in the first postoperative day (8.8±8.4μM versus 1.5±0.2μM control; P=0.15). However this difference failed to reach statistical significance (Figure 4.9). On the other hand, average serum bile acid levels were higher in the IRI group as early as 5 hours post-reperfusion (47.9±21.5μM versus 18.3±9.6μM control; p=0.09). This difference reached statistical significance on postoperative day 1 (152.3±50.7μM versus 9.4±1.4μM control; p=0.008) but resolved by day 3 (Figure 4.10). Serum alkaline phosphatase levels were significantly higher in the IRI group in the early postoperative period and peaked at postoperative day 3 (231.7±50.1U/L versus 95±22.9U/L control; p=0.01). Serum alkaline phosphatase levels in the IRI group returned to baseline control levels by day 6 (Figure 4.11). γ-glutamyl transferase (GGT) levels were, on average, higher in the IRI group at the 5-hour timepoint

(7.5±3.3U/L versus 3.4±1.3U/L control; P=0.11) and up to 24 hours post re-perfusion compared to controls, but this difference was not statistically significant (Figure 4.12).

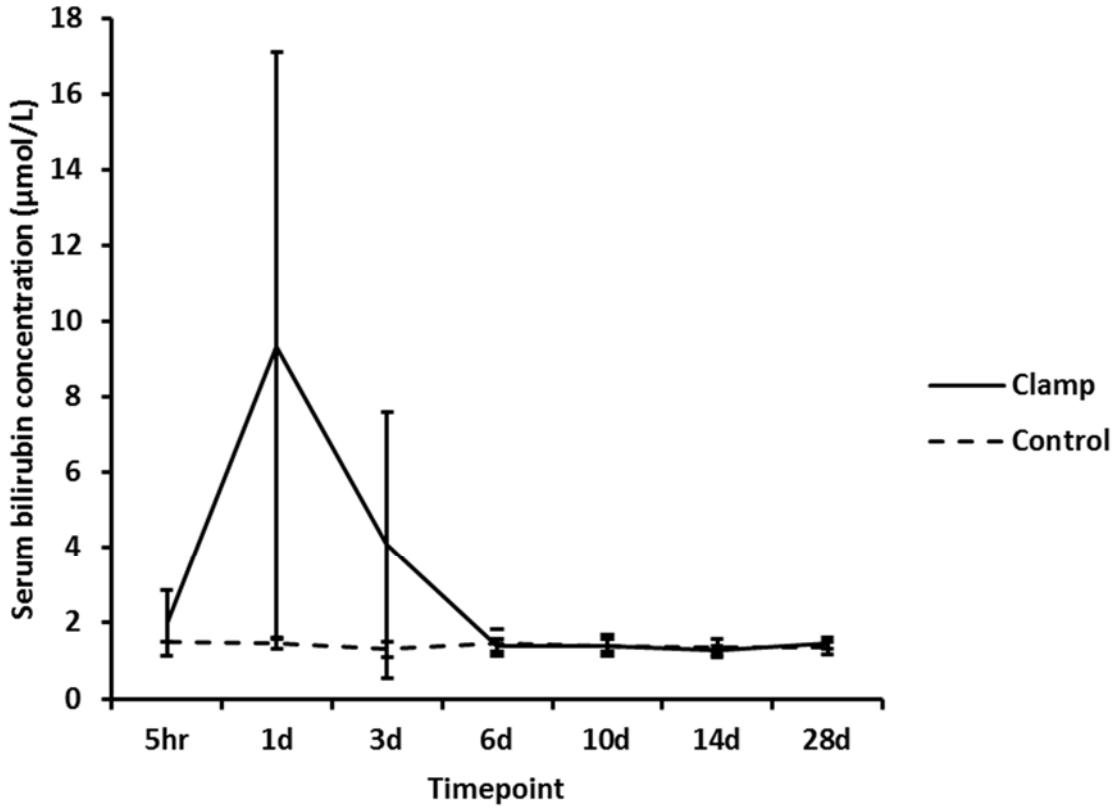

Figure 4.9 A comparison of serum bilirubin concentration between IRI and control groups. Although average bilirubin levels are higher in the IRI group on day 1 the difference is not statistically significant.

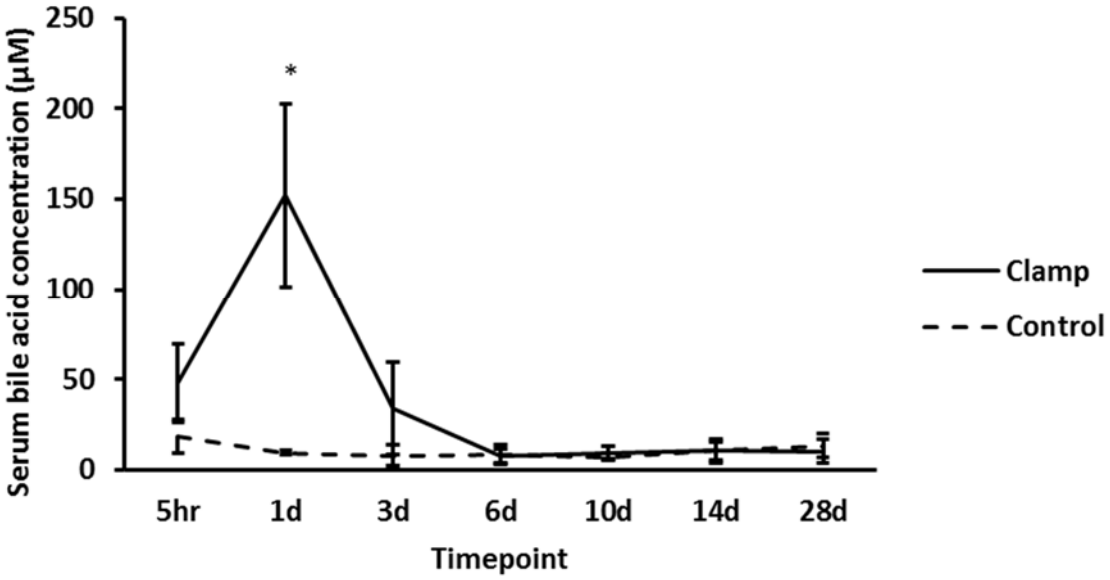

Figure 4.10 A comparison of serum bile acid concentration between the IRI and control groups. Serum bile acids were significantly higher in the IRI group after 1 day of reperfusion. *p<0.01 (versus control).

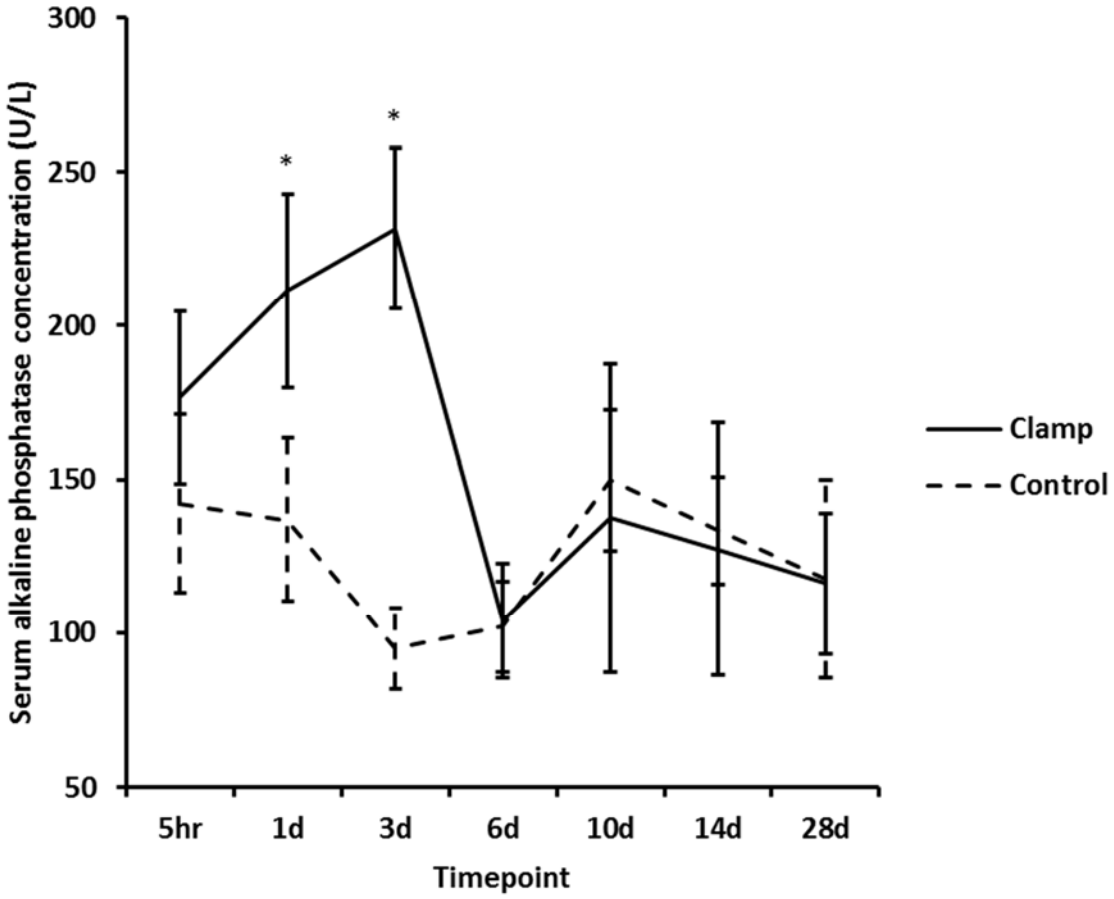

Figure 4.11 A comparison of serum alkaline phosphatase (ALP) activity between the IRI and control groups. Serum ALP activity was significantly higher in the IRI group between postoperative day 1 and 3. *p<0.01 (versus control).

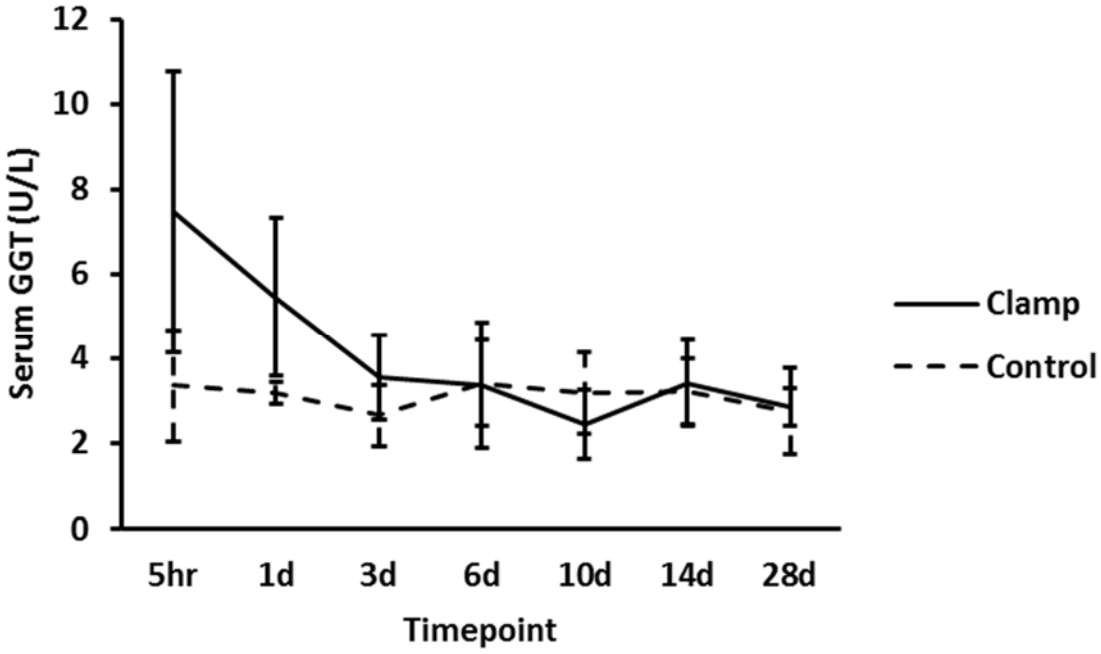

Figure 4.12 A comparison of serum γ-glutamyl transferase (GGT) activity between IRI and control groups. Although average serum GGT activity is higher in the IRI group within the first 24 hours post-reperfusion, the difference is not statistically significant.

Alanine aminotransferase

In the first 3 postoperative days, average serum alanine aminotransferase (ALT) activity was higher in the IRI group compared to the control group. Although the levels peaked 5 hours and 1 day after reperfusion, this difference failed to reach statistical significance due to the large variance in ALT levels in the IRI group at these timepoints (range 1457-13321U/L). ALT activity was significantly higher in the IRI group compared to control immediately post-surgery (1543±689U/L versus 115.7±69.6U/L control; $p<0.0001$) and on postoperative day 3 (317±32.8U/L versus 67±32.9U/L control; $p=0.001$) and returned to baseline control levels by day 6 (Figure 4.13).

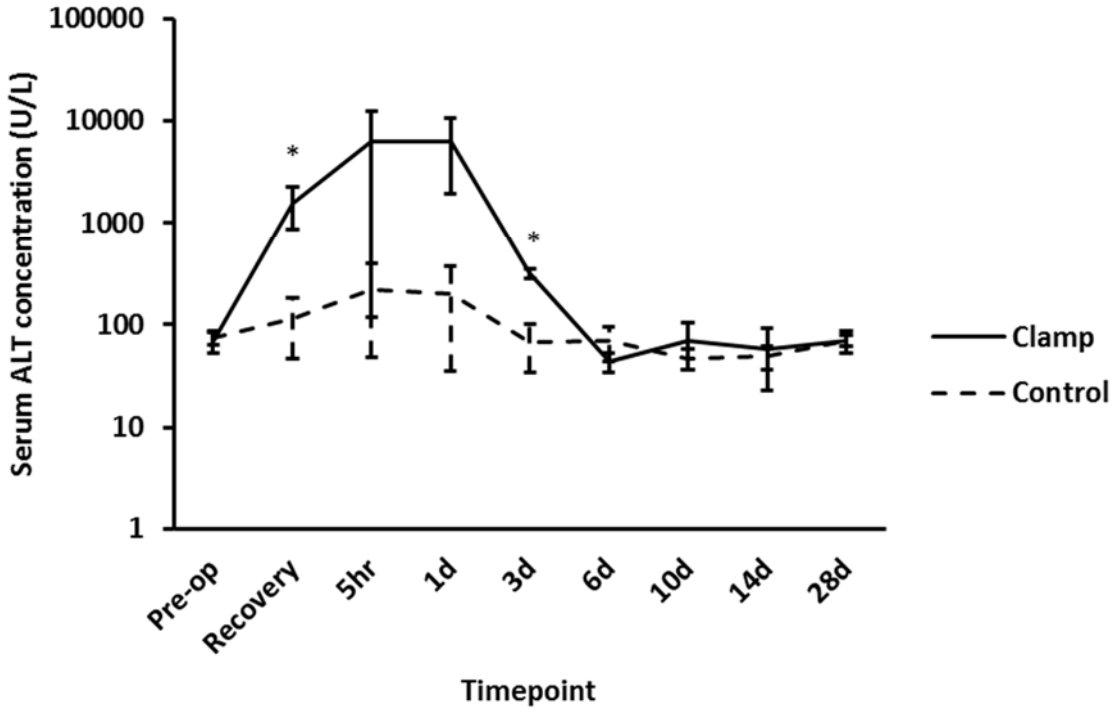

Figure 4.13 A comparison of serum alanine transaminase (ALT) activity between the IRI and control groups (logscale). Higher average serum ALT activity was demonstrated in the IRI group immediately following surgery up until day 3. *p<0.005 (versus control).

Hyaluronic acid concentration

Hyaluronate levels were measured as a marker of sinusoidal endothelial cell damage. Serum hyaluronate levels were -on average- higher in the IRI group than control during the first 3 postoperative days. The levels peaked on day 1 (204.9±137.8ng/ml versus 26.9±8.7ng/ml control; p=0.09) but were only significantly higher on day 3 (53.9±14.4ng/ml versus 14.4±3.7ng/ml control; p=0.01). Once again, serum levels returned to control values by day 6 (Figure 4.14). In comparison, measurement of hyaluronic acid concentrations in liver homogenates of ischaemic and sham ischaemic lobes showed a significant peak rise in the IRI group on day 3 post re-perfusion (11582.5±5693.7ng/ml versus 810.6±225ng/ml control; p=0.03).

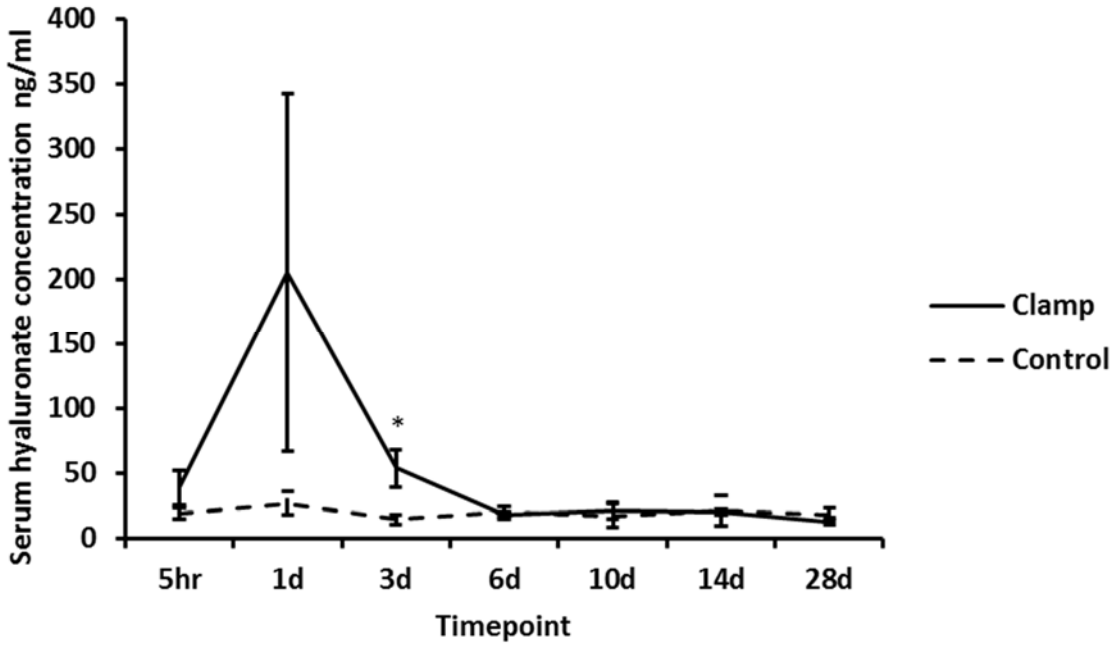

Figure 4.14 A comparison of serum hyaluronate concentration between the IRI and control groups. Higher average hyaluronate concentration was demonstrated in the IRI group on day 1 and 3 postoperatively. *p<0.05 (versus control)

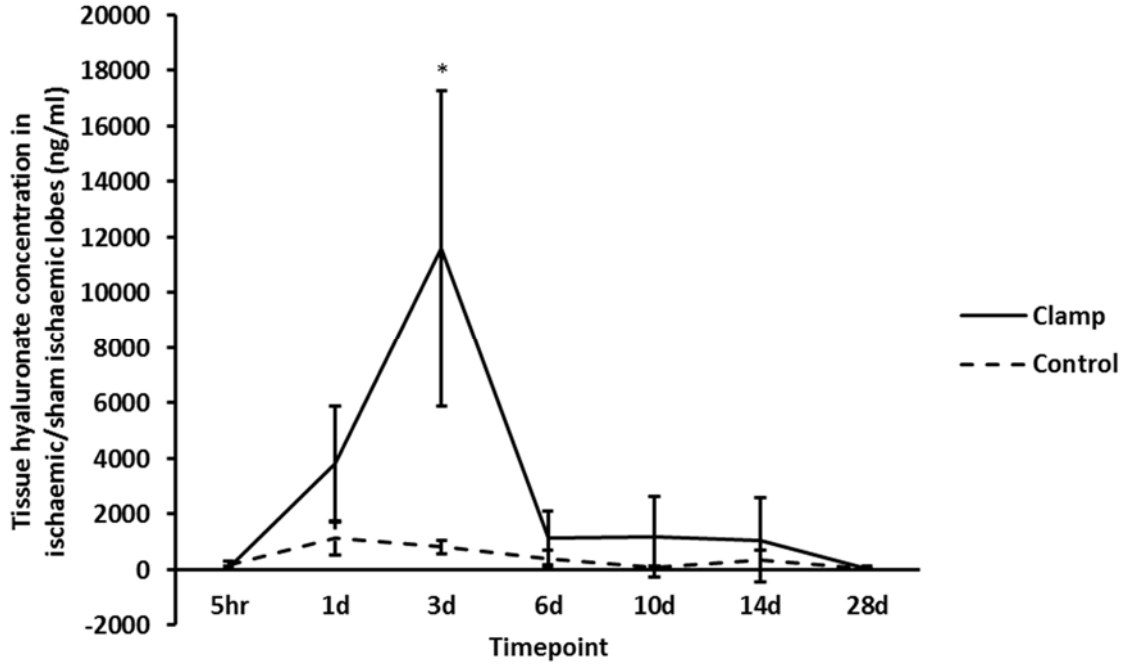

Figure 4.15 A comparison of tissue hyaluronate concentration in ischaemic and sham ischaemic lobes. Average hyaluronate concentration peaked on day 3 in the IRI group. *p<0.05 (versus control)

Biliary bile acid and phospholipid concentration

Total bile acid concentration in bile surged in the IRI group to levels significantly higher than that in the control group on postoperative day 1 (18.6±3.3M versus 11.2±1.5M control; p=0.02). Total biliary bile acid concentrations appeared to rise steadily in both groups from day 3 until day 14 with no significant difference between the two groups (Figure 4.16). It is unclear whether this rise represented an increase from or a return to preoperative baseline since pre-anaesthetic values were not available in view of the requirement for bile duct cannulation to obtain biliary samples.

Biliary phospholipid concentration rose to significantly higher levels in the IRI group compared to the control group, however this only occurred on postoperative day 3 (7.7±1.1mM versus 4.9±0.6mM control; p=0.016) lagging behind the earlier surge in biliary bile acid concentration in that group (Figure 4.16). Measurement of biliary bile salt to phospholipid (BS/PL) ratio demonstrated significantly lower values in the clamp group on day 3 post re-perfusion. In comparison, serum BS/PL ratio measurements highlighted a significant rise on day 1 in the clamp group versus controls.

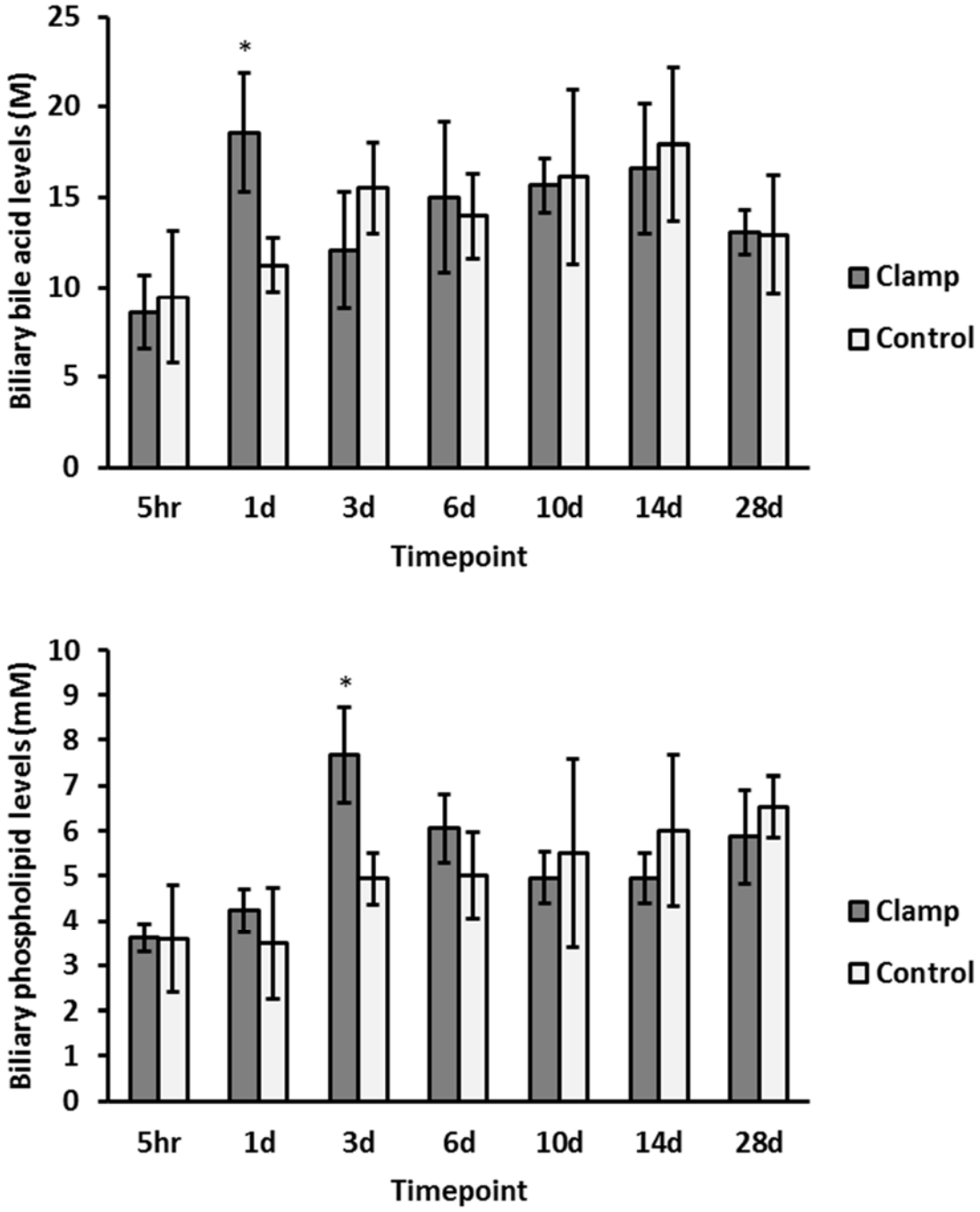

Figure 4.16 A comparison between biliary bile acid (above) and phospholipid (below) concentrations between the IRI and control groups. A significant increase in biliary bile acid in the IRI group (day 1) is followed by a delayed increase in biliary phospholipid in that group (day 3). *p<0.05 (versus control).

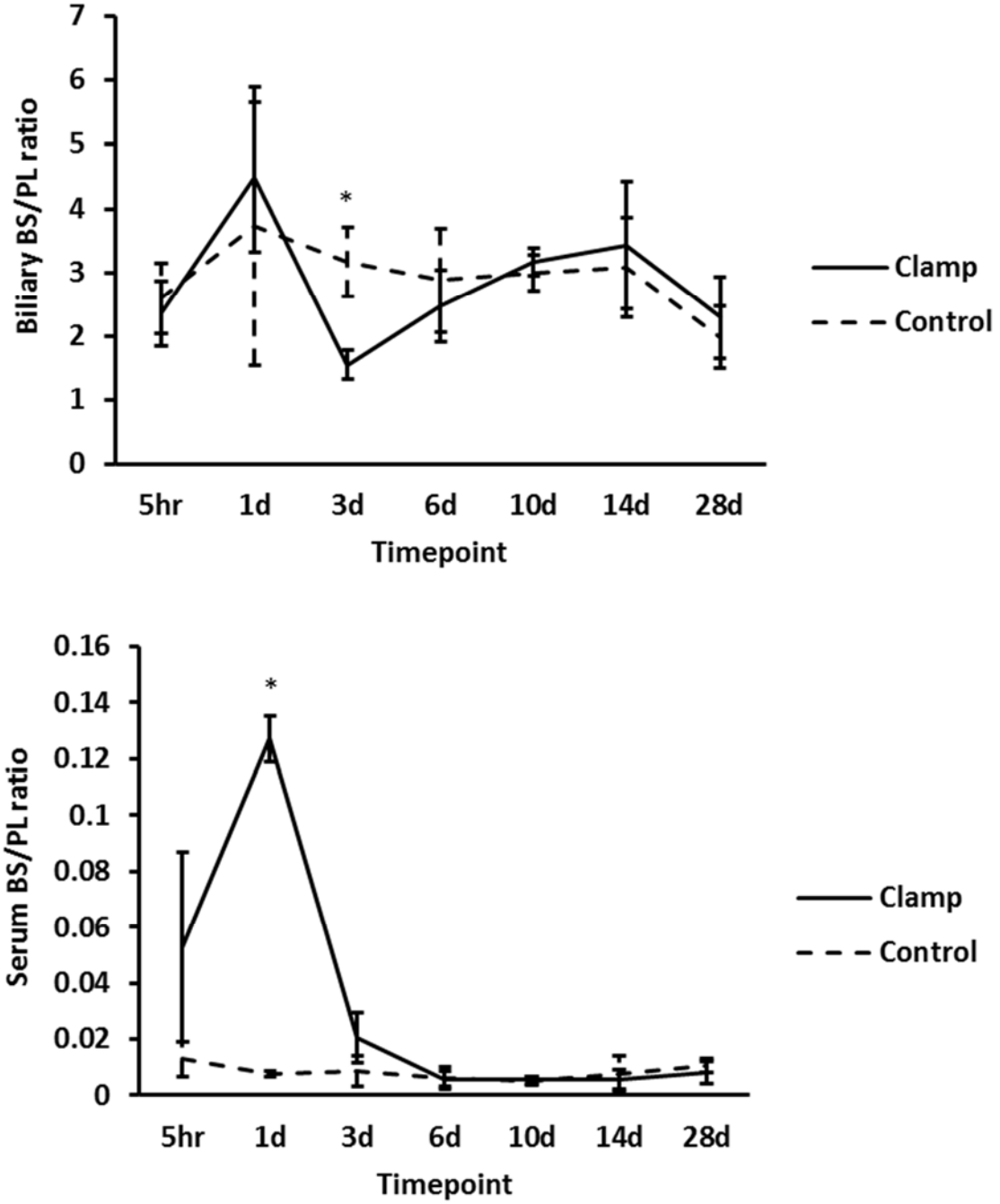

Figure 4.17 A comparison between biliary (above) and serum (below) BS/PL ratios between the IRI and control groups. *p<0.05 (versus control).

Bile salt transporters

The expression of bile salt transporters was examined to further explore the findings related to biliary bile salt levels. RT-PCR was performed to measure Na^+ -

taurocholate co-transporting polypeptide (Ntcp; Slc10a1), bile salt export pump (Bsep; Abcb11) and organic anion transporting polypeptide (Oatp2b1; Slc02b1) mRNA transcript levels in liver homogenates of ischaemic and sham ischaemic lobes.

Ntcp mRNA levels were significantly lower in the IRI group on day 1 post re-perfusion (18-fold reduction compared to controls; p=0.01) and remained significantly lower on day 3 (Figure 4.18). A similar pattern was noted with Oatp2b1 levels, with a 3-fold reduction on day 1 compared to controls (p=0.002) (Figure 4.19). On average, Bsep transcripts were lower in the IRI group between day 1 and 3 compared to controls, but this difference did not reach statistical significance (Figure 4.20). It was also observed that the levels of transcripts for all three transporters became higher in the IRI group on average (though not statistically significant) compared to controls at later timepoints (between day 10 and 14).

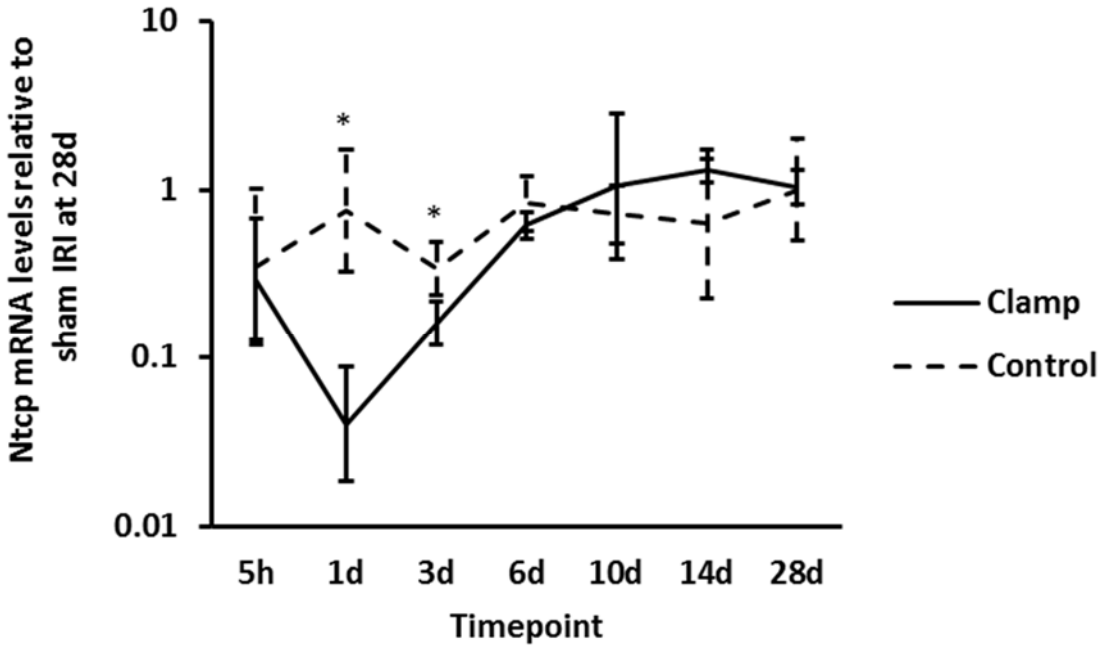

Figure 4.18 RT-PCR analysis in ischaemic and sham ischaemic lobes shows significantly reduced expression of Ntcp in the ischaemic liver lobes between day 1 and 3 post-reperfusion. *p<0.05 versus control

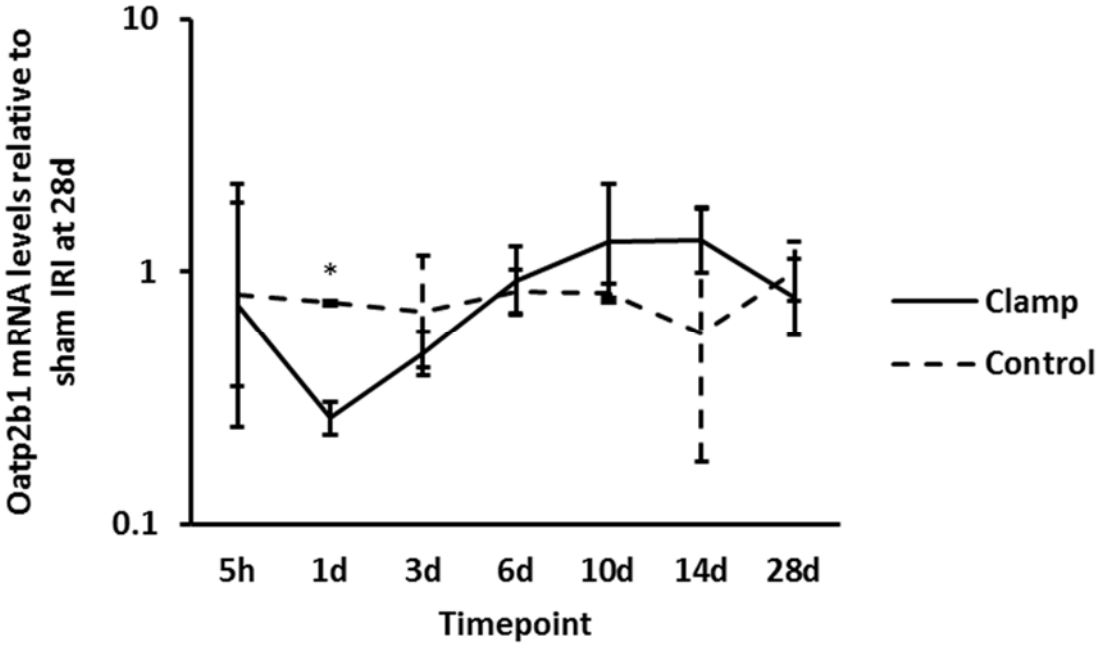

Figure 4.19 RT-PCR analysis in ischaemic and sham ischaemic lobes shows significantly reduced expression of Oatp2b1 in ischaemic liver lobes on day 1 post-reperfusion. *p<0.005 versus control

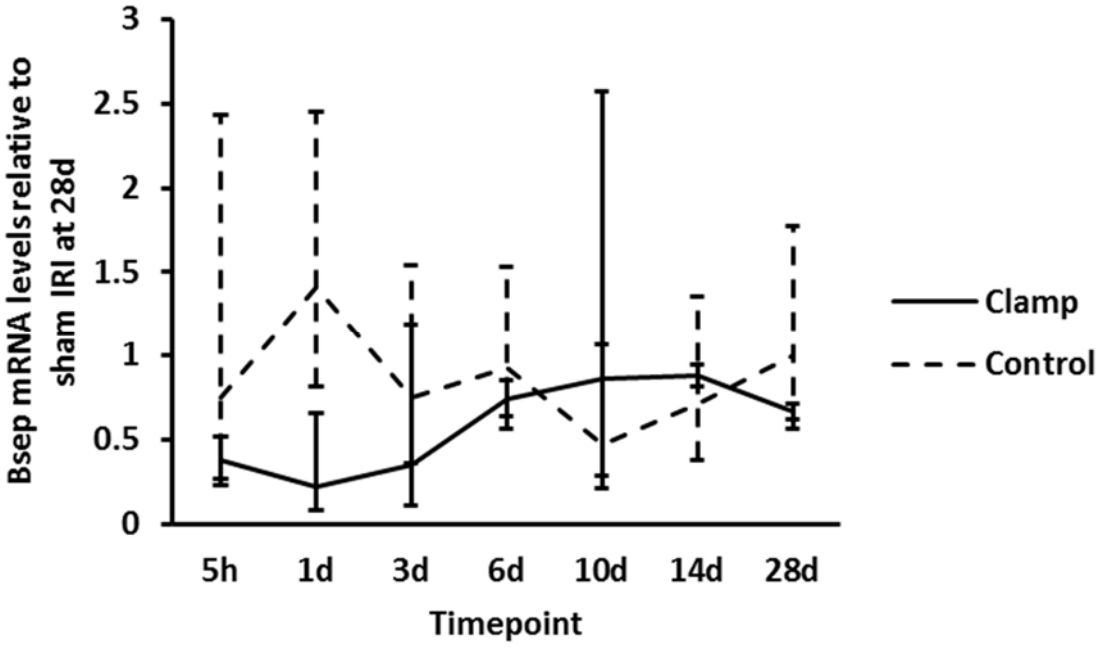

Figure 4.20 RT-PCR analysis comparing the expression of Bsep in ischaemic and sham ischaemic lobes.

Multiplex cytokine array

Serum, bile and liver homogenate samples were analysed to determine levels of the following cytokines: IFN-γ, TNF-α, MCP-1, MIP-1α, MIP-1β, MIP-2, VEGF, RANTES, IP-10, IL-1α, IL-1β, IL-2, IL-4, IL-5, IL-6, IL-12 p70, IL-10 and EGF.

Serum

Of the cytokines measured, serum concentrations of IL-1α, MIP-1α, IL-6, MCP-1, VEGF and MIP-2 were significantly raised in the IRI group compared to control (Figure 4.21). In addition, serum levels of RANTES were lower in the IRI group in the early postoperative days but rose steadily to concentrations higher than those in the control group by postoperative day 10 (Figure 4.22).

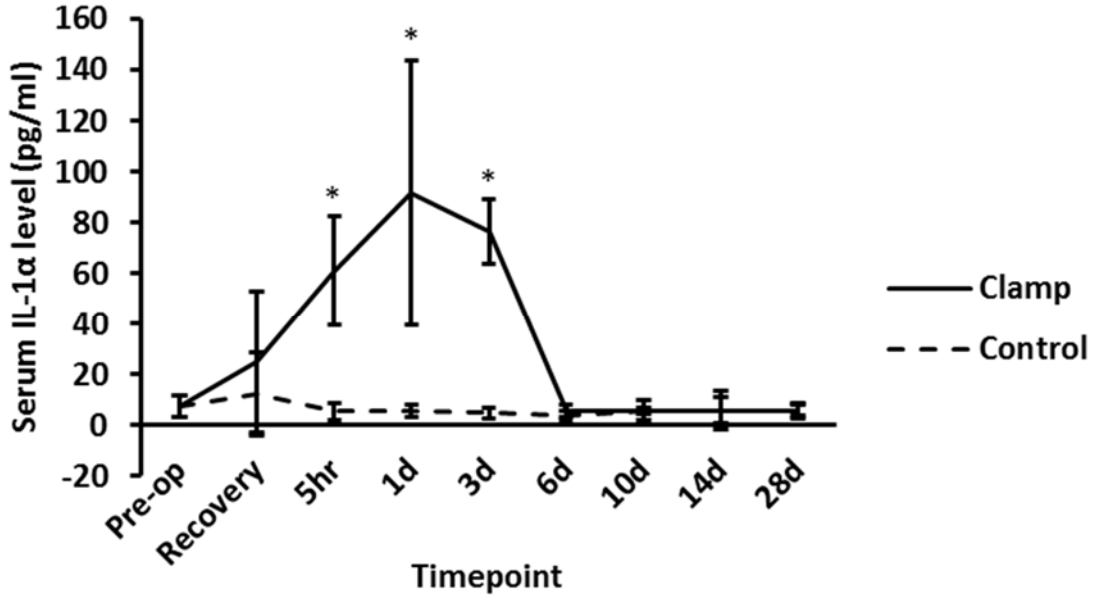
Serum IL-1α level (pg/ml)
160
140
120
100
80
60
40
20
0
-20
*
*
*
Pre-op
Recovery
5hr
1d
3d
6d
10d
14d
28d
Timepoint
Clamp
Control

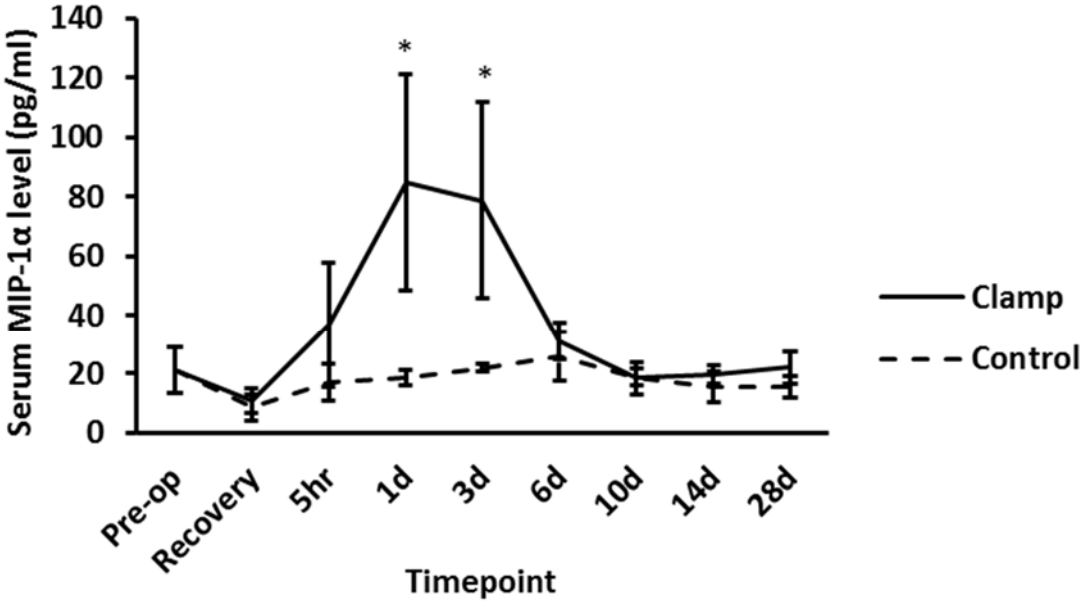
Serum MIP-1α level (pg/ml)
140
120
100
80
60
40
20
0
*
*
Pre-op
Recovery
5hr
1d
3d
6d
10d
14d
28d
Timepoint
Clamp
Control

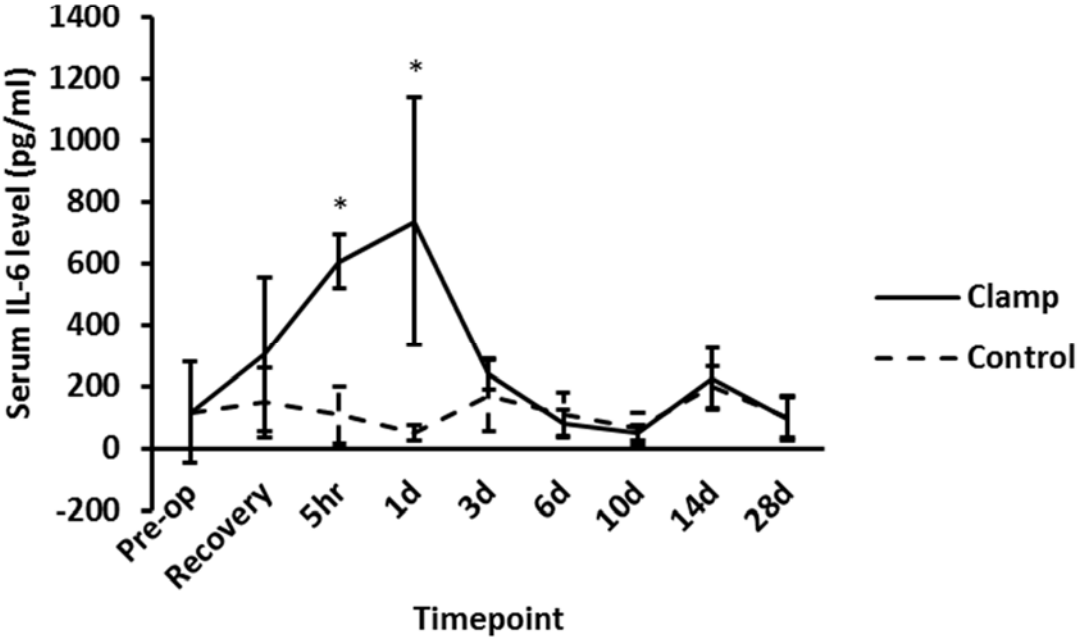
Serum IL-6 level (pg/ml)
1400
1200
1000
800
600
400
200
0
-200
*
*
Pre-op
Recovery
5hr
1d
3d
6d
10d
14d
28d
Timepoint
Clamp
Control

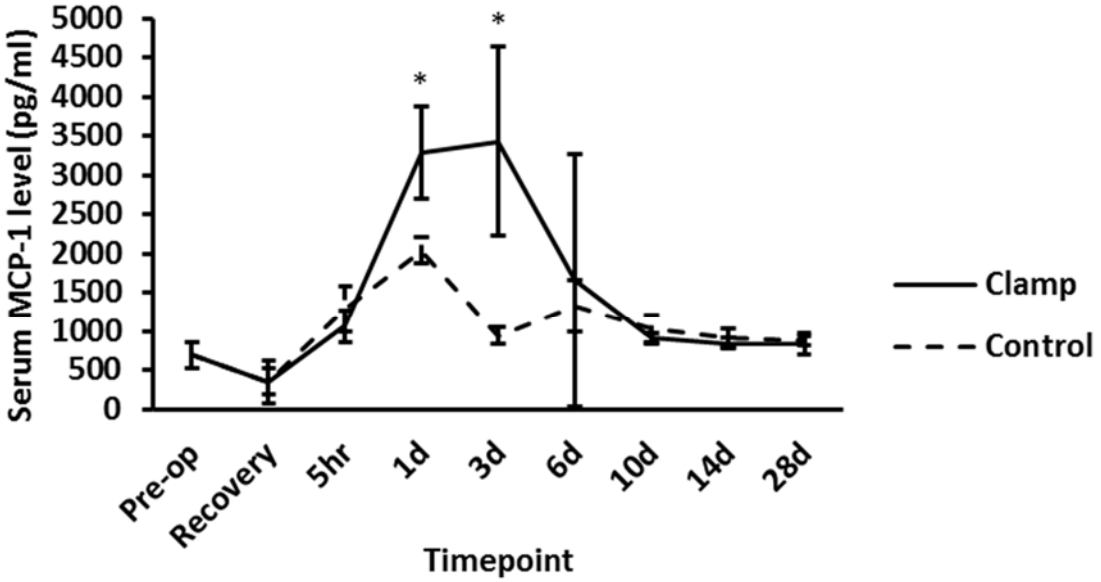
Serum MCP-1 level (pg/ml)
5000
4500
4000
3500
3000
2500
2000
1500
1000
500
0
*
*
Pre-op
Recovery
5hr
1d
3d
6d
10d
14d
28d
Timepoint
Clamp
Control

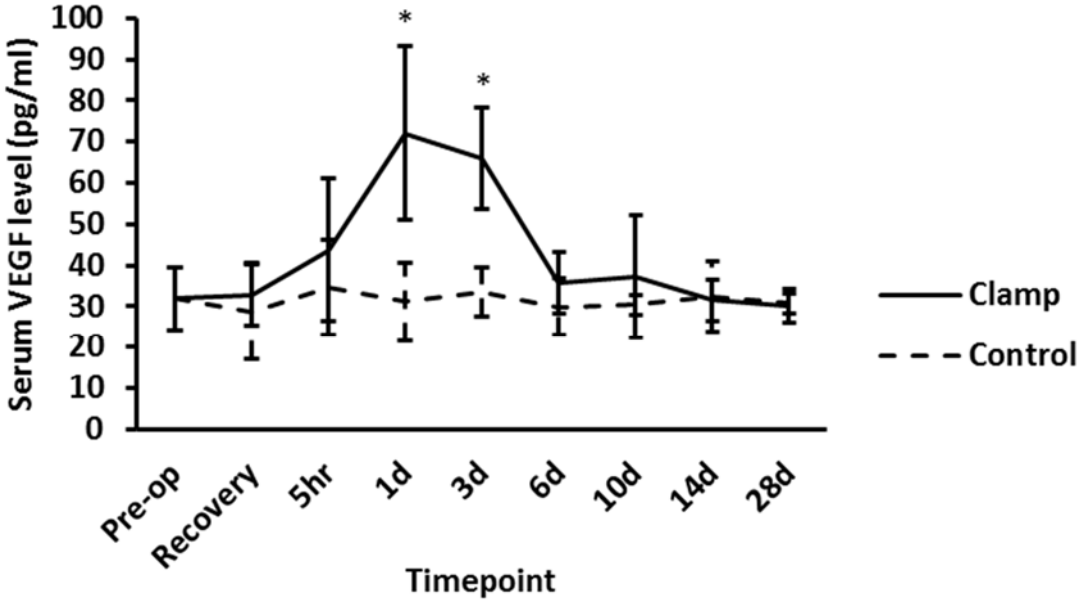
Serum VEGF level (pg/ml)
100
90
80
70
60
50
40
30
20
10
0
*
*
Pre-op
Recovery
5hr
1d
3d
6d
10d
14d
28d
Timepoint
Clamp
Control

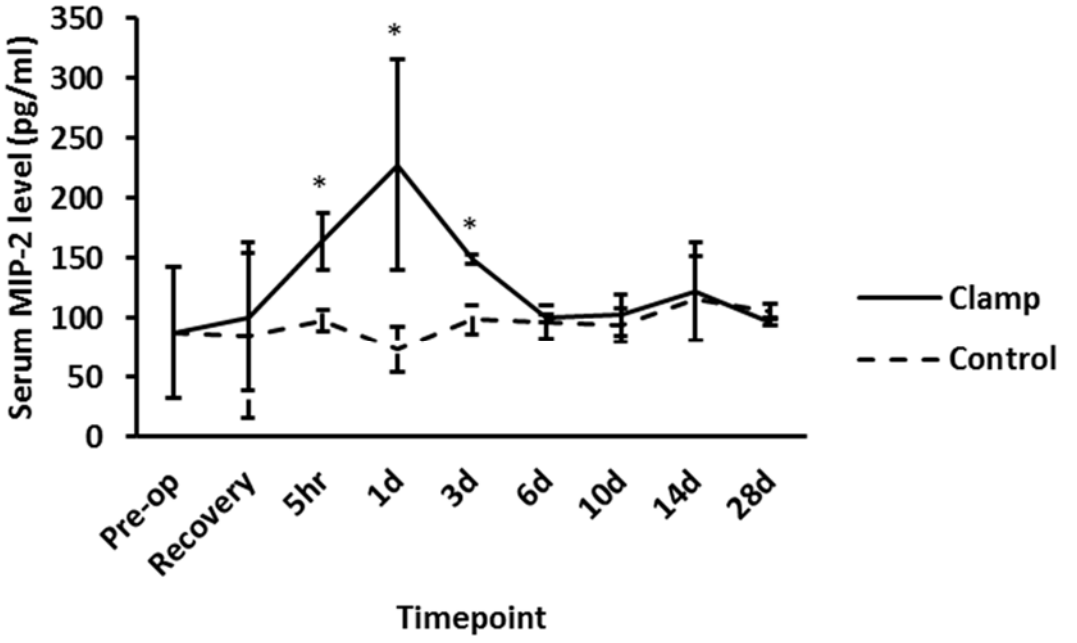
Serum MIP-2 level (pg/ml)
350
300
250
200
150
100
50
0
*
*
*
Pre-op
Recovery
5hr
1d
3d
6d
10d
14d
28d
Timepoint
Clamp
Control

Figure 4.21 Serum levels of IL-1α, MIP-1α, IL-6, MCP-1, VEGF and MIP-2 compared between the two study groups. *p<0.05 (versus control)

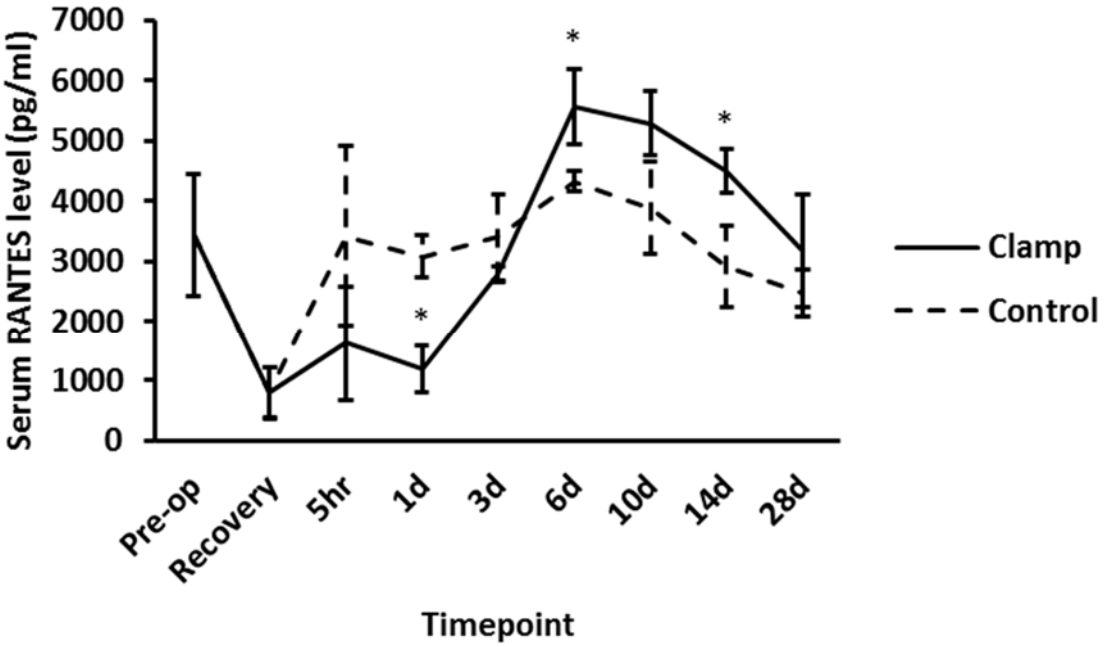

Figure 4.22 Changes in serum RANTES concentration in both the IRI and control groups. *p<0.05 (versus control)

Table 19 summarises the results from cytokines that demonstrated significant differences in concentration between the two study groups at various timepoints.

Table 19 Summary of cytokines that demonstrated significant differences in serum concentrations between the IRI and control groups. Values are reported as mean±SD.

		IRI group (pg/ml)	Control group (pg/ml)	P value
IL-1α	5 hours	60.9±21.4	5.3±3.2	0.01
	Day 1	91.4±51.9	5.6±2.4	0.05

	Day 3	76.2±12.7	4.6±2.1	0.001
IL-6	5 hours	604.9±86.3	107.1±92.9	0.002
	Day 1	736±405.2	47.4±26.7	0.04
MCP-1	Day 1	3292.2±590.8	2038.8±169	0.02
	Day 3	3438.1±1202.8	944.1±103.3	0.02
MIP-1a	Day 1	84.8±36.3	18.5±2.6	0.03
	Day 3	78.6±33.1	21.9±1.3	0.04
MIP-2	5 hours	163.3±23.1	97.3±8.6	0.01
	Day 1	227±87.8	73.1±19.4	0.04
	Day 3	148.3±4.1	98±12.8	0.003
RANTES	Day 1	1190.7±382	3078.4±350.4	0.003
	Day 6	5572.1±627.5	4324±165.3	0.03
	Day 10	5292.2±521.3	3887.1±776.7	0.06
	Day 14	4486±364.3	2922.3±675.5	0.02
VEGF	Day 1	72±21.1	31.1±9.6	0.04
	Day 3	65.9±12.3	33.5±5.9	0.01

Bile

Biliary concentrations of MCP-1 and VEGF were higher in the IRI group compared to control in the early postoperative period (up to day 1 and day 3 respectively) (Figure 4.23). These results appear to mirror those obtained from serum samples and, in the case of VEGF, peaked at higher concentrations than in serum (Figure 4.21). Biliary concentration of EGF in the IRI group was significantly below control baseline on

postoperative days 1 and 3 and rose steadily to baseline average by day 14 (Figure 4.24). Biliary concentrations of RANTES in the IRI group progressively increased and were significantly higher than in the control group by postoperative day 28 (Figure 4.25).

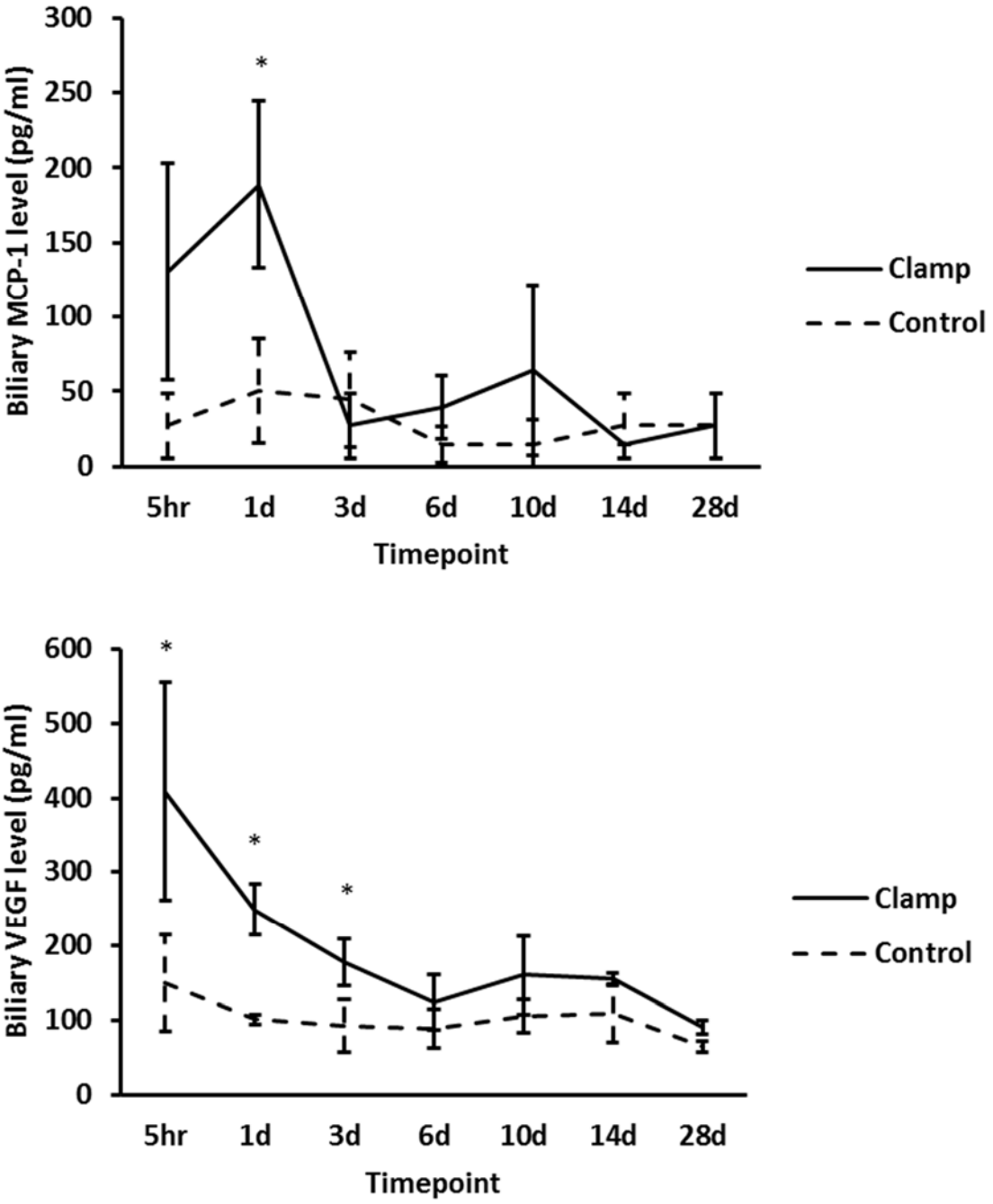

Figure 4.23 Biliary levels of MCP-1 (top) and VEGF (bottom) compared between the two study groups. *p<0.05 (versus control)

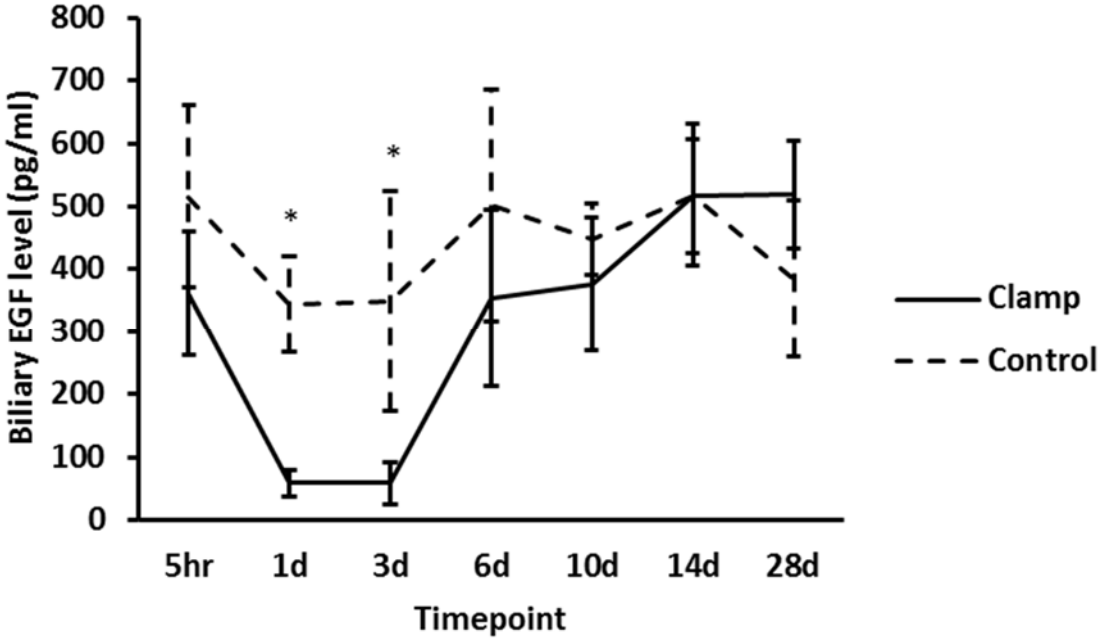

Figure 4.24 Changes in biliary EGF concentration in both the IRI and control groups. *p<0.05 (versus IRI)

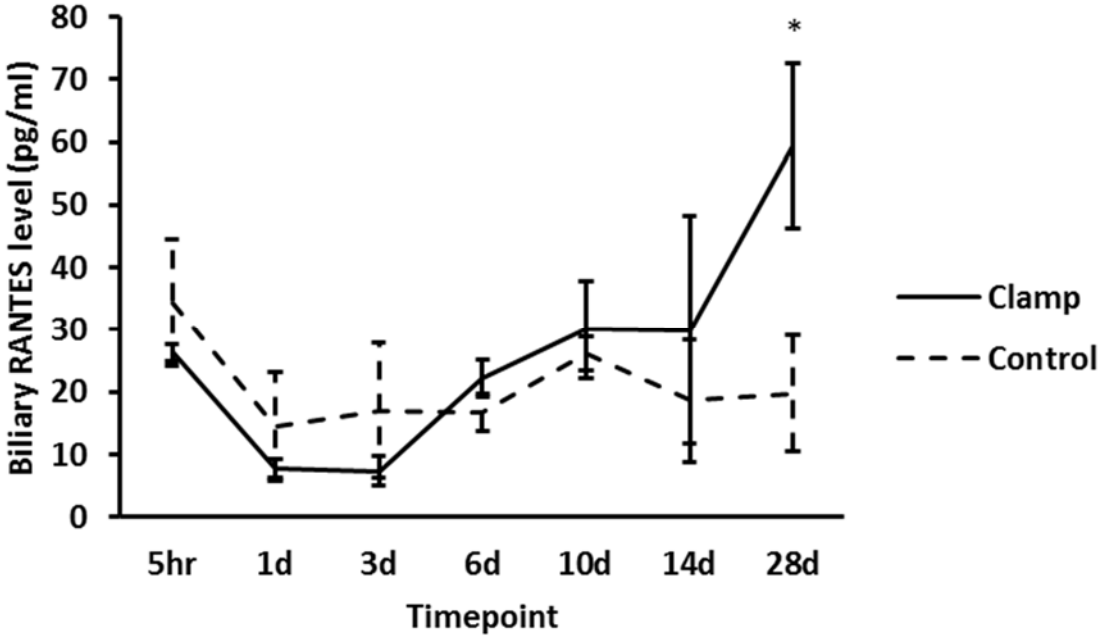

Figure 4.25 Changes in biliary RANTES concentration in both the IRI and control groups. *p<0.05 (versus control)

A summary of the biliary cytokine results is outlined in Table 20

Table 20 Summary of cytokines that demonstrated significant differences in biliary concentrations between the IRI and control groups. Values are reported as mean±SD.

		IRI group (pg/ml)	Control group (pg/ml)	P value
EGF	Day 1	58.6±21.4	343.8±76.1	0.00
	Day 3	58.5±33.4	349.6±176.2	0.05
MCP-1	5 hours	130.6±72.5	27±21.4	0.08
	Day 1	188.9±55.8	50.3±34.9	0.02
RANTES	Day 28	59.4±13.1	19.7±9.3	0.01
VEGF	5 hours	407.7±146.9	149.9±64.9	0.05
	Day 1	249.4±33.6	101±6.4	0.002
	Day 3	177.8±31.7	92.6±35.8	0.04

Liver homogenate

Cytokine levels in liver homogenate were normalised according to the protein concentration of each sample. Of the cytokines measured, significant differences were observed in the ischaemic liver concentrations of IL-1α, IL-1β, IL-2, IL-4, IL-6, IL-10, IL-12p70, IP-10, MIP-1α, MIP-2 and VEGF between the IRI and control groups.

Changes in these cytokines followed one of three patterns:

- Postoperative rise in the IRI group: MIP-1α levels in the IRI group rose to levels significantly higher than control from 5 hours to 3 days postoperatively after which levels returned to baseline control values (Figure 4.26).
- Initial postoperative rise followed by late drop in the IRI group: Levels of IL-6, IL-12p70, MIP-2 and VEGF in ischaemic lobes were initially significantly greater than control values but later dropped significantly to sub-baseline levels by day 3-10 postoperatively. IL-1α followed a similar though less definitive course (Figure 4.27).
- Sustained sub-baseline levels in the IRI group postoperatively: Concentrations of IL-2, IL-4, IL-10 and IP-10 in ischaemic lobes were significantly lower than in sham ischaemic lobes throughout the postoperative period. IL-1β followed a similar though less definitive course (Figure 4.28).

RANTES levels in liver homogenates in the IRI group demonstrated an early sub-baseline production followed by a delayed rise compared to controls after day 6. However, the differences were not statistically significant (Figure 4.29).

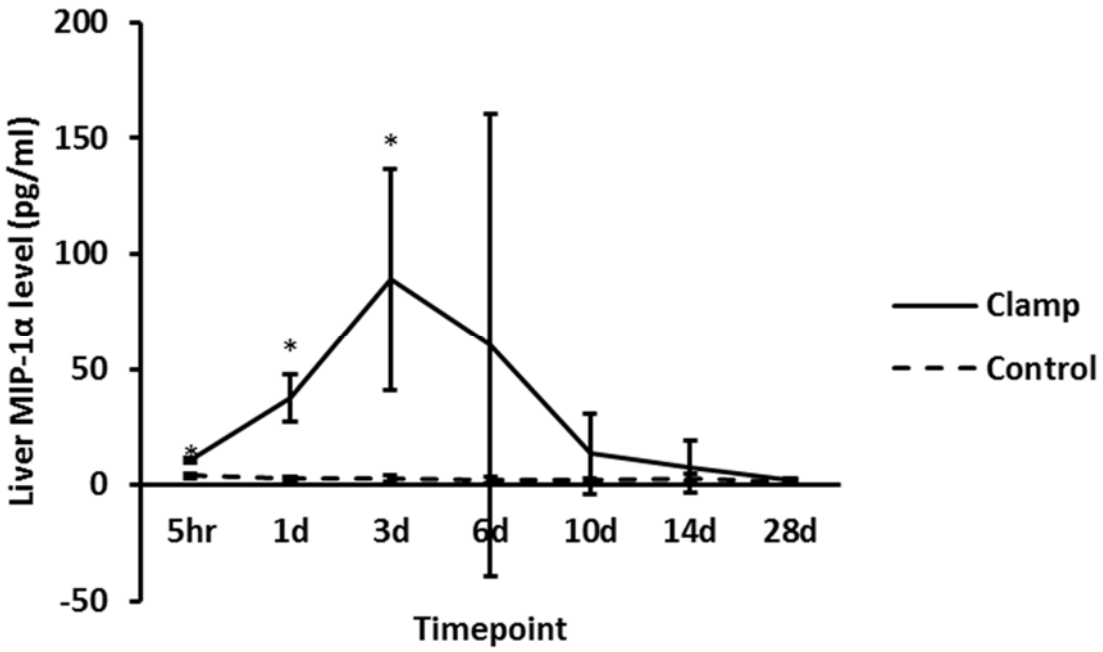

Figure 4.26 Changes in MIP-1α concentration in ischaemic versus sham ischaemic liver tissue. *p<0.05 (versus control)

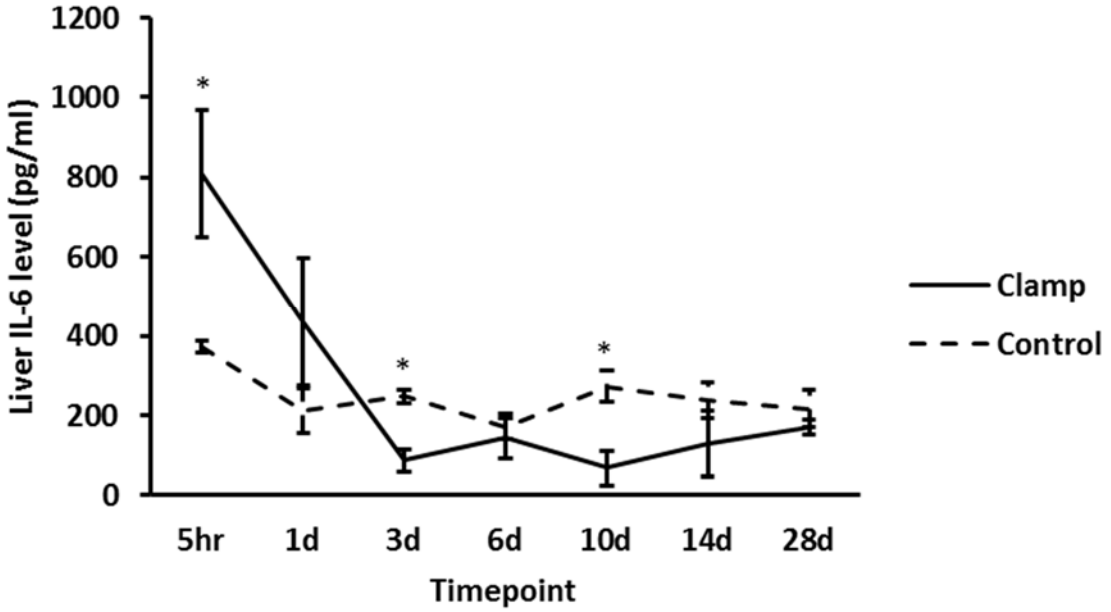
Liver IL-6 level (pg/ml)
1200
1000
800
600
400
200
0
*
*
*
5hr
1d
3d
6d
10d
14d
28d
Timepoint
Clamp
Control

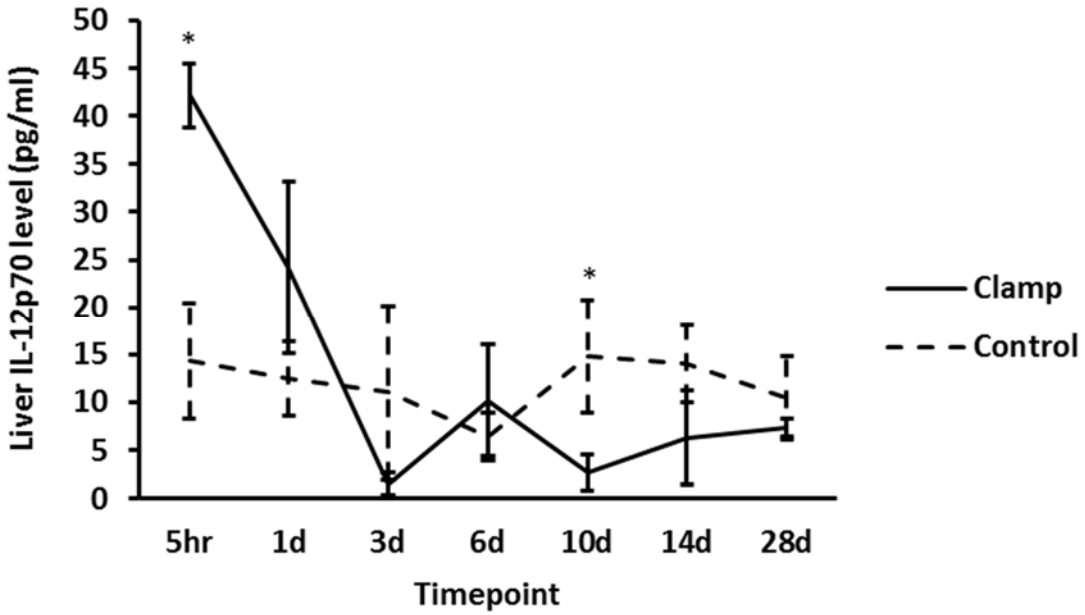
Liver IL-12p70 level (pg/ml)
50
45
40
35
30
25
20
15
10
5
0
*
*
5hr
1d
3d
6d
10d
14d
28d
Timepoint
Clamp
Control

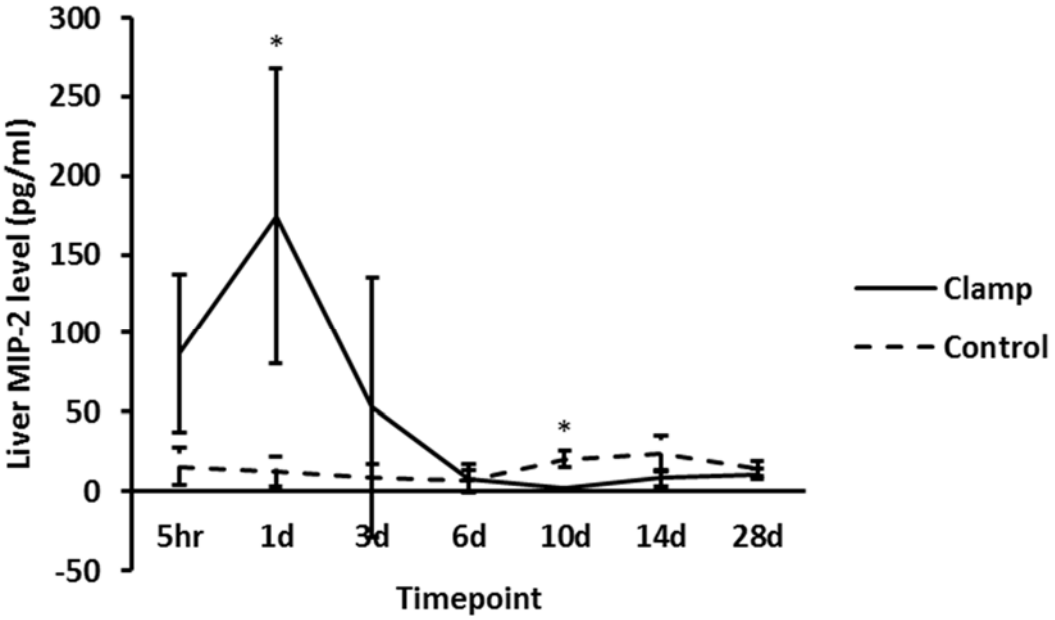
Liver MIP-2 level (pg/ml)
300
250
200
150
100
50
0
-50
*
*
5hr
1d
3d
6d
10d
14d
28d
Timepoint
Clamp
Control

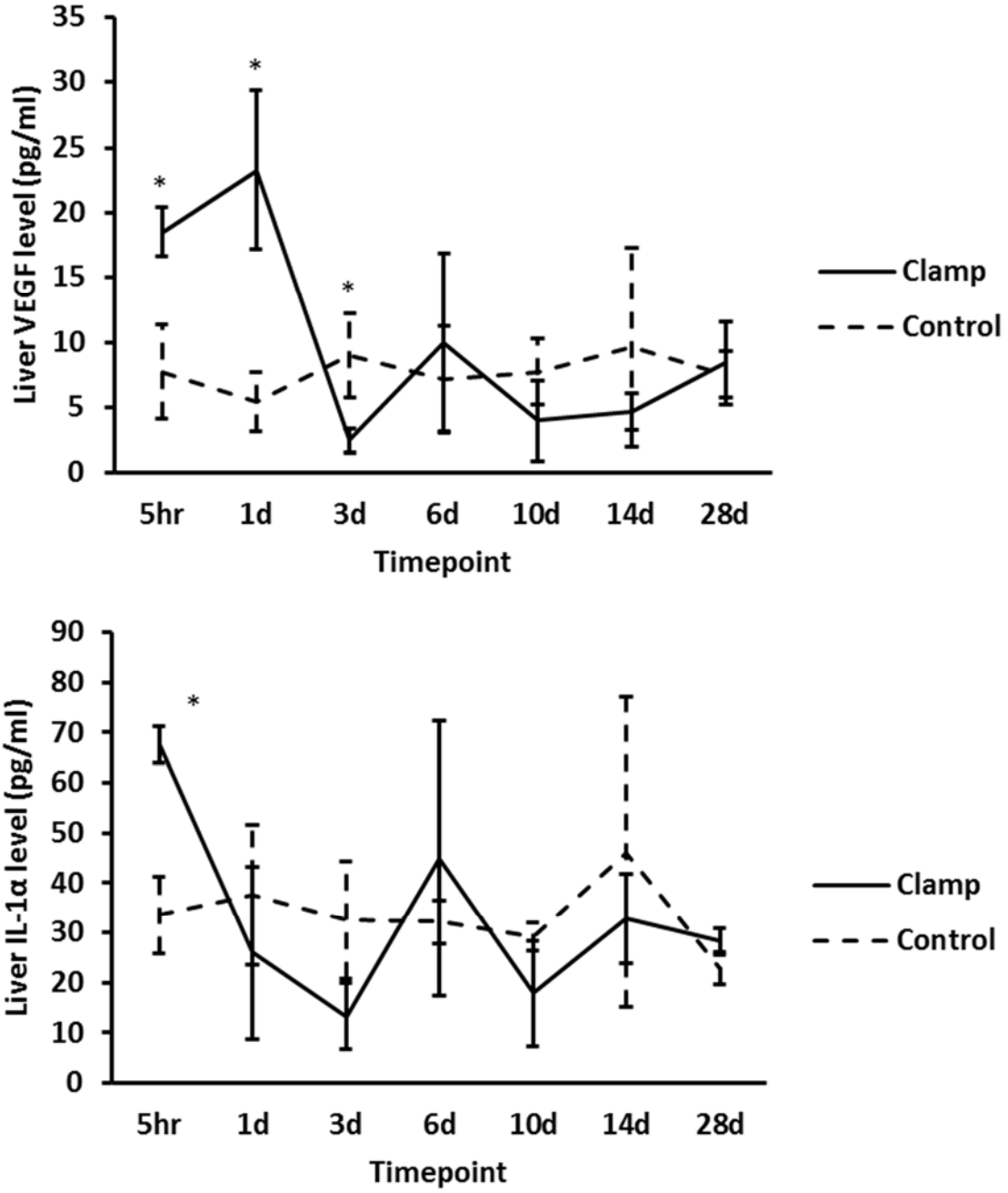

Figure 4.27 Levels of IL-6, IL-12p70, MIP-2, VEGF and IL-1α in ischaemic versus sham ischaemic liver tissue. *p<0.05 (IRI versus control)

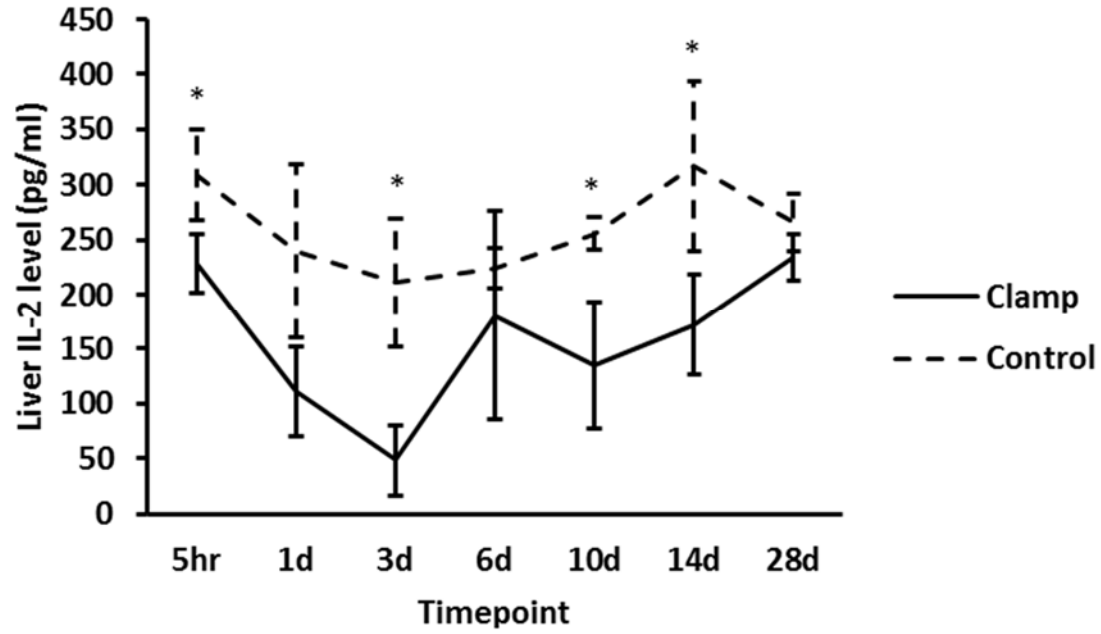
Liver IL-2 level (pg/ml)
450
400
350
300
250
200
150
100
50
0
5hr
1d
3d
6d
10d
14d
28d
Timepoint
Clamp
Control

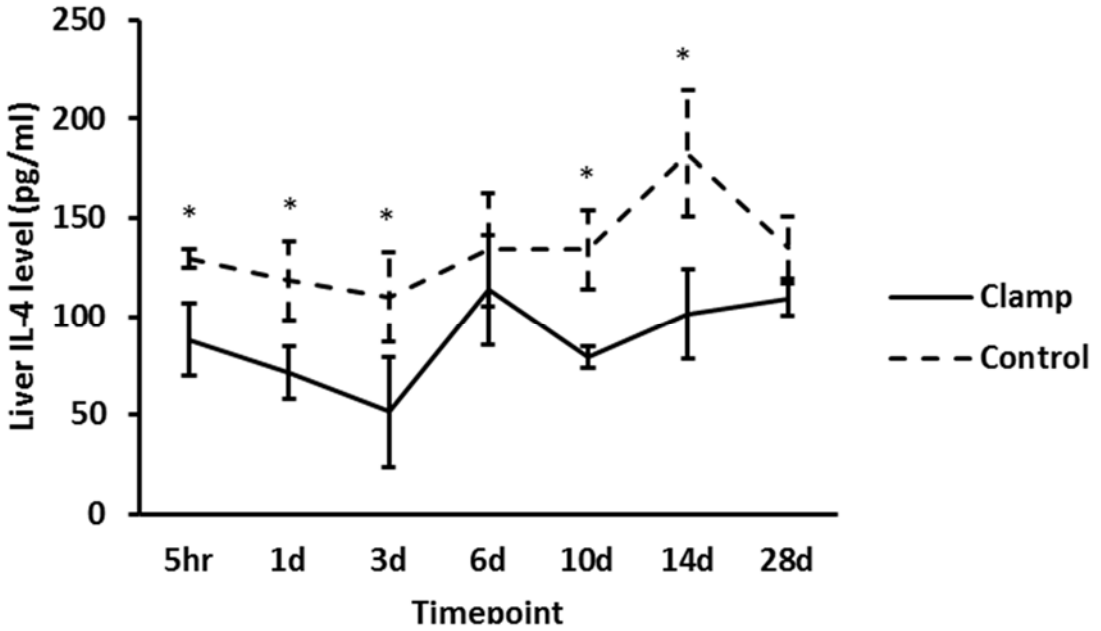
Liver IL-4 level (pg/ml)
250
200
150
100
50
0
5hr
1d
3d
6d
10d
14d
28d
Timepoint
Clamp
Control

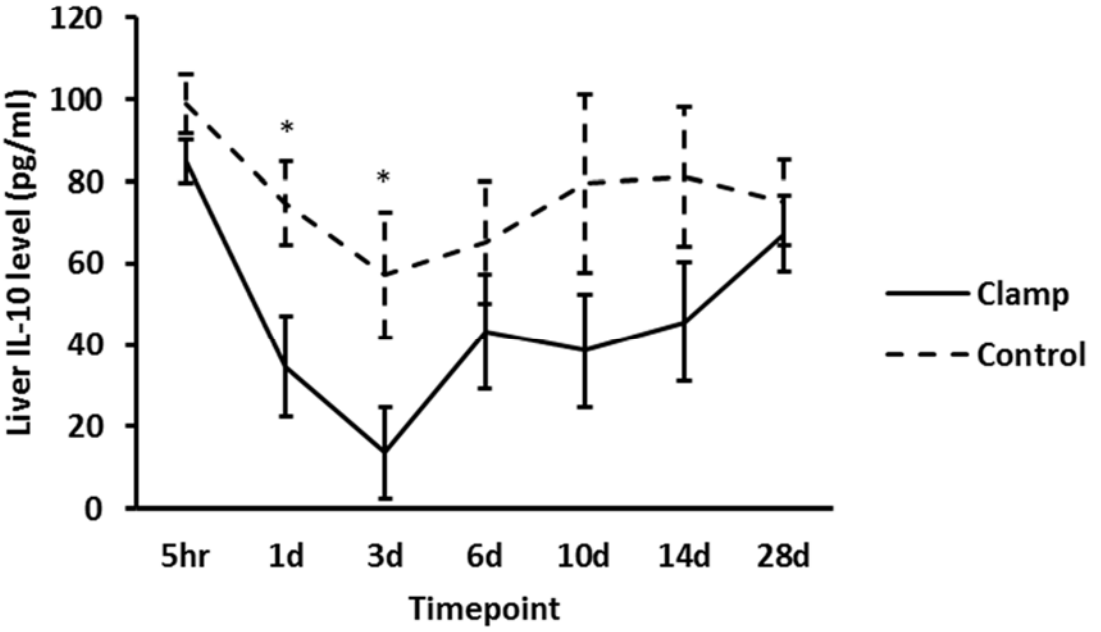
Liver IL-10 level (pg/ml)
120
100
80
60
40
20
0
5hr
1d
3d
6d
10d
14d
28d
Timepoint
Clamp
Control

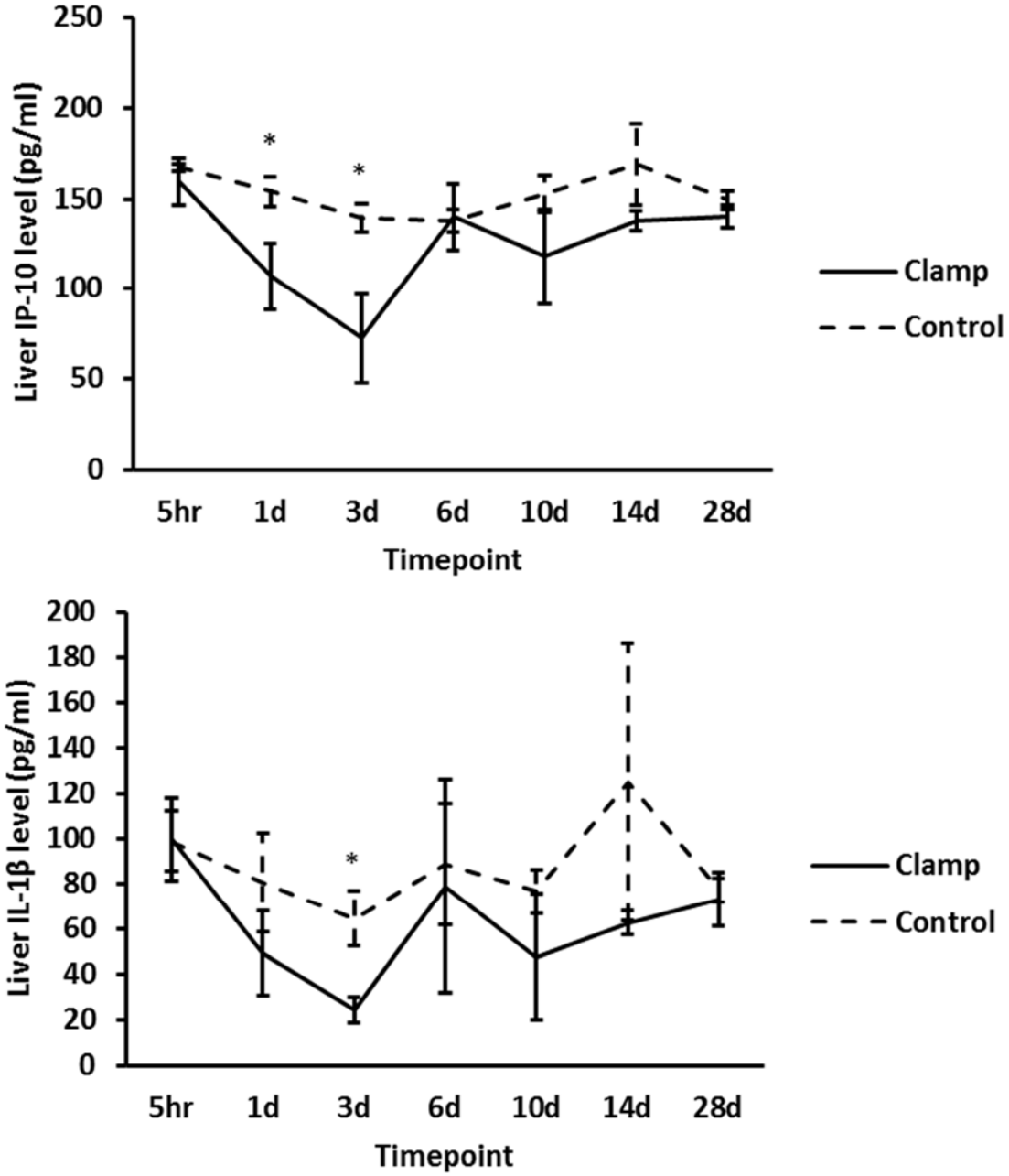

Figure 4.28 Levels of IL-2, IL-4, IL-10, IP-10 and IL-1β in ischaemic versus sham ischaemic liver tissue. *p<0.05 (versus IRI)

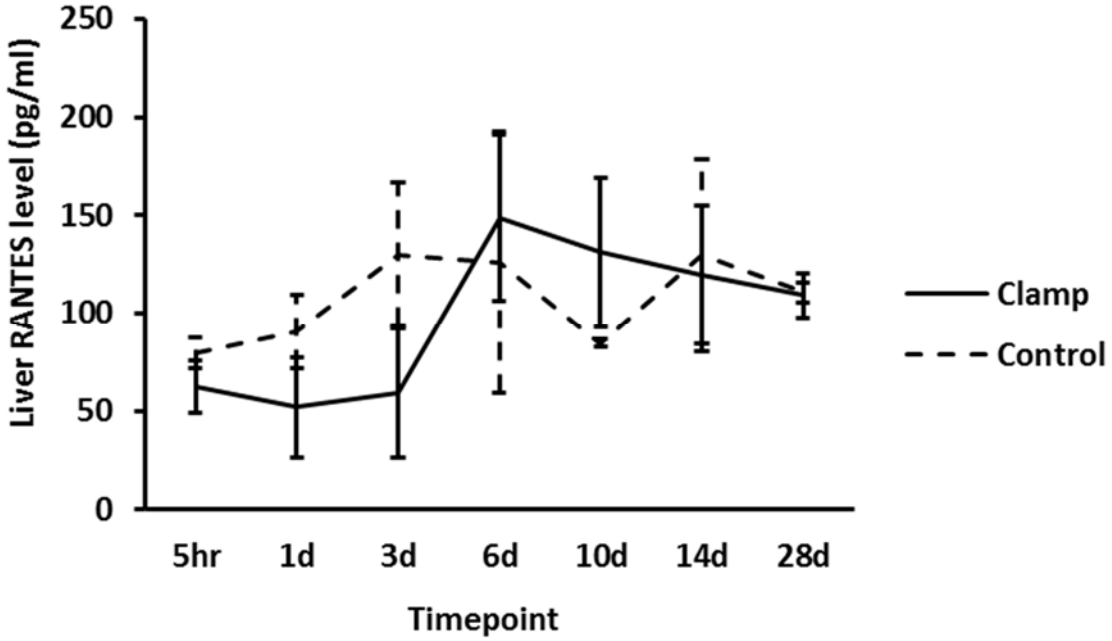

Figure 4.29 Levels of RANTES in ischaemic versus sham ischaemic liver tissue

A summary of the cytokine results in liver homogenate is outlined in Table 21

Table 21 Summary of cytokines that demonstrated significant differences in ischaemic lobe concentration between the IRI and control groups. Values are reported as mean±SD.

		IRI group (pg/ml)	Control group (pg/ml)	P value
IL-1α	5 hours	67.5±3.7	33.6±7.7	0.002345
	Day 3	13.3±6.6	32.5±11.8	0.070376
	Day 28	28.4±2.3	22.6±3	0.05611
IL-1b	Day 3	24.3±5.7	64.6±12.1	0.006482
IL-2	5 hours	228.3±27.1	308.6±40.6	0.046491
	Day 1	111.4±40.9	239.3±79	0.067552

	Day 3	48.8±31.7	210.8±58.3	0.013404
	Day 10	135±57.3	255.2±14.9	0.024523
	Day 14	172.4±45.5	316.6±77.3	0.049568
IL-4	5 hours	88.2±18.7	129.7±4.8	0.020412
	Day 1	71.4±13.6	118.1±20.1	0.028978
	Day 3	51.4±27.7	110.1±22.8	0.047119
	Day 10	79.1±5.7	134±20.1	0.010432
	Day 14	101.3±22.7	182.5±31.8	0.022789
	Day 28	108.7±8.3	135.1±15.8	0.062884
IL-6	5 hours	808.9±160.2	371.1±14.5	0.009206
	Day 1	435.4±162.4	211±54.7	0.085883
	Day 3	85.7±27	247.4±17.6	0.00097
	Day 10	66.8±43.5	272.6±37.9	0.003476
IL-10	5 hours	84.7±5.3	98.7±7.1	0.051705
	Day 1	34.7±12.3	74.6±10.2	0.012256
	Day 3	13.6±11	57.1±15.2	0.015982
	Day 10	38.6±13.8	79.3±21.9	0.052723
	Day 14	45.7±14.5	81.1±17	0.051783
IL-12p70	5 hours	42.1±3.3	14.3±6	0.002221
	Day 10	2.7±1.9	14.8±5.9	0.027277
IP-10	Day 1	107.2±18.2	154.1±8.2	0.015319
	Day 3	72.6±24.7	139.5±7.5	0.01096

	Day 10	118.1±26.1	152.9±10.3	0.098865
	Day 14	138.3±5.5	169±22.4	0.082282
MIP-1α	5 hours	10.7±1	4±0.9	0.000901
	Day 1	37.6±10.2	3±0.7	0.004273
	Day 3	89±47.8	2.8±1.1	0.035397
MIP-2	5 hours	87.4±50.3	15.6±11.8	0.074042
	Day 1	174.2±93.4	12.6±9.2	0.040672
	Day 10	2±0	20.2±5.2	0.003884
VEGF	5 hours	18.5±1.9	7.7±3.6	0.009939
	Day 1	23.3±6.1	5.5±2.3	0.009136
	Day 3	2.5±0.9	9±3.2	0.028403

Histological changes

To determine the histological changes induced by IRI, liver sections from ischaemic and sham ischaemic (control) lobes were stained with H&E. Sections exposed to IRI demonstrated distinct cellular changes compared to the control specimens (Figure 4.30 A&B). Ischaemic changes and spotty hepatocellular necrosis in zones 2 and 3 (mid-zonal and centrilobular, respectively) were evident as early as 5 hours after clamp release. This became more pronounced by day 1. Liver damage severity scores were significantly higher in the IRI group up to day 3 post-reperfusion compared to sham IRI (Figure 4.31). Progressive inflammation was manifest in zone 1 (peri-portal) 5 hours after clamp release and peaked at day 14 (Figure 4.32). Peri-portal inflammatory infiltrates at delayed timepoints contained increasing numbers of mononuclear granulocytes and haemosiderin-laden macrophages (Figure 4.30-B). In contrast, inflammation in zone 3 (centrilobular) was largely composed of acute inflammatory cells and was maximal on day 3 post-reperfusion, returning to baseline

levels by day 6 (Figure 4.33). The inflammatory changes in zone 1 were associated with ductular reaction, neovascularisation and fibrosis from day 3 and led to distortion of the intrahepatic architecture by day 14. Hepatocellular regeneration was marked on day 28 post-reperfusion, and the pathological changes in the peri-portal regions were still evident at this stage (Figure 4.30-B). Non-ischaemic lobes from the clamp and control groups appeared histologically normal and therefore only sham ischaemic (control) sections are shown.

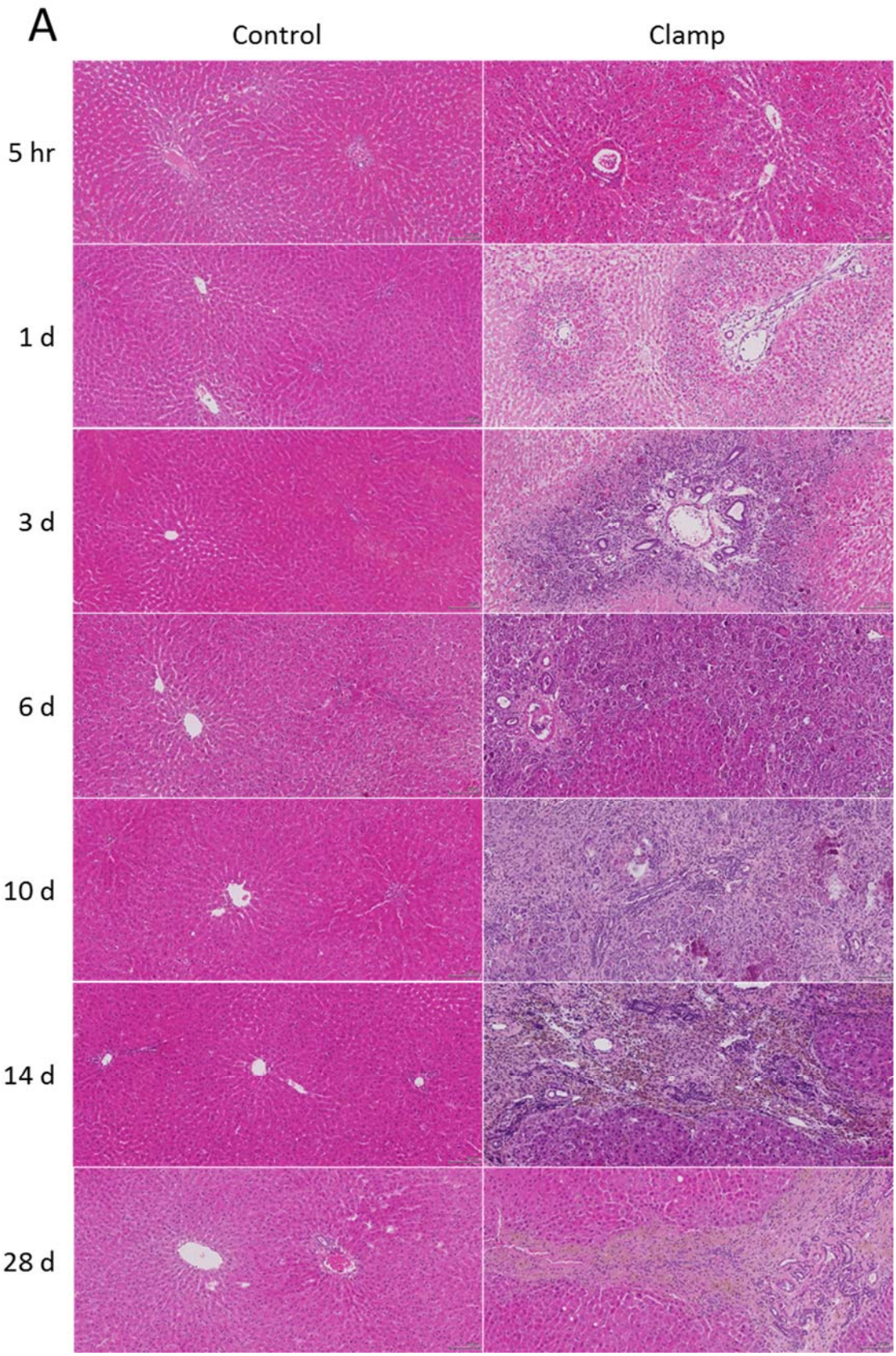
A
Control
Clamp
5 hr
1 d
3 d
6 d
10 d
14 d
28 d

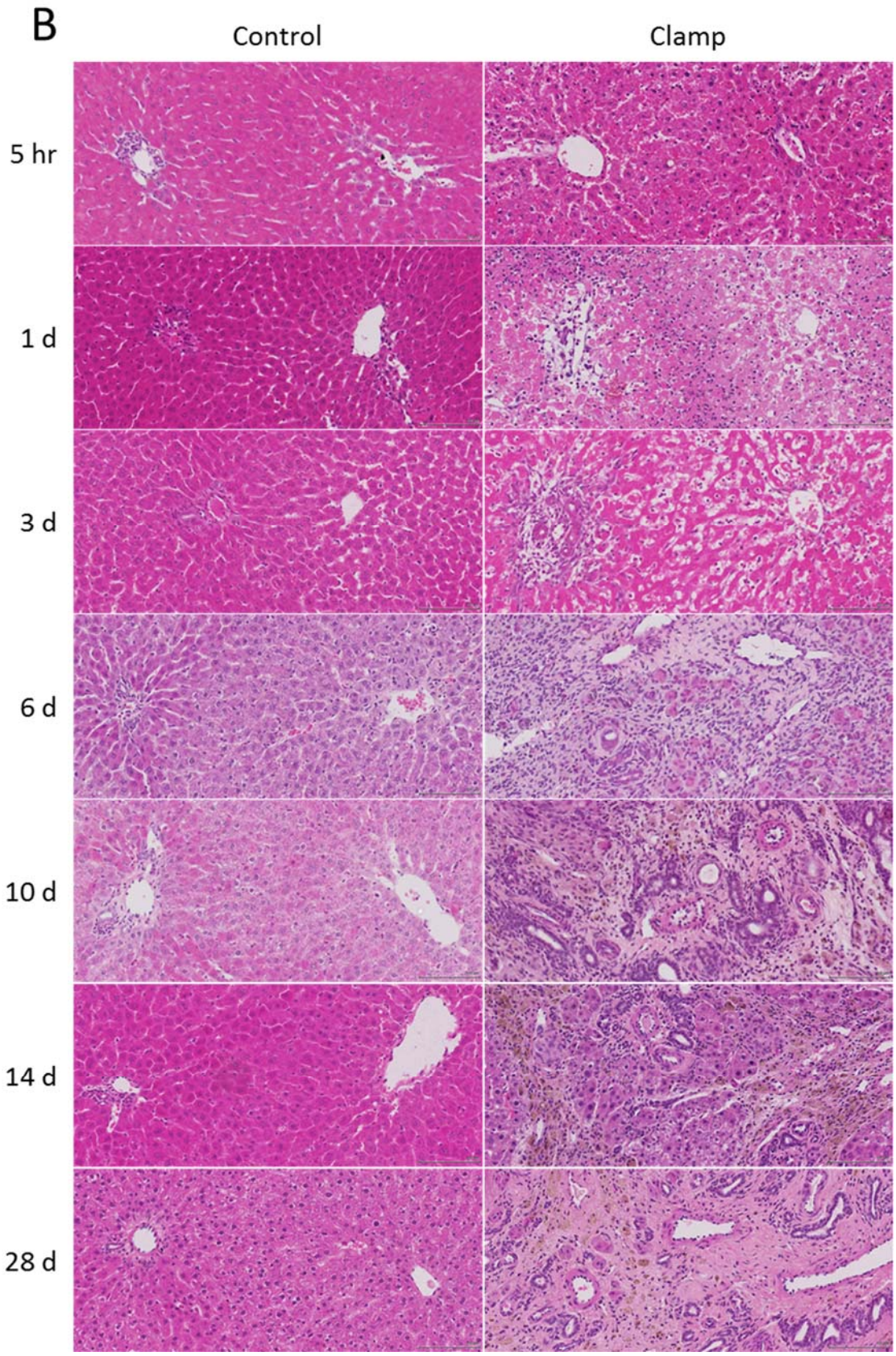

Figure 4.30 H&E staining of liver sections in low (A) and high (B) magnification demonstrates early parenchymal injury followed by ductal proliferation and peri-ductal fibrosis persisting up to 28 days following reperfusion in the IRI group.

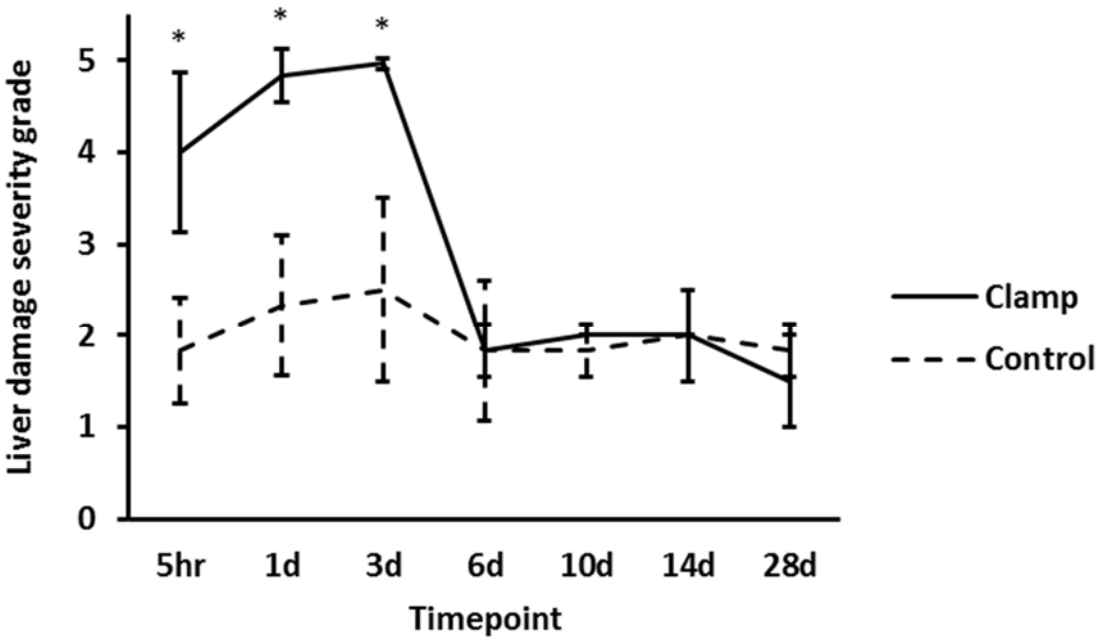

Figure 4.31 Comparison of liver damage severity scores between IRI and control groups assessed on H&E slides (scale of 0–5: normal–extensive damage). *p<0.05 (versus control)

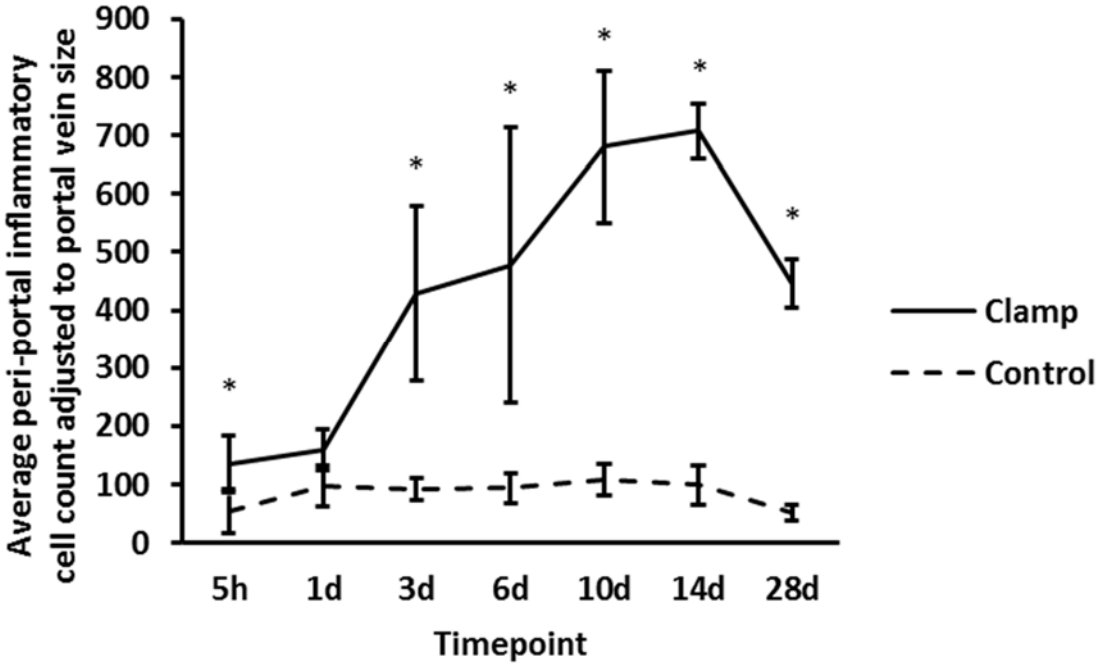

Figure 4.32 Comparison of inflammatory cell counts in peri-portal areas between the IRI and control groups. Inflammatory cell counts are significantly higher in the IRI

group from day 3 and persist for at least 28 days following reperfusion. *p<0.05 (versus control)

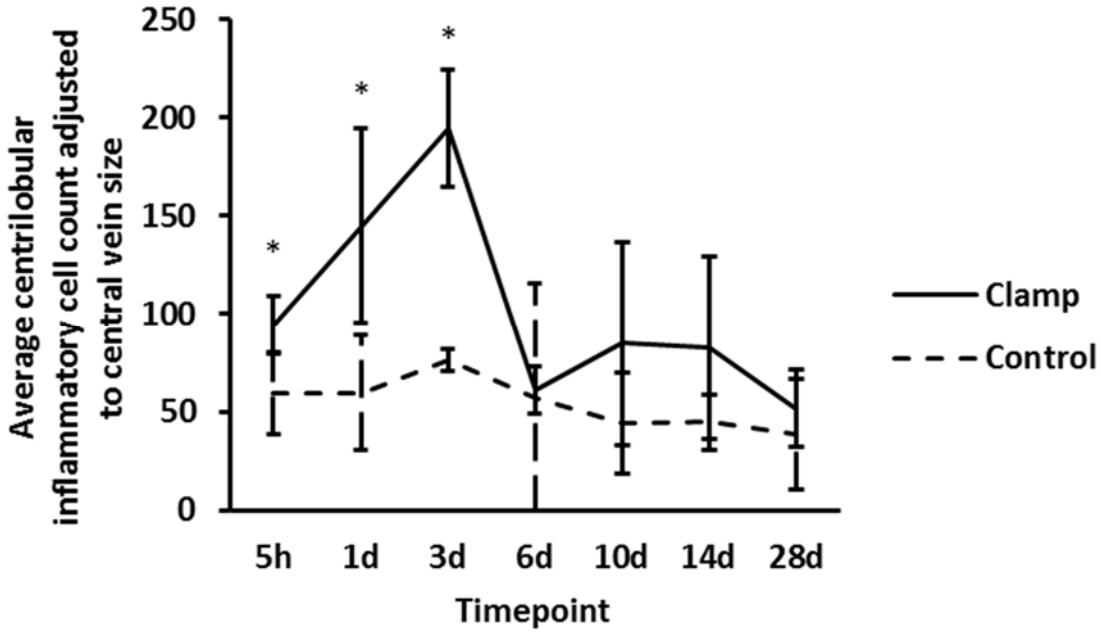

Figure 4.33 Comparison of inflammatory cell counts in centrilobular areas between the IRI and control groups. Inflammatory cell counts in centrilobular areas normalise after day 3. *p<0.05 (versus control)

Peri-portal fibrosis

Since H&E stained sections were suggestive of fibrogenesis, this was investigated further using α-SMA immunohistochemistry staining as a marker of activated myofibroblasts (Figure 4.34). Quantification of positive staining revealed a significant increase in α-SMA staining in ischaemic lobes in the IRI group between day 3 and 14 post-reperfusion, peaking at day 10 (3.2 ± 0.6% versus 0.4 ± 0.1% sham IRI; P=0.001) (Figure 4.35). Staining of liver sections for vimentin demonstrated comparable results (Figure 4.36 and Figure 4.37).

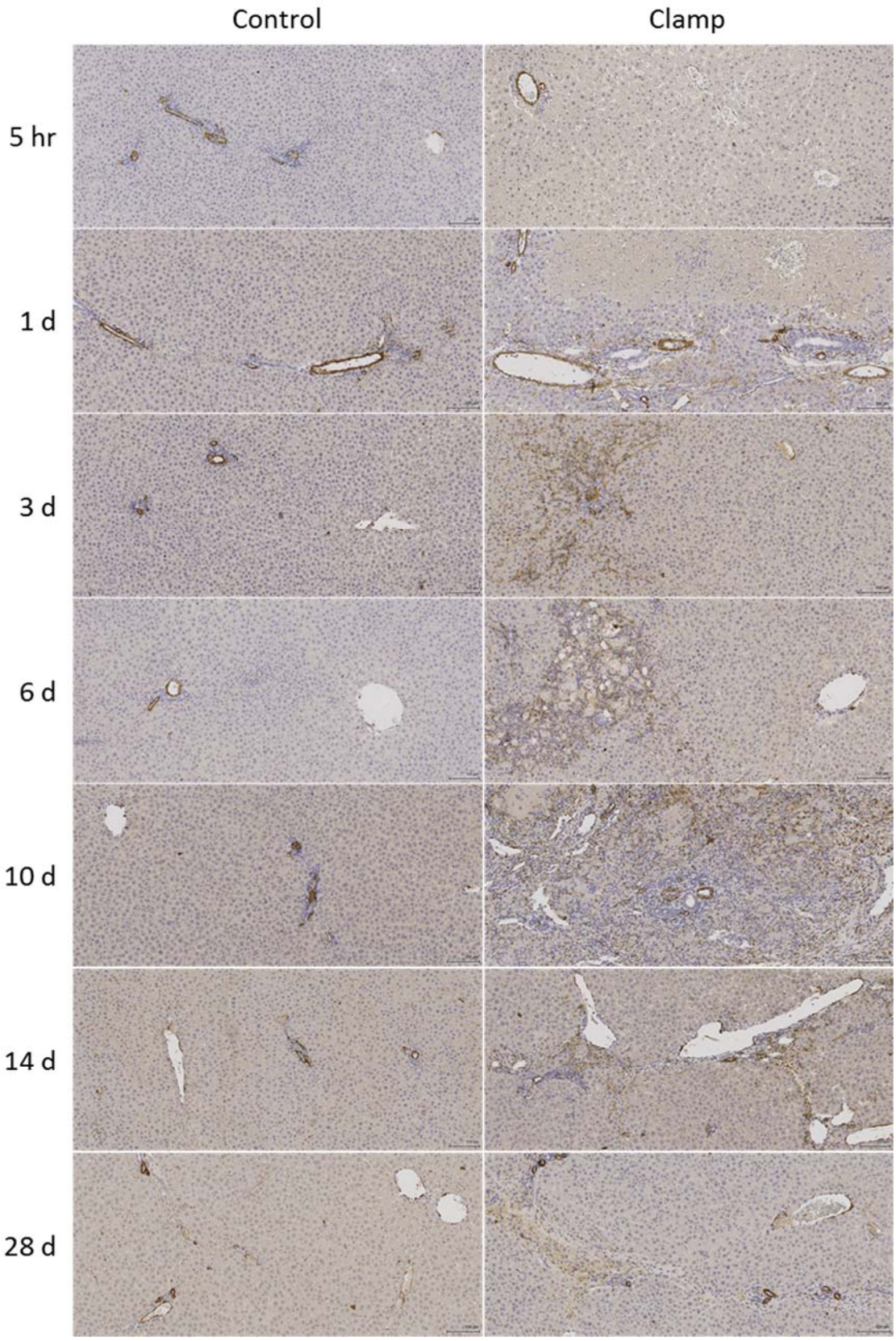

Figure 4.34 Comparison of α-SMA immunohistochemistry staining between IRI and sham IRI groups demonstrates a progressive increase in α-SMA-positive myofibroblasts in the IRI group peaking at day 10.

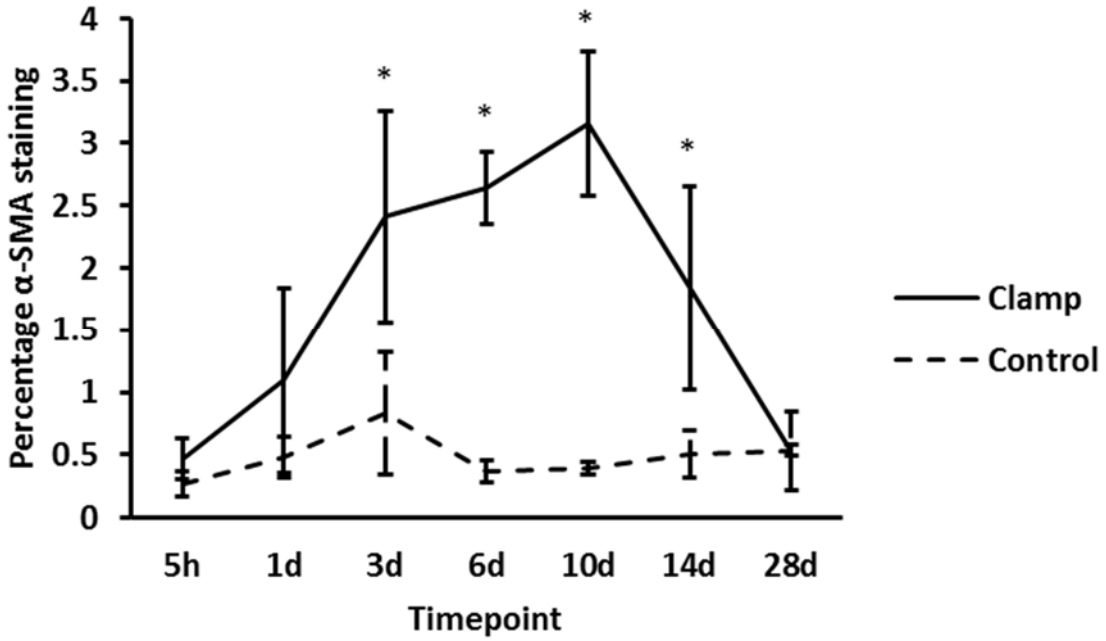

Figure 4.35 Quantification of α-SMA immunohistochemistry staining demonstrates significantly higher α-SMA expression in the IRI group between day 3 and 14 post-reperfusion compared to control. *p<0.05 (versus control)

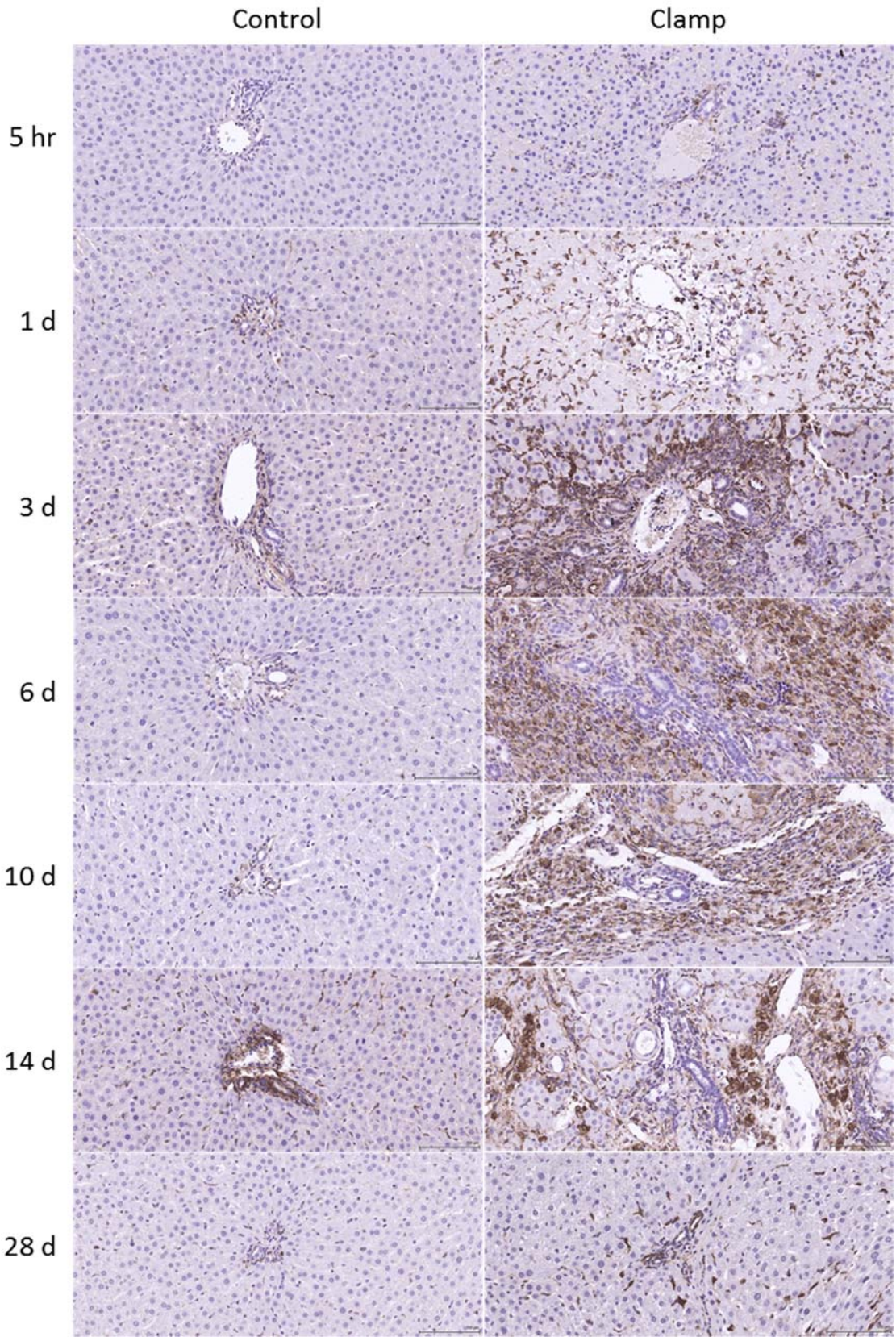

Figure 4.36 Comparison of vimentin staining between IRI and sham IRI groups demonstrates a significant increase in vimentin-positivity in the IRI group

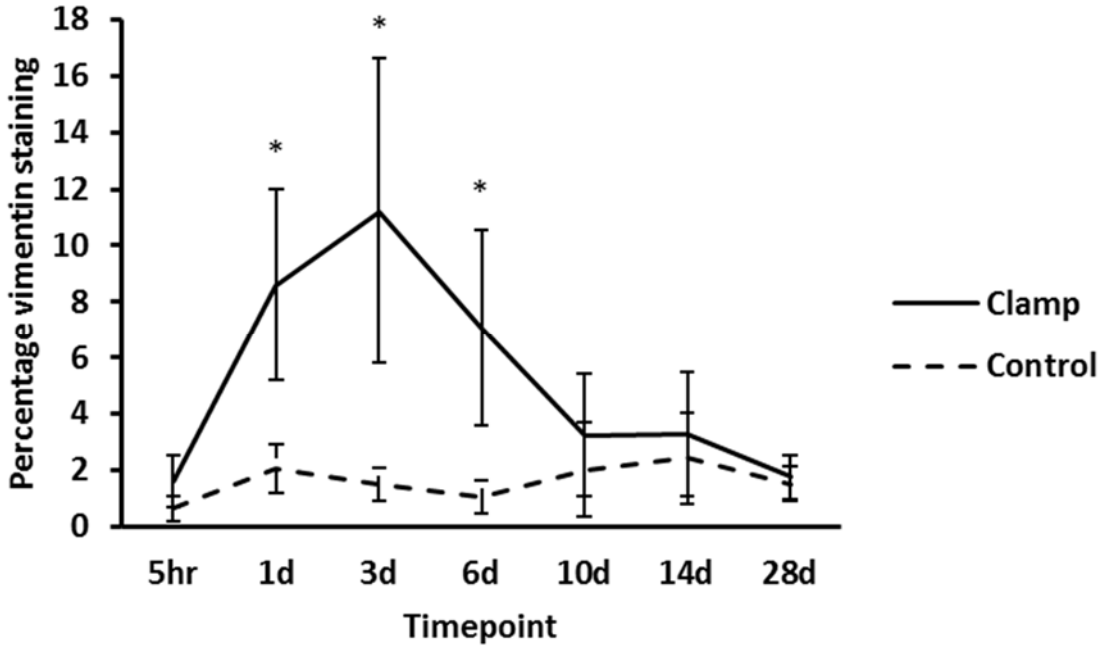

Figure 4.37 Quantification of vimentin immunohistochemistry staining demonstrates significantly higher vimentin expression in the IRI group between day 1 and 6 post-reperfusion compared to control. *p<0.05 (versus control)

The extent of liver fibrosis was assessed by staining serial liver sections from ischaemic and sham ischaemic lobes with sirius red. This analysis revealed severe and progressive peri-portal fibrosis in liver sections of animals in the IRI group, bridging portal tracts at later timepoints and persisting up to 28 days after the initial injury (Figure 4.38). Quantification of the areas stained with sirius red showed that the degree of fibrosis was maximal in the IRI lobes on day 10 post-reperfusion (3.6±1.2% versus 0.8±0.2% in sham IRI lobes; P=0.03). Fibrosis was still significantly present on day 28 post-reperfusion (2.9 ± 1.2%; P=0.26 versus IRI lobes on day 10). Non-ischaemic lobes from the IRI group and sham IRI groups appeared histologically normal and therefore only the sham IRI is shown (Figure 4.39).

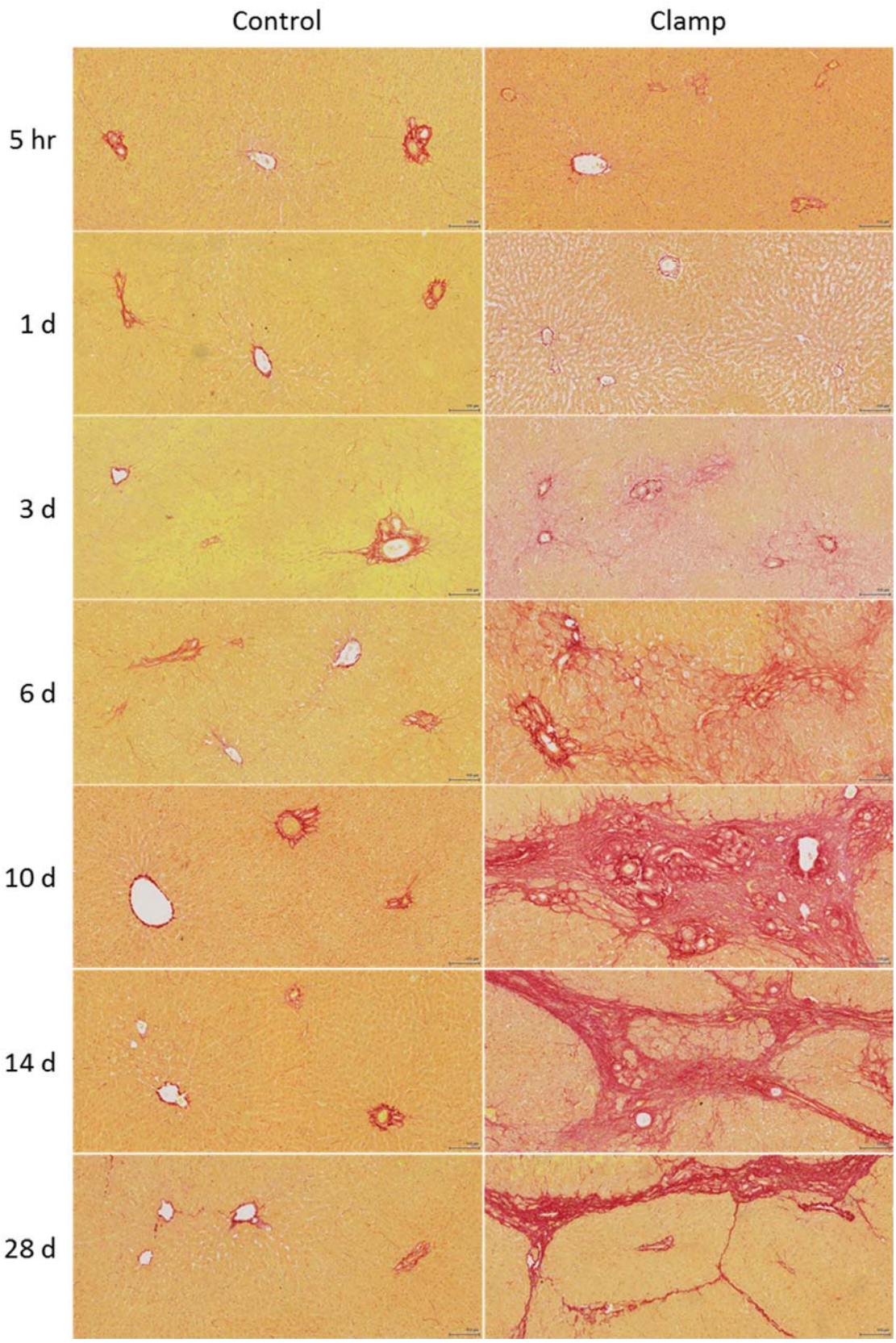

Figure 4.38 Sirius red staining demonstrates progressive peri-portal fibrosis in the IRI group persisting up to 28 days following reperfusion with bridging portal tracts at late timepoints.

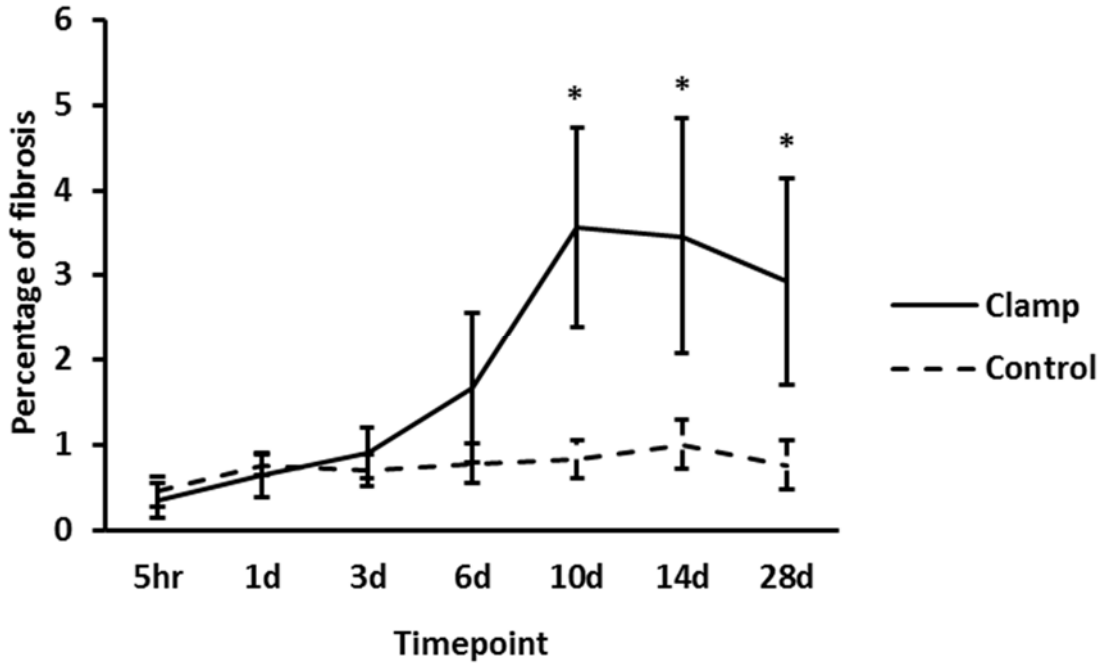

Figure 4.39 Progression of fibrosis in the IRI group compared to control based on quantification of sirius red staining. *p<0.05. *p<0.05 (versus control)

To confirm these findings, mRNA transcript levels of the pro-fibrotic cytokine TGF-β, vimentin and pro-alpha1(I) collagen were measured by RT-PCR in ischaemic and sham ischaemic liver lobes. Sham ischaemic liver lobes at day 28 were used as reference samples. TGF-β and vimentin mRNA transcript levels were significantly higher in the ischaemic lobes between day 1 and 3 post-reperfusion compared to the sham ischaemic lobes. Peak levels were demonstrated at day 1 (13-fold and 53-fold increase in TGF-β and vimentin mRNA levels respectively in ischaemic lobes) (Figure 4.40 and Figure 4.41). COL1A1 mRNA was significantly elevated in the Ischaemic lobes in IRI group between day 3 and 14 after clamp release, peaking at day 6 with a 30-fold increase in COL1A1 mRNA levels compared to sham ischaemic lobes (Figure 4.42).

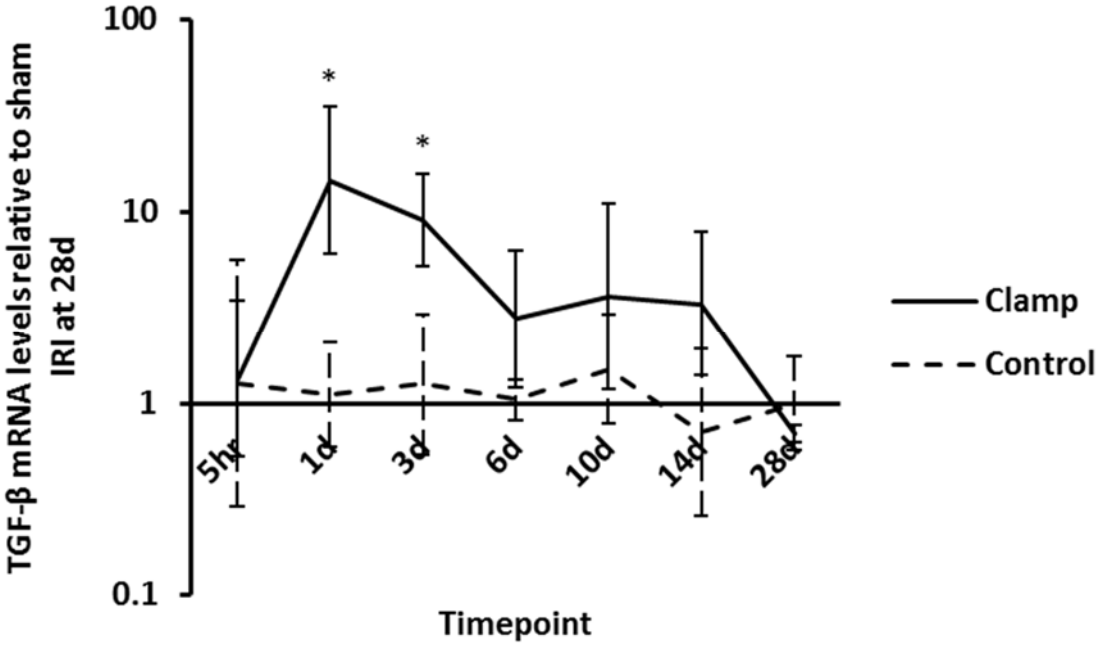

Figure 4.40 RT-PCR analysis in ischaemic and sham ischaemic lobes shows significantly increased expression of TGF-β in the ischaemic liver lobes between day 1 and 3 post-reperfusion. *p<0.05 versus control

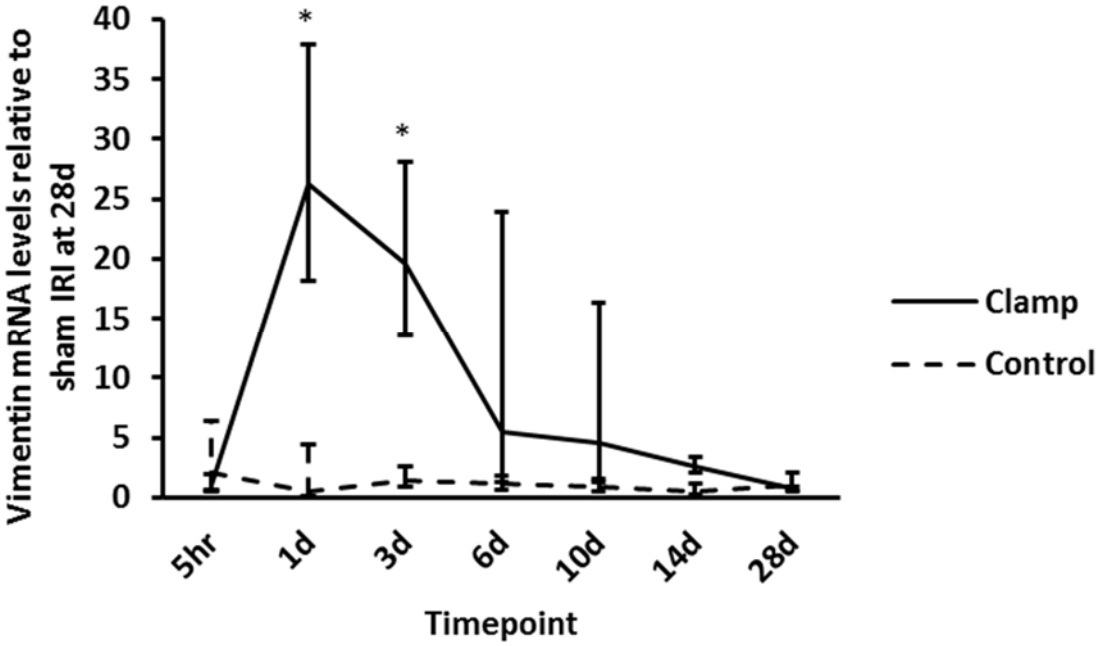

Figure 4.41 RT-PCR analysis in ischaemic and sham ischaemic lobes shows significantly increased expression of vimentin in the ischaemic liver lobes between day 1 and 3 post-reperfusion. *p<0.05 versus control

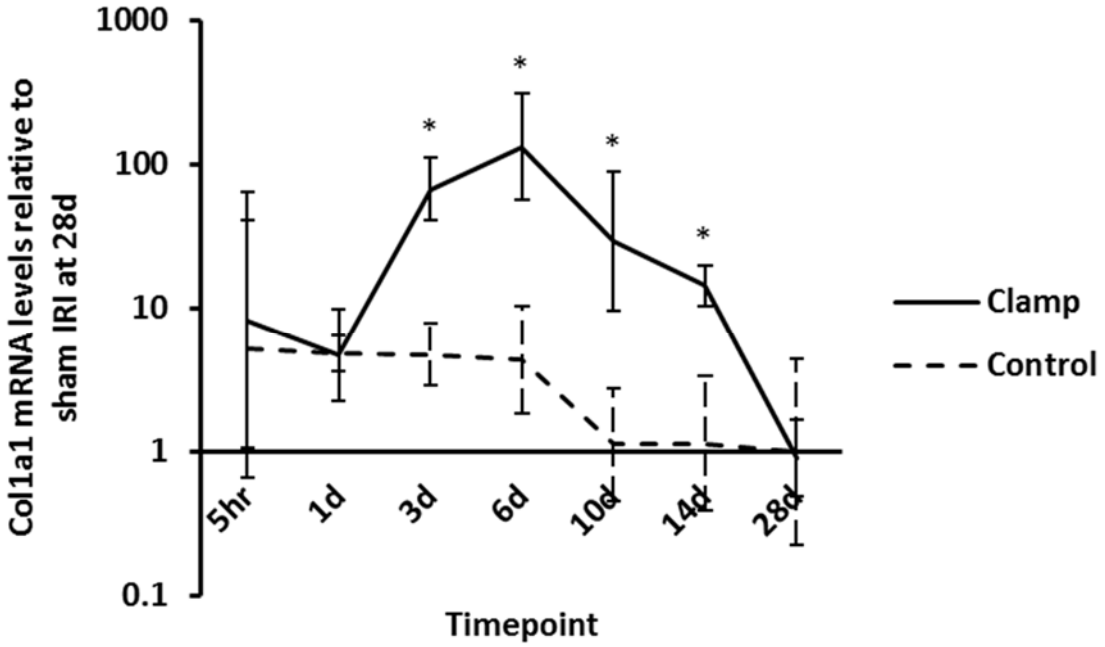

Figure 4.42 RT-PCR analysis in ischaemic and sham ischaemic lobes shows significantly increased expression of Col1A1 in the ischaemic liver lobes between day 3 and 14 post-reperfusion. *p<0.05 versus control

Ductular reaction

Examination of H&E-stained slides suggested the development of a ductular reaction in response to IRI. This was further assessed using immunohistochemistry staining to quantify the expression of cytokeratin 19 (CK19), a marker of both mature and immature biliary epithelial cells ((Zorn, 2008) (Figure 4.43). Quantification of CK19 staining demonstrated a significant increase in positivity following IRI from day 10 up to day 28 post-reperfusion, with peak positivity at day 14 (4.2±1.3% versus 0.3±0.2% in the sham IRI group; P=0.007) (Figure 4.44).

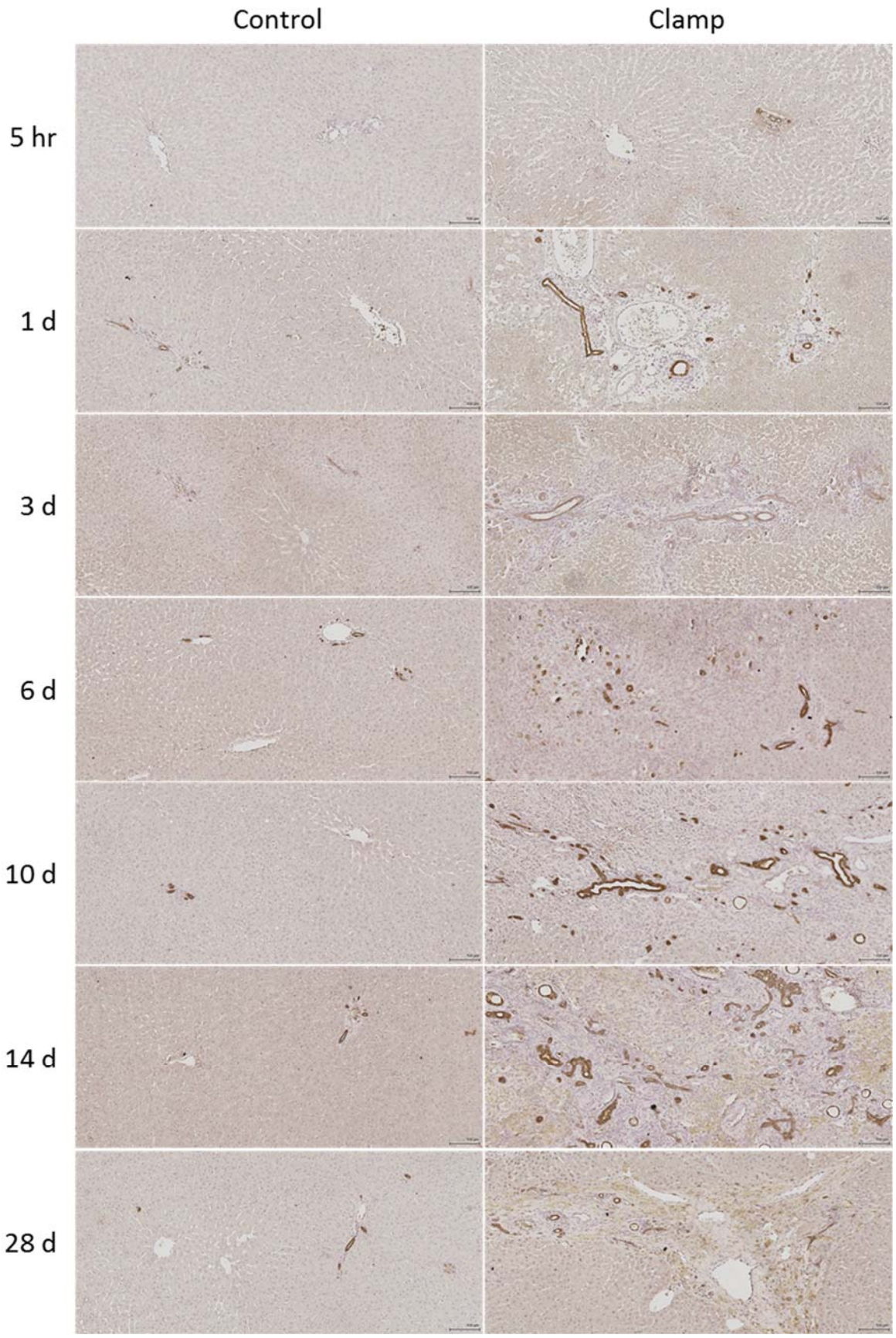

Figure 4.43 Comparison of CK19 staining between IRI and sham IRI groups demonstrates a significant increase in CK19-positivity in the IRI group

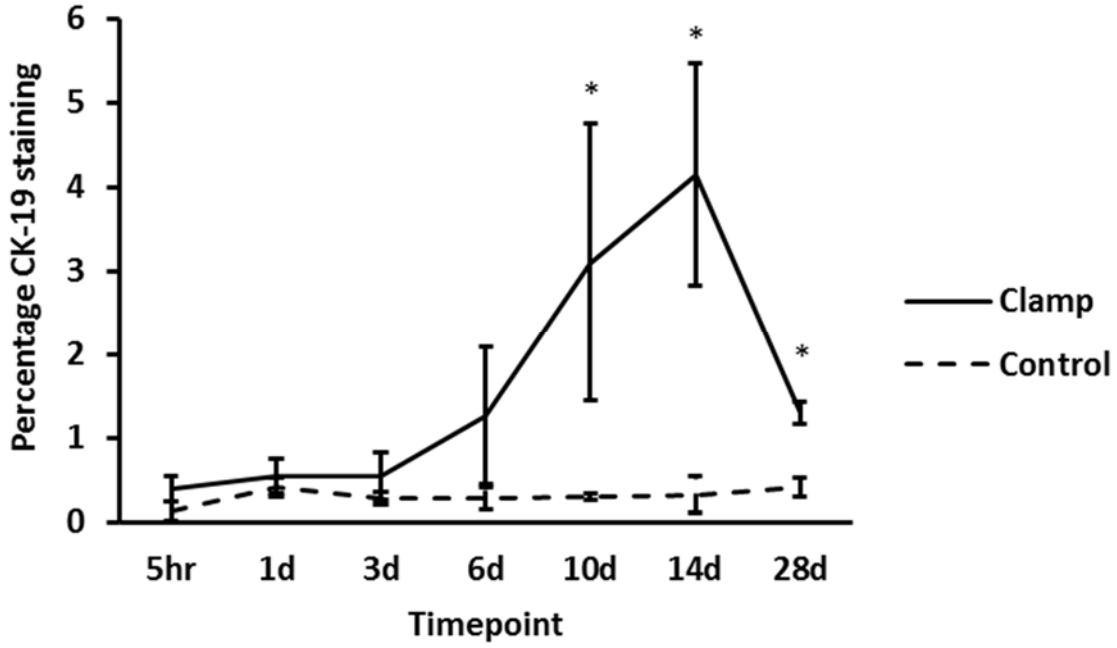

Figure 4.44 Quantification of CK19 immunohistochemistry staining demonstrates significantly higher CK19 expression in the IRI group from day 10 up to day 28 post-reperfusion compared to control. *p<0.05 (versus control)

Biliary epithelial cell microvilli measurements

Based on TEM imaging of bile ducts (Figure 4.45), it was observed that biliary epithelial cells from large ducts demonstrated a significant increase in microvillar height, on postoperative day 1 in the IRI group compared to the control group. This difference was greater on postoperative day 28. Basal width measurements were higher in the IRI group but only reached statistical significance on day 28 (Table 22). Microvillar density was significantly reduced in the IRI group compared to control but increased to a value greater than control on day 28 (Figure 4.46).

Examination of small bile duct (defined as ducts with diameters less than 100μm) showed no significant difference in microvillar measurements between the two groups.

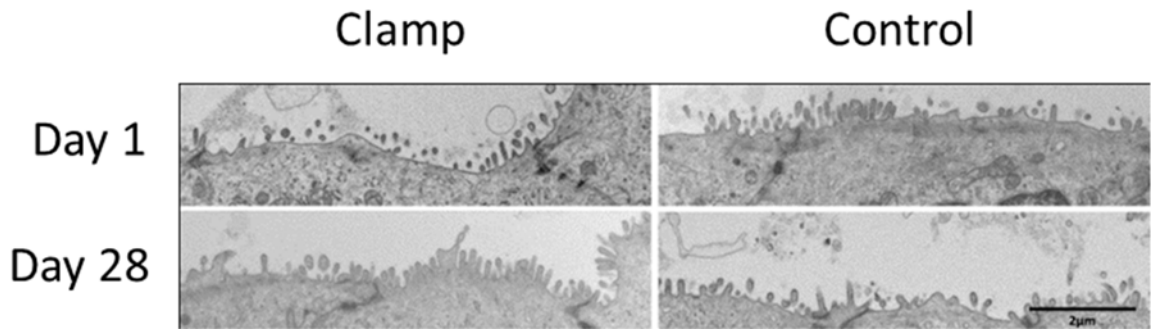

Figure 4.45 TEM images comparing BEC microvilli morphology during early (day 1) and late (day 28) reperfusion timepoints

Table 22 A comparison of BEC microvilli height and width between study groups

	Height*		**Basal width***	
	1d	**28d**	**1d**	**28d**
IRI	213 (271.5)	227 (392)	102 (137)	111 (205.4)
Control	203 (213)	197 (326.5)	96 (125.5)	100 (161.6)
P value	**<0.01**	**<0.0001**	**N/S**	**<0.0001**

*Results expressed as median (mean rank); Unit of measurement=nm

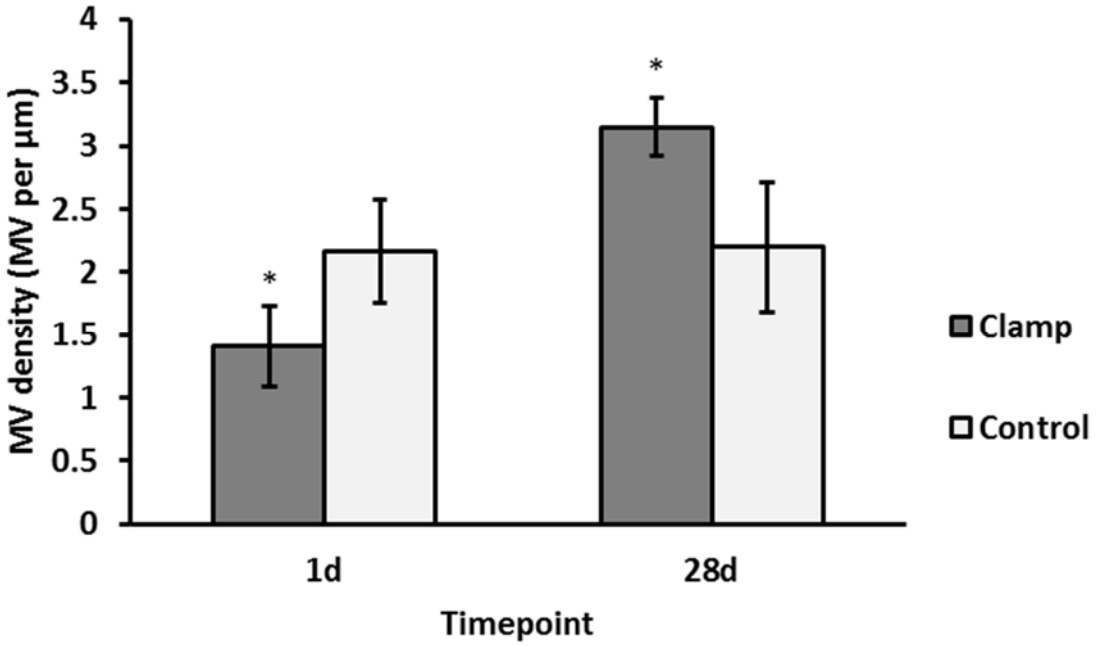

Figure 4.46 Changes in BEC microvillar density following IRI. *p<0.05 (versus control)

4.4. Discussion

The aim of this study was to investigate the short and long-term pro-inflammatory and pro-fibrotic effects of IRI particularly in relation to the intra-hepatic biliary tract.

The majority of the published research on hepatic IRI in animal models focuses on data within the first few hours/days of reperfusion (Zhao et al., 2009, Dusunceli et al., 2008, Ichiki et al., 2008, Liu et al., 2011b, Mochizuki et al., 2007, Pratap et al., 2011, Teoh et al., 2010, Sener et al., 2005, Man et al., 2005). However, since complications following DCD organ donations that occur subsequent to initial liver injury were the focus of this study, a 28-day follow up period was opted for to take into account the delayed clinical presentation of NABS, a more clinically relevant complication in this group of recipients (Ayoub et al., 2010). This has been considered sufficient follow up for long-term complications in an adult rat by previous investigators in view of the relative overall lifespan of adult rats compared to humans (Schlegel et al., 2013).

A modified 70% hepatic IRI model was adopted in this study in order to avoid portal congestion associated with proximal hilar inflow occlusion and cholestatic injury associated with concomitant bile duct clamping. Inflow occlusion of 90 minutes in the pilot phase of model development produced predictable and reproducible damage (4.3.1). An ischaemic period of 90 minutes has previously been shown to induce maximal TNF-α production and inflammation (Colletti et al., 1990).

Adequate radiological visualisation of the biliary tree was not possible in this model due to the unavoidable disruption of ductules and leakage of contrast into the systemic circulation, and due to the suboptimal resolution of the small animal CT scanner imaging. Hence the original plan to investigate potential stenotic lesions within the biliary tree was abandoned.

The initial weight loss experienced in both groups in the early postoperative period was most probably related to the expected increase in catabolism following surgery. Animals in the IRI group appeared to be more affected by this early weight loss. However, the improvement in weights of animals in the IRI group -which was comparable to controls-indicated good recovery from the hepatic IRI. The comparable levels of serum albumin and total protein suggest that there was no significant increase in the negative nitrogen balance above that normally seen following abdominal surgery.

It was evident from this study that bile flow in ischaemic livers was significantly reduced in the early post re-perfusion period. Although the IRI group subsequently achieved bile flow rates comparable to controls from day 3 onwards, it is unclear whether this was due to recovering bile production in ischaemic lobes or a compensatory effect in non-ischaemic lobes since –for practical reasons- total bile flow rather than lobar flow was measured in this study. Nevertheless, the microvilli of BEC exposed to IRI demonstrated a significant increase in surface area with time during this study, suggesting a prolonged adaptive secretory response within ischaemic lobes.

Serum bile acid and ALP levels were found to be significantly higher in the IRI group in the early post re-perfusion period. These results signify cholestasis in the animals exposed to IRI. The prompt resolution of the cholestatic picture within one week of the injury point to a compensatory role probably played by the non-ischaemic lobes. Although serum bilirubin and GGT levels followed a pattern comparable to serum bile acids and ALP, the results were not statistically significant. This was likely due to the large variance observed the IRI group in the face of a small sample size per timepoint (n=3).

Serum hyaluronic acid was measured as a surrogate marker of sinusoidal endothelial cell damage (Shimizu et al., 1994). Levels in this study indicated that sinusoidal endothelial damage occurred mainly between day 1 and 3 post re-perfusion. These findings were confirmed by measuring tissue hyaluronate levels which demonstrated a comparable pattern.

Serum ALT activity was used as a marker of hepatocyte damage uninfluenced by the compensatory effect of non-ischaemic lobes. It provided evidence of hepatocellular damage in the IRI group that was manifest immediately postoperatively and lasted up to 3 days. However, bearing in mind that the average half-life of serum ALT is 47±10 hours (Kim et al., 2008), it is likely that the majority of hepatocellular damage will have occurred within the first 36 hours post re-perfusion.

Hepatocellular necrosis -mostly visible in mid-zonal and centrilobular areas- was evident histologically from 5 hours up to 3 days post re-perfusion in this study. This was associated with an early inflammatory response in the centrilobular areas over the same duration of time. Peri-portal inflammation was also evident shortly after re-perfusion, and in contrast to the centrilobular response, persisted up to 28 days.

Cytokine measurement was subsequently undertaken to shed further light on these histological findings. Interleukins 1α and 6 were found to be expressed at significantly greater levels in the early timepoints following IRI, suggesting an important role for these pro-inflammatory cytokines in the acute inflammatory phase following reperfusion injury. A number of chemokines followed a similar pattern, including MCP-1, MIP-1α and MIP-2. Two particular chemokines were found to be significantly elevated in bile samples following IRI: MCP-1 and VEGF. This suggests increased secretion of these proteins in the vicinity of biliary ductules/ducts, leading to further propagation of a periductal inflammatory response. The early rise in VEGF secretion following IRI suggests that it is produced in response to hypoxia, a known stimulant of VEGF expression (Ziello et al., 2007). VEGF might also play a role in the neovascular and ductular response observed during the latter timepoints post IRI. However, VEGF levels were not found to be significantly higher than controls at these delayed timepoints.

Interestingly, tissue levels of the anti-inflammatory interleukins 4 and 10 were lower in the IRI group throughout the postoperative period, suggesting a prolonged suppression of immunomodulatory pathways following IRI.

The chemokine RANTES has been previously found to be linked to progressive fibrosis (Ramm, 2011). In this study, we have identified a pattern of delayed RANTES production in animals exposed to IRI from day 6 onwards. This correlates with the expression of pro-fibrotic proteins in the affected liver lobes culminating in persistent liver fibrosis. RANTES is likely to be secreted by both lymphocytes and activated hepatic stellate cells (Ramm, 2011). The progressive rise in biliary levels of RANTES suggests considerable peri-biliary fibrosis post-IRI.

Surprisingly, TNF-α levels were not found to be significantly elevated following reperfusion in this study despite evidence in the literature supporting its role in IRI (Datta et al., 2013). TNF-α release has been reported to be detectable in serum samples between 30 minutes and 8 hours of reperfusion (Datta et al., 2013). This window may have been too narrow to enable TNF-α detection at the chosen timepoint in our study.

TGF-β secretion was evident as early as day 1 post re-perfusion. The release of this pro-fibrotic cytokine results in the expression of α-SMA –a marker of activated

hepatic stellate cells- from day 3. Findings from this study suggest that active HSCs persist up to 14 days post re-perfusion.

Although Col1a1 expression persisted up to day 14, fibrosis –manifest as positive Sirius red staining- peaked on day 10 and was still evident on day 28 post re-perfusion. A ductular reaction was closely associated with this fibrotic response, albeit peaking at a slightly later timepoint (day 14).

The hypothesis that IRI could lead to a disturbance in the physiological balance between biliary bile acids and phospholipids was also tested in this study (Buis et al., 2009). Although the findings obtained do not provide a definitive answer to the hypothesis in question, they do shed light on many aspects of it. While biliary bile acids were found to be elevated on day 1 following IRI, biliary phospholipids -which are thought to provide a protective role against the cytotoxic effects of bile salts- peaked on day 3. The resultant lag in the phospholipid response may have allowed enough time for bile salt damage to ensue. Nevertheless, when biliary bile salt/phospholipid ratios were compared between IRI and control groups, the higher ratio in the IRI group on day 1 did not reach statistical significance. Moreover, the ratios were significantly lower in the IRI group on day 3 compared to controls. This may suggest a more consistent and effective biliary phospholipid secretory response on day 3 compared to the presumed earlier bile salt secretory surge. However, both biliary bile acid and phospholipid measurements refer to concentrations from ‘common bile duct’ samples which include mixed bile produced by ischaemic and non-ischaemic lobes and thus are predisposed to the compensatory effect of non-ischaemic lobes. Given that bile composition from non-ischaemic lobes was not examined separately in this study, the magnitude of this possible compensatory response remains unclear.

Measurement of hepatocellular bile salt transporters provided a way to examine this hypothesis from a different angle. Measurement of Ntcp, Bsep and Oatp2b1 transcript levels in liver tissue suggested that the expression of these transporters was greatly reduced between day 1 and 3 post re-perfusion. Regardless of whether this reflected global hepatocellular damage or more selective inhibition of these transporters following IRI, it suggested that the overall picture was more in keeping with cholestasis rather than an increase in biliary bile salt secretion. This was further confirmed on measurement of serum bile salt/phospholipid ratio which was found to

be significantly elevated in the IRI group, in addition to the cholestatic picture noted in the liver function tests described earlier.

This study shows that severe (90 min) hepatic IRI results in progressive peri-portal fibrosis that peaks at day 10 and persists for at least 28 days after reperfusion, following an early period of reversible cholestasis and cellular injury. This contrasts with the injury response following other acute hepatic injuries to CCL4 and methapyriline toxicity where fibrosis only develops through repeated injury over several weeks (Wright et al., 2001, Iredale et al., 1998).

One limitation of this study is the small sample size per timepoint. This was due to the relatively large number of timepoints chosen in order to portray a meaningful sequence to each process examined. The small sample size per timepoint may have resulted in type 2 errors in the reported results, effectively underestimating the effect of IRI for various endpoints and timepoints. Nevertheless, restrictions on experimental animal procedures (NC3Rs/BBSRC/Defra/MRC/NERC/Wellcome Trust, 2013) in addition to time and funding constraints prevented any further meaningful increase in sample size.

Despite the advantages of a partial ischaemic model, one major limitation it presented was the potential compensatory effect of non-ischaemic lobes unaccounted for in various endpoints. This effect was difficult to measure particularly in mixed fluid samples such as serum and bile. The lack of expertise and equipment needed to cannulate and sample smaller vessels posed a major challenge here. In addition to deviating from the classic clinical transplant scenario where all lobes are ischaemic, the systemic effect of non-ischaemic lobes on the behaviour of ischaemic lobes within the same animal in this model remain poorly understood. Previous research has demonstrated stromal morphological alterations in non-ischaemic lobes probably in response to circulating inflammatory cytokines, resulting in activation of KCs and upregulation of MMPs but no evidence of cell death in non-ischaemic lobes (Kitamura et al., 2010, Liu et al., 2011a, Palladini et al., 2012, Nakamitsu et al., 2001)

The lack of cholangiography results in this model precluded the ability to correlate between histological findings and radiological evidence of NABS in this study. As mentioned earlier, this was largely due to the lack of suitable equipment for this planned phase of the study.

Despite these limitations, this study provides significant headway in our knowledge regarding hepatic IRI and its fibrotic and inflammatory effects. The progression of fibrosis following IRI has not been investigated in a sequential manner similar to this study in previously published reports. The results outlined will provide valuable insight into the pathogenesis of biliary lesions several months after liver transplantation (Ayoub et al., 2010, Buis et al., 2006).

Chapter 5. PXR study

5.1. Introduction

Interest in the PXR as a novel therapeutic target has clearly increased over the past 15 years (Banerjee et al., 2015). Figure 5.1 shows the rising number of publications that have investigated the PXR since its discovery in 1998. In order to understand the basis of this growing interest and potential role of the PXR in many clinical conditions including hepatic ischaemia reperfusion injury, it is important to examine the history and biology of this intriguing nuclear receptor in more detail.

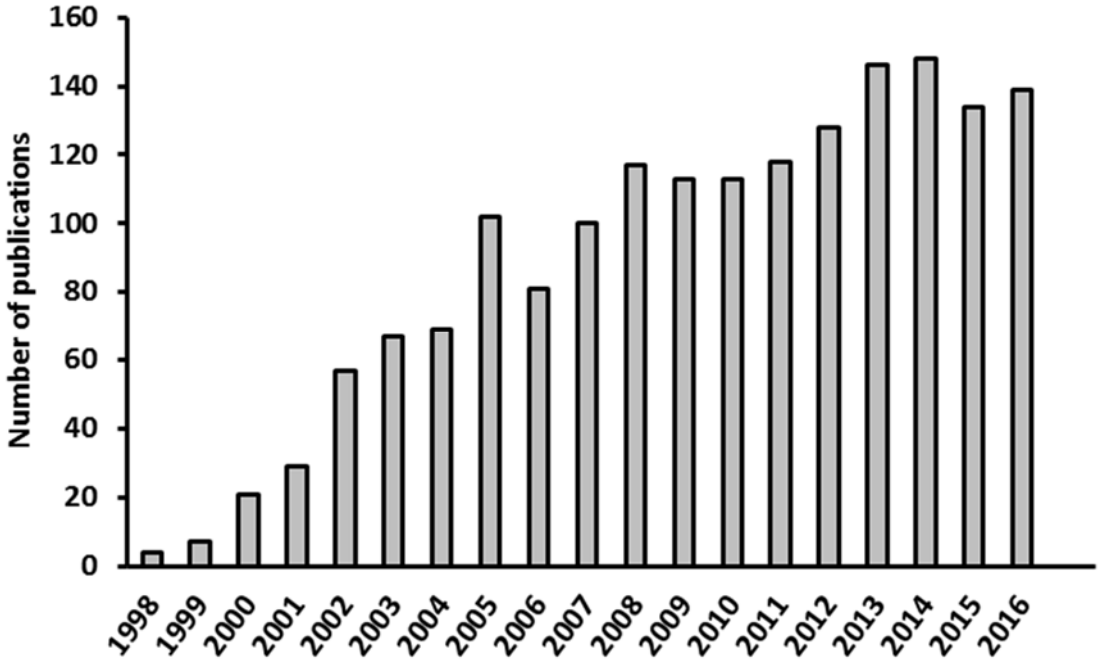

Figure 5.1 Timeline trend for PXR publications

5.1.1. The nuclear receptor superfamily

The PXR belongs to a larger group of receptors collectively known as the nuclear receptor superfamily. This includes receptors for a number of known hormones and endogenous ligands, such as the glucocorticoid receptor (GR), oestrogen receptor (ER), progesterone receptor (PR) and vitamin D receptor (VDR) (Li et al., 2012). In addition, other nuclear receptors have been identified over the years for which a predominant endogenous physiological ligand cannot be identified. These are

referred to as orphan nuclear receptors and include receptors that act as transcriptional regulators (such as the small heterodimer partner (SHP)), cell development stimulators (such as the hepatocyte nuclear factors (HNFs)), regulators of cholesterol metabolism (such as the peroxisome proliferator-activated receptors (PPARs), the liver x receptor (LXR) and the farnesoid x receptor (FXR)) and regulators of xenobiotic metabolism (such as the constitutive androstane receptor (CAR) and the pregnane x receptor (PXR)) (Mullican et al., 2013). In humans, 48 nuclear receptors have been identified, 36 of which are orphan receptors (Li et al., 2012).

The structure of nuclear receptors

Nuclear receptors share a common structural arrangement that is comprised of four major domains (Pawlak et al., 2012, Nikolenko Iu and Krasnov, 2007):

- The N terminal A/B domain is located on the amino terminal of the protein and contains the activation function 1 (AF1) region which can vary in size significantly among orphan nuclear receptors
- The DNA binding domain (DBD- henceforth referred to as DBDnr to avoid confusion with a similar acronym used in this document) is formed by two zinc finger motifs, one of which (known as the P-box) is responsible for the receptor's DNA-binding specificity. This area is typically highly conserved among nuclear receptors
- The ligand-binding domain (LBD) is located on the carboxy terminal of the protein and consists of 11-13 α-helical regions that forma hydrophobic pocket wherein ligand binding takes place. This domain is responsible for the receptor's ligand-binding specificity and therefore varies between receptors in that regard and in the presence or absence of an activation function 2 (AF2) region which gives the receptor the ability to interact with coactivators. This domain also contains a distinct region responsible for dimerisation.
- The hinge domain links the DBDnr to the LBD in a flexible manner and can vary in length between receptors

Figure 5.2 illustrates the overall structure of a nuclear receptor.

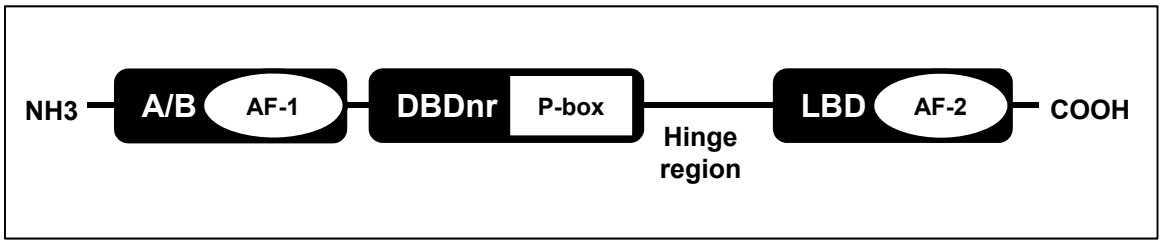

Figure 5.2 The general structure of a nuclear receptor

Mechanism of action of ligand-binding nuclear receptors

The most commonly recognised feature of nuclear receptors is their ability to activate target gene transcription upon binding to ligands (Pawlak et al., 2012). Unbound nuclear receptors can either be cytoplasmic or nuclear in location (Nikolenko Iu and Krasnov, 2007). Cytoplasmic nuclear receptors shuttle to the nucleus following activation by ligand (Mullican et al., 2013). Binding of the ligand induces conformational changes that facilitate dissociation of corepressor molecules (including the silencing mediator for retinoid and thyroid hormone (SMRT) and the nuclear receptor co-repressor (NCoR)) and concomitant changes to the AF-2 region (when present) that allow interaction with various coactivator molecules such as the steroid receptor coactivator (SRC-1) (Pawlak et al., 2012). Ligand binding also induces conformational changes to the DBDnr region that allows binding of the nuclear receptor to sequence-specific hormone-response elements (HREs) on the target DNA and activation of gene transcription (Nikolenko Iu and Krasnov, 2007).

Nuclear receptors bind to DNA either as monomers, homodimers (such as classical steroid receptors) or heterodimers with the retinoid x receptor (RXR) (such as VDR and many orphan nuclear receptors). Some nuclear receptors can function either as homodimers or heterodimers (such as HNFs and RXR) (Pawlak et al., 2012).

Some nuclear receptors can supress target gene transcription when in the ligand-free state through the formation of corepressor complexes (Pawlak et al., 2012)

5.1.2. Discovery of the PXR

The effect of xenobiotics on metabolic enzymes and transporters had been well known but not truly understood until the eventual discovery of the PXR in 1998 (Yan and Xie, 2016).

In 1997, a mouse DNA sequence representing a fragment of a novel nuclear receptor LBD was identified by Kliewer et al (Glaxo Wellcome) while searching the Washington University Expressed Sequence Tag database (Kliewer et al., 1998). With the help of a mouse liver cDNA library, this data was used to clone the full length mouse protein of 431 amino acids, which the Kliewer team labelled PXR. The name was given due to activation of this nuclear receptor by a number of naturally-occurring pregnanes.

Shortly after the discovery of mouse PXR (mPXR), human PXR was isolated independently in 1998 by three research groups: the Kliewer group at Glaxo Wellcome laboratories in North Carolina (Lehmann et al., 1998), the Evans group at the Salk institute in California (Blumberg et al., 1998) and the Berkenstam group at the Pharmacia and Upjohn laboratories in Stockholm (Bertilsson et al., 1998). The newly cloned human nuclear receptor was designated the human pregnane x receptor (hPXR), the steroid and xenobiotic receptor (SXR) and the human pregnane-activated receptor (hPAR) by each of these groups respectively. The receptor became classified as a member of the NR1I group and given the designation NR1I2 in 1999 based on the Unified Nomenclature System for the Nuclear Receptor Superfamily (Nuclear Receptors Nomenclature Committee, 1999). It remains preferentially referred to as the PXR (Ekins, 2007). In addition to mouse and human PXR, monkey, dog, rabbit and rat PXR have since been cloned as well as that of other species (Kliewer et al., 2002).

5.1.3. The structure of the PXR and its mechanism of action

The structure of the PXR follows the structural organisation of nuclear receptors described in 5.1.1. The hPXR is made of 434 amino acids, 3 longer than the mPXR (Lehmann et al., 1998). The 3D structure of the hPXR has previously been determined through x-ray crystallography (Watkins et al., 2001). This has shown the hydrophobic pocket of the LBD to be large, spherical and flexible, in contrast to other nuclear receptors. This allows a number of structurally diverse compounds to bind to

the LBD ranging from 268-823kDa in size, and gives the PXR its known role as a promiscuous xenobiotic receptor (Kliewer et al., 2002, Mullican et al., 2013).

The unbound PXR is located in the cytoplasm and translocates to the nucleus in a ligand-dependent manner (Kawana et al., 2003). The LBD of the PXR includes an AF-2 region which is thought to play a role in nuclear translocation and allows the binding of transcriptional coactivators (di Masi et al., 2009). In the case of CYP3A4 transcription regulation (a known target gene for the PXR), the absence of ligand-bound PXR in the nucleus permits coactivators such as SRC-1, HNF4α and PPARγ-coactivator-1α (PGC-1α) to facilitate the transcription of SHP (a regulatory orphan nuclear receptor) and SMRT (a nuclear receptor corepressor) which in turn suppress the transcription of CYP3A4. Upon translocation of the ligand-bound PXR to the nucleus, it forms a heterodimer with RXRα, which is further stabilised by SRC-1, HFN4α and PGC-1α, and inhibits the transcription of SHP and SMRT. The PXR-RXRα-coactivator complex then binds the xenobiotic responsive enhancer molecule (XREM)/PXRE and promotes transcription of CYP3A4 (Shukla et al., 2011). This process is illustrated in Figure 5.3.

The PXR is mainly expressed in the liver and intestine in human, rabbit, rat and mouse (Kliewer et al., 2002). Unsurprisingly, this distribution is identical to that of CYP3A expression in these species (Lehmann et al., 1998, Kliewer et al., 2002, Savas et al., 2000, Zhang et al., 1999). Although traces of mPXR transcripts have also been identified in the mouse stomach and kidney, this has not been evident in human tissue (Figure 5.4). It is now widely accepted that the PXR acts as a master transcription factor regulating the expression of key phase I and phase II enzymes and transporters in the metabolism of drugs and xenobiotics (Tolson and Wang, 2010, Pavek, 2016). A list of hPXR target genes is summarised in Table 23, highlighting drug-metabolising enzyme and transporter genes.

Other members of the NR1I family are VDR and CAR. The PXR is most closely related to CAR where the two nuclear receptors share 66% and 45% of their DBDnr and LBD amino acid identity respectively. Both function as regulators of xenobiotic metabolism in a coordinative manner and have an overlapping gene target profile although CAR is less promiscuous in binding ligands (Kliewer et al., 2002, Maglich et al., 2002). In contrast to PXR, CAR activation can take place without ligand binding, as its name implies (Tolson and Wang, 2010).

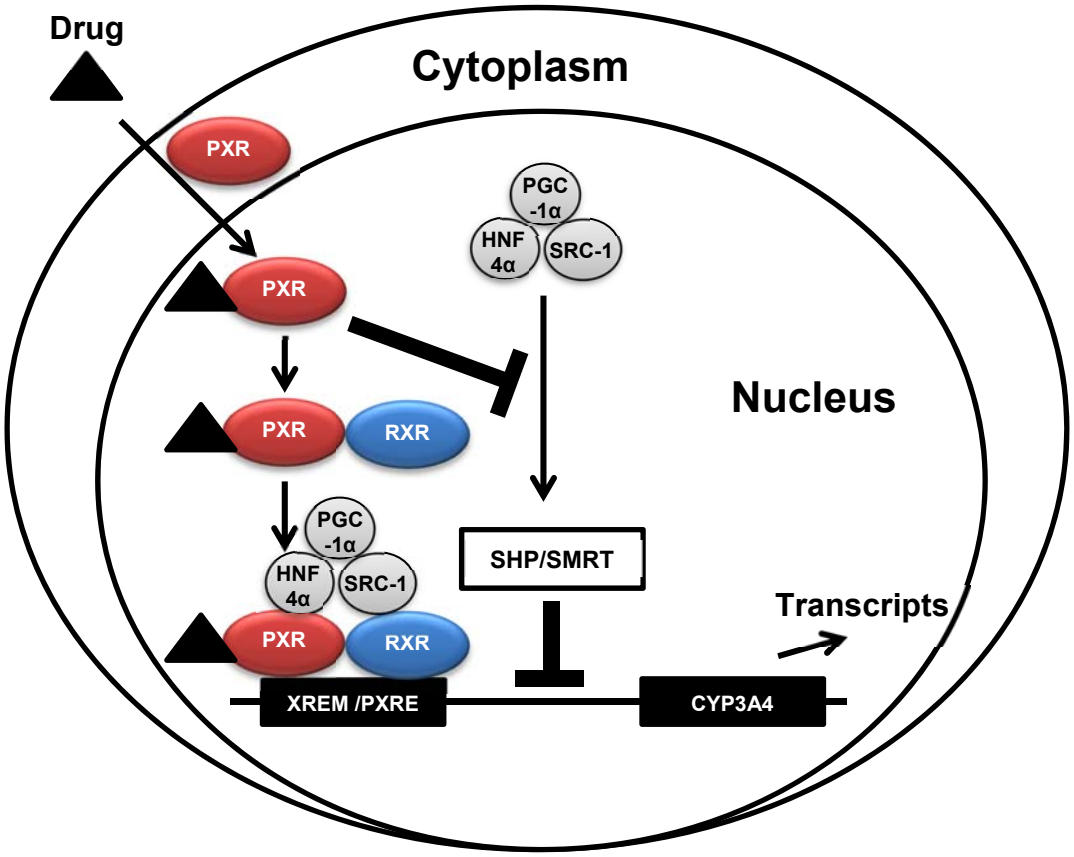

Figure 5.3 Regulation of CYP3A4 transcription by ligand-activation of the PXR. Adapted from Shukla et al (Shukla et al., 2011)

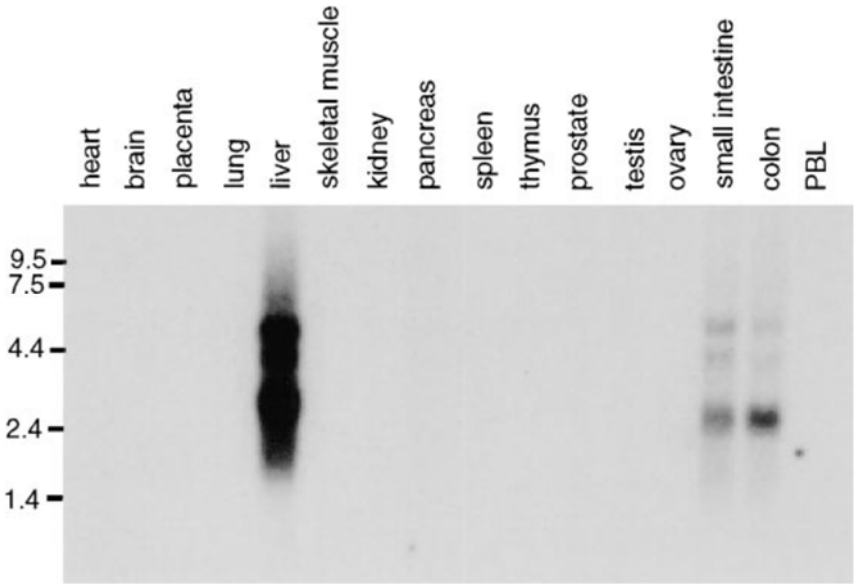

Figure 5.4 Northern blot analysis of hPXR expression in various human tissue. From Lehmann et al (Lehmann et al., 1998)

Table 23 List of PXR target genes and role in xenobiotic metabolism. Corresponding human orthologues of murine genes reported if known. Phase I: Activation; Phase II: Solubilisation; Phase III: Elimination. Adapted from Rosenfeld et al and Hariparsad et al (Rosenfeld et al., 2003, Hariparsad et al., 2009)

Target gene	Role in xenobiotic metabolism	Target gene	Role in xenobiotic metabolism
Abcb1a (Mdr1a)*	Phase III	**CYP3A5**	Phase I
Abcb1b (Mdr1b)*	Phase III	**CYP4F12**	Phase I
ABCB4 (MDR2/3)	Phase III	**ENTPD5**	N/A
ABCB9	Phase III	**FASN**	N/A
ABCC3 (MRP3)	Phase III	**GCKR**	N/A
ABCC4 (MRP4)	Phase III	**GLDC**	N/A
AKR1C1	N/A	**GSTA1**	Phase II
AKR1C2	N/A	**GSTA4**	Phase II
ALDH1a1	Phase I	**GSTM1**	Phase II
Aldh1a7*	Phase I	**GSTM2**	Phase II
ALDH3A2	Phase I	**GSTT1**	Phase II
ARAF	N/A	**HMGCR**	N/A
BMP1	N/A	**INSIG2**	N/A
CARS	N/A	**LTBP1**	N/A
CD36	N/A	**MTTP**	N/A
CD59	N/A	**NR1I2 (PXR)**	All
CES2	Phase I	**NR1I3 (CAR)**	Phase I
CES3	Phase I	**OATP2**	Phase III
CFL1	N/A	**PAPSS2**	Phase II
Cpt1*	N/A	**PDIA4**	N/A
Cyp2a4*	Phase I	**POR**	N/A
Cyp2b10*	Phase I	**S100A8**	N/A
CYP2C8	Phase I	**SLC40A1**	N/A
Cyp3a11*	Phase I	**SULT1B1**	Phase II
CYP3A4	Phase I	**TCN2**	N/A
Abcb1a (Mdr1a)*	Phase III	**UGT1A**	Phase II

*No clear human orthologue

5.1.4. PXR ligand selectivity between species

Orthologues of the PXR from various species display different affinities to ligands. For example, rifampicin is an activator of the human and rabbit PXR but has little effect on the rat and mouse PXR. On the other hand, Pregnenolone-16α-carbonitrile (PCN) is a potent rodent PXR activator that shows little affinity to the human PXR (Kliewer et al., 2002).

As mentioned in 5.1.1, the DBDnr is highly conserved whereas the LBD varies significantly between nuclear receptors. In a similar manner, divergence in the PXR LBD between species provides an explanation for the observed differences in ligand affinity between PXR orthologues. However, while most human and rodent nuclear receptor orthologues share over 90% of the amino acid identity in the LBD, in the case of the PXR, they only share 76-77% (Kliewer et al., 2002). This may indicate an evolutionary divergence in diet and xenobiotic exposure between various species (Li et al., 2012). Despite the divergence in ligand affinities between PXR orthologues, they operate through a common metabolic pathway with comparable target genes given the conserved DBDnr region amongst these orthologues (94-100% amino acid identitiy) (Li et al., 2012, Kliewer et al., 2002).

Figure 5.5 shows a comparison of PXR amino acid sequences between species and with other NR1I members

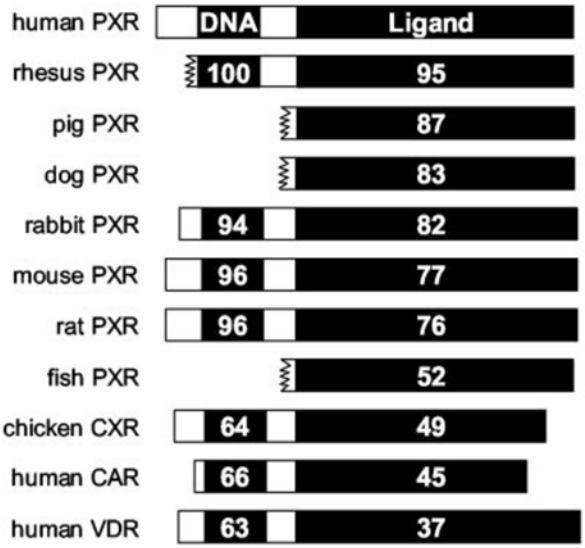

Figure 5.5 Comparison of PXR sequences (DBDnr and LBD) between orthologues and other NR1I members. Numbers indicate percentage similarity of amino acid identity. DBDnr for pig, dog and fish were not cloned at the time the original diagram was published and hence are not shown. From Kliewer et al (Kliewer et al., 2002)

5.1.5. Role of the PXR

Much of what is currently understood about the role of the PXR is owed to research using PXR-null (Staudinger et al., 2001b) and hPXR transgenic mice (Xie et al., 2000a). In normal conditions, PXR-null mice thrive, develop and reproduce normally, and display no obvious phenotypic changes compared to wild type mice. In addition, extensive biochemical testing has shown no significant abnormalities in serum levels of a number of metabolic parameters including glucose, cholesterol and liver enzymes. This suggests that function of the PXR is not vital in baseline conditions and in the absence of a xenobiotic challenge (Kliewer et al., 2002). However, the lack of PXR causes an altered or absent response to various xenobiotic and pathological insults in comparison to wild type mice, thus providing insight into the role of the PXR (Marek et al., 2005, Teng and Piquette-Miller, 2007, Dou et al., 2012).

The ligand-activated PXR commonly carries out its functions through direct induction of target gene expression. In addition, it has also been shown to exert effects through cross-talk with other nuclear receptors usually mediated by interference with or competition for coactivation factors (Pavek, 2016). As new functions of the PXR continue to be unveiled, its currently recognised roles are listed below.

Metabolic roles of the PXR

Regulation of xenobiotic metabolism

As detailed earlier, upon activation by a range of drugs and other xenobiotics, the PXR induces the expression of a number of enzymes and transporters that metabolise and excrete these chemicals, in conjunction with CAR (see section 5.1.3).

Regulation of bile acid metabolism

The PXR is activated by bile acids, most potently lithocholic acid (LCA) (Xie et al., 2001). Similar to its regulatory effect on xenobiotic metabolism, the activated PXR induces the expression of enzymes and transporters, including OATP2, UDP-glucuronosyltransferases (UGTs) and MRP2 that results in the uptake, conjugation and excretion of bile acids into bile. In addition, the PXR can inhibit bile acid synthesis from cholesterol via suppression of CYP7A1 (Jonker et al., 2012). It is debatable whether the PXR exerts its regulatory effect on bile acids in physiological conditions as the normal serum levels of bile acids are at least 10-fold lower than the AC50 of LCA, the most potent PXR activator amongst bile acids. Therefore, it is more likely that the PXR provides a detoxifying mechanism against high bile acid levels present during cholestatic conditions (Copple and Li, 2016). The PXR exerts its regulatory effect in collaboration with the FXR, the main bile acid regulatory nuclear receptor (Jonker et al., 2012).

Regulation of glucose metabolism

Activated PXR has been shown to indirectly suppress the expression of rate-limiting enzymes in gluconeogenesis and glycogenolysis (glucose-6-phosphatase and phosphoenolpyruvate carboxykinase 1) through the inhibition of transcription factors for these enzymes (cAMP-response element binding protein (CEBP) and the forkhead box protein FoxO1) (Zhou et al., 2006b, Kodama et al., 2007, Kodama et al., 2004, Ihunnah et al., 2011)

Regulation of lipid and cholesterol metabolism

PXR activation suppresses the transcription of carnitine palmitoyl transferase 1A (CPT1A) and 3-hydroxy-3-methylgluterate-CoA synthase 2 (HMGCS2) which are key steps in fatty acid oxidation and ketogenesis. This possibly occurs through deactivation of the forkhead box protein FoxA2 (Nakamura et al., 2007, Ihunnah et al., 2011). In addition, PXR activation directly induces the expression of CD36, a membrane glycoprotein that facilitates cellular uptake of circulatory free fatty acids, thus promoting lipogenesis. This effect may explain the potential link between PXR activation and hepatic steatosis (see section 5.1.6) (Zhou et al., 2006b, Koonen et al., 2007, Ihunnah et al., 2011). Evidence for the effects of PXR activation on cholesterol and lipoprotein metabolism is inconsistent and thus its role in this aspect remains unclear (Ihunnah et al., 2011).

Other metabolic roles

PXR activation has also been shown to promote adrenal glucocorticoid and mineralocorticoid hormone synthesis (Zhai et al., 2007) and deactivation of androgens (Zhai et al., 2007). In addition, it directly promotes bilirubin detoxification by inducing the expression of conjugating enzymes (UGTs) and transporter proteins that facilitates its excretion, in a manner similar to that of bile acids (Ihunnah et al., 2011).

Other emerging roles for the PXR

Research in recent years has uncovered evidence of potential value for PXR activation in pathological conditions (Li et al., 2012). In addition to the beneficial effects in cholestatic conditions described earlier in this section, the PXR has been shown to produce a number of potentially useful effects in areas listed below.

Inflammation

Anti-inflammatory properties have been demonstrated following PXR activation in liver, intestinal tissue and articular cartilage in vivo (Wallace et al., 2010, Shah et al.,

2007, Mencarelli et al., 2013). Moreover, a recent study has demonstrated a more regulated and effective immune response to bacterial infection in wild type compared to PXR-null mice (Qiu et al., 2016).

A reciprocal negative regulatory relationship is believed to exist between PXR and NFκB signalling (Zhou et al., 2006a, Gu et al., 2006). Therefore, it is likely that the anti-inflammatory effect of PXR activation is due to suppression of NFκB signalling and the resultant immunomodulatory effect on cytokine expression (Wallace et al., 2010, Shah et al., 2007)

In view of this effect, a number of studies have examined the potential therapeutic effects of PXR activation on various inflammatory conditions over the past decade. Several PXR activators have been shown to improve clinical and biochemical manifestations of inflammatory bowel disease in animal models (Zhang et al., 2015b, Hu et al., 2015, Zhang et al., 2015a, Hu et al., 2014, Shah et al., 2007, Cheng et al., 2010a), while certain PXR gene haplotypes have been found to be associated with increased susceptibility to Crohn's disease (Glas et al., 2011). In addition, a recent study using a murine model of arthritis has demonstrated significant improvement in localised arthritic and systemic inflammation using a PXR activator (Mencarelli et al., 2013).

Fibrogenesis

PXR activation has been shown to ameliorate carbon tetrachloride-induced liver fibrosis and bleomycin-induced skin fibrosis in rodents (Marek et al., 2005, Beyer et al., 2013). The anti-fibrotic action of ligand-activated PXR is thought to be due to a direct effect on myofibroblasts (Haughton et al., 2006) as well as an indirect immunomodulatory effect (Axon et al., 2008, Beyer et al., 2013).

Neoplasia

There is emerging evidence that PXR activation may be beneficial in certain malignancies. A recent study on a murine colon cancer model showed a reduction in tumour burden and improved animal survival following PXR activation through promotion of apoptosis and suppression of proliferation in tumour cells (Cheng et al.,

2014). However, the evidence on this matter is by no means consistent (Zhou et al., 2008). Favourable results with PXR activation have also been noted on cervical and endometrial cancer tissue (Masuyama et al., 2007, Niu et al., 2014).

On the other hand, PXR activation in tumours that express relatively high levels of PXR such as breast, ovarian and prostate cancer can result in increased tumour proliferation and chemoresistance (Meyer zu Schwabedissen et al., 2008, Chen et al., 2009b, Masuyama et al., 2016, Chen et al., 2007).

Growth and healing

PXR activation in mice has been shown to induce hepatocyte growth and liver regeneration (Staudinger et al., 2001a, Marek et al., 2005, Dai et al., 2008). It has also been found to promote intestinal epithelial healing and repair of colitis-induced damage to gut epithelial barrier (Terc et al., 2014). In addition, PXR activation has been found to promote the expression of antiapoptotic proteins in vitro and in vivo (Iannelli et al., 2011).

5.1.6. Risks associated with PXR activation

The use of PXR activators has been found to be associated with a number of potential risks that may limit its applicability in clinical practice.

Drug-drug interactions

Given that the CYP3A family of metabolic enzymes are primary targets of the activated PXR, and that these enzymes are responsible for the metabolism of over 50% of prescription medications, it comes as no surprise that PXR activation can result in significant and occasionally life-threatening drug interactions (Kliewer et al., 2002). A classic example is the herbal remedy and potent PXR activator St John's wort, used as an over-the-counter antidepressant and anxiolytic medication. Its use has been associated with increased metabolism of a number of drugs that are metabolised by CYP3A4 including oral contraceptives, digoxin and warfarin (Kliewer et al., 2002). An extreme case of cardiac transplant rejection due to interaction of this

PXR activator with ciclosporin has been reported in the literature (Ruschitzka et al., 2000). Due to such potentially dangerous interactions, screening for PXR activation occurs at early stages of modern drug development in order to select safer candidate medications less likely to cause such interactions (Willson and Kliewer, 2002, Synold et al., 2001)

On a similar note, PXR activation has been associated with potentiation of paracetamol-induced liver injury through the acceleration of paracetamol metabolism and accumulation of a toxic reactive metabolite N-acetyl-p-benzoquinone imine (NAPQI) in the liver (Guo et al., 2004, Wolf et al., 2005, Cheng et al., 2009)

Steatosis

Research on human hepatocytes and on humanised PXR mice has linked the use of PXR activators to the development of hepatic steatosis (Moya et al., 2010, Lee et al., 2008, Cheng et al., 2012). In theory, this would suggest an increased risk of developing non-alcoholic fatty liver disease (NAFLD) with the use of PXR activators. The intracellular accumulation of triglyceride noted in these studies is thought to be caused by the upregulating action of PXR on of CD36, a fatty acid transporter that has been associated with the development of cardiovascular and metabolic abnormalities (Febbraio and Silverstein, 2007). In addition, two PXR polymorphisms (rs7643645 and rs2461823) have been associated with disease severity in NAFLD (Sookoian et al., 2010). However, the clinical relevance of these findings remains questionable, since no reports of drug-induced steatosis has been reported on PXR activators in clinical use to date (di Masi et al., 2009).

Promotion of neoplastic growth

As detailed in section 5.1.5, activation of the PXR may promote the proliferation and chemoresistance of certain cancer types (e.g. breast, ovarian and prostate).

Other potential risks associated with long-term PXR activation

Growth retardation and liver toxicity has been demonstrated in mice with constitutively-expressed hPXR, suggesting potentially deleterious effects associated with sustained PXR activation (Xie et al., 2000a, Kliewer et al., 2002). However, the clinical significance of these findings is unclear.

5.1.7. Hypothesis and aim of study

Given the potential anti-inflammatory, anti-fibrotic and regenerative effects associated with PXR activation, it was postulated that activation of the PXR would be of benefit in reducing the hepatic damage caused by IRI (see Chapter 4 for details on IRI-related liver damage). Indeed, a beneficial role for PXR activation in hepatic IRI has previously been suggested (Iannelli et al., 2011).

The aim of this study was to investigate the effect of a PXR-activation on IRI-induced hepatic inflammation and fibrosis in a previously validated rat model of hepatic IRI.

5.2. Materials and methods

5.2.1. Ethical considerations

Local Ethical Review Committee (ERC) and Home Office approval for the animal models were obtained (project license PPL 60/3907; protocol 19b9) in this project.

All experiments were carried out in accordance with the Animals (Scientific Procedures) Act 1986 and in strict compliance with other local and national guidelines and policies.

5.2.2. Model to investigate the effect of PXR activation on hepatic ischaemia-reperfusion injury

Rats (male Sprague Dawley, weight 350-500g) were divided into treatment and control groups (n=10 per group). A PXR activator (50 mg/kg Pregnenolone-16α-carbonitrile 30mg/ml in 100% DMSO) or vehicle control was administered subcutaneously to rats in the treatment and control groups respectively for 2 days prior to hepatic ischaemia-reperfusion injury.

Reagents for in vivo PXR model

Pregnenolone-16α-carbonitrile (PCN) is a rodent-specific PXR activator and was purchased from Sigma-Aldrich (product code P0543) along with dimethyl sulfoxide (DMSO) (product code D8418) which was used as solvent vehicle.

Procedure for in vivo PXR model

Pre-operative analgesia, antibiotic and anaesthetic regimes were administered to animals in both groups on the day of the procedure in a manner similar to that described in section 4.2.2.

Upon induction of anaesthesia, animals were shaved, cannulated and exposed to a laparotomy. Using a surgical microscope, lobar vessels to the left and middle hepatic lobes were identified, separated from the corresponding bile duct branch and clamped for 60 min in both groups in order to induce lobar IRI and BEC injury. Intra-

operative heparin (300IU/kg) was administered intravenously immediately prior to clamping. Post-operative analgesia, antibiotic and fluid regimes were administered in line with the hepatic ischaemia-reperfusion injury model. Baseline blood samples were taken pre- and post-operatively in both groups.

Following recovery, animals were weighed on a daily basis and examined for any deviation from normal health. Animals showing signs of ill health were treated by the NVS or, if excessive, killed humanely by a schedule 1 method.

Daily doses of PXR activator (50 mg/kg PCN 30mg/ml in 100% DMSO) or vehicle control were injected subcutaneously in the treatment or control groups respectively for up to day 10 post surgery.

Animal in each group were assigned one of two time points for termination (1 or 10 days postoperatively) where they were exposed to a second laparotomy. Anaesthesia was induced and maintained in a manner similar to the initial procedure. During the termination procedure, the common bile duct was cannulated to enable bile collection into pre-weighted tubes for sampling and bile flow measurement. Blood samples were also taken and the liver lobes were harvested, weighted and preserved for tissue analysis as previously described in section 4.2.2.

Diagrammatic representation of the PXR study is illustrated in Figure 5.6 and Figure 5.7.

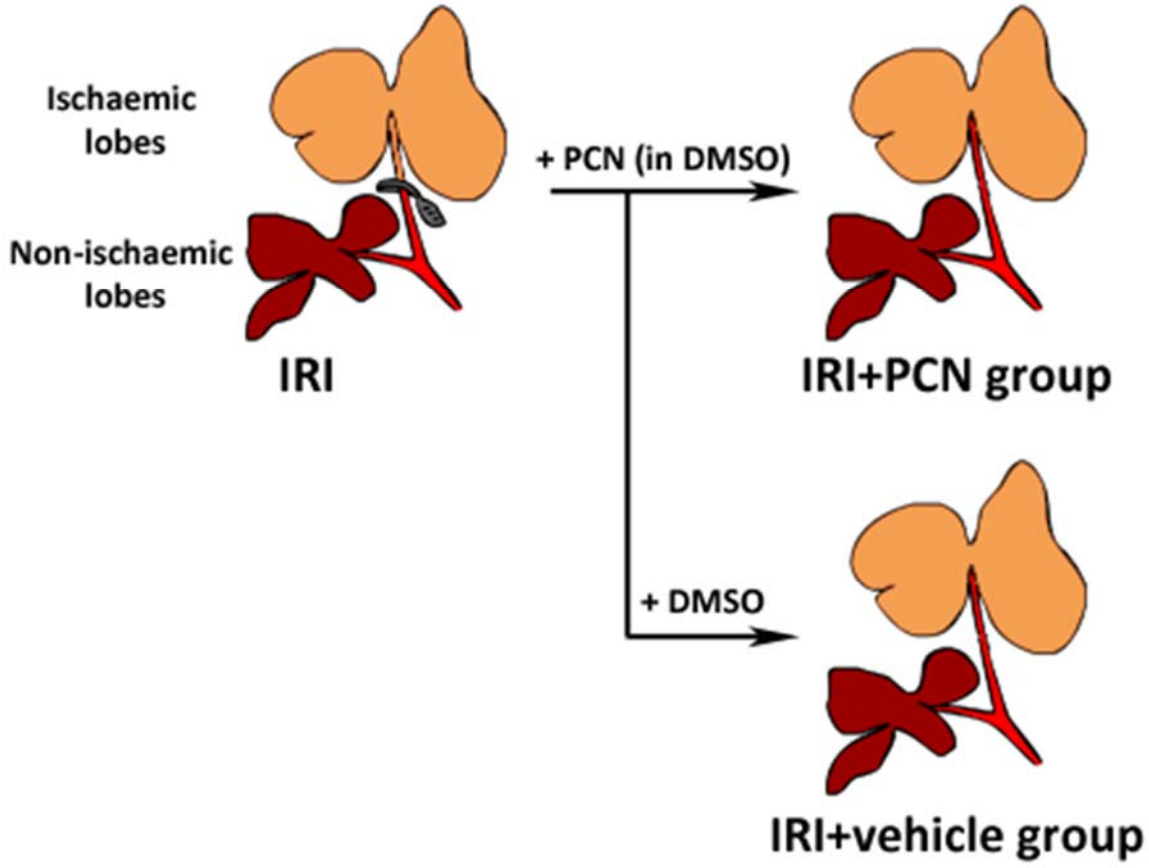

Figure 5.6 In vivo PXR study: treatment and control groups

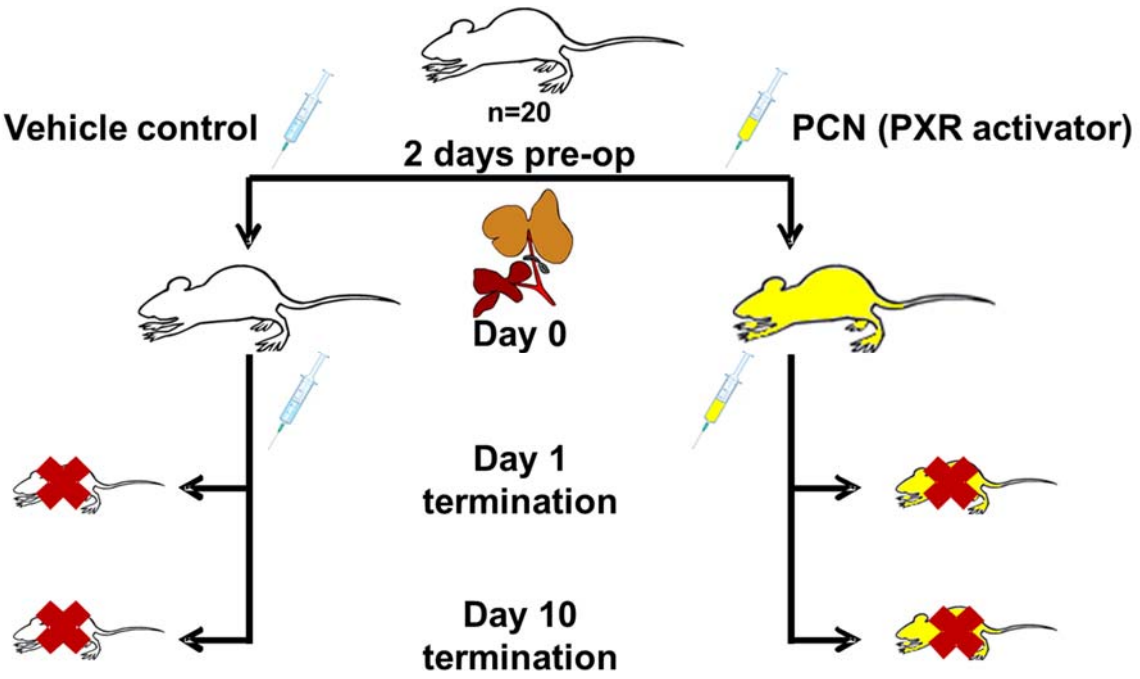

Figure 5.7 PXR study timeframe

5.2.3. Sample processing and preservation

Reagents and techniques used for sample processing, preservation and storage (liver, bile and blood) are similar to those described in section 4.2.3.

5.2.4. Protein analysis

Reagents and methods for the Lowry method, gel electrophoresis and western blot are similar to those described in section 2.2.7.

5.2.5. mRNA quantification

Reagents and methods used for mRNA quantification are as previously described in section 4.2.5.

5.2.6. Methods for tissue staining

Reagents and methods for processing of tissue sections and for H&E, Sirius red and immunohistochemistry staining are similar to those described in section 4.2.6.

5.2.7. Other biochemical analyses

Reagents and methods for the TBARS, bile acid and GluDH assays are similar to those described in section 4.2. Rat serum levels of total protein, bilirubin, alkaline phosphatase, alanine transaminase and γ-glutamyl transferase were performed at the clinical biochemistry laboratories of the Royal Victoria Infirmary in Newcastle upon Tyne.

5.2.8. Statistical analysis

Statistical methods used are those described in section 2.2.9.

5.3. Results

5.3.1. Mortality

In view of the significant risk of death caused by intraoperative bleeding in the IRI model, a small animal surgical microscope was employed for dissection of hilar structures in the PXR activation model. This significantly reduced operating times in this study and reduced mortality to 0%.

5.3.2. Evidence of PXR activation

Induction of cytochrome P450 (Cyp3A1) was used as an indicator of PXR activation. Expression of Cyp3A1 was significantly higher in the treatment group compared to control on day one as demonstrated by western blot analysis (Figure 5.8 and Figure 5.9). This difference increased on day 10. Using RT-PCR analysis, a 3.7 and 24-fold increase in Cyp3A1 mRNA transcripts was evident on day 1 and 10 post-reperfusion respectively in the treatment group relative to day 1 levels in the control group (Figure 5.10).

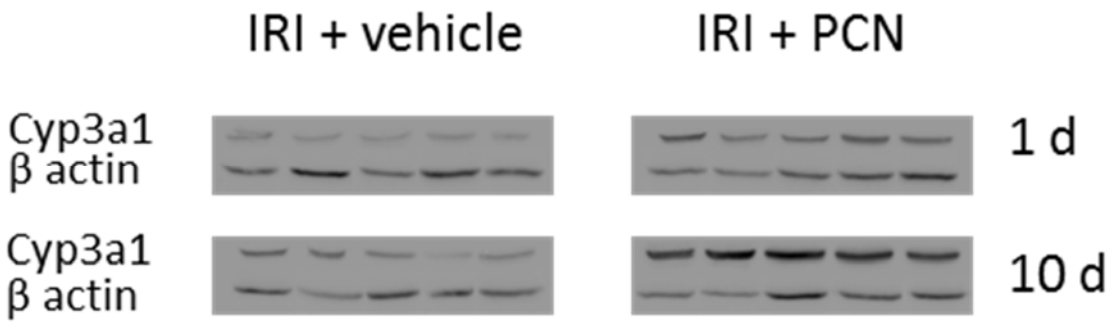

Figure 5.8 Western blot of Cyp3A1 expression on day 1 and 10 in IRI+PCN and IRI+vehicle groups.

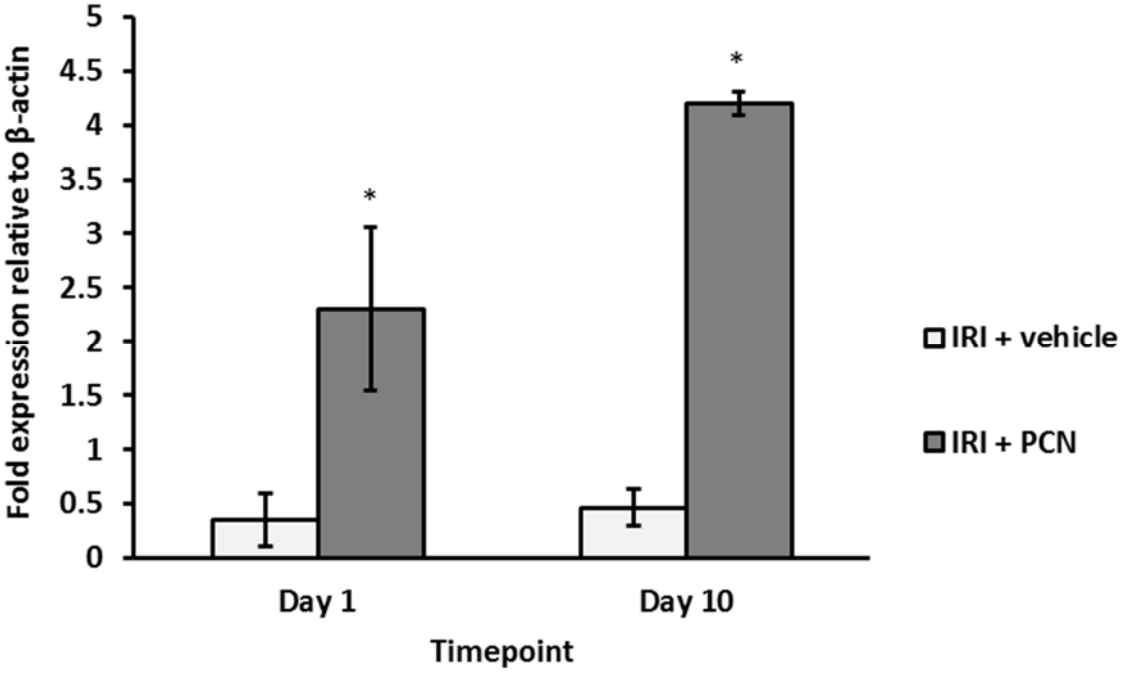

Figure 5.9 Corresponding densitometry analysis of Cyp3A1 western blot results in ischaemic and sham ischaemic lobes. *P<0.05 versus IRI+vehicle

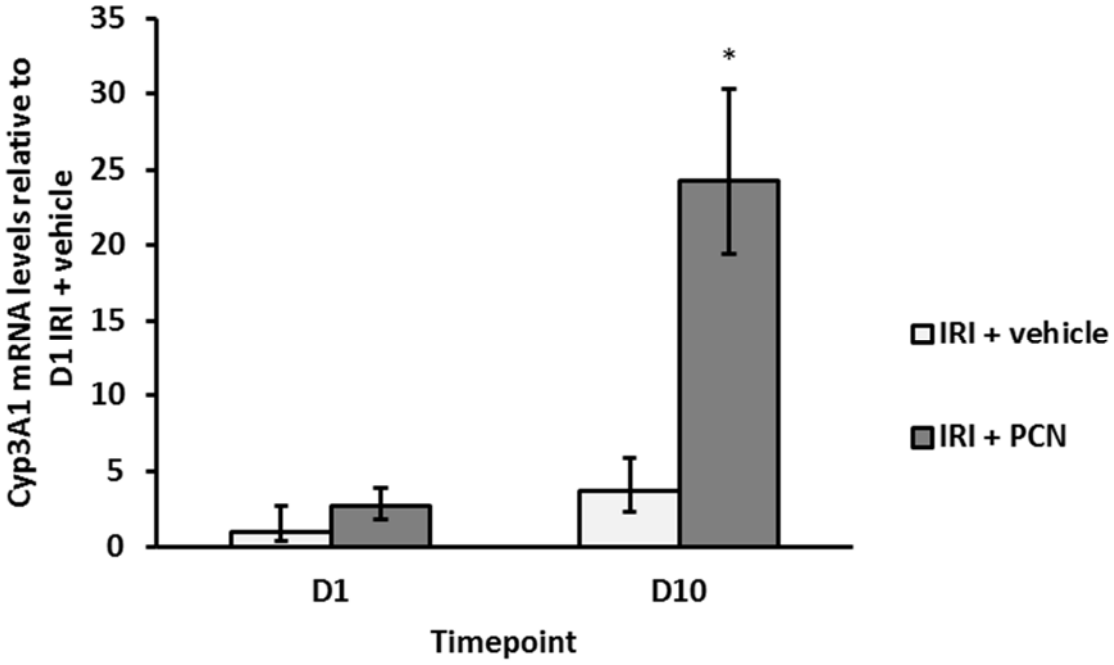

Figure 5.10 RT-PCR analysis of Cyp3A1 mRNA transcripts in ischaemic and sham ischaemic lobes. *P<0.05 versus IRI+vehicle

5.3.3. Effect of PXR activation on lipid peroxidation

Malondialdehyde (MDA) was used as a surrogate marker of lipid peroxidation to test whether or not PXR activation reduces oxidative stress during IRI. MDA levels were measured in liver homogenates from the ischaemic lobes from both the IRI-PCN and IRI-vehicle groups.

Although serum MDA levels were comparable between the two groups, MDA levels in liver homogenates were significantly lower in the ischaemic lobes of the IRI-PCN group on day 1 post-reperfusion (7.9 ± 0.6 μM versus 10.5 ± 1.8 μM in the IRI-vehicle group; P=0.03) (Figure 5.11). No significant differences in MDA levels in non-ischaemic lobes were noted between the two groups on day 1.

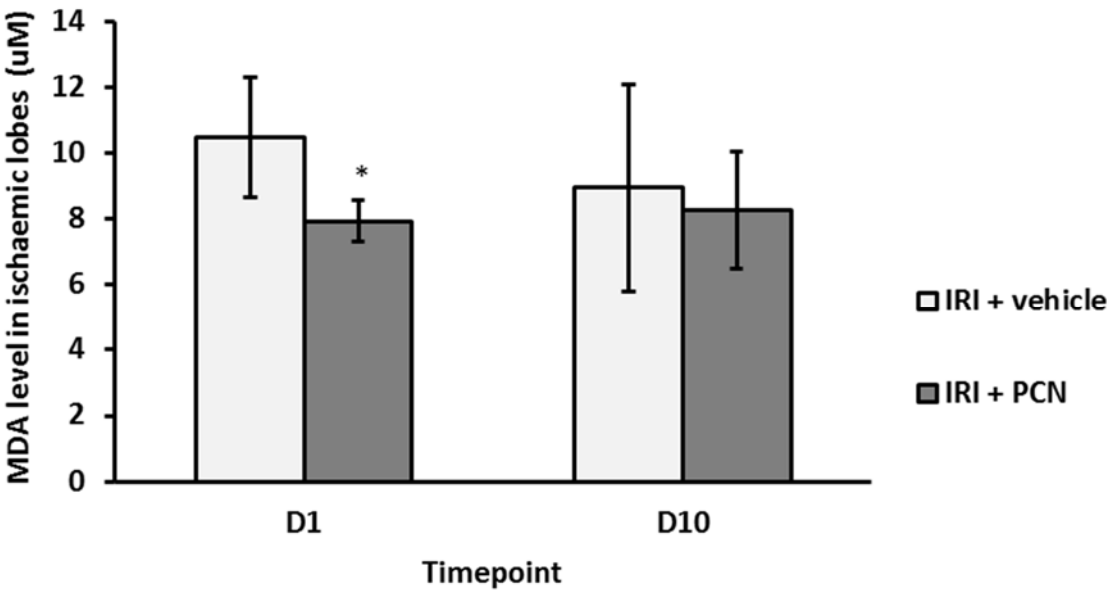

Figure 5.11 Liver MDA levels. PCN treatment compared to control. *P<0.05 versus IRI+vehicle.

5.3.4. Effect of PXR activation on bile flow

PCN treatment significantly increased bile flow rates on day 1 following IRI by 25% compared to the IRI-vehicle group (37.7 ± 2.9 μl/kg/min versus 30.1 ± 2.1 μl/kg/min in the IRI-vehicle group; P=0.001) (Figure 5.12). Average bile flow remained higher in the IRI-PCN group on day 10 post-reperfusion but this effect did not reach statistical

significance. Similarly, serum bile acid levels were significantly lower in the PCN-treated group on day 1 (Figure 5.13).

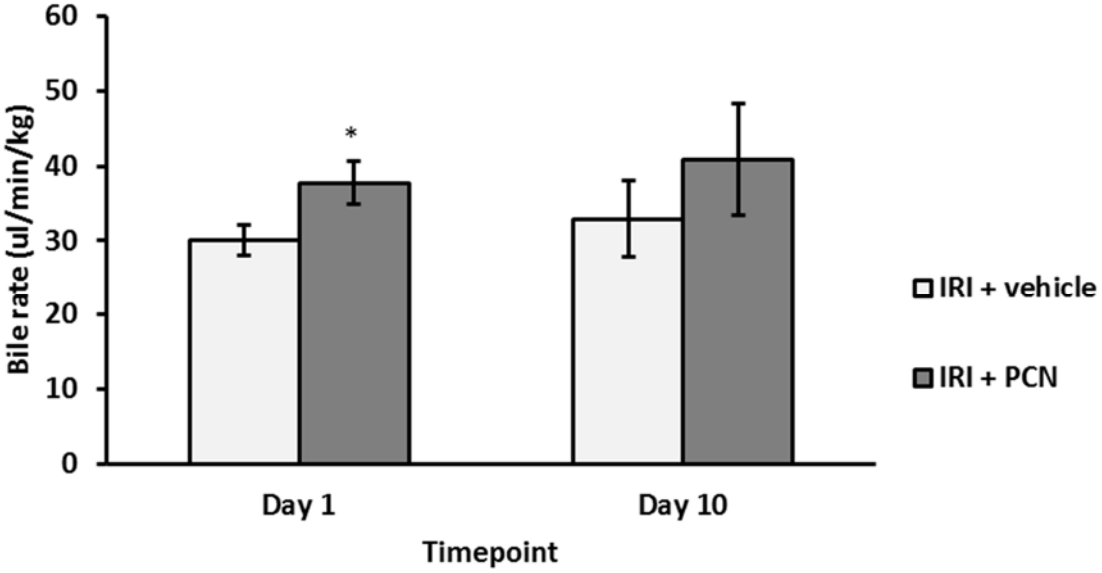

Figure 5.12 Bile flow post-IRI. PCN treatment compared to control. *P<0.005 versus IRI+vehicle.

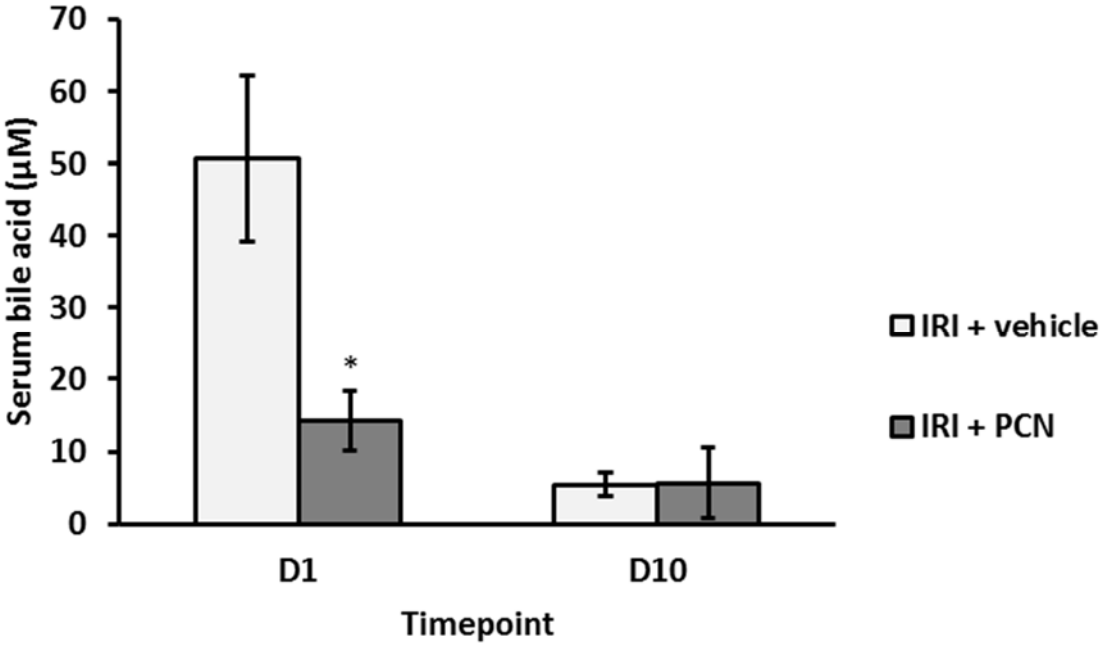

Figure 5.13 Serum bile acid levels post-IRI. PCN treatment compared to control. *P<0.05 versus IRI+vehicle.

5.3.5. Effect of PXR activation on hepatocellular necrosis

The severity of liver damage was quantified in H&E sections in both groups (Figure 5.14). PCN treatment resulted in a significant reduction in liver damage severity scores on day 1 post-reperfusion (Figure 5.15). Evidence of necrosis was minimal in both groups on day 10 after IRI in accordance with the findings in the previous IRI study (Figure 4.31).

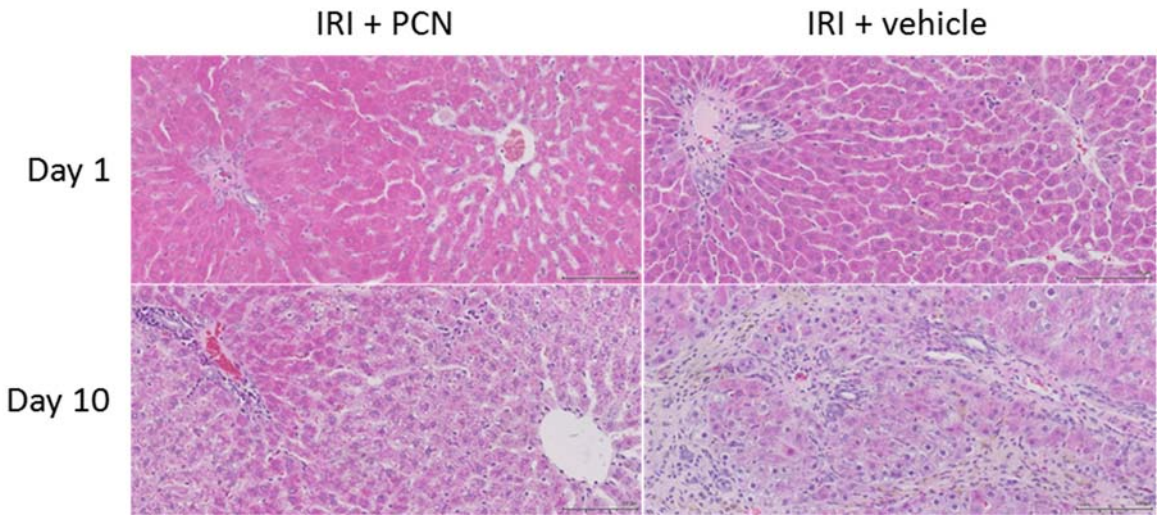

Figure 5.14 H&E staining of liver sections in PXR study. Scale bar represents 100μm at X20 magnification

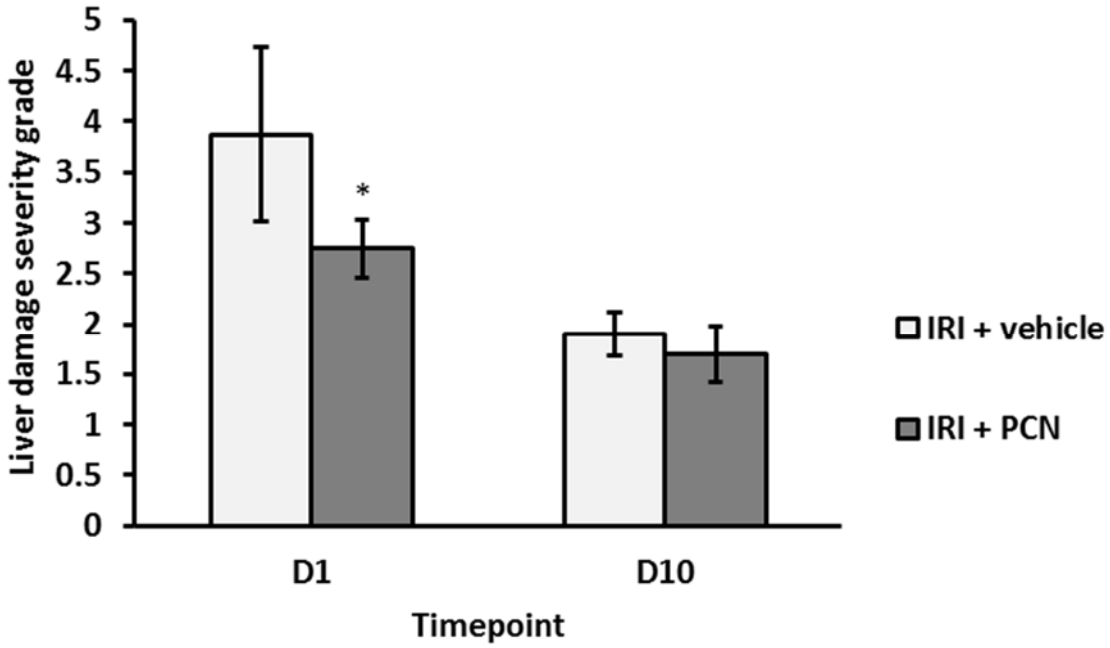

Figure 5.15 Comparison of liver damage severity scores between IRI+PCN and IRI+vehicle groups assessed on H&E slides (scale of 0–5). *P<0.05 versus IRI+vehicle

5.3.6. Effect of PXR activation on liver function tests

PCN treatment resulted in a significant reduction in serum ALT levels in the IRI-PCN group on day 1 post-reperfusion (381.3±62.0U/L versus 970.3±314.5U/L in IRI-vehicle control; P=0.03). Serum ALT levels were similar to pre-operative baseline levels on day 10 in both groups. PCN treatment had no significant effect on serum bilirubin, albumin or ALP levels. Serum ALT, ALP and total protein results are displayed in Figure 5.16, Figure 5.17 and Figure 5.18.

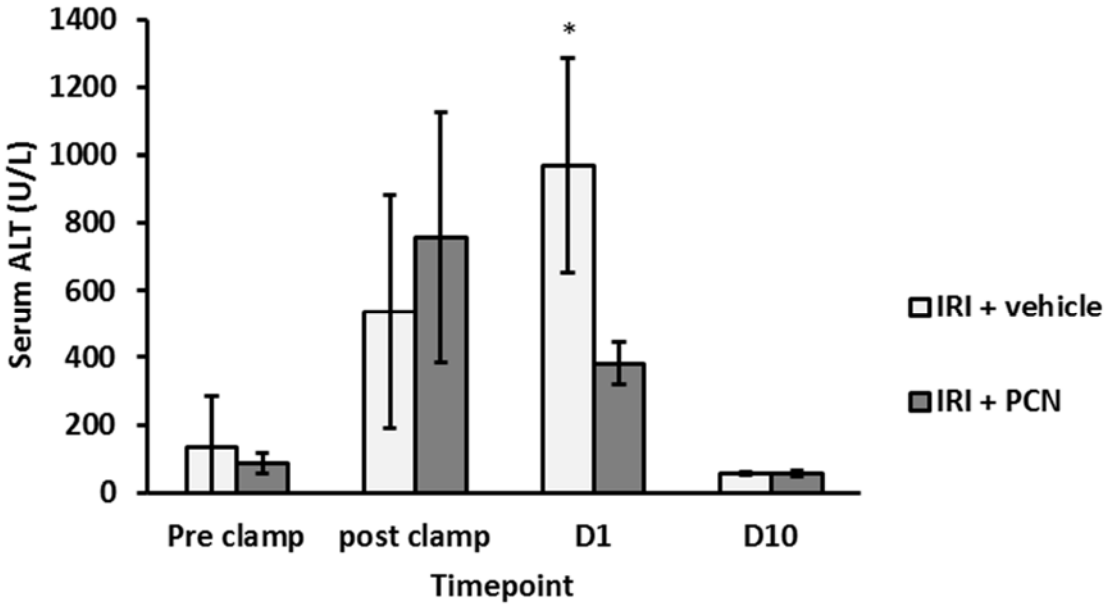

Figure 5.16 Serum ALT pre and post-IRI. PCN treatment compared to control. *P<0.05 versus IRI+vehicle

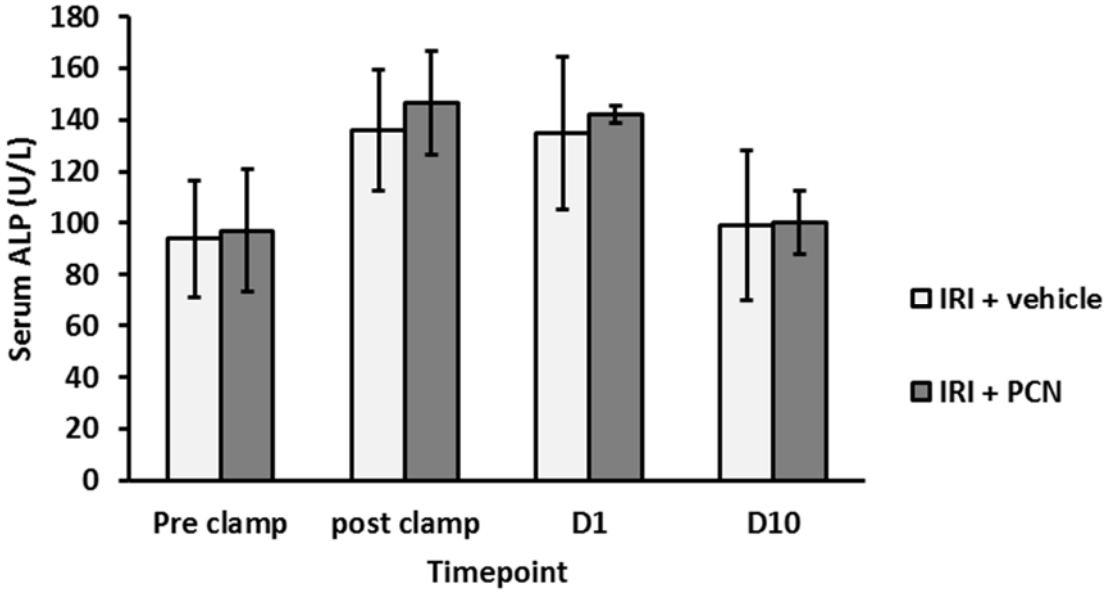

Figure 5.17 Serum ALP levels pre and post-IRI. PCN treatment compared to control.

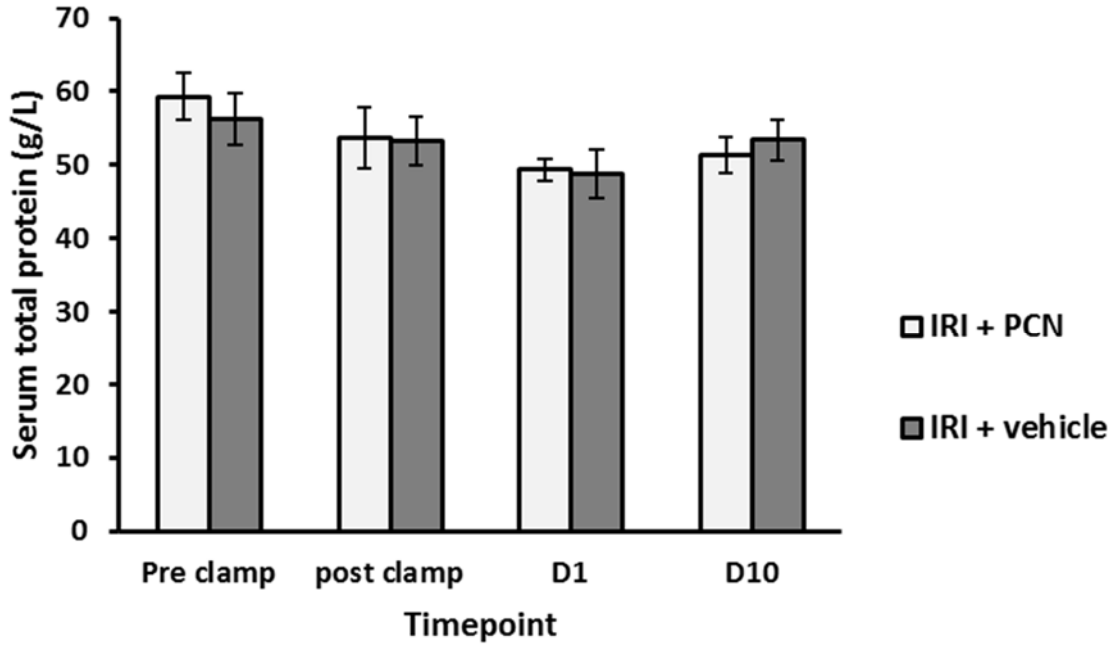

Figure 5.18 Serum total protein levels pre and post-IRI. PCN treatment compared to control.

5.3.7. Effect of PXR activation on inflammatory cell infiltration

PCN treatment significantly reduced the number of peri-portal and centrilobular inflammatory cells on day 1 compared to the IRI-vehicle group (Figure 5.19, Figure 5.20 and Figure 5.21). The inflammatory cell count in the peri-portal areas remained significantly higher in the vehicle control group on day 10 (Figure 5.20).

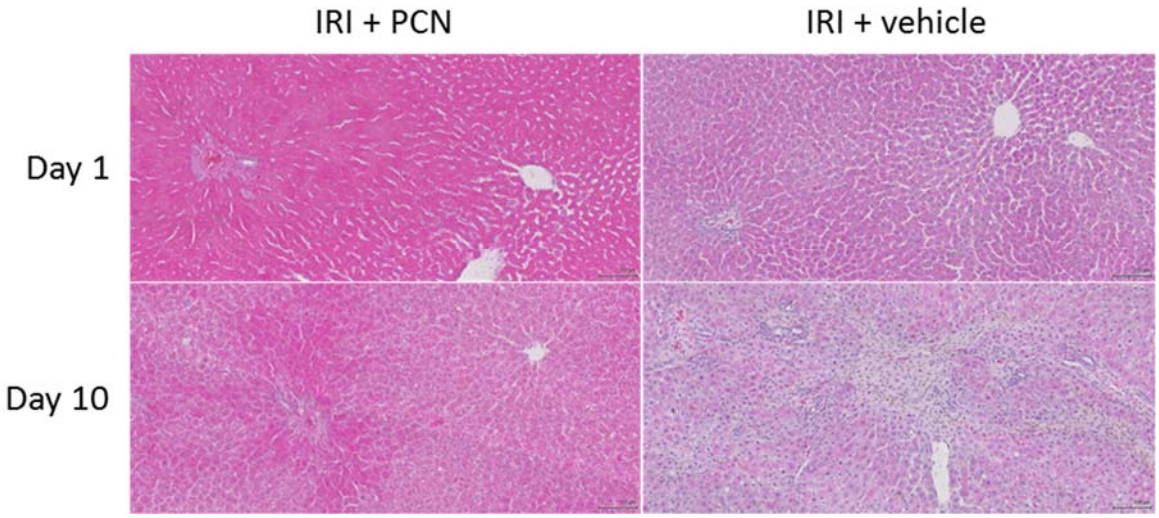

Figure 5.19 A: H&E staining of liver sections in PXR study. Scale bar represents 100μm at X10 magnification

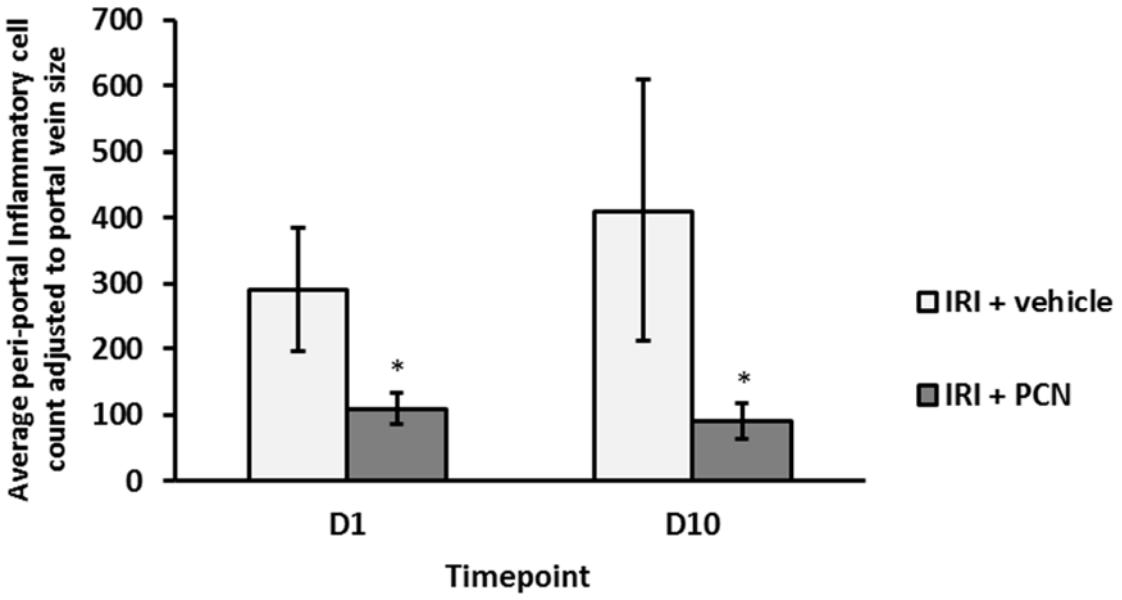

Figure 5.20 Comparison of inflammatory cell counts in peri-portal areas between the IRI+PCN and IRI-vehicle groups. *P<0.05 versus IRI+vehicle

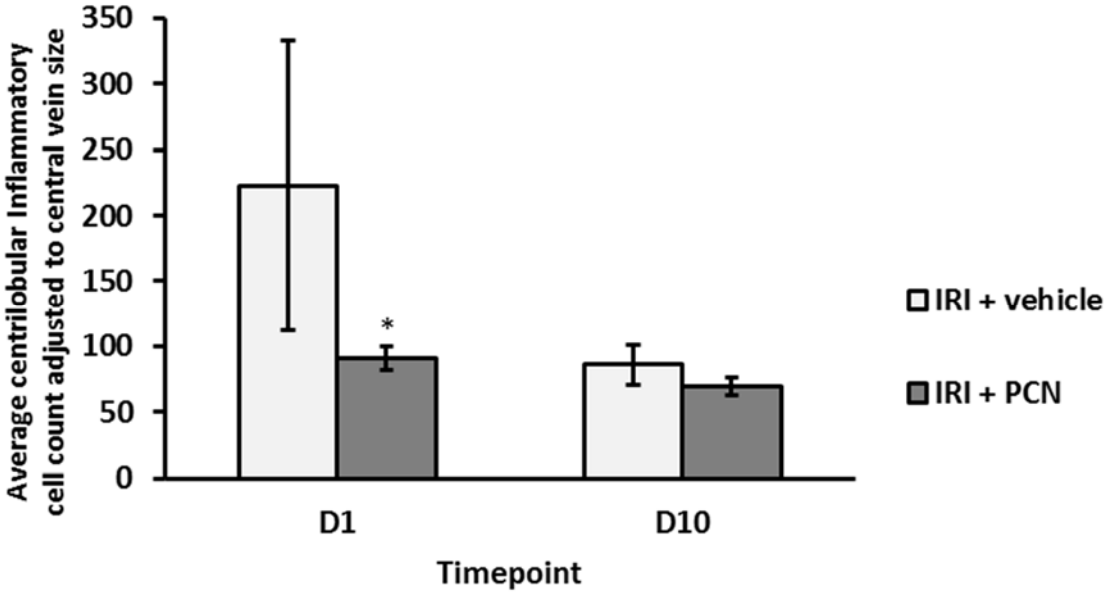

Figure 5.21 Comparison of inflammatory cell counts in centrilobular areas between the IRI+PCN and IRI-vehicle groups. *P<0.05 versus IRI+vehicle

5.3.8. Effect of PXR activation on dry liver weight

Liver lobes in animals treated with PCN showed less signs of damage macroscopically compared to control livers (Figure 5.22). When normalised to total body weight, ischaemic lobes in the PCN group weighed significantly more on day 10 post-reperfusion (2.6±0.1g/100g versus 2.1±0.1g/100g in the control group; P<0.001) (Figure 5.23).

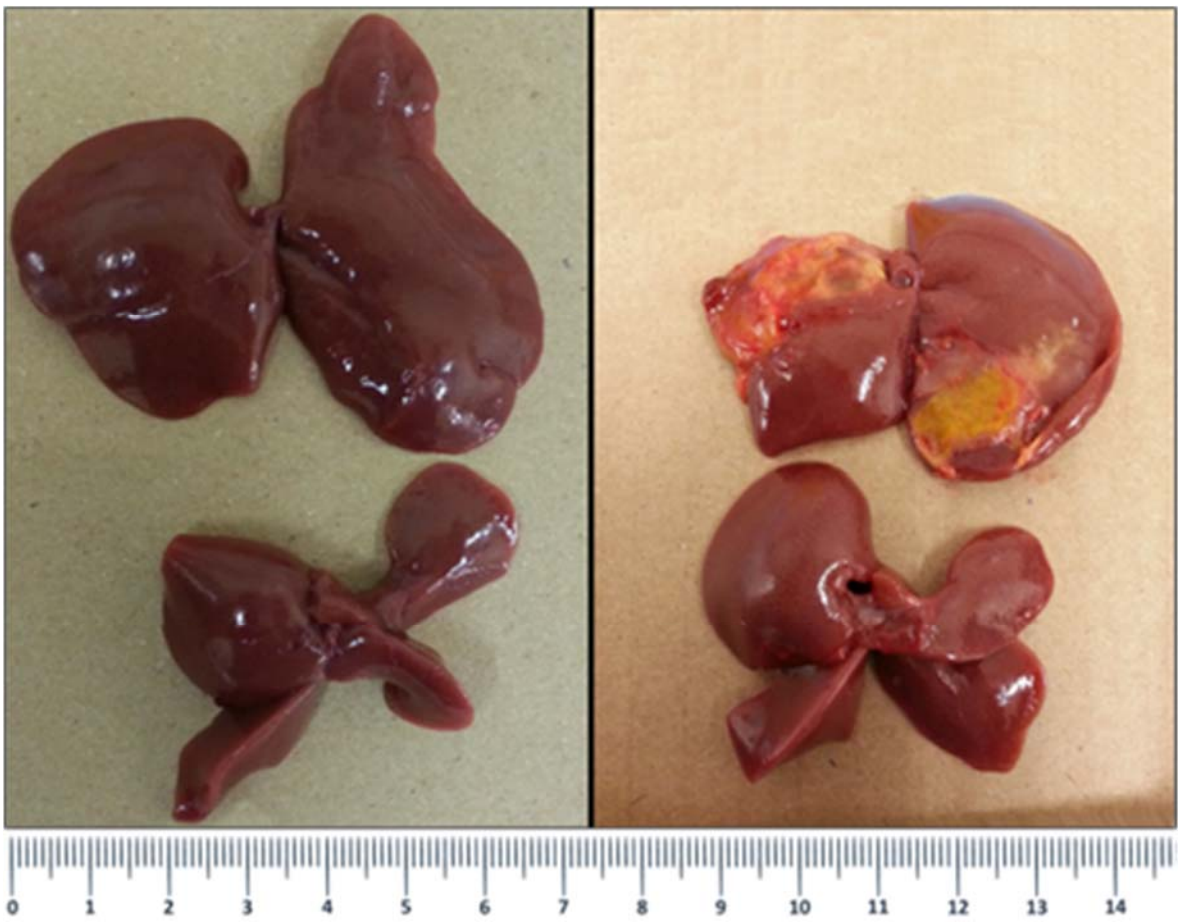

Figure 5.22 Gross changes in size and features of rat liver lobes (top) subjected to 60 min of partial lobar ischaemia followed by reperfusion for 10 days in PCN-treated animals (left) compared to vehicle-treated controls (right). Non-ischaemic lobes (bottom) are shown for comparison.

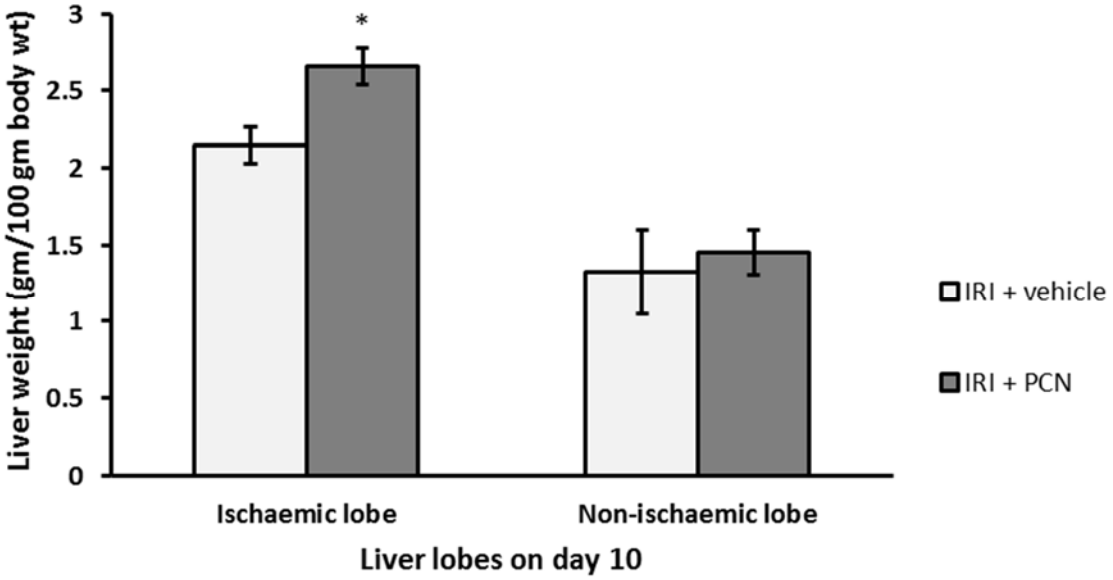

Figure 5.23 Liver lobe weights on day 10 post-IRI. *P<0.05 versus IRI+vehicle

5.3.9. Effect of PXR activation on IRI-induced fibrogenesis

The effect of PCN treatment on IRI-induced fibrogenesis was investigated by quantifying TGF-β, α-SMA, vimentin and collagen levels in ischaemic liver samples through RT-PCR, immunohistochemistry and Sirius red staining.

RT-PCR

Ischaemic lobes from the IRI-PCN group expressed significantly reduced mRNA transcript levels for TGF-β and α-SMA (2.55 and 2.97-fold reduction compared to IRI-vehicle respectively; P<0.05) on day 1 post-reperfusion (Figure 5.24 and Figure 5.25). Vimentin mRNA transcript levels were also lower, while MMP-2 mRNA levels were higher on day 1 in PCN-treated livers, however, these differences did not reach statistical significance (Figure 5.26 and Figure 5.27). No differences in the expression of any of the above genes were identified on day 10 between the two groups.

Hepatic mRNA transcript levels for Col1a1 were expressed in significantly lower levels in the PCN-treated group on day 10 (5-fold reduction compared to IRI-vehicle respectively; P<0.05) (Figure 5.28).

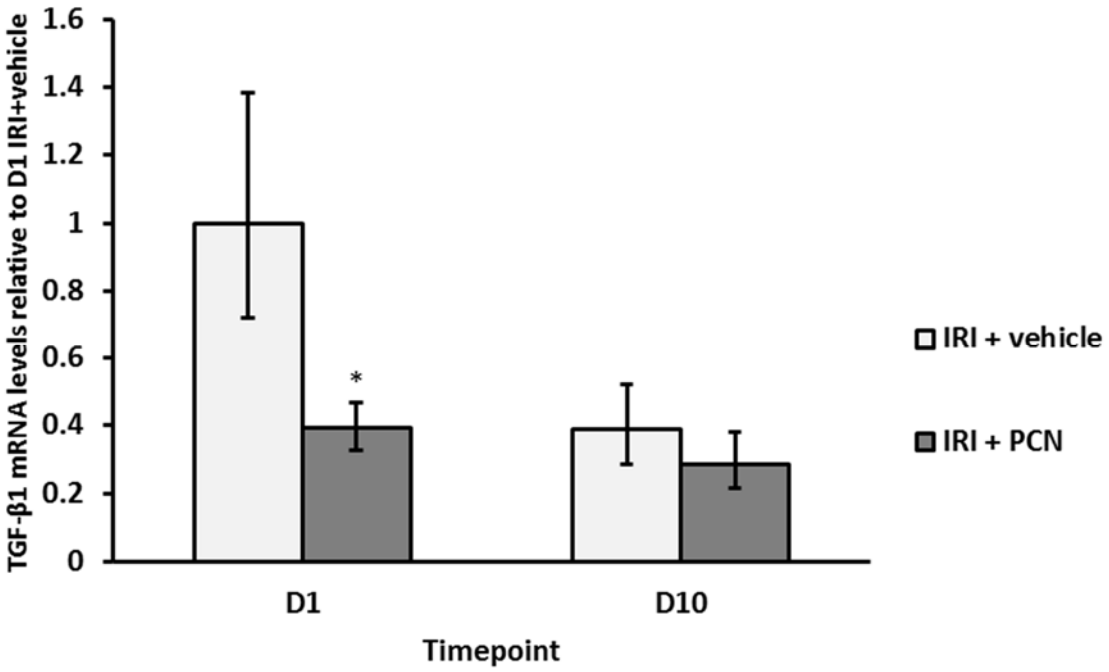

Figure 5.24 RT-PCR analysis comparing TGF- β mRNA expression between the IRI+PCN and IRI-vehicle groups. *p<0.05 versus IRI+vehicle

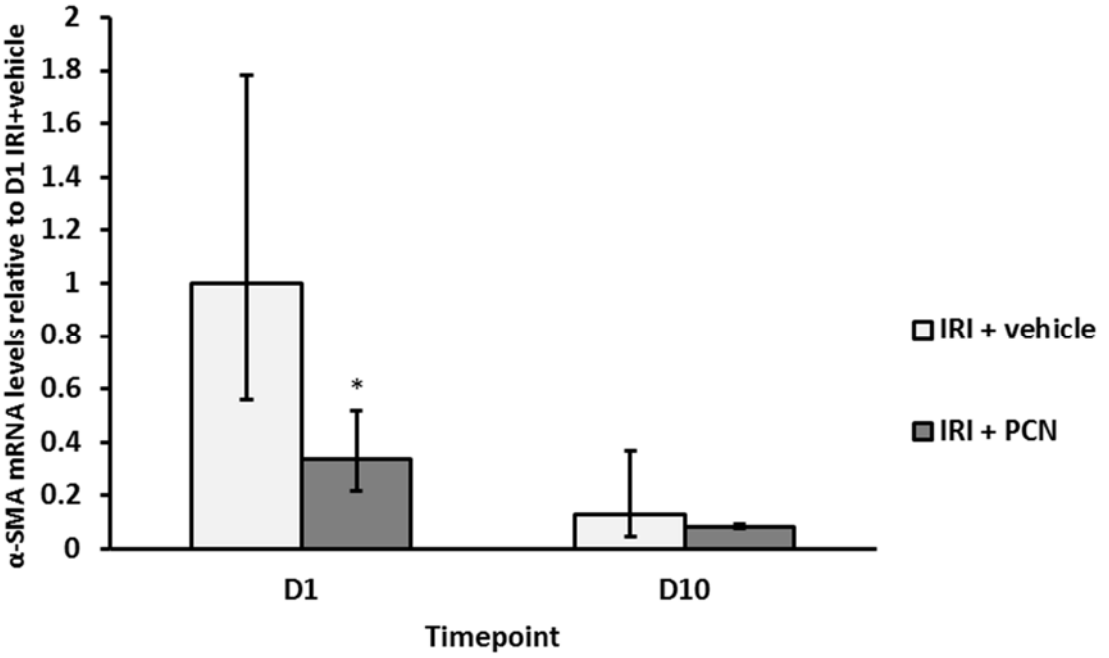

Figure 5.25 RT-PCR analysis comparing α-SMA mRNA expression between the IRI+PCN and IRI-vehicle groups. *p<0.05 versus IRI+vehicle

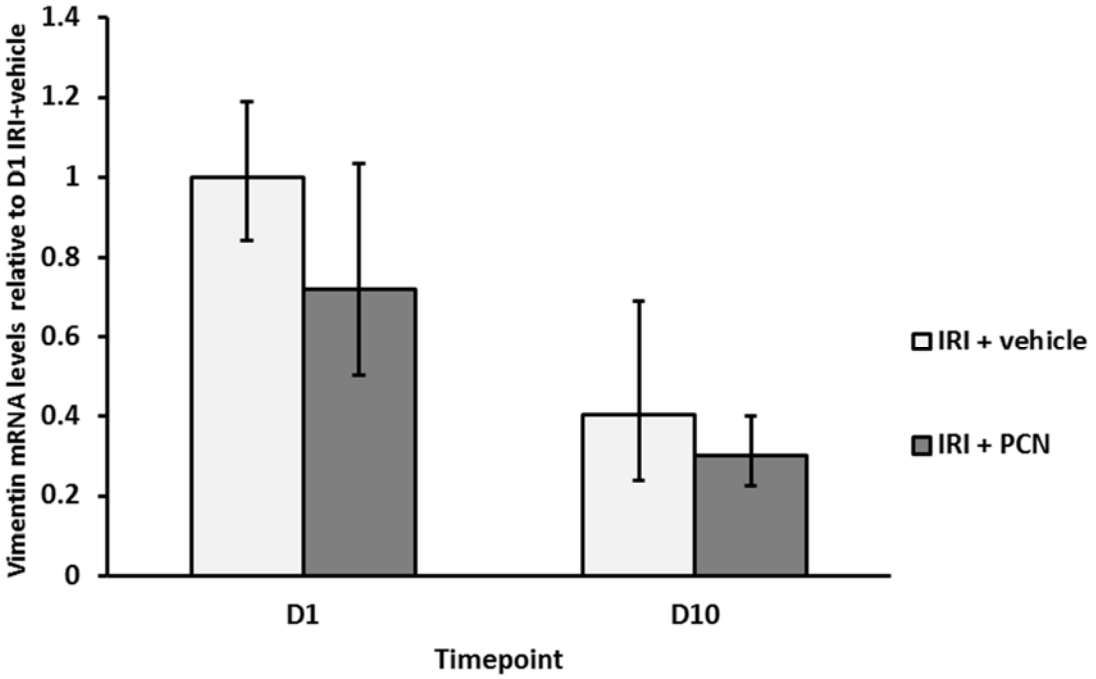

Figure 5.26 RT-PCR analysis comparing vimentin mRNA expression between the IRI+PCN and IRI-vehicle groups.

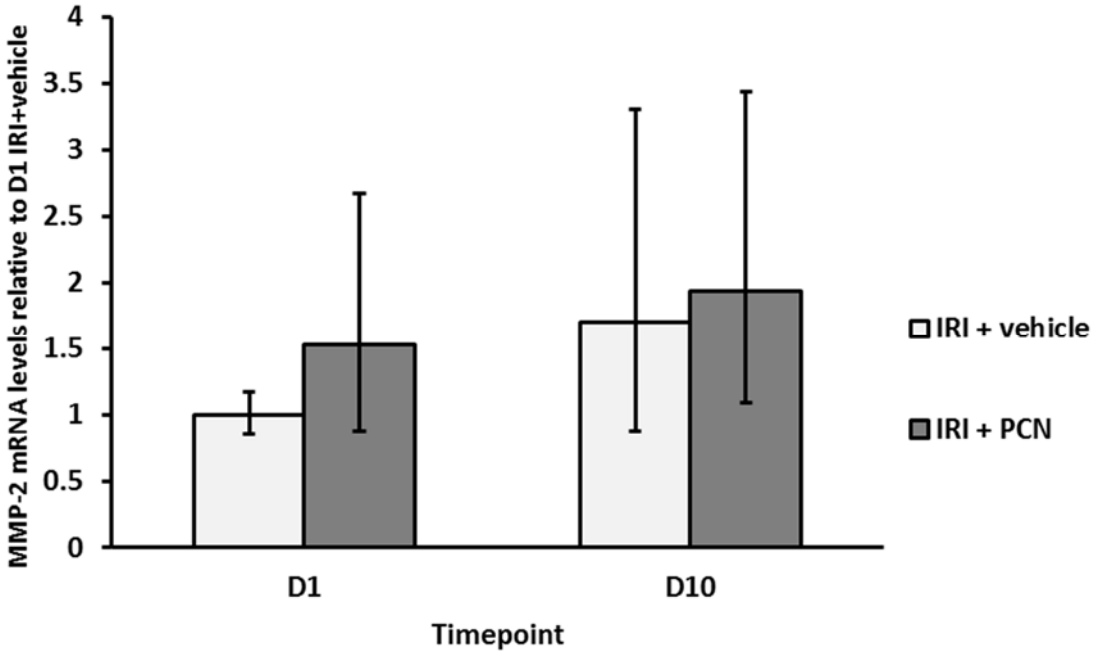

Figure 5.27 RT-PCR analysis comparing MMP-2 mRNA expression between the IRI+PCN and IRI-vehicle groups.

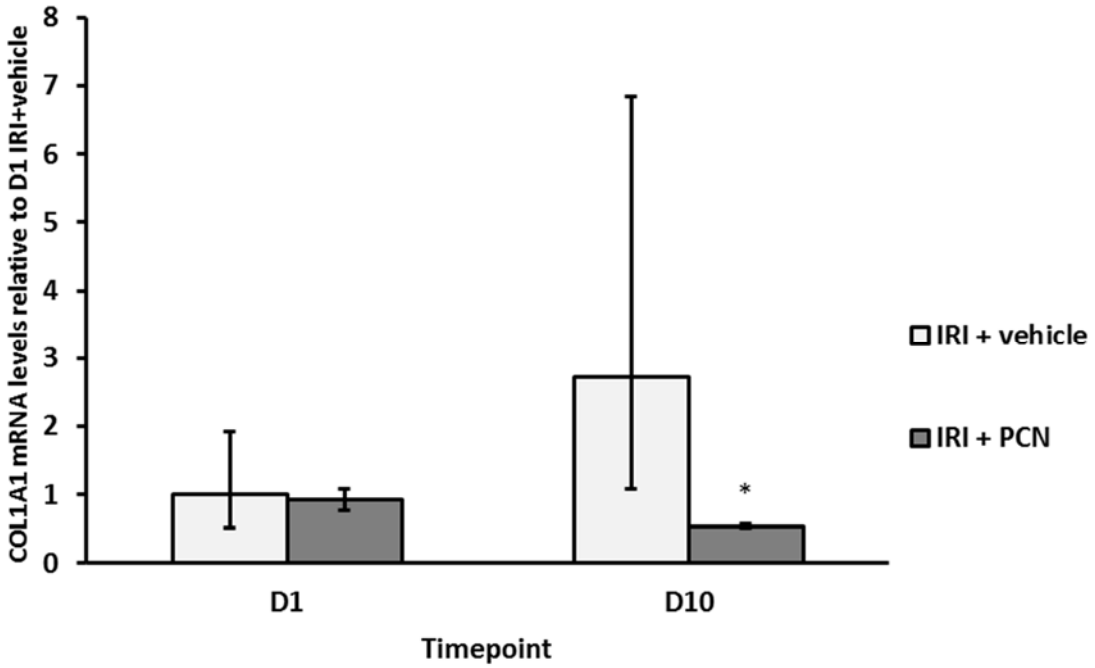

Figure 5.28 RT-PCR analysis comparing Col1a1 mRNA expression between the IRI+PCN and IRI-vehicle groups. *p<0.05 versus IRI+vehicle

Immunohistochemistry staining

Liver sections were probed for vimentin and α-SMA expression in order to quantify the extent of active myofibroblasts following PXR activation. PCN treatment led to a 53% reduction in vimentin expression around portal tracts in ischaemic liver sections on day 10 after clamp release in comparison to controls (3.8±1.4% versus 8.2±1.7% in IRI-vehicle; p=0.002) (Figure 5.29). Peri-portal α-SMA expression in liver sections treated with PCN was reduced by 58% on day 10 (4.6±0.8% versus 11±6% in IRI-vehicle; P=0.047) (Figure 5.30).

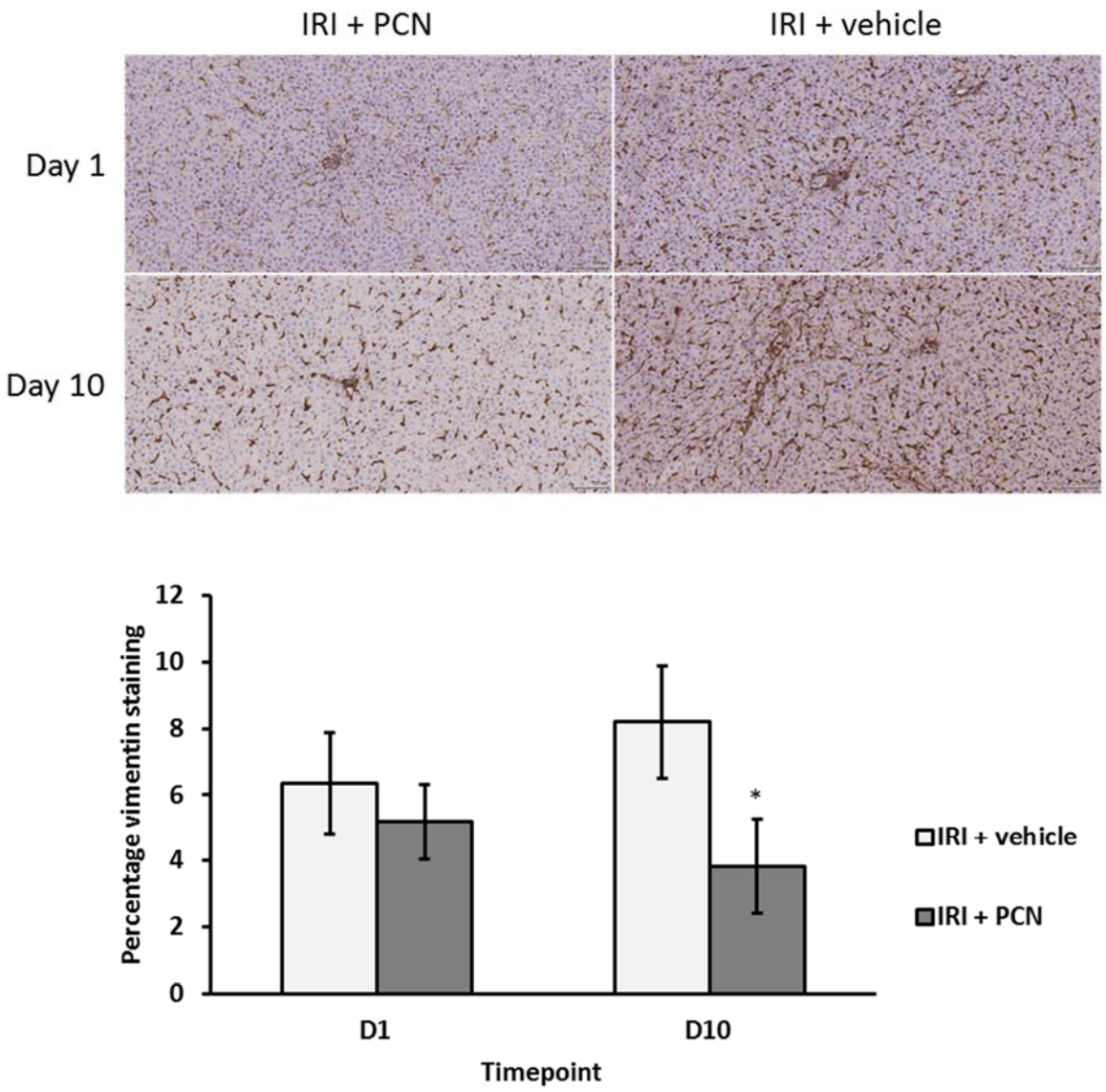

Figure 5.29 Comparison of vimentin staining between IRI+PCN and IRI+vehicle groups on post-reperfusion days 1 and 10 (above) with corresponding stain quantification (below). *P<0.005 versus IRI+vehicle

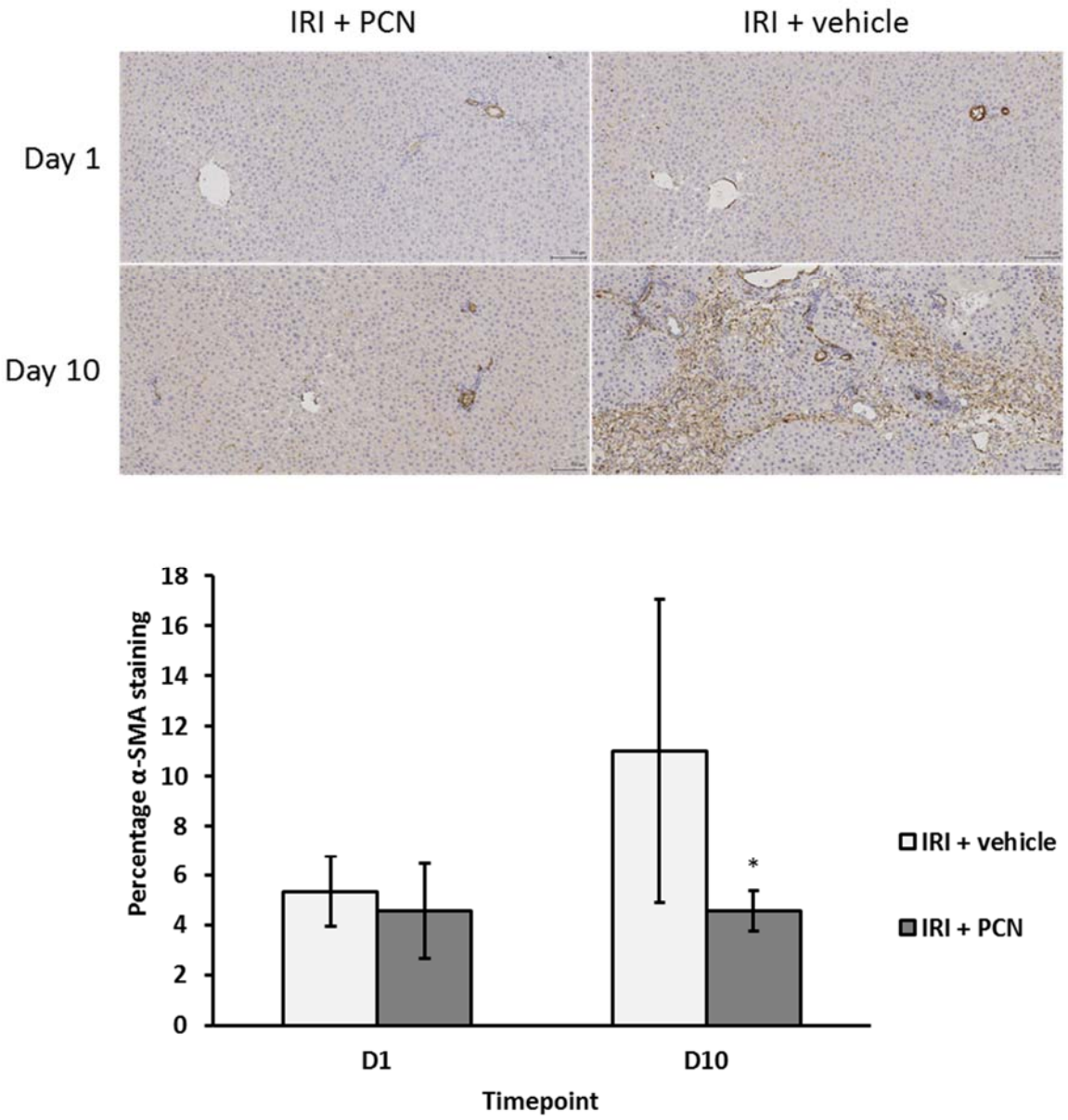

Figure 5.30 Comparison of α-SMA staining between IRI+PCN and IRI+vehicle groups on post-reperfusion days 1 and 10 (above) with corresponding stain quantification (below). *P<0.05 versus IRI+vehicle

Sirius red staining

Liver sections were stained with Sirius red in order to assess the extent of liver fibrosis. PCN treatment was shown to reduce the extent of Sirius red staining in rats treated with PCN by 68% in comparison to vehicle controls on day 10 after clamp release (0.26±0.06% versus 0.84±0.5% in IRI-vehicle; p=0.045) (Figure 5.31).

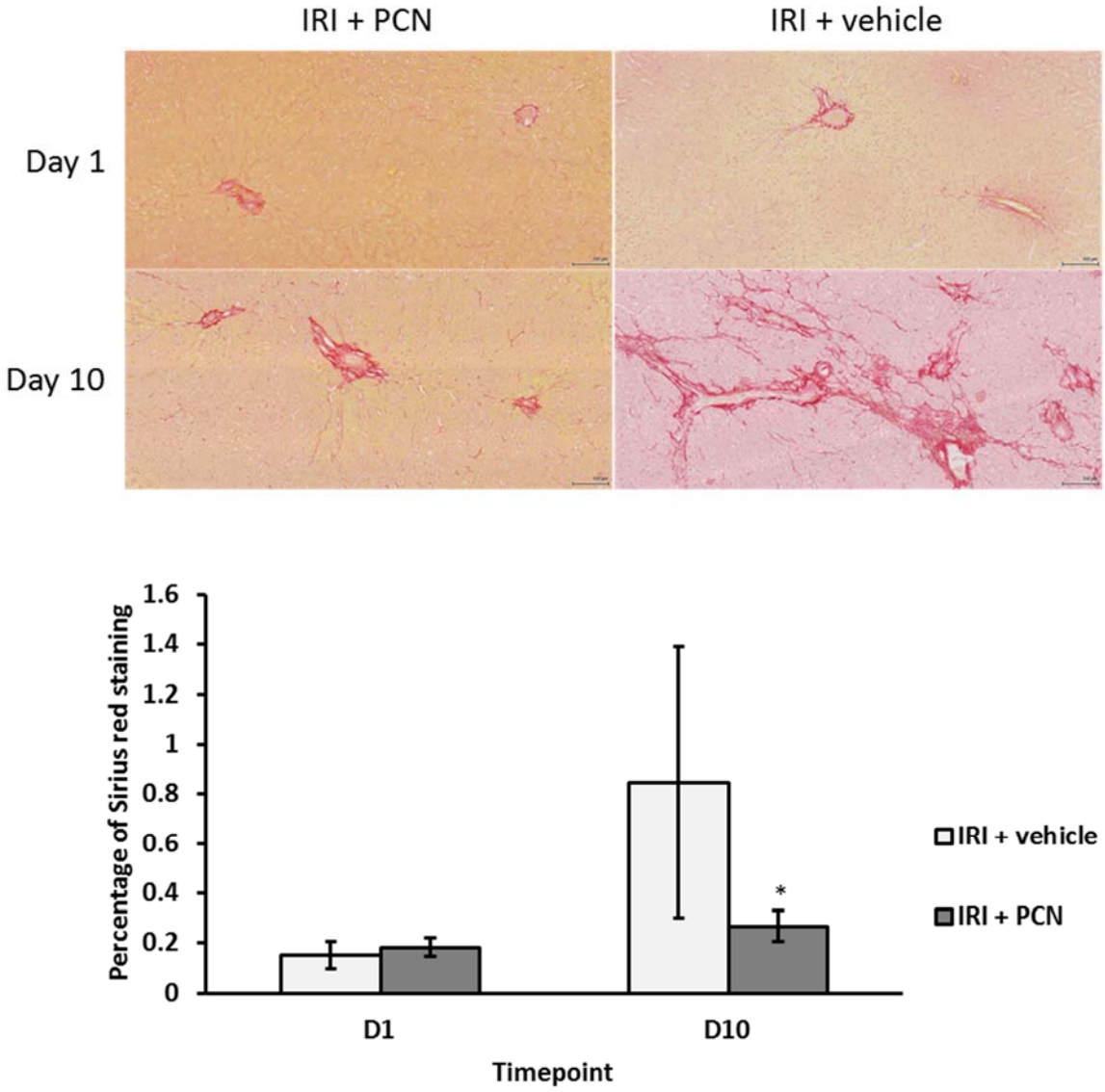

Figure 5.31 Comparison of Sirius red staining between IRI+PCN and IRI+vehicle groups on post-reperfusion days 1 and 10 (above) with corresponding stain quantification (below). *P<0.05 versus IRI+vehicle

5.3.10. Effect of PXR activation on IRI-induced ductular reaction

Liver sections were probed for the expression of CK19 to assess the extent of cholangiocyte proliferation and ductular reaction. CK19 positivity in PCN-treated liver sections on day 10 was comparable to day 1 baseline levels and reduced by 46% compared to day 10 controls (1.4±0.2% versus 2.7±1.1% in IRI-vehicle; p=0.042) (Figure 5.32).

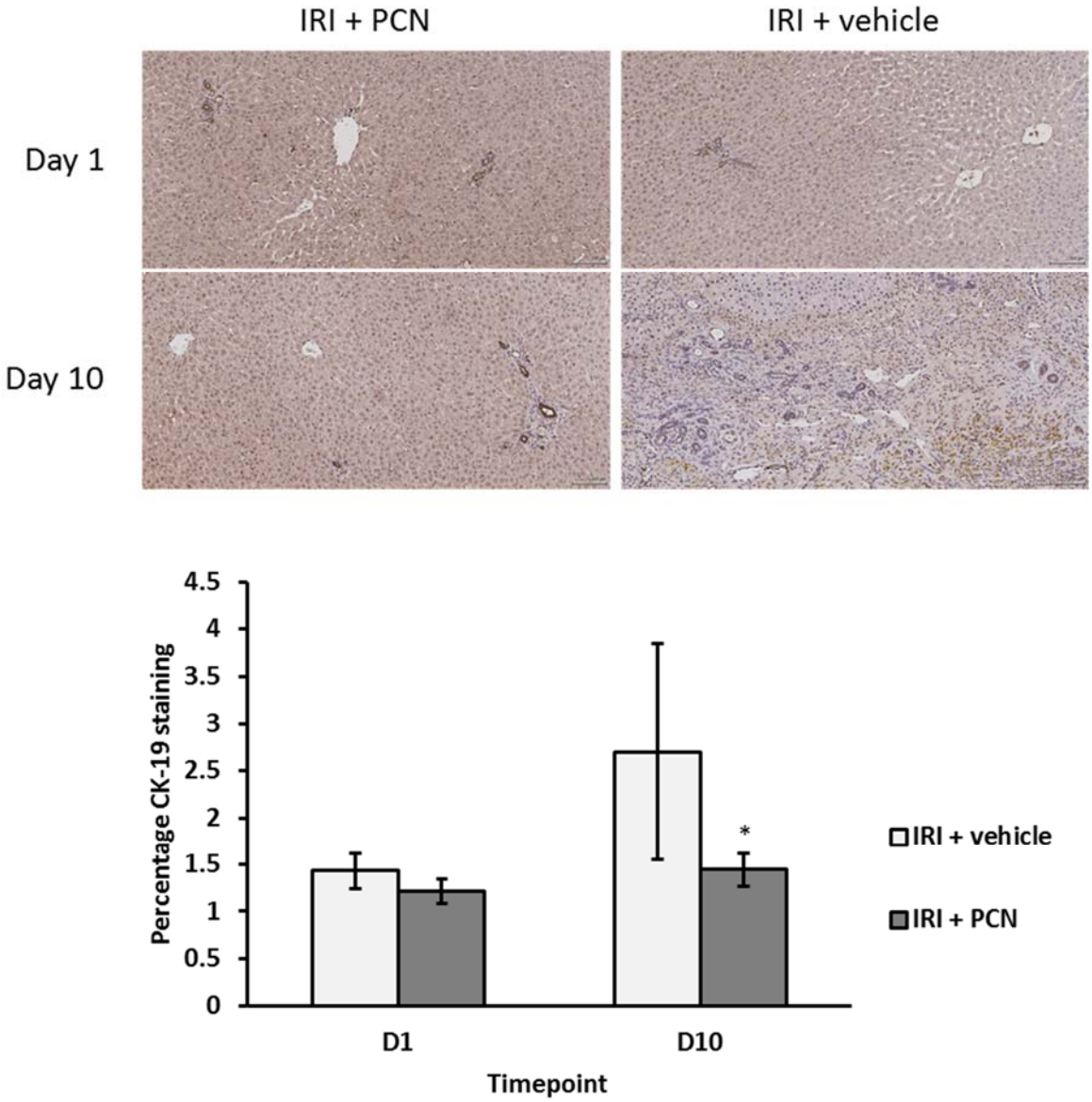

Figure 5.32 Comparison of CK19 staining between IRI+PCN and IRI+vehicle groups on post-reperfusion days 1 and 10 (above) with corresponding stain quantification (below). *P<0.05 versus IRI+vehicle

5.4. Discussion

In view of the cholestatic, inflammatory and fibrotic response to IRI in the liver observed in the initial rat IRI model (Chapter 4), it was hypothesised that a drug intervention targeting activation of the PXR would alleviate these adverse effects, providing proof of principle for a rational treatment to reduce the prevalence of NABS and graft failure in patients undergoing liver transplantation.

To test this hypothesis, rats were subjected to IRI with or without administration of the rodent-specific PXR activator PCN. Once daily subcutaneous PCN treatment significantly induced expression of the Cyp3a1 protein - which is transcriptionally regulated by the activated PXR (Moore and Kliewer, 2000) – demonstrating that hepatic levels of PCN were sufficient to sustain functional PXR activation as early as 48 hours after commencement of PCN treatment.

A modified 70% hepatic IRI model similar to the initial rat IRI model was adopted in the in vivo PXR study to avoid portal congestion and cholestatic injury. The ischaemic period, however, was reduced to 60 minutes in the PXR study in order to better represent the clinical conditions associated with marginal liver transplants. Although the reduction in ischaemia time may have contributed to the dramatic reduction in peri-operative mortality experienced in this study, improved animal survival was most probably related to the employment of a surgical microscope which dramatically reduced operating times and reduced the risk of intraoperative vascular injury and bleeding.

The main endpoints in this experiment were inflammation and fibrosis. Thus only two timepoints were chosen (day 1 and 10). This was based on optimal windows for identifying these endpoints according to data from the optimised hepatic IRI model (Chapter 4).

This study shows that activation of the PXR prior to and after IRI reduces cellular damage, inflammation and fibrosis. This is consistent with results from previous studies which revealed cyto-protective, anti-inflammatory and anti-fibrotic effects of PXR activation in a number of acute and chronic liver injury models (Marek et al., 2005, Wallace et al., 2010, Stedman et al., 2005, Axon et al., 2008, Andrews et al., 2010, Teng and Piquette-Miller, 2007). Iannelli et al (2011) have previously shown that the administration of clotrimazole -a strong PXR activator- prior to IRI resulted in

an anti-apoptotic effect during the first six hours post-reperfusion. The study presented in this chapter demonstrates that the cyto-protective effect of PXR activation extends beyond the first few hours post-reperfusion as evident by reduced necrosis on H&E sections and reduced serum ALT levels on day 1 post-reperfusion when PCN was administered. PXR activation also resulted in a reduction in the degree of lipid peroxidation post IRI. This may be due to the increased expression of PXR-regulated proteins implicated in the oxidative stress response such as glutathione-S-transferase (Rosenfeld et al., 2003) which has previously been shown to play a protective role during reperfusion injury (Romani et al., 1988). Reduced oxidative stress may further explain the enhanced cyto-protection associated with PXR activation in addition to the previously described anti-apoptotic effect (Iannelli et al., 2011).

The choleretic effect of the activated PXR is well described (Jonker et al., 2012, Kakizaki et al., 2009) and was clearly evident in this study. The early reduction in serum bile acids following PCN treatment also highlighted the ameliorating effect of PXR activation on hepatic IRI-induced cholestasis. Whether the improvement of cholestasis in this model further contributed to the reduced cellular damage or was a direct manifestation of hepatocellular survival and function following PXR activation remains to be elucidated. However, it is most likely that the two phenomena are inter-related.

Beyond the initial post-reperfusion period, it was also demonstrate that PXR activation during IRI results in a reduced ductular reaction and an anti-inflammatory effect that persists in peri-portal areas for at least 10 days post-reperfusion. A clear anti-fibrotic effect was also evident by the reduced TGF-β (day 1), α-SMA (day 1) and Col1a1 (day 10) hepatic transcript levels, and reduced α-SMA and Sirius red staining -particularly around portal tracts- on day 10 with PCN treatment. Higher average levels of MMP-2 in that group –though not statistically significant- suggest a trend towards increased extracellular matrix breakdown with PXR activation.

The implications of these findings for graft survival in liver transplantation are far reaching particularly in the case of DCD organs which are particularly predisposed to NABS. In this sense, activation of the PXR during liver transplantation may improve graft outcomes and increase the efficiency of donor liver utilisation.

However, the lack of cholangiography data limit the clinical applicability of the results in relation to the development of NABS. The challenges faced in obtaining cholangiography images have been discussed in the previous chapter (4.4).

It may be argued that the decision to reduce ischaemia time in this study compared to the previous hepatic IRI model may have altered the optimal timepoints for the identification of inflammation and fibrosis. This may be the case. However, based on the results obtained, the chosen timepoints (day 1 and 10) were sufficient to identify differences in the main endpoints as a result of PCN treatment. Furthermore, excessive ischaemia beyond what is relevant clinically could have unnecessarily resulted in non-salvageable hepatic IRI damage and clinically inapplicable results.

The relatively small sample size is a limitation in this study. However, a power analysis was performed a priori based on an expected 50% and 20% reduction in inflammatory and fibrotic markers respectively on day 10 according to previous work in our laboratory (Marek et al., 2005, Wallace et al., 2010). It was identified that a minimum of 4 animals would be required per group assuming a power of 80% and an alpha level of 0.05. Based on that, a sample size of 5 animals per group for each timepoint was adopted in this study in keeping with the National Centre for the Replacement Refinement & Reduction's guidelines to minimise animal use in such experiments (NC3Rs/BBSRC/Defra/MRC/NERC/Wellcome Trust, 2013)

The optimal time point at which the first dose of PXR activator should be administered in relation to reperfusion and the duration of treatment in order to confer any benefit following liver transplantation remains unclear. In the current study, PXR activation was commenced 48 hours prior to IRI as opposed to 72 hours in the study by Iannelli et al (2011) and demonstrated comparably favourable outcomes despite longer ischaemia times. This raises the question of whether pre-IRI treatment with PXR activators provides any added benefit over the commencement of treatment during or following IRI. This question is addressed in the clinical PXR study presented in the following chapter (Chapter 6).

Chapter 6. Clinical PXR study

6.1. Introduction

The results obtained from PXR activation in the rat IRI model are highly encouraging (Chapter 5). Nevertheless, translation of this achievement into clinical practice should follow at this stage in order to test the clinical applicability and relevance of these results and further advance our knowledge on this subject. The benchside to bedside approach however, is rarely a straightforward endeavour and presents multiple challenges and obstacles to overcome (Keramaris et al., 2008). Therefore, it is important to understand key issues that need to be addressed in order to adapt the benchside model to a clinical population.

6.1.1. Rat versus human PXR

As detailed in section 5.1.4, there are key evolutionary differences between PXR orthologues from different species. Varying LBD regions between orthologues mean that their ligand-specificities vary significantly, although it is likely that the regulated target genes and signalling pathways are comparable given the conservative nature of the DBDnr regions amongst orthologues (Kliewer et al., 2002). An understanding of this ligand-specificity is imperative in order to identify clinically-relevant PXR activators.

6.1.2. Identification of clinically relevant PXR activators

In addition to the issue of species-selectivity, it is worth noting that not all ligands that bind to the PXR necessarily lead to its activation (Ekins et al., 2007). Furthermore, in view of its capacity to accept molecules of varying sizes and chemical properties, and an ability to accommodate smaller molecules in different orientations, traditional structure-based virtual screening methods are of little help in identifying potential PXR ligands (Ekins et al., 2009). Therefore, various in vivo and in vitro laboratory techniques have been developed to investigate ligand binding to and activation of the PXR. Key approaches are outlined below.

Human hepatocyte-based assays

The use of cultured primary human hepatocytes is the gold standard in vitro system to assess induction potentials of new drugs (LeCluyse, 2001). It is a system widely accepted by the drug industry, academia and regulatory bodies and enables the investigation of various aspects of drug action and its regulation within an intact cellular system (Sinz et al., 2008). However, the difficulty in obtaining and maintaining primary human hepatocytes in culture has driven researchers towards using immortalised hepatocytes and other in vitro assays for early stages of drug screening (Zhu et al., 2004, Sinz et al., 2008).

Ligand binding assays

A number of ligand binding assays have been employed using isolated PXR receptors in vitro. These include the scintillation proximity assay (SPA) that utilises a radioligand with scintillating effect when bound to the immobilised PXR, an effect that reduces when non-radioactive ligands compete for PXR binding (Kliewer et al., 2002); the coactivator receptor ligand assay (CARLA) where interaction of the PXR with a radioactive coactivator upon ligand binding produces co-precipitation of the complex which can then be measured (Kliewer et al., 2002); and fluorescence resonance energy transfer (FRET) where interaction of a coactivator with a fluorescence-labelled LBD (in the presence of a bound ligand) produces a measurable fluorescence signal (Shukla et al., 2009). These assays can be used to create concentration-response curves and measure binding potencies of various ligands. However, despite their relative simplicity, ligand binding assays lack the structural cellular components that put ligand binding into life-like context and hence data obtained from these assays usually requires further validation (Sinz et al., 2008)

Trans-activation assays

These assays are cell-based; usually involving either primary hepatocytes (Raucy et al., 2002)or cell line derived from immortalised hepatocytes (e.g. HepG2) (Shukla et al., 2011). Cells are co-transfected with a vector containing species-specific PXR coding regions (encoding full or chimeric receptor), and a vector combining a reporter gene, an upstream target gene (e.g. CYP3A4) enhancer and a minimal promoter element. Various ligands can then be assessed for PXR activation (through

measurement of reporter gene output) and/or target gene expression. Similar to ligand-binding assays, trans-activation assays can measure binding potencies of various ligands. Although these assays are more complex and time-consuming, they also provide essential information beyond ligand binding, such as receptor activation and gene expression, differentiating PXR agonists from antagonists or non-functional ligands (Ekins et al., 2007, Sinz et al., 2008). However, one major disadvantage of these assays is that they only assess direct interaction of ligands to the isolated PXR. No account is taken of the interactions and cross talk between ligand-bound PXR and other nuclear receptors, which come into play in real life.

The above assays can be employed in automated high throughput screening (HTS) processes to profile large numbers of potential PXR ligands (Shukla et al., 2011, Raucy and Lasker, 2010).

Transgenic animal models

Humanised hPXR mice were first developed by Xie et al (Xie et al., 2000a). These animals are genetically engineered to express hPXR (rather than mPXR) and therefore respond to human-specific PXR activators allowing the investigation of hPXR-ligand interaction within a complex dynamic living system. This facilitates more detailed assessment of drug pharmacokinetics including drug-drug interactions, particularly in more complex humanised models where human CYP genes are also introduced (Scheer et al., 2015). However, these models are not suitable for screening large numbers of drugs for PXR activation for obvious reasons. In addition, such models result in in vivo interplay between “humanised” gene products and native genes and proteins and therefore does not fully replicate events in an intact unmodified biological system (Sinz et al., 2008).

6.1.3. PXR polymorphism

In addition to variations in PXR response between species, disparate responses can occur within the individuals of the same species. Indeed, the inter-individual variation in response to PXR-activating drugs is well established albeit still poorly understood

(Eichelbaum and Burk, 2001, Kliewer et al., 2002). Various environmental and genetic factors have been implicated in this observation (Rana et al., 2016).

The existence of over 35 single nucleotide polymorphisms (SNP) in the PXR gene may partly explain this variation (Zhang et al., 2001, King et al., 2007). PXR SNPs have been shown to explain variations in response to many drugs including warfarin (Moon et al., 2015), imatinib (Liu et al., 2017) and certain chemotherapeutic regimes (Mbatchi et al., 2015, Revathidevi et al., 2016), and have been linked to susceptibility to conditions such as NAFLD (Sookoian et al., 2010), Crohn's disease (Glas et al., 2011) and colorectal cancer (Ni et al., 2015). However, it is worth noting that, of the multiple SNP identified, only a small proportion are in the PXR protein coding regions resulting in a few variant PXR proteins. The frequency of these variants is very low and is unlikely to account for a significant proportion of variation in drug responses between individuals (Zhang et al., 2001, Kliewer et al., 2002). Other polymorphisms, including that of CAR and various coactivators are likely to be key contributors to this variation (Prakash et al., 2015)

6.1.4. Designing a clinical study

Multiple methodology aspects need to be addressed in order to design a robust translational study based on data from the animal research.

Type of study

Analysis and quantification of the effect of PXR activation in clinical practice is essential to the validation of results from the animal work. The gold standard analytical design in clinical research is the randomised control trial (RCT), where bias is minimised and the controlled benchside research environment is simulated as closely as possible (Grimes and Schulz, 2002). However, such prospective work presents a number of ethical and logistical challenges. For example, based on an annual average of 42 liver transplants at local level (Newcastle upon Tyne NHS Trust local data), it will require at least four years to recruit a sufficient number of patients in order to adequately power such study to detect a generous 50% reduction in a hypothetical commonly occurring risk at an alpha level of 0.05. Given the time restrictions associated with this project, the alternative option is to design a

retrospective cohort study based on previous liver transplantations performed in the trust, accepting the limitations associated with such design (Grimes and Schulz, 2002).

Method for identifying and grading PXR-activating drugs

Various PXR screening studies were examined in order to select the optimal tool for the identification and grading of clinically relevant PXR activators (Persson et al., 2006, Moore et al., 2000, Lehmann et al., 1998, Shukla et al., 2009, Shukla et al., 2011). These were assessed for assay strengths and limitations, reporting of potency profiles, comprehensiveness and inclusion of current drugs. The hPXR activation dataset by Shukla et al (Shukla et al., 2011) was chosen as a reference tool based on its comprehensive assessment of contemporary and clinically relevant drugs.

Prediction of clinical PXR activation status in retrospect

In an ideal situation, PXR activation would be quantified based on prospective tissue analysis of subjects. Given the clear ethical questions that such approach poses, and in the absence of routine tissue collection post transplantation, definitive PXR status quantification was not a viable option. However, the alternative prediction-based approach presents a number of challenges in its own right. Innumerable drug- and patient-related variables dictate individual patient response to PXR activators particularly when given in combination with other PXR-activating and non-activating medications. Only a handful of these variables are available retrospectively (drug dose, route of administration, PXR activating potency and patient weight). Moreover, no validated approaches to the prediction of PXR activation have been reported in the literature to date. Therefore, a prediction tool was developed by the project team based on established pharmacokinetic principles and the availability of retrospective data, accepting that this is an objective yet unvalidated tool with the potential risk of inaccurate estimation. A detailed description of this tool is provided in section 6.2.4.

Outcome measurement

Results from the animal model were based on largely on histological and short-term biochemical data. However, a focus on clinically relevant outcomes is required in a translational study. In the context of liver transplantation, such outcomes include early graft function, procedure-related complications and long term graft and patient survival. Based on results from the animal model, improved outcomes were anticipated in graft survival and the risk of developing NABS.

6.1.5. Hypothesis and aim of study

Based on the animal models, it was hypothesised that hPXR activation in the early post-transplantation period would lead to improved graft survival and a reduction in clinically-relevant complications associated with ischaemia reperfusion injury

The aim of this clinical study was to investigate the effect of early hPXR-activation on procedure-related complications and survival outcomes in a cohort of liver transplantation recipients.

6.2. Methods

6.2.1. Study design

This clinical study was designed as a retrospective cohort study of patients undergoing deceased donor orthotopic liver transplantation (OLT) between October 2010 and September 2016 at the Institute of Transplantation of the Freeman Hospital (Newcastle upon Tyne Hospitals NHS Foundation Trust, UK).

6.2.2. Data extraction

Data for this study was obtained from multiple sources including the Trust's electronic medical record system, eRecord (Cerner, Kansas City, USA); a locally held transplant coordinator database; the NHSBT National Transplant Database (NTxD); the NHSBT Organ Donation and Transplantation Electronic Offering System (EOS); the British National Formulary (BNF 69) (Joint Formulary Committee, 2015); the Merck Index Online and drug profiling data for Human PXR (hPXR) activation obtained from the National Institutes of Health (NIH) (Shukla et al., 2011)

The extracted data was divided into six main domains: Donor, recipient and graft data, admission and transplantation data, medication data, early graft function data, complication data and survival data. Details of the individual variables collected within each domain are outlined in Table 24.

The collected data was entered into a Microsoft Office Excel 2010 spreadsheet (Microsoft Corp., Redmond, WA).

Table 24 Details of variables collected for clinical PXR study

Domain	Variable	Details
Donor, recipient and graft data	Donor age	Age at the time of death (years) Based on EOS data
	Donor gender	Male or Female Based on EOS data
	Donor height	Height at the time of death (cm)

		Based on EOS data
	Donor weight	Weight at the time of death (kg) Based on EOS data
	Donor Body Mass Index (BMI)*	Derived from donor height and weight BMI=Weight (kg)/Height^2 (m)
	Donor ethnicity	Categories Based on EOS data
	Cause of donor death	Categories Based on EOS data
	Donor Cytomegalovirus (CMV) status	IgG positive or negative at the time of death Based on EOS data
	Type of deceased donor	DBD or DCD Based on EOS data
	Recipient age	Age at the time of transplantation (years) Based on eRecord data
	Recipient gender	Male or Female Based on eRecord data
	Donor/recipient gender mismatch*	Derived from donor and recipient gender data Yes=opposite donor/recipient genders
	Recipient height	Height at the time of transplantation (cm) Based on eRecord data
	Recipient weight	Weight at the time of transplantation (kg) Based on eRecord data
	Recipient Body Mass Index (BMI)*	Derived from recipient height and weight BMI=Weight (kg)/Height^2 (m)
	Recpient Cytomegalovirus (CMV) status	IgG positive or negative at the time of transplantation Based on eRecord data
	CMV mismatch*	Derived from donor and recipient gender data Yes=donor CMV positive and recipient CMV negative
	Primary liver pathology of recipient	Categories Based on local database and NTxD data

	Previous liver transplantation	Yes or No Based on local database and NTxD data
	Model for End Stage Liver Disease (MELD) score	Calculated using recipient serum creatinine, bilirubin and international normalized ratio for prothrombin time (INR) at the time of transplantation Based on local database and NTxD data
	Graft type	Whole or split liver graft Based on local database and NTxD data
	Super-urgent status	Yes or No Based on local database and NTxD data
Admission and transplantation data	Date of admission	DD/MM/YYY Based on eRecord data
	Date of transplantation	DD/MM/YYY Date at the start of transplantation Based on eRecord data
	Date of discharge	DD/MM/YYY If readmitted within 48 hours then latest date of discharge Based on eRecord data
	Length of hospital stay (LOS)*	Derived from transplantation and discharge dates (days) LOS=duration of time between transplantation and discharge
	Cold ischaemia time (CIT)	Calculated as the total duration of cold storage of the graft (minutes) Based on NTxD data
	Total Warm ischaemia time (WIT)	Total warm ischaemia time (minutes) is the combined duration of first and second warm ischaemia times First warm ischaemia time is calculated from the time of death to graft procurement (in DCD retrieval) Second warm ischaemia time is calculated from the time of graft removal from cold storage to reperfusion of graft (in both DBD and DCD organ transplantation) Based on NTxD data

	Veno-venous bypass time	Total duration of veno-venous bypass (minutes) Based on NTxD data
	Type of biliary anastomosis	Duct-to-duct anastomosis or Roux-en-Y hepaticojejunostomy Based on NTxD data
	Type of arterial anastomosis	Single or multiple Based on NTxD data
	Number of organs transplanted	Liver alone or multi-organ transplantation Based on local database and NTxD data
	Intraoperative blood transfusion	Number of units transfused intraoperatively Based on NTxD data
	Postoperative blood transfusion	Number of units transfused within 48 hours postoperatively Based on NTxD data
	Operating surgeon	Primary operating surgeon Based on eRecord data
	Duration of intensive care unit (ITU) stay	Postoperative period up to discharge from ITU (days) Based on NTxD data
Medication data	**Collected for each drug administered. Total amount of drug administered within the first 7 days post-transplantation is calculated (in moles) and normalised to total body weight**	
	Drug dose	Amount of drug per dose (mg) Based on eRecord data Drug doses expressed in volumes (ml) or other delivery forms (e.g. puffs) are converted to equivalent weights (mg) based on BNF data
	Route of drug administration	Recorded route of drug administration Based on eRecord data
	Total number of doses administered	Total number of doses administered within first 7 days post-transplantation Based on eRecord data
	Drug molecular weight	From standard molecular formula of drug Based on BNF and Merck Index Online data
	Half-maximal activation value (AC_{50}) of drug to	The concentration of drug which produces 50% of maximal hPXR

	hPXR	activation response on a concentration-response curve (CRC) Based on NIH data
	Class of drug concentration response curve (CRC)	CRC class indicating quality of fit and efficacy of hPXR activation response Based on NIH data
Early graft function data	Serum bilirubin	Serum bilirubin on day 7 post-transplantation (μmol/L) Based on eRecord data
	Serum prothrombin time (PT)	Serum PT on day 7 post-transplantation (seconds) Based on eRecord data
	Serum ALT	Highest level of serum ALT within first 7 days of transplantation (IU/L) Based on eRecord data
	Early Allograft Dysfunction (EAD)*	Derived from early graft function data (serum bilirubin, PT and ALT) See section 6.2.5
Complication data	**See section 6.2.5 for definitions of complications**	
	Primary non-function (PNF)	Yes or No Defined as failure of graft to function immediately after transplantation (where specific technical causes have been excluded) leading to death or requiring re-transplantation (Oh et al., 2004) Based on local database and NTxD data
	Vascular complications	Bleeding, thrombosis or vascular stenosis Type, date of diagnosis (radiological, histological or intraoperative) and intervention details are recorded Based on eRecord and NTxD data
	Biliary complications	Biliary strictures or leaks Type, date of diagnosis (radiological, endoscopic, histological or intraoperative) and intervention details are recorded Based on eRecord and NTxD data
	Infective complications	Yes or No Culture-proven and treated infection regardless of site

		Type, date of first positive culture and type of treatment are recorded Based on eRecord and NTxD data
	Sepsis*	Yes or No Derived from clinical, biochemical and pharmacological data composing the Sequential Organ Failure Assessment (SOFA) score (Sepsis-3 definition) Based on eRecord data
	Return to theatre	Yes or No Number of re-exploration procedures, reason(s) for return to theatre and date(s) of surgery are recorded Based on eRecord data
	T cell-mediated rejection (TCMR)	Yes or No Number of episodes and dates of positive biopsies are recorded Based on eRecord and NTxD data
	Degree of TCMR	Mild, moderate or severe episode based on biopsy report If multiple biopsies are taken within one episode of TCMR, the degree of TCMR is measured according to the highest reported severity Based on eRecord data
	Antibody-mediated rejection (AMR)	Yes or No Number of episodes and dates of positive biopsies are recorded Based on eRecord and NTxD data
	Chronic rejection	Yes or No Date of first suggestive biopsy is recorded Based on eRecord data
	Disease recurrence	Yes or No Based on eRecord data
Survival data	**See section 6.2.5 for definitions of survival data**	
	Occurrence of TCMR	As above Yes or No Based on eRecord data
	Occurrence of graft failure	Yes or No Based on eRecord data
	Occurrence of Death	Yes or No Based on local database and NTxD

		data
	Cause of death	Categories Based on local database and eRecord data
	Date of first TCMR episode	As above DD/MM/YYY Date of first positive biopsy Based on eRecord data
	Date of re-transplantation	DD/MM/YYY Based on eRecord data
	Date of death	DD/MM/YYY Based on local database and NTxD data
	Last date of follow up	DD/MM/YYY Latest review date of patient (in person or via telephone) as of 22/05/2017 Based on eRecord data
	Rejection-free graft survival*	Duration of time between date of transplantation and date of first TCMR episode [otherwise censored at date of re-transplantation, death or last follow up]
	Graft survival (death-censored)*	Duration of time between date of transplantation and date of re-transplantation [otherwise censored at date of death or last follow up whichever the latest]
	Patient survival*	Duration of time between date of transplantation and date of death [otherwise censored at date of last follow up]

*Derived variables

6.2.3. Exclusion criteria

The following exclusion criteria were applied in this study

- Recipients of combined organ transplantation
- Recipients that experienced graft failure within the first 7 days post-transplantation (including primary non-function)
- Recipients that died within the first 7 days post-transplantation

Recipients of DCD organs, split liver transplants, super-urgent transplants and recipients of previous transplants were included in the study if they did not meet the above exclusion criteria.

6.2.4. Calculation of Predicted hPXR activation value on day 7 ($PPAV_7$)

Given the retrospective nature of this study and the lack of consistency in tissue availability in the studied population, hPXR activation in recipients was indirectly assessed based on the total dose and hPXR-activation potency of drugs administered within the first week of transplantation. The 7-day timepoint was chosen to coincide with the early assessment of graft function, one of the main outcomes measured in this study.

For each recipient, the total amount of each drug administered within the first 7 days of transplantation was identified and calculated using the electronic prescription function of eRecord. In order to maintain consistency in measurement between various drugs, the total amount of each drug administered over 7 days was converted to moles based on its average molecular weight obtained from The Merck Index Online (www.rsc.org/merck-index). The molar total was then divided by body weight of recipient at the time of transplantation to take into account the effect of body weight on the pharmacokinetics of each drug (Burton, 2006). Calculation of the weight-normalised 7-day molar total (WTD_7) for each drug is summarised in the following equation:

$$\mathrm{WTD7} = \frac{\mathrm{TD7(gm)}}{\mathrm{MW} * \mathrm{TBW(kg)}}$$

Where TD_7 is the total amount of the corresponding drug administered over 7 days, MW is the molecular weight of that drug and TBW refers to total body weight of the recipient at the time of transplantation.

Data on the Human PXR (hPXR) activation profile of clinically used drugs was based on a dataset kindly provided by researchers at the National Institutes of Health (NIH) (Shukla et al., 2011). According to the data provided, drugs were classified into one of four major concentration-response curve (CRC) classes that correspond to the compound efficacy and quality of curve fit (r^2) derived from the Hill equation (Shukla et al., 2009). Drugs with CRC classes 1.1, 1.2, 2.1 and 2.2 were considered active.

Drugs with class X.4 curves showed poor fit and low efficacy and were considered inconclusive whereas drugs with class 4 curves exhibited no concentration-response relationship and were thus considered inactive. For the purpose of this study, drugs associated with the latter curves were not considered to be hPXR activators at clinically administered doses and were excluded from further measurements. The relative potencies of the remaining drugs were quantified based on the half-maximal activation value (AC_{50}) provided in the NIH datasets.

The predicted hPXR activation value on day 7 ($PPAV_7$) represents an attempt to predictively measure the degree of hPXR activation for an individual recipient on the 7^{th} day post-transplantation based on the weight-normalised total dose (WTD_7) and potency (AC_{50}) of each hPXR activator administered to that recipient during the 7-day period. It was calculated based on the following equation:

$$\mathrm{PPAV7} = \frac{\mathrm{WTD7\ (drug\ A)}}{\mathrm{AC50\ (drug\ A)}} + \frac{\mathrm{WTD7\ (drug\ B)}}{\mathrm{AC50\ (drug\ B)}} + \frac{\mathrm{WTD7\ (drug\ C)}}{\mathrm{AC50\ (drug\ C)}} + \cdots$$

Where drugs A, B, C … are medications associated with CRC classes 1 and 2 administered to the recipient within the first 7 days post-transplantation.

The final $PPAV_7$ value was multiplied by a factor of $1x10^6$ to produce a simpler decimal figure.

Due to the retrospective nature of this study, three unavoidable presumptions were made in the calculation of recipient $PPAV_7$:

1. That the practically unmeasurable inter- and intra-drug variation in pharmacokinetic parameters (such as bioavailability and volume of drug distribution) due to various recipient and drug characteristics would not have a significant impact on hPXR activation after 7 days of drug administration
2. That hPXR activation in vivo was dependent primarily on the hPXR-activation potency of any given drug (inversely related to the AC_{50} value) and not its efficacy (which differs between activators of high and low quality CRC subclasses)
3. That no genetic variation in response to hPXR activator existed between individuals

In reality, it is highly unlikely that any of these presumptions were accurate given the complex nature of mammalian systems. However, since any potential error in $PPAV_7$

measurement arising from these presumptions would be random, it was postulated that inaccurately-predicted values would be randomly distributed between the various study subgroups and would not significantly influence the outcomes.

The study population was divided into low and high hPXR activation groups based on a cut-off median $PPAV_7$ within the cohort.

6.2.5. Outcomes

Early allograft dysfunction

The primary outcome investigated in this study was Early Allograft Dysfunction (EAD) based on the modified definition validated by Olthoff et al (2010). EAD was defined as the presence of at least one of the following criteria:

- Serum bilirubin level ≥10mg/dl (170μmol/L) on day 7 post-transplantation
- International normalised ratio (INR) ≥1.6 on day 7 post-transplantation
- Serum Alanine or Aspartate aminotransferase (ALT or AST) >2000IU/L within the first 7 days post-transplantation

EAD provided an early measure of graft function and has been shown to be associated with graft loss and patient mortality (Olthoff et al., 2010).

Early and late postoperative complications

The incidence of transplant-related vascular, biliary and infective complications was also investigated in this study in addition to the incidence of return to theatre and acute rejection. Late complications including chronic graft rejection and disease recurrence were also examined. These outcomes are listed and defined in Table 25.

Table 25 Definition of liver transplant-related complications

Outcome	Definition
Vascular complication	Bleeding, thrombosis or vascular stenosis (arterial or venous; anastomotic or otherwise), diagnosed radiologically, histologically or intraoperatively and

	requiring pharmacological, radiological or surgical intervention. Equivalent to grade III complications according to the Clavien-Dindo classification (Dindo et al., 2004)
Biliary complication	Bile leak or stricture (anastomotic or NABS; solitary or multiple), diagnosed radiologically, endoscopically, histologically or intraoperatively and requiring operative or endoscopic intervention such as washout, drainage, stenting, dilatation or re-transplantation. Equivalent to grade III complications according to the Clavien-Dindo classification (Dindo et al., 2004)
Infective complication	Culture-proven infection (including wound, biliary tree, gastrointestinal, urinary tract, indwelling catheter, deep-seated infected fluid collection or isolated bacteraemia of unclear source) treated with antibiotics or drainage (radiological or surgical). Equivalent to grade II and III complications according to the Clavien-Dindo classification (Dindo et al., 2004) Antibiotic treatment for positive cultures from donor or preservation fluid specimens is excluded as is prophylactic or empirical antibiotic administration
Sepsis	Evidence of organ dysfunction [quantified as a Sequential Organ Failure Assessment (SOFA) score of 2 or more points] in response to a culture-proven infection (Singer et al., 2016). Equivalent to grade IV complications according to the Clavien-Dindo classification (Dindo et al., 2004)
Return to theatre	Any planned or unexpected return to theatre for re-exploration of the abdomen within the same admission regardless of indication or surgical intervention performed
T cell-mediated rejection (TCMR)	Biopsy-proven T cell-mediated rejection (early or late). Classified as mild, moderate or severe according to maximum severity reported. (Demetris et al., 2016) Repeated episode of rejection is defined as biopsy-proven acute rejection following previous rejection with normalised liver function tests or rejection-negative biopsy in the interim period
Acute antibody-mediated rejection (AMR)	Histopathological, immunohistochemical and serological evidence suggestive of acute antibody-mediated rejection and reasonable exclusion of other pathologies that may lead to a similar pattern of injury (Demetris et al., 2016)
Chronic rejection	Histological evidence suggestive of chronic rejection (early or late) supported by clinical, biochemical or radiological findings (Demetris et al., 2016)
Disease recurrence	A combination of histological, biochemical, immunological and/or radiological evidence consistent with recurrent original liver pathology (Demetris et al., 2006)

Survival outcomes

Delayed outcomes examined in this study were rejection-free survival, graft survival (death-censored) and overall patient survival. Rejection-free survival time was calculated from the date of transplantation to the date of first TCMR episode and censored at re-transplantation, death or last follow up date. Graft survival time was calculated from the date of transplantation to the date of re-transplantation and censored at death or last follow up date. Patient survival time was calculated from the date of transplantation to the date of death and censored at date of last follow up.

6.2.6. Data expression and statistical analysis

Data expression and bivariate statistical analysis for continuous and categorical data is similar to that described in 3.2.6. In addition, correlation between continuous independent variables was performed by measuring Pearson's correlation coefficient. The strength of correlation is described as small, medium or large corresponding to correlation coefficient values below 0.3, between 0.3 and 0.5, and above 0.5 respectively (Cohen, 1988).

Kaplan-Meier statistics were performed for survival analyses. Median time to event (in days) is reported for each group when available [lower, upper bound 95% confidence interval for median time to event]. Log rank test was used to identify differences in survival distribution between groups and results are reported as chi-square statistic (degree of freedom indicated within parenthesis) and P value.

Univariate followed by multivariate Cox regression analyses were performed to identify the relative contribution of multiple independent variables to the prediction of occurrence of rejection-free, graft and patient survival. The univariate analysis was performed to measure the individual effect of independent variables on survival. Independent variables that demonstrated significant effects on survival were then combined in a multivariate regression model to investigate the simultaneous effect of these relevant variables. The ratio of events per variable (EPV) was maintained at acceptable levels in the multivariate regression model in order to preserve validity of the model analysis (van Domburg et al., 2014). The multivariate model was executed using the standard Enter method. Results are reported as hazard ratio [lower, upper

bound 95% confidence interval for hazard ratio] and P value. Multicolinearity diagnostics were performed to identify evidence of linear dependency between independent variables in a multivariate regression model. Variance inflation factor (VIF) values below 4 indicated acceptably low levels of inter-variable multicollinearity.

Statistical test results with p values of less than 0.05 were considered statistically significant. All statistical tests were performed using the Statistical Package for Social Sciences version 19.0 (SPSS Inc., Chicago, IL, USA) and Microsoft Office Excel 2010 (Microsoft Corp., Redmond, WA).

6.3. Results

6.3.1. Overview of patient inclusion

In total, 253 OLT procedures were performed at the Freeman Hospital between October 2010 and September 2016. Of these, 240 were considered eligible for inclusion in this study (228 recipients). The remaining 13 transplant procedures were considered ineligible for inclusion due to reasons outlined in the inclusion flowchart below (Figure 6.1).

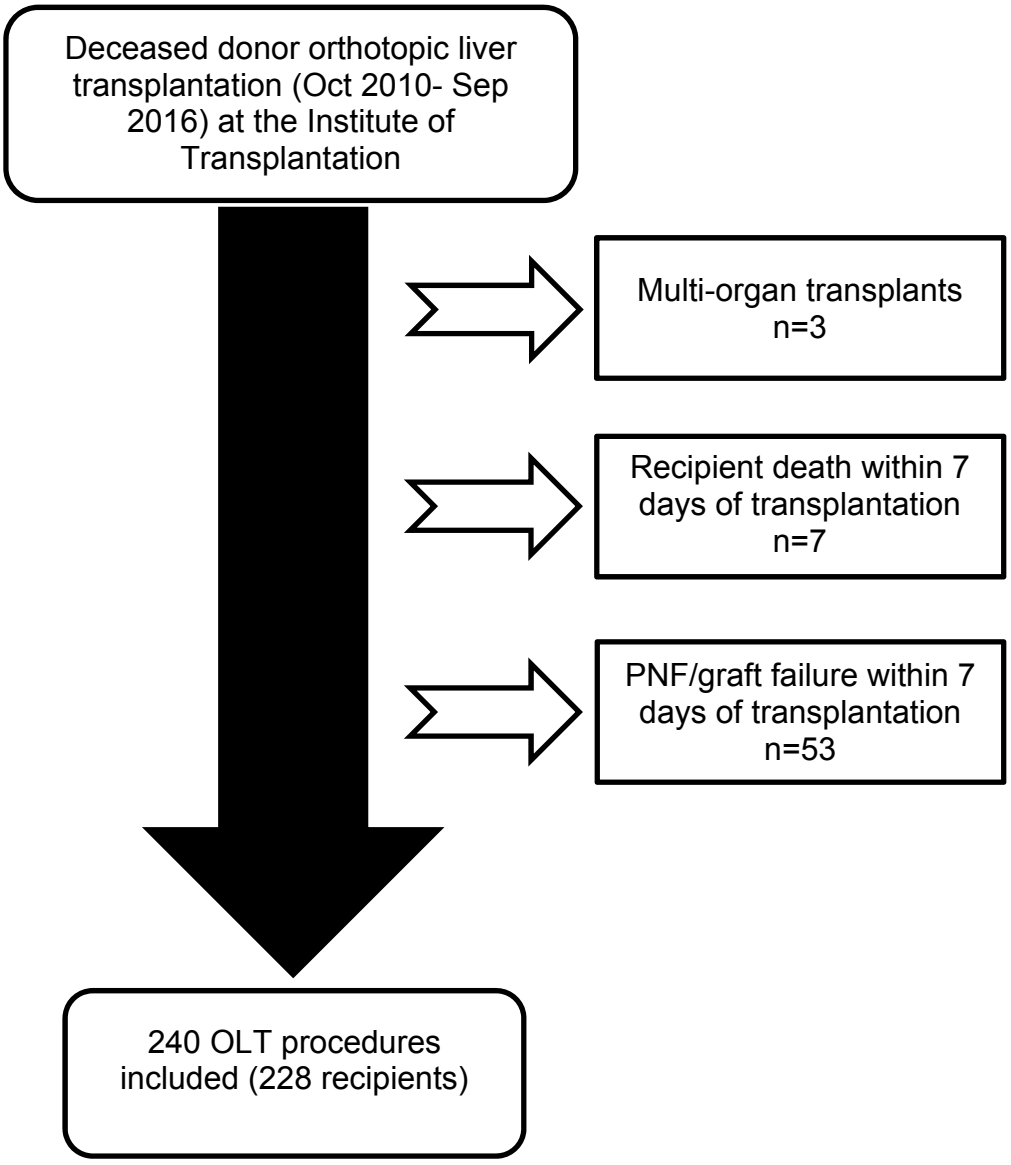

Figure 6.1 Procedure-inclusion flowchart

6.3.2. Characteristics of study population

Recipient characteristics

Two hundred and twenty eight recipients received 240 liver transplants during the study period. Recipients that had received more than one transplant were analysed separately for each transplant episode. Categorical and continuous characteristics of the recipients are summarised in Table 26 and Table 27 respectively.

Table 26 Frequency distribution of recipient characteristics

Recipient characteristic		**Frequency (percentage of total)**
Gender	Female	96 (40)
	Male	144 (60)
Primary liver pathology	ALD	60 (25)
	Autoimmune liver disease	50 (20.83)
	Graft failure -acute	8 (3.33)
	Graft failure -chronic	16 (6.67)
	Liver tumour +/- chronic liver disease	42 (17.5)
	NAFLD	15 (6.25)
	Other -acute	5 (2.08)
	Other -chronic	8 (3.33)
	Paracetamol overdose	11 (4.58)
	Unclear -acute	9 (3.75)
	Unclear -chronic	4 (1.67)
	Viral hepatitis	12 (5)
Previous transplants		30 (12.5)

Table 27 Descriptive statistics of recipient characteristics (continuous variables)

Recipient characteristic	**Average**	**SEM**	**Lowest**	**Highest**

Age (years)	53.2	0.85	17	71
MELD	18.28	0.63	6	65
Height (cm)	169.62	0.6	147	193
Weight (kg)	79.07	1.15	39.1	128.8
BMI	27.3	0.34	16.21	41.44

Donor characteristics

Categorical and continuous characteristics of the donors are summarised in Table 28 and Table 29 respectively. The majority of OLT donors were of the DBD type (88.75%) and of Caucasian ethnicity (97.5%). With the exception of donor gender, overall donor demographics were comparable to those of the recipients. Donor anthropometrics were significantly associated with those of the recipient (weight-weight and height-height correlation coefficients were 0.545 and 0.203 respectively; $P<0.005$). However, donor and recipient ages were not significantly correlated even when super-urgent cases were excluded (correlation coefficient -0.107; $P=0.124$).

Table 28 Frequency distribution of donor characteristics

Donor characteristic		**Frequency (percentage of total)**
Donor Type	DBD	213 (88.75)
	DCD	27 (11.25)
Donor gender	Female	125 (52.08)
	Male	115 (47.92)
Donor COD (grouped)	Hypoxic brain injury/stroke	43 (17.92)
	Intracranial haemorrhage/trauma	187 (77.92)
	Meningitis	5 (2.08)
	Other	2 (0.83)
	Tumour	3 (1.25)
Race	Asian	2 (0.83)
	Black	1 (0.42)

	Chinese	3 (1.25)
	White	234 (97.5)

Table 29 Descriptive statistics of donor characteristics (continuous variables)

Donor characteristic	Average	SEM	Lowest	Highest
Age (years)	50.25	0.95	17	80
Height (cm)	170.21	0.62	149	194
Weight (kg)	75.76	0.95	43.3	125
BMI	26.12	0.29	15.57	42.02

Transplantation characteristics

Categorical and continuous characteristics of the transplantation process (perioperative data) are summarised in Table 30 and Table 31. Super-urgent and redo OLT comprised 13.3% and 12.5% of all included procedures respectively. The majority of procedures were performed using whole liver grafts (95%).

Recipient age was significantly inversely correlated to a number of perioperative variables including MELD score, postoperative transfusion requirement and length of ITU and hospital stay (correlation coefficient -0.267, -0.184, -0.194 and -0.157 respectively; $P<0.05$). Interestingly, recipient preoperative MELD score correlated significantly with postoperative ITU stay (correlation coefficient 0.308; $P<0.0005$). A correlation matrix of all continuous recipient, donor and perioperative variables is reported in Appendix 4.

Table 30 Frequency distribution of transplant characteristics

Transplant characteristic	Frequency (percentage of total)
Super-urgent transplant	32 (13.33)
CMV mismatch	54 (22.5)

Gender mismatch		89 (37.08)
Graft type	Whole	228 (95)
	Split	12 (5)
Primary surgeon	BJ	25 (10.42)
	CHW	14 (5.83)
	DMM	50 (20.83)
	DT	41 (17.08)
	GS	25 (10.42)
	JJF	55 (22.92)
	SAW	30 (12.5)
Biliary anastomosis	End-to-end	181 (75.42)
	Roux-en-Y	54 (22.5)
	Delayed	5 (2.08)
HA anastomosis	Single	206 (85.83)
	Multiple	34 (14.17)

Table 31 Descriptive statistics of transplant characteristics (continuous variables)

Transplant characteristic	**Average**	**SEM**	**Lowest**	**Highest**
Cold ischaemia time (min)	585.75	9.4	128	1043
Veno-venous bypass (min)	136.66	3.5	0	346
Warm ischaemia time (min)	54.31	1.29	19	155
Intraoperative blood transfusion (units)	6.59	0.43	0	40
Postoperative blood transfusion (units)	1.7	0.3	0	53
ITU stay (days)	7.31 (4*)	0.61	1	59
Length of hospital stay (days)	32.95 (25*)	1.49	9	138

*median values

6.3.3. hPXR activation

Identification of hPXR activators used in liver transplantation

A list of hPXR activators used within the first 7 days post-transplantation was generated by comparing eRecord pharmacy data for transplant recipients to the NIH drug hPXR-activation profile database. This list is shown in Table 32. Lower AC50 values indicate higher hPXR activation potencies. As is evident from this data, Rifampicin was the most potent hPXR activator documented to have been administered in the immediate (7-day) post-transplantation period followed by Phytomenadione (vitamin K1). A full list of medications used in the postoperative period for transplant recipients is outlined in Appendix 4.

Table 32 hPXR activators administered within the first 7 days post-transplantation

Drug	**AC50 for hPXR activation (μM)**
Amlodipine	8.91
Azithromycin	35.48
Beclometasone	15.85
Budesonide	8.91
Ciprofloxacin	7.08
Domperidone	25.12
Efavirenz	3.98
Fentanyl	14.13
Haloperidol	14.13
Levothyroxine	25.12
Loperamide	10
Mirtazapine	15.85
Nifedipine	12.59
Phytomenadione	2.51
Rifampicin	0.71
Salmeterol	3.98
Sertraline	28.18
Tolterodine	5.62
Verapamil	12.59

The most commonly administered hPXR activator was Phytomenadione followed by Fentanyl and then Amlodipine (administered to 89.17%, 34.17% and 20% of transplant recipients respectively). Table 33 summarises the administered doses for the commonly received hPXR activators during the study period.

Table 33 Administered doses of common hPXR activators during the first 7 days post-transplantation

hPXR activator *	Number of patients receiving medication (percentage of total)	Median number of doses per patient	Minimum dose	Maximum dose
Amlodipine 5-10 mg PO	48 (20)	3	1	8
Ciprofloxacin 400-500 mg PO	18 (7.5)	4	1	14
Fentanyl infusion 20-50 ml IV	82 (34.17)	1	1	150
Haloperidol 0.5-5 mg PO/SC	23 (9.58)	1	1	10
Levothyroxine 50-300 mcg PO	13 (5.42)	7	2	7
Loperamide 2-4 mg PO	6 (2.5)	1.5	1	3
Phytomenadione 10 mg IV	214 (89.17)	3	1	12
Rifaximin 400-550 mg PO	25 (10.42)	3	1	19

*Excludes drugs received by less than 5 recipients

Predicted hPXR activation status of recipients on day 7 post-transplantation ($PPAV_7$)

The average $PPAV_7$ in this study was 32.5±4.9 and ranged from 0 to 582.1. The median $PPAV_7$ was 8. Given the wide variation in $PPAV_7$, median $PPAV_7$ was used as a cut-off value dividing the study population into low and high hPXR activation groups (n=119 and 121 respectively).

A comparison of recipient, donor and perioperative transplant characteristics between the two groups is outlined in Table 34. This demonstrates a statistically significant difference in recipient gender distribution between the two groups with a relatively higher proportion of female recipients in the high hPXR group. In addition, recipient height, weight and BMI were significantly greater in this group. With the exception of these variables, there were no significant differences between the two groups in other recipient, donor or transplant characteristics.

It is worth noting that no significant difference was noted in average $PPAV_7$ between male and female recipient gender (35.9±7.3 versus 27.3±5.6 respectively; P=0.39). In addition, no significant correlation was observed between $PPAV_7$ and recipient anthropometric measurements (Appendix 4).

Table 34 Comparison of recipient, donor and transplant variables between low and high hPXR activation groups

Variable (units)		**Low hPXR group***	**High hPXR group***	**P value**
		(percentage or mean±SEM)		
Recipient features				
Gender	Female	31.93	47.93	0.013
	Male	68.07	52.07	
Age (years)		53.32±1.11	53.08±1.29	0.88
MELD score		17.47±0.79	19.11±0.98	0.19
Height (cm)		168.31±0.86	170.98±0.83	0.026
Weight (kg)		75.69±1.5	82.51±1.69	0.003
BMI		26.6±0.44	28.03±0.51	0.03
Primary liver pathology				0.38
Re-transplant		11.76	13.22	0.85
Donor features				

Type of donor	DBD	89.92	87.6	0.68
	DCD	10.08	12.4	
Gender	Female	48.74	55.37	0.37
	Male	51.26	44.63	
Age (years)		49.74±1.39	50.77±1.29	0.59
Height (cm)		169.57±0.84	170.88±0.9	0.29
Weight (kg)		75.21±1.32	76.33±1.37	0.56
BMI		26.12±0.4	26.12±0.41	0.99
Cause of death	ICH/Trauma	75.63	80.17	0.4
	HBI/CVA	21.85	15.7	
	Other	2.52	4.13	
Race	White	97.48	97.52	1
	Other	2.52	2.48	
Perioperative features				
Super-urgent transplant		13.4	13.2	1
CMV mismatch		22.69	22.31	1
Gender mismatch		38.66	35.54	0.69
Split graft		5.88	4.13	0.57
Primary surgeon				0.1
CIT (minutes)		592.07±13.5	579.33±13.1	0.5
VV bypass (minutes)		141.88±4.76	131.35±5.1	0.13
WIT (minutes)		54.36±1.79	54.26±1.88	0.97
Biliary anastomosis	End-to-end	73.95	76.86	0.73
	Roux-en-y	24.37	20.66	
	Delayed	1.68	2.48	
Multiple arterial anastomoses		17.65	10.74	0.14

IO blood transfusion (units)	6.89±0.58	6.29±0.62	0.48
PO blood transfusion (units)	1.45±0.19	1.93±0.55	0.42
ITU stay	8.45±0.98	6.14±0.72	0.06
Hospital stay	34.74±2.2	31.13±2.01	0.23

6.3.4. Early allograft dysfunction (EAD) and hPXR activation

EAD was identified in 48 recipients (20%) in this study. This was triggered by high serum ALT levels in over half the cases (54.1%) and by high serum bilirubin in slightly less than half the cases (47.9%). EAD was less commonly triggered by high PT levels (27% of EAD cases). EAD was triggered by more than one factor in 27% of EAD cases.

In order to validate the definition of EAD, graft and patient survival were analysed using EAD as the grouping factor. This demonstrated a significant difference in death-censored graft survival between recipients that showed EAD versus those that did not (1- and 5-year survival: 80.9±5.7% and 77±6.6% versus 95±1.6% and 90.4±2.8% respectively; Log Rank P=0.002) (Figure 6.2). However, no significance difference in patient survival was noted between the EAD and non-EAD groups (1- and 5-year survival: 94.1±1.7% and 77.7±4.2% versus 91.5±4.1% and 87.4±5.6% respectively; Log Rank P=0.48) (Figure 6.3).

The association between hPXR activation and early graft function was subsequently explored. The risk of EAD was found to be comparable between the low and high hPXR groups (18.5% and 21.5% respectively; P=0.629) (Figure 6.4). In addition, the average $PPAV_7$ was 29.3±8.5 in the EAD cohort versus 33.3±5.8 in the cohort that did not experience EAD (P=0.748) (Figure 6.5).

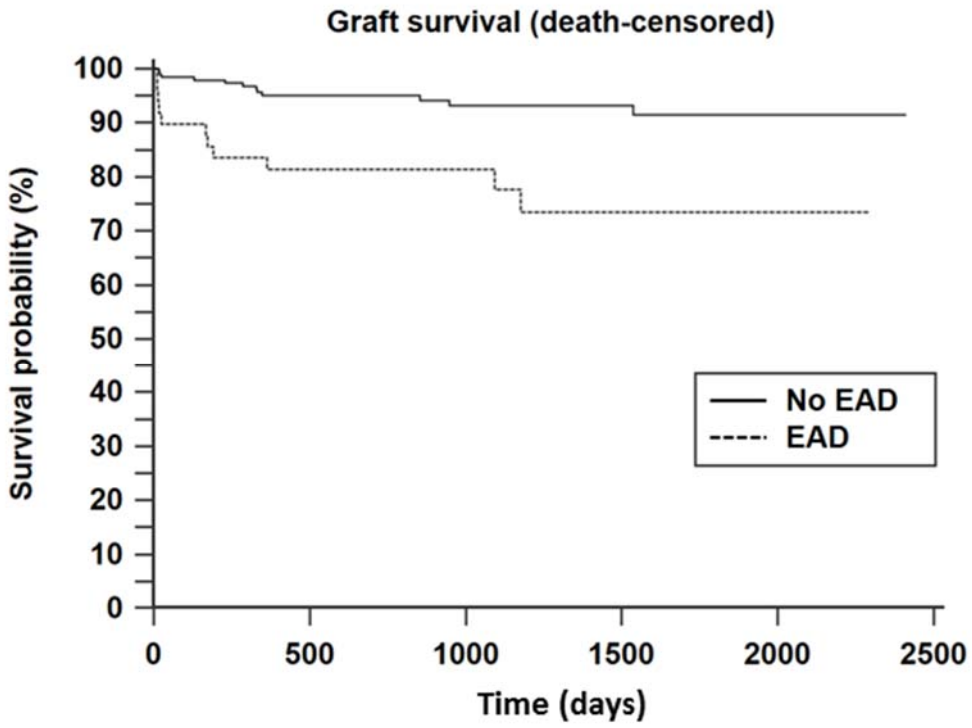

Figure 6.2 Kaplan-Meier curve comparing graft survival (death-censored) between EAD and non-EAD groups

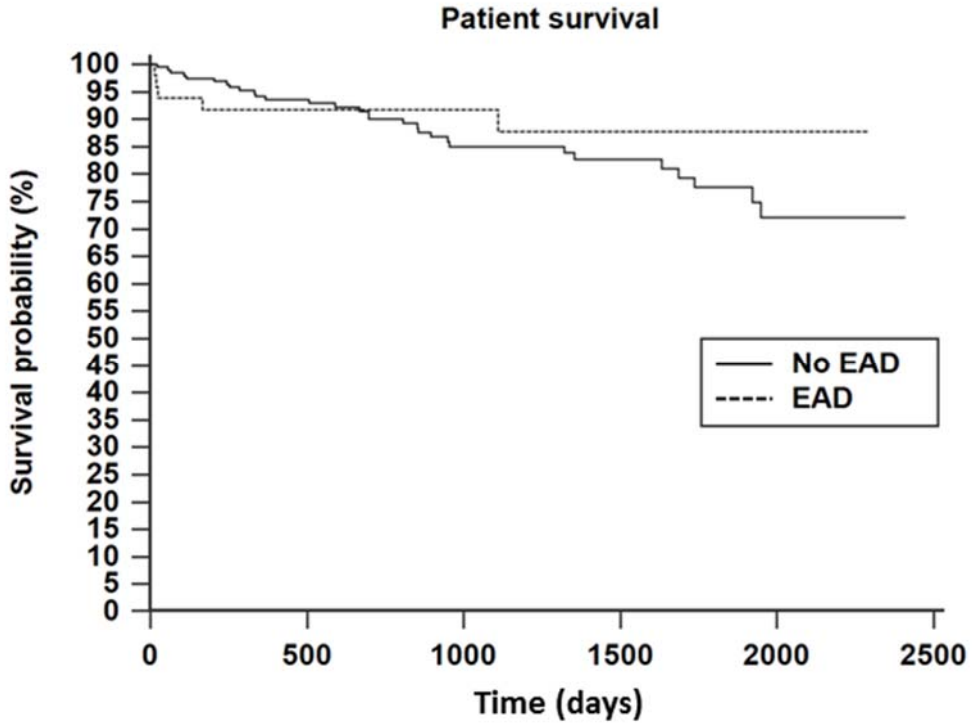

Figure 6.3 Kaplan-Meier curve comparing patient survival between EAD and non-EAD groups

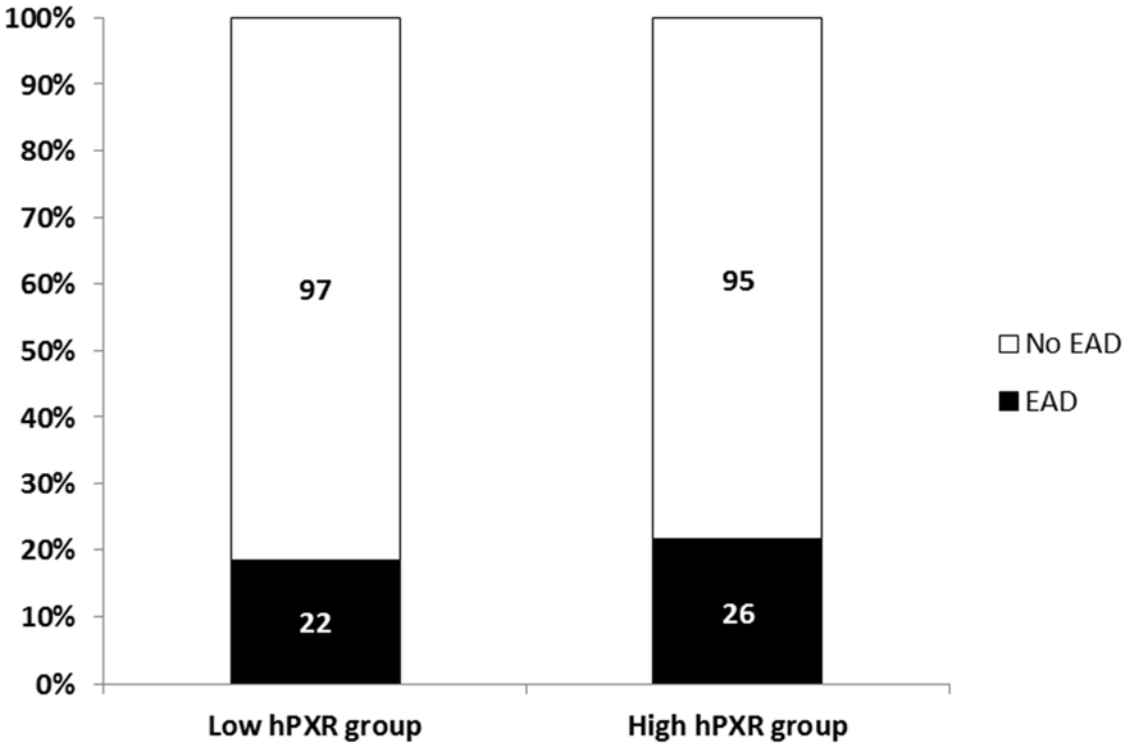

Figure 6.4 Comparison of EAD risk between low and high hPXR activation groups

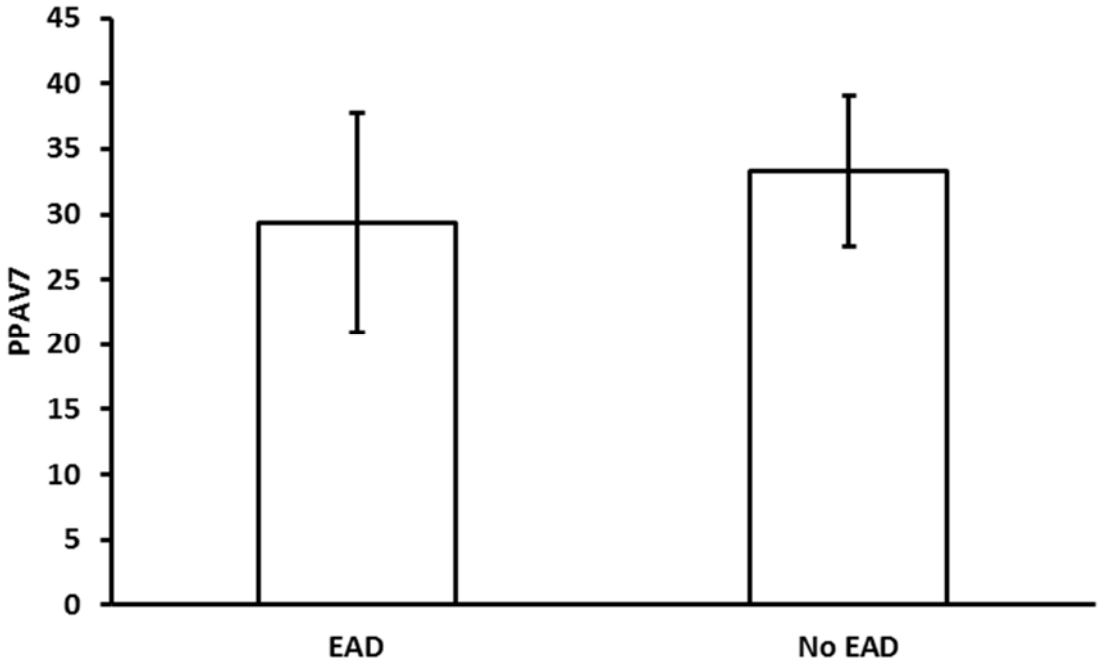

Figure 6.5 Comparison of average $PPAV_7$ between EAD and non-EAD cohorts

6.3.5. Post-transplant complications and hPXR activation

The incidence of post-OLT complications within the study population

The incidence of vascular, biliary and infective complications was analysed amongst the overall study population in addition to the incidence of re-laparotomy, rejection and disease recurrence. The risk of graft failure and death is also briefly outlined in this section but is examined in more detail in 6.3.6.

Postoperative bleeding occurred in 15.8% of the study population and was the most common reason for re-laparotomy (48.7% of all cases returning to theatre). HAT and NABS occurred in 5.8% and 5.4% of the overall cohort respectively. Severe sepsis occurred in 12.9% of cases.

TCMR occurred in 38.8% of cases post-OLT. Of these, 27.9% experienced severe TCMR and 17.2% experienced multiple episodes of rejection. AMR occurred in 4.6% of cases, all of which were associated with TCMR. The primary liver disease recurred in 9.6% of the study population. This was related to recurrent hepatitis C virus infection in 82.6% of cases.

The incidence of graft failure in the study population was 9.6%. Graft failure occurred within 90 days of transplantation in 3.3% of cases (34.8% of graft failure). The 90-day and overall mortality rate post-OLT was 2.5% and 14.6% in the study population. This was most commonly due to sepsis and multi-organ failure (83.3% of 90-day mortalities and 34.3% of overall deaths).

A summary of post-OLT complications is outlined in Table 35. The overall complication rate (including rejection) was 79.6%.

Table 35 Incidence of post-OLT complications in the study population

Complication	Frequency (percentage of total)
Vascular complications	82 (34.2)
Bleeding	38 (15.8)
Vascular stenosis	25 (10.4)
Venous thrombosis	22 (9.2)

	HAT	14 (5.8)
Biliary complications		61 (25.4)
	NABS	13 (5.4)
	Biliary leak	25 (10.4)
	Anastomotic stricture	36 (15)
Infective complications		103 (42.9)
	Sepsis	31 (12.9)
Return to theatre		41 (17.1)
Reason	Bile leak	5 (2.1)
	Bleeding	20 (8.3)
	Perforated viscus	5 (2.1)
	Planned relook	7 (2.9)
	Other	4 (1.7)
T cell-mediated rejection		93 (38.8)
Acute antibody-mediated rejection		11 (4.6)
Chronic rejection		6 (2.5)
Overall complications		191 (79.6)

Associations between post-OLT complications and hPXR activation

The average $PPAV_7$ was compared between recipients experiencing post-OLT complications and those that did not. The results are summarised in Table 36.

The data highlights significantly lower average $PPAV_7$ in recipients that developed anastomotic biliary strictures (17.66±5.49 versus 35.12±5.7 in recipients without strictures; P=0.03) and recipients that had experienced sepsis (16.39±7.14 versus 34.89±5.54 in sepsis-free recipients; P=0.04). Interestingly, the average $PPAV_7$ in patients that developed non-anastomotic biliary strictures (NABS) was higher than in recipients without this complication. However, this difference did not reach statistical significance (43.1±20.27 versus 31.89±5.09 respectively; P=0.61).

There was no significant difference in average $PPAV_7$ between recipients experiencing TCMR and TCMR-free recipients (38.1±9.13 versus 28.96±5.61 respectively; P=0.37). In addition, average $PPAV_7$ was comparable between patients experiencing single and multiple episodes of TCMR and between patients experiencing mild, moderate and severe episodes of TCMR (data not shown). Table 36 also shows lower average $PPAV_7$ in patients experiencing AMR and those experiencing chronic rejection. However, these results did not reach statistical significance.

Table 36 A comparison of average $PPAV_7$ between recipients with and without various post-OLT complications

Complication	Yes*	No*	P value
Vascular complications	31.08±8.4	33.24±6.1	0.84
Bleeding	49.78±17.23	29.25±4.87	0.26
Vascular stenosis	38.06±22.93	31.86±4.84	0.7
Venous thrombosis	37.76±26.1	31.97±4.77	0.74
HAT	27.71±15.72	32.8±5.15	0.81
Biliary complications	29.56±6.94	33.5±6.18	0.73
NABS	43.1±20.27	31.89±5.09	0.61
Biliary leak	33.52±11.46	32.38±5.34	0.94
Anastomotic stricture	17.66±5.49	35.12±5.7	0.03
Infective complications	24.71±6.7	38.36±6.99	0.16
Sepsis	16.39±7.14	34.89±5.54	0.04
Return to theatre	52.78±18.16	28.32±4.59	0.2
T cell-mediated rejection	38.1±9.13	28.96±5.61	0.37
Acute antibody-mediated rejection	19.05±6.08	33.15±5.15	0.55
Chronic rejection	5.75±2.66	33.19±5.05	0.39
Disease recurrence	66.58±28.14	28.89±4.53	0.2
Overall complications	35.49±5.98	20.86±6.05	0.09

*Results expressed as average $PPAV_7$±SEM

6.3.6. The impact of hPXR activation on survival following OLT

Patient, graft and rejection-free survival analysis

A comparison was made between low and high hPXR activation groups to investigate potential differences in patient, graft and rejection-free survival. The resultant Kaplan-Meier survival curves are shown in Figure 6.6, Figure 6.7 and Figure 6.8 respectively.

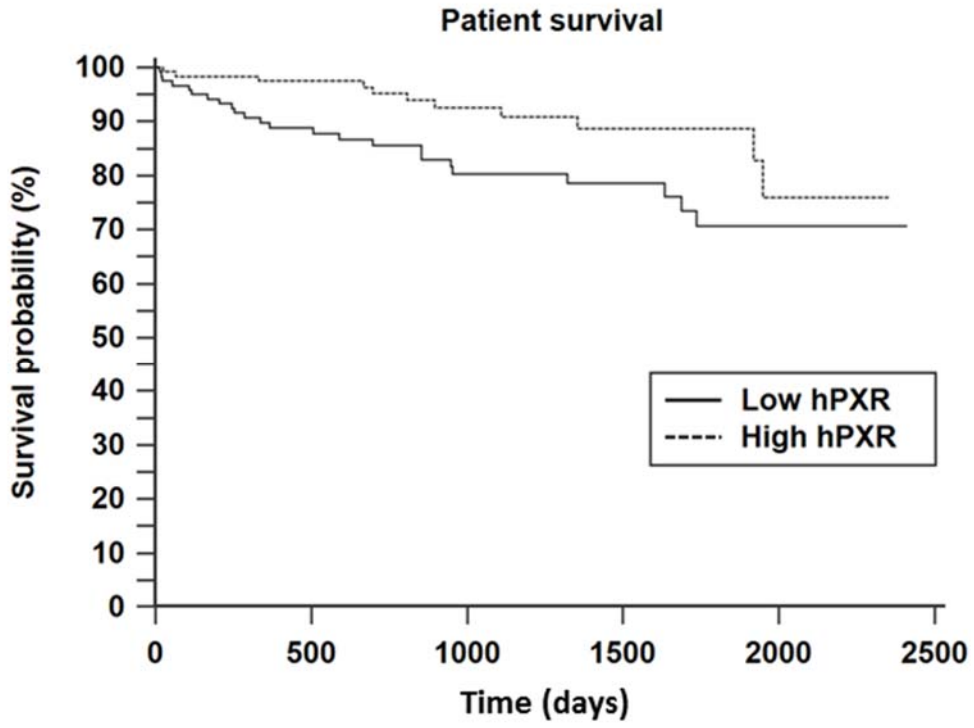

Figure 6.6 Kaplan-Meier curve comparing patient survival between low and high hPXR activation groups

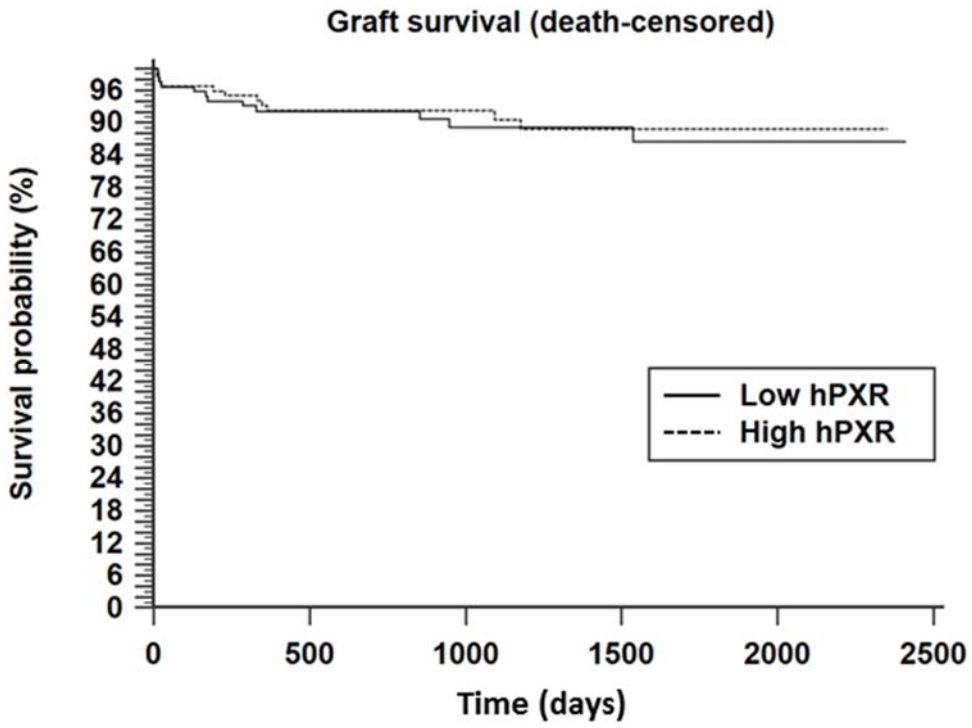

Figure 6.7 Kaplan-Meier curve comparing graft survival (death-censored) between low and high hPXR activation groups

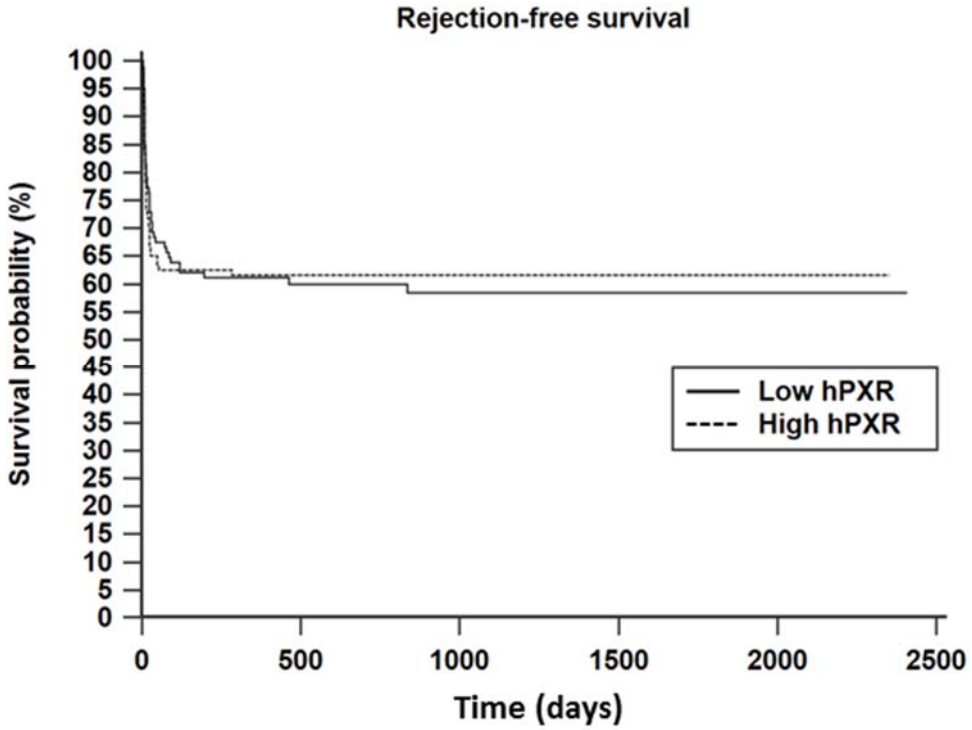

Figure 6.8 Kaplan-Meier curve comparing rejection-free survival between low and high hPXR activation groups

The high hPXR activation group experienced a significant improvement in patient survival compared to the low hPXR group (1- and 5-year survival: 97.4±1.5% and 88.7±3.8% versus 89.9±2.8% and 70.7±5.8% respectively; Log Rank P=0.023). No significant difference in graft or rejection-free survival was evident between the two groups (Log rank P values 0.758 and 0.964 respectively).

Factors that influence patient, graft and rejection-free survival

Univariate and multivariate Cox regression analyses were performed in order to examine the effect of various factors (including hPXR activation) on patient, graft and rejection-free survival.

Patient survival

Results from univariate Cox regression for patient survival are summarised in Table 37. Recipient age, preoperative MELD score, primary liver disease recurrence, graft failure and hPXR activation group were identified as significant independent variables associated with patient survival. These variables were used in the multivariate regression model in addition to overall complications which, as an encompassing variable, was also found to be significantly associated with patient survival. Overall complications included complications such as HAT, sepsis and non-NABS biliary complications which were identified as significant complications independently associated with patient survival but not entered separately into the multivariate regression model to avoid the negative impact of an unacceptably low EPV ratio on model validity. The multivariate Cox regression for patient survival is summarised in Table 38. Based on this model, only preoperative MELD score, graft failure and hPXR activation group retained statistical significance as independent prognostic factors for patient survival.

Multicolinearity diagnostics showed no evidence of linear dependency between the independent variables selected in the multivariate regression model.

Table 37 Univariate Cox regression for patient survival

Independent variable	Hazard ratio	95% CI	P value
Recipient factors			
Male gender	1.56	[0.75, 3.25]	0.23
Age	1.04	[1.01, 1.08]	0.02
MELD	0.94	[0.89, 0.99]	0.01
Height	0.997	[0.96, 1.03]	0.87
Weight	0.999	[0.98, 1.02]	0.94
BMI	1.01	[0.94, 1.07]	0.87
Primary liver pathology			
ALD (ref)			0.14
Autoimmune liver disease	1.005	[0.32, 3.17]	0.99
Liver tumours	2.44	[0.96, 6.19]	0.06
Other causes	1.13	[0.44, 2.9]	0.81
Redo transplant	1.8	[0.74, 4.34]	0.19
Donor factors			
DCD	1.56	[0.6, 4.05]	0.36
Male gender	1.5	[0.77, 2.92]	0.24
Age	0.98	[0.96, 1.002]	0.08
Height	1.03	[0.997, 1.07]	0.07
Weight	1.02	[0.995, 1.04]	0.12
BMI	1.02	[0.95, 1.09]	0.66
Cause of death			
ICH/Trauma (ref)			0.62
HBI/CVA	0.99	[0.41, 2.4]	0.99
Other	2.04	[0.48, 8.57]	0.33

Non-caucasian ethnicity	1.44	[0.2, 10.67]	0.72
Perioperative factors			
Super-urgent transplant	0.19	[0.03, 1.39]	0.1
CMV mismatch	0.96	[0.65, 1.42]	0.83
Split graft	1.43	[0.85, 2.41]	0.18
CIT	0.998	[0.99, 1.001]	0.16
VV bypass	0.99	[0.99, 1.002]	0.15
WIT	0.99	[0.97, 1.01]	0.26
Biliary anastomosis			
End-to-end (ref)			0.63
Roux-en-y	1.44	[0.69, 3.01]	0.34
Delayed	0.00001		0.98
Multiple arterial anastomoses	0.95	[0.59, 1.53]	0.84
IO blood transfusion	0.98	[0.93, 1.04]	0.57
PO blood transfusion	0.87	[0.71, 1.07]	0.18
ITU stay	0.97	[0.92, 1.03]	0.29
Hospital stay	0.998	[0.98, 1.01]	0.84
Complications			
Vascular complications	1.77	[0.91, 3.44]	0.09
Bleeding	0.9	[0.35, 2.33]	0.83
Vascular stenosis	2.19	[0.91, 5.29]	0.08
Venous thrombosis	1.48	[0.57, 3.8]	0.42
HAT	4.68	[1.8, 12.16]	0.002
Biliary complications	1.38	[0.68, 2.82]	0.38
NABS	2.64	[0.93, 7.5]	0.07
Biliary leak	2.03	[0.84, 4.89]	0.11
Anastomotic stricture	1.64	[0.74, 3.6]	0.22
Infective complications	2.94	[1.44, 6]	0.003

Sepsis	5.42	[2.72, 10.79]	<0.001
Return to theatre	0.52	[0.16, 1.72]	0.29
T cell-mediated rejection	0.56	[0.26, 1.19]	0.13
Time to TCMR	1.001	[0.997, 1.01]	0.52
Number of TCMR	0.61	[0.31, 1.19]	0.15
Degree of TCMR	0.79	[0.26, 2.38]	0.68
Acute antibody-mediated rejection	0.85	[0.12, 6.22]	0.87
Chronic rejection	1.03	[0.14, 7.52]	0.98
Overall complications	4.53	[1.09, 18.91]	0.04
Disease recurrence	2.37	[1.08, 5.23]	0.03
Graft failure	5.12	[2.37, 11.06]	<0.001
EAD	1.04	[0.45, 2.38]	0.93
High hPXR group	0.45	[0.22, 0.91]	0.03

Table 38 Multivariate Cox regression for patient survival

Independent variable	Hazard ratio	95% CI	P value
Recipient age	1.03	[0.995, 1.07]	0.09
MELD score	0.94	[0.89, 0.99]	0.01
Overall complications	4.05	[0.95, 17.18]	0.06
Disease recurrence	1.56	[0.69, 3.5]	0.29
Graft failure	3.81	[1.7, 8.53]	0.001
High hPXR group	0.48	[0.23, 0.99]	0.048

Graft survival

Results from univariate Cox regression for graft survival are summarised in Table 39. Autoimmune primary liver pathology, donor male gender, delayed biliary reconstruction, HAT, NABS, sepsis and EAD were identified as factors significantly associated with death-censored graft survival. In order to limit the number of variables carried forward to the multivariate regression model, donor male gender and EAD were excluded from further analysis. The former variable was excluded given the available evidence refuting its significance (Sarkar et al., 2015) while the latter was excluded because further validation of the prognostic value of EAD in graft survival was beyond the scope of this study. Multicolinearity diagnostics showed no evidence of linear dependency between the remaining independent variables selected in the multivariate regression model. The results of this model are summarised in Table 40. Only delayed biliary reconstruction and HAT retained statistical significance as independent prognostic factors for death-censored graft survival in the multivariate model.

As predicted from the lack of association between EAD and hPXR activation described in 6.3.4 and from the non-significant Kaplan-Meier analysis for graft survival (Figure 6.7), hPXR activation groups did not demonstrate a significant association with graft survival on Cox regression analysis.

Table 39 Univariate Cox regression for graft survival

Independent variable	Hazard ratio	95% CI	P value
Recipient factors			
Male gender	0.97	[0.42, 2.25]	0.95
Age	0.99	[0.96, 1.02]	0.62
MELD	0.997	[0.95, 1.04]	0.91
Height	1.001	[0.96, 1.05]	0.95
Weight	1.001	[0.98, 1.02]	0.9

BMI	1.01	[0.93, 1.09]	0.87
Primary liver pathology			
ALD (ref)			0.22
Autoimmune liver disease	9.36	[1.15, 76.15]	0.04
Liver tumours	7.34	[0.86, 62.86]	0.07
Other causes	7.4	[0.95, 57.82]	0.06
Redo transplant	1.16	[0.34, 3.9]	0.81
Donor factors			
DCD	2.53	[0.93, 6.83]	0.07
Male gender	2.68	[1.1, 6.52]	0.03
Age	1.02	[0.99, 1.06]	0.13
Height	1.01	[0.96, 1.05]	0.81
Weight	1.01	[0.98, 1.04]	0.59
BMI	1.01	[0.92, 1.11]	0.81
Cause of death			
ICH/Trauma (ref)			0.45
HBI/CVA	0.39	[0.09, 1.67]	0.2
Other	0.0001		0.98
Non-caucasian ethnicity	1.91	[0.26, 14.24]	0.53
Perioperative factors			
Super-urgent transplant	0.29	[0.04, 2.19]	0.23
CMV mismatch	1.15	[0.67, 1.98]	0.61
Split graft	0.83	[0.35, 1.95]	0.67
CIT	0.89	[0.33, 2.44]	0.83
VV bypass	1.003	[0.999, 1.01]	0.06
WIT	1.003	[0.995, 1.01]	0.47
Biliary anastomosis			

End-to-end (ref)			0.09
Roux-en-y	1.41	[0.55, 3.63]	0.48
Delayed	5.13	[1.17, 22.55]	0.03
Multiple arterial anastomoses	1.1	[0.64, 1.89]	0.72
IO blood transfusion	1.02	[0.96, 1.07]	0.56
PO blood transfusion	0.86	[0.64, 1.14]	0.29
ITU stay	1.02	[0.99, 1.05]	0.27
Hospital stay	1.01	[0.997, 1.02]	0.13
Complications			
Vascular complications	10.33	[3.51, 30.37]	<0.0001
Bleeding	1.86	[0.73, 4.73]	0.19
Vascular stenosis	1.97	[0.67, 5.81]	0.22
Venous thrombosis	1.38	[0.41, 4.63]	0.61
HAT	30.14	[12.61, 72.08]	<0.0001
Biliary complications	1.91	[0.83, 4.41]	0.13
NABS	4.21	[1.43, 12.42]	0.01
Biliary leak	0.86	[0.2, 3.68]	0.84
Anastomotic stricture	1.99	[0.78, 5.04]	0.15
Infective complications	1.69	[0.74, 3.84]	0.21
Sepsis	3.48	[1.43, 8.49]	0.01
Return to theatre	1.05	[0.36, 3.08]	0.94
T cell-mediated rejection	1.01	[0.44, 2.32]	0.99
Time to TCMR	0.99	[0.95, 1.03]	0.53
Number of TCMR	0.95	[0.49, 1.86]	0.89
Degree of TCMR	1.58	[0.51, 4.87]	0.43
Acute antibody-mediated rejection	2.25	[0.53, 9.63]	0.27
Chronic rejection	1.67	[0.23, 12.43]	0.61
Overall complications	29.18	[0.4, 2106.39]	0.12

Disease recurrence	2.3	[0.85, 6.21]	0.1
EAD	3.79	[1.67, 8.6]	0.001
High hPXR group	0.88	[0.39, 1.99]	0.76

Table 40 Multivariate Cox regression for graft survival

Independent variable	Hazard ratio	95% CI	P value
Autoimmune liver disease	0.93	[0.32, 2.69]	0.89
Delayed biliary reconstruction	7.8	[1.7, 35.85]	0.01
HAT	25.99	[10.17, 66.44]	<0.0001
NABS	1.92	[0.52, 7.04]	0.33
Sepsis	2.3	[0.89, 5.96]	0.09

Rejection-free survival

Results from univariate Cox regression for rejection-free survival are summarised in Table 41. Recipient gender, recipient age, alcoholic liver disease, autoimmune liver disease, super-urgent transplant, CIT, venous thrombosis and NABS were identified as independent variables associated with TCMR-free survival. Given the high number of event in the dataset, all the above independent variables were included in the multivariate model with minimal risk to the model validity. As observed in the Cox regression models described earlier, multicolinearity diagnostics showed no evidence of linear dependency between the independent variables selected in the multivariate regression model for rejection-free survival. The results of the multivariate model are summarised in Table 42. Only recipient age, NABS and venous thrombosis retained a significant independent association with rejection-free survival in this model. Interestingly, both recipient age and venous thrombosis appear to confer a protective effect against TCMR (HR [95% CI]: 0.98 [0.96, 0.99] and 0.25 [0.08, 0.8]

respectively; P<0.05), in contrast to NABS which was associated with an increased rejection risk (HR [95% CI]: 2.2 [1.06, 4.57]; P=0.03).

Table 41 Univariate Cox regression for rejection-free survival

Independent variable	Hazard ratio	95% CI	P value
Recipient factors			
Male gender	0.5	[0.33, 0.76]	0.001
Age	0.98	[0.97, 0.99]	0.002
MELD	1.02	[0.995, 1.04]	0.13
Height	0.99	[0.97, 1.02]	0.65
Weight	0.99	[0.98, 1.001]	0.08
BMI	0.96	[0.93, 1.01]	0.09
Primary liver pathology			
ALD (ref)			0.003
Autoimmune liver disease	2.59	[1.42, 4.75]	0.002
Liver tumours	0.89	[0.42, 1.9]	0.76
Other causes	1.68	[0.95, 2.99]	0.08
Redo transplant	1.8	[0.74, 4.34]	0.19
Donor factors			
DCD	1.52	[0.86, 2.68]	0.15
Male gender	0.82	[0.55, 1.24]	0.35
Age	1.01	[0.998, 1.03]	0.1
Height	0.996	[0.98, 1.02]	0.72
Weight	0.996	[0.98, 1.01]	0.55
BMI	0.99	[0.94, 1.04]	0.63

Cause of death			
ICH/Trauma (ref)			0.99
HBI/CVA	1.03	[0.61, 1.72]	0.92
Other	0.93	[0.29, 2.95]	0.9
Non-caucasian ethnicity	0.05	[0.0002, 8.12]	0.25
Perioperative factors			
Super-urgent transplant	1.74	[1.04, 2.91]	0.04
CMV mismatch	1.27	[0.96, 1.67]	0.09
Split graft	0.73	[0.41, 1.29]	0.28
CIT	0.998	[0.997, 0.999]	0.03
VV bypass	1.001	[0.997, 1.005]	0.58
WIT	0.995	[0.98, 1.01]	0.38
Biliary anastomosis			
End-to-end (ref)			0.4
Roux-en-y	0.69	[0.4, 1.19]	0.19
Delayed	1.11	[0.27, 4.54]	0.88
Multiple arterial anastomoses	1.05	[0.8, 1.39]	0.72
IO blood transfusion	0.98	[0.94, 1.01]	0.24
PO blood transfusion	0.88	[0.76, 1.004]	0.06
ITU stay	0.99	[0.96, 1.01]	0.25
Hospital stay	1.004	[0.996, 1.01]	0.36
Complications			
Vascular complications	0.66	[0.42, 1.05]	0.08
Bleeding	0.63	[0.34, 1.19]	0.16
Vascular stenosis	0.92	[0.46, 1.83]	0.82
Venous thrombosis	0.28	[0.09, 0.88]	0.03
HAT	0.57	[0.18, 1.81]	0.34
Biliary complications	1.09	[0.69, 1.72]	0.73

NABS	2.4	[1.21, 4.78]	0.01
Biliary leak	0.64	[0.3, 1.39]	0.26
Anastomotic stricture	1.32	[0.78, 2.24]	0.3
Infective complications	1.37	[0.91, 2.06]	0.13
Sepsis	0.88	[0.47, 1.65]	0.69
Return to theatre	0.997	[0.58, 1.71]	0.99
Disease recurrence	1.37	[0.73, 2.58]	0.32
Graft failure	1.25	[0.63, 2.48]	0.53
EAD	0.94	[0.56, 1.58]	0.82
High hPXR group	0.99	[0.66, 1.49]	0.96

Table 42 Multivariate Cox regression for rejection-free survival

Independent variable	Hazard ratio	95% CI	P value
Recipient gender	1.23	[0.97, 1.57]	0.08
Recipient age	0.98	[0.96, 0.99]	0.003
Alcoholic liver disease	0.9	[0.5, 1.64]	0.74
Autoimmune liver disease	1.63	[0.94, 2.81]	0.08
Super-urgent transplantation	1.14	[0.56, 2.29]	0.72
CIT	0.999	[0.998, 1.0004]	0.17
Venous thrombosis	0.25	[0.08, 0.8]	0.02
NABS	2.2	[1.06, 4.57]	0.03

6.3.7. Subgroup analyses

In order to identify any confounding effect introduced by the inclusion of recipients of DCD organs, split liver transplants, super-urgent transplants and recipients of previous transplants, subgroup analyses of the main outcomes in this study were performed by excluding the abovementioned groups separately.

The effect of hPXR activation on EAD in the subgroups

As demonstrated in the main group analysis, no differences in average $PPAV_7$ was found between recipients with and without EAD when DCD, split organ, super-urgent and redo transplant recipients were excluded separately from the analysis (Table 43).

Table 43 Subgroup analyses comparing average $PPAV_7$ between recipients with and without EAD

Subgroup analysis	Yes*	No*	P value
DCD transplants excluded	30.8±9.7	33.2±6.3	0.86
Split liver transplants excluded	29.7±8.8	34.4±6.1	0.72
Super-urgent transplants excluded	60±17.2	28.9±5.4	0.09
Redo transplants excluded	34.8±10.5	25.9±4.7	0.43

*Results expressed as average $PPAV_7$±SEM

Post-OLT complications

Average $PPAV_7$ remained significantly lower in recipients demonstrating anastomotic biliary strictures and those experiencing sepsis when split liver transplant recipients were excluded. Average $PPAV_7$ values were also significantly lower in the presence of anastomotic biliary strictures when super-urgent recipients were excluded. However, differences In $PPAV_7$ between recipients that experienced sepsis did not reach statistical significance in this subgroup. When DCD or redo transplant recipients were excluded from the analysis, no significant reduction in average

$PPAV_7$ was identified in the presence of anastomotic biliary strictures or sepsis (Table 44 and Table 45)

Table 44 Subgroup analyses comparing average $PPAV_7$ between recipients with and without anastomotic biliary strictures

Subgroup analysis	Yes*	No*	P value
DCD transplants excluded	19.3±6.3	35.1±6.2	0.078
Split liver transplants excluded	18.3±5.8	36.1±6	0.035
Super-urgent transplants excluded	19.4±6.1	37.8±6.5	0.04
Redo transplants excluded	15.9±5.7	29.5±5	0.075

*Results expressed as average $PPAV_7$±SEM

Table 45 Subgroup analyses comparing average $PPAV_7$ between recipients with and without sepsis

Subgroup analysis	Yes*	No*	P value
DCD transplants excluded	17.3±7.9	35.1±6.1	0.079
Split liver transplants excluded	16.4±7.1	36.1±5.9	0.036
Super-urgent transplants excluded	18.2±8.5	37.4±6.2	0.074
Redo transplants excluded	18.4±9.6	28.6±4.7	0.46

*Results expressed as average $PPAV_7$±SEM

Patient survival

Patient survival remained significantly improved in the high hPXR group even when DCD, split or super-urgent liver transplant recipients were excluded from the survival analysis. However, when redo transplant recipients were excluded, statistical significance was lost (Table 46).

Table 46 Subgroup analyses of patient survival (only Log Rank P values reported)

Subgroup analysis	Log Rank P value
DCD transplants excluded	0.024
Split liver transplants excluded	0.013
Super-urgent transplants excluded	0.037
Redo transplants excluded	0.14

6.4. Discussion

This study was performed in order to explore the findings of the animal PXR study (Chapter 5) and to assess the clinical applicability and benefit of PXR activation in liver transplantation. The hypothesis was that hPXR activation in the early post-transplantation period would lead to improved graft survival and a reduction in clinically-relevant complications associated with ischaemia reperfusion injury.

Accurate measurement of pharmacological data was central to this study. Therefore the inclusion period was limited by the timepoint at which the electronic medical record system (eRecord) became fully operational within the trust. The hPXR-activating efficacy and potency of drugs administered within the first week of transplantation was assessed using a comprehensive drug-hPXR activation dataset obtained from an external source (Shukla et al., 2011). This ensured impartiality, consistency and objectivity in hPXR activation assessment particularly during occasions where results from this dataset contradicted sporadic locally-produced PXR-profiling data.

Data on drug administration was limited to the first 7 days following transplantation in this study. This timeframe was chosen to ensure consistent drug data collection during the inpatient period (bearing in mind that some patients were discharged as early as 9 days post-transplantation (Table 31)) and also to coincide with EAD assessment on day 7 post-transplantation.

EAD was included as a measured outcome in this study due to its validated association with graft failure (Olthoff et al., 2010). This association was further validated in our local cohort of liver transplant recipients where the predictive value of EAD in graft survival extended well beyond the originally described 6-month survival (Figure 6.2). However, it is worth noting that, in contrast to the original EAD report, no significant association was found between EAD and recipient mortality (Figure 6.3).

Graft failure and patient death were the main clinically-relevant outcomes measured in this study. Recipients that experienced either of these events within the first week post-transplantation were excluded because 7-day drug data was not fully obtainable in these patients. Other clinically-relevant outcomes measured in this study included various post-OLT complications and disease recurrence.

Survival analyses demonstrated a significant improvement in patient survival in patients estimated to have relatively higher hPXR activation status on day 7 post-transplantation (classified as high hPXR activation group). Subsequent univariate and multivariate Cox regression analysis confirmed the hPXR activation groups to be a significant predictor of patient survival. The lack of association between the hPXR activation groups and graft survival was in keeping with earlier negative results comparing average $PPAV_7$ between recipients with and without EAD. However, the observed lack of improvement in graft survival with hPXR activation may be related to the definition of graft failure applied in this study. Recipients with failing grafts who are deemed ineligible for further transplantation and those that die prior to re-transplantation are not included in this definition. It remains unclear whether or not the inclusion of these subgroups of recipients would have affected the graft survival analysis.

A key finding in this study was that average $PPAV_7$ values were significantly lower in recipients demonstrating anastomotic biliary strictures and those experiencing sepsis post-transplantation compared to recipients that did not experience these complications. Given the previously obtained results from the animal model demonstrating anti-fibrotic effects due to PXR activation (Chapter 5), it would not be unreasonable to suggest a protective effect for hPXR activation against the development of anastomotic biliary strictures in clinical transplantation. The improvement in septic complications may be a direct result of reduced biliary obstruction and, consequently, biliary sepsis. However, further detailed analysis of the studied cohort will be required in order to explore this explanation. Surprisingly, average $PPAV_7$ values showed no significant shifts when examined in the context of NABS. A protective effect of hPXR activation against this complication was anticipated given the potential implication of ischaemia-reperfusion injury in its development (Mourad et al., 2014). However, these results highlight the complexity and heterogeneity in the pathogenesis of these lesions and the pathological distinction from anastomotic biliary strictures (Ryu and Lee, 2011).

It is worth noting that average $PPAV_7$ values were found to be lower in recipients that experienced AMR and in those that developed chronic rejection although the difference were not statistically significant compared to recipients that did not develop these complications. It is possible that a larger sample size was required to uncover significant changes given the low incidence of these complications (4.6% and 2.5%

overall respectively). On the other hand, no significant association was demonstrated between hPXR activation and rejection-free survival defined by TCMR episodes, which excludes a hPXR effect on this type of graft rejection.

The retrospective nature of this study is its main limitation. Recipient hPXR activation status was estimated in this study based on the type and amount of medications received within a pre-determined timeframe. A number of presumptions were made regarding drug action and patient response in order to reach a calculated estimation, and it is highly unlikely that any of these assumptions are accurate. However, inaccurate estimations of hPXR activation would have been consistent and randomly distributed between the study groups and, therefore, would not have significantly influenced the outcomes. A more accurate method for assessing hPXR activation would be based on tissue sample analysis. However, such method is associated with significant ethical and logistical constraints and was thus not pursued in this project.

Potential bias may have been introduced to the results from the presence of a significantly higher proportion of female and obese recipients in the high hPXR group. However, average $PPAV_7$ values were not found to be significantly different between male and female in the overall cohort. The increased average weight noted in the high hPXR group cannot simply be explained by gender difference alone since the average height was also significantly greater in this cohort. It is also worth noting that weight-normalisation in the calculation of $PPAV_7$ would produce relatively lower values in more obese patients. Therefore, larger doses of PXR activators may have been administered to obese patients although no significant correlation was identified between recipient weight and $PPAV_7$ (Appendix 4). Regardless of the explanation for the gender and anthropometric differences between the hPXR groups, neither recipient weight nor gender demonstrated any significant association with graft or recipient survival. In addition, no association was noted between recipient weight or gender and the incidence of anastomotic biliary strictures or sepsis (results not shown).

The potential confounding effect of including DCD, split organ, super-urgent and redo transplant recipients in this study was also addressed. Redo transplantation recipients were found to have a significantly greater risk of sepsis (data not shown). Otherwise, none of these factors were significantly associated with post-OLT complications that were shown to be affected by hPXR activation. Nevertheless, the

effect of hPXR activation on post-OLT complications was lost when either DCD, super-urgent or redo transplant recipients were excluded in separate subgroup analyses. On the other hand, the effect of hPXR activation on patient survival remained significant even when DCD, split graft and super-urgent transplant recipients were separately excluded. Although redo transplantation may have contributed to patient death in view of the higher risk of sepsis in this group, redo transplantation was not a factor significantly associated with patient survival in the Cox regression model. Regardless of the questionable impact of redo transplantation on patient death, hPXR activation was identified as an independent significant prognostic factor in recipient survival.

A remarkable finding in this study was that the apparent short-term exposure to medications that activate the hPXR was associated with a long-term survival benefit. Although this finding may suggest long-lasting effects of hPXR activation, it is equally plausible that the greater short-term exposure underlines a propensity to longer-term exposure to the same hPXR-activating medications.

Interestingly, clinically-relevant hPXR activators identified in this study (including Amlodipine, Nifedipine and Verapamil) were previously shown to have beneficial effects in animal models of liver ischaemia reperfusion injury as demonstrated during the literature review stage of this project (Chattopadhyay et al., 2010, Hardy et al., 1995, Oliveira et al., 2001, Erdogan et al., 2001, Pronobesh et al., 2008). Although the beneficial effects in those studies were not attributed to PXR activation, this may have played a significant role.

In conclusion, this study highlights the beneficial role for hPXR activation in reducing anastomotic biliary strictures, sepsis and ultimately improving patient survival following liver transplantation, in keeping with results from the earlier animal PXR model. However, further research would be required to address issues such as the accuracy of assessing PXR activation and the role of longer term PXR activation

Conclusion

This project included a number of studies that were aimed at investigating the development and resolution of biliary pathology due to ischaemia reperfusion injury following liver transplantation. Although inconclusive, the initial in vitro assays suggested an active pro-inflammatory role for biliary epithelial cells when subjected to oxygen after a period of hypoxia and prompted a focus on ischaemia reperfusion injury in vivo.

Following a comprehensive review of the literature, an in vivo model of rat hepatic ischaemia reperfusion injury was developed. This examined the progression of fibrosis following hepatic IRI in a sequential manner not previously explored, and demonstrated that hepatic IRI causes persistent inflammatory and fibrotic changes beyond the initial ischaemic insult, although radiological evidence for the presence of NABS could not be obtained in this study due to the lack of appropriate equipment.

Seen as a promising therapeutic target in inflammatory liver conditions, activation of the pregnane x receptor was investigated in a separate study using the same rat model of hepatic IRI. Consistent with previous results from our group, this new study demonstrated a reduction in post-IRI cellular damage, inflammation and fibrosis following activation of the PXR, and suggested a positive effect in reducing biliary complications following liver transplantation. These findings were subsequently verified in a retrospective clinical study that highlighted a beneficial role for PXR activation in reducing anastomotic biliary strictures and ultimately improving patient survival following liver transplantation

These studies provide further insight into the pathogenesis of biliary lesions following reperfusion injury and shed further light on the potential role for PXR activation in improving graft outcomes following liver transplantation. However, as with most research, new questions have emerged from these studies including the potential role of chemokines such as MCP-1 in post-reperfusion biliary pathology and the optimal duration of PXR activation following transplantation. This research also opens the door for innovative therapies such as the use of PXR activators in preservation and perfusion fluid prior to liver transplantation. Further research is required to address these and other outstanding questions.

Appendices

Appendix 1

Antibodies used in experiments

Antibody	Species raised in	Product code	Dilution (IHC/ICC)	Dilution (WB)	Manufacturer
a-SMA	Mouse	Ab134813	1:250-500		Abcam
Vimentin	Rabbit	ab92547	1:250-500		Abcam
CK19	Rabbit	Ab84632	1:250-500		Abcam
Cyp3A1	Mouse	ab22724		1:3000	Abcam
b-Actin	Mouse	A5441		1:3000	Sigma
Synaptophysin	Mouse	Ab8049	1:500		Abcam
GFAP	Rabbit	Ab7260	1:500		Abcam
CD163	Rabbit	Ab213612	1:250		Abcam
Elastin	Rabbit	Ab217356	1:500		Abcam
OSTa	Rabbit	Ab103442	1:500		Abcam
AE2	Rabbit	Ab191189	1:500		Abcam
CFTR	Mouse	Ab2784	1:500		Abcam
ZO1	Rabbit	Ab216880	1:500		Abcam
MRP3	Mouse	Ab3376	1:500		Abcam
PDGFR	Rabbit	Ab62437	1:500		Abcam
Anti-mouse HRP	Goat	P0447	1:200	1:3000	DAKO
Anti-rabbit HRP	Goat	P0448	1:200	1:3000	DAKO
Anti-rabbit TRITC	Goat	T6778	1:200		Sigma
Anti-rabbit FITC	Sheep	F7512	1:200		Sigma
Anti-mouse FITC	Rabbit	F9137	1:250		Sigma

Appendix 2

The distribution of model adoption in rat hepatic IRI studies over time

IRI model	Period							
	Pre 1981	1981-1985	1986-1990	1991-1995	1996-2000	2001-2005	2006-2010	2011-2015
Total hepatic exclusion	0	0	0	1	3	2	2	1
Total inflow occlusion	1	1	3	19	47	62	62	73
Portosystemic shunt	1	4	5	13	26	11	3	0
Portosystemic anastomosis	0	0	0	0	2	2	0	0
Splenic transposition	0	0	1	7	10	3	0	0
92% inflow occlusion (excluding caudate)	0	0	0	0	0	0	0	2
92% inflow occlusion + caudate resection	0	0	0	0	0	2	1	2
20% inflow occlusion (right)	0	0	0	2	11	10	3	1
20% inflow occlusion + 80% resection	0	0	1	5	2	2	3	2
70% inflow occlusion (Left/median)	4	10	24	81	77	93	128	131
70% inflow occlusion + 30% resection	0	0	4	20	21	12	11	10
70% inflow occlusion + 30% ligation	0	1	3	4	7	12	9	3
40% inflow occlusion (middle)	0	0	0	0	1	0	0	0
40% inflow	0	0	0	0	1	0	3	3

occlusion + 60% resection								
50% inflow occlusion (right/right middle)	0	0	0	0	0	0	0	1
30% inflow occlusion (left)	0	0	0	0	0	0	2	2
Portal vein occlusion	0	0	2	5	13	3	3	6
Hepatic artery occlusion	0	0	1	3	5	3	5	4

The distribution of anaesthetic use in rat hepatic IRI studies over time

IRI model	**Period**							
	Pre 1981	**1981-1985**	**1986-1990**	**1991-1995**	**1996-2000**	**2001-2005**	**2006-2010**	**2011-2015**
Chloral hydrate	0	0	0	4	6	4	4	16
Ether/ pentobarbital	0	2	0	4	5	1	1	0
Ketamine/ xylazine	0	0	2	1	8	19	42	60
Ketamine/ barbiturate	0	0	0	3	7	1	6	3
Ether	4	7	11	41	56	38	23	8
Enflurane	0	0	0	2	5	3	0	0
Halothane	0	0	0	3	2	2	2	1
Isoflurane	0	0	0	0	7	16	26	29
Ketamine	0	1	3	8	11	14	11	7
Pentobarbital	2	3	18	61	66	83	68	50
Thiopental	0	0	0	0	2	2	5	6
Urethane	0	0	0	2	11	14	15	11

The distribution of ischaemia time in rat hepatic IRI studies over time

IRI model	Period							
	Pre 1981	1981-1985	1986-1990	1991-1995	1996-2000	2001-2005	2006-2010	2011-2015
15 min	1	3	1	12	15	3	5	5
30 min	0	3	12	29	53	49	54	60
45 min	0	0	3	17	14	31	33	39
60 min	1	6	15	54	69	80	92	100
90 min	1	11	9	32	38	31	33	23
120 min	1	4	11	15	14	15	8	2
180 min	1	4	11	15	14	15	8	2

The distribution of minimum reperfusion time in rat hepatic IRI studies over time

IRI model	Period							
	Pre 1981	1981-1985	1986-1990	1991-1995	1996-2000	2001-2005	2006-2010	2011-2015
0 min	2	1	6	23	42	34	30	7
1-60 min	2	4	24	71	95	82	75	78
61-120 min	1	4	6	13	28	49	39	37
121-240 min	0	5	0	5	15	20	31	42
241-360 min	0	0	1	4	17	22	25	40
361-720 min	0	0	0	6	4	5	7	6
721-1440 min	1	6	4	21	11	14	32	25

The distribution of short-term maximum reperfusion time in rat hepatic IRI studies over time

IRI model	Period							
	Pre 1981	1981-1985	1986-1990	1991-1995	1996-2000	2001-2005	2006-2010	2011-2015

01-60 min	0	1	14	47	46	36	39	45
61-120 min	2	4	6	14	35	38	35	33
121-240 min	0	6	1	6	15	12	31	32
241-360 min	0	0	0	4	11	30	21	32
361-720 min	0	0	0	7	6	10	13	6
721-1440 min	2	8	11	32	36	40	55	56

The distribution of long-term maximum reperfusion time in rat hepatic IRI studies over time

IRI model	**Period**							
	Pre 1981	**1981-1985**	**1986-1990**	**1991-1995**	**1996-2000**	**2001-2005**	**2006-2010**	**2011-2015**
1441-2880 min	1	0	3	5	5	5	4	8
3d	0	0	0	4	10	1	6	2
4-7d	0	0	1	8	13	7	17	15
8-14d	0	0	0	3	6	8	3	0
15-30d	0	0	2	6	1	7	1	4
>30d	0	0	0	0	0	0	1	2

Appendix 3

Primers used in experiments (rat)

Primer ID	Primer sequence 5'-3'	Experiment
18s rRNA	US CCCGAAGCGTTTACTTTGAA DS CCCTCTTAATCATGGCCTCA	IRI/PXR
Ntcp	US GCATCATGCCCCTCGCTGCT DS GGTGGTCATCACGATGCTGAGGT	IRI
Bsep	US GCCAGGGGAAACGACGGCTC DS GGCCGTCCAGAGTCACCATGC	IRI
Abcb4	US AGCGAGAAACGGAACAGCACGG DS AGCTATGGCCATGAGGGTGCC	IRI
Tgfβ1	US CGAGCCCGAGGCGGACTACT DS ATAGATTGCGTTGTTGCGGTCCACC	IRI/PXR
Acta2 (α-SMA)	US TGCCATGTATGTGGCTATTCA DS ACCAGTTGTACGTCCAGAAGC	IRI/PXR
Col1a1	US TGTGTTGCTGAAAGACTACCTCGT DS AGTTGCCCCGGTGACACACAA	IRI/PXR
Mmp2	US GCACCGTCGCCCATCATCAAGT DS TTGCGGGGAAAGAAGTTGTAGT	IRI/PXR
Vimentin	US CAGGCCACCTCGTCCTTCGAAG DS TGTGCCGGAGCCACCGAACAT	IRI/PXR
Cyp3A1	US TGGCCCAGTGGGGATTATGGGG DS GGGACAGGTTTGCCTTTCTCTTGCC	IRI/PXR
Nr1i2 (PXR)	US GCTCCTGCTGGACCCGTTGA DS GCCAGGGCGATCTGGGGAGAA	IRI/PXR
Nr1i3 (CAR)	US CTCTCCTGACAGGCCTGGGGT DS CGAAGCTCAGCTAGCAGGCCC	IRI/PXR

Appendix 4

Correlation matrix of continuous recipient, donor and perioperative variables in clinical PXR study*

		PPAV7	Age	LOS	MELD	Ht	Wt	BMI	D-Age	D-Ht	D-Wt	D-BMI	CIT	VV	WIT	IOB	POB	ITU stay
PPAV7	PC	1.000	-0.028	0.111	-0.059	0.065	0.043	0.012	0.003	0.016	0.108	0.098	0.076	0.074	-0.055	0.204	-0.030	0.173
	Sig		0.663	0.085	0.372	0.324	0.503	0.853	0.968	0.801	0.098	0.131	0.238	0.255	0.394	0.002	0.668	0.007
Age	PC	-0.028	1.000	-0.157	-0.267	-0.030	0.104	0.147	-0.126	0.046	-0.002	-0.035	-0.001	-0.195	0.042	-0.113	-0.184	-0.194
	Sig	0.663		0.015	0.000	0.644	0.107	0.024	0.051	0.482	0.981	0.589	0.993	0.002	0.516	0.081	0.008	0.003
LOS	PC	0.111	-0.157	1.000	0.220	0.025	0.032	0.022	-0.111	0.100	0.048	-0.009	0.080	0.184	0.097	0.294	0.171	0.695
	Sig	0.085	0.015		0.001	0.707	0.617	0.733	0.085	0.125	0.466	0.893	0.216	0.004	0.135	0.000	0.014	0.000
MELD	PC	-0.059	-0.267	0.220	1.000	-0.114	-0.173	-0.176	0.146	-0.027	-0.062	-0.048	0.064	0.257	0.067	0.163	0.173	0.308
	Sig	0.372	0.000	0.001		0.086	0.008	0.008	0.025	0.682	0.351	0.469	0.329	0.000	0.308	0.013	0.014	0.000
Ht	PC	0.065	-0.030	0.025	-0.114	1.000	0.552	0.096	0.069	0.203	0.389	0.299	0.026	0.079	0.002	0.122	0.169	-0.038
	Sig	0.324	0.644	0.707	0.086		0.000	0.142	0.291	0.002	0.000	0.000	0.690	0.226	0.980	0.063	0.017	0.561
Wt	PC	0.043	0.104	0.032	-0.173	0.552	1.000	0.877	0.070	0.233	0.545	0.458	0.163	0.031	0.151	-0.048	0.071	-0.026
	Sig	0.503	0.107	0.617	0.008	0.000		0.000	0.280	0.000	0.000	0.000	0.011	0.636	0.019	0.464	0.313	0.683
BMI	PC	0.012	0.147	0.022	-0.176	0.096	0.877	1.000	0.061	0.138	0.408	0.371	0.162	-0.011	0.217	-0.113	-0.003	-0.010
	Sig	0.853	0.024	0.733	0.008	0.142	0.000		0.348	0.036	0.000	0.000	0.013	0.865	0.001	0.084	0.967	0.875
D-Age	PC	0.003	-0.126	-0.111	0.146	0.069	0.070	0.061	1.000	-0.238	0.039	0.190	0.151	0.039	0.055	-0.034	0.110	-0.021
	Sig	0.968	0.051	0.085	0.025	0.291	0.280	0.348		0.000	0.549	0.003	0.020	0.549	0.396	0.599	0.115	0.745
D-Ht	PC	0.016	0.046	0.100	-0.027	0.203	0.233	0.138	-0.238	1.000	0.488	-0.105	0.062	-0.005	-0.008	0.043	-0.076	0.010
	Sig	0.801	0.482	0.125	0.682	0.002	0.000	0.036	0.000		0.000	0.107	0.343	0.938	0.902	0.508	0.285	0.875
D-Wt	PC	0.108	-0.002	0.048	-0.062	0.389	0.545	0.408	0.039	0.488	1.000	0.811	0.081	0.003	0.023	0.008	0.023	-0.020
	Sig	0.098	0.981	0.466	0.351	0.000	0.000	0.000	0.549	0.000		0.000	0.214	0.958	0.725	0.902	0.743	0.763
D-BMI	PC	0.098	-0.035	-0.009	-0.048	0.299	0.458	0.371	0.190	-0.105	0.811	1.000	0.050	0.006	0.034	-0.021	0.079	-0.022
	Sig	0.131	0.589	0.893	0.469	0.000	0.000	0.000	0.003	0.107	0.000		0.445	0.928	0.607	0.744	0.265	0.734
CIT	PC	0.076	-0.001	0.080	0.064	0.026	0.163	0.162	0.151	0.062	0.081	0.050	1.000	0.194	0.089	0.129	0.061	-0.002
	Sig	0.238	0.993	0.216	0.329	0.690	0.011	0.013	0.020	0.343	0.214	0.445		0.003	0.171	0.046	0.384	0.977
VV	PC	0.074	-0.195	0.184	0.257	0.079	0.031	-0.011	0.039	-0.005	0.003	0.006	0.194	1.000	0.198	0.288	0.137	0.233
	Sig	0.255	0.002	0.004	0.000	0.226	0.636	0.865	0.549	0.938	0.958	0.928	0.003		0.002	0.000	0.051	0.000
WIT	PC	-0.055	0.042	0.097	0.067	0.002	0.151	0.217	0.055	-0.008	0.023	0.034	0.089	0.198	1.000	0.201	0.029	0.153
	Sig	0.394	0.516	0.135	0.308	0.980	0.019	0.001	0.396	0.902	0.725	0.607	0.171	0.002		0.002	0.677	0.017
IOB	PC	0.204	-0.113	0.294	0.163	0.122	-0.048	-0.113	-0.034	0.043	0.008	-0.021	0.129	0.288	0.201	1.000	0.227	0.256
	Sig	0.002	0.081	0.000	0.013	0.063	0.464	0.084	0.599	0.508	0.902	0.744	0.046	0.000	0.002		0.001	0.000
POB	PC	-0.030	-0.184	0.171	0.173	0.169	0.071	-0.003	0.110	-0.076	0.023	0.079	0.061	0.137	0.029	0.227	1.000	0.181
	Sig	0.668	0.008	0.014	0.014	0.017	0.313	0.967	0.115	0.285	0.743	0.265	0.384	0.051	0.677	0.001		0.009
ITU stay	PC	0.173	-0.194	0.695	0.308	-0.038	-0.026	-0.010	-0.021	0.010	-0.020	-0.022	-0.002	0.233	0.153	0.256	0.181	1.000
	Sig	0.007	0.003	0.000	0.000	0.561	0.683	0.875	0.745	0.875	0.763	0.734	0.977	0.000	0.017	0.000	0.009	

*Abbreviations: LOS: Length of hospital stay; Ht: recipient height; Wt: recipient weight; D-Age: donor age; D-Ht: donor height; D-wt: donor weight; D-BMI: donor BMI; CIT: cold ischaemia time; VV: veno-venous bypass time; WIT: warm ischaemia time; IOB: intraoperative blood transfusion; POB: postoperative blood transfusion.

PXR activation profile of drugs used in the post-transplantation period*

Drug	**ac50**	**class**	**Drug**	**ac50**	**class**
Abacavir	0	4	Hyoscine butylbromide	0	4
Acetazolamide	0	4	Ibuprofen	0	4
Acetylcysteine	0	4	Insulin soluble human	0	4
Aciclovir	0	4	Ipratropium	0	4
Adenosine	0	4	Irbesartan	0	4
Alendronic acid	0	4	Isosorbide mononitrate	0	4
Alginate sodium	0	0	Ketamine	19.95	2.4
Allopurinol	0	4	Labetalol	0	4
AMILORide	0	4	Lactulose	0	4
Amiodarone	15.85	2.4	Lamivudine	0	4
Amitriptyline	0	4	Lansoprazole	0	4
AMLODipine	8.91	1.2	Latanoprost	0	4
Amoxicillin	0	4	Leflunomide	0.79	4
Amphotericin B	0	4	Lercanidipine	0	4
Amphotericin B liposomal	0	4	Levothyroxine	25.12	2.1
Anidulafungin	0	4	Linezolid	0	4
Argipressin	0	4	Liothyronine	3.16	1.1
Aripiprazole	0	4	Lisinopril	0	4
Aspirin	0	4	Loperamide	10	2.1
Atenolol	0	4	Lorazepam	10	2.4
Atorvastatin	0.04	1.4	Lymecycline	0	4
AzathioPRINE	0	4	Melatonin	0	4
AzithroMYCIN	35.48	3	Meropenem	0	4
Aztreonam	0	4	Mesalazine	0	4
Beclometasone	15.85	2.1	Metformin	0	4

Benzydamine	5.62	2.4	Methadone	0	4
Bimatoprost + Timolol	0	4	MethylPREDNISOLONE	0	4
Bisacodyl	0	4	Metoclopramide	0	4
Bisoprolol	0	4	Metoprolol	0	4
Budesonide + Formoterol	8.91	1.3	Metronidazole	0	4
Bumetanide	0	4	Metronidazole topical	0	4
Calcium carbonate	0	4	Midazolam	0	4
Calcium carbonate + Colecalciferol	0	4	Midodrine	0	4
Calcium carbonate + lactate + gluconate	0	4	Mirtazapine	15.85	2.2
Calcium chloride	0	4	Mometasone nasal	0	4
Calcium glubionate + Calc. lactobionate	0	4	Morphine	0	4
Calcium gluconate	0	4	Mupirocin	0	4
Carbocisteine	0	4	Mycophenolate mofetil	0	4
Carbomer 980	0	4	Mycophenolic acid	0	4
Carvedilol	0	4	Naloxone	0	4
Caspofungin	0	4	Naltrexone	0	4
Ceftazidime	0	4	Nateglinide	19.95	2.4
Ceftriaxone	0	4	Nefopam	0	4
Cefuroxime	0	4	Neomycin	0	4
Cetirizine	0	4	Nicotine	0	4
Chloramphenicol	0	4	Nifedipine	12.59	3
Chloramphenicol ophthalmic	0	4	Nitrazepam	0	4
Chlordiazepoxide	0	4	Noradrenaline	0	4
Chlorhexidine	0	4	Norfloxacin	0	4
Chlorhexidine + Neomycin	0	4	Nystatin	0	4
Chlorphenamine	0	4	Olanzapine	0	4
Ciprofloxacin	7.08	3	Omeprazole	0	4
Cisatracurium	0	4	Ondansetron	0	4
Citalopram	0	4	Orlistat	0	4

Clarithromycin	0	4	Oseltamivir	0	4
Clindamycin	0	4	Oxethazaine	14.13	3
Clonazepam	0	4	Oxycodone	0	4
Clonidine	0	4	Paracetamol	0	4
Co-amoxiclav	0	4	Perindopril	0	4
Co-beneldopa	0	4	Phenoxymethylpenicillin	0	4
Codeine	0	4	Phytomenadione	2.51	1.1
Colecalciferol	0	4	Pioglitazone	0	4
Colistin	0	4	Piperacillin + Tazobactam	0	4
Co-trimoxazole	0	4	Pravastatin	0	4
Crotamiton	0	4	PrednisoLONE	0.18	1.4
Cyclizine	0	4	Pregabalin	0	4
Dalteparin	0	4	Prochlorperazine	0	4
Dapsone	0	4	Propofol	0	4
Daptomycin	0	4	Propranolol	3.98	2.4
Dequalinium dichloride	0	4	Pyridoxine	0	4
Desmopressin	0	4	Quetiapine	19.95	2.4
Diazepam	0	4	Quinine	0	4
Digoxin	1.58	5	Ramipril	0	4
Diltiazem	0	4	Ranitidine	0	4
Docusate	0	4	Remifentanil	0	4
Domperidone	25.12	3	Ribavirin	0	4
Dopexamine	0	4	Rifampicin	0.71	1.2
Dosulepin	0	4	Rifaximin	10	2.3
Doxazosin	0	4	Risperidone	0	4
Doxycycline	0	4	Salbutamol	0	4
Efavirenz	3.98	2.2	Salmeterol	3.98	2.2
Emtricitabine + Tenofovir	0	4	Sertraline	28.18	2.1
Entecavir	0	4	Sildenafil	0	4
Eplerenone	0	4	Simvastatin	0.79	1.4
Epoprostenol	0	4	Sitagliptin	0	4
Ertapenem	0	4	Sodium valproate	0	4
Erythromycin	0	4	Spironolactone	0	4

Erythromycin lactobionate	0	4	Tacrolimus	0	4
Escitalopram	0	4	Tamsulosin	0	4
Fenofibrate micronised	0	4	Teicoplanin	0	4
Fentanyl	14.13	2.1	Temazepam	0	4
Finasteride	0	4	Tenofovir	0	4
Flucloxacillin	0	4	Terlipressin	0	4
Fluconazole	0	4	Thiamine	0	4
Fludrocortisone	0	4	Thiopental	25.12	2.4
Fluoxetine	3.16	2.4	Tibolone	0	4
Fluticasone + Salmeterol	3.98	2.2	Tinzaparin	0	4
Folic acid	0	4	Tiotropium	0	4
Fosfomycin	0	4	Tolbutamide	0	4
Furosemide	0	4	Tolterodine	5.62	1.3
Gabapentin	0	4	Tramadol	0	4
Gentamicin	0	4	Tranexamic acid	0	4
GliCLAzide	0	4	Trazodone	4.47	1.4
Glyceryl trinitrate	0	4	Trimethoprim	0	4
Glycopyrronium	0	4	Ursodeoxycholic acid	0	4
Halibut liver oil	0	4	ValGANciclovir	0	4
Haloperidol	14.13	2.1	Vancomycin	0	4
Heparin	0	4	Venlafaxine	0	4
Hydrocortisone	0.08	2.2	VERAPAMIL	12.59	2.1
Hydromorphone	0	4	Vitamin E	0	4
HydrOXYzine	0	4	Zopiclone	0	4

*Excludes immunotherapy and nutrition/electrolyte supplements

References

ABDO, E. E., CUNHA, J. E., DELUCA, P., COELHO, A. M., BACCHELLA, T. & MACHADO, M. C. 2003. Protective effect of N2-mercaptopropionylglycine on rats and dogs liver during ischemia/reperfusion process. *Arquivos de gastroenterologia,* 40, 177-80.

ABE, T., LYNCH, S., BALDERSON, G., PILLAY, P., AKIYAMA, T., INUZUKA, S., MATSUNAMI, H. & STRONG, R. 1993. The effects of prostacyclin analog OP-41483 on normothermic liver ischemia and reperfusion injury in rats. *Prostaglandins Leukot Essent Fatty Acids,* 48, 417-22.

ABOU-REBYEH, H., VELTZKE-SCHLIEKER, W., RADKE, C., STEINMULLER, T., WIEDENMANN, B. & HINTZE, R. E. 2003. Complete bile duct sequestration after liver transplantation, caused by ischemic-type biliary lesions. *Endoscopy,* 35, 616-20.

ABT, P., CRAWFORD, M., DESAI, N., MARKMANN, J., OLTHOFF, K. & SHAKED, A. 2003. Liver transplantation from controlled non-heart-beating donors: an increased incidence of biliary complications. *Transplantation,* 75, 1659-63.

ACCATINO, L., PIZARRO, M., SOLIS, N., ARRESE, M. & KOENIG, C. S. 2003. Bile secretory function after warm hepatic ischemia-reperfusion injury in the rat. *Liver Transpl,* 9, 1199-210.

ADKISON, D., HOLLWARTH, M. E., BENOIT, J. N., PARKS, D. A., MCCORD, J. M. & GRANGER, D. N. 1986. Role of free radicals in ischemia-reperfusion injury to the liver. *Acta physiologica Scandinavica. Supplementum,* 548, 101-7.

ALLER, M. A. & ARIAS, J. 2009. *Microsurgery in Liver Research*, Bentham Science Publishers.

ANDREWS, E., ARMSTRONG, M., TUGWOOD, J., SWAN, D., GLAVES, P., PIRMOHAMED, M., AITHAL, G. P., WRIGHT, M. C., DAY, C. P. & DALY, A. K. 2010. A role for the pregnane X receptor in flucloxacillin-induced liver injury. *Hepatology,* 51, 1656-64.

ARAB, H. A., SASANI, F., RAFIEE, M. H., FATEMI, A. & JAVAHERI, A. 2009. Histological and biochemical alterations in early-stage lobar ischemia-reperfusion in rat liver. *World journal of gastroenterology : WJG,* 15, 1951-7.

ARII, S., MONDEN, K., ADACHI, Y., ZHANG, W., HIGASHITSUJI, H., FURUTANI, M., MISE, M., FUJITA, S., NAKAMURA, T. & IMAMURA, M. 1994. Pathogenic role of Kupffer cell activation in the reperfusion injury of cold-preserved liver. *Transplantation,* 58, 1072-7.

ASAKAWA, H., JEPPSSON, B., MACK, P., HULTBERG, B., HAGERSTRAND, I. & BENGMARK, S. 1989. Acute ischemic liver failure in the rat: a reproducible model not requiring portal decompression. *Eur Surg Res,* 21, 42-8.

AXON, A., COWIE, D. E., MANN, D. A. & WRIGHT, M. C. 2008. A mechanism for the anti-fibrogenic effects of the pregnane X receptor (PXR) in the liver: inhibition of NF-kappaB? *Toxicology,* 246, 40-4.

AYOUB, W. S., ESQUIVEL, C. O. & MARTIN, P. 2010. Biliary complications following liver transplantation. *Digestive diseases and sciences,* 55, 1540-6.

BANERJEE, M., ROBBINS, D. & CHEN, T. 2015. Targeting xenobiotic receptors PXR and CAR in human diseases. *Drug discovery today,* 20, 618-28.

BERNARD, C. 1855. *Leçons de physiologie expérimentale appliquée à la médecine, faites au Collège de France,* Paris,, J.B. Baillière et fils; etc.

BERTILSSON, G., HEIDRICH, J., SVENSSON, K., ASMAN, M., JENDEBERG, L., SYDOW-BACKMAN, M., OHLSSON, R., POSTLIND, H., BLOMQUIST, P. & BERKENSTAM, A. 1998. Identification of a human nuclear receptor defines a new signaling pathway for CYP3A induction. *Proceedings of the National Academy of Sciences of the United States of America,* 95, 12208-13.

BESSEMS, M., T HART, N. A., TOLBA, R., DOORSCHODT, B. M., LEUVENINK, H. G., PLOEG, R. J., MINOR, T. & VAN GULIK, T. M. 2006. The isolated perfused rat liver: standardization of a time-honoured model. *Laboratory animals,* 40, 236-46.

BEYER, C., SKAPENKO, A., DISTLER, A., DEES, C., REICHERT, H., MUNOZ, L., LEIPE, J., SCHULZE-KOOPS, H., DISTLER, O., SCHETT, G. & DISTLER, J. H. 2013. Activation of pregnane X receptor inhibits experimental dermal fibrosis. *Annals of the rheumatic diseases,* 72, 621-5.

BLUMBERG, B., SABBAGH, W., JR., JUGUILON, H., BOLADO, J., JR., VAN METER, C. M., ONG, E. S. & EVANS, R. M. 1998. SXR, a novel steroid and xenobiotic-sensing nuclear receptor. *Genes & development,* 12, 3195-205.

BORCHARDT, R. T., SMITH, P. L. & WILSON, G. 1996. *Models for assessing drug absorption and metabolism,* New York, Plenum Press.

BRICENO, J., CIRIA, R., DE LA MATA, M., RUFIAN, S. & LOPEZ-CILLERO, P. 2010. Prediction of graft dysfunction based on extended criteria donors in the model for end-stage liver disease score era. *Transplantation,* 90, 530-9.

BROCKMANN, J. G., AUGUST, C., WOLTERS, H. H., HOMME, R., PALMES, D., BABA, H., SPIEGEL, H. U. & DIETL, K. H. 2005. Sequence of reperfusion influences ischemia/reperfusion injury and primary graft function following porcine liver transplantation. *Liver transplantation : official publication of the American Association for the Study of Liver Diseases and the International Liver Transplantation Society,* 11, 1214-22.

BUCK, D. G. & ZAJKO, A. B. 2008. Biliary complications after orthotopic liver transplantation. *Tech Vasc Interv Radiol,* 11, 51-9.

BUIS, C. I., GEUKEN, E., VISSER, D. S., KUIPERS, F., HAAGSMA, E. B., VERKADE, H. J. & PORTE, R. J. 2009. Altered bile composition after liver transplantation is associated with the development of nonanastomotic biliary strictures. *Journal of hepatology,* 50, 69-79.

BUIS, C. I., HOEKSTRA, H., VERDONK, R. C. & PORTE, R. J. 2006. Causes and consequences of ischemic-type biliary lesions after liver transplantation. *Journal of hepato-biliary-pancreatic surgery,* 13, 517-24.

BUIS, C. I., VERDONK, R. C., VAN DER JAGT, E. J., VAN DER HILST, C. S., SLOOFF, M. J., HAAGSMA, E. B. & PORTE, R. J. 2007. Nonanastomotic biliary strictures after liver transplantation, part 1: Radiological features and risk factors for early vs. late presentation. *Liver transplantation : official publication of the American Association for the Study of Liver Diseases and the International Liver Transplantation Society,* 13, 708-18.

BURRA, P. & FREEMAN, R. 2012. Trends in liver transplantation 2011. *Journal of hepatology,* 56 Suppl 1, S101-11.

BURTON, M. E. 2006. *Applied pharmacokinetics & pharmacodynamics : principles of therapeutic drug monitoring,* Baltimore, Lippincott Williams & Wilkins.

CALDWELL-KENKEL, J. C., CURRIN, R. T., TANAKA, Y., THURMAN, R. G. & LEMASTERS, J. J. 1989. Reperfusion injury to endothelial cells following cold ischemic storage of rat livers. *Hepatology,* 10, 292-9.

CALNE, R. Y. 1977. The present status of liver transplantation. *Transplant Proc,* 9, 209-16.

CAMERON, A. M. & BUSUTTIL, R. W. 2005. Ischemic cholangiopathy after liver transplantation. *Hepatobiliary Pancreat Dis Int,* 4, 495-501.

CHATTOPADHYAY, P., CHAUDHURY, P. & WAHI, A. K. 2010. Ca2+ concentrations are key determinants of ischemia-reperfusion-induced apoptosis: significance for the molecular mechanism of Bcl-2 action. *Applied biochemistry and biotechnology,* 160, 1968-77.

CHEN, G., WANG, S., BIE, P., LI, X. & DONG, J. 2009a. Endogenous bile salts are associated with bile duct injury in the rat liver transplantation model. *Transplantation,* 87, 330-9.

CHEN, Y., TANG, Y., CHEN, S. & NIE, D. 2009b. Regulation of drug resistance by human pregnane X receptor in breast cancer. *Cancer biology & therapy,* 8, 1265-72.

CHEN, Y., TANG, Y., WANG, M. T., ZENG, S. & NIE, D. 2007. Human pregnane X receptor and resistance to chemotherapy in prostate cancer. *Cancer research,* 67, 10361-7.

CHEN, Y. X., SATO, M., KAWACHI, K. & ABE, Y. 2006. Neutrophil-mediated liver injury during hepatic ischemia-reperfusion in rats. *Hepatobiliary & pancreatic diseases international : HBPD INT,* 5, 436-42.

CHENG, J., FANG, Z. Z., NAGAOKA, K., OKAMOTO, M., QU, A., TANAKA, N., KIMURA, S. & GONZALEZ, F. J. 2014. Activation of intestinal human pregnane X receptor protects against azoxymethane/dextran sulfate sodium-induced colon cancer. *The Journal of pharmacology and experimental therapeutics,* 351, 559-67.

CHENG, J., KRAUSZ, K. W., TANAKA, N. & GONZALEZ, F. J. 2012. Chronic exposure to rifaximin causes hepatic steatosis in pregnane X receptor-humanized mice. *Toxicological sciences : an official journal of the Society of Toxicology,* 129, 456-68.

CHENG, J., MA, X., KRAUSZ, K. W., IDLE, J. R. & GONZALEZ, F. J. 2009. Rifampicin-activated human pregnane X receptor and CYP3A4 induction enhance acetaminophen-induced toxicity. *Drug metabolism and disposition: the biological fate of chemicals,* 37, 1611-21.

CHENG, J., SHAH, Y. M., MA, X., PANG, X., TANAKA, T., KODAMA, T., KRAUSZ, K. W. & GONZALEZ, F. J. 2010a. Therapeutic role of rifaximin in inflammatory bowel disease: clinical implication of human pregnane X receptor activation. *The Journal of pharmacology and experimental therapeutics,* 335, 32-41.

CHENG, L., ZHAO, L., LI, D., LIU, Z., CHEN, G., TIAN, F., LI, X. & WANG, S. 2010b. Role of cholangiocyte bile Acid transporters in large bile duct injury after rat liver transplantation. *Transplantation,* 90, 127-34.

CHIEN, K. R., ABRAMS, J., PFAU, R. G. & FARBER, J. L. 1977. Prevention by chlorpromazine of ischemic liver cell death. *The American journal of pathology,* 88, 539-57.

CHIEN, K. R., ABRAMS, J., SERRONI, A., MARTIN, J. T. & FARBER, J. L. 1978. Accelerated phospholipid degradation and associated membrane dysfunction in irreversible, ischemic liver cell injury. *The Journal of biological chemistry,* 253, 4809-17.

CHOI, N. K., HWANG, S., KIM, K. W., PARK, G. C., YU, Y. D., JUNG, S. H., PARK, P. J., CHOI, Y. I., SONG, G. W., JUNG, D. H., HONG, S. K., AHN, C. S., KIM, K. H., MOON, D. B., HA, T. Y. & LEE, S. G. 2012. Intensive pulmonary support using extracorporeal membrane oxygenation in adult patients undergoing liver transplantation. *Hepato-Gastroenterology,* 59, 1189-93.

CHOMCZYNSKI, P. & SACCHI, N. 1987. Single-step method of RNA isolation by acid guanidinium thiocyanate-phenol-chloroform extraction. *Analytical biochemistry,* 162, 156-9.

CHUN, K., ZHANG, J., BIEWER, J., FERGUSON, D. & CLEMENS, M. G. 1994. Microcirculatory failure determines lethal hepatocyte injury in ischemic/reperfused rat livers. *Shock,* 1, 3-9.

CLEMENS, M. G., MCDONAGH, P. F., CHAUDRY, I. H. & BAUE, A. E. 1985. Hepatic microcirculatory failure after ischemia and reperfusion: improvement with ATP-MgCl2 treatment. *The American journal of physiology,* 248, H804-11.

CLOTMAN, F., LIBBRECHT, L., GRESH, L., YANIV, M., ROSKAMS, T., ROUSSEAU, G. G. & LEMAIGRE, F. P. 2003. Hepatic artery malformations associated with a primary defect in intrahepatic bile duct development. *Journal of hepatology,* 39, 686-92.

COHEN, J. 1988. *Statistical power analysis for the behavioral sciences,* Hillsdale, N.J., L. Erlbaum Associates.

COLLETTI, L. M., REMICK, D. G., BURTCH, G. D., KUNKEL, S. L., STRIETER, R. M. & CAMPBELL, D. A., JR. 1990. Role of tumor necrosis factor-alpha in the pathophysiologic alterations after hepatic ischemia/reperfusion injury in the rat. *The Journal of clinical investigation,* 85, 1936-43.

COPPLE, B. L. & LI, T. 2016. Pharmacology of bile acid receptors: Evolution of bile acids from simple detergents to complex signaling molecules. *Pharmacological research,* 104, 9-21.

CUTRIN, J. C., CANTINO, D., BIASI, F., CHIARPOTTO, E., SALIZZONI, M., ANDORNO, E., MASSANO, G., LANFRANCO, G., RIZZETTO, M., BOVERIS, A. & POLI, G. 1996. Reperfusion damage to the bile canaliculi in transplanted human liver. *Hepatology,* 24, 1053-7.

D'ALESSANDRO A, M., HOFFMANN, R. M., KNECHTLE, S. J., ODORICO, J. S., BECKER, Y. T., MUSAT, A., PIRSCH, J. D., SOLLINGER, H. W. & KALAYOGLU, M. 2000. Liver transplantation from controlled non-heart-beating donors. *Surgery,* 128, 579-88.

D'ALESSANDRO, A. M., FERNANDEZ, L. A., CHIN, L. T., SHAMES, B. D., TURGEON, N. A., SCOTT, D. L., DI CARLO, A., BECKER, Y. T., ODORICO, J. S., KNECHTLE, S. J., LOVE, R. B., PIRSCH, J. D., BECKER, B. N., MUSAT, A. I., KALAYOGLU, M. & SOLLINGER, H. W. 2004. Donation after cardiac death: the University of Wisconsin experience. *Annals of transplantation,* 9, 68-71.

DAI, G., HE, L., BU, P. & WAN, Y. J. 2008. Pregnane X receptor is essential for normal progression of liver regeneration. *Hepatology,* 47, 1277-87.

DARILMAZ, G., TOPALOGLU, S., TOPALOGLU, E., OZEL, H., SAYGUN, O., AVSAR, F. M., SOKMENSUER, C., UCAR, G., SAHIN, M. & HENGIRMEN, S. 2005. Evaluation of liver damage after application of TVE in the rat model. *Transplant Proc,* 37, 4550-2.

DATTA, G., FULLER, B. J. & DAVIDSON, B. R. 2013. Molecular mechanisms of liver ischemia reperfusion injury: insights from transgenic knockout models. *World J Gastroenterol,* 19, 1683-98.

DE BAKER, H. C. 1956. Ischaemic necrosis in the rat liver. *The Journal of pathology and bacteriology,* 71, 135-43.

DELTENRE, P. & VALLA, D. C. 2006. Ischemic cholangiopathy. *Journal of hepatology,* 44, 806-17.

DEMETRIS, A. J., ADEYI, O., BELLAMY, C. O., CLOUSTON, A., CHARLOTTE, F., CZAJA, A., DASKAL, I., EL-MONAYERI, M. S., FONTES, P., FUNG, J., GRIDELLI, B., GUIDO, M., HAGA, H., HART, J., HONSOVA, E., HUBSCHER, S., ITOH, T., JHALA, N., JUNGMANN, P., KHETTRY, U., LASSMAN, C., LIGATO, S., LUNZ, J. G., 3RD, MARCOS, A., MINERVINI, M. I., MOLNE, J., NALESNIK, M., NASSER, I., NEIL, D., OCHOA, E., PAPPO, O., RANDHAWA, P., REINHOLT, F. P., RUIZ, P., SEBAGH, M., SPADA, M., SONZOGNI, A., TSAMANDAS, A. C., WERNERSON, A., WU, T. & YILMAZ, F. 2006. Liver biopsy interpretation for causes of late liver allograft dysfunction. *Hepatology,* 44, 489-501.

DEMETRIS, A. J., BELLAMY, C., HUBSCHER, S. G., O'LEARY, J., RANDHAWA, P. S., FENG, S., NEIL, D., COLVIN, R. B., MCCAUGHAN, G., FUNG, J. J., DEL BELLO, A., REINHOLT, F. P., HAGA, H., ADEYI, O., CZAJA, A. J., SCHIANO, T., FIEL, M. I., SMITH, M. L., SEBAGH, M., TANIGAWA, R. Y., YILMAZ, F., ALEXANDER, G., BAIOCCHI, L., BALASUBRAMANIAN, M., BATAL, I., BHAN, A. K., BUCUVALAS, J., CERSKI, C. T. S., CHARLOTTE, F., DE VERA, M. E., ELMONAYERI, M., FONTES, P., FURTH, E. E., GOUW, A. S. H., HAFEZI-BAKHTIARI, S., HART, J., HONSOVA, E., ISMAIL, W., ITOH, T., JHALA, N. C., KHETTRY, U., KLINTMALM, G. B., KNECHTLE, S., KOSHIBA, T., KOZLOWSKI, T., LASSMAN, C. R., LERUT, J., LEVITSKY, J., LICINI, L., LIOTTA, R., MAZARIEGOS, G., MINERVINI, M. I., MISDRAJI, J., MOHANAKUMAR, T., MOLNE, J., NASSER, I., NEUBERGER, J., O'NEIL, M., PAPPO, O., PETROVIC, L., RUIZ, P., SAGOL, O., SANCHEZ FUEYO, A., SASATOMI, E., SHAKED, A., SHILLER, M., SHIMIZU, T., SIS, B., SONZOGNI, A., STEVENSON, H. L., THUNG, S. N., TISONE, G., TSAMANDAS, A. C., WERNERSON, A., WU, T., ZEEVI, A. & ZEN, Y. 2016. 2016 Comprehensive Update of the Banff Working Group on Liver Allograft Pathology: Introduction of Antibody-Mediated Rejection. *American journal of transplantation : official journal of the American Society of Transplantation and the American Society of Transplant Surgeons,* 16, 2816-2835.

DEMETRIS, A. J., MARKUS, B. H., SAIDMAN, S., FUNG, J. J., MAKOWKA, L., GRANER, S., DUQUESNOY, R. & STARZL, T. E. 1988. Isolation and primary cultures of human intrahepatic bile ductular epithelium. *In vitro cellular & developmental biology : journal of the Tissue Culture Association,* 24, 464-70.

DI MASI, A., DE MARINIS, E., ASCENZI, P. & MARINO, M. 2009. Nuclear receptors CAR and PXR: Molecular, functional, and biomedical aspects. *Molecular aspects of medicine,* 30, 297-343.

DIANAT, N., DUBOIS-POT-SCHNEIDER, H., STEICHEN, C., DESTERKE, C., LECLERC, P., RAVEUX, A., COMBETTES, L., WEBER, A., CORLU, A. & DUBART-KUPPERSCHMITT, A. 2014. Generation of functional cholangiocyte-like cells from human pluripotent stem cells and HepaRG cells. *Hepatology,* 60, 700-14.

DINDO, D., DEMARTINES, N. & CLAVIEN, P. A. 2004. Classification of surgical complications: a new proposal with evaluation in a cohort of 6336 patients and results of a survey. *Annals of surgery,* 240, 205-13.

DONG, J. H., HE, X. D., LI, K., DUAN, H. C., PENG, Z. M. & CAI, J. X. 2002. Tolerance limit of rats to normothermic hepatic inflow occlusion under portal blood bypass. *Hepatobiliary Pancreat Dis Int,* 1, 57-62.

DOU, W., MUKHERJEE, S., LI, H., VENKATESH, M., WANG, H., KORTAGERE, S., PELEG, A., CHILIMURI, S. S., WANG, Z. T., FENG, Y., FEARON, E. R. & MANI, S. 2012. Alleviation of gut inflammation by Cdx2/Pxr pathway in a mouse model of chemical colitis. *PloS one,* 7, e36075.

DUSUNCELI, F., ISERI, S. O., ERCAN, F., GEDIK, N., YEGEN, C. & YEGEN, B. C. 2008. Oxytocin alleviates hepatic ischemia-reperfusion injury in rats. *Peptides,* 29, 1216-22.

EICHELBAUM, M. & BURK, O. 2001. CYP3A genetics in drug metabolism. *Nature medicine,* 7, 285-7.

EKINS, S. 2007. *Computational toxicology : risk assessment for pharmaceutical and environmental chemicals,* Hoboken, N.J., Wiley-Interscience.

EKINS, S., CHANG, C., MANI, S., KRASOWSKI, M. D., RESCHLY, E. J., IYER, M., KHOLODOVYCH, V., AI, N., WELSH, W. J., SINZ, M., SWAAN, P. W., PATEL, R. & BACHMANN, K. 2007. Human pregnane X receptor antagonists and agonists define molecular requirements for different binding sites. *Molecular pharmacology,* 72, 592-603.

EKINS, S., KORTAGERE, S., IYER, M., RESCHLY, E. J., LILL, M. A., REDINBO, M. R. & KRASOWSKI, M. D. 2009. Challenges predicting ligand-receptor interactions of promiscuous proteins: the nuclear receptor PXR. *PLoS computational biology,* 5, e1000594.

EL-BENNA, J., DANG, P. M. & GOUGEROT-POCIDALO, M. A. 2008. Priming of the neutrophil NADPH oxidase activation: role of p47phox phosphorylation and NOX2 mobilization to the plasma membrane. *Seminars in immunopathology,* 30, 279-89.

ERDOGAN, O., YILDIZ, S., BASARAN, A., DEMIRBAS, A. & YESILKAYA, A. 2001. Effect of intraportal verapamil infusion on hepatic ischemia-reperfusion injury. *Polish journal of pharmacology,* 53, 137-41.

ESMAEILZADEH, M., NICKKHOLGH, A., MAJLESARA, A., HAFEZI, M., GAROUSSI, C., GHAZI-MOGHADDAM, K., FARIDAR, A., GOLRIZ, M., FONOUNI, H. & MEHRABI, A. 2012. Technical guidelines for porcine liver allo-transplantation: a review of literature. *Annals of transplantation,* 17, 101-10.

EXPERT WORKING GROUP ON SEVERITY CLASSIFICATION OF SCIENTIFIC PROCEDURES 2009. Expert Working Group on Severity Classification of Scientific Procedures Performed on Animals: Final Report. Brussels: European Commission, 2009.

FABRIS, L., CADAMURO, M., FIOROTTO, R., ROSKAMS, T., SPIRLI, C., MELERO, S., SONZOGNI, A., JOPLIN, R. E., OKOLICSANYI, L. & STRAZZABOSCO, M. 2006. Effects of angiogenic factor overexpression by human and rodent cholangiocytes in polycystic liver diseases. *Hepatology,* 43, 1001-12.

FEBBRAIO, M. & SILVERSTEIN, R. L. 2007. CD36: implications in cardiovascular disease. *The international journal of biochemistry & cell biology,* 39, 2012-30.

FLYE, M. W. & YU, S. 1987. The synergistic effect of superoxide dismutase and adenosine triphosphate-MgCl2 on acute hepatic ischemia. *Transplant Proc,* 19, 1324-6.

FOLEY, D. P., FERNANDEZ, L. A., LEVERSON, G., CHIN, L. T., KRIEGER, N., COOPER, J. T., SHAMES, B. D., BECKER, Y. T., ODORICO, J. S., KNECHTLE, S. J., SOLLINGER, H. W., KALAYOGLU, M. & D'ALESSANDRO, A. M. 2005. Donation after cardiac death: the University of Wisconsin experience with liver transplantation. *Annals of Surgery,* 242, 724-31.

FORMAN, H. J. & TORRES, M. 2002. Reactive oxygen species and cell signaling: respiratory burst in macrophage signaling. *American journal of respiratory and critical care medicine,* 166, S4-8.

FRIEDMAN, S. L. 2008. Hepatic stellate cells: protean, multifunctional, and enigmatic cells of the liver. *Physiological reviews,* 88, 125-72.

GASBARRINI, A., ADDOLORATO, G., DI CAMPLI, C., SIMONCINI, M., MONTEMAGNO, S., CASTAGNETO, M., PADALINO, C., POLA, P. & GASBARRINI, G. 2001. Gender affects reperfusion injury in rat liver. *Digestive diseases and sciences,* 46, 1305-12.

GAUDIO, E., ONORI, P., PANNARALE, L. & ALVARO, D. 1996. Hepatic microcirculation and peribiliary plexus in experimental biliary cirrhosis: a morphological study. *Gastroenterology,* 111, 1118-24.

GEUKEN, E., VISSER, D., KUIPERS, F., BLOKZIJL, H., LEUVENINK, H. G., DE JONG, K. P., PEETERS, P. M., JANSEN, P. L., SLOOFF, M. J., GOUW, A. S. & PORTE, R. J. 2004. Rapid increase of bile salt secretion is associated with bile duct injury after human liver transplantation. *J Hepatol,* 41, 1017-25.

GLAS, J., SEIDERER, J., FISCHER, D., TENGLER, B., PFENNIG, S., WETZKE, M., BEIGEL, F., OLSZAK, T., WEIDINGER, M., GOKE, B., OCHSENKUHN, T., FOLWACZNY, M., MULLER-MYHSOK, B., DIEGELMANN, J., CZAMARA, D. & BRAND, S. 2011. Pregnane X receptor (PXR/NR1I2) gene haplotypes modulate susceptibility to inflammatory bowel disease. *Inflammatory bowel diseases,* 17, 1917-24.

GOTO, M., TAKEI, Y., KAWANO, S., NAGANO, K., TSUJI, S., MASUDA, E., NISHIMURA, Y., OKUMURA, S., KASHIWAGI, T., FUSAMOTO, H. & ET AL. 1994. Endothelin-1 is involved in the pathogenesis of ischemia/reperfusion liver injury by hepatic microcirculatory disturbances. *Hepatology,* 19, 675-81.

GRACIA-SANCHO, J., CASILLAS-RAMIREZ, A. & PERALTA, C. 2015. Molecular pathways in protecting the liver from ischaemia/reperfusion injury: a 2015 update. *Clinical science,* 129, 345-62.

GRACIA-SANCHO, J., VILLARREAL, G., JR., ZHANG, Y., YU, J. X., LIU, Y., TULLIUS, S. G. & GARCIA-CARDENA, G. 2010. Flow cessation triggers endothelial dysfunction during organ cold storage conditions: strategies for pharmacologic intervention. *Transplantation,* 90, 142-9.

GRANT, A. G. & BILLING, B. H. 1977. The isolation and characterization of a bile ductule cell population from normal and bile-duct ligated rat livers. *British journal of experimental pathology,* 58, 301-10.

GREGERSON, H., JENSEN, S. L., MOODY, F. & SHOKOUH-AMIRI, M. 1996. *Essentials of Experimental Surgery: Gastroenterology*, Taylor & Francis.

GRIMES, D. A. & SCHULZ, K. F. 2002. An overview of clinical research: the lay of the land. *Lancet,* 359, 57-61.

GU, X., KE, S., LIU, D., SHENG, T., THOMAS, P. E., RABSON, A. B., GALLO, M. A., XIE, W. & TIAN, Y. 2006. Role of NF-kappaB in regulation of PXR-mediated gene expression: a mechanism for the suppression of cytochrome P-450 3A4 by proinflammatory agents. *The Journal of biological chemistry,* 281, 17882-9.

GUICHELAAR, M. M., BENSON, J. T., MALINCHOC, M., KROM, R. A., WIESNER, R. H. & CHARLTON, M. R. 2003. Risk factors for and clinical course of non-anastomotic biliary strictures after liver transplantation. *American journal of transplantation : official journal of the American Society of Transplantation and the American Society of Transplant Surgeons,* 3, 885-90.

GUO, G. L., MOFFIT, J. S., NICOL, C. J., WARD, J. M., ALEKSUNES, L. A., SLITT, A. L., KLIEWER, S. A., MANAUTOU, J. E. & GONZALEZ, F. J. 2004. Enhanced acetaminophen toxicity by activation of the pregnane X receptor. *Toxicological sciences : an official journal of the Society of Toxicology,* 82, 374-80.

HAHN, O., SZIJARTO, A., LOTZ, G., SCHAFF, Z., VIGVARY, Z., VALI, L. & KUPCSULIK, P. K. 2007. The effect of ischemic preconditioning prior to intraoperative radiotherapy on ischemic and on reperfused rat liver. *J Surg Res,* 142, 32-44.

HAMADA, T., DUARTE, S., TSUCHIHASHI, S., BUSUTTIL, R. W. & COITO, A. J. 2009. Inducible nitric oxide synthase deficiency impairs matrix metalloproteinase-9 activity and disrupts leukocyte migration in hepatic ischemia/reperfusion injury. *The American journal of pathology,* 174, 2265-77.

HARADA, H., BHARWANI, S., PAVLICK, K. P., KORACH, K. S. & GRISHAM, M. B. 2004. Estrogen receptor-alpha, sexual dimorphism and reduced-size liver ischemia and reperfusion injury in mice. *Pediatric research,* 55, 450-6.

HARADA, H., PAVLICK, K. P., HINES, I. N., HOFFMAN, J. M., BHARWANI, S., GRAY, L., WOLF, R. E. & GRISHAM, M. B. 2001. Selected contribution: Effects of gender on reduced-size liver ischemia and reperfusion injury. *Journal of applied physiology,* 91, 2816-22.

HARADA, K., SHIMODA, S., IKEDA, H., CHIBA, M., HSU, M., SATO, Y., KOBAYASHI, M., REN, X. S., OHTA, H., KASASHIMA, S., KAWASHIMA, A. & NAKANUMA, Y. 2011. Significance of periductal Langerhans cells and biliary epithelial cell-derived macrophage inflammatory protein-3alpha in the pathogenesis of primary biliary cirrhosis. *Liver international : official journal of the International Association for the Study of the Liver,* 31, 245-53.

HARADA, N., OKAJIMA, K. & UCHIBA, M. 2006. Dalteparin, a low molecular weight heparin, attenuates inflammatory responses and reduces ischemia-reperfusion-induced liver injury in rats. *Critical care medicine,* 34, 1883-91.

HARDY, K. J., TANCHEROEN, S. & SHULKES, A. 1995. Hepatic ischemia-reperfusion injury modification during liver surgery in rats: pretreatment with nifedipine or misoprostol. *Liver transplantation and surgery : official publication of the American Association for the Study of Liver Diseases and the International Liver Transplantation Society,* 1, 302-10.

HARIPARSAD, N., CHU, X., YABUT, J., LABHART, P., HARTLEY, D. P., DAI, X. & EVERS, R. 2009. Identification of pregnane-X receptor target genes and

coactivator and corepressor binding to promoter elements in human hepatocytes. *Nucleic acids research,* 37, 1160-73.

HAUGHTON, E. L., TUCKER, S. J., MAREK, C. J., DURWARD, E., LEEL, V., BASCAL, Z., MONAGHAN, T., KORUTH, M., COLLIE-DUGUID, E., MANN, D. A., TRIM, J. E. & WRIGHT, M. C. 2006. Pregnane X receptor activators inhibit human hepatic stellate cell transdifferentiation in vitro. *Gastroenterology,* 131, 194-209.

HAYASHI, H., CHAUDRY, I. H., CLEMENS, M. G. & BAUE, A. E. 1986. Hepatic ischemia models for determining the effects of ATP-MgCl2 treatment. *J Surg Res,* 40, 167-75.

HERTL, M., HARVEY, P. R., SWANSON, P. E., WEST, D. D., HOWARD, T. K., SHENOY, S. & STRASBERG, S. M. 1995. Evidence of preservation injury to bile ducts by bile salts in the pig and its prevention by infusions of hydrophilic bile salts. *Hepatology,* 21, 1130-7.

HERTL, M., HERTL, M. C., KLUTH, D. & BROELSCH, C. E. 2000. Hydrophilic bile salts protect bile duct epithelium during cold preservation: a scanning electron microscopy study. *Liver Transpl,* 6, 207-12.

HIRASAWA, H., CHAUNDRY, I. H. & BAUE, A. E. 1978. Improved hepatic function and survival with adenosine triphosphate-magnesium chloride after hepatic ischemia. *Surgery,* 83, 655-62.

HISAMA, N., YAMAGUCHI, Y., ISHIKO, T., MIYANARI, N., ICHIGUCHI, O., GOTO, M., MORI, K., WATANABE, K., KAWAMURA, K., TSURUFUJI, S. & OGAWA, M. 1996. Kupffer cell production of cytokine-induced neutrophil chemoattractant following ischemia/reperfusion injury in rats. *Hepatology,* 24, 1193-8.

HOEKSTRA, H., PORTE, R. J., TIAN, Y., JOCHUM, W., STIEGER, B., MORITZ, W., SLOOFF, M. J., GRAF, R. & CLAVIEN, P. A. 2006. Bile salt toxicity aggravates cold ischemic injury of bile ducts after liver transplantation in Mdr2+/- mice. *Hepatology,* 43, 1022-31.

HU, D., WANG, Y., CHEN, Z., MA, Z., YOU, Q., ZHANG, X., LIANG, Q., TAN, H., XIAO, C., TANG, X. & GAO, Y. 2015. The protective effect of piperine on dextran sulfate sodium induced inflammatory bowel disease and its relation with pregnane X receptor activation. *Journal of ethnopharmacology,* 169, 109-23.

HU, D., WANG, Y., CHEN, Z., MA, Z., YOU, Q., ZHANG, X., ZHOU, T., XIAO, Y., LIANG, Q., TAN, H., XIAO, C., TANG, X., ZHANG, B. & GAO, Y. 2014. Artemisinin protects against dextran sulfate-sodium-induced inflammatory bowel disease, which is associated with activation of the pregnane X receptor. *European journal of pharmacology,* 738, 273-84.

HUANG, H., EVANKOVICH, J., YAN, W., NACE, G., ZHANG, L., ROSS, M., LIAO, X., BILLIAR, T., XU, J., ESMON, C. T. & TSUNG, A. 2011. Endogenous histones function as alarmins in sterile inflammatory liver injury through Toll-like receptor 9 in mice. *Hepatology,* 54, 999-1008.

HUANG, H., TOHME, S., AL-KHAFAJI, A. B., TAI, S., LOUGHRAN, P., CHEN, L., WANG, S., KIM, J., BILLIAR, T., WANG, Y. & TSUNG, A. 2015. Damage-associated molecular pattern-activated neutrophil extracellular trap exacerbates sterile inflammatory liver injury. *Hepatology,* 62, 600-14.

HUET, P. M., NAGAOKA, M. R., DESBIENS, G., TARRAB, E., BRAULT, A., BRALET, M. P. & BILODEAU, M. 2004. Sinusoidal endothelial cell and hepatocyte death following cold ischemia-warm reperfusion of the rat liver. *Hepatology,* 39, 1110-9.

HUGUET, C., GAVELLI, A., CHIECO, P. A., BONA, S., HARB, J., JOSEPH, J. M., JOBARD, J., GRAMAGLIA, M. & LASSERRE, M. 1992. Liver ischemia for hepatic resection: where is the limit? ***Surgery,*** **111, 251-9.**

IANNELLI, A., DE SOUSA, G., ZUCCHINI, N., SAINT-PAUL, M. C., GUGENHEIM, J. & RAHMANI, R. 2011. Anti-apoptotic pro-survival effect of clotrimazole in a normothermic ischemia reperfusion injury animal model. ***J Surg Res,*** **171, 101-7.**

ICHIKI, A., MIYAZAKI, T., NODERA, M., SUZUKI, H. & YANAGISAWA, H. 2008. Ascorbate inhibits apoptosis of Kupffer cells during warm ischemia/reperfusion injury. ***Hepato-gastroenterology,*** **55, 338-44.**

IHUNNAH, C. A., JIANG, M. & XIE, W. 2011. Nuclear receptor PXR, transcriptional circuits and metabolic relevance. ***Biochimica et biophysica acta,*** **1812, 956-63.**

IKEDA, T., YANAGA, K., KISHIKAWA, K., KAKIZOE, S., SHIMADA, M. & SUGIMACHI, K. 1992. Ischemic injury in liver transplantation: difference in injury sites between warm and cold ischemia in rats. ***Hepatology,*** **16, 454-61.**

IREDALE, J. P., BENYON, R. C., PICKERING, J., MCCULLEN, M., NORTHROP, M., PAWLEY, S., HOVELL, C. & ARTHUR, M. J. 1998. Mechanisms of spontaneous resolution of rat liver fibrosis. Hepatic stellate cell apoptosis and reduced hepatic expression of metalloproteinase inhibitors. ***The Journal of clinical investigation,*** **102, 538-49.**

ISHII, M., VROMAN, B. & LARUSSO, N. F. 1989. Isolation and morphologic characterization of bile duct epithelial cells from normal rat liver. ***Gastroenterology,*** **97, 1236-47.**

ISSE, K., HARADA, K., ZEN, Y., KAMIHIRA, T., SHIMODA, S., HARADA, M. & NAKANUMA, Y. 2005. Fractalkine and CX3CR1 are involved in the recruitment of intraepithelial lymphocytes of intrahepatic bile ducts. ***Hepatology,*** **41, 506-16.**

JAESCHKE, H. 2002. Xanthine oxidase-induced oxidant stress during hepatic ischemia-reperfusion: are we coming full circle after 20 years? ***Hepatology,*** **36, 761-3.**

JAESCHKE, H., FARHOOD, A., BAUTISTA, A. P., SPOLARICS, Z. & SPITZER, J. J. 1993. Complement activates Kupffer cells and neutrophils during reperfusion after hepatic ischemia. ***The American journal of physiology,*** **264, G801-9.**

JAY, C., LADNER, D., WANG, E., LYUKSEMBURG, V., KANG, R., CHANG, Y., FEINGLASS, J., HOLL, J. L., ABECASSIS, M. & SKARO, A. I. 2011a. A comprehensive risk assessment of mortality following donation after cardiac death liver transplant - an analysis of the national registry. ***Journal of hepatology,*** **55, 808-13.**

JAY, C. L., LYUKSEMBURG, V., LADNER, D. P., WANG, E., CAICEDO, J. C., HOLL, J. L., ABECASSIS, M. M. & SKARO, A. I. 2011b. Ischemic cholangiopathy after controlled donation after cardiac death liver transplantation: a meta-analysis. ***Annals of Surgery,*** **253, 259-64.**

JIMENEZ-GALANES, S., MENEU-DIAZ, M. J., ELOLA-OLASO, A. M., PEREZ-SABORIDO, B., YILIAM, F. S., CALVO, A. G., USERA, M. A., GONZALEZ, M. C., GONZALEZ, J. C. & GONZALEZ, E. M. 2009. Liver transplantation using uncontrolled non-heart-beating donors under normothermic extracorporeal membrane oxygenation. ***Liver transplantation : official publication of the American Association for the Study of Liver Diseases and the International Liver Transplantation Society,*** **15, 1110-8.**

JOINT FORMULARY COMMITTEE 2015. ***British national formulary*****, London : British Medical Association : Pharmaceutical Society of Great Britain.**

JONKER, J. W., LIDDLE, C. & DOWNES, M. 2012. FXR and PXR: potential therapeutic targets in cholestasis. ***The Journal of steroid biochemistry and molecular biology,*** **130, 147-58.**

JOPLIN, R. 1994. Isolation and culture of biliary epithelial cells. ***Gut,*** **35, 875-8.**

JOPLIN, R. & KACHILELE, S. 2009. Human intrahepatic biliary epithelial cell lineages: studies in vitro. ***Methods in molecular biology,*** **481, 193-206.**

JOPLIN, R., STRAIN, A. J. & NEUBERGER, J. M. 1989. Immuno-isolation and culture of biliary epithelial cells from normal human liver. ***In vitro cellular & developmental biology : journal of the Tissue Culture Association,*** **25, 1189-92.**

KACZMAREK, B., MANAS, M. D., JAQUES, B. C. & TALBOT, D. 2007. Ischemic cholangiopathy after liver transplantation from controlled non-heart-beating donors-a single-center experience. ***Transplantation Proceedings,*** **39, 2793-5.**

KAKIZAKI, S., TAKIZAWA, D., TOJIMA, H., YAMAZAKI, Y. & MORI, M. 2009. Xenobiotic-sensing nuclear receptors CAR and PXR as drug targets in cholestatic liver disease. ***Current drug targets,*** **10, 1156-1163.**

KAMIHIRA, T., SHIMODA, S., NAKAMURA, M., YOKOYAMA, T., TAKII, Y., KAWANO, A., HANDA, M., ISHIBASHI, H., GERSHWIN, M. E. & HARADA, M. 2005. Biliary epithelial cells regulate autoreactive T cells: implications for biliary-specific diseases. ***Hepatology,*** **41, 151-9.**

KAMINSKI, M., WIADERKIEWICZ, R. & SIEKIERSKA, E. 1997. Effect of chlorfenvinphos on rat liver subjected to ischemia and reperfusion. ***Przegl Lek,*** **54, 693-701.**

KANAZAWA, H., FUJIMOTO, Y., TERATANI, T., IWASAKI, J., KASAHARA, N., NEGISHI, K., TSURUYAMA, T., UEMOTO, S. & KOBAYASHI, E. 2011. Bone marrow-derived mesenchymal stem cells ameliorate hepatic ischemia reperfusion injury in a rat model. ***PloS one,*** **6, e19195.**

KARATZAS, T., NERI, A. A., BAIBAKI, M. E. & DONTAS, I. A. 2014. Rodent models of hepatic ischemia-reperfusion injury: time and percentage-related pathophysiological mechanisms. ***The Journal of surgical research,*** **191, 399-412.**

KARWINSKI, W., BOLANN, B., ULVIK, R., FARSTAD, M. & SOREIDE, O. 1993. Normothermic liver ischemia in rats: xanthine oxidase is not the main source of oxygen free radicals. ***Research in experimental medicine. Zeitschrift fur die gesamte experimentelle Medizin einschliesslich experimenteller Chirurgie,*** **193, 275-83.**

KAWAMOTO, M., MATSUNAMI, T., ERTL, R. F., FUKUDA, Y., OGAWA, M., SPURZEM, J. R., YAMANAKA, N. & RENNARD, S. I. 1997. Selective migration of alpha-smooth muscle actin-positive myofibroblasts toward fibronectin in the Boyden's blindwell chamber. ***Clinical science,*** **93, 355-62.**

KAWANA, K., IKUTA, T., KOBAYASHI, Y., GOTOH, O., TAKEDA, K. & KAWAJIRI, K. 2003. Molecular mechanism of nuclear translocation of an orphan nuclear receptor, SXR. ***Molecular pharmacology,*** **63, 524-31.**

KAYA, H., KARADEMIR, S., TUNCEL, P., ASTARCIOGLU, H., SAGOL, O. & ASTARCIOGLU, I. 2008. The comparative effects of total hepatic vascular isolation techniques performed at different durations in rat. ***J Surg Res,*** **145, 223-8.**

KERAMARIS, N. C., KANAKARIS, N. K., TZIOUPIS, C., KONTAKIS, G. & GIANNOUDIS, P. V. 2008. Translational research: from benchside to bedside. *Injury,* 39, 643-50.

KIM, J. S., HE, L. & LEMASTERS, J. J. 2003. Mitochondrial permeability transition: a common pathway to necrosis and apoptosis. *Biochemical and biophysical research communications,* 304, 463-70.

KIM, J. S., WANG, J. H. & LEMASTERS, J. J. 2012. Mitochondrial permeability transition in rat hepatocytes after anoxia/reoxygenation: role of Ca2+-dependent mitochondrial formation of reactive oxygen species. *American journal of physiology. Gastrointestinal and liver physiology,* 302, G723-31.

KIM, W. R., FLAMM, S. L., DI BISCEGLIE, A. M. & BODENHEIMER, H. C. 2008. Serum activity of alanine aminotransferase (ALT) as an indicator of health and disease. *Hepatology,* 47, 1363-70.

KING, C. R., XIAO, M., YU, J., MINTON, M. R., ADDLEMAN, N. J., VAN BOOVEN, D. J., KWOK, P. Y., MCLEOD, H. L. & MARSH, S. 2007. Identification of NR1I2 genetic variation using resequencing. *European journal of clinical pharmacology,* 63, 547-54.

KITAMURA, Y., WASHINO, Y., KOGA, E., ITO, A., KAWAGOE, M., NAKAZAKI, C., KISO, K., ICHI, I., MATSURA, T. & KOJO, S. 2010. Oxidative stress in the ischemic and non-ischemic parts of the rat liver after two-thirds ischemia/reperfusion. *Biosci Biotechnol Biochem,* 74, 979-83.

KLIEWER, S. A., GOODWIN, B. & WILLSON, T. M. 2002. The nuclear pregnane X receptor: a key regulator of xenobiotic metabolism. *Endocrine reviews,* 23, 687-702.

KLIEWER, S. A., MOORE, J. T., WADE, L., STAUDINGER, J. L., WATSON, M. A., JONES, S. A., MCKEE, D. D., OLIVER, B. B., WILLSON, T. M., ZETTERSTROM, R. H., PERLMANN, T. & LEHMANN, J. M. 1998. An orphan nuclear receptor activated by pregnanes defines a novel steroid signaling pathway. *Cell,* 92, 73-82.

KNOOP, M., SCHNOY, N., KECK, H. & NEUHAUS, P. 1993. Morphological changes of human common bile ducts after extended cold preservation. *Transplantation,* 56, 1572-3.

KODAMA, S., KOIKE, C., NEGISHI, M. & YAMAMOTO, Y. 2004. Nuclear receptors CAR and PXR cross talk with FOXO1 to regulate genes that encode drug-metabolizing and gluconeogenic enzymes. *Molecular and cellular biology,* 24, 7931-40.

KODAMA, S., MOORE, R., YAMAMOTO, Y. & NEGISHI, M. 2007. Human nuclear pregnane X receptor cross-talk with CREB to repress cAMP activation of the glucose-6-phosphatase gene. *The Biochemical journal,* 407, 373-81.

KOGURE, K., ISHIZAKI, M., NEMOTO, M., KUWANO, H. & MAKUUCHI, M. 1999. A comparative study of the anatomy of rat and human livers. *Journal of hepato-biliary-pancreatic surgery,* 6, 171-5.

KONERU, B., REDDY, M. C., DELA TORRE, A. N., PATEL, D., IPPOLITO, T. & FERRANTE, R. J. 1995. Studies of hepatic warm ischemia in the obese Zucker rat. *Transplantation,* 59, 942-6.

KOONEN, D. P., JACOBS, R. L., FEBBRAIO, M., YOUNG, M. E., SOLTYS, C. L., ONG, H., VANCE, D. E. & DYCK, J. R. 2007. Increased hepatic CD36 expression contributes to dyslipidemia associated with diet-induced obesity. *Diabetes,* 56, 2863-71.

KUKAN, M. & HADDAD, P. S. 2001. Role of hepatocytes and bile duct cells in preservation-reperfusion injury of liver grafts. *Liver transplantation :*

official publication of the American Association for the Study of Liver Diseases and the International Liver Transplantation Society, 7, 381-400.
KUKAN, M., VAJDOVA, K., HORECKY, J., NAGYOVA, A., MEHENDALE, H. M. & TRNOVEC, T. 1997. Effects of blockade of Kupffer cells by gadolinium chloride on hepatobiliary function in cold ischemia-reperfusion injury of rat liver. *Hepatology,* 26, 1250-7.
LAEMMLI, U. K. 1970. Cleavage of structural proteins during the assembly of the head of bacteriophage T4. *Nature,* 227, 680-5.
LANGLE, F., ROTH, E., STEININGER, R., WINKLER, S. & MUHLBACHER, F. 1995. Arginase release following liver reperfusion. Evidence of hemodynamic action of arginase infusions. *Transplantation,* 59, 1542-9.
LECLUYSE, E. L. 2001. Human hepatocyte culture systems for the in vitro evaluation of cytochrome P450 expression and regulation. *European journal of pharmaceutical sciences : official journal of the European Federation for Pharmaceutical Sciences,* 13, 343-68.
LECLUYSE, E. L., WITEK, R. P., ANDERSEN, M. E. & POWERS, M. J. 2012. Organotypic liver culture models: meeting current challenges in toxicity testing. *Critical reviews in toxicology,* 42, 501-48.
LEE, J. H., ZHOU, J. & XIE, W. 2008. PXR and LXR in hepatic steatosis: a new dog and an old dog with new tricks. *Molecular pharmaceutics,* 5, 60-6.
LEHMANN, J. M., MCKEE, D. D., WATSON, M. A., WILLSON, T. M., MOORE, J. T. & KLIEWER, S. A. 1998. The human orphan nuclear receptor PXR is activated by compounds that regulate CYP3A4 gene expression and cause drug interactions. *The Journal of clinical investigation,* 102, 1016-23.
LEMASTERS, J. J., NIEMINEN, A. L., QIAN, T., TROST, L. C., ELMORE, S. P., NISHIMURA, Y., CROWE, R. A., CASCIO, W. E., BRADHAM, C. A., BRENNER, D. A. & HERMAN, B. 1998. The mitochondrial permeability transition in cell death: a common mechanism in necrosis, apoptosis and autophagy. *Biochimica et biophysica acta,* 1366, 177-96.
LEMASTERS, J. J., THERUVATH, T. P., ZHONG, Z. & NIEMINEN, A. L. 2009. Mitochondrial calcium and the permeability transition in cell death. *Biochimica et biophysica acta,* 1787, 1395-401.
LENTINE, K. L. & SCHNITZLER, M. A. 2011. The economic impact of addressing the organ shortage with clinically high-risk allografts. *Missouri medicine,* 108, 275-9.
LENTSCH, A. B., YOSHIDOME, H., CHEADLE, W. G., MILLER, F. N. & EDWARDS, M. J. 1998. Chemokine involvement in hepatic ischemia/reperfusion injury in mice: roles for macrophage inflammatory protein-2 and Kupffer cells. *Hepatology,* 27, 507-12.
LI, G. L., LIN, H. M., LONG, T. Z., LV, L. H., YU, J. D., HUANG, Y. H., MIN, J. & WAN, Y. L. 2011. High incidence of biliary complications in rat liver transplantation: can we avoid it? *World journal of gastroenterology : WJG,* 17, 3140-4.
LI, T., YU, R. T., ATKINS, A. R., DOWNES, M., TUKEY, R. H. & EVANS, R. M. 2012. Targeting the pregnane X receptor in liver injury. *Expert opinion on therapeutic targets,* 16, 1075-83.
LICHTMAN, S. N. & LEMASTERS, J. J. 1999. Role of cytokines and cytokine-producing cells in reperfusion injury to the liver. *Seminars in liver disease,* 19, 171-87.

LINBERG, R., JOHNSON, M., NHO, K., GILBERT, C. & SHORR, R. 1994. Normal oxygen tension restored in the ischemic rat liver model by PEG-hemoglobin. ***Artif Cells Blood Substit Immobil Biotechnol,*** **22, 805-12.**

LIU, A., DIRSCH, O., FANG, H., SUN, J., JIN, H., DONG, W. & DAHMEN, U. 2011a. HMGB1 in ischemic and non-ischemic liver after selective warm ischemia/reperfusion in rat. ***Histochem Cell Biol,*** **135, 443-52.**

LIU, D. L., JEPPSSON, B., HAKANSSON, C. H. & ODSELIUS, R. 1996. Multiple-system organ damage resulting from prolonged hepatic inflow interruption. ***Arch Surg,*** **131, 442-7.**

LIU, J., CHEN, Z., CHEN, H., HOU, Y., LU, W., HE, J., TONG, H., ZHOU, Y. & CAI, W. 2017. Genetic Polymorphisms Contribute to the Individual Variations of Imatinib Mesylate Plasma Levels and Adverse Reactions in Chinese GIST Patients. ***International journal of molecular sciences,*** **18.**

LIU, L., JEPPSSON, B. & BENGMARK, S. 1992. Bacterial Translocation into Portal Blood from the Gut during Portal Triad Occlusion. ***Digestive Surgery,*** **9, 95-101.**

LIU, Y., SUN, X. J., LIU, J., KANG, Z. M. & DENG, X. M. 2011b. Heme oxygenase-1 could mediate the protective effects of hyperbaric oxygen preconditioning against hepatic ischemia-reperfusion injury in rats. ***Clinical and experimental pharmacology & physiology,*** **38, 675-82.**

LOWRY, O. H., ROSEBROUGH, N. J., FARR, A. L. & RANDALL, R. J. 1951. Protein measurement with the Folin phenol reagent. ***The Journal of biological chemistry,*** **193, 265-75.**

MADRAHIMOV, N. 2006. ***Vascular anatomy of the rat liver and its implications for extended hepatectomy and the determination of the minimal liver mass.*** **Universität Duisburg-Essen, Medizinische Fakultät» Universitätsklinikum Essen» Klinik für Allgemeinchirurgie, Viszeral-und Transplantationschirurgie.**

MADRAHIMOV, N., DIRSCH, O., BROELSCH, C. & DAHMEN, U. 2006. Marginal hepatectomy in the rat: from anatomy to surgery. ***Annals of surgery,*** **244, 89-98.**

MAGLICH, J. M., STOLTZ, C. M., GOODWIN, B., HAWKINS-BROWN, D., MOORE, J. T. & KLIEWER, S. A. 2002. Nuclear pregnane x receptor and constitutive androstane receptor regulate overlapping but distinct sets of genes involved in xenobiotic detoxification. ***Molecular pharmacology,*** **62, 638-46.**

MAN, K., NG, K. T., LEE, T. K., LO, C. M., SUN, C. K., LI, X. L., ZHAO, Y., HO, J. W. & FAN, S. T. 2005. FTY720 attenuates hepatic ischemia-reperfusion injury in normal and cirrhotic livers. ***American journal of transplantation : official journal of the American Society of Transplantation and the American Society of Transplant Surgeons,*** **5, 40-9.**

MANCINELLI, R., GLASER, S., FRANCIS, H., CARPINO, G., FRANCHITTO, A., VETUSCHI, A., SFERRA, R., PANNARALE, L., VENTER, J., MENG, F., ALPINI, G., ONORI, P. & GAUDIO, E. 2015. Ischemia reperfusion of the hepatic artery induces the functional damage of large bile ducts by changes in the expression of angiogenic factors. ***Am J Physiol Gastrointest Liver Physiol,*** **309, G865-73.**

MAREK, C. J., TUCKER, S. J., KONSTANTINOU, D. K., ELRICK, L. J., HAEFNER, D., SIGALAS, C., MURRAY, G. I., GOODWIN, B. & WRIGHT, M. C. 2005. Pregnenolone-16alpha-carbonitrile inhibits rodent liver fibrogenesis via PXR (pregnane X receptor)-dependent and PXR-independent mechanisms. ***The Biochemical journal,*** **387, 601-8.**

MARTINS, P. N. & NEUHAUS, P. 2007. Surgical anatomy of the liver, hepatic vasculature and bile ducts in the rat. ***Liver international : official journal of the International Association for the Study of the Liver,*** **27, 384-92.**

MASSIP-SALCEDO, M., ROSELLO-CATAFAU, J., PRIETO, J., AVILA, M. A. & PERALTA, C. 2007. The response of the hepatocyte to ischemia. ***Liver international : official journal of the International Association for the Study of the Liver,*** **27, 6-16.**

MASUYAMA, H., NAKAMURA, K., NOBUMOTO, E. & HIRAMATSU, Y. 2016. Inhibition of pregnane X receptor pathway contributes to the cell growth inhibition and apoptosis of anticancer agents in ovarian cancer cells. ***International journal of oncology,*** **49, 1211-20.**

MASUYAMA, H., NAKATSUKASA, H., TAKAMOTO, N. & HIRAMATSU, Y. 2007. Down-regulation of pregnane X receptor contributes to cell growth inhibition and apoptosis by anticancer agents in endometrial cancer cells. ***Molecular pharmacology,*** **72, 1045-53.**

MASYUK, T. V., RITMAN, E. L. & LARUSSO, N. F. 2003. Hepatic artery and portal vein remodeling in rat liver: vascular response to selective cholangiocyte proliferation. ***Am J Pathol,*** **162, 1175-82.**

MATSUI, K. & KOJIMA, M. 1991. Effect of phosphoenolpyruvate on energy metabolism of ischemic liver in anesthetized rats--31P-MRS study. ***Biochem Int,*** **24, 1025-31.**

MATSUMOTO, K., FUJII, H., MICHALOPOULOS, G., FUNG, J. J. & DEMETRIS, A. J. 1994. Human biliary epithelial cells secrete and respond to cytokines and hepatocyte growth factors in vitro: interleukin-6, hepatocyte growth factor and epidermal growth factor promote DNA synthesis in vitro. ***Hepatology,*** **20, 376-82.**

MBATCHI, L. C., SCHMITT, A., THOMAS, F., CAZAUBON, Y., ROBERT, J., LUMBROSO, S., BROUILLET, J. P., POURQUIER, P., CHATELUT, E., BOYER, J. C. & EVRARD, A. 2015. Polymorphisms in SLCO1B3 and NR1I2 as genetic determinants of hematotoxicity of carboplatin and paclitaxel combination. ***Pharmacogenomics,*** **16, 1439-50.**

MCKEOWN, C. M., EDWARDS, V., PHILLIPS, M. J., HARVEY, P. R., PETRUNKA, C. N. & STRASBERG, S. M. 1988. Sinusoidal lining cell damage: the critical injury in cold preservation of liver allografts in the rat. ***Transplantation,*** **46, 178-91.**

MCMASTER, P. D. 1922. Do Species Lacking a Gall Bladder Possess Its Functional Equivalent? ***The Journal of experimental medicine,*** **35, 127-40.**

MENCARELLI, A., D'AMORE, C., RENGA, B., CIPRIANI, S., CARINO, A., SEPE, V., PERISSUTTI, E., D'AURIA, M. V., ZAMPELLA, A., DISTRUTTI, E. & FIORUCCI, S. 2013. Solomonsterol A, a marine pregnane-X-receptor agonist, attenuates inflammation and immune dysfunction in a mouse model of arthritis. ***Marine drugs,*** **12, 36-53.**

MENDES-BRAZ, M., ELIAS-MIRO, M., JIMENEZ-CASTRO, M. B., CASILLAS-RAMIREZ, A., RAMALHO, F. S. & PERALTA, C. 2012. The current state of knowledge of hepatic ischemia-reperfusion injury based on its study in experimental models. ***Journal of biomedicine & biotechnology,*** **2012, 298657.**

MERION, R. M., PELLETIER, S. J., GOODRICH, N., ENGLESBE, M. J. & DELMONICO, F. L. 2006. Donation after cardiac death as a strategy to increase deceased donor liver availability. ***Annals of Surgery,*** **244, 555-62.**

MEYER ZU SCHWABEDISSEN, H. E., TIRONA, R. G., YIP, C. S., HO, R. H. & KIM, R. B. 2008. Interplay between the nuclear receptor pregnane X receptor and the uptake transporter organic anion transporter polypeptide 1A2 selectively enhances estrogen effects in breast cancer. *Cancer research,* 68, 9338-47.

MILANI, S., HERBST, H., SCHUPPAN, D., STEIN, H. & SURRENTI, C. 1991. Transforming growth factors beta 1 and beta 2 are differentially expressed in fibrotic liver disease. *The American journal of pathology,* 139, 1221-9.

MOCHIZUKI, K., OHNO, Y., KANEMATSU, T., SAKURAI-YAMASHITA, Y., NIWA, M., HISHIKAWA, Y. & KOJI, T. 2007. Possible protection of sinusoidal endothelial cells by endothelin B receptor during hepatic warm ischemia-reperfusion. *Surgery today,* 37, 460-7.

MONTALVO-JAVE, E. E., ESCALANTE-TATTERSFIELD, T., ORTEGA-SALGADO, J. A., PINA, E. & GELLER, D. A. 2008. Factors in the pathophysiology of the liver ischemia-reperfusion injury. *The Journal of surgical research,* 147, 153-9.

MONTERO, E. F., QUIREZE, C., JR. & D'OLIVEIRA, D. M. 2005. Bile duct exclusion from selective vascular inflow occlusion in rat liver: role of ischemic preconditioning and N-acetylcysteine on hepatic reperfusion injury. *Transplant Proc,* 37, 425-7.

MOON, J. Y., CHANG, B. C., LEE, K. E., BANG, J. S. & GWAK, H. S. 2015. Effects of Pregnane X Receptor Genetic Polymorphisms on Stable Warfarin Doses. *Journal of cardiovascular pharmacology and therapeutics,* 20, 532-8.

MOORE, J. T. & KLIEWER, S. A. 2000. Use of the nuclear receptor PXR to predict drug interactions. *Toxicology,* 153, 1-10.

MOORE, L. B., PARKS, D. J., JONES, S. A., BLEDSOE, R. K., CONSLER, T. G., STIMMEL, J. B., GOODWIN, B., LIDDLE, C., BLANCHARD, S. G., WILLSON, T. M., COLLINS, J. L. & KLIEWER, S. A. 2000. Orphan nuclear receptors constitutive androstane receptor and pregnane X receptor share xenobiotic and steroid ligands. *The Journal of biological chemistry,* 275, 15122-7.

MORLAND, C. M., FEAR, J., MCNAB, G., JOPLIN, R. & ADAMS, D. H. 1997. Promotion of leukocyte transendothelial cell migration by chemokines derived from human biliary epithelial cells in vitro. *Proceedings of the Association of American Physicians,* 109, 372-82.

MOURAD, M. M., ALGARNI, A., LIOSSIS, C. & BRAMHALL, S. R. 2014. Aetiology and risk factors of ischaemic cholangiopathy after liver transplantation. *World journal of gastroenterology,* 20, 6159-69.

MOYA, M., GOMEZ-LECHON, M. J., CASTELL, J. V. & JOVER, R. 2010. Enhanced steatosis by nuclear receptor ligands: a study in cultured human hepatocytes and hepatoma cells with a characterized nuclear receptor expression profile. *Chemico-biological interactions,* 184, 376-87.

MULLICAN, S. E., DISPIRITO, J. R. & LAZAR, M. A. 2013. The orphan nuclear receptors at their 25-year reunion. *Journal of molecular endocrinology,* 51, T115-40.

NAKAMITSU, A., HIYAMA, E., IMAMURA, Y., MATSUURA, Y. & YOKOYAMA, T. 2001. Kupffer cell function in ischemic and nonischemic livers after hepatic partial ischemia/reperfusion. *Surg Today,* 31, 140-8.

NAKAMURA, K., MOORE, R., NEGISHI, M. & SUEYOSHI, T. 2007. Nuclear pregnane X receptor cross-talk with FoxA2 to mediate drug-induced

regulation of lipid metabolism in fasting mouse liver. *The Journal of biological chemistry,* 282, 9768-76.

NC3RS/BBSRC/DEFRA/MRC/NERC/WELLCOME TRUST 2013. Responsibility in the use of animals in bioscience research: expectations of the major research councils and charitable funding bodies. London: NC3Rs.

NELSON, J. D., DENISENKO, O. & BOMSZTYK, K. 2006. Protocol for the fast chromatin immunoprecipitation (ChIP) method. *Nature protocols,* 1, 179-85.

NHSBT 2015. Organ donation and transplantation. Activity report 2014/2015.

NI, H., SU, B., PAN, L., LI, X., ZHU, X. & CHEN, X. 2015. Functional variants inPXRare associated with colorectal cancer susceptibility in Chinese populations. *Cancer epidemiology,* 39, 972-7.

NIKOLENKO IU, V. & KRASNOV, A. N. 2007. [Nuclear receptors: structure and mechanisms of action]. *Genetika,* 43, 308-16.

NISHIDA, S., NAKAMURA, N., KADONO, J., KOMOKATA, T., SAKATA, R., MADARIAGA, J. R. & TZAKIS, A. G. 2006. Intrahepatic biliary strictures after liver transplantation. *J Hepatobiliary Pancreat Surg,* 13, 511-6.

NIU, Y., WANG, Z., HUANG, H., ZHONG, S., CAI, W., XIE, Y. & SHI, G. 2014. Activated pregnane X receptor inhibits cervical cancer cell proliferation and tumorigenicity by inducing G2/M cell-cycle arrest. *Cancer letters,* 347, 88-97.

NOACK, K., BRONK, S. F., KATO, A. & GORES, G. J. 1993. The greater vulnerability of bile duct cells to reoxygenation injury than to anoxia. Implications for the pathogenesis of biliary strictures after liver transplantation. *Transplantation,* 56, 495-500.

NORTHOVER, J. M. & TERBLANCHE, J. 1979. A new look at the arterial supply of the bile duct in man and its surgical implications. *Br J Surg,* 66, 379-84.

NUCLEAR RECEPTORS NOMENCLATURE COMMITTEE 1999. A unified nomenclature system for the nuclear receptor superfamily. *Cell,* 97, 161-3.

NYKONENKO, A., VAVRA, P. & ZONCA, P. 2017. Anatomic Peculiarities of Pig and Human Liver. *Experimental and clinical transplantation : official journal of the Middle East Society for Organ Transplantation,* 15, 21-26.

OH, C. K., SAWYER, R. G., PELLETIER, S. J., PRUETT, T. L. & SANFEY, H. A. 2004. Independent predictors for primary non-function after liver transplantation. *Yonsei medical journal,* 45, 1155-61.

OLIVEIRA, C. P., LOPASSO, F. P., LAURINDO, F. R., LEITAO, R. M. & LAUDANNA, A. A. 2001. Protection against liver ischemia-reperfusion injury in rats by silymarin or verapamil. *Transplantation proceedings,* 33, 3010-4.

OLTHOFF, K. M., KULIK, L., SAMSTEIN, B., KAMINSKI, M., ABECASSIS, M., EMOND, J., SHAKED, A. & CHRISTIE, J. D. 2010. Validation of a current definition of early allograft dysfunction in liver transplant recipients and analysis of risk factors. *Liver transplantation : official publication of the American Association for the Study of Liver Diseases and the International Liver Transplantation Society,* 16, 943-9.

OMENETTI, A., PORRELLO, A., JUNG, Y., YANG, L., POPOV, Y., CHOI, S. S., WITEK, R. P., ALPINI, G., VENTER, J., VANDONGEN, H. M., SYN, W. K., BARONI, G. S., BENEDETTI, A., SCHUPPAN, D. & DIEHL, A. M. 2008. Hedgehog signaling regulates epithelial-mesenchymal transition during

biliary fibrosis in rodents and humans. *The Journal of clinical investigation,* 118, 3331-42.

OP DEN DRIES, S., SUTTON, M. E., LISMAN, T. & PORTE, R. J. 2011. Protection of bile ducts in liver transplantation: looking beyond ischemia. *Transplantation,* 92, 373-9.

OTERO, A., GOMEZ-GUTIERREZ, M., SUAREZ, F., ARNAL, F., FERNANDEZ-GARCIA, A., AGUIRREZABALAGA, J., GARCIA-BUITRON, J., ALVAREZ, J. & MANEZ, R. 2003. Liver transplantation from Maastricht category 2 non-heart-beating donors. *Transplantation,* 76, 1068-73.

PALLADINI, G., FERRIGNO, A., RIZZO, V., BONCOMPAGNI, E., RICHELMI, P., FREITAS, I., PERLINI, S. & VAIRETTI, M. 2012. Lobe-specific heterogeneity and matrix metalloproteinase activation after ischemia/reperfusion injury in rat livers. *Toxicologic pathology,* 40, 722-30.

PALMEIRA, C. M. & ROLO, A. P. 2004. Mitochondrially-mediated toxicity of bile acids. *Toxicology,* 203, 1-15.

PAVEK, P. 2016. Pregnane X Receptor (PXR)-Mediated Gene Repression and Cross-Talk of PXR with Other Nuclear Receptors via Coactivator Interactions. *Frontiers in pharmacology,* 7, 456.

PAWLAK, M., LEFEBVRE, P. & STAELS, B. 2012. General molecular biology and architecture of nuclear receptors. *Current topics in medicinal chemistry,* 12, 486-504.

PERALTA, C., JIMENEZ-CASTRO, M. B. & GRACIA-SANCHO, J. 2013. Hepatic ischemia and reperfusion injury: effects on the liver sinusoidal milieu. *Journal of hepatology,* 59, 1094-106.

PERSSON, K. P., EKEHED, S., OTTER, C., LUTZ, E. S., MCPHEAT, J., MASIMIREMBWA, C. M. & ANDERSSON, T. B. 2006. Evaluation of human liver slices and reporter gene assays as systems for predicting the cytochrome p450 induction potential of drugs in vivo in humans. *Pharmaceutical research,* 23, 56-69.

PORTMANN, B. & ZEN, Y. 2012. Inflammatory disease of the bile ducts-cholangiopathies: liver biopsy challenge and clinicopathological correlation. *Histopathology,* 60, 236-48.

PRAKASH, C., ZUNIGA, B., SONG, C. S., JIANG, S., CROPPER, J., PARK, S. & CHATTERJEE, B. 2015. Nuclear Receptors in Drug Metabolism, Drug Response and Drug Interactions. *Nuclear receptor research,* 2.

PRATAP, A., PANAKANTI, R., YANG, N., LAKSHMI, R., MODANLOU, K. A., EASON, J. D. & MAHATO, R. I. 2011. Cyclopamine attenuates acute warm ischemia reperfusion injury in cholestatic rat liver: hope for marginal livers. *Molecular pharmaceutics,* 8, 958-68.

PRINGLE, J. H. 1908. V. Notes on the Arrest of Hepatic Hemorrhage Due to Trauma. *Annals of surgery,* 48, 541-9.

PRONOBESH, C., DAGAGI, A. V., PALLAB, C. & KUMAR, W. A. 2008. Protective role of the calcium channel blocker amlodipine against mitochondrial injury in ischemia and reperfusion injury of rat liver. *Acta pharmaceutica,* 58, 421-8.

QIU, Z., CERVANTES, J. L., CICEK, B. B., MUKHERJEE, S., VENKATESH, M., MAHER, L. A., SALAZAR, J. C., MANI, S. & KHANNA, K. M. 2016. Pregnane X Receptor Regulates Pathogen-Induced Inflammation and Host Defense against an Intracellular Bacterial Infection through Toll-like Receptor 4. *Scientific reports,* 6, 31936.

RAMM, G. A. 2011. Anti-chemokine therapy for the treatment of hepatic fibrosis: an attractive approach. *Hepatology,* 54, 354-8.

RANA, M., DEVI, S., GOURINATH, S., GOSWAMI, R. & TYAGI, R. K. 2016. A comprehensive analysis and functional characterization of naturally occurring non-synonymous variants of nuclear receptor PXR. *Biochimica et biophysica acta,* 1859, 1183-97.

RAUCY, J. L. & LASKER, J. M. 2010. Current in vitro high throughput screening approaches to assess nuclear receptor activation. *Current drug metabolism,* 11, 806-14.

RAUCY, J. L., MUELLER, L., DUAN, K., ALLEN, S. W., STROM, S. & LASKER, J. M. 2002. Expression and induction of CYP2C P450 enzymes in primary cultures of human hepatocytes. *The Journal of pharmacology and experimental therapeutics,* 302, 475-82.

REVATHIDEVI, S., SUDESH, R., VAISHNAVI, V., KALIYANASUNDARAM, M., MARYHELEN, K. G., SUKANYA, G. & MUNIRAJAN, A. K. 2016. Screening for the 3'UTR Polymorphism of the PXR Gene in South Indian Breast Cancer Patients and its Potential Role in Pharmacogenomics. *Asian Pacific journal of cancer prevention : APJCP,* 17, 3971-7.

RHEE, J. E., JUNG, S. E., SHIN, S. D., SUH, G. J., NOH, D. Y., YOUN, Y. K., OH, S. K. & CHOE, K. J. 2002. The effects of antioxidants and nitric oxide modulators on hepatic ischemic-reperfusion injury in rats. *J Korean Med Sci,* 17, 502-6.

ROMANI, F., VERTEMATI, M., FRANGI, M., ASENI, P., MONTI, R., CODEGHINI, A. & BELLI, L. 1988. Effect of superoxide dismutase on liver ischemia-reperfusion injury in the rat: a biochemical monitoring. *European surgical research. Europaische chirurgische Forschung. Recherches chirurgicales europeennes,* 20, 335-40.

ROSENFELD, J. M., VARGAS, R., JR., XIE, W. & EVANS, R. M. 2003. Genetic profiling defines the xenobiotic gene network controlled by the nuclear receptor pregnane X receptor. *Molecular endocrinology,* 17, 1268-82.

RUSCHITZKA, F., MEIER, P. J., TURINA, M., LUSCHER, T. F. & NOLL, G. 2000. Acute heart transplant rejection due to Saint John's wort. *Lancet,* 355, 548-9.

RUSSO, L., GRACIA-SANCHO, J., GARCIA-CALDERO, H., MARRONE, G., GARCIA-PAGAN, J. C., GARCIA-CARDENA, G. & BOSCH, J. 2012. Addition of simvastatin to cold storage solution prevents endothelial dysfunction in explanted rat livers. *Hepatology,* 55, 921-30.

RYU, C. H. & LEE, S. K. 2011. Biliary strictures after liver transplantation. *Gut and liver,* 5, 133-42.

SAIMAN, Y. & FRIEDMAN, S. L. 2012. The role of chemokines in acute liver injury. *Frontiers in physiology,* 3, 213.

SANGER, C., SCHENK, A., SCHWEN, L. O., WANG, L., GREMSE, F., ZAFARNIA, S., KIESSLING, F., XIE, C., WEI, W., RICHTER, B., DIRSCH, O. & DAHMEN, U. 2015. Intrahepatic Vascular Anatomy in Rats and Mice--Variations and Surgical Implications. *PloS one,* 10, e0141798.

SARKAR, M., WATT, K. D., TERRAULT, N. & BERENGUER, M. 2015. Outcomes in liver transplantation: does sex matter? *Journal of hepatology,* 62, 946-55.

SATO, T., ASANUMA, Y., KUSANO, T., SASAKI, N., SHINDO, Y. & KOYAMA, K. 1998. Difference in hepatic tissue oxygenation between total vascular exclusion and inflow occlusion of the liver and the possible role of hepatic venous blood under liver ischemia. *Digestive Surgery,* 15, 15-20.

SAVAS, U., WESTER, M. R., GRIFFIN, K. J. & JOHNSON, E. F. 2000. Rabbit pregnane X receptor is activated by rifampicin. *Drug metabolism and disposition: the biological fate of chemicals,* 28, 529-37.

SAWAYA, D. E., JR., ZIBARI, G. B., MINARDI, A., BILTON, B., BURNEY, D., GRANGER, D. N., MCDONALD, J. C. & BROWN, M. 1999. P-selectin contributes to the initial recruitment of rolling and adherent leukocytes in hepatic venules after ischemia/reperfusion. *Shock,* 12, 227-32.

SCHEER, N., KAPELYUKH, Y., RODE, A., OSWALD, S., BUSCH, D., MCLAUGHLIN, L. A., LIN, D., HENDERSON, C. J. & WOLF, C. R. 2015. Defining Human Pathways of Drug Metabolism In Vivo through the Development of a Multiple Humanized Mouse Model. *Drug metabolism and disposition: the biological fate of chemicals,* 43, 1679-90.

SCHLEGEL, A., GRAF, R., CLAVIEN, P. A. & DUTKOWSKI, P. 2013. Hypothermic oxygenated perfusion (HOPE) protects from biliary injury in a rodent model of DCD liver transplantation. *Journal of hepatology,* 59, 984-91.

SCHMUCKER, D. L., OHTA, M., KANAI, S., SATO, Y. & KITANI, K. 1990. Hepatic injury induced by bile salts: correlation between biochemical and morphological events. *Hepatology,* 12, 1216-21.

SCHON, M. R., KOLLMAR, O., AKKOC, N., MATTHES, M., WOLF, S., SCHREM, H., TOMINAGA, M., KEECH, G. & NEUHAUS, P. 1998. Cold ischemia affects sinusoidal endothelial cells while warm ischemia affects hepatocytes in liver transplantation. *Transplantation Proceedings,* 30, 2318-20.

SCHRUMPF, E., TAN, C., KARLSEN, T. H., SPONHEIM, J., BJORKSTROM, N. K., SUNDNES, O., ALFSNES, K., KASER, A., JEFFERSON, D. M., UENO, Y., EIDE, T. J., HARALDSEN, G., ZEISSIG, S., EXLEY, M. A., BLUMBERG, R. S. & MELUM, E. 2015. The biliary epithelium presents antigens to and activates natural killer T cells. *Hepatology,* 62, 1249-59.

SEMENZA, G. L. 2000. Cellular and molecular dissection of reperfusion injury: ROS within and without. *Circulation research,* 86, 117-8.

SENER, G., SEHIRLI, O., ERCAN, F., SIRVANCI, S., GEDIK, N. & KACMAZ, A. 2005. Protective effect of MESNA (2-mercaptoethane sulfonate) against hepatic ischemia/reperfusion injury in rats. *Surgery today,* 35, 575-80.

SENGA, S., ONITUKA, A., HIROSE, H., YAMAMOTO, K. & NIWA, K. 1990. Protective effect of liposomal encapsulated superoxide dismutase on ischemically injured liver in the rat. *Transplant Proc,* 22, 2025-6.

SHAH, Y. M., MA, X., MORIMURA, K., KIM, I. & GONZALEZ, F. J. 2007. Pregnane X receptor activation ameliorates DSS-induced inflammatory bowel disease via inhibition of NF-kappaB target gene expression. *American journal of physiology. Gastrointestinal and liver physiology,* 292, G1114-22.

SHARMA, S., GURAKAR, A. & JABBOUR, N. 2008. Biliary strictures following liver transplantation: past, present and preventive strategies. *Liver Transpl,* 14, 759-69.

SHI, H., YANG, G., ZHENG, T., WANG, J., LI, L., LIANG, Y., XIE, C., YIN, D., SUN, B., SUN, J., WANG, H., PAN, S., JIANG, H., LAU, W. & LIU, L. 2015. A preliminary study of ALPPS procedure in a rat model. *Scientific reports,* 5, 17567.

SHIBAYAMA, Y., ASAKA, S. & NISHIJIMA, A. 1991. Mechanism of liver injury following ischemia. *Exp Mol Pathol,* 55, 251-60.

SHIMIZU, H., HE, W., GUO, P., DZIADKOVIEC, I., MIYAZAKI, M. & FALK, R. E. 1994. Serum hyaluronate in the assessment of liver endothelial cell

function after orthotopic liver transplantation in the rat. *Hepatology,* 20, 1323-9.

SHUKLA, S. J., NGUYEN, D. T., MACARTHUR, R., SIMEONOV, A., FRAZEE, W. J., HALLIS, T. M., MARKS, B. D., SINGH, U., ELIASON, H. C., PRINTEN, J., AUSTIN, C. P., INGLESE, J. & AULD, D. S. 2009. Identification of pregnane X receptor ligands using time-resolved fluorescence resonance energy transfer and quantitative high-throughput screening. *Assay and drug development technologies,* 7, 143-69.

SHUKLA, S. J., SAKAMURU, S., HUANG, R., MOELLER, T. A., SHINN, P., VANLEER, D., AULD, D. S., AUSTIN, C. P. & XIA, M. 2011. Identification of clinically used drugs that activate pregnane X receptors. *Drug metabolism and disposition: the biological fate of chemicals,* 39, 151-9.

SILVER, E. H. & SZABO, S. 1983. Role of lipid peroxidation in tissue injury after hepatic ischemia. *Exp Mol Pathol,* 38, 69-76.

SINGER, M., DEUTSCHMAN, C. S., SEYMOUR, C. W., SHANKAR-HARI, M., ANNANE, D., BAUER, M., BELLOMO, R., BERNARD, G. R., CHICHE, J. D., COOPERSMITH, C. M., HOTCHKISS, R. S., LEVY, M. M., MARSHALL, J. C., MARTIN, G. S., OPAL, S. M., RUBENFELD, G. D., VAN DER POLL, T., VINCENT, J. L. & ANGUS, D. C. 2016. The Third International Consensus Definitions for Sepsis and Septic Shock (Sepsis-3). *JAMA,* 315, 801-10.

SINZ, M., WALLACE, G. & SAHI, J. 2008. Current industrial practices in assessing CYP450 enzyme induction: preclinical and clinical. *The AAPS journal,* 10, 391-400.

SIRICA, A. E. & GAINEY, T. W. 1997. A new rat bile ductular epithelial cell culture model characterized by the appearance of polarized bile ducts in vitro. *Hepatology,* 26, 537-49.

SJOVALL, S., AHREN, B. & BENGMARK, S. 1990. Intermittent hepatic dearterialization induces glucose intolerance: an experimental study in the rat. *Br J Surg,* 77, 405-8.

SOOKOIAN, S., CASTANO, G. O., BURGUENO, A. L., GIANOTTI, T. F., ROSSELLI, M. S. & PIROLA, C. J. 2010. The nuclear receptor PXR gene variants are associated with liver injury in nonalcoholic fatty liver disease. *Pharmacogenetics and genomics,* 20, 1-8.

SPIEGEL, H. U. & BAHDE, R. 2006. Experimental models of temporary normothermic liver ischemia. *J Invest Surg,* 19, 113-23.

STAUDINGER, J., LIU, Y., MADAN, A., HABEEBU, S. & KLAASSEN, C. D. 2001a. Coordinate regulation of xenobiotic and bile acid homeostasis by pregnane X receptor. *Drug metabolism and disposition: the biological fate of chemicals,* 29, 1467-72.

STAUDINGER, J. L., GOODWIN, B., JONES, S. A., HAWKINS-BROWN, D., MACKENZIE, K. I., LATOUR, A., LIU, Y., KLAASSEN, C. D., BROWN, K. K., REINHARD, J., WILLSON, T. M., KOLLER, B. H. & KLIEWER, S. A. 2001b. The nuclear receptor PXR is a lithocholic acid sensor that protects against liver toxicity. *Proceedings of the National Academy of Sciences of the United States of America,* 98, 3369-74.

STEDMAN, C. A., LIDDLE, C., COULTER, S. A., SONODA, J., ALVAREZ, J. G., MOORE, D. D., EVANS, R. M. & DOWNES, M. 2005. Nuclear receptors constitutive androstane receptor and pregnane X receptor ameliorate cholestatic liver injury. *Proceedings of the National Academy of Sciences of the United States of America,* 102, 2063-8.

STEENKS, M., VAN BAAL, M. C., NIEUWENHUIJS, V. B., DE BRUIJN, M. T., SCHIESSER, M., TEO, M. H., CALLAHAN, T., PADBURY, R. T. & BARRITT,

G. J. 2010. Intermittent ischaemia maintains function after ischaemia reperfusion in steatotic livers. *HPB : the official journal of the International Hepato Pancreato Biliary Association,* 12, 250-61.

STEPHEN, M. S., GALLAGHER, P. J., SHEIL, A. G., SHELDON, D. M. & STOREY, D. W. 1996. Hepatic resection with vascular isolation and routine supraceliac aortic clamping. *American journal of surgery,* 171, 351-5.

STRAZZABOSCO, M. & FABRIS, L. 2008. Functional anatomy of normal bile ducts. *Anat Rec (Hoboken),* 291, 653-60.

STRAZZABOSCO, M., FABRIS, L. & SPIRLI, C. 2005. Pathophysiology of cholangiopathies. *J Clin Gastroenterol,* 39, S90-S102.

SUSZYNSKI, T. M., RIZZARI, M. D., SCOTT, W. E., 3RD, TEMPELMAN, L. A., TAYLOR, M. J. & PAPAS, K. K. 2012. Persufflation (or gaseous oxygen perfusion) as a method of organ preservation. *Cryobiology,* 64, 125-43.

SUZUKI, S., NAKAMURA, S., SAKAGUCHI, T., MITSUOKA, H., TSUCHIYA, Y., KOJIMA, Y., KONNO, H. & BABA, S. 1998. Pathophysiological appraisal of a rat model of total hepatic ischemia with an extracorporeal portosystemic shunt. *J Surg Res,* 80, 22-7.

SYAL, G., FAUSTHER, M. & DRANOFF, J. A. 2012. Advances in cholangiocyte immunobiology. *American journal of physiology. Gastrointestinal and liver physiology,* 303, G1077-86.

SYNOLD, T. W., DUSSAULT, I. & FORMAN, B. M. 2001. The orphan nuclear receptor SXR coordinately regulates drug metabolism and efflux. *Nature medicine,* 7, 584-90.

TAKEDA, K., JIN, M. B., FUJITA, M., FUKAI, M., SAKURAI, T., NAKAYAMA, M., TANIGUCHI, M., SUZUKI, T., SHIMAMURA, T., FURUKAWA, H. & TODO, S. 2003. A novel inhibitor of Rho-associated protein kinase, Y-27632, ameliorates hepatic ischemia and reperfusion injury in rats. *Surgery,* 133, 197-206.

TENG, S. & PIQUETTE-MILLER, M. 2007. Hepatoprotective role of PXR activation and MRP3 in cholic acid-induced cholestasis. *British journal of pharmacology,* 151, 367-76.

TEOH, N. C. 2011. Hepatic ischemia reperfusion injury: Contemporary perspectives on pathogenic mechanisms and basis for hepatoprotection-the good, bad and deadly. *Journal of gastroenterology and hepatology,* 26 Suppl 1, 180-7.

TEOH, N. C. & FARRELL, G. C. 2003. Hepatic ischemia reperfusion injury: pathogenic mechanisms and basis for hepatoprotection. *Journal of gastroenterology and hepatology,* 18, 891-902.

TEOH, N. C., WILLIAMS, J., HARTLEY, J., YU, J., MCCUSKEY, R. S. & FARRELL, G. C. 2010. Short-term therapy with peroxisome proliferation-activator receptor-alpha agonist Wy-14,643 protects murine fatty liver against ischemia-reperfusion injury. *Hepatology,* 51, 996-1006.

TERADA, R., YAMAMOTO, K., HAKODA, T., SHIMADA, N., OKANO, N., BABA, N., NINOMIYA, Y., GERSHWIN, M. E. & SHIRATORI, Y. 2003. Stromal cell-derived factor-1 from biliary epithelial cells recruits CXCR4-positive cells: implications for inflammatory liver diseases. *Laboratory investigation; a journal of technical methods and pathology,* 83, 665-72.

TERC, J., HANSEN, A., ALSTON, L. & HIROTA, S. A. 2014. Pregnane X receptor agonists enhance intestinal epithelial wound healing and repair of the intestinal barrier following the induction of experimental colitis. *European journal of pharmaceutical sciences : official journal of the European Federation for Pharmaceutical Sciences,* 55, 12-9.

THERUVATH, T. P., ZHONG, Z., CURRIN, R. T., RAMSHESH, V. K. & LEMASTERS, J. J. 2006. Endothelial nitric oxide synthase protects transplanted mouse livers against storage/reperfusion injury: Role of vasodilatory and innate immunity pathways. *Transplantation proceedings,* 38, 3351-7.

THETHY, S., THOMSON, B., PLEASS, H., WIGMORE, S. J., MADHAVAN, K., AKYOL, M., FORSYTHE, J. L. & JAMES GARDEN, O. 2004. Management of biliary tract complications after orthotopic liver transplantation. *Clin Transplant,* 18, 647-53.

THULUVATH, P. J., GUIDINGER, M. K., FUNG, J. J., JOHNSON, L. B., RAYHILL, S. C. & PELLETIER, S. J. 2010. Liver transplantation in the United States, 1999-2008. *American journal of transplantation : official journal of the American Society of Transplantation and the American Society of Transplant Surgeons,* 10, 1003-19.

TOLSON, A. H. & WANG, H. 2010. Regulation of drug-metabolizing enzymes by xenobiotic receptors: PXR and CAR. *Advanced drug delivery reviews,* 62, 1238-49.

TOPALOGLU, S., IZCI, E., OZEL, H., TOPALOGLU, E., AVSAR, F. M., SAYGUN, O., UCAR, G., SOKMENSUER, C. & HENGIRMEN, S. 2005. Effects of TVE application during 70% hepatectomy on regeneration capacity of rats. *The Journal of surgical research,* 124, 139-45.

TRALHAO, J. G., ABRANTES, A. M., GONCALVES, A. C., HOTI, E., LARANJO, M., MARTINS, R., OLIVEIROS, B., CARDOSO, D., SARMENTO-RIBEIRO, A. B., BOTELHO, M. F. & CASTRO-SOUSA, F. 2013. Study of hepatocellular function in the murine model following hepatic artery selective clamping. *Acta Cir Bras,* 28, 657-63.

TSUBOI, K., TAZUMA, S., NISHIOKA, T. & CHAYAMA, K. 2004. Partial characterization of cytoprotective mechanisms of lecithin against bile salt-induced bile duct damage. *J Gastroenterol,* 39, 955-60.

TSUCHIYA, Y., SUZUKI, S., INABA, K., SAKAGUCHI, T., BABA, S., MIWA, M., KONNO, H. & NAKAMURA, S. 2003. Impact of endothelin-1 on microcirculatory disturbance after partial hepatectomy under ischemia/reperfusion in thioacetamide-induced cirrhotic rats. *J Surg Res,* 111, 100-8.

TZAKIS, A. G., GORDON, R. D., SHAW, B. W., JR., IWATSUKI, S. & STARZL, T. E. 1985. Clinical presentation of hepatic artery thrombosis after liver transplantation in the cyclosporine era. *Transplantation,* 40, 667-71.

UPPAL, H., TOMA, D., SAINI, S. P., REN, S., JONES, T. J. & XIE, W. 2005. Combined loss of orphan receptors PXR and CAR heightens sensitivity to toxic bile acids in mice. *Hepatology,* 41, 168-76.

VAN AS, A. B., LOTZ, Z., TYLER, M. & KAHN, D. 2002. Reperfusion injury associated with portal venous and hepatic arterial perfusion in liver transplantation. *Transplantation,* 74, 158-63.

VAN DER MEER, C., FABER, E. G. & VALKENBURG, P. W. 1971. Experiments on the cause of death in rats after permanent and temporary occlusion of the portal vein. *Proceedings of the Koninklijke Nederlandse Akademie van Wetenschappen. Series C. Biological and medical sciences,* 74, 76-91.

VAN DOMBURG, R., HOEKS, S., KARDYS, I., LENZEN, M. & BOERSMA, E. 2014. Tools and techniques--statistics: how many variables are allowed in the logistic and Cox regression models? *EuroIntervention : journal of*

EuroPCR in collaboration with the Working Group on Interventional Cardiology of the European Society of Cardiology, **9, 1472-3.**

VDOVIAKOVA, K., PETROVOVA, E., MALOVESKA, M., KRESAKOVA, L., TELEKY, J., ELIAS, M. Z. & PETRASOVA, D. 2016. Surgical Anatomy of the Gastrointestinal Tract and Its Vasculature in the Laboratory Rat. *Gastroenterology research and practice,* **2016, 2632368.**

VIGNAIS, P., VIGNAIS, P. M. & GRENOBLE SCIENCES (ORGANISATION) 2010. *Discovering life, manufacturing life : how the experimental method shaped life sciences,* **Dordrecht the Netherlands ; New York, Springer.**

VOLLMAR, B., GLASZ, J., LEIDERER, R., POST, S. & MENGER, M. D. 1994. Hepatic microcirculatory perfusion failure is a determinant of liver dysfunction in warm ischemia-reperfusion. *The American journal of pathology,* **145, 1421-31.**

VOLLMAR, B., RICHTER, S. & MENGER, M. D. 1996. Leukocyte stasis in hepatic sinusoids. *The American journal of physiology,* **270, G798-803.**

WALD, O., PAPPO, O., SAFADI, R., DAGAN-BERGER, M., BEIDER, K., WALD, H., FRANITZA, S., WEISS, I., AVNIEL, S., BOAZ, P., HANNA, J., ZAMIR, G., EID, A., MANDELBOIM, O., SPENGLER, U., GALUN, E. & PELED, A. 2004. Involvement of the CXCL12/CXCR4 pathway in the advanced liver disease that is associated with hepatitis C virus or hepatitis B virus. *European journal of immunology,* **34, 1164-74.**

WALLACE, K., BURT, A. D. & WRIGHT, M. C. 2008. Liver fibrosis. *The Biochemical journal,* **411, 1-18.**

WALLACE, K., COWIE, D. E., KONSTANTINOU, D. K., HILL, S. J., TJELLE, T. E., AXON, A., KORUTH, M., WHITE, S. A., CARLSEN, H., MANN, D. A. & WRIGHT, M. C. 2010. The PXR is a drug target for chronic inflammatory liver disease. *The Journal of steroid biochemistry and molecular biology,* **120, 137-48.**

WANG, L., BROWN, J. R., VARKI, A. & ESKO, J. D. 2002. Heparin's anti-inflammatory effects require glucosamine 6-O-sulfation and are mediated by blockade of L- and P-selectins. *The Journal of clinical investigation,* **110, 127-36.**

WANG, L. Q., ROOS, G., ANDERSSON, B., RENFJARD, E., PERSSON, B. & STENRAM, U. 1995. Tumour S-phase activity, nucleotide profile and RNA levels after hepatic artery occlusion and reperfusion in an experimental model of secondary liver carcinoma. *Br J Surg,* **82, 963-7.**

WATKINS, R. E., WISELY, G. B., MOORE, L. B., COLLINS, J. L., LAMBERT, M. H., WILLIAMS, S. P., WILLSON, T. M., KLIEWER, S. A. & REDINBO, M. R. 2001. The human nuclear xenobiotic receptor PXR: structural determinants of directed promiscuity. *Science,* **292, 2329-33.**

WERTHEIM, J. A., PETROWSKY, H., SAAB, S., KUPIEC-WEGLINSKI, J. W. & BUSUTTIL, R. W. 2011. Major challenges limiting liver transplantation in the United States. *American journal of transplantation : official journal of the American Society of Transplantation and the American Society of Transplant Surgeons,* **11, 1773-84.**

WILLSON, T. M. & KLIEWER, S. A. 2002. PXR, CAR and drug metabolism. *Nature reviews. Drug discovery,* **1, 259-66.**

WITTHAUT, R., FARHOOD, A., SMITH, C. W. & JAESCHKE, H. 1994. Complement and tumor necrosis factor-alpha contribute to Mac-1 (CD11b/CD18) up-regulation and systemic neutrophil activation during endotoxemia in vivo. *Journal of leukocyte biology,* **55, 105-11.**

WOLF, K. K., WOOD, S. G., HUNT, J. A., WALTON-STRONG, B. W., YASUDA, K., LAN, L., DUAN, S. X., HAO, Q., WRIGHTON, S. A., JEFFERY, E. H., EVANS, R. M., SZAKACS, J. G., VON MOLTKE, L. L., GREENBLATT, D. J., COURT, M. H., SCHUETZ, E. G., SINCLAIR, P. R. & SINCLAIR, J. F. 2005. Role of the nuclear receptor pregnane X receptor in acetaminophen hepatotoxicity. *Drug metabolism and disposition: the biological fate of chemicals,* 33, 1827-36.

WRIGHT, M. C. 2006. The impact of pregnane X receptor activation on liver fibrosis. *Biochemical Society transactions,* 34, 1119-23.

WRIGHT, M. C., ISSA, R., SMART, D. E., TRIM, N., MURRAY, G. I., PRIMROSE, J. N., ARTHUR, M. J., IREDALE, J. P. & MANN, D. A. 2001. Gliotoxin stimulates the apoptosis of human and rat hepatic stellate cells and enhances the resolution of liver fibrosis in rats. *Gastroenterology,* 121, 685-98.

XIANG, Y., JOHNSON, E. A., ZHANG, C., HUANG, G., HAYES, R. L., WANG, K. K. & SVETLOV, S. I. 2006. Generation of aberrant forms of DFF40 concurrent with caspase-3 activation during acute and chronic liver injury in rats. *Biochemical and biophysical research communications,* 350, 457-62.

XIE, W., BARWICK, J. L., DOWNES, M., BLUMBERG, B., SIMON, C. M., NELSON, M. C., NEUSCHWANDER-TETRI, B. A., BRUNT, E. M., GUZELIAN, P. S. & EVANS, R. M. 2000a. Humanized xenobiotic response in mice expressing nuclear receptor SXR. *Nature,* 406, 435-9.

XIE, W., RADOMINSKA-PANDYA, A., SHI, Y., SIMON, C. M., NELSON, M. C., ONG, E. S., WAXMAN, D. J. & EVANS, R. M. 2001. An essential role for nuclear receptors SXR/PXR in detoxification of cholestatic bile acids. *Proceedings of the National Academy of Sciences of the United States of America,* 98, 3375-80.

XIE, X., RIVIER, A. S., ZAKRZEWICZ, A., BERNIMOULIN, M., ZENG, X. L., WESSEL, H. P., SCHAPIRA, M. & SPERTINI, O. 2000b. Inhibition of selectin-mediated cell adhesion and prevention of acute inflammation by nonanticoagulant sulfated saccharides. Studies with carboxyl-reduced and sulfated heparin and with trestatin a sulfate. *The Journal of biological chemistry,* 275, 34818-25.

XU, W. H., YE, Q. F. & XIA, S. S. 2004. Apoptosis and proliferation of intrahepatic bile duct after ischemia-reperfusion injury. *Hepatobiliary Pancreat Dis Int,* 3, 428-32.

YAMADA, F., SAITO, T., ABE, T., TSUCHIYA, T., SATO, Y., KENJO, A., KIMURA, T. & GOTOH, M. 2007. Ischemic preconditioning enhances regenerative capacity of hepatocytes in long-term ischemically damaged rat livers. *Journal of gastroenterology and hepatology,* 22, 1971-7.

YAN, J. & XIE, W. 2016. A brief history of the discovery of PXR and CAR as xenobiotic receptors. *Acta pharmaceutica Sinica. B,* 6, 450-452.

YASOSHIMA, M., KONO, N., SUGAWARA, H., KATAYANAGI, K., HARADA, K. & NAKANUMA, Y. 1998. Increased expression of interleukin-6 and tumor necrosis factor-alpha in pathologic biliary epithelial cells: in situ and culture study. *Laboratory investigation; a journal of technical methods and pathology,* 78, 89-100.

YASWEN, P., HAYNER, N. T. & FAUSTO, N. 1984. Isolation of oval cells by centrifugal elutriation and comparison with other cell types purified from normal and preneoplastic livers. *Cancer research,* 44, 324-31.

YOUNG, C. S., PALMA, J. M., MOSHER, B. D., HARKEMA, J., NAYLOR, D. F., DEAN, R. E. & CROCKETT, E. 2001. Hepatic ischemia/reperfusion injury in P-selectin and intercellular adhesion molecule-1 double-mutant mice. *The American surgeon,* 67, 737-44.

YSKA, M. J., BUIS, C. I., MONBALIU, D., SCHUURS, T. A., GOUW, A. S., KAHMANN, O. N., VISSER, D. S., PIRENNE, J. & PORTE, R. J. 2008. The role of bile salt toxicity in the pathogenesis of bile duct injury after non-heart-beating porcine liver transplantation. *Transplantation,* 85, 1625-31.

ZAJKO, A. B., CAMPBELL, W. L., BRON, K. M., LECKY, J. W., IWATSUKI, S., SHAW, B. W., JR. & STARZL, T. E. 1985. Cholangiography and interventional biliary radiology in adult liver transplantation. *AJR Am J Roentgenol,* 144, 127-33.

ZAJKO, A. B., CAMPBELL, W. L., LOGSDON, G. A., BRON, K. M., TZAKIS, A., ESQUIVEL, C. O. & STARZL, T. E. 1987. Cholangiographic findings in hepatic artery occlusion after liver transplantation. *AJR. American journal of roentgenology,* 149, 485-9.

ZENG, W. Q., ZHANG, J. Q., LI, Y., YANG, K., CHEN, Y. P. & LIU, Z. J. 2013. A new method to isolate and culture rat kupffer cells. *PloS one,* 8, e70832.

ZHAI, Y., BUSUTTIL, R. W. & KUPIEC-WEGLINSKI, J. W. 2011. Liver ischemia and reperfusion injury: new insights into mechanisms of innate-adaptive immune-mediated tissue inflammation. *American journal of transplantation : official journal of the American Society of Transplantation and the American Society of Transplant Surgeons,* 11, 1563-9.

ZHAI, Y., PAI, H. V., ZHOU, J., AMICO, J. A., VOLLMER, R. R. & XIE, W. 2007. Activation of pregnane X receptor disrupts glucocorticoid and mineralocorticoid homeostasis. *Molecular endocrinology,* 21, 138-47.

ZHANG, H., LECULYSE, E., LIU, L., HU, M., MATONEY, L., ZHU, W. & YAN, B. 1999. Rat pregnane X receptor: molecular cloning, tissue distribution, and xenobiotic regulation. *Archives of biochemistry and biophysics,* 368, 14-22.

ZHANG, J., DING, L., WANG, B., REN, G., SUN, A., DENG, C., WEI, X., MANI, S., WANG, Z. & DOU, W. 2015a. Notoginsenoside R1 attenuates experimental inflammatory bowel disease via pregnane X receptor activation. *The Journal of pharmacology and experimental therapeutics,* 352, 315-24.

ZHANG, J., KUEHL, P., GREEN, E. D., TOUCHMAN, J. W., WATKINS, P. B., DALY, A., HALL, S. D., MAUREL, P., RELLING, M., BRIMER, C., YASUDA, K., WRIGHTON, S. A., HANCOCK, M., KIM, R. B., STROM, S., THUMMEL, K., RUSSELL, C. G., HUDSON, J. R., JR., SCHUETZ, E. G. & BOGUSKI, M. S. 2001. The human pregnane X receptor: genomic structure and identification and functional characterization of natural allelic variants. *Pharmacogenetics,* 11, 555-72.

ZHANG, X., WANG, Y., MA, Z., LIANG, Q., TANG, X., HU, D., TAN, H., XIAO, C. & GAO, Y. 2015b. Tanshinone IIA ameliorates dextran sulfate sodium-induced inflammatory bowel disease via the pregnane X receptor. *Drug design, development and therapy,* 9, 6343-62.

ZHAO, D. F., CHEN, D. Z., LV, J. S., LANG, R., JIN, Z. K. & QING, H. 2008. Establishment of an animal model of biliary ischemic stenosis with clamping in mice. *Transplantation proceedings,* 40, 1303-5.

ZHAO, H. F., ZHANG, G. W., ZHOU, J., LIN, J. H., CUI, Z. L. & LI, X. H. 2009. Biliary tract injury caused by different relative warm ischemia time in

liver transplantation in rats. *Hepatobiliary & pancreatic diseases international : HBPD INT,* 8, 247-54.

ZHOU, C., TABB, M. M., NELSON, E. L., GRUN, F., VERMA, S., SADATRAFIEI, A., LIN, M., MALLICK, S., FORMAN, B. M., THUMMEL, K. E. & BLUMBERG, B. 2006a. Mutual repression between steroid and xenobiotic receptor and NF-kappaB signaling pathways links xenobiotic metabolism and inflammation. *The Journal of clinical investigation,* 116, 2280-2289.

ZHOU, J., LIU, M., ZHAI, Y. & XIE, W. 2008. The antiapoptotic role of pregnane X receptor in human colon cancer cells. *Molecular endocrinology,* 22, 868-80.

ZHOU, J., ZHAI, Y., MU, Y., GONG, H., UPPAL, H., TOMA, D., REN, S., EVANS, R. M. & XIE, W. 2006b. A novel pregnane X receptor-mediated and sterol regulatory element-binding protein-independent lipogenic pathway. *The Journal of biological chemistry,* 281, 15013-20.

ZHOU, T., CHEN, J. L., SONG, W., WANG, F., ZHANG, M. J., NI, P. H. & GENG, J. G. 2002. Effect of N-desulfated heparin on hepatic/renal ischemia reperfusion injury in rats. *World J Gastroenterol,* 8, 897-900.

ZHU, Z., KIM, S., CHEN, T., LIN, J. H., BELL, A., BRYSON, J., DUBAQUIE, Y., YAN, N., YANCHUNAS, J., XIE, D., STOFFEL, R., SINZ, M. & DICKINSON, K. 2004. Correlation of high-throughput pregnane X receptor (PXR) transactivation and binding assays. *Journal of biomolecular screening,* 9, 533-40.

ZIELLO, J. E., JOVIN, I. S. & HUANG, Y. 2007. Hypoxia-Inducible Factor (HIF)-1 regulatory pathway and its potential for therapeutic intervention in malignancy and ischemia. *The Yale journal of biology and medicine,* 80, 51-60.

ZOGRAFOS, G. N., KAKAVIATOS, N. D., SKIATHITIS, S. & HABIB, N. 1999. Total vascular exclusion for liver resections: pros and cons. *Journal of surgical oncology,* 72, 50-5; discussion 55-6.

ZORN, A. M. 2008. Liver development. *StemBook.* Cambridge (MA).